32nd Annual Combustion Research Meeting

Airlie Conference Center
Warrenton, Virginia
May 31 – June 3, 2011

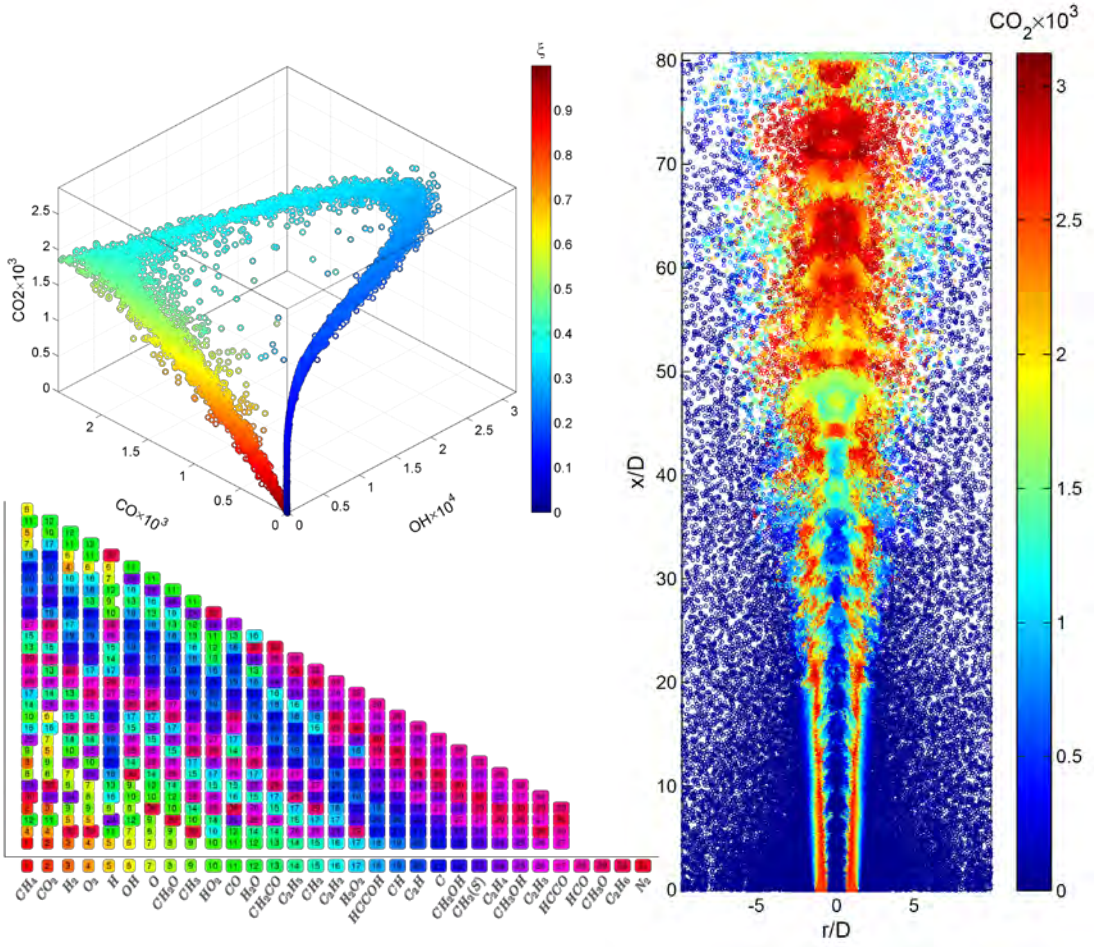

U.S. DEPARTMENT OF ENERGY | Office of Science

Office of Basic Energy Sciences
Chemical Sciences, Geosciences & Biosciences Division

32nd Annual Combustion Research Meeting

DOE Contractors' Meeting Program and Abstracts

Airlie Conference Center
Warrenton, Virginia
May 31 – June 3, 2011

Chemical Sciences, Geosciences, and Biosciences Division
Office of Basic Energy Sciences
Office of Science
U.S. Department of Energy

Cover Graphics:
Simulations of turbulent methane flames using large-eddy simulation (LES) and probability density function (PDF) methods. From the particles in an LES/PDF simulation of the Barlow & Frank flame D: (right) scatter plot in an axial-radial plane of CO_2; and (top left) scatter plot of CO, CO_2 and OH , color coded by mixture fraction. Bottom: species in order of importance (as determined by the GALI algorithm) for use in the RCCE reduced description of methane combustion. The columns show the ordering of the species considered for addition at each stage.

Haifeng Wang, Varun Hiremath & Stephen Pope, Cornell University

This document was produced under contract number DE-AC05-06OR23100 between the U.S. Department of Energy and Oak Ridge Associated Universities.

The research grants and contracts described in this document are supported by the U.S. DOE Office of Science, Office of Basic Energy Sciences, Chemical Sciences, Geosciences and Biosciences Division.

Foreword

This abstract booklet provides a record of the thirty-second U.S. Department of Energy principal investigators' meeting focused on gas-phase chemical physics. The reports appearing in this volume present work in progress in basic research contributing to the development of a predictive capability for combustion processes. The work reported herein is supported by the Department of Energy's Office of Basic Energy Sciences (BES) and, in large measure, by the chemical physics program. The long-term objective of this effort is the provision of theories, data, and procedures to enable the development of reliable computational models of combustion processes, systems, and devices.

The objective of this meeting is to provide a fruitful environment in which researchers with common interests will present and exchange information about their activities, will build collaborations among research groups with mutually reinforcing strengths, will identify needs of the research community, and will uncover opportunities for future research directions. The agenda consists of an invited keynote talk, oral presentations by program PIs and invited poster presentations from junior level researchers in an effort to increase the awareness of the Gas Phase Chemical Physics program. Approximately one third of the PIs in the program speak each year in rotation. With ample time for discussion and interactions, we emphasize that this is an informal meeting for exchange of information and building of collaborations; it is not a review of researchers' achievements or a forum to define the future direction of the program.

We appreciate the privilege of serving in the management of this research program. In carrying out these tasks, we learn from the achievements and share the excitement of the research of the many sponsored scientists and students whose work is summarized in the abstracts published on the following pages.

We thank all of the researchers whose dedication and innovation have advanced DOE BES research and made this meeting possible and productive. We hope that this conference will help you will build on your successes and we look forward to our assembly next year for our 33rd annual meeting.

We thank Diane Marceau of the Chemical Sciences, Geosciences and Biosciences Division, and Connie Lansdon and Tim Ledford of the Oak Ridge Institute for Science and Education for their important contributions to the technical and logistical features of this meeting.

Michael Casassa
Mark Pederson
Wade Sisk

Agenda

32nd Annual Combustion Research Meeting
U.S. Department of Energy
Office of Basic Energy Sciences

Agenda

Tuesday, May 31, 2011

3:00 pm *Registration*

5:00 pm *No-host Reception at The Whistling Swan Pub*

7:00 pm *Dinner*

Wednesday, June 1, 2011

7:00 am *Breakfast*

Session I
David J. Nesbitt, Chair & Meeting Co-Chair

8:00 am Welcome and Introduction – Wade Sisk, DOE/BES
Introduction of Invited Poster Presenters – Jacqueline Chen, Meeting Co-chair

8:30 am **Keynote Speaker** "Laser Diagnostics at High Repetition Rates: Progress and Challenges," Andreas Dreizler, Technische Universität Darmstadt..... 1

9:30 am "Advanced Nonlinear Optical Methods for Quantitative Measurements in Flames," Robert Lucht, Purdue University..... 193

10:00 am "Computational and Experimental Study of Flames," Mitchell D. Smooke and Marshall B. Long, Yale University..... 295

10:30 am *Break*

Session II
Habib Najm, Chair

11:00 am "Theory and Modeling of Small Scale Processes in Turbulent Flow," Alan R. Kerstein, Sandia National Laboratories 157

11:30 am "Investigation of Non-premixed Turbulent Combustion," Stephen B. Pope, Cornell University..... 263

12:00 pm *Lunch*

Session III
Nancy Brown, Chair

4:00 pm "Modeling Reactions in High-Pressure Turbulence in the Cold Ignition Regime," Josette Bellan, California Institute of Technology.....37

4:30 pm "LES of Turbulence-Chemistry Interaction in Reacting Multiphase Flows," Joseph Oefelein, Sandia National Laboratories.....241

5:00 pm Poster Session / Reception (Garden Room)

"Multi-scale Simulation of Turbulent Flames—Soot, Fire, and Flame Extinction and Re-ignition," David O. Lignell, Brigham Young University 3

"Elucidating the Initial Steps of Combustion at a Detailed Molecular Level," Michael C. McCarthy, Harvard-Smithsonian Center for Astrophysics 5

"Characterization of Combustion Radicals via Matrix-Isolation FTIR," Laura R. McCunn, Marshall University.....9

"Improving Our Understanding of Turbulent Combustion Physics," Carlos A. Pantano-Rubino, University of Illinois.....11

"Addressing Complexity in Combustion Simulation: From Model Reduction to Software Design," James C. Sutherland, University of Utah.....13

"Threshold and Imaging Photoelectron Photoion Coincidence Spectroscopy Experiments for High-Accuracy Thermochemistry," Bálint Sztáray, University of the Pacific.....17

6:00 pm *Dinner*

Thursday, June 2, 2011

7:00 am *Breakfast*

Session IV
Carol Parish, Chair

8:00 am "Chemical Accuracy from Ab Initio Molecular Orbital Calculations," Martin Head-Gordon, University of California Berkeley 129

Session V
Robert Continetti, Chair

Session VI
Amy Mullin, Chair

Session VII
David Osborn, Chair

6:00 pm "Hydrocarbon Radical Thermochemistry: Gas-Phase Ion Chemistry Techniques," Kent M. Ervin, University of Nevada..... 85

6:30 pm "Determination of Accurate Energetic Database for Combustion Chemistry by High-Resolution Photoionization and Photoelectron Methods," Cheuk-Yiu Ng, University of California Davis.....237

7:00 pm *Dinner at the Pavilion*

Friday, June 3, 2011

7:00 am *Breakfast*

Session VIII
Wesley Allen, Chair

8:00 am "The Dynamics of Large-Amplitude Motion in Energized Molecules," David S. Perry, University of Akron 251

8:30 am "Theoretical Studies in Spectroscopy and Chemical Dynamics," Hua-Gen Yu, Brookhaven National Laboratory 339

9:00 am "Time-Resolved Infrared Absorption Studies of Radical Reactions," R. Glen Macdonald, Argonne National Laboratory 197

9:30 am *Break*

Session IX
William Green, Chair

10:00 am "Experimental Ignition Studies of Oxygenated Hydrocarbons," Margaret S. Wooldridge, University of Michigan 331

10:30 am "Chemical Kinetic Modeling of Combustion Chemistry," W. J. Pitz and C. K. Westbrook, Lawrence Livermore National Laboratory.....259

11:00 am "Elementary Reaction Kinetics of Combustion Species," Craig A. Taatjes, Sandia National Laboratories.....307

11:30 am Closing Remarks

12:00 pm *Lunch*

Table of Contents

Table of Contents

Abstracts of Invited Presentations

32nd Annual Combustion Research Conference
May 31st – June 3rd 2011
Airline Conference Center, Warrenton,Virginia, USA

Laser combustion diagnostics at high repetition rates: progress and challenges

Andreas Dreizler
Inst. Reactive Flows and Diagnostics, Center of Smart Interfaces, Mechanical Engineering, Technische Universität Darmstadt, Germany, email: dreizler@csi.tu-darmstadt.de

Laser diagnostics guide an improved understanding of turbulent combustion processes. Until recently data rates were too low to resolve transients. Although low data rates are suited for determining statistical moments, highly dynamic processes being far from statistically stationary are in this way not accessible. Hence much shorter pulse-to-pulse separations are essential resolving ideally Kolmogorov time-scales.

Significant improvements in laser and CMOS detector technology enabled transfer of well-established planar laser diagnostics such as particle image velocimetry (PIV), laser-induced fluorescence (LIF), or Rayleigh scattering into the regime of multiple kHz repetition rates. Applied to highly dynamic processes such as flame extinction, ignition processes, flash back into nozzles, cyclic variations in internal combustion engines, or lifted flames a growing fraction of the combustion-community demonstrated that high speed diagnostics actually does support an improved physical understanding of transient processes providing a complementary view at complex combustion phenomena that is not accessible by sampling statistically independent.

Most of these studies at kHz data rates, however, were based on qualitative detector signals. Such information is sufficient for calculating cross-correlations in PIV or tracking flame fronts using for example OH PLIF. For quantitative temperature, mixture fraction, or concentration measurements at high sampling rates a linear response, reproducible offsets, and long term stability are crucial attributes for quantifying CMOS detector signals and calibration procedures. State-of-the-art CMOS cameras and image intensifiers designed for high frame rates suffer either from physical constraints or from not being designed for scientific imaging. These short comings need to be addressed in much more detail before reliable quantitative scalar imaging becomes trustworthy.

Another shortcoming of present high speed imaging is the restriction to two spatial directions and time resulting in three-dimensional sampling. As turbulent combustion is spatially three-dimensional a challenge for future is (quasi) four-dimensional imaging. In fluid dynamics tomographic approaches already emerged allowing for volumetric velocimetry (Tomo-PIV). For scalar imaging multiple-sheet approaches were used but not yet temporally tracked. Even higher pulse repetition rates in combination with adequate laser pulse energies and very fast scanning devices may offer one possibility to tackle this challenge.

In this contribution some selected examples are reviewed exemplifying the potential of planar diagnostics at kHz repetition rates. Towards quantitative imaging limitations of state-of-the art CMOS detectors are addressed and first attempts for planar temperature measurements are discussed. Finally, initial steps towards quasi-4D-imaging are presented.

References

- V. Weber, J. Brübach, R.L. Gordon, A. Dreizler: Pixel-based non-linear characterisation of CMOS high speed camera systems; Appl. Phys. B, DOI: 10.1007/s00340-011-4443-1
- B. Böhm, C. Heeger, R. Gordon, A. Dreizler: New perspectives on turbulent combustion: Multi-parameter high-speed laser diagnostics; Flow Turbulence and Combustion, DOI 10.1007/s10494-010-9291-2
- C. Heeger, R.L. Gordon, M.J. Tummers, T. Sattelmayer, A. Dreizler: Experimental analysis of flashback in lean premixed swirling flames: upstream flame propagation; Exp. in Fluids 49, 853 – 864 (2010)
- B. Bork, B. Böhm, C. Heeger, S.R. Chakravarthy, A. Dreizler: 1D high-speed Rayleigh measurements in turbulent flames; Appl. Phys. B 101, 487 – 491 (2010)

Multi-scale simulation of turbulent flames—soot, fire, and flame extinction and reignition

David O. Lignell

32nd Annual Combustion Research Meeting,
May 31-June 3, 2011, Warrenton, Virginia
U.S. Department of Energy, Office of Science, Office of Basic Energy

A great challenge of turbulent combustion simulation is the problem of the wide range of time and length scales present. Resolution of all continuum scales is not possible at the high Reynolds numbers of practical flows that exist in, e.g., engines, combustors, furnaces, and fires. A quantitative understanding of the reacting flows in these devices and environments is crucial to enable next-generation predictivity and design capabilities. This is especially true for devices requiring improved efficiency and reduced emissions, under increasingly complex conditions such as high pressure, vitiated flows, with complex fuels.

The research presented is the simulation of reacting flows to provide insight into fundamental turbulence-chemistry interactions; to develop and validate combustion models; and to advance multi-scale simulation techniques. The goals of the work are to develop affordable multi-scale simulation approaches that can be applied to complex flow configurations, and that are regime independent (for example, not requiring separate models for premixed or non-premixed flames).

Simulation results are presented of flames with significant scale-overlap and finite rate chemistry: soot formation, and flame extinction and reignition. Results from direct numerical simulations (DNS) are presented that provide insight into these processes, and numerical data for model validation. The DNS highlight the importance of fine structures on the impact of reactive scalars. Flame topology is an important factor in soot formation due to differential diffusion effects that dictate soot-flame interactions including enhanced growth and oxidation. These interactions, however, depend on the relation of the mixing timescale to the soot reaction and coagulation rates. Similarly, local flow structures significantly impact flame extinction, and the subsequent reignition processes. Flames are initially extinguished in regions of flame curvature centered in the fuel stream where scalar dissipation rates are higher. As extinction is more pervasive, this dependence becomes less important. During reignition, the competition between flame folding and edge propagation is important, with the latter an inherently multi-dimensional process.

DNS cannot be extended to flows of practical interest due to high computational costs, and is limited in the number of simulations that can be performed, and in the range of parameters that can be varied (costs scale with Re^3, limiting the range of scales accessible). The one-dimensional turbulence (ODT) model allows extension to a broader range of flow parameters, such as higher Reynolds numbers or Schmidt

numbers while resolving the fine scales, but only in one dimension, and requires modeling of large-scale advection. Results of ODT applied to fire and DNS of flame extinction are presented. In some fires, flame propagation is observed to occur by direct contact of flames with the unburnt fuel. However, direct resolution of flames is not computationally efficient. The ODT model is being applied to investigate flame propagation in fires through statistics of the turbulent flame brush in vertical ethylene wall fires. This configuration is used as a canonical flow for an advancing vertical fire through a fuel bed, such as grass or brush. A validation study comparing ODT to DNS of flame extinction and reignition has also been performed in an effort to quantify the capabilities and limitations of the ODT model for resolving flames in a most challenging configuration. Three simulations are performed with increasing levels of extinction of 40%, 70%, and nearly 100%. The final case begins as a nonpremixed flame, and reignites as a premixed flame through a stratified mixture of fuel, oxidizer, and combustion products. ODT results show good agreement for flow evolution and extinction processes, but a significant under prediction of reignition in the first two cases due to the inability of ODT to capture edge flame propagation for configurations in which edge flames are important. Preliminary results indicate that ODT captures the premixed reignition process.

The abilities of ODT to resolve fine scale processes, along with its limitations to canonical configurations and inability to capture large-scale flow dynamics motivates the extension of the model to three-dimensional formulations. This approach is termed autonomous microstructure evolution, or AME, and consists of a lattice of ODT lines spaced at a nominal LES level or greater (since ODT captures large scales, just not three dimensional large scales). AME has the potential to offer regime-independent simulations of complex turbulent flows at a cost comparable to (or somewhat higher than) LES, but significantly less than DNS, and at high Reynolds numbers. The resolution of fine scales (albeit at lower dimensionality) in the physical coordinate is a potential advantage over most current subgrid models that operate in a state space, and are difficult to extend beyond their originally intended use.

Elucidating the Initial Steps of Combustion at a Detailed Molecular Level

Michael C. McCarthy
Harvard-Smithsonian Center for Astrophysics
Cambridge, MA 02138
mccarthy@cfa.harvard.edu

I. Program Scope

A research program using broadband and cavity rotational spectroscopy to elucidate the chemical pathways and reactive intermediates in combustion processes is proposed. Using an array of sensitive spectroscopic tools and production methods, oxidation pathways that involve reactions between hydrocarbons and the OH and HO_2 radicals to produce reactive oxygen species (ROS) will be explored. One important objective of this effort is to clarify the role that water seems to play in enhancing ROOH formation. In a separate, but related effort, we seek to detect and structurally characterize key intermediates whose geometries are either unknown at high spectral resolution or are uncertain on the basis of theoretical calculations (e.g., linear heavy atom versus branched backbones). Such studies are needed because differences in geometry can strongly affect reactivity, such as barriers to intramolecular H-abstractions. As part of this effort, precise experimental structures and dipole moments will be determined for several well-known hydrocarbon radicals and carbenes that are important intermediates in combustion environments. Such measurements provide needed benchmarks for quantum chemical calculations, so that theoretical predictions of similar-sized and larger reactive molecules can be made more accurate. Preliminary experiments have been undertaken with good success in each of the two proposed areas of endeavor, suggesting that with additional effort, significant advances should be possible.

II. Recent Progress

A. Characterizing oxygen-chain intermediates at high-spectral resolution

Producing key ROS such as R•, RO•, and ROO• in high concentrations has often proved challenging, but we have recently demonstrated that the combination of Fourier transform microwave rotational spectroscopy and an electrical discharge through H_2 and O_2 is a very efficient way to produce and detect the weakly-bound HO•••OO complex at very high spectral resolution. The H_2/O_2 discharge also produces OH (from direct detection of its strong, low-frequency lambda-doublet transitions) and HO_2 (and likely H_2O) in high concentration, as evidenced from detection of modestly strong lines of the H_2O•••HO_2 complex under the same experimental conditions (see Fig. 1). A plausible inference of this work is that the introduction of hydrocarbon fuels might efficiently produce oxy, peroxyl, and carbon-containing radicals, and that these can be detected with the same instrumentation. Owing to the high abundance of HO•••OO in our molecular beam, we have recently undertaken isotopic studies of this important intermediate [1] which establish: (1) it is formed via the reaction OH + O_2, (2) it possesses a long central O—O bond (about 1.68 Å), in agreement with earlier work [2], but one that deviates significantly from high-level theoretical calculations [3] which predict a much shorter O—O bond length (in the range 1.58—1.62 Å), and (3) it possesses a surprisingly short O—H bond distance (0.93 Å), which is also in poor agreement with theory (0.97 Å).

HO•••OO serves as a specific example of a more general phenomenon, and one that demonstrates the need for high-resolution spectroscopic investigations: the difficulty that prereactive complexes pose for ab initio theory, even when high-level quantum chemical methods (e.g. coupled cluster) are employed. For this reason, considerable care is required to accurately calculate molecular properties at present. Because small alkyl peroxy radicals often undergo low-barrier conformational rearrangements (see Ref. 4 and references therein), the same situation may also apply to these molecular systems. Structural information inferred from optical measurements may be of limited utility in some instances, owing to the substantially

lower spectral resolution of laser spectroscopy relative to microwave spectroscopy. We note, for example, that the derived rotational constants of CH_3OO• (the simplest alkyl peroxy radical) from laser [5] and microwave experiments [6] can different considerably (i.e. by more than 5%).

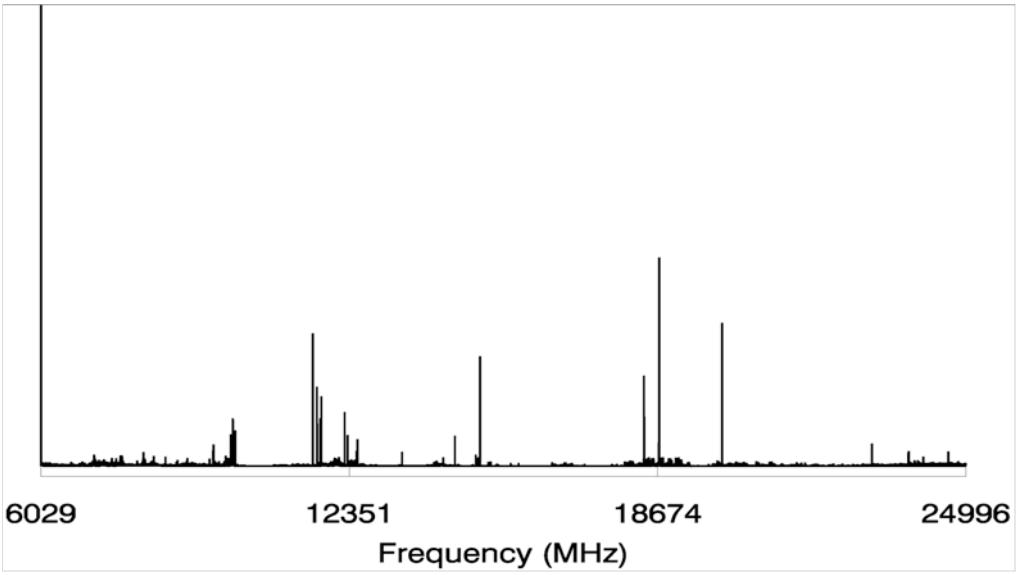

Fig. 1. The broadband rotational spectrum (6-25 GHz) through a discharge of H_2 and O_2. Strong lines near 6 and 13.4 GHz arise from OH, and those near 18.8 GHz are from HOOO•; many of the remaining lines are presently unassigned.

B. Providing Structural Information on Key Radicals: Implications for Reactivity and Kinetic Modeling

Knowledge of molecular properties is crucial in combustion chemistry. For example, bond dissociation energies aid in predicting relative reactivities, and are widely used in rationalizing the importance of specific reactions that occur for a particular fuel [4]. More generally, chemical networks of combustion are based on extensive theoretical calculations, of which only a small fraction are directly corroborated by experiment. Free radicals play a central role in these networks, but often represent the greatest challenge to theory owing to well-known difficulties that an unpaired electron sometimes induces. Although direct measurement of the properties of many free radicals are probably impractical because of their short chemical lifetimes, the means are now at hand to structurally characterize a number of reactive intermediates whose geometries are either unknown at high spectral resolution or are uncertain on the basis of theoretical calculations. Basic structural information (e.g., a linear heavy atom versus a branched backbone) provides a firm foundation by which corresponding properties of these radicals, such as reactivity (barrier heights for H-atom abstraction) and dipole moments, can then be incorporated into kinetic modeling on the basis of calculation. For example, self-destruction reaction rates of different butyl peroxyl isomers have been shown to vary by more than 100 [7]; establishing that C_6H radical has a $^2\Pi$ rather than a $^2\Sigma$ ground state [8] implies a much larger dipole moment (5.6 D vs. 0.8 D; Ref. [9]), which has implications to energy-transfer calculations. Detailed structural analysis of a small number of prototypical radicals that are known to be present in high abundance under a wide range of combustion conditions will also be undertaken as part of this effort.

Work is now underway to precisely determine the structure and dipole moments of six key free radicals: propargyl (H_2C_3H•), phenyl (C_6H_5•), benzyl ($C_6H_5CH_2$•), fulvenyl, and phenoxy (C_6H_5O•), by

means of rotational spectroscopy at centimeter and millimeter wavelengths, and Stark measurements. By providing these benchmarks for theory, calculations of related radicals and still larger systems can be based on a very firm foundation using the right combination of level of theory and basis set. In addition to their use in energy-transfer calculations, dipole moments provide an important check of the electronic wavefunction, and therefore represent a sensitive and simple test of theory.

From prior or preliminary experiments in our laboratory, isotopic spectroscopy of each radical should be straightforward. For instance, some time ago ^{13}C lines of H_2C_3H• were detected by our group using propargyl chloride as a precursor, despite the very small dipole moment (of order 0.15 D) of this radical. In the case of ortho-benzyne, a complete structural analysis was undertaken by isotopic spectroscopy [10], yield precise bond lengths and angles for this simple enediyne (see Fig. 2). Following our work on the rotational spectrum of the phenyl [11] radical, additional searches were undertaken, yielding evidence for at least one vibrationally excited state. The ^{13}C species are predicted to be detectible at only one-half the intensity of these rotational satellites, implying that with dedicated searches, these too can be found. If necessary, the isotopic investigations proposed here can likely be extended to other hydrocarbon and ROS, as they have already for a number of carbon chain radicals [12].

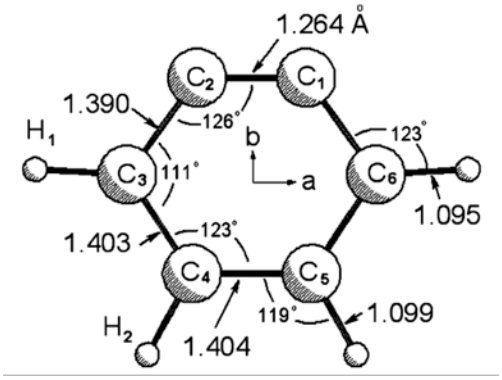

Fig. 2. The experimental structure of ortho-benzyne as determined by microwave spectroscopy of its rare isotopic species (Ref. 10). We find most importantly that the C_1-C_2 bond length, is 1.264(3) Å, only 0.057 Å longer than the free acetylene bond. Similar structural analyses for other combustion intermediates such as propargyl and phenyl radicals can likely be undertaken with present techniques, allowing electronic structure theorists to validate their calculations.

III. Future Work

Looking forward, a major thrust of our research effort is to undertake rotational studies of water and closely-related complexes of HO_2, to determine precise molecular structures for these long-lived intermediates, and to provide accurate transitions frequencies for use in direct detection, using both broadband chirped and cavity FT microwave spectroscopies. Some of the most immediate goals are to derive a precise experimental structure for the H_2O•••HO_2 complex and to detect larger complexes. Because of intrinsically high sensitivity and spectral resolution of our techniques, the rotational studies of a number of oxy and peroxy reactive intermediates RO• and ROO• will likely be an important by-product of this work.

We also intend to target specific classes of ROS where the location of the radical site (i.e. an unsaturated carbon atom) may introduce a structural ambiguity, or radicals which may possess several distinct, low-lying isomers. Vinylic radicals such as CH_2CHCCH_2, for example, may possess either a linear CCC backbone like allene or a bent backbone like the parent butadiene. Determining the most stable isomer for the various butyl peroxyl isomers and its structure by microwave spectroscopy of a supersonic molecular beam establishes the ground state energy, provides clear benchmarks for theory, and has important implications for reactivity — all of which can be used to improve chemical modeling. Our group has considerable experience in reactive molecule spectroscopy and structural analysis: nearly 200

entirely new species, including ions, branching chains, reactive hydrocarbon rings, etc. have been detected at high spectral resolution in our laboratory during the past 15 years.

IV. References

1. Derro, E. L.; Murray C.; Sechler, T. D.; Lester, M. I. *J. Phys. Chem. A* **2007**, *111*, 11592.
2. Suma, K.; Sumiyoshi, Y.; Endo, Y. *Science* **2005**, *308*, 1885.
3. Varner, M. E.; Harding, M. E.; Gauss, J.; Stanton, J. F. *Chem. Phys. Lett.* **2006**, *346*, 53.
4. Sharma, S. **2009**, Ph.D. Thesis, MIT, entitled ``Predictive Modeling of Combustion Processes''.
5. Chung, C.-Y.; Cheng, C.-W.; Lee, Y.-P.; Liao, H.-Y.; Sharp, E. N.; Rupper, P.; Miller, T. A. *J. Chem. Phys.* **2007**, *127*, 044311.
6. Endo, Y. private communication; Katoh, K., **2007**, Ph.D. Thesis, University of Tokyo.
7. Glover, B. G.; Miller, T. A. *J. Phys. Chem. A* **2005**, *109*, 11191.
8. Pearson, J. C.; Gottlieb, C. A.; Woodward, D. R.; Thaddeus, P. *Astron. Astrophys.* **1988**, *189*, L13.
9. Woon, D. E. *Chem. Phys. Lett.* **1995**, *244*, 45.
10. Kukolich, S. G.; McCarthy, M. C.; Thaddeus, P. *J. Phys.* Chem. A **2004**, *108*, 2645.
11. McMahon, R. J.; McCarthy, M. C.; Gottlieb, C. A.; Dudek, J. B.; Stanton, J. F.; Thaddeus, P. *Ap. J. Lett. 2003*, **590**, L61.
12. McCarthy, M. C.; Thaddeus, P. *J. Chem. Phys.* **2005**, *122*, 174308.

Characterization of Combustion Radicals Via Matrix-Isolation FTIR

Laura R. McCunn
Department of Chemistry, Marshall University
One John Marshall Drive
Huntington, WV 25755-2520
mccunn@marshall.edu

I. Program Scope

We aim to characterize radicals that are formed during combustion processes by matrix-isolation spectroscopy. A significant part of our work is the identification of molecules that may serve as clean precursors to selected radicals through pyrolysis or photolysis. Our initial focus is on the $C_2H_3O_2$ radical isomers, which occur as intermediates in the reaction of the vinyl radical and O_2.[i,ii] Our experiments are designed to trap radicals in a low-temperature argon matrix and to record their vibrational spectra. The data will serve as experimental benchmarks for the structures of these radicals by comparison to *ab initio* calculations. We also aim to probe the reactivity of the radicals within the matrix by irradiating them with broadband UV light. Identification of the photolysis products by FTIR may offer insight to the fate of such radicals formed during combustion.

II. Recent Progress

In 2009, a matrix-isolation FTIR apparatus was constructed in collaboration with undergraduate research students at Marshall University. We have since investigated several molecules that could serve as precursors to the methoxycarbonyl radical, CH_3OCO. Methyl chloroformate, $CH_3OC(O)Cl$ is known to be a photolytic precursor to methoxycarbonyl in the gas phase,[iii] so we attemped broadband UV irradiation of this molecule isolated in argon, but no photochemical reactions were observed. Dimethyl oxalate, $CH_3OC(O)C(O)OCH_3$, was investigated with similar results. We have also recorded the FTIR spectrum of methyl pyruvate isolated in an argon matrix. To aid in identification of the *cis*- and *trans*- isomers, we have performed calculations using Gaussian 09. Matrix-isolated methyl pyruvate was irradiated to probe for conformational changes.

III. Future Work

A hyperthermal nozzle[iv] has recently been added to the matrix-isolation FTIR apparatus. Research efforts are now devoted to testing halogenated hydrocarbons and other molecules which are likely to generate the $C_2H_3O_2$ radical isomers. We are attempting pyrolysis of methyl chloroformate to produce the methoxycarbonyl radical. Dimethyl oxalate will also be investigated as a possible precursor to methoxycarbonyl as cleavage of the central carbon-carbon bond in this symmetric molecule would produce two methoxycarbonyl radicals.

IV. References

i. A. M. Mebel, E. W. Diau, M. C. Lin, and K. Morokuma, *J. Am. Chem. Soc.* **1996**, 118, 9759.
ii. R. Yang, L. Yu, X. Jin, M. Zhou, and B. K. Carpenter, *J. Chem. Phys.* **2005**, *122*, 014511.
iii. L. R. McCunn, K.-C. Lau, M. J. Krisch, L. J. Butler, J.-W. Tsung and J. J. Lin, *J. Phys. Chem. A* **2006**, *110*, 1625.
iv. X. Zhang, A. V. Friderichsen, S. Nandi, G. B. Ellison, D. E. David, J. T. McKinnon, T. G. Lindeman, D. C. Dayton, and M. R. Nimlos, *Rev. Sci. Instrum.* **2003**, *74*, 3077.

Improving our understanding of turbulent combustion physics

Carlos Pantano (cpantano@illinois.edu)
Department of Mechanical Science and Engineering
University of Illinois at Urbana-Champaign

The poster describes results from very large-scale computational fluid dynamics simulations applied to the study of turbulent nonpremixed combustion. The research focuses on the physics of turbulence, turbulent-combustion interaction, and flame structure using techniques borrowed from applied mathematics, fluid physics, and high-performance simulation. The results of these detailed studies are then used to develop dynamical reduced-order flame models for more comprehensive, and practical, simulation tools that are capable of representing all aspects of the design and optimization of energy conversion systems; i.e., fluid, thermal, structural, etc. The main difficulty of turbulent combustion modeling is the presence of chemical reactions that even for the simplest hydrocarbons, such as methane, can involve hundreds of species. More practical liquid hydrocarbons involve multiple phases and thousands of reactions. Therefore, it is important to establish an accurate way to model the turbulence and chemistry interaction without having to compute all the details of the chemistry. Our work tries to improve understanding of the relevant aspects of turbulence physics for combustion applications (density variation and mixing rates), coupled with the development of flame models that extract their internal structure, where the energy conversion happens. The flame models then interact with turbulence in a dynamic manner and are general enough but computationally tractable to affect engineering practice.

Simulating turbulent flows is generally very challenging, and our work does not attempt to address all the questions encountered in these flows. Instead, we focus on the differences that combustion introduces in turbulent flows. One can identify several hierarchies of interactions within the flow. At the lowest level, flames alter the transport properties of the fluid, primarily by changing the temperature, and modifying the rate at which concentration fluctuations are destroyed in the flow (scalar dissipation). At the intermediate level, variations of density imply different exchanges of momentum in the flow even when the velocities are very similar (this affects mixing). Finally, at the highest level, the intrinsic coupling between the small and intermediate scales of the flow leads to changes in the large-scale behavior of the turbulence; e.g., changes in coherent structures, entrainment rates, etc. Our research focuses on the smallest and intermediate scales and attempts to answer questions pertaining to the differences between reacting and non-reacting turbulent flows with regards to mixing rates and velocity and temperature spectra scaling.

At the lowest level of description in the regime of interest, a nonpremixed combusting flow consists of flames residing at the location where fuel and oxidizer meet in stoichiometic proportions. These flames are generally unable to survive large levels of strain owing to the competition between the rate at which reaction products can be produced, determined by chemical kinetics, with the rate at which the heat flux leaves the flame (having a strong nonlinear Arrhenius-like dependence). In addition, the chaotic nature of turbulent flows generally results in some portions of a flame that burn in sustained and stable mode while other regions can be extinguished producing holes. The most challenging problem is the understanding of the dynamics of the boundary that separate the burning from the

quenched regions. These boundaries respond dynamically as a function of the rate of strain and variations in transport properties. We focus on the understanding of the statistics of the propagation of the boundaries and in improving approaches to model their behavior.

Modeling the dynamics of flame holes is a difficult problem that involves the propagation of curves (the flame boundary) of variable length constrained to a moving stoichiometric surface (the nominal flame mid-surface). The flame-hole boundary experiences variable rates of propagation within the stoichiometric surface. Modeling this dynamic phenomenon involves approximating the boundary-propagation speed with that of an equivalent edge flame. An edge flame is a canonical two-dimensional boundary value problem involving detailed chemical kinetics but simple flows. This allows effective chemistry abstraction, since the model edge flame contains all the details of the stoichiometry and chemical mechanism, and it can be solved a priori; outside the turbulent flow simulation. Similar established approaches are used to model the actively burning regions of the flame using flamelet ideas. We strive to isolate the chemistry details by pre-calculating the relevant flame structures and only introducing the relevant hydrodynamic models in the variable-density turbulent flow.

Addressing Complexity in Combustion Simulation: From Model Reduction to Software Design

James C. Sutherland

Department of Chemical Engineering, University of Utah
Salt Lake City, UT, 84112
James.Sutherland@utah.edu

I. Dimension Reduction in Combustion Modeling

Turbulent combustion simulation is a particularly challenging example of multiscale, multiphysics modeling where multiple physical processes couple nonlinearly over a vast range of length and time scales. Currently, Direct Numerical Simulation (DNS) is the only methodology that directly captures the full range of continuum length and time scales, but it is limited to small problems due to the exceptional cost. Large Eddy Simulation (LES), on the other hand, resolves length and time scales larger than some filter scale, and must resort to modeling unresolved terms - particularly the advective and source terms. Both LES and DNS remain highly expensive computational tools due to the requirement of resolution in four independent variables.

Increasing the complexity for combustion simulation is the number of thermochemical degrees of freedom that are present. In general, the thermochemical state of a single-phase reacting system with n_s chemical species is uniquely determined by n_s+1 parameters (*e.g.* T, p, and n_s-1 mass fractions, Y_i). However, it is widely recognized that in turbulent combustion, lower dimensional manifolds exist in this (n_s+1)-dimensional space [1]. All of the models which reduce the number of thermochemical degrees of freedom rely, either directly or indirectly, on the existence of a low-dimensional attractive manifold to which the state quickly relaxes. Among the most common approaches to reducing the number of thermochemical degrees of freedom are mechanism reduction and state-space parameterization.

We address both the spatial resolution problem as well as the thermochemical dimensionality problem below.

A. Physical Dimension Reduction

The One-Dimensional Turbulence (ODT) model originally proposed by Kerstein [3] resolves the full range of length and time scales in the flow (analogous to DNS), but in one spatial dimension. This means that only two independent variables (rather than four in DNS and LES) must be handled.

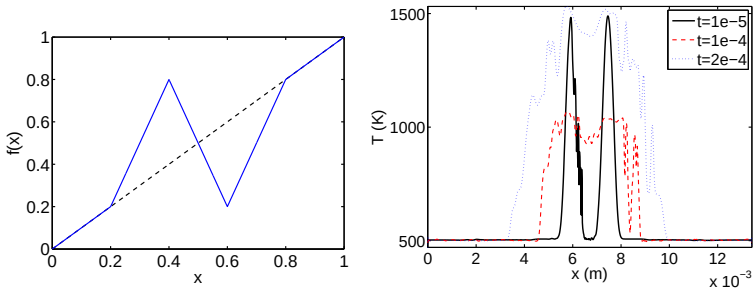

Figure 1: Left: example of a triplet-map (defining an "eddy") applied to a linear function. Right: instantaneous realizations of ODT simulations of extinction and reignition in a syngas jet flame [2].

In ODT, turbulent mixing is represented by instantaneous, stochastic rearrangement events that are driven by velocity gradients. These "eddy events" cause a rearrangement of the fields in a way that mimics the action of a three-dimensional eddy (see Figure 1). The triplet map that defines an eddy has many desirable properties to ensure conservation, preserve scale locality, *etc.* [3, 4]. Despite its one-dimensional nature, ODT has been shown to be highly effective at reproducing statistics from three dimensional flows and has been successfully applied to a wide variety of applications including homogenous turbulence, wall-bounded flows, free shear flows, buoyant-driven flows, particle-laden flows (with and without reaction) and turbulent combustion. In ODT, eddy events are driven by the local energetics of the flow field, and the ODT model can accurately reproduce critical features of the flow field such as the $-5/3$ energy cascade [3].

The poster will present results of ODT simulations of turbulent nonpremixed CO/H_2 flames with extinction and reignition as well as coal gasification processes.

B. State Space Dimension Reduction

PCA has recently been used to identify manifolds in state space [5–7]. Consider m observations of n variables arranged in an $n \times m$ matrix $\mathbf{X}$ whose columns represent individual observations and rows correspond to different variables. PCA determines a basis for the data $\mathbf{X}$ such that the data are well-represented by a truncated basis.

In the context of combustion applications, the n variables comprising the rows of $\mathbf{X}$ are the n_s+1 variables $[T,\ p,\ Y_1,\ Y_2, \ldots, Y_{n_s-1}]$. Performing a PCA on this set of variables yields a new (n_s+1)-dimensional basis, $\boldsymbol{\eta}$, which is a rotation of the original basis. Retaining $n_\eta < (n_s+1)$ of these defines a basis for a n_η-dimensional parameterization of the thermochemical state of the system.

Once a PCA has been defined, transport equations for the PCs may be derived by applying the PCA transformation to the original governing equations as described in [6]. Initial and boundary conditions may be likewise transformed to be expressed in terms of the PCs. However, for such an approach to succeed, the truncated basis (where $n_\eta < n_s+1$) must not only parameterize the thermochemical state (which has been successfully demonstrated) but the source terms as well. This remains an area where further research is required.

Results show that PCA can be used to obtain models that not only provide identify manifolds in turbulent combustion systems, but that are also insensitive to filtering, *i.e.*, they do not require explicit closure.

In summary, for a PCA to be used as a combustion modeling approach, a canonical system (*e.g.* opposed jet flame, ODT, DNS, *etc.*) is chosen to produce data, $\boldsymbol{\phi}$, to be used as a surrogate for the true system of interest. This system is solved over the relevant range of its natural parameters to obtain a large set of data. This data is then gathered in its entirety to define $\mathbf{X}$ and PCA is applied to $\mathbf{X}$ to determine the PCs, which are the parameterizing variables. A truncated set of PCs, $\boldsymbol{\eta}$, is then defined (with $n_\eta \ll n_s$), along with the mapping between $\boldsymbol{\phi}$ and $\boldsymbol{\eta}$, and $\boldsymbol{\eta}$ is then transported in the CFD application.

II. Multiphysics Software Design

Multiphysics simulation software is plagued by complexity stemming from nonlinear coupling. In addition to nonlinear coupling, such software often must support many models, each of which may require a different set of transport equations, constitutive models, and equations of state. Strong coupling, together with a multiplicity of models, leads to complex algorithms and rigid software. The rigid, complex software is due to design that focuses on algorithms.

In this poster we present an alternative programming paradigm where programmers focus not on the algorithm, but on the data. Mathematical expressions are reflected in software in a way that directly exposes data dependencies through a directed acyclic graph and graph theory is employed to *automatically* generate an algorithm. This allows programmers to avoid the complexity of ordering operations, and allows problems with very complex dependencies to become entirely tractable, and removes virtually all logic from the algorithm itself. Changes are highly localized, allowing model developers to implement code without requiring a detailed understanding of the couplings that may be implied by a given model. It provides a natural framework to achieve model adaptivity, where one model suite may be substituted for another dynamically, allowing for addition or removal of transport equations, modifying constitutive models, *etc*. and allows us to automatically generate a new algorithm.

Unlike traditional programming models, this approach naturally handles complexity associated with multiple modeling options (which may imply different nonlinear coupling and may require solution of different sets of PDEs, equations of state, or constitutive relationships).

Furthermore, this approach enables efficient algorithmic parallelization via threads. By exposing dependencies in the algorithm explicitly, thread-based parallelism can be implemented through algorithm decomposition, thus providing a basis for exploiting parallelism that is independent from and complimentary to domain decomposition approaches.

References

[1] U. Maas and S. B. Pope. Implementation of simplified chemical kinetics based on intrinsic low-dimensional manifolds. In *Proc. Combust. Inst.*, volume 24, pages 103–112. The Combustion Institute,

1992.

[2] N Punati, J C Sutherland, A R Kerstein, E R Hawkes, and J H Chen. An Evaluation of the One-Dimensional Turbulence Model: Comparison with Direct Numerical Simulations of CO/H2 Jets with Extinction and Reignition. In *Proc. Combust. Inst.*, page to appear, 2011.

[3] A. R. Kerstein. One-dimensional turbulence: model formulation and application to homogeneous turbulence, shear flows, and buoyant stratified flows. *J. Fluid Mech.*, 392:277–334, 1999.

[4] A. R. Kerstein, W. T. Ashurst, S. Wunsch, and V. Nilsen. One-dimensional turbulence: vector formulation and application to free shear flows. *J. Fluid Mech.*, 447:85–109, 2001.

[5] A Parente, J C Sutherland, P J Smith, and L Tognotti. Identification of Low-Dimensional Manifolds in Turbulent Flames. In *Proc. Combust. Inst.*, volume 32, pages 1579–1586. The Combustion Institute, 2009.

[6] J Sutherland and A Parente. Combustion modeling using principal component analysis. *Proc. Combust. Inst.*, 32(1):1563–1570, 2009.

[7] A Parente, J C Sutherland, B B Dally, L Tognotti, and P J Smith. Investigation of the MILD combustion regime via Principal Component Analysis. *Proc. Combust. Inst.*, 33(2):3333–3341, 2011.

[8] T. Echekki, A. R. Kerstein, T. D. Dreeben, and J.Y. Chen. One-dimensional turbulence simulation of turbulent jet diffusion flames: Model formulation and illustrative applications. *Combust. Flame*, 125:1083–1105, 2001.

[9] K. N. C. Bray. The challenge of turbulent combustion. In *Proc. Combust. Inst.*, volume 26, pages 1–26. The Combustion Institute, 1996.

[10] S. B. Pope. Computations of turbulent combustion: Progress and challenges. In *Proc. Combust. Inst.*, volume 23, pages 591–612. The Combustion Institute, 1990.

[11] James C Sutherland. Programming paradigms for multiphysics simulation at petascale and exascale. In *AIChE Annual Meeting*, Salt Lake City, November 2010.

[12] Patrick K. Notz, Roger P. Pawlowski, and James C. Sutherland. Graph-based software design for managing complexity and enabling concurrency in multiphysics PDE software. *ACM Transactions on Mathematical Software*.

[13] Patrick Notz, Roger Pawlowski, and James C. Sutherland. A Software Design for Solving Coupled Multiphysics Equations in a Dynamic, Extensible and Efficient Way. In *European Conference on Computational Mechanics*, Paris, France, May 2010.

[14] James C Sutherland. Automated Algorithm Generation and Thread Paralellism in Complex Scientific Computing Applications. In *SIAM Parallel Processing Conference*, Seattle, WA, March 2010.

[15] J. C. Sutherland, N. Punati, and A. R. Kerstein. A Unified Approach to the Various Formulations of the One-Dimensional Turbulence Model. Technical Report ICSE091201, Institute for Clean and Secure Energy, The University of Utah, Salt Lake City, UT, 2010.

[16] T. Echekki, A. R. Kerstein, and J. C. Sutherland. *The One-Dimensional Turbulence (ODT) Model*, chapter 11. Springer, 2011.

[17] N Punati, J C Sutherland, A R Kerstein, E R Hawkes, and J H Chen. An Evaluation of the One-Dimensional Turbulence Model: Comparison with Direct Numerical Simulations of CO/H2 Jets with Extinction and Reignition. *Proc. Combust. Inst.*, 33(1):1515–1522, 2010.

Threshold and Imaging Photoelectron Photoion Coincidence Spectroscopy Experiments for High-Accuracy Thermochemistry

Bálint Sztáray
Department of Chemistry, University of the Pacific
Stockton, CA-95211
bsztaray@pacific.edu

I. Program Scope

Using laboratory based Threshold Photoelectron Photoion Coincidence (TPEPICO) and synchrotron-based Imaging PEPICO (iPEPICO) Spectroscopy, we are determining high-accuracy thermochemical data on intermediate size molecules and radicals that can be used as input in modeling combustion and atmospheric processes. Our research is built on both the recent experimental improvements and on our constantly improving modeling tools based on statistical rate theories. The experiments are carried at the University of the Pacific, on the TPEPICO experiment that was designed and built with DOE support and at the Swiss Light Source. The iPEPICO apparatus at the latter is or will be utilized in the following cases: a) for small molecules, where fast dissociation allows the determination of ionic dissociation energies to sub-kJ mol^{-1} accuracy; b) for systems where dissociative photoionization requires photon energies in excess of 13.5 eV; c) to measure dissociative photoionization onsets of radicals produced in small concentrations by the soon-to-be-built laser-photolysis source; and d) to determine very accurate kinetic energy release (KER) data using the double (electron + ion) velocity map imaging setup.

II. Recent Progress

Photoelectron photoion coincidence (PEPICO) spectroscopy is a marriage of photoelectron spectroscopy and mass spectrometry. Electron / ion pairs are created by single photon ionization and the two charged species are measured in delayed coincidence with each other. Ions are selected in narrow range of internal energy by collecting only ions created in delayed coincidence with the photoelectrons. In threshold PEPICO, only the initially zero-energy electrons are detected, while in imaging PEPICO (iPEPICO), the electron velocity image is detected in coincidence with the photoions. These photoelectrons provide the start signal for measuring the ion time of flight (TOF) distributions. Kinetics information about dissociation rate constants and translational energy release in the dissociation is contained in the TOF distributions. Recent developments in the experimental technique, including the use of velocity map imaging electron optics to account for the contamination of energetic electrons, as well as advances in data analysis that take into account the initial thermal energy distribution of the molecules, has permitted the extraction of dissociation limits and, therefore, bond energies to within 10 meV (0.5 kJ/mol) using the lab-based TPEPICO experiment. With the recent commissioning of the VUV beamline at the Swiss Light Source (SLS) synchrotron, both the energy resolution and the photon energy range of these experiments have been considerably extended, allowing bond energies to be determined with close to meV accuracy.

The use of the PEPICO technique is demonstrated on a few selected systems, where the existing gaps in high-accuracy thermochemistry is filled using the numbers from T- and i-PEPICO.

The dissociative photoionization onsets of Br and I loss reactions were measured for C_2H_5Br and C_2H_5I respectively in order to establish the heats of formation of these two basic ethyl halides. The appearance energy of ethyl cation from ethyl bromide was found to be 1074.2 $\pm$ 0.8 kJ mol^{-1} and that from ethyl iodide was found to be 1016.4 $\pm$ 0.8 kJ mol^{-1}. The heats of formation of ethyl bromide and ethyl iodide are interconnected through the ethyl cation. In establishing the thermochemistry of the ethyl halides, the ethyl cation heat of formation was concluded to be 915.5 ± 1.3 kJ mol^{-1} based on a recent value for ethyl radical heat of formation and the well-established ionization energy and on ab initio isodesmic calculations using recent PEPICO data. Using this anchor, the following heats of formations were obtained: $\Delta_f H^\circ_{0K}$ [EtBr] = –40.8 $\pm$ 1.5 kJ mol^{-1} and $\Delta_f H^\circ_{0K}$ [EtI] = 6.3 $\pm$ 1.5 kJ mol^{-1}. These results

are more consistent with the higher EtBr heats of formation values in the literature, contrary to recent findings. For ethyl iodide, the latest calorimetric value does not agree within the claimed accuracy.

1,1-dimethylhydrazine was measured to study entropy effects in the unimolecular dissociation of its energy selected molecular ions. 0 K appearance energies of the fragment ions were extracted by modeling the experimental data with rigid activated complex (RAC-) RRKM theory. It was found that the data could be well reproduced with a single TS for each dissociation channel if two different H-loss channels were assumed: one corresponding to a C–H, the other to an N–H bond dissociation. Once the appearance energies were established, heats of formation of the fragment ions was derived. The heat of formation of the neutral molecule was computed by applying composite ab initio methods (G3, CBS-APNO, W1U) on a series of isodesmic reactions between methyl hydrazines and methyl amines.

The dissociative photoionization of four compounds, SCl_2, S_2Cl_2, $SOCl_2$, and SO_2Cl_2, were measured with both threshold and imaging PEPICO. In all systems, the molecular ion loses a chlorine atom in a fast dissociation. The 0 K appearance energies of the first chlorine-loss fragment ions were determined to be 12.252 ± 0.012 eV, 11.205 ± 0.003 eV, 11.709 ± 0.003 eV, and 12.505 ± 0.003 eV, respectively. SCl_2 was measured on the laboratory-based TPEPICO instrument, in which the second Cl-loss dissociation could not be observed within the available photon energy. For $S_2Cl_2^+$ and $SOCl_2^+$, the appearance energy of the fragment ion after two chlorine-loss dissociations were determined to be 13.32 ± 0.02 eV, and 14.88 ± 0.02 eV, respectively. Based on the analysis of the breakdown curves, it was concluded that assuming three-dimensional translational degrees of freedom yields a more reliable statistical model of the product energy distributions. The literature heat of formation of the neutral precursor molecule thionyl chloride, $SOCl_2$ does not agree with our results based on the SO^+ cation, and is revised by more than 10 kJ mol^{-1} to –198.2 ± 2.4 kJ mol^{-1}. A particularly broad Franck–Condon gap with vanishingly small threshold electron signal in the photon energy range for the second Cl-loss reaction in $SO_2Cl_2^+$ is discussed with regard to the mechanism of threshold ionization.

In the dissociative photoionization of energy selected methanol isotopologues (CH_3OH, CD_3OH, CH_3OD and CD_3OD), the first dissociation is predominantly an H/D-atom loss from the carbon, also confirmed by partial deuteration. At photon energies between 14–15 eV, in a subsequent hydrogen molecule loss, the formation of CHO^+/CDO^+ dominates as opposed to COH^+/COD^+ formation. In both of these processes we see little evidence for H-atom scrambling. In the photon energy range corresponding to the $\tilde{B}$ and $\tilde{C}$ ion states, a hydroxyl radical loss appears yielding CH_3^+. Based on the branching ratios as a function of ion internal energy, statistical considerations and ab initio calculations, this process is suggested to take place on the first electronically excited $\tilde{A}\,^2\mathrm{A}'$ ion state. Uncharacteristically, internal conversion is outcompeted by unimolecular dissociation due to the apparently weak Renner–Teller-like coupling between the $\tilde{X}$ and the $\tilde{A}$ ion states. The 0 K appearance energies of the ions CH_2OH^+, CD_2OH^+, CH_2OD^+ and CD_2OD^+ are measured to be 11.6454 ± 0.0017 eV, 11.739 ± 0.003 eV, 11.642 ± 0.003 eV and 11.737 ± 0.003 eV respectively. The 0 K heat of formation of CH_2OH^+, protonated formaldehyde, was determined to be 717.7 ± 0.7 kJ mol^{-1}. This yields a 0 K heat of formation of CH_2OH of −11.1 ± 0.9 kJ mol^{-1} and a 298 K proton affinity of formaldehyde of 711.60 ± 0.71 kJ mol^{-1}. The reverse barrier to homonuclear H_2-loss from CH_3OH^+ is determined to be 36 kJ mol^{-1}, whereas for heteronuclear H_2-loss from CH_2OH^+ it is found to be 210 kJ mol^{-1}.

III. Future Plans

Combustion and atmospheric models are only as accurate as the input parameters that are either experimentally determined or calculated. With the continuation of the PEPICO project, we offer significant improvements to three important sets of parameters: accurate thermochemical data, reaction rates, and energy distributions. Therefore, our future research is aimed at a) determining highly accurate experimental thermochemical information on neutral and ionic species directly related to combustion and atmospheric processes; b) advancing our understanding of statistical rate and energy distribution theories to improve on the kinetics modeling tools used in combustion and atmospheric models.

IV. References

- Dissociative photoionization mechanism of methanol isotopologues (CH_3OH, CD_3OH, CH_3OD and CD_3OD) by iPEPICO: energetics, statistical and non-statistical kinetics and isotope effects, Sampada Borkar, Bálint Sztáray and Andras Bodi, Phys Chem Chem Phys, *submitted*
- Modeling Unimolecular Reactions in Photoelectron Photoion Coincidence Experiments, Bálint Sztáray,* Andras Bodi, and Tomas Baer, Journal of Mass Spectrometry, 45 (2010) 1233–1245
- Dissociative Photoionization of Sulfur Chlorides and Oxochlorides: Thermochemistry and Bond Energies Based on Accurate Appearance Energies, Sampada Borkar, Lauren Ooka, Andras Bodi, Thomas Gerber and Bálint Sztáray*, Journal of Physical Chemistry A, 114 (2010) 9115–9123
- Self-consistent Heats of Formation for the Ethyl Cation, Ethyl Bromide and Ethyl Iodide from Threshold Photoelectron Photoion Coincidence Spectroscopy, Sampada Borkar, and Bálint Sztáray*, Journal of Physical Chemistry A, 114 (2010) 6117–6123
- Dissociation of Energy-Selected 1,1-Dimethylhydrazine Ions, Zsolt Gengeliczki, Sampada N. Borkar, Bálint Sztáray*, Journal of Physical Chemistry A, 114 (2010) 6103–6110

Abstracts of Principal Investigator Presentations

The relaxation of methylene in collisions with He

Millard H. Alexander (mha@umd.edu),[1] LiFang Ma,[2] Jacek Klos[3]
Department of Chemistry and Biochemistry, University of Maryland, College Park, MD 20742-2021
Paul J. Dagdigian[4]
Department of Chemistry, The Johns Hopkins University, Baltimore, MD 21218-2685

I. Program Scope

Our group studies inelastic and reactive collisions of small molecules, focusing on radicals important in combustion environments. Our goal is the better understanding of kinetic processes which may be difficult to access experimentally.

An essential component is the accurate determination of potential energy surfaces (PES's), using multi-reference, configuration-interaction and coupled-cluster techniques. After fitting the *ab initio* points to obtain global PESs, we treat the dynamics using time-independent (close-coupling) methods.

II. Recent Progress

Since inception of our DOE-funded program (fall, 2009) we have focused on the study of the methylene radical (CH_2) in the $\tilde{a}^1A_1$ state. Inelastic collisions of methylene are currently under experimental study at Brookhaven. [1-3] Our work is one of the first detailed simulations of state-to-state relaxation of an asymmetric top in collisions with an atom.

We have determined a highly-accurate PES for the interaction of $CH_2(\tilde{a})$ with He, using CCSD(T) calculations with correlation-consistent basis sets, extrapolated to the complete basis set limit. The calculations were carried out on a large grid of CH_2–He orientations and separation distances. These *ab initio* points were then fitted,[4] by an expansion in spherical harmonics in the appropriate inertial frame of CH_2, in which the *z* axis lies perpendicular to the C_2 axis, but in the plane of the triatomic (Fig. 1).

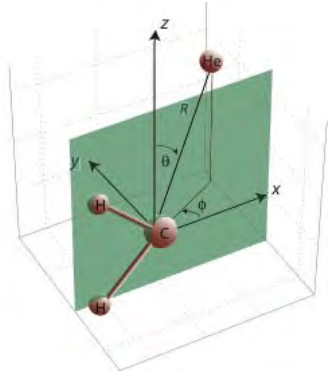

Fig. 1. Geometry of the $CH_2(\tilde{a})$–He system, with the *z* axis aligned along the *a* inertial axis, perpendicular to the C_2 axis.

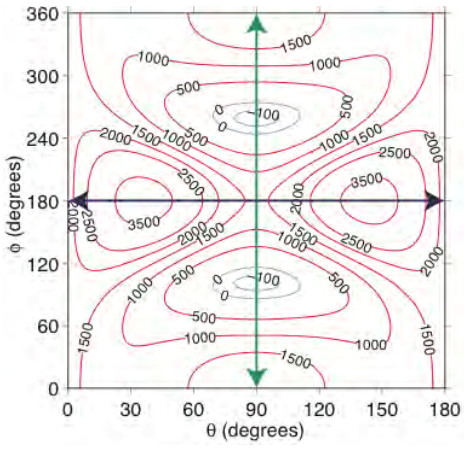

Fig. 2. Contour plot of the $CH_2(\tilde{a})$–He PES for the He atom fixed at a distance of R=4.58 bohr (the CH_2–He separation at the global minimum). The heavy blue (horizontal) line delineates semicircular motion in the *xz*-plane from +*z* to – *z*; the two highly-positive regions at $\theta \cong 35^\circ$ and 145° correspond to repulsion between the He atom and the two H nuclei. The heavy green (vertical) line delineates circular motion in the *xz*-plane. The minima at $\phi \cong 90^\circ$ and 270° correspond to a decrease in electron repulsion due to the double vacancy in the $2p_y$ (b_1) orbital of CH_2 in the $\tilde{a}$ state.

A contour plot of the $CH_2(\tilde{a})$–He potential energy surface is shown in Fig. 2. In the $\tilde{a}$ state the $2p_y$ orbital (the non-bonding orbital perpendicular to the plane of the molecule) is unoccupied. Thus, $CH_2(\tilde{a})$ behaves

[1] Principal investigator; [†]Graduate student; [‡]Research Assistant Professor; [§] Senior collaborator.

as an amphoteric Lewis acid/base. When He approaches perpendicular to the molecular plane, the interaction is substantially less repulsive than when He approaches in the molecular plane.

The energies of the lower rotational levels of $CH_2(\tilde{a})$ are displayed in Fig. 3, for both nuclear spin modifications. Collisions with He can not cause transitions between these two species of different nuclear permutation symmetry. For an asymmetric top, even for a given J and K, the energy gaps in the *ortho* as compared with *para* rotational ladders can be quite different, especially for K=1.

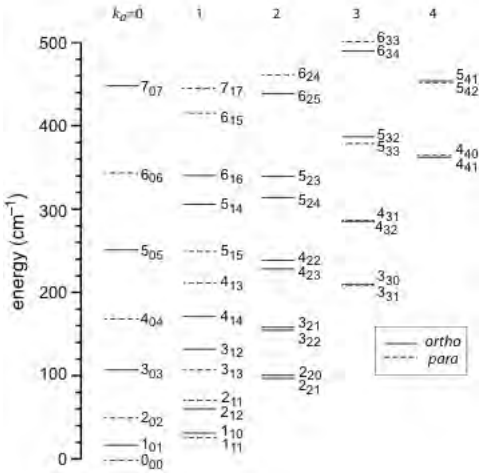

Fig. 3. Rotational levels of the *ortho* (blue, solid) and *para* (red, dashed) isotopomers of $CH_2(\tilde{a})$ with energies less than 500 cm^{-1}. The levels are grouped by column according to the value of the prolate-limit body-frame projection quantum number k_a. The individual rotational levels are labeled by the total angular momentum j and by its projections along the a and c inertial axes: k_a and k_c.

To determine cross sections and rate constants we utilize our recent extension of the Hibridon program suite[5] to inelastic collisions of asymmetric top molecules.[4] Figure 4 reveals the inelastic cross sections for scattering out of the j=4 level of both *ortho* (left panel) and *para* (right panel). We observe that

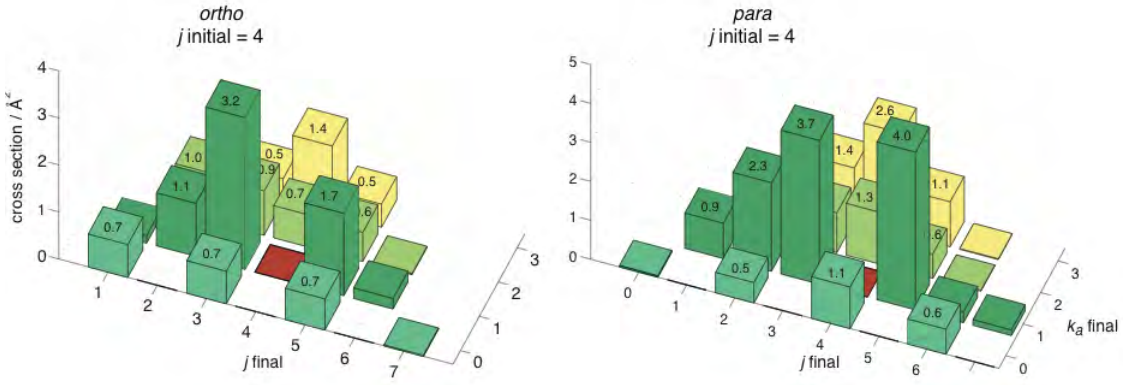

Fig. 4. Bar plot of the cross sections for rotationally inelastic scattering of *ortho* (left panel) and *para* (right panel) $CH_2(\tilde{a})$ in the j = 4, k_a = 1 levels by collision with He at a collision energy of 300 cm^{-1}. The red square denotes the initial level.

the dominant cross sections and the overall relaxation efficiency are both greater for the *para* isotopomer. This is reversed for transitions out of the j=5 levels (not shown). In part, this difference can be explained by the non-uniform energy gaps seen in Fig. 3. For a symmetric top molecule (such as NH_3) the relaxation of the *ortho* and *para* levels would be identical (except for k=0). There is a similar *ortho*/*para* propensity for the Δk_a = +2 transitions which reverses also for transitions out of odd j levels. This is a consequence of the strong electronic anisotropy in the $CH_2(\tilde{a})$–He PES (see Fig. 2), which is due to the Lewis amphoterism.

There have been a number of papers in the literature in which the relative magnitude of cross sections for rotationally-inelastic collisions of a diatomic molecule have been modeled entirely by a (negative) exponential or inverse power-law dependence on the magnitude of the energy gap. Our simulations reveal that overall, rotationally-inelastic collisions in a bent triatomic, at least in the case of $CH_2(\tilde{a})$–He collisions, cannot be fit by either an exponential or power-law dependence on the energy gap.

Figure 5 compares the rate constants for collisional removal (summed over all final states) for the k_a=1 levels of *ortho*-$CH_2(\tilde{a})$ with experimental results from Brookhaven.[3] The experiments monitor the rate of infilling of an initially depleted rotational level. This rate can be shown to be equivalent to the rate of collisional removal for the same level.[6]

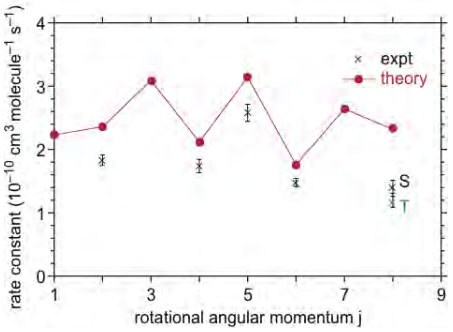

Fig. 5. Rate constants for collisional removal by rotational transitions for $CH_2(\tilde{a})$ *ortho* k_a = 1 levels in collisions with helium. Our theoretical values are compared with the experimental results of Hall, Sears, and their co-workers (Ref. 3). The j = 8 level of this manifold is known to be strongly perturbed by a vibration-rotation level of the $\tilde{X}^3B_1$ state (Ref. 7). The labels "*S*" and "*T*" denote the experimentally observed rate constants for the two perturbed levels of predominantly singlet and triplet character, respectively.

The agreement with experiment is excellent. In particular a substantial modulation appears between the relaxation of the even-j as contrasted with the odd-j levels, which is also seen experimentally. This is a consequence both of the non-uniform energy gaps in the k_a=1 manifold (Fig. 3) as well as the strength of the electronic anisotropy. A similar modulation is seen in the rates for collisional depolarization (not shown here).

III. Future Work

a. Electronic-rotational relaxation involving the $\tilde{X}$ state of methylene

We plan to investigate collisional energy transfer between the $\tilde{a}$ state and the ground $\tilde{X}^3B_1$ state of CH_2. Experimentally, facile energy transfer has been observed.[8, 9] We will model this process by the "gateway" mechanism of Gelbart and Freed,[10] whereby singlet-triplet energy transfer occurs through discrete vibration-rotation levels of the $\tilde{a}$ and $\tilde{X}$ states with the same total angular momentum and parity, which are coincidentally nearly degenerate and hence strongly-mixed by the weak spin-orbit coupling. The consequence of this electronic mixing is seen in Fig. 5 in the experimental j=8 points marked "*S*" and "*T*". Cross sections (and, subsequently, rate constants) can be obtained by taking linear combinations of the *S*-matrix elements for scattering of the CH_2 molecule in either one or the other of these two states.

In the $\tilde{X}$ state, the out-of-plane $2p_y$ orbital is singly occupied, thus the electronic anisotropy of the state is reduced, compared to that in the $\tilde{a}$ state. We have determined an *ab initio* PES for the interaction of He with $CH_2(\tilde{X})$. By Walsh's rules the barrier to nonlinearity in the $\tilde{X}$ state is lower than in the $\tilde{a}$ state. The $\tilde{a}$–$\tilde{X}$ spin-orbit mixing involves the v=3 bend level of the $\tilde{X}$ state, which lies above this barrier (as well as other levels), we need to average the $CH_2(\tilde{X})$–He PES over the bending motion of the triatomic, making use of a rigid bender model.[11] Figure 6 presents contour plots of the $CH_2(\tilde{X})$–He PES, which can be compared with the $CH_2(\tilde{X})$–He PES shown in Fig. 2.

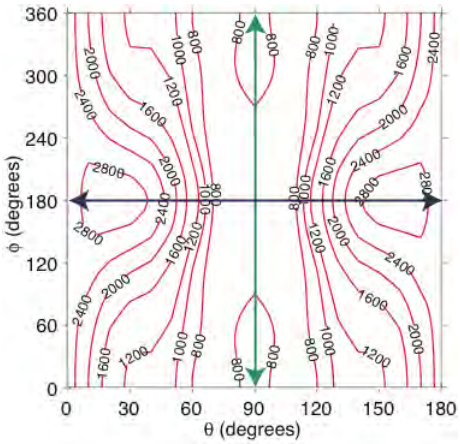

Fig. 6. Contour plot of the $CH_2(\tilde{X})$–He potential energy surface, for the He atom fixed at a distance of R=4.58 bohr (the same distance as in Fig. 2) and the H–C–H equilibrium bond angle. The heavy blue (horizontal) line delineates semicircular motion in the *xz*-plane (see Fig. 1) from +*z* to – *z*; the two highly-positive regions at $\theta \cong 35^\circ$ and 145° correspond repulsion between the He atom and the two H atoms. The heavy green (vertical) line delineates circular motion in the *xz*-plane.

As can be seen by comparing this figure with Fig. 2, the electronic anisotropy is far smaller, since the out-of-plane 2*p* orbital on the C atom is singly occupied in the $\tilde{X}$ state.

Because the v=3 bending vibrational level of the $\tilde{X}$ state lies above the barrier to linearity, to simulate inelastic scattering, we calculated *ab initio* points on the $CH_2(\tilde{X})$–He PES at a number of

bending angles and then averaged the interaction energy over the wavefunction for the v=3 bending vibration. In fact, the vibrationally-averaged PES, even for this excited bending mode, differs little from the PES determined for $CH_2(\tilde{X})$ at its equilibrium bond angle.

We are initiating calculations of rotational relaxation cross sections and rate constants for rotational energy transfer within the $\tilde{X}$ state. Then, within the gateway model discussed above, we will extend these calculations to $\tilde{a} \rightarrow \tilde{X}$ relaxation. In particular, we will focus on relaxation out of the few rotational levels in the $\tilde{a}$ state which are strongly mixed.

b. Vibrational relaxation in methylene

Having determined the $CH_2(\tilde{X})$–He potential energy surface as a function of the methylene bending angle, we will modify our Hibridon[5] inelastic scattering code to allow the determination of cross sections for (bending) vibrationally-inelastic processes. Our goal is to obtain an estimate of the relative efficiency of these processes to aid, eventually, in developing more accurate kinetic models for simulations of combustion environments involving methylene. Because the calculated $CH_2(\tilde{X})$–He PES depends little on the bending angle, we anticipate that vibrational relaxation will be relatively inefficient.

c. Rotational relaxation in the methyl radical

We plan also to carry out similar quantum scattering calculations for rotational relaxation of the planar CH_3 radical, in its ground $\tilde{X}^2A_2''$ electronic state, in which the singly-filled 2*p* orbital of the C atom projects out of the plane, using a RCCSD(T) calculation of the CH_3–He PES.

IV. Publications and submitted journal articles supported by this project to date

1. L. Ma, M. H. Alexander, and P. J. Dagdigian, "Theoretical investigation of rotationally-inelastic collisions of $CH_2(\tilde{a})$ with helium," J. Chem. Phys. **XX**, yyyy (2011) (in press).
2. M. H. Alexander, G. Hall, and P. J. Dagdigian, "The Approach to Equilibrium: Detailed Balance and the Master Equation," J. Chem. Educ. (submitted).

V. References

1. Y. Kim, A. V. Komissarov, G. E. Hall, and T. J. Sears, "Observation of the $c\ ^1A_1$ state of methylene by optical-optical double resonance," J. Chem. Phys. **123**, 24306 (2005).
2. Z. Wang, Y. Kim, G. E. Hall, and T. J. Sears, "State mixing and predissociation in the $c \leftrightarrow a$ band system of singlet methylene studied by optical-optical double resonance," J. Phys. Chem. A **112**, 9248-9254 (2008).
3. S. K. Lee, Y. Kim, T. J. Sears, and G. E. Hall, private communication.
4. P. J. Dagdigian and M. Alexander, "Depolarization in H_2O-He collisions," Mol. Phys. **108**, 1159-1169 (2010).
5. HIBRIDON is a package of programs for the time-independent quantum treatment of inelastic collisions and photodissociation written by M. H. Alexander, D. E. Manolopoulos, H.-J. Werner and others. More information and/or a copy of the code can be obtained from the website http://www2.chem.umd.edu/groups/alexander/hibridon/hib43.
6. M. H. Alexander, G. Hall, and P. J. Dagdigian, "The Approach to Equilibrium: Detailed Balance and the Master Equation," J. Chem. Ed. (2011).
7. U. Bley and F. Temps, "Collision-induced intersystem crossing of CH_2 from a^1A_1 to $X\ ^3B_1$: A case-study of the mixed-state model," J. Chem. Phys. **98**, 1058-1072 (1993).
8. A. V. Komissarov, A. Lin, T. J. Sears, and G. E. Hall, "State-resolved thermalization of singlet and mixed singlet-triplet states of CH_2," J. Chem. Phys. **125**, 084308 (5 pages) (2006).
9. D. Patel-Misra and P. J. Dagdigian, "State-resolved electronic quenching of NH($a\ ^1\Delta$) by Xe and CO," J. Chem. Phys. **97**, 4871-4880 (1992).
10. W. M. Gelbart and K. F. Freed, "Intramolecular perturbations and quenching of luminescence in small molecules," Chem. Phys. Lett. **18**, 470-475 (1973).
11. J. T. Hougen, P. R. Bunker, and J. W. C. Johns, "The vibration-rotation problem in triatomic molecules allowing for a large amplitude bending vibration," J. Mol. Spectrosc. **34**, 136-172 (1970).

Theoretical Studies of Elementary Hydrocarbon Species and Their Reactions

Wesley D. Allen and Henry F. Schaefer III
Center for Computational Chemistry and Department of Chemistry
University of Georgia, Athens, GA 30602-2525
E-mail: wdallen@uga.edu and sch@uga.edu; Phone: (706) 542-7729

Explicitly Correlated R12 Methods for Radicals

Conventional electron correlation methods converge to the complete basis set (CBS) limit only as $t^{-1/4}$ in the computational time (t). This torpid convergence arises from the inability of one-particle functions (orbitals) to describe the coalescence region between two electrons. The Coulomb singularities in the electronic Hamiltonian require the exact wave function to display a cusp and corresponding depletion of electron density (Coulomb hole) when any interelectronic distance (r_{12}) approaches zero. Two-particle functions that depend explicitly on r_{12} can effectively treat the cusp region without large orbital basis sets. Much progress has been made recently in the development of explicitly correlated methods such as MP2-R12 and CCSD(T)-R12 that incorporate r_{12} terms directly into the electronic wave function. While closed-shell and spin-orbital R12 methodologies for coupled-cluster theory have been well studied, open-shell, spin-restricted R12 methods are lacking, which is problematic for the free-radical chemistry predominant in combustion applications. An ideal starting point for open-shell R12 methods is the symmetric exchange or Z-averaged approach. By introducing a symmetric exchange operator for α and β electrons, the number of wave function parameters is drastically reduced. This formalism has negligible spin contamination compared to unrestricted methods, and the imposed spin constraints do not introduce size-consistency errors as in many other spin-adapted schemes. Building on our previous work on ZAPT2-R12 perturbation theory for open-shell systems,[8] we have now developed capabilities for the more complicated and robust ZA-CCSD-R12 method.[24] A practical approach has been achieved by using only the Fock operator rather than the full similarity-transformed Hamiltonian to incorporate the R12 corrections. We have demonstrated the excellent basis set convergence of our ZA-CCSD-R12 method for a series of atomization energies. Specifically, with only a triple-ζ (TZ) quality basis, ZA-CCSD-R12 surpasses the accuracy of conventional computations with augmented sextuple-ζ (aV6Z) basis sets (Fig. 1). This performance is remarkable given the simplicity of the final ansatz: Fock operator commutations only, Hermitian cluster operator, and extended Brillouin condition for simplifying the coupling of explicitly-correlated and conventional terms.

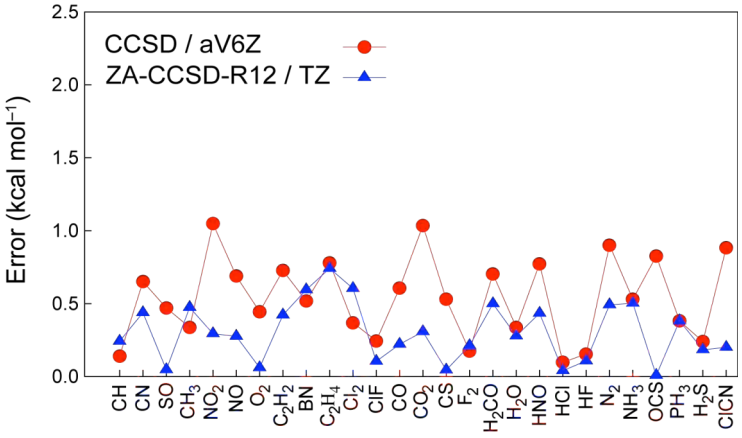

Figure 1. Comparison of conventional (aV6Z) and explicitly correlated (R12/TZ) CCSD incremental correlation energy errors for the atomization energies of 27 molecules; referenced to CCSD/CBS benchmarks derived from (aV5Z, aV6Z) extrapolations.

Methylhydroxycarbene: Tunneling Control of a Chemical Reaction

In joint work[25] with the experimental group of Peter Schreiner (Giessen, Germany), methylhydroxycarbene (**1**, Me–C–OH) was generated for the first time by high vacuum flash pyrolysis (HVFP) of pyruvic acid (at 900 °C) and spectroscopically (IR, UV/Vis) characterized via immediate matrix isolation in solid Ar at 11 K. The identity of **1** was unequivocally confirmed by precise agreement between observed IR bands and theoretical anharmonic

vibrational frequencies computed from an all-electron (AE) CCSD(T)/cc-pCVTZ complete quartic force field. The UV/Vis spectrum of **1** displays a broad band with maximum absorption at 393 nm (3.2 eV) that extends to around 460 nm (2.7 eV), in full accord with our aug-cc-pVTZ multireference coupled cluster [Mk-MRCCSD(T)] computations that gave a gas-phase vertical (adiabatic) excitation energy of 3.4 (2.7) eV. Surprisingly, we observed rapid disappearance **1** after cryogenic trapping. Upon standing in Ar at 11 K in the dark, the IR peaks of **1** decayed gradually via first-order kinetics with a half-life of $t_{1/2}$ = 66 (± 5) min. In stark contrast, the bands of the deuterium isotopologue Me–C–OD (**d-1**) did not change under identical conditions for extended periods of time (at least 16 h). The kinetic experiments thus revealed that **1** isolated in its ground vibrational and electronic state exhibits facile [1,2]-hydrogen tunneling and that two conspicuous phenomena occur simultaneously: efficient penetration of a formidable 28.0 kcal mol^{-1} barrier to yield acetaldehyde (**3**), and complete obstruction of the formation of vinyl alcohol (**4)** despite a much lower 22.6 kcal mol^{-1} barrier.

We established the theoretical basis for the remarkable behavior of methylhydroxycarbene by computing pure tunneling rates for both **1** → **3** and **1** → **4**. The AE-CCSD(T)/cc-pCVTZ method was employed to precisely map out the associated intrinsic reaction paths (IRPs) descending from transition states $\mathbf{TS_{1t\text{-}3}}$ and $\mathbf{TS_{1t\text{-}4t}}$ (Fig. 2) and to determine zero-point vibrational energies (ZPVEs) along these steepest-descent routes. Final potential energy curves for the isomerization paths were then constructed from high-quality AE-CCSD(T)/cc-pCVQZ energy points appended with the ZPVEs. Within a reaction-path Hamiltonian model, WKB tunneling probabilities were evaluated from barrier penetration integrals computed numerically from our highly accurate electronic structure results. This theoretical analysis yielded a tunneling half-life of 71 min for **1** → **3**, in close agreement with the observed rate of decay. Moreover, the computed half-life for **1** → **4** was 190 days, nicely explaining why vinyl alcohol is not the preferred product of methylhydroxycarbene isomerization, despite the lower barrier for formation of **4**. Finally, we obtained a tunneling half-life for **d-1** of 4000 years, consistent with the observed shutdown of the methylhydroxycarbene decay mechanism upon deuterium substitution.

Methylhydroxycarbene demonstrates the need to consider *tunneling control* in addition to classical kinetic or thermodynamic control in order to analyze, predict, and understand the full diversity of chemical reactivity. Our work highlights the possibility of reactions in which the observed product is neither the one requiring the lowest activation barrier nor the one with the lowest free energy but rather the one most readily reached by quantum mechanical tunneling.

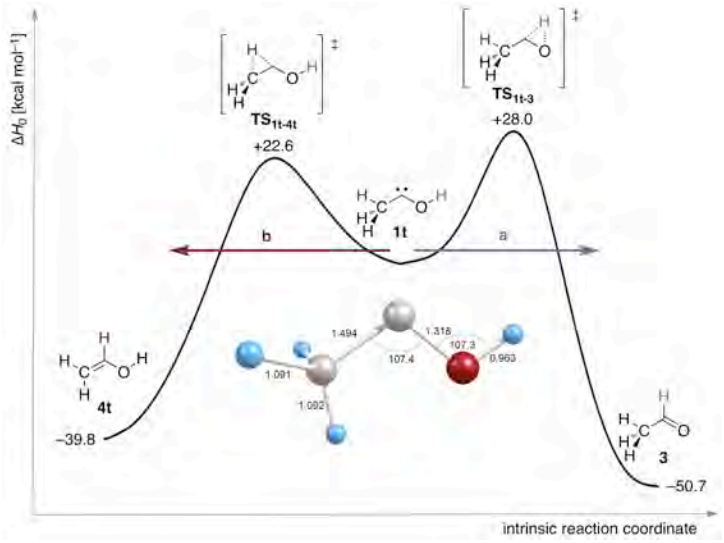

Figure 2. Energetic profiles for [1,2]H-shift isomerizations of *trans*-methylhydroxycarbene (**1t**); relative energies ΔH_0 (in kcal mol^{-1}) pinpointed from our convergent focal-point analysis (FPA) computations. The bond lengths (Å) and angles (°) given for **1t** are ground-state optimum geometrical parameters given by AE-CCSD(T)/cc-pCVQZ theory. The curves are drawn quantitatively with the intrinsic reaction coordinate (IRC) in mass-weighted Cartesian space as the abscissa in order to reflect the proper barrier heights and widths for the two competing reactions. Simple visual inspection thus indicates a higher hydrogen tunneling probability for the more narrow energy profile of path **a**.

The Propyl + O_2 Reaction System

Reactions of alkyl radicals (R·) with O_2 are ubiquitous in combustion, atmospheric chemistry, and biological processes. As the size of the alkyl radical grows, R + O_2 reactions rapidly become more complex, and isomerizations to hydroperoxyalkyl radicals (QOOH) can increase in importance relative to concerted elimination of HO_2. The need for definitive *ab initio* theoretical research on propyl + O_2 is demonstrated by the disparity between the reaction energetics from the best existing electronic structure computations and parameters derived from master equation

kinetic models that best reproduce the available body of experimental measurements. In a herculean investigation, we have fully optimized geometries at the CCSD(T)/cc-pVTZ level of theory for all chemically relevant minima and transition states of the *n*-propyl and *i*-propyl + O_2 systems (Fig. 3). Final energetics were derived from explicit computations with basis sets as large as cc-pV5Z and correlation treatments as extensive as coupled cluster through full triples with perturbative inclusion of quadruple excitations [CCSDT(Q)]. Focal point analyses (FPA) targeting the complete basis set (CBS) limit of CCSDT(Q) theory were executed with inclusion of auxiliary corrections for core correlation, relativistic effects, and first-order non-Born-Oppenheimer terms. For the *n*-propyl + O_2 system, we find the critical transition state (**TS1**) for concerted elimination of HO_2 to lie 3.9 kcal mol^{-1} below the reactants and 3.1 kcal mol^{-1} lower than the key isomerization transition state (**TS2**) for CH_3CHCH_2OH radical formation. Even the robust CCSD(T)/cc-pVQZ method yields a concerted elimination barrier that is 1.8 kcal mol^{-1} too high, a striking result because such shifts of barrier heights in R + O_2 reactions can change branching fractions by an order of magnitude. Our definitive energetics for propyl + O_2 provide benchmarks for assessing the accuracy of master equation kinetic models.

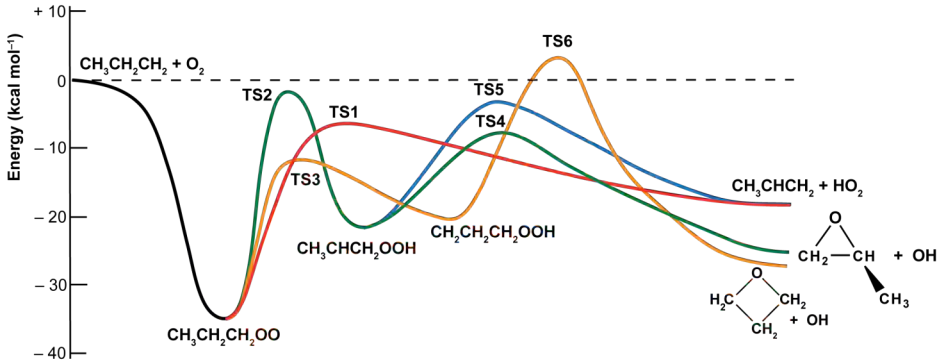

Figure 3. Schematic potential energy surfaces for the reactions of the *n*-propyl radicals with molecular oxygen.

Benzene + OH Surface: Intermediates and Transition States

Myriad experimental and theoretical studies have established the importance of hydroxyl radicals (HO·) in combustion, atmospheric chemistry, and the environmental sciences. The primary mechanism for removal of benzene pollutants from the troposphere is thought to start with attack by the hydroxyl radical. This process is key to understanding the degradation of polycyclic aromatic hydrocarbons (PAHs) in various environments. Accurate energetics for aromatic–radical systems are crucial for atmospheric simulation and macroscale kinetic modeling of hydrocarbon combustion. The scheme below shows the two lowest-energy reaction pathways on the benzene + OH potential energy surface. Pathway **II** dominates at lower temperatures, but the hydroxycyclohexadienyl radical (**I3**) is not stable above about 500 K, so that pathway **I** takes precedence at higher temperatures. In our very recent computational research,[23] Pathways **I** and **II** have been investigated using convergent focal-point analyses (FPA) to obtain CCSD(T)/CBS energetics for nine distinct stationary points as well as three additional conjectured intermediates. DFT methods alone proved insufficient to quantitatively characterize this potential energy surface. Refinements of DFT energetics within the G3 composite scheme in earlier papers gave results closer to our benchmarks, but with less theoretical rigor and greater statistical uncertainty. A number of nearly isoenergetic structures for **I1** and **I2** exist with binding energies less than 3 kcal mol^{-1}, as a consequence of the flat potential energy surfaces for the associated noncovalent interactions. Our computations find a surprisingly low transition state ($\mathbf{TS_2}$) for the addition pathway, lying only 1.8 kcal mol^{-1} above the separated reactants. The competing transition state ($\mathbf{TS_1}$) for hydrogen abstraction is 4.2 kcal mol^{-1} above reactants.

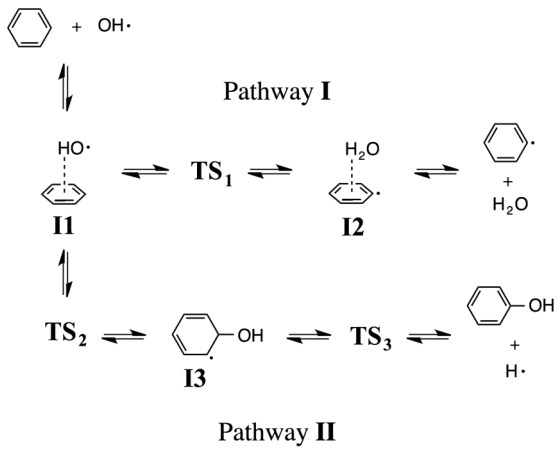

Publications Supported by DOE: 2009-2011

1. S. E. Wheeler, K. N. Houk, P. v. R. Schleyer, and W. D. Allen, "A Hierarchy of Homodesmotic Reactions," *J. Am. Chem. Soc*. **131**, 2547 (2009).
2. P. R. Schreiner, H. P. Reisenauer, E. Mátyus, A. G. Császár, A. Siddiqi, A. C. Simmonett, and W. D. Allen, "Infrared Signatures of the NCCO Radical," *Phys. Chem. Chem. Phys*. **11**, 10385 (2009).
3. A. C. Simmonett, H. F. Schaefer, and W. D. Allen, "The Enthalpy of Formation and Anharmonic Force Field of Diacetylene," *J. Chem. Phys*. **130**, 044301 (2009).
4. A. C. Simmonett, N. J. Stibrich, B. N. Papas, H. F. Schaefer, and W. D. Allen, "The Barrier to Linearity and Anharmonic Force Field of the Ketenyl Radical," *J. Phys. Chem. A* **113**, 11643 (2009).
5. S. E. Wheeler and H. F. Schaefer, "Thermochemistry of the HOSO Radical, a Key Intermediate in Fossil Fuel Combustion," *J. Phys. Chem. A* **113**, 6779 (2009).
6. Q. Hao, A. C. Simmonett, Y. Yamaguchi, D.-C. Fang, and H. F. Schaefer, "Structures and Energetics of H_6^+ Clusters," *J. Phys. Chem. A* **113**, 13608 (2009).
7. Q. Cheng, F. A. Evangelista, A. C. Simmonett, Y. Yamaguchi, and H. F. Schaefer, "The Water Dimer Radical Cation: Structures, Vibrational Frequencies, and Energetics," *J. Phys. Chem. A* **113**, 13779 (2009).
8. J. J. Wilke and H. F. Schaefer, "The Subtleties of Explicitly Correlated *Z*-Averaged Perturbation Theory: Choosing an R12 Method for High-Spin Open-Shell Molecules," *J. Chem. Phys*. **131**, 244116 (2009).
9. J. C. Hargis, H. F. Schaefer, K. N. Houk, and S. E. Wheeler, "Non-Covalent Interactions of a Benzo[a]pyrene Diol Epoxide with DNA Base Pairs: Insight into the DNA Intercalation of (+) – B*a*P DE-2," *J. Phys. Chem. A* **114**, 2038 (2010).
10. J. A. Miller, S. J. Klippenstein, Y. Georgievskii, L. B. Harding, W. D. Allen, and A. C. Simmonett, "Reactions between Resonance-Stablized Radicals: Propargyl + Allyl," *J. Phys. Chem. A* **114**, 4881 (2010).
11. Q. Wu, Y. Yamaguchi, Q. Li, and H. F. Schaefer, "Unusual Isomers of Disilacyclopropenylidene (Si_2CH_2)," *J. Phys. Chem. A* **114**, 7102 (2010).
12. T. Lu. Q. Hao, A. C. Simmonett, F. A. Evangelista, Y. Yamaguchi, D.-C. Fang, and H. F. Schaefer, "Low-Lying Triplet States of Diphosphene and Diphosphinylidene," *J. Phys. Chem. A* **114**, 9617 (2010).
13. Q. Wu, A. C. Simmonett, Y. Yamaguchi, Q. Li, and H. F. Schaefer, "Silacyclopropenylidene and its Most Important SiC_2H_2 Isomers," *Barbara J. Garrison Special Issue, J. Phys. Chem. C* **114**, 5447 (2010).
14. E. Mátyus, C. Fábri, T. Szidarovszky, G. Czakó, W. D. Allen, and A. G. Császár, "Assigning Quantum Labels to Variationally Computed Rotational-Vibrational Eigenstates of Polyatomic Molecules," *J. Chem. Phys*. **133**, 034113 (2010).
15. Q. Wu, Q. Cheng, Y. Yamaguchi, Q. Li, and H. F. Schaefer, "Triplet States of Cyclopropenylidene and its Isomers," *J. Chem. Phys.* **132**, 044308 (2010).
16. U. Bozkaya, J. M. Turney, Y. Yamaguchi, and H. F. Schaefer, "The Barrier Height, Unimolecular Rate Constant, and Lifetime for the Decomposition of HN_2," *J. Chem. Phys*. **132**, 064308 (2010).
17. H. Feng and W. D. Allen, "The Problematic $F_2 + C_2H_4$ Reaction Barrier," *J. Chem. Phys*. **132**, 094304 (2010).
18. Q. Cheng, A. C. Simmonett, F. A. Evangelista, Y. Yamaguchi, and H. F. Schaefer, "Characterization of the BNNO Radical," *J. Chem. Theory Comput.* **6**, 1915 (2010).
19. Q. Wu, Q. Hao, J. J. Wilke, A. C. Simmonett, Y. Yamaguchi, Q. Li, D.-C. Fang, and H. F. Schaefer, "Anharmonic Vibrational Analysis for the Propadienylidene Molecule ($H_2C=C=C$)," *J. Chem. Theory Comput.* **6**, 3122 (2010).
20. D. Gerbig, H. P. Reisenauer, C.-H. Wu, D. Ley, W. D. Allen, and P. R. Schreiner, "Phenylhydroxycarbene," *J. Am. Chem. Soc.* **132**, 7273 (2010).
21. Q. Hao, A. C. Simmonett, Y. Yamaguchi, D. Fang, and H. F. Schaefer, "From Acetylene Complexes to Vinylidene Structures: The GeC_2H_2 Systems," *J. Comp. Chem.* **32**, 15 (2011).
22. Y. Yamaguchi and H. F. Schaefer, "Analytic Derivative Methods in Molecular Electronic Structure Theory and its Applications to Spectroscopy," in press, *Handbook of High Resolution Spectroscopy*, Editors M. Quack and F. Merkt (Wiley, Chichester, 2011).
23. D. S. Hollman, A. C. Simmonett, and H. F. Schaefer, "The Benzene + OH Potential Energy Surface: Intermediates and Transition States," *Phys. Chem. Chem. Phys.* **13**, 2214 (2011).
24. J. J. Wilke and H. F. Schaefer, "Spin-Restricted Explicity Correlated Coupled Cluster for High-Spin Open-Shell Molecules. The *Z*-Averaged CCSD-R12 Approach," *J. Chem. Phys.*, submitted (2011).
25. P. R. Schreiner, H. P. Reisenauer, D. Ley, D. Gerbig, C.-H. Wu, and W. D. Allen, "Methylhydroxycarbene: Tunneling Control of a Chemical Reaction," *Science*, under final review for publication (2011).

Annual Progress report April 2011

Threshold Photoelectron Photoion Coincidence (TPEPICO) Studies: The Road to ± 0.1 kJ/mol Thermochemistry

Tomas Baer (baer@unc.edu)
Department of Chemistry
University of North Carolina
Chapel Hill, NC 27599-3290
DOE Grant DE-FG02-97ER14776

Program Scope

The threshold photoelectron photoion coincidence (TPEPICO) technique is utilized to investigate the dissociation dynamics and thermochemistry of energy selected medium to large organic molecular ions. The reactions include parallel and consecutive steps that are modeled with the statistical theory in order to extract dissociation onsets for multiple dissociation paths. These studies are carried out with the aid of molecular orbital calculations of both ions and the transition states connecting the ion structure to their products. The results of these investigations yield accurate heats of formation of ions, free radicals, and stable molecules. In addition, they provide information about the potential energy surface that governs the dissociation process. Isomerization reactions prior to dissociation are readily inferred from the TPEPICO data.

The TPEPICO Experiment

The threshold photoelectron photoion coincidence (TPEPICO) experiment in Chapel Hill is carried out with a laboratory H_2 discharge light source. Threshold electrons are collected by velocity focusing them into a 1.5 mm hole on a mask located at the end of the 12 cm drift tube. Some hot electrons pass through a 2x5 mm opening located next to the central 1.5 mm hole. In this fashion, two TPEPICO spectra are simultaneously collected, one for threshold and one for hot electrons. Hot electron free data are obtained by subtracting a fraction of the hot from the threshold TPEPICO data. The ion TOF is either a linear version or a reflectron for studying H loss processes. The electrons provide the start signal for measuring the ion time of flight distribution. When ions dissociate in the microsecond time scale, their TOF distributions are asymmetric. The dissociation rate constant can be extracted by modeling the asymmetric TOF distribution. A high-resolution version of this experiment with a molecular beam source and an electron imaging detector at the Swiss Light Source (SLS) has been constructed and has been collecting data since August, 2008. Because of the high photon flux, we have implemented the first multi-start multi-stop coincidence scheme using a master clock as the time base. The maximum photon resolution and flux have not yet been achieved due to some alignment issues. However, 2 meV resolution (0.2 kJ/mol) is routinely available, which is yielding very precise heats of formation of some key molecules, radicals and ions.

Recent Results

Dissociation dynamics of energy selected *i*-$C_3H_7X^+$ ions by iPEPICO: Accurate Heats of Formation of *i*-$C_3H_7^+$, *i*-C_3H_7Cl, *i*-C_3H_7Br, and *i*-C_3H_7I: The dissociation dynamics of energy selected *i*-C_3H_7X (X = H,Cl, Br, and I) ions have been investigated by imaging photoelectron-photoion coincidence (iPEPICO) spectroscopy using synchrotron radiation from the X04DB VUV beam line in the Swiss Light Source of the Paul Scherrer Institut. The 0 K dissociation energy (E_0) for *i*-C_3H_8 was determined to be 11.624 ± 0.002 eV. This leads to a 298 K isopropyl

ion heat of formation of 805.9 ± 0.5 kJ mol^{-1}. The $\Delta_f H^o_{298K}(i\text{-}C_3H_7^+)$ combined with the measured 0 K onsets for $i\text{-}C_3H_7^+$ formation from isopropyl chloride (11.065 ± 0.004 eV), isopropyl bromide (10.454 ± 0.008 eV), and isopropyl iodide (9.812 ± 0.008 eV), yields the 298 K isopropyl chloride, bromide and iodide heats of formation of –145.7 ± 0.7 kJ mol^{-1}, –95.6 ± 0.9 kJ mol^{-1} and –38.5 ± 0.9 kJ mol^{-1} respectively. These values provide a significant correction to literature values and reduce the error limits. Finally, the new $i\text{-}C_3H_7^+$ heat of formation leads to a predicted adiabatic ionization energy for the isopropyl radical of 7.430 ± 0.012 eV, and a 298 K proton affinity for propene of 744.1 ± 0.8 kJ mol^{-1}. The determination of the $i\text{-}C_3H_7^+$ heat of formation, based on the H loss onset from propane, was not straightforward for interesting reasons. A room temperature experiment with 80 V/cm ion extraction resulted in an onset of 11.640 ± 0.005 eV, whereas a 20 V/cm extraction as well as a molecular beam experiment reduced the onset to the reported 11.624 ± 0.002 eV. RRKM modeling of this reaction suggested that the rate constant should be fast. However, this did not take into account the possibility of a centrifugal barrier for H loss, through which tunneling can result in slow reaction. Thus, the 80 V/cm extraction experiment did not permit the ions sufficient time to dissociate and thus shifted the onset energy to higher energies, whereas the 20 V/cm experiment did. The molecular beam data suppressed high J values, thus eliminating the centrifugal barrier, thereby yielding the lower energy onset in agreement with the 20 V/cm data.

Tunneling in a simple bond scission: The surprising barrier in the H loss from HCOOH$^+$: In a joint study with John Stanton (UT-Austin) the dissociation dynamics of gas phase formic acid ions (HCOOH$^+$, DCOOD$^+$, HCOOD$^+$, DCOOH$^+$) were investigated by Threshold Photoelectron-Photoion Coincidence (TPEPICO) spectroscopy and high level ab initio calculations. The slow rate constants for this seemingly simple H loss reaction and the large onset energy shifts due to isotopic substitution point to a substantial exit barrier through which the H or D atoms tunnel. Modeling of the HCOOH$^+$ experimental data using RRKM theory with tunneling through an Eckart potential are best fitted with a barrier of about 17 kJ mol^{-1}. High level ab initio calculations support the experimental findings with a computed barrier of 15.9 kJ mol^{-1}, which is associated with the substantial geometry change between the product HOCO$^+$ cation and the corresponding HCOOH$^+$ molecular ion. Because of this exit channel barrier, the formic acid ion dissociation does not provide a route for determination of the HOCO$^+$ heat of formation. Rather, the most accurate value comes from the calculations employing the High Accuracy Extrapolated *ab initio* Thermochemistry (HEAT) scheme, which yields a $\Delta_f H^o_{0K}[HOCO^+]$ = 600.3 ±1.0 kJ mol^{-1} ($\Delta_f H^o_{298K}[HOCO^+]$ = 597.3 ±1.0 kJ mol^{-1}). The calculated proton affinity of CO_2 is thus 534.7 ± 1.0 kJ mol^{-1} at 0 K and 539.3 ± 1.0 kJ mol^{-1} at 298.15 K.

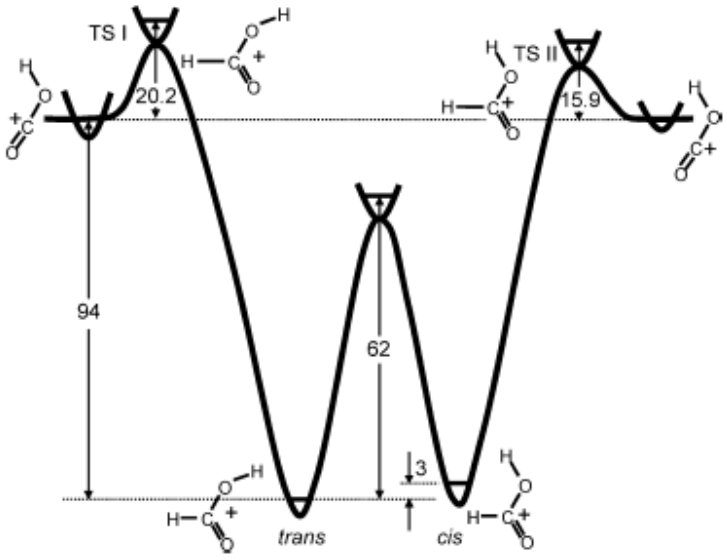

The heats of formation of $C_6H_5^{\bullet}$ $C_6H_5^+$ and C_6H_5NO by TPEPICO and Active Thermochemical Tables Analysis: In a joint study with Branko Ruscic (Argonne National Laboratory) the threshold photoelectron photoion coincidence has been used to prepare selected internal energy distributions of nitrosobenzene ions [$C_6H_5NO^+$]. Dissociation to $C_6H_5^+$ + NO products was measured over a range of internal energies and rate constants from 10^3 to 10^7 s^{-1} and fitted with the statistical theory of unimolecular decay. A 0 K dissociative photoionization onset energy of 10.607 ± 0.020 eV was derived by using the simplified statistical adiabatic channel model. The thermochemical network of Active Thermochemical Tables (ATcT) was expanded to include phenyl and phenylium, as well as nitrosobenzene. The current ATcT heats of formation of these three species at 0 K (298.15 K) are 350.6 (337.3) ±0.6, 1148.7 (1136.8) ±1.0, and 215.6 (198.6) ±1.5 kJ mol-1, respectively. The resulting adiabatic ionization energy of phenyl is 8.272 ± 0.010 eV. The new ATcT thermochemistry for phenyl entails a 0 K (298.15 K) C-H bond dissociation enthalpy of benzene of 465.9 (472.1) ± 0.6 kJ mol^{-1}. Several related thermochemical quantities from ATcT, including the current enthalpies of formation of benzene, monohalobenzenes, and their ions, as well as interim ATcT values for the constituent atoms, are also given.

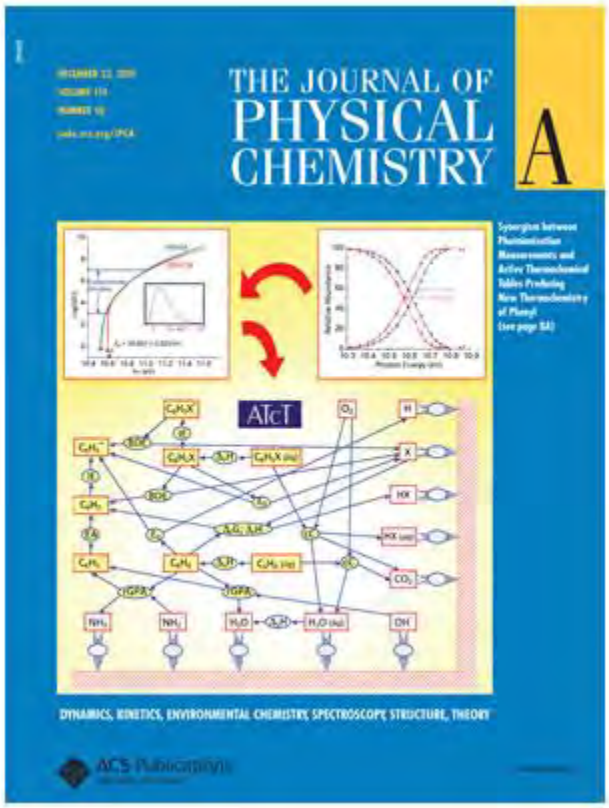

Work in Progress and Future Plans

Some work in progress include the study of the translational dimnesionality in dissociation reactions. We have found that I loss from $C_2H_4I_2^+$ proceeds with I atoms leaving the ion in a 1-D translational energy distribution. Phase space theory predicts a 2-D distribution.

Publications from DOE supported work 2009 – 2011

William Stevens, Bálint Sztáray, Nicholas S. Shuman, Tomas Baer, and Jürgen Troe, Specific Rate Constants k(E) of the Dissociation of Halobenzene Ions: Analysis by Statistical Unimolecular Rate Theories. *J. Phys. Chem. A* **113** 573-582 (2009)

Balázs Hornung, Andras Bodi, Csaba Pongor, Zsolt Gengeliczki, Tomas Baer, and Bálint Sztáray, Dissociative photoionization of $X(CH_3)_3$ (X = N, P, As, Sb, Bi): mechanism, trends and accurate energetics, *J. Phys. Chem. A* **113** 8091-8098 (2009)

Andras Bodi, Melanie Johnson, Thomas Gerber, Zsolt Gengeliczki, Bálint Sztáray, and Tomas Baer, Imaging photoelectron photoion coincidence spectroscopy with velocity focusing electron optics, *Rev. Sci. Instrum*. **80** 034101/1 - 7 (2009)

Nicholas S. Shuman, Austin Spencer, and Tomas Baer, Experimental thermochemistry of $SiCl_3R$ (R = Cl, H, CH_3, C_2H_5, C_2H_3, CH_2Cl, $SiCl_3$), $SiCl_3^+$, and $SiCl_3^\bullet$, J.Phys.Chem. A **113** 9458 – 9466 (2009)

Nicholas S. Shuman, William R. Stevens, Katherine E. Lower, and Tomas Baer, The heat of formation of the allyl ion by TPEPICO spectroscopy, J.Phys.Chem. A **113** 10710-10717 (2009)

Andras Bodi, Nicholas S. Schuman, and Tomas Baer, On the ionization and dissociative photoionization of iodomethane: a definitive experimental enthalpy of formation of CH_3I, *Phys. Chem. Chem. Phys* **11** 11013-11021 (2009)

Nicholas S. Shuman, Andras Bodi, and Tomas Baer, Heats of formation of t-butyl peroxy radical and t-butyl diazyl ion: RRKM vs SSCAM rate theories in systems with kinetic and competitive shifts, *J. Phys. Chem. A* **114** 232-240 (2010)

William R. Stevens, S. Hunter Walker, Nicholas S. Shuman[†], and Tomas Baer, Dissociative Photoionization Study of Neopentane:A path to an accurate heat of formation of the *t*-butyl ion, t-butyl iodide, and t-butyl hydroperoxide, *J. Phys. Chem. A* **114** 804 – 810 (2010)

Nicholas S. Shuman, William R. Stevens, and Tomas Baer, Dissociation dynamics of energy selected acetic acid ions: The gas phase heat of formation of the acetyl ion, *Int.J.Mass Spectrom.*, **294**, 88-92 (2010)

William R. Stevens, Andras Bodi, and Tomas Baer, Dissociation dynamics of energy selected, propane, and i-$C_3H_7X^+$ ions by iPEPICO: Accurate Heats of Formation of i-$C_3H_7^+$, i-C_3H_7Cl, i-C_3H_7Br, and i-C_3H_7I, *J. Phys. Chem. A*, **114**, 11285-11291 (2010)

Nicholas S. Shuman, Melanie Johnson, William R. Stevens, Michael E. Harding, John F. Stanton, and Tomas Baer, Tunneling in a simple bond scission: The surprising barrier in the H loss from $HCOOH^+$, *J. Phys. Chem. A.*, **114**, 10016-10023 (2010)

William R. Stevens, Branko Ruscic, and Tomas Baer, The heats of formation of $C_6H_5^\bullet$, $C_6H_5^+$, and C_6H_5NO by TPEPICO and Active Thermochemical Tables analysis, *J. Phys. Chem. A.*, **114**, 13134-13145 (2010)

Ágnes Révész**,** László Szepes, Tomas Baer, and Bálint Sztáray, Binding energies and isomerization in metallocene ions from threshold photoelectron photoion concidence spectroscopy, *J.Am. Chem.Soc.* **132**, 17795-17803 (2010)

Bálint Sztáray, Andras Bodi, and Tomas Baer, Modeling unimolecular reactions in photoelectron photoion coincidence experiments, *J.Mass Spectrom*. **45**, 1233-1245 (2010)

Juan Z. Davalos, Nicholas S. Shuman, Rebeca Herrero, and Tomas Baer, Dissociation Dynamics and Thermochemistry of Tin Species, $(CH_3)_4Sn$ and $(CH_3)_6Sn_2$, by Threshold Photoelectron-Photoion Coincidence Spectroscopy, *J. Phys. Chem. A*. **115**, 402-409 (2011).

Andras Bodi, William R. Stevens, and Tomas Baer, Understanding the Complex Dissociation Dynamics of Energy Selected Dichloroethylene Ions: Neutral Isomerization Energies and Heats of Formation by Imaging-Photoelectron-Photoion-Coincidence, J. Phys. Chem. A, **115**, 726-734 (2011)

Turbulence-Chemistry Interactions in Reacting Flows

Robert S. Barlow
Combustion Research Facility
Sandia National Laboratories, MS 9051
Livermore, California 94550
barlow@sandia.gov

Program Scope

This program is directed toward achieving a more complete understanding of turbulence-chemistry interactions in flames and providing detailed measurements for validation of combustion models. In the Turbulent Combustion Laboratory (TCL), simultaneous line imaging of spontaneous Raman scattering, Rayleigh scattering, and two-photon laser-induced fluorescence (LIF) of CO is applied to obtain spatially and temporally resolved measurements of temperature, the concentrations of all major species, mixture fraction, and reaction progress, as well as gradients in these quantities in hydrocarbon flames. The instantaneous three-dimensional orientation of the turbulent reaction zone is also measured by imaging of OH LIF (or Rayleigh scattering at 355 nm) in two crossed planes, which intersect along the laser axis for the multiscalar measurements. These combined data characterize both the thermo-chemical state and the instantaneous flame structure, such that the influence of turbulent mixing on flame chemistry may be quantified. Our experimental work is closely coupled with international collaborative efforts to develop and validate predictive models for turbulent combustion. This is accomplished through our visitor program and through the TNF Workshop series. Although the past emphasis has been on nonpremixed and partially premixed combustion, the workshop and this program have expanded their scope to address a broad range of combustion modes, including premixed and stratified flames. We are also working to extend our quantitative multiscalar diagnostics to more complex hydrocarbon fuels. Entry into these new research areas has prompted developments in both hardware and methods of data analysis to achieve unprecedented spatial resolution and precision of multiscalar measurements. Within the CRF we collaborate with Joe Oefelein to use highly-resolved large-eddy simulations (LES) of our experimental flames in order to gain greater fundamental understanding of the dynamics of multi-scale flow-chemistry interactions. We also collaborate with Tom Settersten and Jonathan Frank to refine our quantitative LIF methods and to apply complementary imaging diagnostics to selected turbulent flames.

Recent Progress

Preferential Transport Effects in Turbulent Premixed Flames

New insights were gained on physical mechanisms contributing to the previously reported large effects of preferential species transport measured in turbulent, bluff-body-stabilized, premixed methane-air flames. Experiments on pilot-stabilized laminar and turbulent premixed flames failed to show transport effects anywhere near the magnitude observed in the original Cambridge burner experiments. Subsequent experiments on a simple annular bluff-body burner revealed that the preferential transport effect is amplified by the presence of a strong recirculation zone.

Multiscalar line measurements were obtained in a series of six premixed CH_4/air flames ($\phi = 0.77$) stabilized on the burner shown in Fig. 1a. The bulk velocity of the annular reactant flow was increased from 1.3 m/s to 7.7 m/s, with the highest value being similar to the 7.5 m/s inner annular bulk velocity in the original Cambridge burner experiments. The four graphs in Fig. 1b show measured conditional means (blue) of the mass fractions of CO_2 and O_2, along with equivalence ratio and the carbon-to-hydrogen atom ratio measured across the reaction zone at a distance of 10 mm above the bluff body surface. Measurements are compared with results from a Chemkin calculation of an unstrained premixed flame at $\phi = 0.77$ (red), using GRI Mech 3.0 and multi-component transport. In the lower range of velocity (1.3 to 2.6 m/s) measured scalar profiles are consistent with the laminar 1D flame calculation (within the accuracy of the measurements). However, with further increases in velocity the measured scalar profiles move progressively toward trajectories observed in the original experiments on the Cambridge/Sandia burner. This change in scalar structure occurs as the turbulent flame brush becomes more tightly constrained between the reactant stream and the bluff-body recirculation zone.

These new experimental results, combined with analysis of preferential diffusion effects in the 1D laminar flame calculations, indicate that the H_2 and H_2O are preferentially transported toward the reactant side of the flame and then convectively carried downstream, while excess CO_2 is accumulated within the recirculation zone. Similar effects of preferential transport may be present in any turbulent premixed or stratified hydrocarbon flame stabilized in a shear flow by a strong recirculation zone. Further work is planned to investigate a range of CH_4/air equivalence ratios and to look at CH_4/H_2 fuel blends.

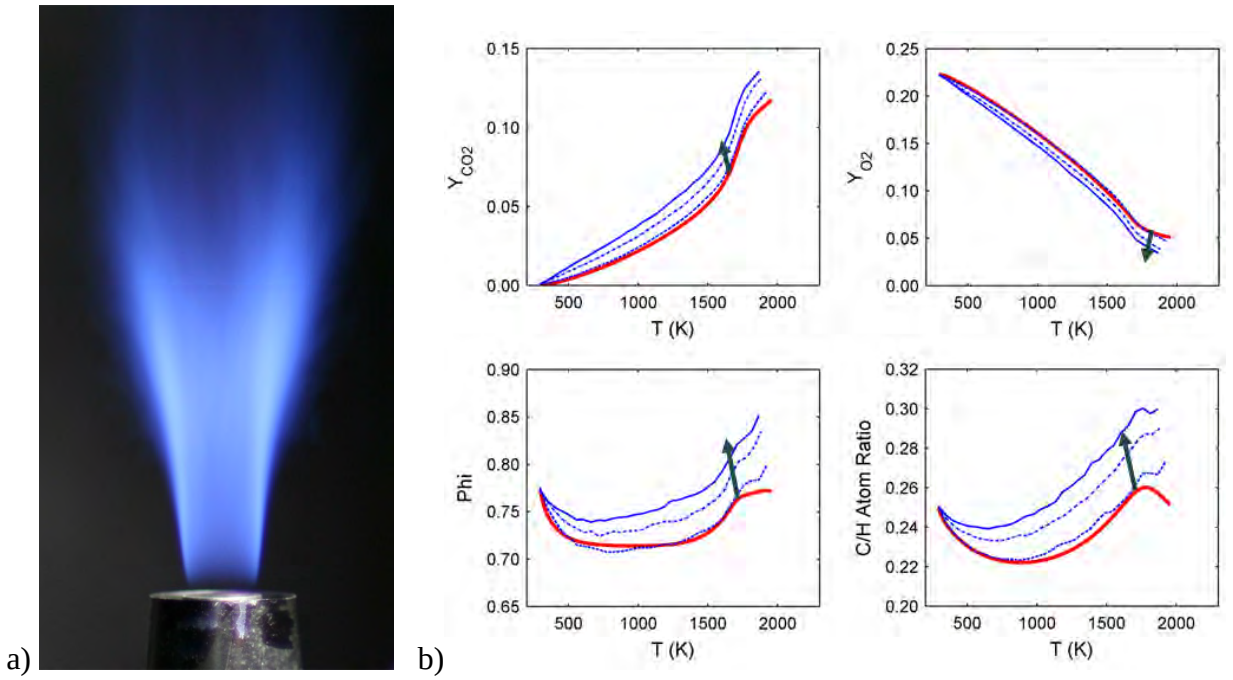

Figure 1. a) Premixed CH_4-air flame at $\phi = 0.77$ stabilized on a simple annular bluff-body burner. b) Conditional mean mass fractions of CO_2 and O_2, equivalence ratio ϕ, and C/H atom ratio plotted against temperature. The measurements (blue) reveal a clear trend of increasing deviation of the from an unstrained laminar flame calculation (red) as the velocity of the annular reactant flow is increased. Bulk reactant velocities were 2.6 m/s (dash), 5.1 m/s (dot-dash), 7.7 m/s (solid).

Oxy-Fuel Combustion

In collaboration with A. Sevault (Norwegian University of Science and Technology) and M. Ditaranto (SINTEF), we conducted experiments on jet flames of methane/hydrogen mixtures in a coflow of 32% O_2 (mole fraction) in CO_2. This mode of oxy-fuel combustion is of interest in the context of research on combustion technologies that could allow for carbon capture and sequestration. Two series of flames were measured in which the probability of localized was influenced by first varying the H_2 volume fraction, while holding jet Reynolds number constant at 15,000, and then varying the jet Reynolds number, while holding the hydrogen volume fraction constant at 55%. Oxy-fuel combustion presents some interesting challenges for multiscalar laser diagnostics, particularly with regard to fluorescence interferences, radiative loading on the optical system due to high CO_2 levels, and strong variation in collisional quenching rates for CO and OH compared to methane-air flames. With appropriate accounting for these challenges, the resulting data are of high quality, as illustrated in Fig. 2, and will be useful for evaluating the ability models to predict strong effects of turbulence-chemistry interaction in oxy-fuel combustion.

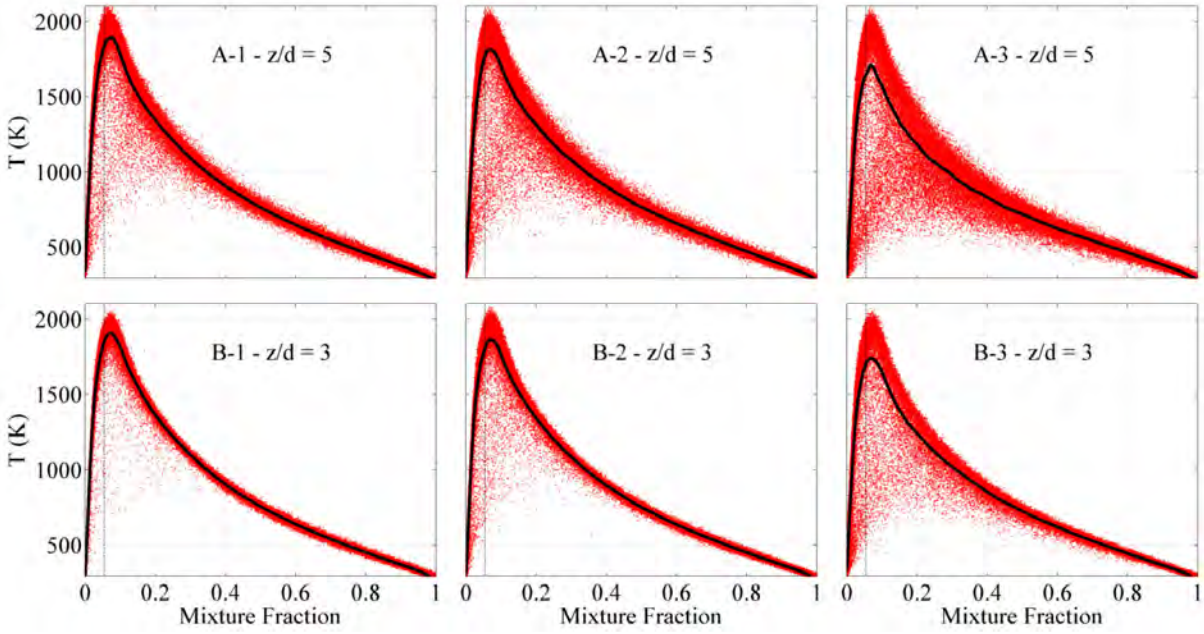

Figure 2. Scatter plots and conditional means of temperature measured in two series of jet flames CH_4/H_2 mixtures burning in a coflow of CO_2/O_2. The probability of local extinction increases with decreasing H_2 mole fraction (series A: 55%, 45%, 37% H_2 at Re = 15,000) or with increasing jet Reynolds number (series B: Re = 12,000, 15,000, 18,000 with 55% H_2 mole fraction).

Future Plans

We are currently implementing a change from crossed-planar imaging of OH LIF to crossed planar imaging of Rayleigh scattering at 355 nm. This will allow more accurate determination of local 3D gradients of temperature and progress variable in turbulent premixed and stratified flames. Other work in progress or planned includes further investigation of preferential transport in premixed CH_4 and CH_4/H_2 flames, further development of Raman

scattering methods for multiscalar measurements in DME flames, experiments on a series of piloted DME jet flames, and new scalar experiments on the Sydney Bluff Body Burner.

BES Supported Publications (2009 - present)

R.S. Barlow, G.H. Wang, P. Anselmo-Filho, M.S. Sweeney, S. Hochgreb, "Application of Raman/Rayleigh/LIF Diagnostics in Turbulent Stratified Flames," *Proc. Combust. Inst*. **32,** 945-953 (2009).

P. Anselmo-Filho, S. Hochgreb, R.S. Barlow, R.S. Cant, "Experimental Measurements of Geometric Properties of Turbulent Stratified Flames," *Proc. Combust. Inst*. **32,** 1763-1770 (2009).

M.J. Dunn, A.R. Masri, R.W. Bilger, R.S. Barlow, G.H. Wang, "The Compositional Structure of Highly Turbulent Piloted Premixed Flames Issuing into Hot Coflow," *Proc. Combust. Inst*. **32**, 1779-1786 (2009).

J. Cai, D.H. Wang, C. Tong, R.S. Barlow, A.N. Karpetis, "Investigation of sub-grid-scale mixing of mixture fraction and temperature in turbulent partially premixed flames," *Proc. Combust. Inst.*, **32**, 1517-1525 (2009).

R.S. Barlow, H.C. Ozarovsky, A.N. Karpetis, R.P. Lindstedt, "Piloted Jet Flames of CH_4/H_2/Air: Experiments on Localized Extinction in the Near Field at High Reynolds Numbers," *Combust. Flame* **156**, 2117-2128 (2009).

M.J. Dunn, A.R. Masri, R.W. Bilger, R.S. Barlow. "Finite Rate Chemistry Effects in Highly Sheared Turbulent Premixed Flames," *Flow. Turb. Combust.* **85**, 621-648 (2010).

J. Cai, C. Tong, R.S. Barlow, A.N. Karpetis, "Noise Correction and Length Scale Estimation for Scalar Dissipation Rate Measurements in Turbulent Partially Premixed Flames," *Flow. Turb. Combust.* **85**, 309-332 (2010).

F. Fuest, R.S. Barlow, D. Geyer, F. Seffrin, A. Dreizler, "A Hybrid Method for Evaluation of 1D Raman Spectroscopy," *Proc. Combust. Inst.* **33**, 815–822 (2011).

J. Cai, C. Tong, R.S. Barlow, A.N. Karpetis, "Conditionally filtered diffusion of mixture fraction and temperature in turbulent partially premixed flames," *Proc. Combust. Inst.*, **33**, 1505-1513 (2011).

M.S. Sweeney, S. Hochgreb, M.J. Dunn, R.S. Barlow, "A comparative analysis of flame surface density metrics in premixed and stratified flames," *Proc. Combust. Inst.* **33**, 1419–1427 (2011).

TNF Workshop Information: http://www.sandia.gov/TNF

Modeling Reactions in High-Pressure Turbulence in the Cold Ignition Regime

Josette Bellan
Mechanical Engineering Department, California Institute of Technology
Pasadena, CA 91125
Josette.Bellan@jpl.nasa.gov

I. Program Scope

This study addresses issues highlighted in the Basic Energy Needs for Clean and Efficient Combustion of 21st Century Transportation Fuels (DOE BES, 2003) under the topic of Combustion under Extreme Pressure. It is there noted that "the most basic concepts of thermal autoignition" are "based on experience and theory at near atmospheric pressures" and that "as pressure increases significantly…, many of these conceptual pictures begin to change or disappear". It is also stated "A better description of the coupling and interaction of high pressure flow and molecular transport processes with chemistry is also necessary", particularly because "Ignition and flame propagation of alternative and renewable fuels, as well as of the changing feed stocks of conventional fossil-based fuels, are very likely to be much different at very high pressures than under the more familiar, lower pressure conditions of current engines." Recognizing that "Under such *(increasing pressure)* conditions distinctions between gas and liquid phases become moot, new equations of state must be used…", it is immediately apparent that there must be "a re-examination of the basic assumptions that govern the physics and chemistry related to combustion; and the need for this type of re-examination increases as the combustion pressure increases." This recognition is also stated under the topic of Multiscale Modeling since due to the new equations of state "The combination of unexplored thermodynamic environments and new physical and chemical fuel properties results in complex interactions among multiphase *(according to the above, the multiphase distinction becomes moot with increasing pressure)* fluid dynamics, thermodynamic properties, heat transfer, and chemical kinetics that are not understood even at a fundamental level." From the theoretical viewpoint for "systems at high pressure, fluid dynamic time scales can be comparable to chemical time scales." and therefore "completely diffusion-controlled reactions … can become important".

Thus, the objective of this study is the investigation of the coupling among thermodynamics, transport properties, intrinsic kinetics and turbulence under the high-pressure and the relatively (with respect to combustion) low-temperature conditions typical of the auto-ignition regime, with particular emphasis on the manifestation of this coupling on the effective kinetic rate. It is also planned to establish collaboration with Dr. Joseph Oefelein of the Combustion Research Facility at Sandia Livermore to work together towards implementing the models developed in this research into the high-pressure Large Eddy Simulation (LES) code under development by him at Sandia.

II. Recent Progress

This study was initiated in September 2009 and began in earnest with the arrival of the Post Doc at the end of July 2010. The report thus contains results obtained during the last eight months of full-pace study. The focus of this year was on two facets of high-pressure combustion: (a) examination of the subgrid-scale (SGS) scalar variance, as related to the potential utilization of flamelet models under supercritical conditions, and (b) developing a

model of reacting flow under supercritical conditions suitable for Direct Numerical Simulation (DNS).

(a) The SGS scalar variance under supercritical conditions.

We first addressed the issue of the SGS scalar variance, σ_Z, as related to the LES modeling of the turbulent reaction through the flamelet model. Although we do not have yet a database of reactive turbulent supercritical flows, since the flamelet model relies on the definition of a conserved scalar Z, we have the necessary information from our previous species-mixing study to perform the investigation; if a conserved scalar can be defined for the reactive flow situation, because of the additional coupling due to reaction, this scalar is expected to have a more complex behavior than the present one resulting only from mixing, so the results of this study are conservative in terms of the level of difficulty to model the scalar variance.

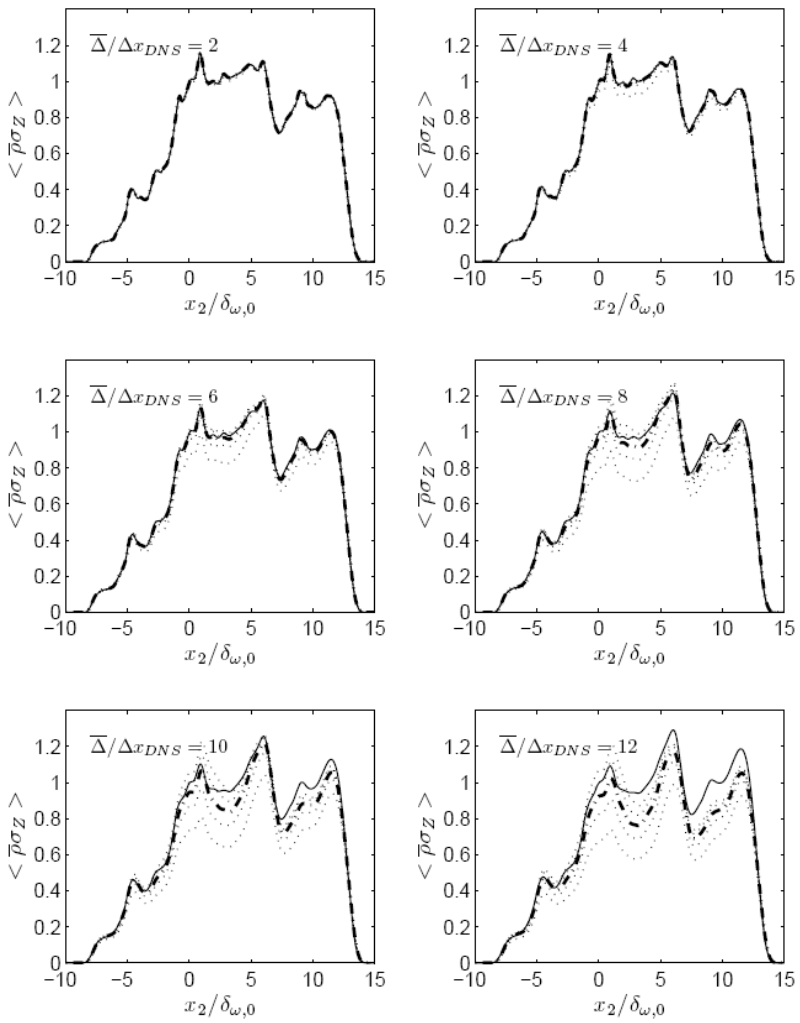

Figure 1. Predictions of the Favre SGS scalar variance using ADM applied to conservative quantities. Several orders of approximation are shown for different filter widths at the transitional time for the HN600 mixing layer. Exact SGS scalar variance: solid line. Dotted lines are the first to fifth order approximations, the third order being distinguished by a dash-dotted line. Variances are non-dimensionalized by the exact value at the center of the mixing layer.

In a first step of the study, we derived the σ_Z equation [1, 2] in two forms. The first form highlighted the new terms in the equation with respect to the atmospheric-pressure conditions case, and the second form emphasized the new SGS terms in the equation that would require modeling, as well as identified the nature of each term (i.e. production or dissipation). The result of assessing the activity of all terms in the two equations was to identify two new SGS terms that are have comparable magnitude to the classical terms and thus cannot be neglected: (i) a SGS diffusion term, and (ii) a SGS Soret term that has a dissipative effect. Given the lack of models for these terms, it was decided that tying to model them in the σ_Z equation for the purpose of solving the equation was bound to be an unrewarding approach, and instead, it was decided to propose direct models for σ_Z. Examination of the database over several binary-species systems revealed that indeed the PDF of Z is best approximated by a β PDF, which

justified investing time in modeling σ_Z since the PDF can be constructed from its mean provided by the LES solution and a model of σ_Z.

Thus, in the second step of the study we explored two models for σ_Z: (1) the approximate deconvolution model (ADM), and (2) a dynamic gradient-based (GRD) model. These models are conceptually different as ADM relies on a mathematical derivation with no assumptions required regarding the nature of the scale interactions, while the GRD relies on the mixing-length hypothesis in conjunction with an equilibrium assumption. Figure 1 illustrates the Favre SGS scalar variance modeled for a heptane/nitrogen (HN) mixing layer using ADM applied to the conservative variables, for several orders of ADM approximation and for several filter widths, including some very large widths compared to the DNS grid-spacing. The model is generally very good to excellent at relatively small filter widths, but as the filter width becomes large, there is evidence that the series expansion on which ADM relies does not converge with increasing order of approximation, as an overshoot becomes increasingly visible with increasing filter width. Thus, ADM should be considered here as an approximation rather than a converging procedure to obtain σ_Z, and in this particular case an approximation order of 3 is recommended. For the GRD-based model, we formulated a new model which we exercised and compared to the results obtained with a classical model in conjunction with two approximations for the filter width; representative results are depicted in Fig. 2. Compared to the classical model which increasingly departs from the filtered DNS template with either type of filter approximation, our model maintains high fidelity even at very large filter widths and in a range where test filtering is performed close to the production range of wavenumbers.

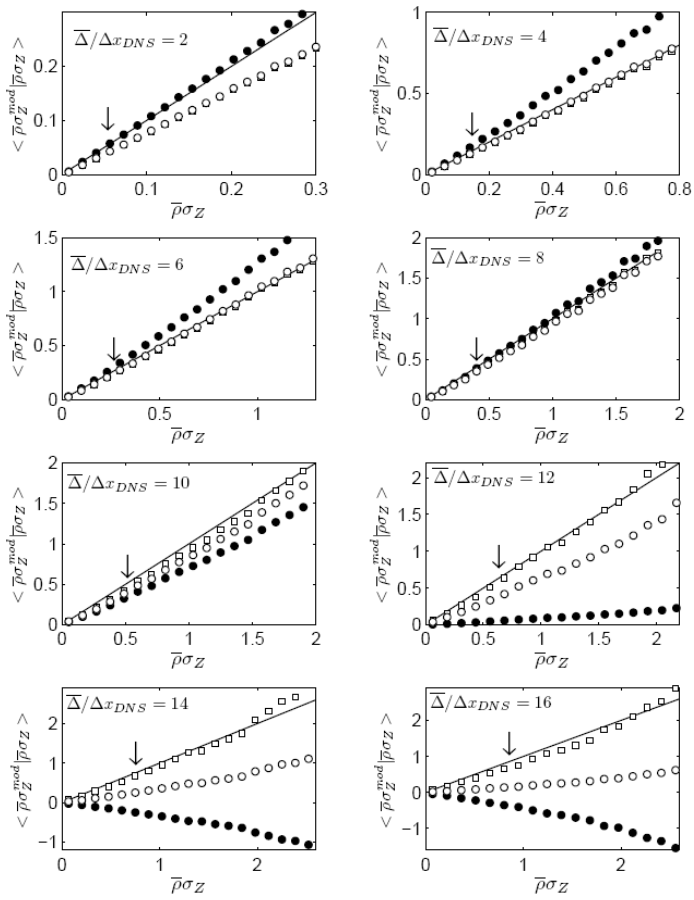

Figure 2. Planar averages of modeled SGS scalar variances conditioned in the exact ones, evaluated using the filtered HN600 DNS at the transitional time over a specific x_2 plane. Coefficients are computed using the new model (squares), and the classical model with two filter approximations (empty circles and filled circles). The arrow indicates the mean quantity.

A manuscript has been submitted for publication [1] and a presentation [2] has been made at a national conference of this subject.

(b) Development of a model and code describing reactions under supercritical-pressure conditions

The second step in this study is the development of a model and code to explore the specific aspects of turbulent combustion under supercritical conditions. As the model will be exercised in DNS, it is only a transitional rather than fully turbulent state that can be reproduced. To capture the physics of fully turbulent reaction using a transitional state, it is

clear that realistic reaction rates cannot be used because the reaction time would be considerably shorter than the turbulence time; thus, in DNS, reactions must be artificially delayed to enable coupling between reaction and turbulence. It seems then reasonable that in DNS one should have a global reaction as a first stage towards more complicated systems. Thus, a five-species one-step reaction rate was here chosen.

Beside the reaction rate, there are several other ingredients to this model, including the transport properties and the equation of state. Using a previously published methodology [i], an equation of state has been derived and coded for the species system of *n*-heptane, nitrogen, oxygen, carbon dioxide and water. For this system of species, the diffusion matrix is 5×5. We do not adopt here the diagonal matrix approximation typically used in combustion problems; this is first because that approach is problematic for rich mixtures and second because it is clear from the study of the SGS scalar variance that diffusion will be an important SGS process (as already seen from detailed analysis of the DNS database [ii]) and missing it or misreproducing it would impact the accuracy of the DNS. Thus, we have computed the complete matrix of pair-wise diffusion coefficients [iii] using as building blocks the binary diffusion coefficients [iv]. Similarly, the thermal diffusion factors were also modeled [iii]. The thermal conductivity was modeled as per Reid et al. [v]. These submodels have all been coded and the supercritical-mixing code has been modified to incorporate these changes and accommodate the larger number of species. The code is now in the debugging mode.

The PI has continued the collaboration established last year with Dr. Oefelein by transmitting additionally to the new SGS model necessary in the momentum equation [vi], a new SGS model describing the small-scale molecular flux effect [vii]. Both of these models were found in *a posteriori* studies essential for reproducing the filtered DNS template [vi,vii].

III. Future Plans

The following activities are planned for the near future:

- Complete the debugging of the code to render it operational.
- By changing the initial conditions, conduct a series of DNS to create a database.
- Analyze *a priori* the database and propose models for the turbulent reaction terms.

IV. References

i. Harstad, K; Miller, R. S.; Bellan, J. *A.I.Ch.E. J*. **1997**, *43(6)*, 1605

ii. Okong'o, N.; Bellan, J. *J. Fluid Mech.* **2002**, *464*, 1

iii. Harstad, K; Bellan, J. *Journal of Chemical Physics* **2004,** *120(12)*, 5664

iv. Harstad, K; Bellan, J. *Ind. & Eng. Chem. Res.* **2004**, *43(2)*, 645

v. Reid, R. C.; Prausnitz, J. M.; Poling, B. E. The Properties of Gases and Liquids, 4th edition, McGraw-Hill, NY, **1987**.

vi. Taşkinoğlu, E. S.; Bellan, J. *J. Fluid Mech.* **2010**, *645*, 211

vii. Taşkinoğlu, E. S.; Bellan, J. accepted in the *J. Fluid Mech.*, **2011**.

V. Publications and submitted articles supported by this project September 2009-March 2011

[1] Masi, E.; Bellan J. The subgrid-scale scalar variance under supercritical pressure conditions, submitted for publication February 2011

[2] Masi, E.; Bellan J. The subgrid scalar variance equation under supercritical pressure conditions, paper 1C04 presented at the 7th US National Combustion meeting, Atlanta, GA., March 21-23, 2011

Theoretical Studies of Combustion Dynamics (DE-FG02-97ER14782)

Joel M. Bowman
Cherry L. Emerson Center for Scientific Computation and Department of Chemistry,
Emory University Atlanta, GA 30322, jmbowma@emory.edu

Program Scope

The research program supported by this Department of Energy grant focuses on the development of rigorous computational methods to model the chemical and physical processes of importance in gas-phase combustion. These includes the development of full-dimensional, global, *ab initio*-based potential energy surfaces (PESs) that describe complex unimolecular and bimolecular reactions. Dynamics on these potentials, which may contain multiple minima and saddle points, are done for long times and these often reveal new pathways and mechanisms of chemical reactions. Large amplitude motion, including isomerization, "roaming", energy transfer in collisions with atoms and molecules can be studied with these potentials. The choice of reaction system to study is always motivated by experiments that challenge and ultimately advance basic understanding of combustion reaction dynamics.

Recent projects

Allyl Photodissociation

In collaboration with Paul Houston, we have developed a global PES describing allyl dissociation to a variety of products. The PES is a permutationally invariant fit to roughly 100 000 *ab initio* energies, computed at the CCSD(T)/aug-cc-pVTZ method/basis. Below is the usual schematic of the PES that indicates a number of minima, saddle points and products, the major one being H+ isomers of C_3H_4.

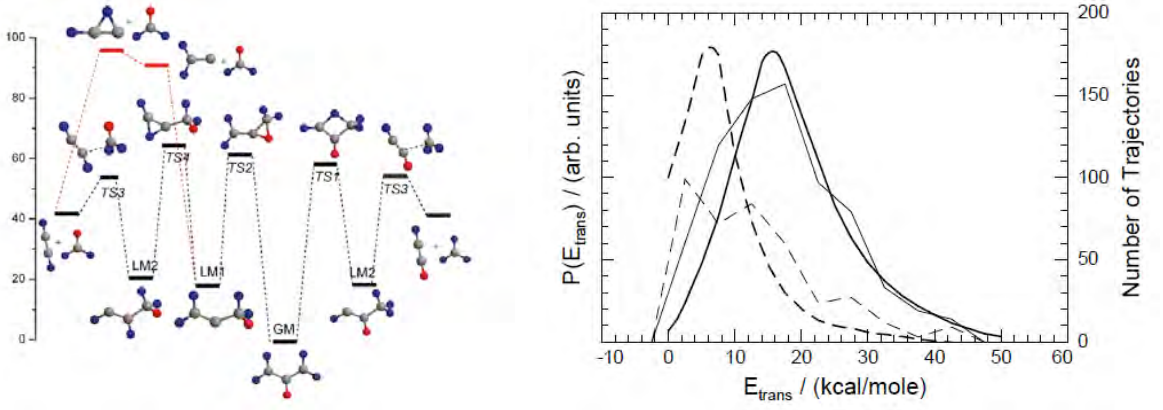

Another pathway, leading to C_2H_2+CH_3 presented a puzzling translational energy distribution upon deuteration [D. Stranges, *et al*. J. Chem. Phys. **128**, 151101 (2008)]. These products can be formed by two pathways, both of which, in the conventional picture, visit LM2 before dissociating to the products. Thus, the translational energy distributions were expected to be equal, at odds with experiment. We were able to explain this by running many thousands of quasiclassical trajectories on the global PES, and observing some dissociation directly from LM1 to vinylidene + CH_3. These

trajectories, as expected, result in a slow translational energy distribution. Thus, this surprising pathway was able to rationalize the experimental result.

Electronic Quenching of OH* by H_2

We continue to work on this quenching process, stimulated by experiments of the Lester group and the Davis group. We developed global PESs for the ground electronic state and electronically excited states by fitting roughly 20 000 MRCI/aug-cc-pVTZ energies. Thousands of trajectories were initiated in the vicinity of thirteen conical intersections identified previously by Hoffman and Yarkony. This simple approach bypasses the need to do surface-hopping calculations, and gives what we terms "post quenching" dynamical predictions of the reactive to non-reactive branching and final state distributions of the products. A summary of some of the results are these calculations is given below, where the final ro-vibrational distribution of the OH product is shown as well as the distribution of bending overtone states of the reactive H_2O product. The former results are in very good agreement with the experiments of Lester and co-workers and the latter results are a prediction, which hopefully will stimulate new experiments. These results do indicate a large degree of internal excitation of H_2O (and largely in the bending mode) and are certainly consistent with a slow translational energy distribution of the $H+H_2O$ products, which has been measured experimentally.

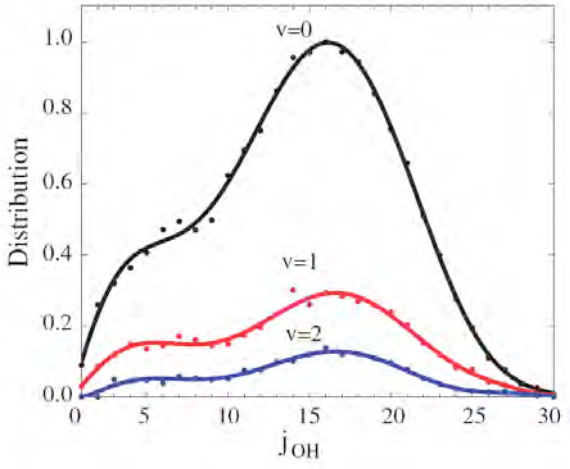

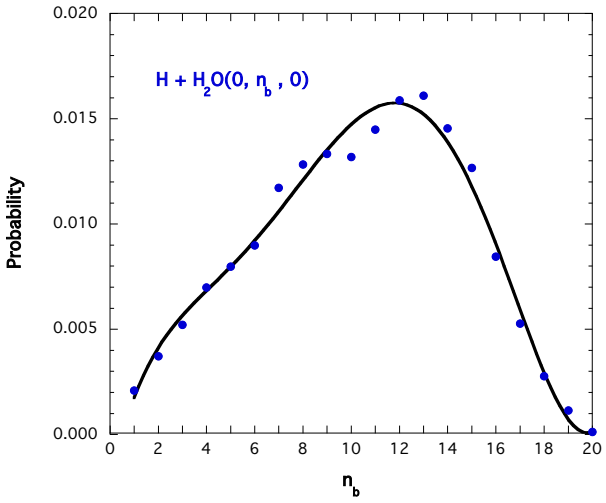

F+CD_3H reaction

We developed a full-dimensional, *ab initio*-based PES for the $F+CH_4$ reaction, based on fitting roughly 20 000 highly accurate electronic energies. This PES is the most accurate one currently available and has been used by us in dynamics calculations of HF final state distributions, which agree well with experimental results of Nesbitt and co-workers. More recently, we reported a study of interesting and surprising mode-specific effects in the $F+CD_3H(v_{CH} = 0,1)$ reaction. This was motivated by crossed molecular beam experiments, reporting these effects, by Liu and co-workers. Specifically excitation of this mode did not lead to enhancement of H-atom transfer, but instead to the D-atom transfer. This surprising result appears to be attributable to the steering effect of the entrance channel van der Waals well. However, this result, while

probably qualitatively correct really does need to be verified by quantum calculations because there is substantial evidence to suppose that the well support resonances that cannot be described by trajectory calculations. Such calculations are extremely demanding; however, they will be attempted by others (see below).

Future Plans

(1) We have made good progress on the study of multi-electronic state dynamics calculations of the H_2CO photodissociation that will explicitly consider the spin-orbit coupling and expect to have results to report shortly. (2) We continue to work on the reactions of CH_4 with F and Cl using global PESs. This work is motivated primarily by recent product-correlated measurements in crossed molecular beam experiments of Kopin Liu at IAMS. We are collaborating with Dong Hui Zhang and Dunyou Wang who are doing quantum wavepacket calculations, which are needed to explore the possible resonances in these reactions. (3) We have begun quasiclassical trajectory calculations of energy transfer in fast H-atom collisions with C_2H_2, using our global *ab initio* PES for C_2H_3, in collaboration with Jonathan Smith at Temple University. (4) We are collaborating with Don Truhlar to fit diabatic potentials and couplings for the 3-state OH^*+H_2 quenching.

PUBLICATIONS SUPPORTED BY THE DOE (2009-present)

1. Three Reaction Pathways in the H+HCO → H_2+CO reaction, K. M. Christoffel and J. M. Bowman, Three reaction pathways in the H + HCO → H_2 + CO reaction, K. Christoffel and J. M. Bowman, Phys. Chem. A, **113**, 4138 (2009).
2. Accurate ab initio potential energy surface, dynamics, and thermochemistry of the F + CH_4 → HF + CH_3 reaction, G. Czakó, B. C. Shepler, B. J. Braams, and J. M. Bowman, J. Chem. Phys. **130** 084301 (2009).
3. Quasiclassical Trajectory Calculations of the HO_2+NO Reaction on a Global Potential Surface, C. Chen, B. C. Shepler, B. J. Braams and J. M. Bowman, Phys. Chem. Chem. Phys. **11**, 4722 (2009).
4. Production of vibrationally excited H_2O from charge exchange of H_3O^+ with cesium, J. E. Mann, Z. Xie, J. D. Savee, J. M. Bowman, and R. Continetti, J. Chem. Phys. **130**, 041102 (2009).
5. Full-dimensional *ab initio* potential energy surface and vibrational configuration interaction calculations for vinyl. A. R. Sharma, B. J. Braams, S. Carter, B. C. Shepler, and J. M. Bowman, J. Chem. Phys. **130**, 174301 (2009).
6. CH stretching excitation steers the F atom to the CD bond in the F + CHD_3 reaction, G. Czakó and J. M. Bowman, J. Am. Chem. Soc. **131**, 17534 (2009).
7. Roaming dynamics in formaldehyde-d2 dissociation, V. Goncharov, S. A. Lahankar, J. D. Farnum, J. M. Bowman, and A. G. Suits, J. Phys. Chem. A **113** (52), 15315 (2009).
8. Permutationally invariant potential energy surfaces in high dimensionality, B. J. Braams and J. M. Bowman, Int. Rev. Phys. Chem. **28**, 577 (2009).
9. Permutationally invariant polynomial basis for molecular energy surface fitting via monomial symmetrization, Z. Xie and J. M. Bowman, J. Chem. Theo Comp. **6** (1), 26 (2010).
10. Seven-degree-of-freedom, quantum scattering dynamics study of the H_2D^++H_2 reaction, D. Y. Wang, Z. Xie, and J. M. Bowman, J. Chem. Phys. **132** (8) (2010).

11. Communications: Classical trajectory study of the postquenching dynamics of OH A $^2\Sigma^+$ by H_2 initiated at conical intersections, E. Kamarchik, B. N. Fu, and J. M. Bowman, J. Chem. Phys. **132** (9) (2010).
12. *Ab Initio*-Based Potential Energy Surfaces for Complex Molecules and Molecular Complexes, J. M. Bowman, B. J. Braams, S. Carter, C. Chen, G. Czakó, B. Fu, X. Huang, E. Kamarchik, A. R. Sharma, B. C. Shepler, Y. Wang, and Z. Xie, J. Phys. Chem. Lett. **1**, 1866 (2010).
13. Evidence for Vinylidene Production in the Photodissociation of the Allyl Radical, C. Chen, B. Braams, D. Y. Lee, J. M. Bowman, P. L. Houston, and D. Stranges, J. Phys. Chem. Lett. **1**, 1875 (2010).
14. Depression of reactivity by the collision energy in the single barrier H + $CD_4 \rightarrow$ HD + CD_3 reaction, W. Q. Zhang, Y. Zhou, G. R. Wu, Y. P. Lu, H. L. Pan, B. N. Fu, Q. A. Shuai, L. Liu, S. Liu, L. L. Zhang, B. Jiang, D. X. Dai, S. Y. Lee, Z. Xie, B. J. Braams, J. M. Bowman, M. A. Collins, D. H. Zhang, and X. M. Yang, PNAS **107**, 12782 (2010).
15. Roaming Pathway Leading to Unexpected Water + Vinyl Products in C_2H_4OH Dissociation, E. Kamarchik, L. Koziol, H. Reisler, J. M. Bowman, and A. I. Krylov, J. Phys. Chem. Lett. **1**, 3058-3065 (2010).
16. Collisional quenching of OD $A^2\Sigma^+$ by H_2: Experimental and theoretical studies of the state-resolved OD $X^2\Pi$ product distribution and branching fraction, J. H. Lehman, L. P. Dempsey, M. I. Lester, B. Fu, E. Kamarchik, and J. M. Bowman, J. Chem. Phys. **133**, 164307 (2010).
17. Quasiclassical trajectory study of the postquenching dynamics of $OH(A)^2\Sigma^+$ by H_2/D_2 on a global potential energy surface, B. Fu, E. Kamarchik, and J. M. Bowman J. Chem. Phys. **133**, 164306 (2010).
18. Roaming Radicals, J. M. Bowman and B. C. Shepler, Annu. Rev. Phys. Chem. **62**, 531 (2011).
19. High-dimensional *ab initio* potential energy surfaces for reaction dynamics calculations, J. M. Bowman, G. Czakó, and B. Fu, Phys. Chem. Chem. Phys. **Advance Article** (2011). DOI: 10.1039/C0CP02722G.
20. An *ab initio* spin-orbit-corrected potential energy surface and dynamics for the F + CH_4 and F + CHD_3 reactions, G. Czakó and J. M. Bowman, Phys. Chem. Chem. Phys. **Advance Article** (2011). DOI: 10.1039/C0CP02456B.
21. The Dynamics of Allyl Radical Dissociation, C. Chen, B. Braams, D. Y. Lee, J. M. Bowman, P. L. Houston, and D. Stranges, J. Phys. Chem. A Article ASAP **DOI:** 10.1021/jp109344g
22. Are Roaming and Conventional Saddle Points for H_2CO and CH_3CHO Dissociation to Molecular Products Isolated from Each Other? B. C. Shepler, Y. Han, and J. M. Bowman, J. Phys. Chem. Lett. **2**, 834 (2011).

COMBUSTION CHEMISTRY

Principal Investigator: Nancy J. Brown
Environmental Energy Technologies Division
Lawrence Berkeley National Laboratory
Berkeley, California, 94720
510-486-4241
NJBrown@lbl.gov

PROJECT SCOPE

Combustion processes are governed by chemical kinetics, energy transfer, transport, fluid mechanics, and their complex interactions. Understanding the fundamental chemical processes offers the possibility of optimizing combustion processes. The objective of our research is to address fundamental issues of chemical reactivity and molecular transport in combustion systems. Our long-term research objective is to contribute to the development of reliable combustion models that can be used to understand and characterize the formation and destruction of combustion-generated pollutants. We emphasize studying chemistry at both the microscopic and macroscopic levels. Our current work is concerned with improving the calculation of transport properties for combustion modeling.

RECENT PROGRESS

Current Research

We have shown that a Lennard-Jones 12-6 (LJ) potential is adequate for the calculation of viscosity of simple molecules considered as pure species and binary mixtures. Viscosity measurements of a single chemical species allow direct estimation of the parameters that describe the interaction between two molecules of the same species, ε_{ii} and σ_{ii}, the conventional energy and length scaling parameters associated with the L-J potential. We found that many different ($\varepsilon_{ii,}$ σ_{ii}) pairs can yield predicted viscosities that agree with experimental values with less than 1% error over a wide range of temperatures. The potential parameters must be corrected according to the approach in TRANLIB if one or both molecules are polar, and this is especially important for radical species.

In order to explore the consequences of this finding which suggests a significant insensitivity of transport to the intermolecular surface, we conducted sensitivity studies of the deflection function, cross section and collision integrals to the intermolecular potential. The sensitivity analysis was accomplished using the “brute force” approach where a localized perturbation in the form of a narrow Gaussian was added to the potential and the calculation was re-run to evaluate the change in the deflection angle under the perturbation. Normalized sensitivities of different powers (l= 1-3) of the cosine of the deflection angle (X), were calculated as a function of reduced energy for different values of reduced impact parameter and energy. Powers of the cosine are selected because these are used in the calculation of the cross sections for different transport properties (l=1 for diffusion and l=2 for viscosity and thermal conductivity).

Sensitivity magnitudes were large near the distance of closest approach. Figure 1 is plot of the normalized maximum sensitivity of $\cos^2$ (X) to the potential as a function of the square of the reduced impact parameter, B*, and reduced energy, G*. The magnitude of the maximum (and minimum) sensitivities is order unity and greater. Sensitivities are

largest at moderate values of B*and small values of G* and they are also significant at lower values of B* (B*<2) and moderate values of G* (G*<8). The trough noted for B* ~ 1 occurs because all trajectories with B*=1 have the same distance of closest approach, and the magnitude of the sensitivities is large there. If the distance of closest approach is less than 1.0 and is decreasing, the magnitude of the sensitivities decreases. Under these conditions, the energy is increasing, the repulsive portion of the potential is most influential, and the corresponding sensitivities are unremarkable.

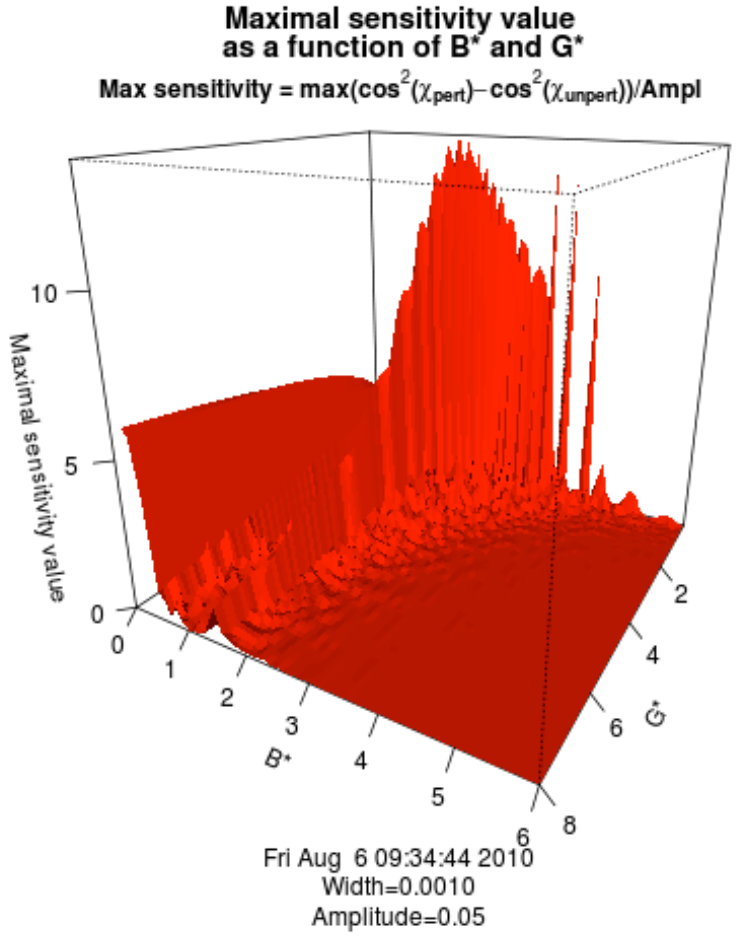

The calculation of transport coefficients requires that two integrals be performed: the first is the evaluation of the cross section, which is an integral over the impact parameter weighted by it; and the second is the evaluation of the collision integral, which is an integral of the cross section over the energy weighted by appropriate powers of a Boltzmann distribution. Figure 2 is a plot of the normalized sensitivity of the collision integral for viscosity with respect to the potential energy (in blue) as a function of reduced distance, r*, for a reduced temperature, T*=8.0. Also shown in the figure is a plot of the LJ potential in red. Most of the sensitivity is in the purely repulsive portion of

the potential, where r*<1.0. The result of the two integrations is to reduce the sensitivity extrema by two orders of magnitude. The shift of the sensitivity into the purely repulsive region occurs as the value of T* increases. Substantial sensitivity structure is found at r*>1 for lower values of T*. In general, there is a decline in sensitivity magnitudes as we progress from the deflection angle to the cross section to the collision angle.

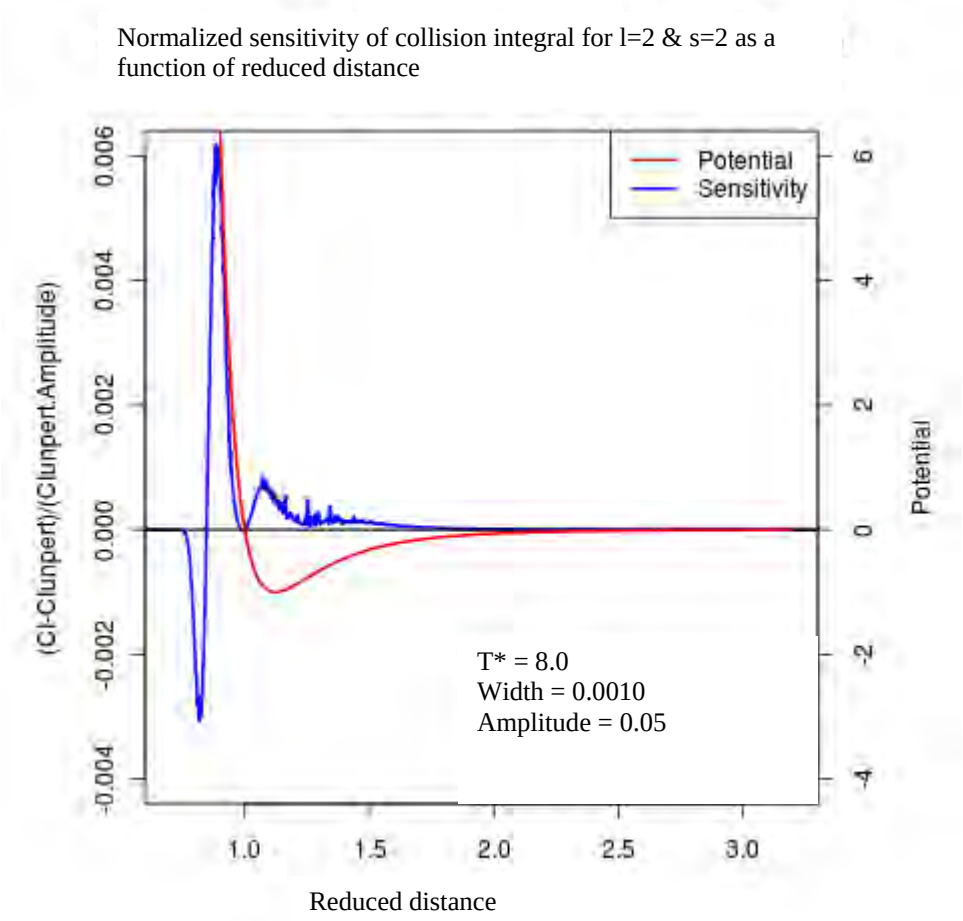

Since combustion occurs at larger values of T*, transport coefficient at those temperatures tend to be very insensitive to the intermolecular potential and mostly to the repulsive portion. Transport coefficients at the higher values of T* are not good candidates for potential inversion studies.

We initiated a study of thermal diffusion, the Soret effect. Thermal diffusion is a second order transport property, and as such, it depends on the nature of the molecular collisions, whereas first order properties depend primarily on the mere occurrence of collisions and only secondarily on the details of the collisions. Thermal diffusion is the relative motion of the components of a mixture arising from a temperature gradient. The resulting composition gradients in the mixture lead to ordinary diffusion, which tends to eliminate gradients. A steady state is reached when the separating effect of thermal diffusions is balanced by the remaining effects of ordinary diffusion, and the components of a mixture will be partially separated. The heavier component is usually concentrated in the colder region, and when this occurs, the thermal diffusion coefficient is positive.

We are reviewing the literature associated with thermal diffusion with the goal of improving the calculation of thermal diffusion factors for light species for combustion modeling. We will calculate the sensitivity of thermal diffusion coefficients to the intermolecular potential to determine how much knowledge of the potential is required to obtain reliable values.

We continue to assemble a set of supporting data for flame studies of H_2/air and CH_4/air flames using a variety of techniques: ab initio calculations, correlations, and literature searches, and are examining the reliability of thermal diffusion calculations. We will use the new transport data in flame modeling studies with Bell and Cheng.

Publications supported by DOE for last two years:

Ling Jin, Nancy Brown, Robert A. Harley, Jian-Wen Bao, Sarah Michelson, James M. Wilzak, Seasonal versus Episodic Performance Evaluation for an Eulerian Photochemical Model, Journal Geophysical Research Atmospheres 115 DO9302,doi:10.1029/2009JDO12680, 2010

Bastien, L.A.J., Price, P.N. and Brown, N.J. "Intermolecular Potential Parameters and Combining Rules Determined from Viscosity Data," International Journal of Chemical Kinetics 42, DOI 10.1002/kin.20521, pp 713-723 (2010).

Brown, N.J., Bastien, L.A.J., and Price, P.N. "Transport Properties for Combustion Modeling." Progress in Energy and Combustion Science doi.org/10.1016/j.pecs.2010.12.001 (2010) .

Jin, L., Harley, R.A., Brown, N.J.,, "Meteorology-induced Variations in the Spatial Behavior of Summer Ozone Pollution in Central California" submitted to Atmospheric Environment (2010)

Sharon M. Shearer, S.M., Harley, R.A., Jin L., and Brown, N.J., "Evaluation of the Condensed SAPRC07 Chemical Mechanism: Predictions of Photochemical Air Pollution in Central California," submitted to Atmospheric Environment, 2010

Dynamics of Product Branching in Elementary Combustion Reactions

Laurie J. Butler
The University of Chicago, The James Franck Institute
5640 South Ellis Avenue, Chicago, IL 60637
L-Butler@uchicago.edu

I. Program Scope

The elementary reactions that determine the performance of a combustion system range from direct H-atom abstraction reactions to complex reactions involving competing addition/elimination mechanisms. While the total rate constant for many elementary reactions is well-characterized, understanding the product branching in complex reactions presents a formidable challenge. To study such reactions, our experiments directly probe the dynamics of the product channels that arise from long-lived radical intermediates along the bimolecular reaction coordinates. The work uses the methodology developed in my group in the last ten years, using both imaging and scattering apparatuses. The experiments generate a particular isomeric form of an unstable radical intermediate along a bimolecular reaction coordinate and investigate the branching between the ensuing product channels of the energized radical as a function of its internal energy under collision-less conditions.

The experiments[1-5] use a combination of: 1) measurement of product velocity and angular distributions in a crossed laser-molecular beam apparatus, with electron bombardment detection in my lab and with tunable vacuum ultraviolet photoionization detection at Taiwan's National Synchrotron Radiation Research Center (NSRRC), and 2) velocity map imaging using state-selective REMPI ionization and single photon VUV ionization of radical intermediates and reaction products. Our publications this year[3-5] include a computational investigation of the product branching in the O + allyl reaction[4] (to complement our prior experimental results[2]), a study[3] to refine our model for partitioning of internal energy between vibration and rotation in radicals produced photolytically, but upon excitation to a predissociative excited state rather than a directly repulsive one, and a comprehensive study[5] of the product branching from the addition mechanism for the OH + ethene reaction, starting from the 2-hydroxyethyl radical. Our results develop insight on product channel branching in reactions that proceed via an addition/ elimination mechanism and provide a key benchmark for theoretical predictions of polyatomic reactions that proceed through unstable radical intermediates.

II. Recent Progress and Ongoing Work

A. Minima and Transition States on the C_3H_5O Potential Energy Surface: O + Allyl

Our prior experimental work (J. Chem. Phys. 129, 084301 (2008) and Ref 2 below) on the O + allyl reaction included imaging and scattering experiments in our lab at Chicago and extensive scattering experiments at the NSRRC in Taiwan in collaboration with J. J. Lin on the product channels accessed from the radical intermediate formed when the O atom adds to a terminal C atom. To measure the branching between product channels accessed from this intermediate, our experiments corrected the relative signal levels by calibrating, in separate experiments, the photoionization cross sections of some of the radical and molecular products with respect to Cl atoms, ethene and vinyl. Measuring the relative signal levels from H_2CO and vinyl produced in a 1:1 ratio allowed us to use Taatjes' photoionization cross section for vinyl to derive a photoionization cross section for formaldehyde. This turned out to be essential for analyzing the branching to the $H_2CO + CH_3$ channel in the OH + ethene system we studied this year (described in Section C below). Likewise, we used the integrated signals

from the ethene + HCO product channel in conjunction with the literature photoionization cross section of ethene to determine the absolute photoionization cross section of HCO radicals from 9 to 11.3 eV. Our determination agrees with the HCO photoionization cross section at 10.3 eV measured by Steve Pratt (J. Phys. Chem A. 114, 11238 (2010).

This year, my former Ph.D. student Benj FitzPatrick published[4] CCSD(T) calculations on the relevant radical intermediates and transition states on the path to the energetically allowed product channels in the O + allyl reaction on the global C_3H_5O potential energy surface. The energetics calculated include those for twenty-three minima, twenty-nine product channels, and all the transition states between them, so also offer insight into other reactions on the C_3H_5O potential energy surface, including OH + allene reaction. He used coupled-cluster theory and a modest basis set, aug-cc-pVDZ, to calculate both structures and harmonic vibrational frequencies of local minima and transition states. Accurate energies were computed using explicitly correlated coupled-cluster methods and a large basis set, cc-pVQZ-F12, to approach the one-particle basis set limit. He used his calculated transition states in conjunction with statistical transition-state theory results to show that energetically small barriers connect many of the alkenol and epoxide intermediates to the straight-chain alkoxy isomers, leading to significant branching to these alkoxy radical intermediates. Facile isomerization to these alkoxy intermediates is significant because the barrier heights leading to H + acrolein and HCO + C_2H_4 product channels are energetically accessible even at low vibrational energies. The low dissociation barrier heights and loose transition states of these pathways result in unimolecular dissociation as opposed to isomerization to a different C_3H_5O intermediate, in agreement with the prior experimental results.

This system serves as a key benchmark to theoretical studies designed to predict product branching in combustion systems. The O + allyl elementary reaction includes two key dynamical features that control the product branching in reactions of radicals with unsaturated hydrocarbon species. First, the initial radical adduct in the addition/elimination channel has direct bond fission channels that compete with isomerization of the radical intermediate via an H atom transfer. This makes the product branching sensitive to quantum tunneling. Second, the intermediate isomerization pathway may not be dynamically separated from the simple bond fission dynamics to H + acrolein; this renders some of the assumptions made in predicting product branching with statistical theories invalid.

B. Modeling the Partitioning of Internal Energy to Vibration vs. Rotation in Radicals Produced Photolytically

Our prior work[2] characterized the internal energy distribution of the nascent CH_2CH_2OH radicals produced in the 193 nm photodissociation of 2-bromoethanol. To model the partitioning of this energy between rotation and vibration, the paper used the measured recoil kinetic energy distribution and the conservation of angular momentum to model the rotational energy imparted to the radicals. Instead of estimating the mean rotational energy with an impulsive model from the equilibrium geometry of 2-bromoethanol, our model explicitly includes weighting over geometries across the quantum wavefunction with zero, one, and two quanta in the harmonic mode that most strongly alters the exit impact parameter. The model gives a nearly perfect prediction of the measured velocity distribution of stable radicals near the dissociation onset using a G4 prediction of the C-Br bond energy and the dissociation barrier for the OH + ethene channel calculated by Senosiain et al., J. Phys. Chem. A 110, 6960 (2006).

In our publication this year,[3] we assess our new model for its predictive ability when the excited state reached in the photodissociation of the radical precursor is not repulsive in the Franck-Condon region. The results on acetyl chloride dissociation show that, as expected, if

the molecule moves outside the Franck-Condon region before experiencing a repulsive force in the C-halogen bond, this alters the predicted partitioning to rotational energy. With the help of trajectory calculations by our co-author W. Fang, we were able identify the region of the S_1 excited state of acetyl chloride in which the repulsive force acts; using this geometry in conjunction with our model gave a good representation of the spectrum of stable acetyl radicals measured experimentally.

C. Product Channel Branching in the OH + Ethene Reaction

Our most substantial work this year, Publication 5 below, presents the first definitive measurements of product branching to all energetically allowed channels from the CH_2CH_2OH radical intermediate of the OH + ethene reaction. The total rate constant OH + ethene reaction has been very well characterized and it has been long understood that H atom abstraction competes with an addition mechanism in this reaction (some of the best work was published by Frank Tully in Chem. Phys. Lett. 96, 14 (1983) and 143, 510 (1988)). In contrast, studies of the product branching from the vibrationally excited radical intermediate formed in the addition mechanism are incomplete at best. Using tunable VUV photoionization in the scattering apparatus at the NSRRC, we detected the products from radicals with the vibrational energy distribution characterized in Fig. 1, right. The data shows the radicals dissociate to three major product channels, H + ethenol (2.6%), CH_3 + formaldehyde (6.3%), vinyl + H_2O (14.5%) as well as to the OH + ethene reactant asymptote (76.5%). The H + acetaldehyde channel contributes less than 1%. Deriving the product branching fractions from the measured relative signals in our scattering experiments rely on accurate measurements of the relative photoionization cross sections of formaldehyde, vinyl, and ethene averaged over the NSRRC bandwidth, as described in Ref. 2 (using Taatjes' absolute vinyl cross section we can also get an absolute cross section for H_2CO from this data), as well as the photoionization cross section of ethenol, determined by Cool et al (J. Chem. Phys. 119, 8356 (2003); accurate to about 25%). The most surprising result is the substantial branching to the H_2O + vinyl channel. The vinyl signal fit in green shown in Fig. 1 (left) evidence the forward/backward symmetric scattering expected for the dissociation of a rotationally and vibrationally CH_2CH_2OH radical. That channel is expected if one begins from the OH + ethene reactants (it is the direct H-atom abstraction channel), but our experiments begin with

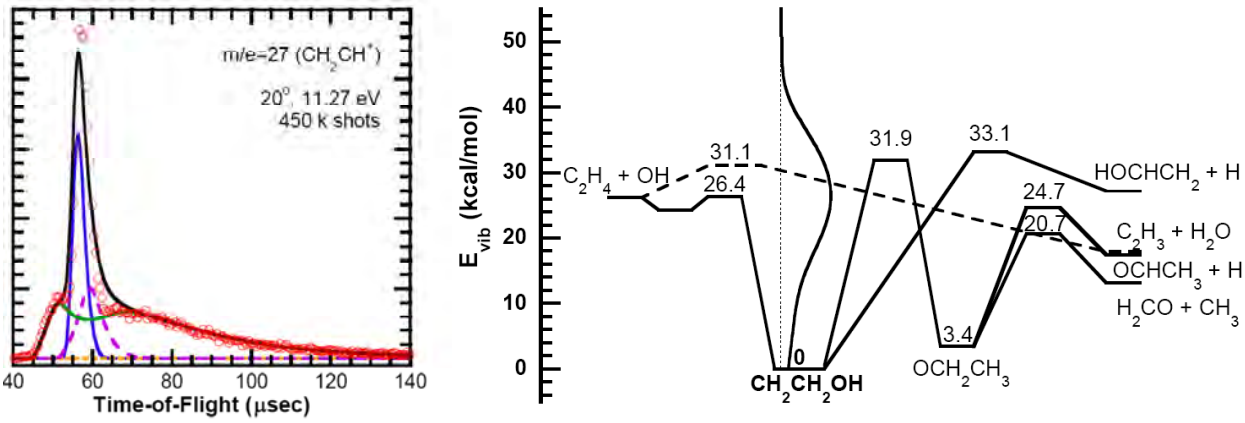

(PES from Senosiain et al., J. Phys. Chem. A 110, 6960 (2006)
Fig. 1. Products from the CH_2CH_2OH radical intermediate of OH + ethene

the CH_2CH_2OH radical intermediate. I asked J. Bowman whether the radical might begin to dissociate to the OH + ethene reactant asymptote but return to instead abstract an H atom. Indeed, he had, before my inquiry, identified such trajectories (subsequently reported in J. Phys. Chem. Lett. 1, 3058 (2010)) on the global potential energy surface calculated with A.

Krylov. To assess the importance of tunneling in this unexpected reaction, we are currently investigating the product channels from the CD_2CD_2OH radical intermediate (H. Reisler alerted us to the commercial availability of the photolytic precursor to this deuterated radical; she recently reported the velocity distributions of the D atom products from the CD_2CD_2OH radical intermediate).

III. Ongoing Work

We are currently analyzing the data on the product channels from the CD_2CD_2OH radical intermediate that we took in February, 2011 at the NSRRC as well as imaging and scattering data we took last summer in my lab at Chicago. Our synthetic collaborator Fran Blase has also taught us the synthesis of a great photolytic precursor to the CH_2CH_2CHO radical, the key radical intermediate on the O + allyl potential energy surface leading to the C_2H_4 + HCO product channel, so we plan work on this system in the coming year. Finally, we have initiated the study of a radical intermediate in the OH + propene reaction, beginning with imaging experiments to characterize the nascent radicals produced from the 193 nm photodissociation of a brominated photolytic precursor.

IV. Publications Acknowledging DE-FG02-92ER14305 (2009 or later)

1. Modeling the Rovibrationally Excited C_2H_4OH Radicals from the Photodissociation of 2-Bromoethanol at 193 nm, B. J. Ratliff, C. C. Womack, X. N. Tang, W. M. Landau, L. J. Butler, and D. E. Szpunar, J. Phys. Chem. A 114, 4934-4945 (2010).
2. Primary Photodissociation Pathways of Epichlorohydrin and Analysis of the C-C Bond Fission Channels from an $O(^3P)$ + Allyl Radical Intermediate, B. L. FitzPatrick, B. W. Alligood, L. J. Butler, S. -H. Lee, and J. J. Lin, J. Chem. Phys. 133, 094306 (2010).
3. Assessing an Impulsive Model for Rotational Energy Partitioning to Acetyl Radicals from the Photodissociation of Acetyl Chloride at 235 nm, C. C. Womack, W. H. Fang, D. B. Straus, and L. J. Butler, J. Phys. Chem. A 114, 13005-10 (2010).
4. Theoretical Study of Isomerization and Dissociation Transition States of C_3H_5O Radical Isomers: Ab Initio Characterization of the Critical Points and Statistical Transition-State Theory Modeling of the Dynamics, B. L. FitzPatrick, J. Phys. Chem. A 115, 1701 (2011). (Work completed as a Ph.D. student with L. J. Butler.)
5. Product Branching from the CH_2CH_2OH Radical Intermediate of the OH + Ethene Reaction, B. J. Ratliff, B. W. Alligood, L. J. Butler, S. –H. Lee, and J. J. Lin, submitted to J. Phys. Chem. A (2011).

Collision Dynamics Studied in Crossed Molecular Beams: Excited Electronic States.

David W. Chandler
Combustion Research Facility
Sandia National Laboratory
Livermore, CA 94551-0969
Email:chand@sandia.gov

Program Scope:

My research focuses on the chemical dynamics of gas phase molecular species. Chemical dynamics is the detailed study of the motion of molecules and atoms on potential energy surfaces in order to learn about the details of the surface as well as the dynamics of their interactions. We have begun study of the collision dynamics of electronically excited state molecules. We excite a molecule at the crossing of the molecular beams (or atomic beams) in order to create an electronically excited state molecule in a particular ro-vibrational state. Within the radiative lifetime (200 ns for NO(A)) the molecule undergoes elastic, rotationally or vibrationally inelastic, or electronically nonadiabatic collisions producing new quantum states of the molecule. Quantum-state-selective ionization of the product molecules and projection of those ions onto an imaging detector allow us to observe, for the first time, differential cross sections and alignment moments for electronically excited state species. In another set of experiments a new concept for Fourier transform spectroscopy was explored and the first experiments have been performed.

Progress Report:
Scattering of Electronically Excited State Molecules.

Measurements of differential cross sections have been generally restricted to ground state molecules or long lived metastable states that can be entrained into a molecular beam source. Here we report on the measurement of inelastic scattering differential cross sections for electronically excited states with very short lifetimes for the first time. By exciting a molecule into an electronically excited state while it is at the crossing point of a second atomic or molecular beam, scattering of the electronically excited state molecules can be studied if the lifetime of the electronic state is sufficiently long. The NO(A) state has a lifetime of 200 ns and we generated it with near-UV light around 226 nm at the crossing of a 5%NO/He beam and a neat beam of Ar atoms. A 400 ns delay between the initial excitation and subsequent state-selective REMPI of the NO(A) state molecules provides sufficient time to allow for collisions in the crossed molecular / atomic beams. In this amount of time 90% of the NO(A) state has decayed back to the ground state and of those molecules remaining in the excited state approximately 1% have had a collision. Those collisions have caused rotational energy transfer to ~20 possible quantum states.

The excitation and detection scheme is shown in Figure 1. After a 400 ns delay the NO(A, j=>0) molecules are selectively ionizing the by (1 + 1) REMPI through the NO(E) state at ~620 nm and those ions are velocity-mapped Ion Imaged. Rotational state-selective imaging of the inelastic collisions allows us to determine the state-specific differential cross sections. In Fig 2 are images of NO(A, J=2,7,14) from such an experiment where one beam containing 5%NO in He intersects a beam containing Ar. This detection scheme is highlighted in Figure 1.

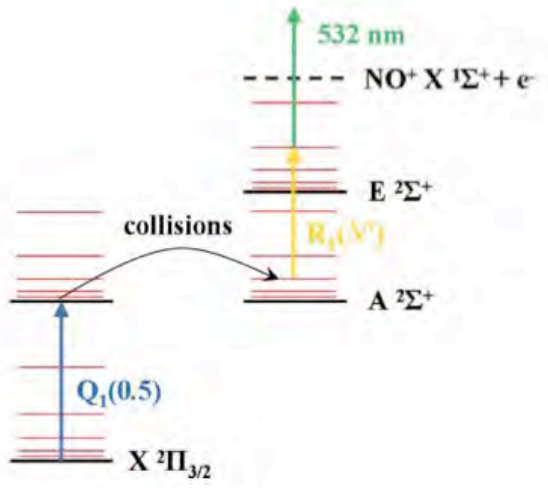

Figure 1: Schematic of detection scheme for measuring quantum state selected differential cross sections for electronically excited state NO.

A major advantage of measuring the scattering of the NO(A) excited state is the reduction of background in the forward-scattering region. Because there are no electronically excited states in the original molecular beams the only way for a molecule to populate a high J state of the beam is by collision. This allows one, in principle, to measure the entire scattering sphere. This ability to measure the entire scattering sphere is seen in the data of Figure 2 and Figure 3.
These truly are background free experiments except at the very front portion of the images where non-resonant ionization of the NO(j=0) is seen as a spot in the images sitting off of the scattering sphere. Because of this we can measure the entire forward scattering differential cross section with no interference and are able to see structure, as predicted, in the Fraunhofer scattering.

This advantage of reduced background can be applied to the study of the collision-induced rotational alignment of the NO(A) molecules as well. By changing the polarization of the light that does the resonant ionization step of the detection one is sensitive to the alignment of the NO molecules after the collision. In Fig 3 are images of NO(A, J=4,9) from such an experiment where one beam containing 5%NO in Ar intersects a beam containing Ne. The experimental images on the left side of the figure were generated by combining two images acquired with different polarizations of the 620-nm light. The images show structure as a function of scattering angle because the NO(A, j= 4, 9) molecules are aligned by the collision in an angle-dependent manner. (Note that our scheme allows us to align the NO(A) molecule before the collision as well!) This rotational alignment can be modeled according to various theoretical approaches. As demonstrated by the middle and right column images of Fig. 3, the classical model recovers the basic trends but misses the interesting oscillations in the direction of the alignment that the 'exact' quantum mechanical model correctly predicts. There are significant non-classical features in the forward scattering that we can investigate experimentally due to our ability to reduce the background in this very interesting region. This work is being done in collaboration with the groups of Ken McKendrick and Matt Costen (Harriott-Watt Univeristy), as well as the groups of B. Friedrich (Fritz-Haber Institute) and Millard Alexander (University of Maryland.)

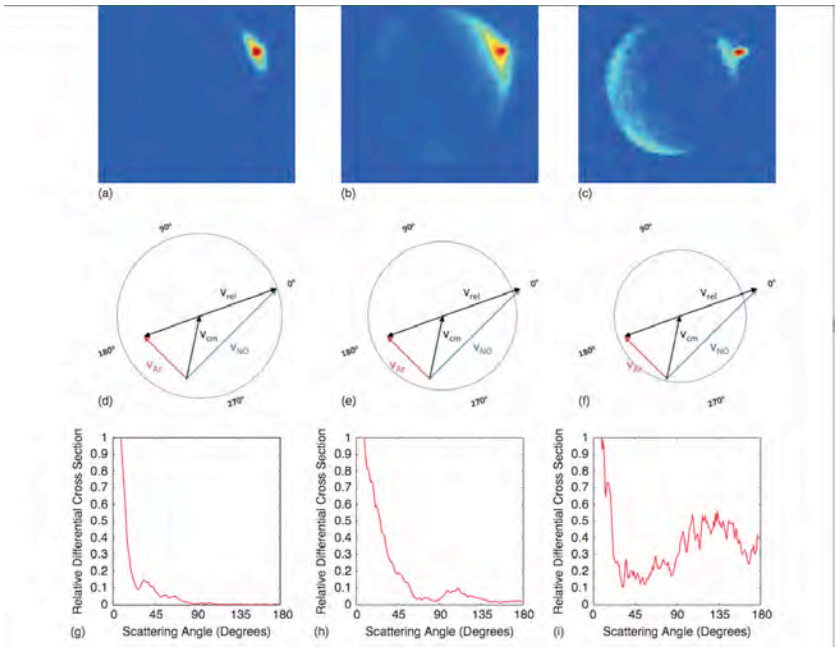

Figure 2: Experimental images (a-c), Newton Diagrams (d-f), and cross sections (g-i) for rotationally inelastic collisions between NO(A) molecules and argon atoms. (a), (d), (g):N=0➔N'=2; (b), (e), (h): N=0➔N'=7;(c), (f), (i):N=0➔N'=14.

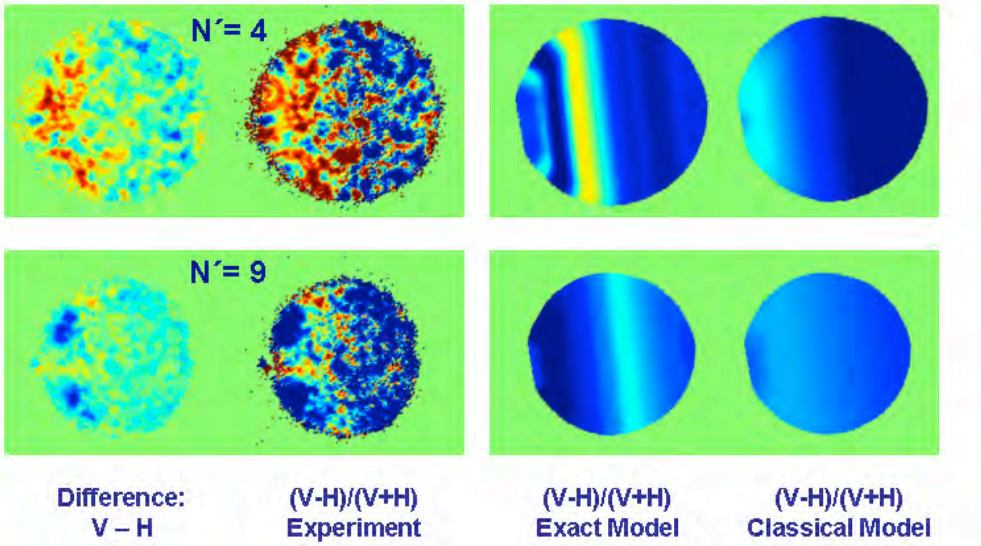

Figure 3: Collisional alignment measurements and theory for NO(A)(j=0) + Ne → NO(A)(j=4,9) + Ne where detection is via 1 + 1 REMPI through the E state of NO.

In figure 3 are shown measured alignment data and corresponding theory. The experimental image on the far left is generated by subtracting an image acquired with vertically-polarized E←A light from an image acquired with horizontally polarized light. Dividing the difference image by the summation of the two to essentially normalize out the differential cross-section and instrument function generates the image at the middle left. Images generated by theoretical models are shown to the right: the 'Exact' model is a quantum scattering calculation on an *ab initio* potential energy surface, and the classical model is based on conservation of angular

momentum for hard-shell collisions. The predominance of a negative value in the images implies the generation of more molecules in an alignment that is sensitive to horizontal light than vertical for our experimental geometry. The sharp oscillations in the sign for the quantum model is obviously a non-classical feature that is evident in the experimental result.

Proposed Work:

Over the next funding period we plan on finishing the analysis of the data our study of inelastic energy transfer in electronically excited state molecules. We are beginning a new set of experiments to measure the entire collisional energy transfer function, P(E,E'), of a very vibrationally excited molecule. We will accomplish this by excitation of a molecule just below its dissociation energy followed by collision induced dissociation and velocity map imaging of the collision product fragments. NO_2 is the first molecule we will study. This study will provide both a direct measure of the entire P(E, E') excitation curve of a dissociating molecule and provide information on a process that is the microscopic reverse of a three body recombination process.

Publications 2009-2011:

1) Direct Angle Resolved Measurements of collision dynamics with electronically excited state molecules :NO(A2S+)+Ar, Kay J.J., Paterson G., Costgen M.L., Strecker K.E., McKendrick K.G., Chandler D.W., J Chem Phys 134,091101 (2011)
2) Cold and Ultracold molecules: Spotlight on Orbiting Resonances, Chandler DW, J Chem. Phys. Vol.132 110901 (2010).
3) Cold atoms by kinematic cooling, Kay, JJ; Klos, J; Alexander, MH, Strecker KE, Chandler DW, Phys. Rev. A A Vol.82(3) 032709 (2010)
4) Differential Cross Sections for Rotational Excitation of ND3 by Ne, Kay JJ, van de Meerakker SYT, Wade EA, Chandler DW et al., J. Phys. Chem. A Vol. 113 (52) 14800-14806 (2009).
5) A compact molecular beam machine, Jansen P, Chandler DW, Strecker KE, Rev. Sci. Instru. Vol. 80 (8) Article Number: 083105 (2009).
6) Production of cold ND3 by kinematic cooling, Kay JJ, van de Meerakker SYT, Strecker KE, Chandler DW et al., Faraday Disc. Vol. 142, 143-153 (2009).
7) The kinematic cooling of molecules with laser-cooled atoms, Takase K, Rahn LA, Chandler DW, et al., New J. of Phys. Vol.11 Article Number: 055033(2009).
8) Imaging the rotationally state-selected NO(A,n) product from the predissociation of the A state of the NO-Ar van der Waals cluster Roeterdink WG, Strecker KE, Hayden CC, Chandler DW, et al., J. Chem. Phys. Vol.130 (13Article Number: 134305 (2009).
9) The Quest for Cold and Ultracold Molecules, Chandler DW, Strecker KE, ChemPhysChem Vol 10(5) 751-754 (2009)

Petascale Direct Numerical Simulation and Modeling of Turbulent Combustion

Jacqueline H. Chen (PI) and Ed Richardson[1]
Sandia National Laboratories, Livermore, California 94551-0969
Email: jhchen@sandia.gov

Program Scope

In this research program we have developed and applied massively parallel three-dimensional direct numerical simulation (DNS) of building-block, laboratory scale flows that reveal fundamental turbulence-chemistry interactions in combustion. The simulation benchmarks are designed to expose and emphasize the role of particular physical subprocesses in turbulent combustion. The simulations address fundamental issues associated with chemistry-turbulence interactions at atmospheric pressure that underly all practical combustion devices: extinction and reignition, premixed and stratified flame propagation and structure, flame stabilization in autoignitive coflowing jet flames and reactive jets in crossflow, and flame propagation in boundary layers. In addition to the new understanding provided by these simulations, the resultant DNS data are being used to develop and validate predictive models required in engineering Reynolds-Averaged Navier Stokes (RANS) and large-eddy (LES) simulations.

Recent Progress

In the past year, computer allocations from a 2010 DOE Innovative and Novel Computational Impact on Theory and Experiment (INCITE) grant have enabled us to perform petascale three-dimensional direct numerical simulations of turbulent flames with detailed chemistry. These studies focused on understanding: 1) Stabilization of lifted turbulent hydrogen jet flames in cross-flow at different fuel injection angles [1], and 2) Turbulent premixed flame structure and propagation in the presence of intense turbulence generated by mean shear [2]. The DNS data were also used to develop and validate mixing and combustion models for RANS and LES [3,4,5]. Highlights of our accomplishments in the past year are summarized below, followed by a summary of future research directions.

Effect of injection angle on stabilization of a reacting turbulent hydrogen jet in cross-flow

With the urgent need to reduce global greenhouse-gas emissions, hydrogen-rich fuels are becoming increasingly relevant in industrial and power generation sectors. The higher reactivity of hydrogen makes it a challenge to design fuel injectors with desired characteristics. For instance, for gas turbines operating in the lean premixed mode (LPM), it is desirable to have an injector design that enables rapid fuel air mixing while not being susceptible to flame flashback. Fully-resolved 3D DNS can illuminate the mechanisms that aid or disrupt flame stabilization and help determine an optimal injection angle, which is the motivation for the present work.

The influence of injection angle on the flame stabilization in a reactive transverse fuel jet in crossflow (JICF) configuration was studied using three-dimensional DNS with detailed chemical kinetics. The case of a nitrogen-diluted hydrogen jet exiting a round nozzle into a cross-flow of heated air is considered and the injection angle is varied from 90 degrees (perpendicular to cross-flow) to 75 degrees relative to cross

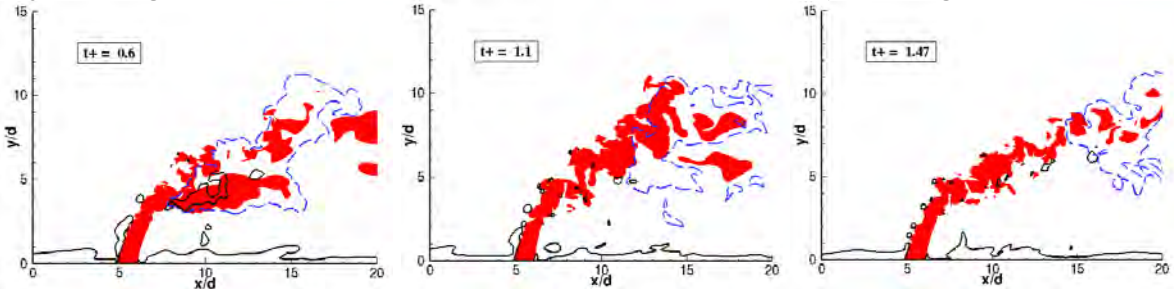

Figure 1. Instantaneous contours on the z-midplane showing the envelope of stoichiometric mixture fraction (red), iso-line of low velocity magnitude of 25 m/s (black) and envelope of 90% peak heat release

[1] Present address University of Southampton, UK

rate (dashed blue). The left figure corresponds to the phase prior to blowoff and the middle and right figures correspond to the blowoff phase. Note the disappearance of the low velocity region during flame blowoff. The quantity t+ is the time elapsed from the start of the simulation normalized by the flow through time.

flow direction. In the 90 degree case where a stable flame was observed Reynolds averaged quantities reveal that the mean location of the flame base coincides with a region of low velocity magnitude that develops on the leeward side of the jet where the local mixture fraction is close to stoichiometric (Grout *et al.* [6]). On the other hand a transient flame blowoff was observed in the 75 degree case (Kolla *et al.* [1]). The onset of blowoff in this case appears to be strongly correlated with the presence/absence of a low velocity region sufficiently close to stoichiometric mixture and this is thought to be the critical mechanism determining flame stabilization. This is evident from the time series of instantaneous snapshots of heat release, low velocity region, and stoichiometric mixture fraction envelope on the spanwise z-midplane shown in Fig.1.

Probability Density Function modeling of molecular mixing in flames with differential diffusion

Modeling of turbulent reacting flows requires closure for averaged or filtered chemical source terms. Probability density function (PDF) methods [7] provide an exact closure for chemical reaction rates but molecular mixing terms remain unclosed and must be modeled. Under particular conditions, for example in the presence of flames, modeling for the effects of molecular mixing on the composition PDF may require improvement. Attempts have been made to address aspects of mixing associated with flames, such as scalar-localness and differential diffusion. In the present study we present a new variant of the Euclidean Minimum Spanning Tree (EMST) mixing model [8] which accounts for differential diffusion while satisfying appropriate realizability constraints. We then use DNS data for a turbulent premixed Bunsen flame [9] to compare the performance of the new EMST model, EMST-DD [3], with the standard EMST and Interaction by Exchange with the Mean (IEM) models [8,10]. Unlike the IEM model, The EMST models describe the structure of mixing through the flame correctly. Combining the EMST description of scalar localness with differential mixing rates, the EMSTDDmodel, predicts mixing rate ratios similar to those in the DNS. A novel feature of the EMST-DD model is that it permits differential diffusion to produce scalar variance, e.g. the model correctly predicts that variance of the nitrogen diluent mass fraction is produced in the premixed combustion DNS.

Modeling transport and scalar dissipation rate in an LES of an autoigniting jet flame

DNS of a non-premixed auto-igniting C_2H_4 jet fame with Re=10,000 and heated co-flow was recently performed by Yoo *et al.* [11]. This DNS was designed to investigate turbulence and ignition interaction, and provides a platform for advancing the fidelity of turbulent ignition models. Recent large eddy simulations of this case with a multi-regime unsteady flamelet model demonstrated that the flame's lift-off height is sensitive to the modeling of scalar dissipation rate, and that a traditional algebraic LES model for this quantity was inaccurate [4]. In the present study the modeling of the scalar dissipation rate is investigated. A transport equation is developed to describe the dissipation rate in an LES of the C_2H_4 jet flame [4]. The term describing dissipation of the dissipation rate is modeled by taking information from the dynamically determined coefficient used to compute scalar variance. The transport equation approach is shown to significantly improve agreement with the dissipation rate observed in the DNS, and to improve predictions of the flame's lift-off height.

Future Work:

Modeling of flame wrinkling for large eddy simulations in intense sheared turbulence

In collaboration with Evatt Hawkes of New South Wales University, a new set of petascale Direct Numerical Simulations (DNS) modeling lean hydrogen combustion with detailed chemistry in a temporally evolving slot-jet configuration is presented as a target data-base for the development and validation of models for premixed turbulent combustion. The jet Reynolds numbers is up to 10,000,

requiring 7 billion grid points, and producing ¾'s petabyte of raw field data. In contrast to prior DNS, a mean shear exists which drives strong turbulent mixing within the flame structure. Three cases have been simulated with different Damköhler number, while Reynolds number is held fixed. Basic statistics will be examined showing the effect of filter-size on unresolved flame wrinkling as was done previously with a lower Reynolds number DNS data set [2], and contrasting this with the effect of filter-size on the resolution of kinetic energy and progress-variable fluctuations. The data-base will then be used to test a range of turbulent premixed flame wrinkling models, including a new model of flame wrinkling for LES applicable at higher Karlovitz number [2], where a range of scales penetrates the internal structure of the flame. The models will be validated against the DNS and and their performance determined as the filter size, downstream distance, and Damköhler number are varied.

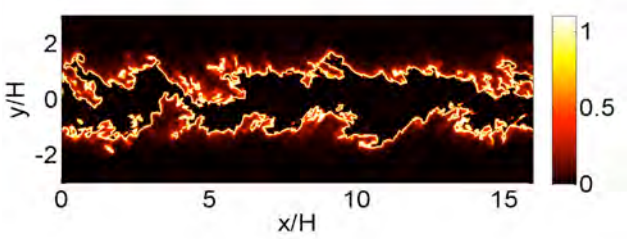

Figure 2: A spanwise cut from the hydrogen premixed turbulent DNS showing heat release normalised by the maximum value in the laminar flame, Re_j = 10,000.

Understanding transient extinction/reignition in di-methyl ether(DME) laminar counterflow flames

We will perform joint experiments/axisymmetric DNS to investigate transient extinction and re-ignition in DME laminar heated nonpremixed counterflow flames with Jonathan Frank. DME is a good proxy for an oxygenated fuel for which mechanisms have been validated [12,13]. Depending on DME and oxygen concentrations, and temperature of the hot oxidizer stream, various flame extinction and re-ignition scenarios may be observed. In particular, we will analyse results for two cases: (a) global extinction and re-ignition via autoignition, (b) local extinction and re-ignition via edge flame propagation. In depth thermochemical analysis will be conducted to elucidate the physics behind the observed phenomena. Detailed comparisons in the time-history of intermediate species, OH and CH_2O, will be made to better understand shortcomings in the chemical mechanism and its coupling with molecular transport models in predicting transient extinction and reignition phenomena.

References:

1. H. Kolla, R. W. Grout, A. Gruber, and J. H. Chen, "Effect of Injection Angle on Stabilization of a Reacting Turbulent Hydrogen Jet in Cross-flow," *7th US National Technical Meeting of the Combustion Institute*, Atlanta, GA March 20-23, 2011.
2. O. Chatakonda, E. R. Hawkes, M. J. Brear, J.H. Chen, E. Knudsen, and H. Pitsch, *Proceedings of the Summer Program 2010*, Center for Turbulence Research, Stanford University, Stanford, USA.
3. E. S. Richardson and J. H. Chen, "Probability Density Function modelling of molecular mixing in flames with differential diffusion," *Proceedings of the European Combustion Meeting*, 2011.
4. E. Knudsen, E. S. Richardson, Shashank, E. M. Doran, H. Pitsch, and J. H. Chen, "Modeling transport and scalar dissipation in an LES of an auto-igniting jet flame," *7th US National Technical Meeting of the Combustion Institute*, Atlanta, GA March 20-23, 2011.
5. N. Punati, J. C. Sutherland, A. R. Kerstein, E. R. Hawkes, and J. H. Chen, *Proc. Combust. Inst*. **33** (2011)1515-1522.
6. R. W. Grout, A. Gruber, J. H. Chen and C. S. Yoo, "Direct Numerical Simulation of Flame Stabilization Downstream of a Transverse Fuel Jet in Cross-Flow," *Proc. Combust. Inst.* **33** (2011), 1629-1637.
7. S.B. Pope, Prog. Energy Combust. Sci. **11** (1985) 119-192.
8. S. Subramaniam, S.B. Pope, *Combust. Flame* **115**(1998) 487-514.
9. R. Sankaran, E.R. Hawkes, J.H. Chen, T. Lu, C.K. Law, *Proc. Combust. Inst*. **31** (1) (2007) 1291-1298.
10. C. Dopazo, Phys. Fluids A **18 (4)** (1975) 397-404.
11. C. S. Yoo, E. S. Richardson, R. Sankaran, and J. H. Chen, *Proc. Combust. Inst*. **33** (2011)1619-1627.
12. Z. Zhao, M. Chaos, A. Kazakov, and F.L. Dryer, *Int J. Chem. Kin*., **40**, 1 (2008) 1–18.
13. Curran, H. J.; Fischer, S. L.; Dryer, F. L. *Int J Chem Kin* **32**, (2000) 741–759.

BES Publications (2009-2011):

1. E. R. Hawkes, R. Sankaran, J. H. Chen, S. Kaiser, and J. H. Frank, "An Analysis of Lower-Dimensional Approximations to the Scalar Dissipation Rate using DNS of Plane Jet Flames," *Proceedings of the Combustion Institute*, **32(1):**1455-1463 (2009).
2. E. S. Richardson, C. S. Yoo, and J. H. Chen, "Analysis of Second-Order Conditional Moment Closure Applied to an Autoignitive Lifted Hydrogen Jet Flame," *Proceedings of the Combustion Institute*, **32(2):**1695-1703 (2009).
3. U. D. Lee, C. S. Yoo, J. H. Chen, and J. H. Frank, "Effects of H_2O and NO on Extinction and Reignition of Vortex-Perturbed Hydrogen Counterflow Flames," *Proceedings of the Combustion Institute*, **32(1):** 1059-1066 (2009).
4. D. Lignell, J. C. Hewson, and J. H. Chen, "Apriori Analysis of Conditional Moment Closure Modeling of a Temporal Ethylene Jet Flame with Soot Formation using DNS," *Proceedings of the Combustion Institute*, **32(1):**1491-1498 (2009).
5. F. Bisetti, J. Y. Chen, E. R. Hawkes, and J. H. Chen, "Differential Diffusion Effects During the Ignition of a Thermally Stratified Premixed Hydrogen-Air Mixture Subject to Turbulence," *Proceedings of the Combustion Institute*, **32(1):** 1465-1472 (2009).
6. T. Lu, C. K. Law, C. S. Yoo, and J. H. Chen "Dynamic Stiffness Removal for Direct Numerical Simulation," *Combust. Flame*, **156(8):**1542-1551 (2009).
7. C. S. Yoo, R. Sankaran, and J. H. Chen "3D Direct Numerical Simulation of a Turbulent Lifted Hydrogen/Air Jet Flame in Heated Coflow:Stabilization and Structure," *J. Fluid Mech.* **460**:453-481 (2010).
8. T. Lu, C. S. Yoo, J. H. Chen, and C. K. Law, "3D Direct Numerical Simulation of a Turbulent Lifted Hydrogen/Air Jet Flame in Heated Coflow: Explosive Mode Analysis," *J. Fluid Mech.* **652** (2010) 45-64.
9. A. Gruber, R. Sankaran, E. R. Hawkes and J. H. Chen, "A Flame-Wall Interaction: A DNS Study," *J. Fluid Mech.* (2010), vol**. 658**, pp. 5–32.
10. U. Lee, C. S. Yoo, J. H. Chen, J. H. Frank, "Effect of NO on Extinction and Reignition of Vortex-Perturbed Hydrogen Flames," *Combust. Flame* **157(2)**: 217-229 (2010).
11. E. S. Richardson, R. Sankaran, R. W. Grout, and J. H. Chen, "Numerical Analysis of Reaction-Diffusion Effects in Turbulent Premixed Methane-Air Combustion," *Combust. Flame* **157**:506-515 (2010).
12. J. H. Chen, A. Choudhary, B. de Supinski, M. DeVries, E. R. Hawkes, S. Klasky, W. K. Liao, K. L. Ma, J. Mellor-Crummey, N. Podhorszki, R. Sankaran, S. Shende, C. S. Yoo, Comput. Sci. Disc**. 2** (2009) 015001.
13. E. S. Richardson, V. E. Granet, A. Eyssartier, and J. H. Chen, "Effects of Equivalence Ratio Variation on Lean, Stratified Methane-Air Laminar Counterflow Flames," *Combust. Theory and Modeling* (2010) **14:6,** 775 – 792.
14. O. Chatakonda, E. R. Hawkes, M. J. Brear, J.H. Chen, E. Knudsen, and H. Pitsch, *Proceedings of the Summer Program 2010*, Center for Turbulence Research, Stanford University, Stanford, USA.
15. R. W. Grout, A. Gruber, J. H. Chen and C. S. Yoo, "Direct Numerical Simulation of Flame Stabilization Downstream of a Transverse Fuel Jet in Cross-Flow," *Proc. Combust. Inst.* **33** (2011), 1629-1637.
16. C. S. Yoo, E. S. Richardson, R. Sankaran, and J. H. Chen, "A DNS Study of the Stabilization Mechanism of a Turbulent Lifted Ethylene Jet Flame in Highly-Heated Coflow, " *Proc. Combust. Inst*. **33** (2011)1619-1627.
17. L. Wang, E. R. Hawkes, and J. H. Chen, "Flame Edge Statistics in Turbulent Combustion," *Proc. Combust. Inst.***33** (2011) 1439-1446.
18. E. R. Hawkes, R. Sankaran, and J. H. Chen, "Estimates of the Three-Dimensional Flame Surface Density and All Terms in its Transport Equation from Two-Dimensional Measurements," *Proc. Combust. Inst*. **33** (2011) 1447-1454.
19. N. Punati, J. C. Sutherland, A. R. Kerstein, E. R. Hawkes, and J. H. Chen, "An Evaluation of the One-Dimensional Turbulence Model: Comparison with Direct Numerical Simulations of CO/H2 Jets with Extinction and Reignition," *Proc. Combust. Inst*. **33** (2011)1515-1522.
20. J. H. Chen, *Plenary Paper* "Petascale Direct Numerical Simulation of Turbulent Combustion – Fundamental Insights Towards Predictive Models," *Proc. Combust. Inst*. **33**(2011) 99-123.
21. D. Lignell and J. H. Chen, "A DNS parametric study of flame extinction and reignition in planar jet flames with varying Damkohler number, in press *Combust. Flame* (2011).
22. C. S. Yoo, T. Lu, J. H. Chen, and C.K. Law, "Direct numerical simulations of ignition of a lean n-heptane/air mixture with temperature inhomogeneities at constant volume: parametric study," in press *Combust. Flame* (2011).

Dynamics and Energetics of Elementary Combustion Reactions and Transient Species
Grant DE-FG03-98ER14879

Robert E. Continetti
Department of Chemistry and Biochemistry
University of California San Diego
9500 Gilman Drive
La Jolla, CA 92093-0340
rcontinetti@ucsd.edu

I. Program Scope

This research program examines the energetics and dynamics of transient neutral species and collision complexes relevant to combustion phenomena. The experimental approach used in these studies involves measurement of the photodetachment and dissociative photodetachment (DPD) of negative ion precursors of important neutral combustion intermediates using photoelectron-photofragment coincidence (PPC) spectroscopy. This year we have exploited the new cryogenic electrostatic ion beam trap (CEIBT) commissioned last year to study the photoelectron spectra and examine DPD processes on cooled anion precursors of species important to combustion processes. Using the CEIBT we have carried out studies of the decomposition of HOCO/DOCO to H/D + CO_2 via tunneling, allowing experimental extraction of the barrier to CO_2 production. High-resolution photoelectron spectroscopy measurements have been performed on $HOCO^-$ and $DOCO^-$ at a number of wavelengths. In collaboration with Stanton's group at UT Austin, this has allowed revision of the electron affinities for both *cis*- and *trans*- isomers of HOCO. We also report on studies of the dissociation dynamics of NO(H_2O) and NO(CD_4) complexes produced by photodetachment. Finally, ongoing experiments on the tert-butoxy radical as well as plans to carry out studies of vibrationally excited anion precursors are discussed.

The PPC spectrometer is capable of a whole new generation of experiments with the trap installed. Both the sensitivity and resolution of the new trap are *higher* than the old single-pass configuration of the spectrometer.[1] One of the key features is that use of the trap allows these *high* duty cycle coincidence experiments to be carried out in conjunction with *low* duty cycle ion sources. In the next year we plan on taking advantage of this by using a tunable IR laser system to selectively excite vibrational modes in precursor anions and influence the branching ratios in radical dissociation. This aids our overall goal of determination of the energetics and reaction dynamics of important combustion intermediates, allowing more quantitative evaluation of their roles in combustion and validation of theoretical approaches to predicting the dynamics of combustion reactions.

II. Recent Progress

A. Energy resolved branching fractions of HOCO

During the past year, we have continued to probe the dynamics of the OH + CO → H + CO_2 reaction by DPD of the $HOCO^-$ anion. Our earlier experiments, conducted with a photon energy of 3.2 eV, yielded evidence for the formation of H + CO_2 below the calculated barrier to formation from the *cis*-HOCO channel.[1] Now with cold precursor ions removing possible contributions from hot bands, these new data provide strong evidence for a tunneling mechanism in the formation of CO_2. The PPC spectra for $HOCO^- + h\nu \rightarrow H + CO_2 + e^-$ and the deuterated analog, shown in Figure 1, provide the primary evidence for tunneling in the exit channel. The horizontal lines in the spectra indicate the maximum eKE expected for dissociation above the calculated barrier to formation of H + CO_2. For both HOCO and DOCO, all dissociation to H + CO_2 or D + CO_2, respectively, occurs above this maximum and

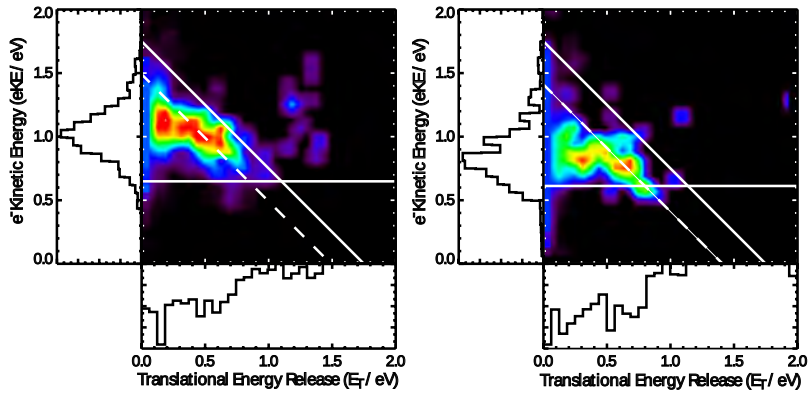

Figure 1. PPC spectrum of HOCO→H+CO_2 (left) and DOCO→D+CO_2 (right). The horizontal lines denote the maximum available eKE expected for dissociation occurring above the barrier, while diagonal lines denote thetotal energy available to *cis*- and *trans*-HOCO(DOCO)

is entirely due to tunneling. The transition from diagonal to horizontal structure in both spectra is indicative of the tunneling lifetime approaching the time-of-flight of the ions at the experimental beam energy. The transition to horizontal character appearing at lower eKE for DOCO compared to HOCO is consistent with a reduction in tunneling probability to D+CO_2 due to the larger reduced mass.

By treating the dissociation using a quasi-1D model, we have successfully determined an effective barrier to formation of H(D) + CO_2. The form of the barrier extracted from the experimental data is shown in Figure 2 compared with theory. The two barriers are in good agreement for the bound part of the surface and the disagreement on the dissociative part results from the significant distortion of nascent CO_2 required for tunneling.

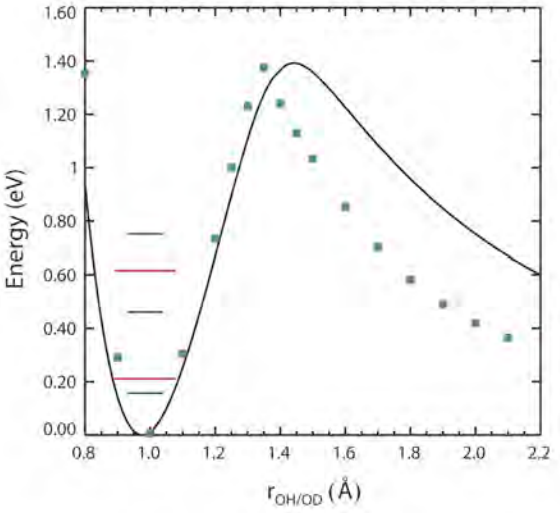

Figure 2. Calculated (green squares) and experimental (solid line) barriers to formation of H + CO_2 from HOCO.

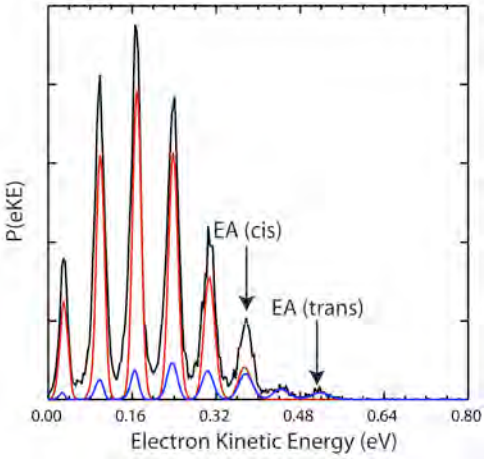

Figure 3. Experimentally obtained photoelectron spectrum of DOCO at a photon energy of 1.88 eV (black) overlaid with calculated vibrational progressions from *cis*- (red) and *trans*- DOCO (blue). The EA for the *cis*- (1.50 eV) and *trans*- (1.37 eV) isomers are indicated.

One major outstanding question is the relative contributions from *cis*- and *trans*-isomers to the observed dynamics of HOCO. To address this question, high-resolution photoelectron spectra of both HOCO and DOCO have been measured at a number of wavelengths near threshold. Comparison of the experimental data with Franck-Condon simulations for *cis*- and *trans*-HOCO and DOCO carried out in collaboration with Stanton's group at UT Austin have provided the first concrete values for the electron affinity (EA) for the two isomers.

B. Probing the interactions of NOx with neutral molecules

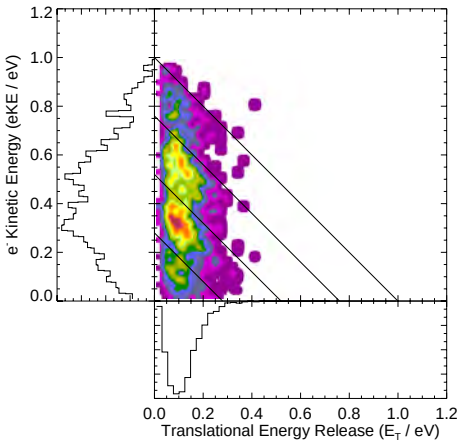

Figure 4. PPC spectrum of $NO^-(H_2O)$. Diagonal lines indicate the maximum E_{TOT} values for different quanta in the NO stretch.

The interactions of NO with simple neutral molecules such as H_2O and CH_4 play an important role in combustion chemistry, given the significance of the oxides of nitrogen as pollutants. Using PPC spectroscopy in our cryogenically cooled EIBT, we have probed the interaction between the NO radical and H_2O and CD_4 by DPD, showing two distinctly different modes of interaction between the species.[2]

Dissociative photodetachment of $NO^-(H_2O)$ has shown evidence for coupling between the NO vibrational and the dissociation coordinate, illustrated in Figure 4 by the diagonal bands present in the correlation spectrum. The ~0.23 eV separation between adjacent ridges is in agreement with the known energy of the NO vibrational mode, and implies that this vibrational mode contributes to the dissociation of the neutral complex. Notably, these features are not apparent from the photoelectron or kinetic energy release spectra alone, highlighting the value of the coincidence technique.

In contrast, the PPC spectrum of $NO(CD_4)$ exhibits no correlation between the photodetached electron kinetic energy and the kinetic energy release from the neutral fragments. The larger total kinetic energy release observed in this spectrum is consistent with a smaller cluster binding energy compared to the $NO(H_2O)$ system, with $NO(CD_4)$ accessing a narrower range of repulsive energies. This difference between $NO(H_2O)$ and $NO(CD_4)$ PPC spectra arises from the interaction between the respective neutral species, with the permanent dipole in water perturbing the NO more than the CD_4.

C. Dissociative processes of alkoxide radicals

We continue to be interested in the decomposition pathways of oxygenated organic radical species. Now, using the CEIBT, we have extended experiments carried out some years ago on the two-body dissociation of the tert-butoxy radical using the single-pass apparatus with a 1 kHz pulsed ion beam. In the early experiments there was some ambiguity as to the identity of the fragments produced, in particular as to whether the neutral fragments arose from loss of a CH_3, O or OH from DPD of a carbanion. Revisiting this set of experiments has allowed us to more thoroughly probe the possible dissociation pathways. The preliminary DPD results show evidence for excitation for a CO vibrational mode in the nascent neutral fragments, implying that the likely fragmentation pathway involves loss of a methyl radical from DPD of a carbanion species $(CH_3)_2COHCH_2^-$.

III. Future Work

In the past year, significant strides have been made towards our intended goal of understanding energetics and dynamics of radical combustion intermediates. Work is now underway to expand our experimental repertoire so that we may probe the reaction dynamics of these species further. The installation of a new ns pulsed laser has allowed construction of an optical parametric oscillator capable of producing mid-infrared light to begin. This

development will allow us to explore the effects of vibrational excitation and photoisomerization of anion precursors on the dynamics of the photodetached radicals and potentially allow control of the product branching ratios in DPD processes with multiple dissociation pathways. In addition, construction has commenced on an electrospray ionization source that can be interfaced with the CEIBT. With this new source, studies of large oxygenated organic molecules important to the combustion of biofuels will be possible, providing new insight into the important emerging field of biofuel energetics.

IV. References

1. Johnson, C.J. & Continetti, R.E. Dissociative photodetachment of cold $HOCO^-$ and below barrier dissociation to $H+CO_2$. *Journal of Physical Chemistry Letters* **1**, 1895-1899 (2010).

2. Poad, B.L.J., Johnson, C.J. & Continetti, R.E. Photoeectron-photofragment coincidence studies of NO-X clusters (X = H_2O, CD_4). *Faraday Discussions* **150**, in press (2011).

V. Publications and submitted journal articles supported by this project 2008-2011

1. Z. Lu, Q. Hu, J.E. Oakman and R.E. Continetti, "Photoelectron-photofragment angular correlations in the dissociative photodetachment of $HOCO^-$ " Mol. Phys. **106,** 595-606 (2008).
2. C.J. Johnson and R.E. Continetti, "Dissociative photodetachment of cold $HOCO^-$ and below-barrier dissociation to H + CO_2" J. Phys Chem. Lett. **1**, 1895-1899 (2010).
3. B.L.J. Poad, C.J. Johnson and R.E. Continetti, "Photoelectron-photofragment coincidence studies of NO^--X clusters (X = H_2O, CD_4)" Faraday Discussions, **150**, in press (2011).
4. C.J. Johnson, B.L.J. Poad, B.B. Shen and R.E.Continetti "New insight into the barrier governing CO_2 formation from OH + CO" Submitted to J. Chem. Phys. (2011).

Studies of the Chemistry of Oxygenated Fuels with Photoionization Mass Spectrometry

Terrill A. Cool
School of Applied and Engineering Physics
Cornell University, Ithaca, New York 14853
tac13@cornell.edu

I. Project Scope

Clean-burning oxygenated bio-derived fuels, such as bio-ethanol, bio-butanol, and biodiesel are of increasing interest as alternatives to petroleum-based transportation fuels. Liquid fuels are likely to be necessary long into the future because of their portability and high energy density. Renewable biomass-derived liquid fuels may reduce dependence on imported petroleum and lower net greenhouse-gas emissions. Many current studies focus on the competition between biofuel and food production, new methods for the formation of such alternative fuels and fuel additives, and engine performance. The combustion chemistry of typical biofuels, including alcohols, ethers, and esters has only recently begun to receive the attention required for predictive descriptions of the combustion of practical bio-derived fuels. Flame-sampling molecular-beam mass spectrometry, with synchrotron photoionization, is an efficient, quantitative tool for studies of premixed, laminar, low-pressure flat flames. Our current research focuses on the chemistry of 13 simple methyl and ethyl esters, dimethoxymethane (DMM), and dimethyl carbonate (DMC). Principal goals of these studies are: (1) show how fuel-specific structural differences including degree of unsaturation, linear vs branched chain structures, and methoxy vs ethoxy functions affect fuel-destruction pathways, (2) understand the chemistry leading to potential increases in the emissions of hazardous air pollutants, including aldehydes and ketones, inherent in the use of biodiesel fuels, and (3) define the key chemical reaction mechanisms responsible for observed reductions in polycyclic aromatic hydrocarbons and particulate matter when oxygenated fuels are used as replacements for conventional fuels. Experimental measurements are combined with comprehensive kinetic modeling.

II. Recent Progress

A. The Effect of Carbon-Carbon Double Bonds on the Combustion Chemistry of Fatty Acid Esters. Bin Yang, Terrill A. Cool, Charles K. Westbrook, Nils Hansen, Katharina Kohse-Höinghaus.

Environmentally friendly biodiesel is a mixture of saturated and unsaturated methyl (or ethyl) esters of long-chain fatty acids. To experimentally examine the effect of unsaturation on the combustion chemistry of fatty acid esters, low-pressure premixed laminar flames of four prototypical small esters have been studied using flame-sampling molecular-beam mass spectrometry. Mole fraction profiles of reactants, products, and well-identified stable and reactive combustion intermediates in flames of methyl propanate ($C_4H_8O_2$) and its isomer ethyl acetate ($C_4H_8O_2$) have been compared with results from methyl propenate ($C_4H_6O_2$) and vinyl acetate ($C_4H_6O_2$) flames, respectively. A total of eight flames have been studied; for each fuel two fuel-rich flame conditions were chosen (phi =1.2 and 1.56). In addition, the underlying oxidation chemistry for these premixed flame conditions has been studied using a detailed

chemical kinetic reaction set, which is largely based on a previously proposed model for saturated esters. The combined results provide a detailed understanding of the similarities and differences between the combustion of saturated vs. unsaturated esters.

Our focus in this study is on the effect of carbon-carbon double bonds on the combustion chemistry of these four simple ester fuels. The structures of these isomers, displayed below, differ in ester function position and degree of unsaturation.

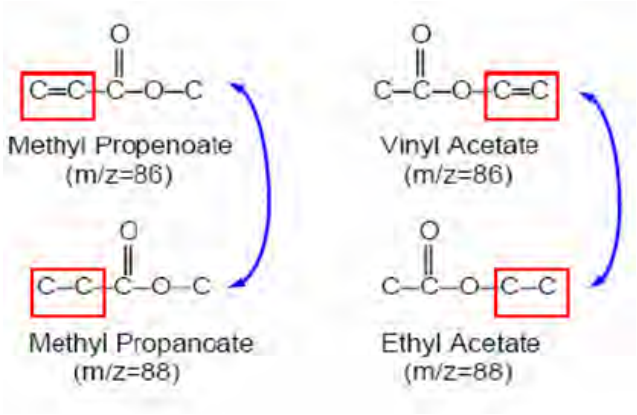

B. The Combustion of Dimethyoxymethane (DMM) and Dimethyl Carbonate (DMC). Bin Yang, Terrill A. Cool, Charles K. Westbrook, Nils Hansen, Katharina Kohse-Höinghaus.

We use flame-sampling synchrotron PIMS to validate and refine current kinetic models for the combustion of dimethoxymethane, $CH_3OCH_2OCH_3$ (DMM), and dimethyl carbonate, $CH_3O(C=O)OCH_3$ (DMC). Our approach, recently used for studies of low-pressure flames of dimethyl ether, CH_3OCH_3 (DME), DME/propene, ethanol/propene, and thirteen esters, provides uniquely detailed descriptions of the compositions of stable and radical intermediates. Measurements of these compositions reveal fuel-specific influences on the fuel destruction mechanisms of unimolecular decomposition and H-atom abstraction followed by β-scissions. Kinetic modeling, accounting for measured compositions of reaction intermediates, yields valuable information concerning the identity and rate constants for these fuel-specific decomposition processes. Extended reaction mechanisms, based on these results, will be incorporated in current kinetic models for combustion of DMM and DMC.

C. **Absolute Cross-Sections for Photoionization of Oxygenated Hydrocarbons. Bin Yang, Terrill A. Cool, David Osborn, Nils Hansen**

Absolute cross-sections for molecular and dissociative photoionization are needed for quantitative flame-sampling molecular beam PIMS studies of the flame chemistry of oxygenated fuels. Dissociative ionization of several small oxygenated hydrocarbons has been extensively studied by several groups, using a full range of experimental techniques. These studies have focused on the measurement of appearance energies for photofragment ions, the structural identities of these fragments, and the dynamic mechanisms responsible for their formation. Dissociative ionization channels often arise from complex isomerization processes in competition with direct bond scission of the parent molecular ion.

We have now completed unpublished measurements of absolute cross-sections for near-threshold molecular and dissociative photoionization for over two dozen oxygenated hydrocarbons (esters, ethers, alcohols, aldehydes, ketones, ketene). Additional measurements for a variety of alkenes and alkynes are also complete and await publication.

III. Future Plans

The principal investigator will retire at the end of calendar year 2011. During this period he will complete flame studies of DMM, DMM/ethane, DMC, and DMC/ethane flames, and make additional measurements of photoionization cross sections. This work will be published in in collaboration with Bin Yang, Charlie Westbrook, Nils Hansen, Katharina Kohse-Höinghaus, and David Osborn. Three additional collaborative papers with Charlie Westbrook, Bin Yang, Nils Hansen and Katharina Kohse-Höinghaus will complete our series of studies of 13 ester flames. The principal investigator also plans to work at the CRF with Nils Hansen to improve the resolution of the mass spectrometer and resolve present uncertainties in the identification of reaction intermediates of key importance in determinations of detailed reaction pathways.

IV. DOE Publications, 2009-present

1. B. Yang, C. K. Westbrook, T. A. Cool, N. Hansen, K. Kohse-Höinghaus "Fuel-Specific Influences on the Composition of Reaction Intermediates in Premixed Flames of Three C5H10O2 Ester Isomers", Phys. Chem. Chem. Phys., 2011, 13(15), 6901-6913.

2. S. Dooley, F. L. Dryer, B. Yang, J. Wang, T. A. Cool, T. Kasper, N. Hansen "An Experimental and Kinetic Modeling Study, of Methyl Formate Low-Pressure Flames", Combust. Flame, 2011, 158(4), 732-741.

3. N. Hansen, T. Kasper, B. Yang, T. A. Cool, W. Li, P. R. Westmoreland, P. Oßwald, K. Kohse-Höinghaus "Fuel-Structure Dependence of Benzene Formation Processes in Premixed Flames Fueled by C6H12 Isomers", Proc. Combust. Inst., 2011, 33(1), 585-592.

4. N. Hansen, W. Li, M. E. Law, T. Kasper, P. R. Westmoreland, B. Yang, T. A. Cool, A. Lucassen "The Importance of Fuel Dissociation and Propargyl + Allyl Association for the Formation of Benzene in a Fuel-Rich 1-Hexene Flame" Phys. Chem. Chem. Phys., 2010, 12(38), 12112-12122.

5. K. Kohse-Höinghaus, P. Oßwald, T. A. Cool, T. Kasper, N. Hansen, F. Qi, C. K. Westbrook, P. R. Westmoreland "Biofuel Combustion Chemistry: From Ethanol to Biodiesel", Angew. Chem. Int. Ed., 2010, 49(21), 3572-3597.

6. J. Wang, B. Yang, T. A. Cool, N. Hansen "Absolute Cross-Sections for Dissociative Photoionization of Some Small Esters", Int. J. Mass Spectrom., 2010, 292(1-3), 14-22.

7. J. Wang, M. Chaos, B. Yang, T. A. Cool, F. L. Dryer, N. Hansen, P. Oßwald, K. Kohse-Höinghaus, P. R. Westmoreland, "Composition of reaction intermediates for stoichiometric and fuel-rich dimethyl ether flames: Flame-sampling mass spectrometry and modeling studies", Physical Chemistry Chemical Physics, 2009, 11, 1328-1339, DOI: 10.1039/B815988B.

8. N. Hansen, T.A. Cool, P.R. Westmoreland, K. Kohse-Höinghaus,"Recent Contributions of Flame-Sampling Molecular-Beam Mass Spectrometry to a Fundamental Understanding of Combustion Chemistry", Progress in Energy and Combustion Science, 2009, 35, 168-191.

9. C. K. Westbrook, W. J. Pitz, P. R. Westmoreland, F. L. Dryer, M. Chaos, P. Oßwald, K. Kohse-Höinghaus, T. A. Cool, J. Wang, B. Yang, N. Hansen, T. Kasper, "A Detailed Chemical Kinetic Mechanism for Oxidation of Four Small Alkyl Esters in Laminar Premixed Flames", Proc. Combust. Inst., 2009, 32, 221-228.

10. A Lucassen, P. Oßwald, U. Struckmeier, K. Kohse-Höinghaus, T. Kasper, N. Hansen, T.A Cool, P. R.Westmoreland, “Species identification in a laminar premixed low-pressure flame of morpholine as a model substance for oxygenated nitrogen-containing fuels”, Proc. Combust. Inst., 2009, 32, 1269-1276.
11. N. Hansen, J. A. Miller, T. Kasper, K. Kohse-Höinghaus, P. R. Westmoreland, J. Wang, T. A. Cool, “Benzene Formation in Premixed Fuel-Rich 1,3-Butadiene Flames“, Proc. Combust. Inst., 2009, 32, 623-630.

12. N. Hansen, J. A. Miller, P R. Westmoreland, T. Kasper, K. Kohse-Höinghaus, J. Wang, T. A. Cool, “Isomer-Specific Combustion Chemistry in Allene and Propyne Flames”, Combust. Flame, 2009, 156(11), 2153-2164.

13. T. Kasper, P. Oßwald, U. Struckmeier, K. Kohse-Höinghaus, C. A. Taatjes, J. Wang, T. A. Cool, M. E. Law, A. Morel, P. R. Westmoreland, “Combustion Chemistry of the Propanol Isomers—investigated by electron ionization and VUV-photoionization molecular-beam mass spectrometry, Combust. Flame, 2009, 156 (6), 1181-1201.

Dissociation Pathways and Vibrational Dynamics in Excited Molecules and Complexes

F.F. Crim
Department of Chemistry
University of Wisconsin–Madison
Madison, Wisconsin 53706
fcrim@chem.wisc.edu

Our research investigates the chemistry of vibrationally excited molecules. The properties and reactivity of vibrationally energized molecules are central to processes occurring in environments as diverse as combustion, atmospheric reactions, and plasmas and are at the heart of many chemical reactions. The goal of our work is to unravel the behavior of vibrationally excited molecules and to exploit the resulting understanding to determine molecular properties and to control chemical processes. A unifying theme is the preparation of a molecule in a specific vibrational state using one of several excitation techniques and the subsequent photodissociation of that prepared molecule. Because the initial vibrational excitation often alters the photodissociation process, we refer to our double-resonance photodissociation scheme as *vibrationally mediated photodissociation.* In the first step, fundamental or overtone excitation prepares a vibrationally excited molecule, and then a second photon, the photolysis photon, excites the molecule to an electronically excited state from which it dissociates. Vibrationally mediated photodissociation provides new vibrational spectroscopy, measures bond strengths with high accuracy, alters dissociation dynamics, and reveals the properties of and couplings among electronically excited states.

Our recent experiments have used ion imaging to follow the adiabatic and nonadiabatic dissociation pathways in ammonia, to study the influence of vibrational excitation on the dynamics at conical intersections in phenol, and to obtain new vibrational spectroscopy on the formic acid dimer. These studies have set the stage for our newest measurements on complexes. We have just completed a detailed study of the spectroscopy and vibrational predissociation dynamics of the ammonia dimer and are beginning experiments on its vibrationally mediated photodissociation. The goals of these studies are to understand and prepare vibrations in the ground electronic state, to study the vibrational structure of the electronically excited molecule, and to probe and control the dissociation dynamics of the excited state in clusters.

Spectroscopy of Ammonia Dimers and Predissociation Products

The detailed insights that have come from our experiments on the influence of vibrational excitation on the excited state dynamics of ammonia suggest that the vibrationally mediated photodissociation of ammonia dimers and complexes of ammonia with other small molecules could reveal novel behavior. Our two central concerns are the influence of complexation on the dynamics at the conical intersection and the changes that complexation produces in the vibrationally mediated photodissociation of ammonia. There are detailed studies of the photodissociation of bare ammonia molecules that provide a starting point for our work. New studies of the vibrational predissociation of ammonia complexes with C_2H_2 and with H_2O by Reisler and coworkers[1,2] provide a similar starting point for understanding the ground-electronic state behavior in some of the complexes we intend to investigate.

We have studied the ammonia dimer to understand its ground-electronic state vibrational dynamics as a prelude to electronic excitation. A supersonic expansion of ammonia in He produces the oligomers we study. Exciting the N-H stretching vibration in an oligomer produces vibrationally and rotationally excited ammonia fragments that we detect by (2+1) REMPI through the $\tilde{B}$ state. The figure shows the infrared action spectrum obtained by observing production of NH_3 fragments with one or two quanta of excitation in the umbrella bending vibration (ν_2). These features are consistent with the transitions observed in He droplets[3] and show that excitation of either the symmetric N-H stretch or the antisymmetric N-H stretch initiates vibrational predissociation.

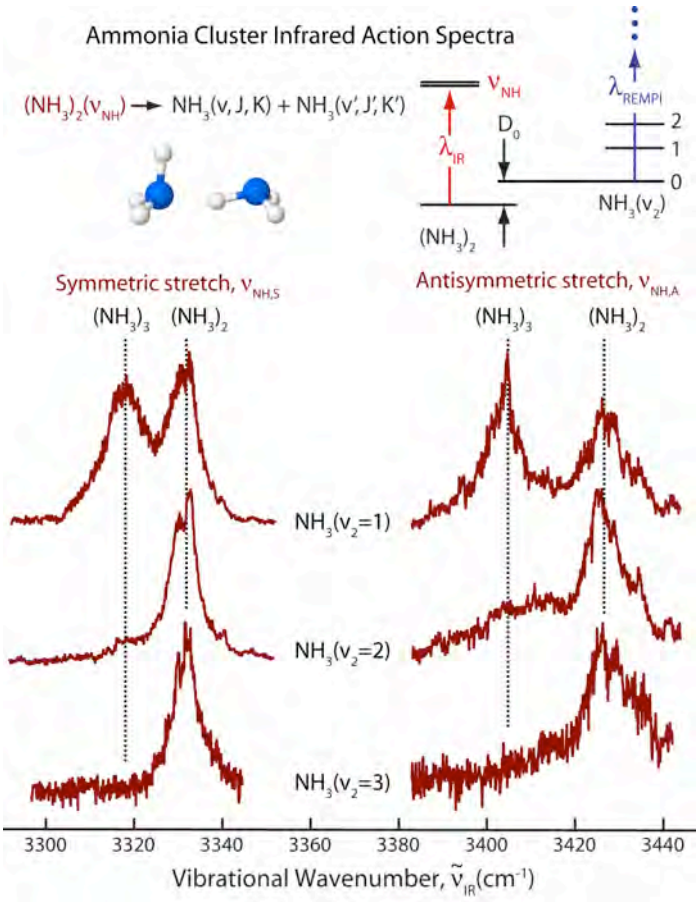

The action spectrum for detection of ammonia products with one quantum of umbrella bending excitation, $NH_3(\upsilon_2=1)$, has prominent features for both the dimer and the trimer. However, the signal from the dimer dominates the action spectrum for products with two quanta of bending excitation $NH_3(\upsilon_2=2)$. Apparently, fragmenting the trimer requires so much energy that there is only enough left to populate umbrella bending states of the monomer with one quantum of excitation. The effect is even more pronounced detecting $NH_3(\upsilon_2=3)$, the production of which ties up still more of the energy that would go to breaking bonds in the trimer.

The key to obtaining these action spectra and to the analysis of the predissociation dynamics described below is the ability to interrogate individual vibrational rotational states (υ, J, K) of the ammonia products using REMPI detection. A collaboration with Dr. Collin Western at the University of Bristol has been critical to simulating and assigning the spectra. Along the way, we have been able to identify new transitions and refine some spectroscopic constants.[4]

Dissociation Energy and Dynamics of Ammonia Dimers

Velocity-map ion-imaging detection of fragments $NH_3(\upsilon, J, K)$ directly provides the distribution of recoil speeds of the undetected partner fragment $NH_3(\upsilon', J', K')$ formed in the vibrational predissociation of the dimer,

$$(NH_3)_2 + h\nu_{IR} \rightarrow NH_3(\upsilon, J, K) + NH_3(\upsilon', J', K'),$$

where J and K are the quantum numbers for the total angular momentum and its projection on the symmetry axis, respectively. The distribution of recoil energies T_{recoil} mirrors the distribution of internal energies $E'_{int}(NH_3)$ of the undetected fragment through the conservation of energy,

$$h\nu_{IR} + E_{int}(NH_3\text{-}NH_3) = D_0 + T_{recoil} + E_{int}(NH_3) + E'_{int}(NH_3),$$

where E_{int} (NH_3-NH_3) is the initial internal energy of the dimer and D_0 is its dissociation energy. Thus, analysis of the recoil distributions is a route to an experimental determination of the binding energy of the dimer.[5]

Even though there are many available states, clear patterns of state population are apparent in the distribution of recoil speeds. The figure shows the distribution extracted from the ion image of the product, $NH_3(\upsilon_2=2^+, J=6, K=6)$. As the vertical lines indicate, the maxima in the distribution align with recoil speeds corresponding to the formation of the undetected product in various J' states with $K'=0$. The identification of the features marked in the figure comes from using conservation of energy and a dissociation energy of 658 cm^{-1}. (The coalescence of the levels with small values of K' make the features near $K'=0$ the most prominent.) Introducing all of the possible values of K' in the analysis produces the simulation of the recoil speed distribution shown as the dashed line in the figure. Performing this same analysis self-consistently for a total of 17 different detected rovibrational states (υ, J, K) produces comparably good fits to all of the data and yields a dissociation energy for the dimer of D_0 = 660±20 cm^{-1}. This value is much more precise than previous experimental estimates and is consistent with recent calculations. Calculating the dissociation energy is challenging because of the large contribution of zero-point energy (about 40% of the well depth D_e) in this loosely bound complex

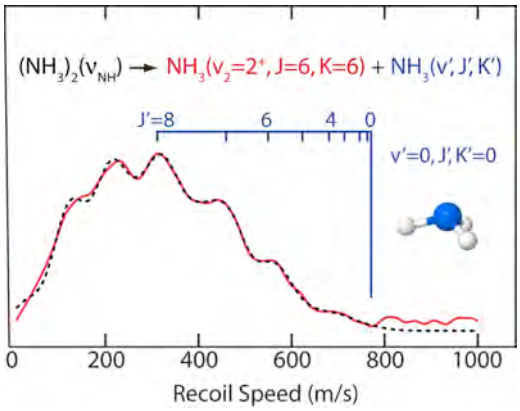

The analysis of the images also shows that most of the available energy appears as vibrational excitation, with there being at least two quanta of umbrella bending excitation distributed between the fragments. Producing $NH_3(\upsilon_2=3^+)$ requires almost all of the available energy and leaves the undetected partner with no vibrational energy. In many cases, $NH_3(\upsilon_2=2^+)$ appears in partnership with $NH_3(\upsilon'=0)$ although there are cases where it is possible to make $NH_3(\upsilon_2'=1)$. In cases where the detected product is $NH_3(\upsilon_2=1^+)$, the distributions suggest that the partner is born with a quantum of umbrella bending excitation as well, reflecting the transfer of vibrational energy between the two moieties during dissociation. Although the antisymmetric umbrella bending vibration (ν_4) is energetically accessible, we see no evidence of its formation, perhaps reflecting a dynamical bias in the vibrational predissociation.

Future Directions

We are completing manuscripts on the spectroscopy[4] and dynamics[5] of the ammonia dimer described above and are preparing to do our first vibrationally mediated photodissociation experiments on that cluster. Our goal is to study complexes with ammonia as well as other bare and complexed molecules where we can use vibrational excitation to influence the passage through conical intersections. The variety of complexes available, including ones with different bonding motifs, offers a rich array of possibilities in which to study the influence of an adduct and initial vibrational excitation.

1. J. A. Parr, G. Li, I. Fedorov, A. J. McCaffery, and H. Reisler, J. Phys. Chem. A **111**, 7589 (2007).
2. A. K. Mollner, B. E. Casterline, L. C. Ch'ng, and H. Reisler, J. Phys. Chem. A **113**, 10174 (2009).
3. S. Kuma, M. N. Slipchenko, T. Momose, and A. F. Vilesov, Chem. Phys. Lett. **439**, 265 (2007).
4. A. S. Case, C. G. Heid, C. M. Western, and F. F. Crim, J. Chem. Phys., (in preparation) (2011).
5. A. S. Case, C. G. Heid, S. H. Kable, and F. F. Crim, J. Chem. Phys., (in preparation) (2011).

PUBLICATIONS SINCE 2009 SUPPORTED BY DOE

Reactive Scattering: Quantum-State-Resolved Chemistry, F. Fleming Crim, in *Tutorials in Molecular Reaction Dynamics*, Eds. Mark Brouard and Claire Vallance (Royal Society of Chemistry, London, 2010).

Bimolecular Dynamics of Combustion Reactions

H. Floyd Davis
Department of Chemistry and Chemical Biology
Baker Laboratory, Cornell University, Ithaca NY 14853-1301
hfd1@Cornell.edu

I. Program Scope:

The aim of this research program is to better understand the mechanisms and product energy disposal in elementary bimolecular reactions fundamental to combustion chemistry. Using the crossed molecular beams method, a molecular beam containing highly reactive free radicals is crossed with a molecular beam. The angular and velocity distributions of the neutral products from single reactive collisions are measured using "universal" mass spectrometry with single photon pulsed vacuum ultraviolet (VUV) photoionization, or for reactions leading to H, D, or O products, by Rydberg tagging time-of-flight (TOF) methods.

II. Recent Progress:

To substantially improve the sensitivity in O atom Rydberg time of flight (ORTOF) experiments, and to greatly expand the range of systems that can be studied using universal pulsed photoionization detection[1] (previously limited to 7.9 eV using an F_2 excimer), we have implemented new VUV light sources (8-11 eV) on two different crossed beams machines in our laboratory. The highest possible efficiency for VUV generation using pulsed nanosecond lasers involves a method first proposed by Smith and Alford[2] and then demonstrated experimentally by Muller and coworkers.[3] It employs 4-wave mixing of collimated *(i.e., unfocussed)* nanosecond pulses in a 1m long cell containing mercury (Hg) vapor. In the following, we illustrate some recent results on two different machines using high-brightness VUV pulsed light sources employing collimated laser beams.

i. $H + O_2 \rightarrow OH\ (^2\Pi) + O\ (^3P_J)$.

The $H + O_2 \rightarrow OH\ (^2\Pi) + O\ (^3P_J)$ reaction is generally considered to be among the most important in combustion.[4,5] It is well-known that the OH is preferentially formed in high-N levels in v = 0 and 1. Some time ago, prior to the implementation of our new VUV source, we attempted to study this reaction in crossed beams using ORTOF employing fast photolytic H atoms produced by photodissociation of HI at 248 nm. However, we were unsuccessful in observing signal, largely due to the small VUV intensity using Kr as the nonlinear medium, small cross section for reaction, and necessarily weak photolytic H atom source.

The title reaction is endothermic by 16.6

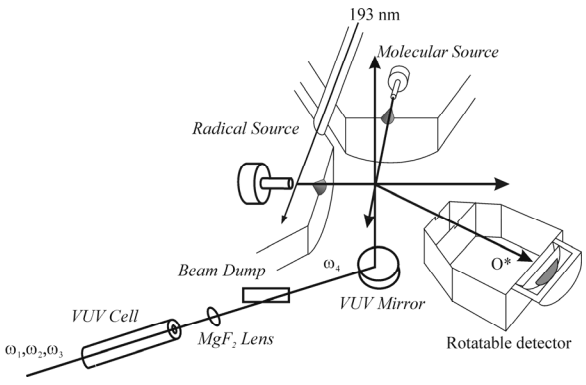

Fig. 1: Schematic of newly-configured Rydberg Tagging Apparatus (not to scale). VUV (ω_4) produced in 1m long Hg cell passes beam dump whereas fundamental beams (ω_1, ω_2, and ω_3) are dumped.

kcal/mole and has been studied by a number of groups at various collision energies using LIF detection of the OH product. The reaction cross section is only on the order of 0.2 A^2, which is about a factor of 5 smaller than H + D_2. Consequently, this reaction is quite challenging from an experimental standpoint. Using our greatly improved VUV source, we have successfully observed reactive scattering signal for the reaction using photolysis of HBr at 193 nm for production of H atoms. These conditions correspond to a collision energy of ~2.5 eV. Our preliminary observations suggest that at this high collision energy the O atoms are primarily backscattered relative to the incoming O_2 molecules. This indicates that the reaction is direct, with the reaction most favored by small impact parameter collisions in which the incoming H atom abstracts an O atom from O_2 and rebounds in the backward direction. We also observe some O atom signal forward scattered relative to the O_2 molecules, corresponding to reactions at larger impact parameters.

From our preliminary results, it is certain that our experimental sensitivity is sufficient to study this reaction, especially at lower collision energies near 1.0 eV and 1.8eV which may be accessed using H atoms produced by photodissociation of HI at 248 nm (corresponding to the I* and I channels, respectively, each contributing about 50%). As indicated in the recent literature, a particularly interesting feature of this system is that while complex-forming dynamics play an important role, there is strong evidence for nonstatistical behavior, particularly at higher collision energies[5] A series of angularly-resolved measurements at well-defined collision energies provided by photolysis of HI or HBr will provide valuable experimental benchmarks against which theoretical predictions on accurate potential energy surfaces may be compared.

ii. Crossed Beams Study of Phenyl Oxidation:

Phenyl radicals (C_6H_5) react with oxygen molecules (O_2) to form phenylperoxy radicals (C_6H_5OO). These intermediates have been calculated to decompose either through O-O bond fission forming C_6H_5O + O, or through isomerization producing C_5H_5 + CO_2, C_5H_5O + CO or $C_6H_4O_2$ + H [6]

Last year, we published an account of the reaction of phenyl radicals with molecular oxygen at a mean collision energy of 64 kJ/mol using the crossed molecular beams technique, employing detection via pulsed single photon ionization at 9.9 eV. In that work, we monitored the formation of phenoxy radicals (C_6H_5O) from the C_6H_5O + O channel, providing insight into the lifetimes of the C_6H_5OO intermediates. The measured distributions implied that the C_6H_5OO lifetimes (τ) are at least comparable to their rotational timescales, i.e. $\tau \geq 1$ ps. Our lower limit for τ was at least 100 times longer than an upper limit inferred from a previous crossed beams experiment carried out at a collision energy of 107 kJ/mol employing a pyrolytic phenyl radical source.[7]

In order to understand the significantly different reaction dynamics for phenyl + O_2 reported in the two laboratories, we have set up a heated pulsed nozzle source capable of reaching temperatures up to 400^{o}C. To reach collision energies above 100 kJ/mol, either the phenyl beam or the O_2 beam can be heated. While heating the O_2 beam is most desirable as it increases the angle of the CM of the system, we have begun by heating the C_6H_5 nozzle so as to increase the vibrational temperature of the C_6H_5 reactant. We have studied the reaction at E_{coll} ~ 120 kJ/mol, which is ~10 kJ/mole higher than that used by Kaiser's group. We find that even at this high collision energy, the C_6H_5O product angular distribution still indicates significant participation of $C_6H_5O_2$ complexes, with no evidence for the onset of the sharply forward peaked angular distribution reported in Ref. 7.

iii. Competing Pathways in the Reaction $C_6H_5 + CH_2CHCH_3$ (Propene):

Previous studies of the reactions of a wide range of unsaturated systems (including propene) with phenyl radicals have been carried out by Kaiser's group using the method of crossed molecular beams.[8,9] To better assess the performance of our apparatus employing pulsed VUV photoionization detection, we studied the title reaction using the same photolytic C_6H_5 source employed in our study of the $C_6H_5 + O_2$ reaction.

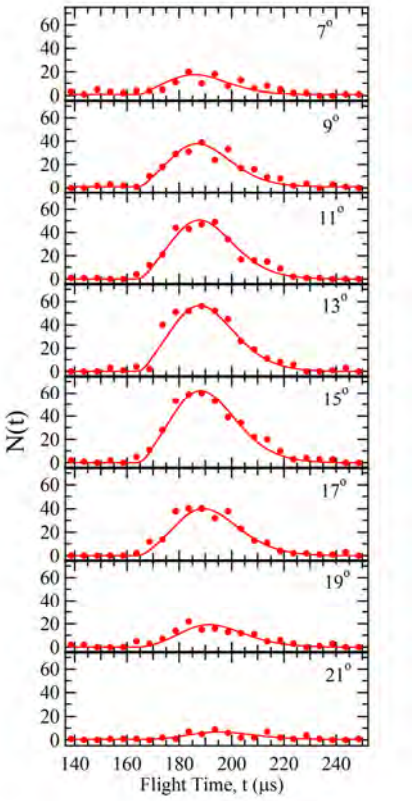

Fig. 2: Laboratory TOF spectra at m/e = 118 for C_9H_{10} + H channel in phenyl + propene reaction at E = 80 kJ/mol.

In the previous work,[9] the only observed product channel in the propene reaction (and in reactions of a series of other unsaturated hydrocarbons), was H atom elimination. For the propene reaction, this was taken as evidence that reaction occurred exclusively by addition of the phenyl radical to the α-carbon atom (*i.e.*, to the CH_2 group) rather than to the methyl substituted central carbon atom. This behavior was attributed to steric effects and a propensity for the electron deficient phenyl radical to attack the carbon with a greater electron density. From the signal to noise calculations, it was concluded that the CH_3 elimination channel cannot account for more than 10% of the total reaction cross section.

We studied the title reaction at collision energy of 80 kJ/mol, which is considerably less than that employed in the previous work (130 and 186 kJ/mol). Not surprisingly, we observed the H atom elimination channel, corresponding to production of C_9H_{10}, which we monitored at its parent m/e = 118 (Fig. 2). We also observed strong signal at m/e = 104, corresponding to C_8H_8 resulting from methyl radical elimination, *i.e.*, $C_6H_5 + CH_2CHCH_3 \rightarrow C_6H_5CHCH_2 + CH_3$. Representative TOF spectra for the $C_8H_8 + CH_3$ channel (Fig. 3) were accumulated using 30,000 laser shots, corresponding to about 20 minutes of averaging each.

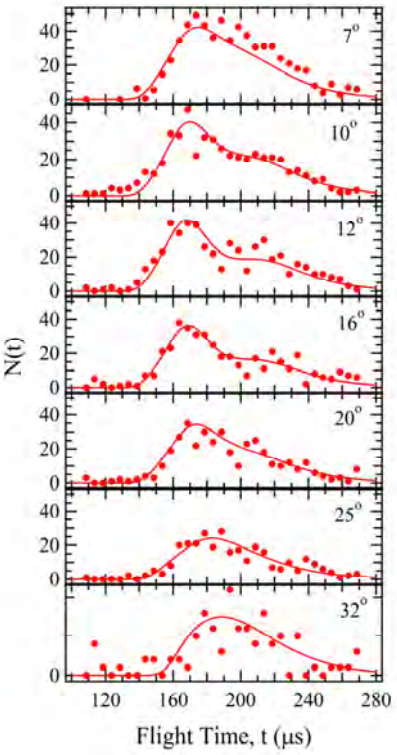

Fig. 3: Laboratory TOF spectra at m/e = 104 for the $C_8H_8 + CH_3$ channel in phenyl + propene reaction at E = 80 kJ/mol.

As can be seen from the figures, we find that the absolute signal level for the C_8H_8 channel (CH_3 elimination) is nearly as large as that for H atom elimination. The Newton sphere for C_9H_{10} channel is very small (due to the light H atom counterfragment), so products are constrained to a small laboratory angular range. The C_8H_8, on the other hand, recoils from CH_3 and is scattered over a relatively large Newton sphere. The substantial signal levels seen suggest that CH_3 elimination is very significant in this system, and may actually be dominant.

In the near future, we plan to directly calibrate the

photoionization detection sensitivity of our apparatus for the different chemical product channels by carrying out parallel experiments involving the photoionization of various stable product molecules commercially available. A particularly interesting question that we hope to address is how ionization and possible VUV fragmentation depends upon the vibrational energy of the product. This should allow us to determine the branching ratios for competing reaction pathways.

III. Future Studies:

During the upcoming year, we plan to continue our studies of the $R + O_2 \rightarrow RO + O$ reactions ($R = H, CH_3$) using ORTOF. The tunable high brightness pulsed VUV source (8-11eV) will be used to study oxidation reactions of other hydrocarbon free radicals (C_2H_3, C_2H_5, C_3H_7, C_4H_9, *etc*.). Finally, to better understand the competing reaction channels producing enols in combustion, bimolecular reactions of OH with ethene and propene will be studied.

IV. Publications citing DOE Support for 2008-Present:

1. Daniel R. Albert and H. Floyd Davis, "Collision Complex Lifetimes in the Reaction $C_6H_5 + O_2 \rightarrow C_6H_5O + O$", *J. Phys. Chem. Lett.* 1, 1107 (2010).
2. David L. Proctor, Daniel R. Albert and H. Floyd Davis, "Improved piezoelectric actuators for use in high-speed pulsed valves", *Rev. Sci. Instrum.* 81, 023106 (2010).

V. References:

1. D. Proctor and HF Davis, *Proc. Nat. Acad. Sci. Am.* **105**, 12673 (2008).
2. A.V. Smith and W.J. Alford, *J. Opt. Soc. Am. B.* **4**, 1765 (1987).
3. H. Muller, D.D. Lowenthal, M.A. DeFaccio, and A. V. Smith, *Opt. Lett.* **13**, 651 (1988).
4. M. A. Bajeh, E.M. Goldfield, A. Hanf, C. Kappel, A.J.H.M. Meijer, H. –R. Volpp and J. Wolfrum, *J. Phys. Chem. A.* **105**, 3359 (2001).
5. Z. Sun, D.H. Zhang, C. Xu, S. Zhou, D. Xie, G. Lendvay, S-Y. Lee,Y. Shi, H. Guo *J.Am.Chem.Soc.* **130**, 14962 (2008).
6. Tokmakov, I.V.; Kim, G.S.; Kislov, V.V.; Mebel, A.M.; Lin, M.C. *J. Phys. Chem. A***, 109**, 6114 (2005).
7. Gu, X.; Zhang, F.; Kaiser, R.I. *Chem. Phys. Lett. 448*, 7 (2007).
8. X. Gu and R.I. Kaiser, *Acc. Chem. Res.* **42**, 290 (2009).
9. F. Zhang, X. Gu, Y. Guo, and R.I. Kaiser, *J. Phys. Chem. A.* **112**, 3284 (2008).

Exploration and validation of chemical-kinetic mechanisms

Michael J. Davis

Chemical Sciences and Engineering Division
Argonne National Laboratory
Argonne, IL 60439
Email: davis@tcg.anl.gov

The main focus of the work is on the exploration and theoretical validation of chemical-kinetic mechanisms, which combines global sensitivity analysis with the exploration of the characteristics of the sensitivity analysis over the physical and chemical parameters. The tools used for generating these sensitivity maps can be applied to other types of fitting and optimization problems. We are in the process of implementing several of these procedures for fitting potential energy surfaces.

Recent Progress

Application of Global Sensitivity Analysis to a New Comprehensive Mechanism for Ethanol Combustion

Global sensitivity analysis has been applied to a new mechanism for ethanol combustion in collaboration with Raghu Sivaramakrishnan and Zhou and Skodje (Colorado). Figure 1 shows results for global sensitivity analysis applied to an ignition-delay target for two different initial mixtures. The results in Figure 1 are first-order sensitivity indices, which is generally all that is needed in our validation tests (higher order terms are often small). The left panel in Figure 1 shows results for undiluted stoichiometric mixtures of ethanol and oxygen and the right shows a mixture of ethanol and oxygen dilute in Ar. The left panel shows results generated from an ignition simulation started at much higher pressure than the right, 20 atm vs. 1 atm. In the left panel of Figure 1 the ignition delay times are most sensitive to the reaction: $C_2H_5OH + HO_2 =$

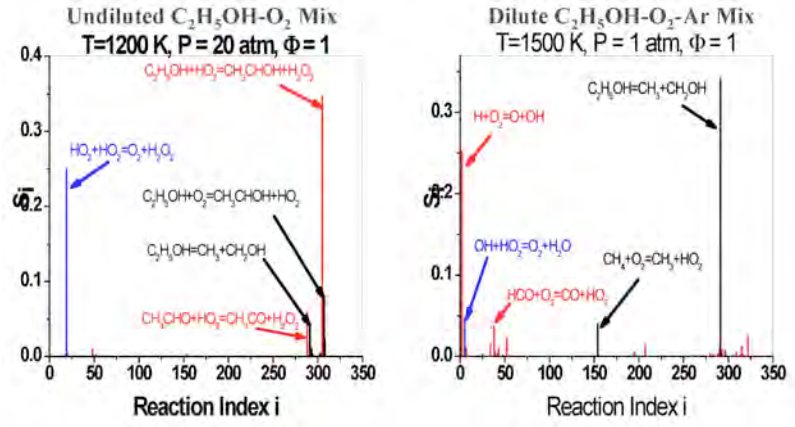

Figure 1. Global sensitivity analysis for two mixtures of ethanol in O_2 and O_2/Ar is shown.

$CH_3CHOH + H_2O_2$. This has led us to theoretically characterize the rate coefficient for this

reaction. The preliminary estimates of the rate coefficient are similar to previous rate coefficients, estimated by analogy, but will now have a lower uncertainty. This new rate coefficient and its uncertainty will be incorporated into future calculations of global sensitivity analysis and may lead to the re-evaluation of other rate coefficients.

The left panel also demonstrates that the reaction $HO_2 + HO_2 = H_2O_2 + O_2$ has high sensitivity at elevated pressure under non-dilute conditions. We have found this reaction has high global sensitivity for many chemical models. This has led to an ongoing project to calculate the rate coefficient for this reaction, which involves a collaboration with Zhou and Skodje (Colorado) and Larry Harding.

The right panel in Figure 1 shows that the most sensitive reaction for ignition under dilute conditions is the dissociation of ethanol. The rate coefficient for this reaction has recently been calculated and its uncertainty is relatively low (2.0). The results in the right panel demonstrate that very accurate calculations of rate coefficients beyond what is generally undertaken would be very productive. For example, a calculation to reduce the uncertainty for this reaction to 1.3 or so would be very useful.

In our study of ethanol combustion we have added several new targets to the ignition-delay target previously used. Figure 2 shows results for species targets for the modeling of the Princeton flow reactor. Here global sensitivity analysis has been applied to the uncertainty of species profiles at specific times. The plot in Figure 2 shows the global sensitivity of the concentration of acetaldehyde to all the reactions in the mechanism. As in the left panel of Figure 1, the reaction with the highest sensitivity is $C_2H_5OH + HO_2 = CH_3CHOH + H_2O_2$. This reaction carries most of the variance for the first order sensitivity coefficients, 0.65 out of 0.83, and is more dominant than in Figure 1. It is also interesting that the other abstraction of a hydrogen from a carbon atom, $C_2H_5OH+HO_2 = CH_2CH_2OH+H_2O_2$ has a low first-order sensitivity coefficient of 0.0032

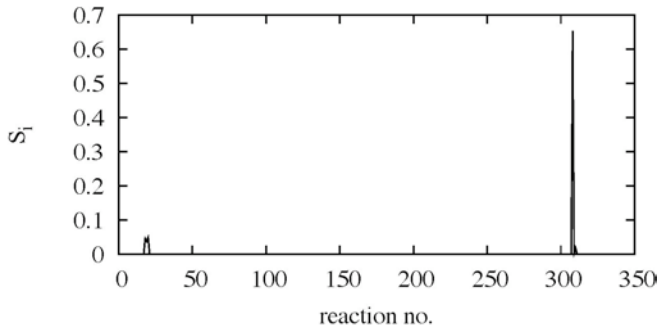

Figure. 2. Global sensitivity analysis is applied to the Princeton flow reactor. The sensitivity of the acetaldehyde concentration at t = 0.1 s is calculated for all the reactions. The large peak on the right is for the reaction $C_2H_5OH + HO_2 = CH_3CHOH + H_2O_2$.

The sum of the first order sensitivity coefficients in the example of Fig. 2 is 0.83. The sum of all sensitivity coefficients is 1.0, and this indicates that there are higher-order sensitivity coefficients that contribute. Because second-order coefficients involve pairs of reactions, we expect that there is a reaction with low first-order sensitivity that pairs with the reaction $C_2H_5OH + HO_2 = CH_3CHOH + H_2O_2$ to give a large second-order coefficient. Calculations are underway to investigate this.

Application of Glonal Sensitivity Analysis to Butanol Oxidation

The study of butanol oxidation is continuing with Zhou and Skodje. Global sensitivity analysis indicated that the most sensitive reaction for ignition was the hydrogen abstraction by HO_2 from butanol, with the highest sensitivity by a significant amount due to the abstraction of the α-hydrogen. New rate coefficients for all the hydrogen abstractions are being calculated by C.-W. Zhou, Simmie, and Curran (Galway). These rate coefficients have smaller uncertainties

than the previous ones. We are running global sensitivity analysis for the mechanism with the updated rate coefficients and uncertainties, with results for the abstraction of the α-hydrogen complete. This update has led to a reduced uncertainty of the overall ignition delay time and the fractionation of the variance decomposition as demonstrated in Figure 3. As indicated in the figure, the highest sensitivity indices are the HO_2 + HO_2 reaction and the abstraction by HO_2 of the γ-hydrogen from butanol, both of which are being re-calculated, as described. These new rate coefficients with new uncertainties are being incorporated into the global sensitivity analysis at this time.

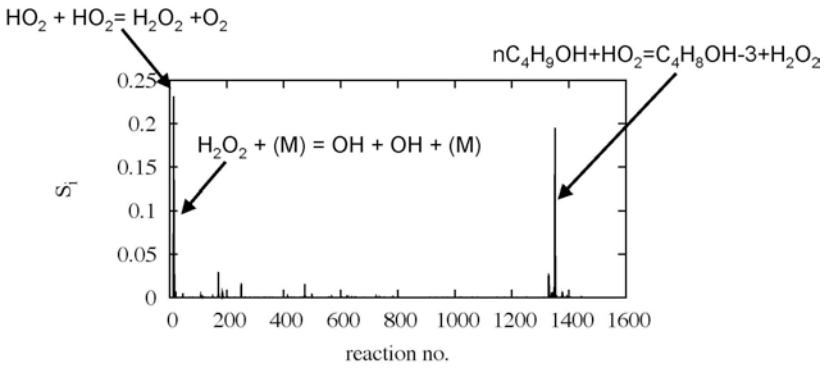

Figure 3. Global sensitivity analysis for ignition of stoichiometric butanol/oxygen mixtures oxidation. P_0 = 10 bar, T_0 = 1200 K.

Theoretical Advances: Hydrogen Oxidation

In collaboration with Skodje and Tomlin we have performed global sensitivity analysis on the H_2/O_2 combustion mechanism. This work has two goals. The H_2/O_2 mechanism is a component of any mechanism for hydrocarbon combustion, and the first goal was to see if global sensitivity analysis could be used to improve this mechanism. The second goal of this work is to develop a detailed understanding of the probability density function (pdf) that describes the uncertainty of targeted observables (e.g., the ignition delay) induced by the uncertainties in specific rate coefficients.

An HDMR expansion of the ignition delay time allows for a detailed understanding of the probability density function in terms of individual reactions, through the deconstruction of the probability density function. Figure 4 shows a one-reaction deconstruction in the top panel, a two-reaction deconstruction in the middle panel and a three-reaction deconstruction in the bottom panel. This type of deconstruction allows for the features of the time pdf to be understood in terms of the individual reactions. Sharp changes in the time pdf can be understood in terms of the shifting importance of individual reactions or groups of reactions.

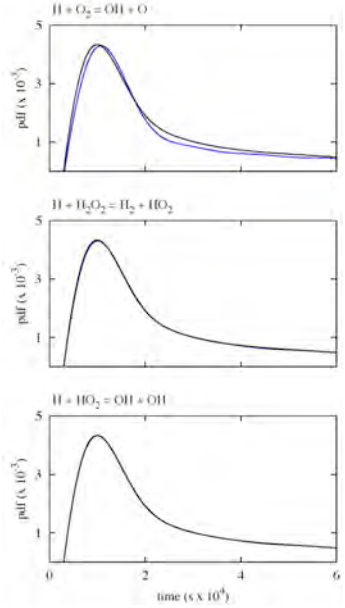

Figure 4. One-reaction (top), two-reaction (middle) and three-reaction (bottom) deconstructions of the ignition delay time pdf for hydrogen oxidation).

Future Plans

Decomposition of the Uncertainty: A Tool for Parallel Updating.

The theoretical validation procedure developed over the last two years is serial, i.e., rate coefficients are updated one at a time for a particular target and for a specific range of initial conditions. We have developed a method for generating parallel updates of the rate coefficients under these same constraints. The parallel updating procedure for a single target at a specific set of initial conditions requires the "decomposition of the uncertainty". The decomposition picks out those reactions that are most likely to become the most sensitive reactions if the current reactions that are most sensitive are updated. The procedure involves a "decomposition" of the hyper-surface describing the response of a specific target to changes in the rate coefficients. Thus, by updating both the most sensitive reactions and those most likely to become sensitive in parallel, the "calendar time" required to theoretically validate the mechanism will be considerably reduced.

Multi-fidelity fitting of sensitivity maps and potential surfaces.

We have used the Gaussian process model to generate sensitivity maps for the analysis of chemical kinetic mechanisms. In collaboration with Miller and Gray (ANL-CNM), as well as Larry Harding, this work is being extended to the calculation of potential energy surfaces. In particular, we have implemented a multi-fidelity version of this procedure, with the different levels of fidelity referring to different levels of electronic structure calculations. We have tested the techniques on the fitting of a portion of a potential energy surface for H + HCO. The results of the initial fitting of potential surfaces in a multi-fidelity fashion is promising, and we intend to pursue this avenue of research more fully in the course of the coming year.

Publications

M. J. Davis and A. S. Tomlin, "Spatial dynamics of steady flames 1. Phase space structure and the dynamics of individual trajectories", J. Phys, Chem. A. **112**, 7768 -7783 (2008).

M. J. Davis and A. S. Tomlin, "Spatial dynamics of steady flames 2. Low-dimensional manifolds and the role of transport processes", J. Phys, Chem. A. **112**, 7784-7805 (2008).

R. T. Skodje, A. S. Tomlin, S. J. Klippenstein, L. B. Harding, and M. J. Davis, "Theoretical validation of chemical-kinetic mechanisms: Combustion of methanol", J. Phys. Chem. A **114**, 8286-8301 (2010).

S. J. Klippenstein, L. B. Harding, M. J. Davis, R. T. Skodje, and A. S. Tomlin, "Uncertainty driven theoretical kinetics studies of CH_3OH ignition: HO_2 + CH_3OH and O_2 + CH_3OH", Proc. Combust. Inst. **33**, 351-357 (2011).

M. J. Davis, R. T. Skodje, and A. S. Tomlin, "Global sensitivity analysis of chemical-kinetic reaction mechanisms: Construction and deconstruction of the probability density function", J. Phys. Chem A **115**, pp 1556–1578 (2011).

R. Sivaramakrishnan, D. Y. Zhou, R. T. Skodje, and M. J. Davis, "A comprehensive mechanism for ethanol combustion", Proceedings of the 7th US National Technical Meeting of the Combustion Institute, Georgia Institute of Technology, Atlanta, GA

PROJECT NARRATIVE

Dynamics of Radical Reactions in Biodiesel Combustion

Theodore S. Dibble
Chemistry Department
SUNY-Environmental Science and Forestry
Syracuse, NY 13210
tsdibble@syr.edu

PROJECT SCOPE

The ignition of diesel fuel depends on isomerization of peroxy radicals (ROO•) via a hydrogen shift reaction:

$$ROO\bullet \rightarrow QOOH \qquad (1)$$

Production of multiple OH radicals (chain branching) in the chemistry following reaction (1) leads to autoignition. Processes such as reaction (2):

$$ROO\bullet \rightarrow Products + HOO \qquad (2)$$

compete with chain branching. Experimentalists face several difficulties in gaining an understanding of this chemistry, and no QOOH species has ever been detected by experiment! This has inspired many computational studies of these processes.

Biodiesel fuel is increasingly being used worldwide. Although we have a fair understanding of the molecular details of the chemistry of peroxy radicals derived from alkanes, biodiesel fuels contain ester and olefin groups which significantly impact the thermodynamics and kinetics of biodiesel ignition.[1] The broader goal of this research is to carry out systematic computational studies of the elementary kinetics of this chemistry for compounds that are models for biodiesel ignition. This includes not only reactions (1) and (2), but also reactions leading to chain branching. In addition, the research will:

- include rigorous treatments of tunneling effects
- quantify the effect of chemically activated processes
- synthesize the results into structure-activity relations (SARs)

RECENT PROGRESS

Tunneling Corrections in Unimolecular Reactions of Peroxy Radicals. Tunneling corrections were investigated for three unimolecular reactions of 1-propylperoxy radical, shown in Scheme 1. These three reactions are prototypes for autoignition reactions in diesel fuel. The goal is to rigorously determine the extent of tunneling and determine which computationally inexpensive tunneling corrections can be used in computational kinetics without significant loss of accuracy.

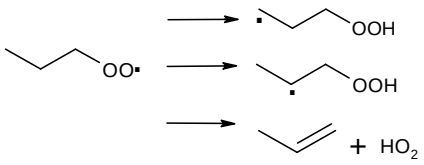

1, 5 H-shift (R1)

1, 4 H-shift (R2)

HO_2 elimination (R3)

Benchmark calculations were carried out at the CCSD(T)/maug-cc-pVTZ [2] //M05-2X/6-311+G(2df,2p) level of theory in GAUSSIAN09[3] To determine accurate barrier heights and reaction energies for each reaction. After testing a number of combinations of DFT methods and basis sets, the M05-2X, B3LYP and B1B95 methods were selected to perform the tunneling calculations for 1,5 H-shift, 1,4 H-shift and HO_2 elimination reactions, respectively. The 6-311+G(2df,2p) basis set was used in all DFT calculations.

Canonical variational transition state theory and small curvature tunneling (SCT) calculations were carried out using the POLYRATE[4] and GAUSSRATE[5] programs. Interpolated variational transition state theory by mapping was used to extend the reaction paths based on small-range straight direct dynamics calculations, which were carried out for -0.5 Å < *s* <0.5 Å with the step size 0.0025 Å, where *s* is the reaction coordinate. The path was extended to -3 Å < *s* < 3 Å with the same step size. A Hessian matrix was calculated every 9 points. The hindered-rotor partition functions were computed using the full torsional eigenvalue summation method[6] based on 10° resolution relaxed scanning of the torsional angle.

High-pressure limiting rate constants were determined for each reaction, and are shown in Figure 1. As expected, the 1,5 H-shift reaction dominates at the lower temperatures. Tunneling correction factors, Γ(T), are depicted in Figure 2. Tunneling corrections are significantly higher

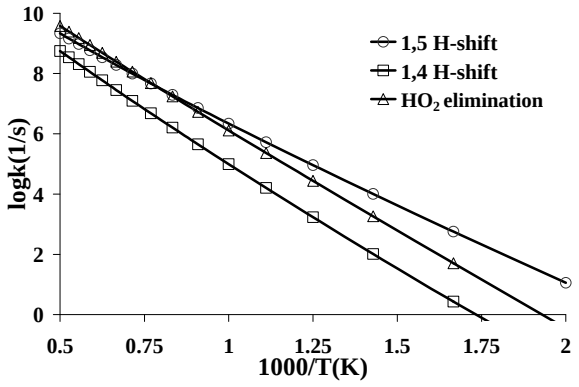

Figure 1. High-pressure limiting rate constants for three reactions of 1-propylperoxy radical.

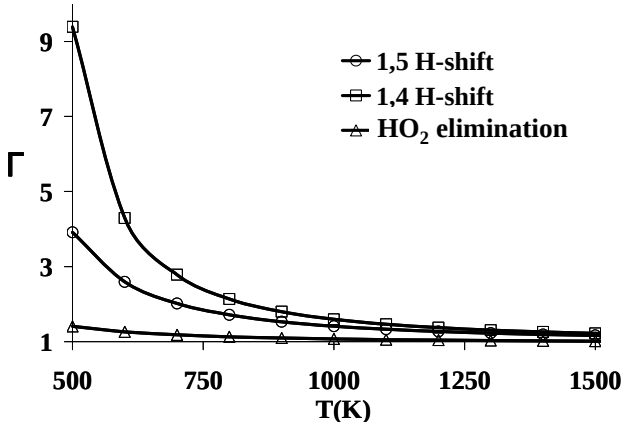

Figure 2. SCT tunneling correction factors, Γ(T), for three reactions of 1-propylperoxy radical.

for the 1,4 H-shift than the 1,5 H-shift reaction. This is consistent with the higher imaginary frequency of the 1,4 H-shift (2172 cm^{-1}) than the 1,5 H-shift (1837 cm^{-1}).

The results of various tunneling treatments were compared; results for the 1,4 H-shift are shown in Figure 3. The Eckart tunneling correction was fairly consistent with the SCT correction, and much better than the Wigner or zero-curvature (ZCT) tunneling models. If these results could be generalized to larger peroxy radical radicals, then one would conclude that the Eckart method is the method of choice.

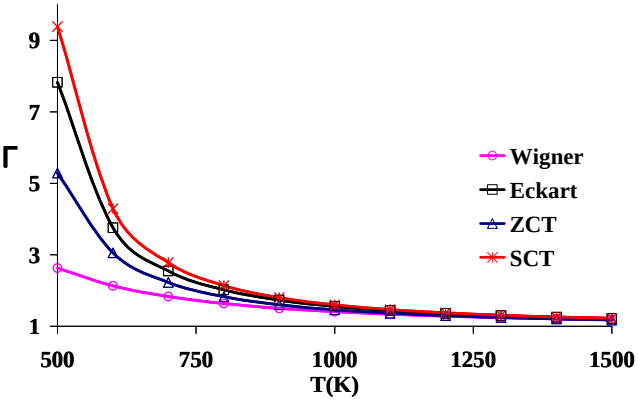

Figure 3. Comparison of tunneling correction factors, Γ(T), for the 1,4 H-shift of 1-propylperoxy radical .

Cis-trans Isomerization of Allylic Radicals and Unimolecular Reactions of the Resulting Peroxy Radicals. Biodiesel fuel is composed largely of fatty acid methyl esters. The fatty acids are composed of long hydrocarbon chains, which are usually unsaturated. These double bonds are almost exclusively in *cis* configurations, whereas gaseous alkenes studied in combustion are mostly *trans*. Bounaceur, et al,[7] argued that the thermal *cis-trans* isomerization was unimportant to the chemistry of small alkenes, but did not consider the chemically activated isomerization. The potential energy profile for production of the 2-butenyl radical ($CH_3CHCHCH_2$) is shown from OH + 2-butene is shown at right. RRKM-Master Equation calculations were carried out with the MultiWell program[8] to determine the fate of chemically activated 2-butenyl radical formed from OH + *trans*-2-butene. In simulations at a range of pressures and temperatures, the *cis* isomer was generally the dominant isomer. Table 1, below, offers a few of those results.

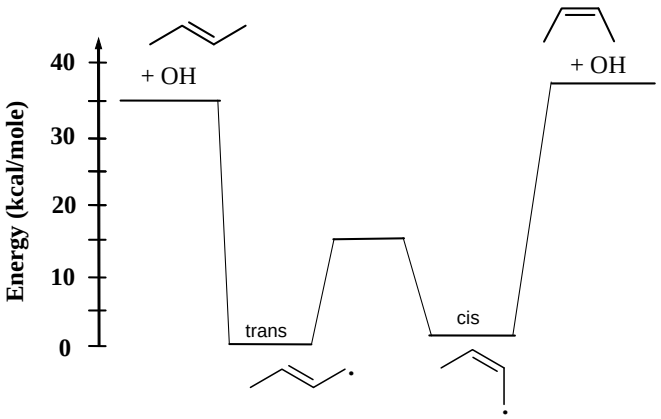

Figure 4. Potential energy profile for 2-butene + OH at M05-2X/6-311+G(2df,2p).

This result is counterintuitive, because it shows that the thermodynamically less stable (at low temperature) isomer is preferred. In this problem, the key factor is the density of states of the two isomers at a range of energies above the isomerization barrier at which the isomerization rate constant becomes slower than quenching. This density of states generally favors the *cis* isomer.

We have carried out DFT calculations on the reactions of the *cis*- and *trans*-but-2-en-1-peroxy radical formed by O_2 addition to C_1 of 2-butenyl radical. This is a larger analog of allyl radical, itself. Allyl radical adds O_2 but the resulting peroxy radical back-dissociates rather than reacting further. The 1,6 H-shift of *cis*-but-2-en-1-peroxy radical may compete with dissociation. CBS-QB3 calculations will be used to refine the relative energies, followed by RRKM/Master Equation calculations to determine if reactions other than dissociation are important. RRKM/Master Equation calculations will be extended to larger (more reactive) analogs.

Method M05-2X/6-311+G(2df,2p) unless specified	**% cis**
300 K, harmonic oscillator	71.7
1500 K, harmonic oscillator	75.0
300 K, anharmonic (through quartic terms)	65.6
300 K harmonic oscillator M06-2X	61.2
300 K harmonic oscillator, B3LYP	64.7

Table 1. Percent production of *cis*-2-butenyl radical upon quenching of chemically activated *trans*-2-butenyl radical produced in reaction with OH. P=1 atm, initial energy =35 kcal/mole.

Autoignition mechanism of methyl butanoate Methyl butanoate (MB) is composed of a methyl ester group and a short alkyl group (see Figure 5). MB oxidation mechanism has been studied as the starting point for understanding biodiesel combustion for a decade.[9] The CBS-QB3 composite method is used to determine reaction energies and activation barriers to reactions of peroxy radicals and the corresponding QOOH species. We include all four peroxy radicals formed subsequent to H-atom abstraction from MB (sites 1-4 in Figure 5). Reactions treated include H-shift and HO_2 elimination of ROO•, and decomposition of QOOH by C-C,

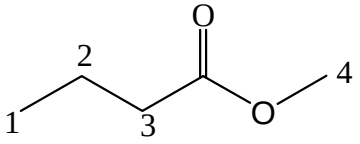

Figure 5. Methyl butanoate

C-O, and O-O scission. Our goal is to compute pressure and temperature dependent rate coefficients in order to test and validate kinetic models of MB autoignition.

Chemically Activated reactions of X• + HOCO. We carried out the first quantum chemical study of the N + HOCO system and RRKM/Master Equation calculations to determine the ultimate products of the reactions N + HOCO and H + HOCO.

FUTURE PLANS

Future work will include examining structure-activity relationships for peroxy radical reactions involving the ester group of model compounds for biodiesel fuel; this complements our recently published work on structure-activity relationships for peroxy radicals with C=C double bonds. The reliability of Eckart tunneling corrections will be investigated in these systems by comparison to SCT. RRKM/Master Equation simulations will be carried out for a wide range of pressures and temperatures to determine rate constants for use in kinetic modeling. .

PUBLICATIONS ACKNOWLEDGING BES SUPPORT 2009-PRESENT

F. Zhang and T. S. Dibble, Effects of ester and olefin functional groups on kinetics of unimolecular reactions of peroxy radicals, **2011**, *115*, 655-663.

T. S. Dibble and Yue Zeng, Potential energy profiles for the N + HOCO reaction and products of the chemically activated reactions N + HOCO and H + HOCO. *Chem. Phys. Letts.*, **2010**, 495 170-174.

REFERENCES

[1] R. Sumathi and W. H. Green, Oxygenate. *Phys. Chem. Chem. Phys*., **2003**, *5*, 3402-17.

[2] E. Papajak, H. R. Leverentz, J. Zheng, and D. G. Truhlar *J. Chem. Theory Comput.* **2009**, *5*, 1197–1202.

[3] M. J. Frisch, et al., Gaussian 09, Revision A.02, Gaussian, Inc., Wallingford CT, 2009.

[4] J. Zheng, S. Zhang, B. J. Lynch, J. C. Corchado, Y.-Y. Chuang, P. L. Fast, W.-P. Hu, Y.-P. Liu, G. C. Lynch, K. A. Nguyen, C. F. Jackels, A. F. Ramos, B. A. Ellingson, V. S. Melissas, J. Villa, I. Rossi, E. L. Coitino, J. Pu, T. V. Albu, R. Steckler, B. C. Garrett, A. D. Isaacson and D. G. Truhlar, POLYRATE-version 2010-A, University of Minnesota, Minneapolis.

[5] J. Zheng, S. Zhang, J. C. Corchado, Y. Chuang, E. L. Coitiño, B. A. Ellingson, and D. G. Truhlar, GAUSSRATE-version 2009-A, University of Minnesota, Minneapolis.

[6] C. Y. Lin, E. I. Izgorodina, M. L. Coote, *J. Phys. Chem. A* **2008**, *112*, 1956-64.

[7] R. Bounaceur, V. Warth, B. Sirjean, P.A. Glaude, R. Fournet, and F. Battin-Leclerc, F. *Proc. Combust. Inst.* **2009**, *32*, 387.

[8] MultiWell-2011, Jan 2011, designed and maintained by J.R. Barker with contributors N.F. Ortiz, J.M. Preses, L.L. Lohr, A. Maranzana, P.J. Stimac, T. L. Nguyen, and T. J. Dhilip Kumar, University of Michigan, Ann Arbor, MI; http://aoss.engin.umich.edu/multiwell/ b) J.R. Barker, *Int. J. Chem. Kinet.*, **2001**, *33*, 232-45. c) J.R. Barker, *Int. J. Chem. Kinet.*, **2009**, *41*, 748-763.

[9] S. Dooley, H. J. Curran, and J. M. Simmie, *Combustion and Flame* **2008**, *153*, 2–32.

Hydrocarbon Radical Thermochemistry: Gas-Phase Ion Chemistry Techniques

Kent M. Ervin
Department of Chemistry and Chemical Physics Program
University of Nevada, Reno
Reno, NV 89557-0216
ervin@unr.edu

I. Program Scope

Gas-phase ion chemistry and mass spectrometry techniques are employed to determine the energetics of hydrocarbon radicals that are important in combustion processes and to investigate the dynamics of ion–molecule reactions. Tandem mass spectrometry is used to measure the activation of endoergic ion-molecule reactions as a function of kinetic energy. Modeling the measured reaction cross sections using statistical rate theory[1] and empirical reaction models allows extraction of reaction threshold energies. These threshold energies yield relative gas-phase acidities, proton affinities, or absolute dissociation energies, which may then be used in thermochemical cycles to derive neutral R–H bond dissociation enthalpies and radical enthalpies of formation.[2] The reactive systems employed in these studies include endoergic bimolecular proton transfer reactions, hydrogen-atom transfer reactions, and collision-induced dissociation of heterodimer complex anions. Electronic structure calculations are used to evaluate the possibility of potential energy barriers or dynamical constrictions along the reaction path, and as input for RRKM and phase space theory calculations. Existing guided ion beam tandem mass spectrometry experiments in the Ervin group are being complemented by development of a Quadrupole Ion Trap/Time-of-Flight tandem mass spectrometer.

II. Recent Progress

A. Energy-Resolved Collision-Induced Dissociation

We continue work to measure gas-phase acidities and other thermochemical properties of oxygen-containing hydrocarbons and of highly unsaturated hydrocarbons that are of interest in combustion kinetic systems. Energy-resolved threshold collision induced dissociation (TCID) is used to measure energetics of ion systems that can be related to neutral hydrocarbon molecules and radicals via thermochemical cycles.

Since the last meeting's report, our guided ion beam tandem mass spectrometer suffered from a fire in the data acquisition computer. The fire did not spread, fortunately, but ancillary damage to some of the detection electronics occurred. As a stop-gap measure the old DOS-based system was reproduced with legacy interface cards, while we are also developing a more modern LabView/USB-based system. The instrument is running again and producing high-quality data.

We are currently completing work[3] on the threshold collision-induced dissociation of peroxyformate anion, $HC(O)OO^-$. Figure 1 shows the threshold fit for the cross section for dissociation to form formate anion, HCO_2^-, with loss of O atom. Using the measured threshold energy and recent measurements[4] of the gas-phase acidity of HCO_3H, we can obtain the first experimental values for the enthalpies of formation of the neutral peroxyformic acid, HCO_3H, and neutral peroxyformyl radical, HC(O)OO, which is an intermediate of combustion interest.

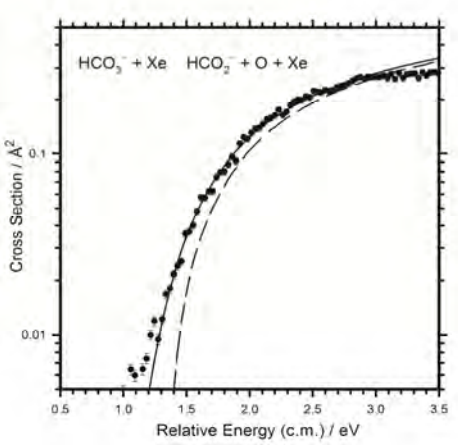

Fig. 1. Cross section and threshold fit for TCID of peroxyformate anion.

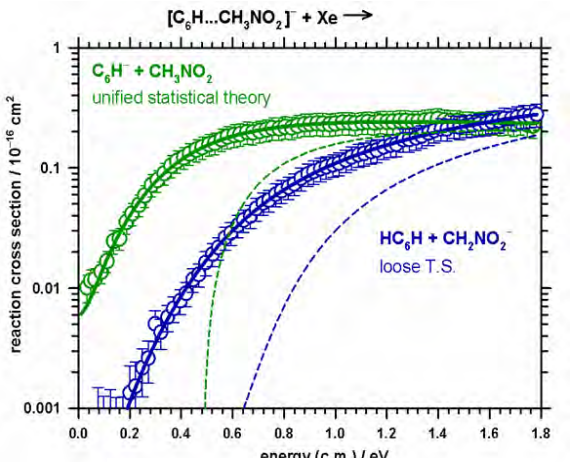

Fig. 2. Potential energy surface for TCID of $HC_6^-(CH_3NO_2)$.

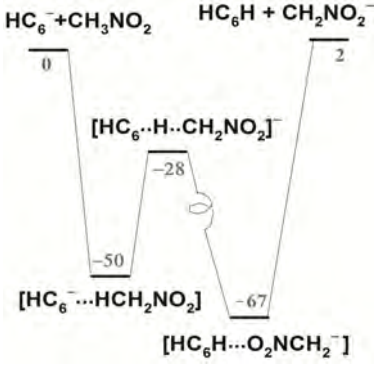

Fig. 3. Potential energy surface for TCID of $HC_6^-(CH_3NO_2)$. B3LYP/ 6-311++G** energies in kJ/mol.

We have also returned to studies of the gas-phase of acidities of polyynes, $HC_{2n}H$ (n=2,3,4), following up on butadiyne (diacetylene) reported previously in our laboratory.[5] Figure 2 shows the cross section and fit for the complex of HC_6^- with nitromethane, undergoing competitive collision-induced dissociation into either $HC_6^- + CH_3NO_2$ (lower threshold) or $HC_6H + CH_2NO_2^-$ (higher threshold) following energy-resolved collisions with xenon target gas. The crossing of the two product channels at higher energies, where the cross-section for the higher-energy channel exceeds that of the lower-energy channel, is evidence of a complex dissociation process. A schematic diagram of the potential energy surface and intermediates is shown in Figure 3. A multiple transition state model (unified statistical theory[6]) of the dissociation process via these intermediates is used to account for the observed behavior and to obtain energetic information.

B. Instrumental Development

Development has continued on a Quadrupole Ion Trap/Time-of-Flight tandem mass spectrometer[7-9] for future ion-molecule reaction kinetics and product velocity distribution measurements. A novel bipolar, short-pulse extraction method[9] has been developed for characterization of the size of the trapped ion cloud in the QIT source. This mode of operation was shown to produce a narrow, well-defined energy distribution of the ion packet. Energy spreads of less than 0.1 eV may be achieved, which will allow high energy resolution in future pulsed ion beam kinetics experiments. Current work on this instrument focuses on a new design for the quadrupole ion trap to improve ion extraction efficiency and the time-of-flight mass resolution.[10] In the conventional design of the quadrupole ion trap with hyperbolic electrodes (which are ideal for radio-frequency trapping and conventional QIT mass spectrometry by resonant ejection), the TOF mass resolution is limited by the spatial extent of the ion cloud because of the curved fields in QIT, which also serves as the first acceleration region of the TOF mass spectrometer. Our new design employs parallel-plate electrodes for a uniform extraction

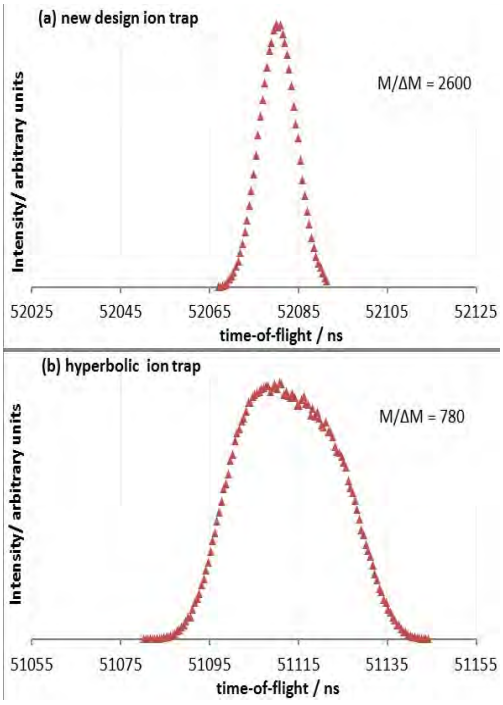

Fig. 4. Comparison of simulated reflectron TOF mass spectrum peaks for QIT designs.

field, with a dual-center-ring electrode design that also maintains good rf trapping. Simulations show that the TOF mass resolution for the new QIT design is limited by the thermal velocity spread of the ions rather than the spatial extent. The velocity spread can be corrected with the reflectron region of the time-of-flight, and is expected to yield a substantial improvement in mass resolution ($M/\Delta M$) from the previous set-up.[9] Figure 4 compares simulated time-of-flight peak profiles for the two designs. A further advantage of the new design is more space for apertures between the two ring electrodes for better ion/laser overlap for photoactivation experiments and a larger collection angle for fluorescence experiments, as compared with the previous design.[7, 8]

C. Franck-Condon Analysis of Photoelectron Spectra

Continuing previous collaborations,[11-14] we have further developed the PESCAL program for Franck-Condon simulations of photoelectron spectra and photodetachment threshold spectra.[15] Minor revisions were implemented in 2009 and 2010. In collaboration with the Carl Lineberger group and Anne McCoy,[16] we have reported the photoelectron spectra and Franck-Condon analyses for CHX_2^- (X=F, Cl, Br, I) anions. The CHX_2^- is pyramidal while the neutral is near-planar. This extreme geometry change causes the standard Franck-Condon simulation using normal mode vibrational eigenvectors in a Cartesian atomic displacement basis to fail utterly. Use of internal coordinates with Wilson FG matrix methods greatly improves the agreement with the experimental band profiles, but the harmonic approximation is still unsatisfactory. Better agreement is obtained using the non-harmonic multidimensional treatment of McCoy.[16] This is a cautionary tale for those using the standard methods and computational geometries to model experiments for systems with large geometry changes. The PESCAL code has become increasingly popular, recently for analysis of photoionization threshold data from synchrotron facilities. Additional citations since 2009 include references17-26.

III. Future Work

Experimental work will continue on the ion thermochemistry experiments detailed above and related work involving proton affinities in cationic systems. In the near term, we plan to extend the work on peroxyformate anion to the similar peroxyacetate system and investigate the thermochemistry of morpholine. We are also further developing our quadrupole ion trap/time-of-flight mass spectrometer apparatus with future applications related to combustion systems.

IV. References

(1) Armentrout, P. B.; Ervin, K. M.; Rodgers, M. T. *J. Phys. Chem. A* **2008**, *112*, 10071.
(2) Ervin, K. M. *Chem. Rev.* **2001**, *101*, 391.
(3) Nickel, A. A.; Lanorio, J. G.; Ervin, K. M. **2010**, (work in progress).
(4) Villano, S. M.; Eyet, N.; Wren, S. W.; Ellison, G. B.; Bierbaum, V. M.; Lineberger, W. C. *J. Phys. Chem. A* **2010**, *114*, 191.

(5) Angel, L.; Ervin, K. *J. Phys. Chem. A* **2001**, *105*, 4042.
(6) Miller, W. H. *J. Chem. Phys.* **1976**, *65*, 2216.
(7) Sassin, N. A.; Everhart, S. C.; Cline, J. I.; Ervin, K. M. *J. Chem. Phys* **2008**, *128*, 234305.
(8) Sassin, N. A.; Everhart, S. C.; Dangi, B. B.; Ervin, K. M.; Cline, J. I. *J. Am. Soc. Mass Spectrom.* **2009**, *20*, 96.
(9) Dangi, B. B.; Sassin, N. A.; Ervin, K. M. *Rev. Sci. Instrum.* **2010**, *81*, 063302.
(10) Dangi, B. B.; Ervin, K. M. **2011**, (manuscript in preparation).
(11) Wren, S. W.; Vogelhuber, K. M.; Ervin, K. M.; Lineberger, W. C. *Phys. Chem. Chem. Phys.* **2009**, *11*, 4745.
(12) Ervin, K. M.; Anusiewicz, I.; Skurski, P.; Simons, J.; Lineberger, W. C. *J. Phys. Chem. A* **2003**, *107*, 8521.
(13) Ervin, K. M.; Ramond, T. M.; Davico, G. E.; Schwartz, R. L.; Casey, S. M.; Lineberger, W. C. *J. Phys. Chem. A.* **2001**, *105*, 10822.
(14) Adams, C. L.; Schneider, H.; Ervin, K.M.; Weber, J.M. *J. Chem. Phys.* **2009**, *130*, 074307.
(15) Ervin, K. M. PESCAL, Fortran program, University of Nevada, Reno, 2010.
(16) Vogelhuber, K. M.; Wren, S. W.; McCoy, A. B.; Ervin, K. M.; Lineberger, W. C. *J. Chem. Phys.* **2011**, (submitted).
(17) Ichino, T.; Villano, S. M.; Gianola, A. J.; Goebbert, D. J.; Velarde, L.; Sanov, A.; Blanksby, S. J.; Zhou, Hrovat, D. A.; Bordern, W. T.; Lineberger, W. C. *J. Phys. Chem. A* **2011**, *115*, 1634.
(18) Vogelhuber, K. M.; Wren, S. W.; Sheps, L.; Lineberger, W. C. *J. Chem. Phys.* **2011**, *134*, 064302.
(19) Wu, X.; Qin, Z.; Xie, H.; Cong, R.; Wu, X.; Tang, Z.; Fan, H. *J. Chem. Phys.* **2010**, *133*, 044303.
(20) Zhou, J.; Takahashi, L. K.; Wilson, K. R.; Leone, S. R.; Ahmed, M. *Anal. Chem.* **2010**, *82*, 3905.
(21) Yacovitch, T. I.; Garand, E.; Neumark, D. M. *J. Phys. Chem. A* **2010**, *114*, 11091.
(22) Yen, T. A.; Garane, E.; Shreve, A. T.; Neumark, D. M. *J. Phys. Chem. A* **2010**, *114*, 3215.
(23) Soorkia, S.; Trevitt, A. J.; Selby, T. M.; Osborn, D. L.; Taatjes, C. A.; Wilson, K. R.; Leone, S. R. *J. Phys. Chem. A* **2010**, *114*, 3340.
(24) Trevitt, A. J.; Goulay, F.; Meloni, G.; Osborn, D. L.; Taatjes, C. A.; Leone, S. R. *Int. J. Mass Spectrom.* **2009**, *280*, 113.
(25) Goulay, F.; Trevitt, A. J.; Meloni, G.; Selby, T. M.; Osborn, D. L.; Taatjes, C. A.; Vereecken, L.; Leone, S. R. *J. Am. Chem. Soc.* **2009**, *131*, 993.
(26) Villalta, P. W.; Leopold, D. G. *J. Chem. Phys.* **2009**, *130*, 024303.

V. Publications supported by this project 2009-2011

1. Adams, C. L.; Schneider, H.; Ervin, K. M.; Weber, J. M. "Low-energy photoelectron imaging spectroscopy of nitromethane anions: Electron affinity, vibrational features, anisotropies and the dipole-bound state", *J. Chem. Phys.* **2009**, *130*, 074307:1-10.

2. S. W. Wren, K. M. Vogelhuber, K. M. Ervin, and W. C. Lineberger, "The photoelectron spectrum of CCl_2^-: The convergence of theory and experiment after a decade of debate", *Phys. Chem. Chem. Phys.* **2009,** *11*, 4745-4753.

3. Dangi, B. B.; Sassin, N. A.; Ervin, K. M. "Pulsed ion extraction diagnostics in a quadrupole ion trap linear time-of-flight mass spectrometer", *Rev. Sci. Instrum.* **2010,** *81*, 063302:1-10.

4. K. M. Ervin, PESCAL, Fortran program for Franck-Condon simulation of photoelectron spectra, *http://wolfweb.unr.edu/~ervin/pes/* (revised 2010).

Spectroscopic and Dynamical Studies
of Highly Energized Small Polyatomic Molecules

Robert W. Field
Massachusetts Institute of Technology
Cambridge, MA 02139
rwfield@mit.edu

I. Program Scope

The fundamental goal of this program is to develop the experimental techniques, diagnostics, interpretive concepts, and pattern-recognition schemes needed to reveal and understand how large-amplitude motions are encoded in the vibration-rotation energy level structure of small, gas-phase, combustion-relevant polyatomic molecules. We are focusing our efforts on unimolecular isomerization in several prototypical systems, including the HNC $\leftrightarrow$ HCN and HCCH $\leftrightarrow$ CCH_2 isomerization systems. We are developing chirped-pulse millimeter wave (CPmmW) spectroscopy as a technique that can be used in conjunction with Stimulated Emission Pumping (SEP) and the Stark effect to populate and identify molecular states with high excitation in *local* vibrational modes, which are of key importance in understanding isomerization processes. In addition, we are attempting to demonstrate the capability of CPmmW spectroscopy to determine the structure of molecular fragmentation transition states by measurement of fragment species/vibrational level populations.

II. Recent Progress

A. CPmmW Spectroscopy

1. Chirped Pulse/Slit jet spectrometer

Chirped-Pulse Millimeter-Wave (CPmmW) spectroscopy is the first truly broadband and high resolution technique for spectroscopy in the millimeter wave region. We designed the technique in collaboration with the Brooks Pate research group at the University of Virginia, based on their pioneering Chirped-Pulse Fourier-Transform Microwave (CP-FTMW) spectrometer, which operates at frequencies up to 20 GHz. We have built and tested a CPmmW spectrometer that operates in the 70–102 GHz frequency range. The spectrometer can acquire up to 12 GHz of spectral bandwidth at better than 100 kHz resolution in a single shot, and initial tests indicate significant advantage over existing millimeter-wave spectrometers in sensitivity times spectral bandwidth. We expect that the slit-jet apparatus we are currently testing and optimizing will increase the sensitivity of our CPmmW experiments by at least a factor of 100, due to increased number density and reduced Doppler profile. Improvements of the CPmmW detection electronics (mmW switches and low noise amplifiers) are expected to yield an additional factor of 10. The sensitivity and accurate relative intensities of the CPmmW technique will translate into new classes of spectral diagnostics that will enable us to attack new regimes of spectral congestion and dynamical complexity in combustion-relevant species.

2. Pyrolysis

Measurement of the nascent vibrational population distribution of unimolecular fragmentation reaction products can reveal reaction mechanisms and quantitative information about their transition states. We have combined our CPmmW spectroscopy with a Peter Chen pyrolysis nozzle to measure the pyrolysis product branching ratios and vibrational population distributions. Spectra of formaldehyde produced by pyrolysis of methyl nitrite

$$CH_3ONO + \Delta \rightarrow [CH_3O] + NO \rightarrow H + CH_2O + NO$$

and of formaldehyde and acetaldehyde produced by pyrolysis of ethyl nitrite

$$CH_3CH_2ONO + \Delta \rightarrow [CH_3CH_2O] + NO \rightarrow H + CH_3CHO + NO \text{ or } H + CH_3 + CH_2O + NO$$

were recorded. Fig. 1a shows the pure rotational CPmmW spectrum of formaldehyde produced by pyrolysis of methyl nitrite. Relative intensities of transitions assigned to the ground and various excited vibrational states

report the mode-specific vibrational temperatures in formaldehyde. Only two of six vibrational modes of formaldehyde are significantly populated in both pyrolysis decomposition reactions as well as in an expansion of pure formaldehyde, suggesting that it is post-nozzle collisional energy transfer that primarily determines the vibrational population distribution. The non-Boltzmann population distribution among the observed vibrational modes demonstrates non-statistical vibrational energy transfer in formaldehyde. This result is in sharp contrast with the equilibrated population distribution that we have measured in OCS and the almost complete vibrational relaxation observed in acetaldehyde.

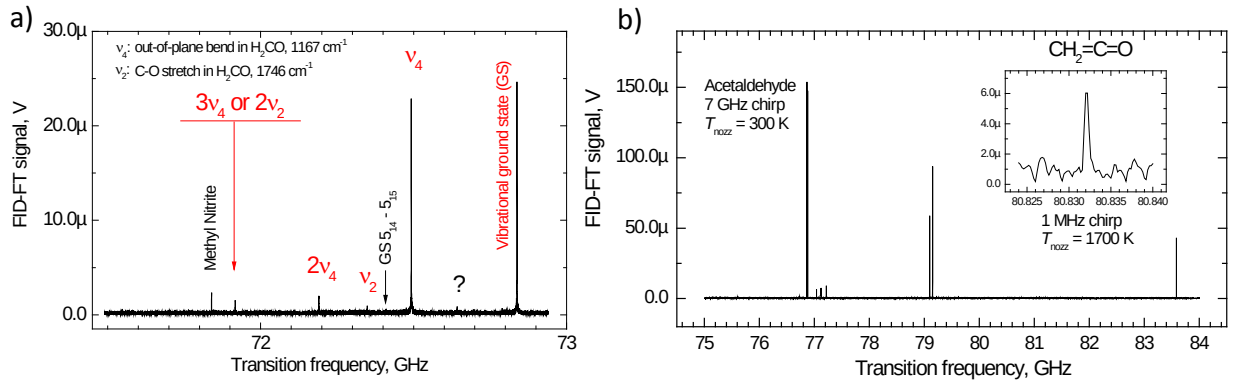

Figure 1: CPmmW pyrolysis experiments. a) Formaldehyde produced by thermal decomposition of methyl nitrite. Several rotational transitions are assigned to formaldehyde molecules in excited vibrational states; b) CPmmW spectrum of acetaldehyde expanded from the heated pyrolysis nozzle. The insert shows a separate measurement in which ketene, produced by thermal cracking of acetaldehyde, was detected.

A new mechanism for thermal cracking of acetaldehyde has been discovered by Ellison and coworkers, who observed ketene as one of acetaldehyde's pyrolysis products in recent experiments. Figure 1b shows ketene produced by pyrolysis of acetaldehyde, as detected by CPmmW. We plan to expand this study by looking at pyrolysis of other aldehydes and additional products in collaboration with the Ellison group.

B. High- and low-barrier unimolecular isomerization in S_0 and S_1 HCCH

The goal of our studies on the acetylene ↔ vinylidene system is to observe barrier-proximal vibrational states. Many studies have demonstrated that the vibrational eigenstates of acetylene and similar molecules undergo a normal-to-local transition in which the normal modes appropriate to describe small displacements from the equilibrium geometry evolve into local modes in which the excitation is isolated in a single C-H bond stretch or ∠CCH bend. The evolution of vibrational character is of particular interest in the acetylene bending system, because the local-bending vibration bears a strong resemblance to the reaction coordinate for isomerization from acetylene to vinylidene, with one hydrogen moving a large distance off of the C-C bond axis while the other hydrogen remains nearly stationary.

1. Observation and theoretical treatment of vibrational levels of S_1 *cis* acetylene

Aside from its utility as an intermediate for studying highly excited vibrational states of the S_0 surface, the S_1 state also presents the possibility of characterizing low-barrier isomerization from its *trans*-geometry minimum to a local minimum at the *cis*-bent geometry. This isomerization has been the focus of many theoretical studies, but it has been difficult to study experimentally because, though the *trans* minimum has been exhaustively characterized, the transition from the ground electronic state to the S_1 *cis* geometry is electronically forbidden and no transitions to this conformer have previously been observed. In the course of characterizing the S_1 surface, several vibrational levels were observed which could not be ascribed to S_1-*trans* or other electronic states. S_1-*cis* seems a likely candidate for explaining these interloper levels, which were, surprisingly, observed below the energy of the calculated barrier to *trans*-*cis* isomerization, and must therefore owe their observed intensity to mixing via tunneling with *trans*-geometry-localized states.

We are now confident that these puzzling aspects of the S_1-S_0 spectrum are manifestations of the *cis*-*trans* isomerization. Measurements of the $^{13}C^{12}CH_2$ and $^{13}C_2H_2$ isotope shifts of the "extra" bands,

in conjunction with *ab initio* calculations, demonstrate that these "extra" levels constitute the first direct observation of the *cis* conformer. Reduced dimension DVR calculations show that the unusual anharmonic behavior of the stretch-bend combination polyads is a consequence of the double minimum in the PES (Figure 2). The unexpected and rapid decrease in the effective vibrational frequencies indicates the approach to the transition state and is reproduced surprisingly well by the reduced dimension calculation. The calculations also confirm our *cis* conformer vibrational assignments. Most importantly, they provide insight into the interaction mechanism between levels of the two conformers and the universal spectroscopic signature for such nonsymmetric isomerizations.

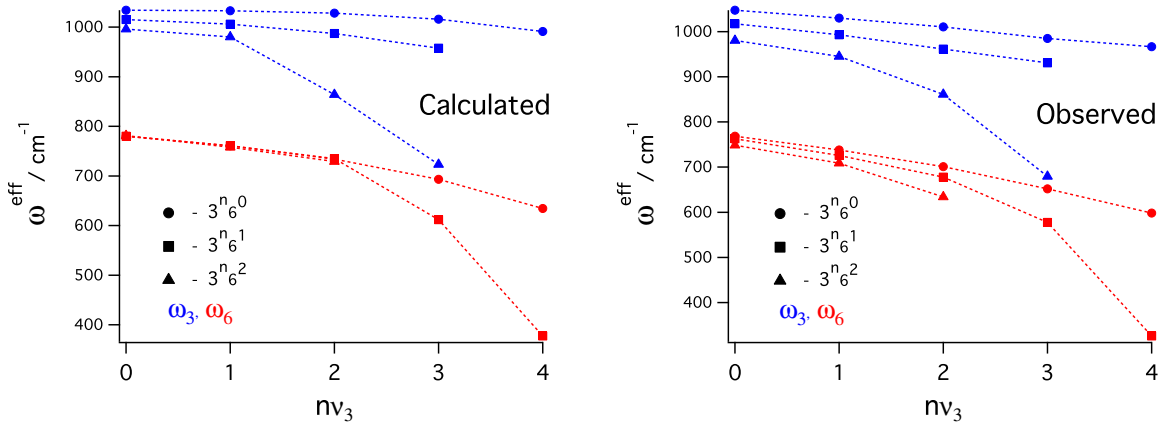

Figure 2: Plots of ω_3^{eff} (*trans*-bend) and ω_6^{eff} (*cis*-bend) vs. v_3 derived from the observed and calculated S_1 level structure. Different marker styles denote data from different values of v_6. Deperturbed values for T_0 are used, except for the 3^36^2 and 3^46^2 levels, which have not yet been deperturbed. (In those cases the energies of the observed $J = K = 0$ states are used instead.)

Our current goal is to consolidate what is known about the S_1 state into a fit model that reproduces the observed spectra with a parsimonious set of parameters. To that end we have recorded new even higher sensitivity LIF spectra of the most troublesome region near the transition state energy, which is fraught with predissociation, pattern-breaking and poor Franck-Condon factors, but contains vital information about the isomerization dynamics. Many new bands have been revealed, including several members of the families of large amplitude motion eigenstates with wavefunctions localized along the minimum energy isomerization path. We have also calculated high-level full-dimensional *ab initio* anharmonic force fields for both *trans*- and *cis*-bent conformers to guide the development of the global model.

Important new insights into the predissociation mechanism on the S_1 state have been revealed by our recent spectra. Our new data includes lifetime measurements of every state observed in the one photon spectrum spanning from just below the predissociation threshold to >1000 cm^{-1} above it. We intend to perform tunable photolysis experiments to combine data on lifetime variation due to parent molecule rovibrational character with CPmmW analysis of the vibrational distribution in the C_2H photofragment.

III. Future Work

We expect to achieve a >100-fold improvement of the signal:background ratio of our CPmmW spectrometer by taking advantage of new millimeter-wave technology and by use of a custom designed slit-jet molecular beam chamber. These enhancements will enable us to measure the populations of vibrationally-excited photolysis and pyrolysis products and locate additional acetylene local-bender vibrational states. The combination of our S_1 DVR results with the high resolution/survey capability of CPmmW/DF spectra will guide us towards conclusive SEP expriments. We will record Stark effect spectra of the S_0 highly vibrationally excited levels, in order to measure the large predicted vibrationally-averaged dipole moments of the local-bender barrier-proximal states and to use these measured dipole moments as a measure of progress along the large amplitude local-bender isomerization coordinate. CPmmW measurements of product state distributions will allow us to extract information about transition states for fragmentation and photodissociation.

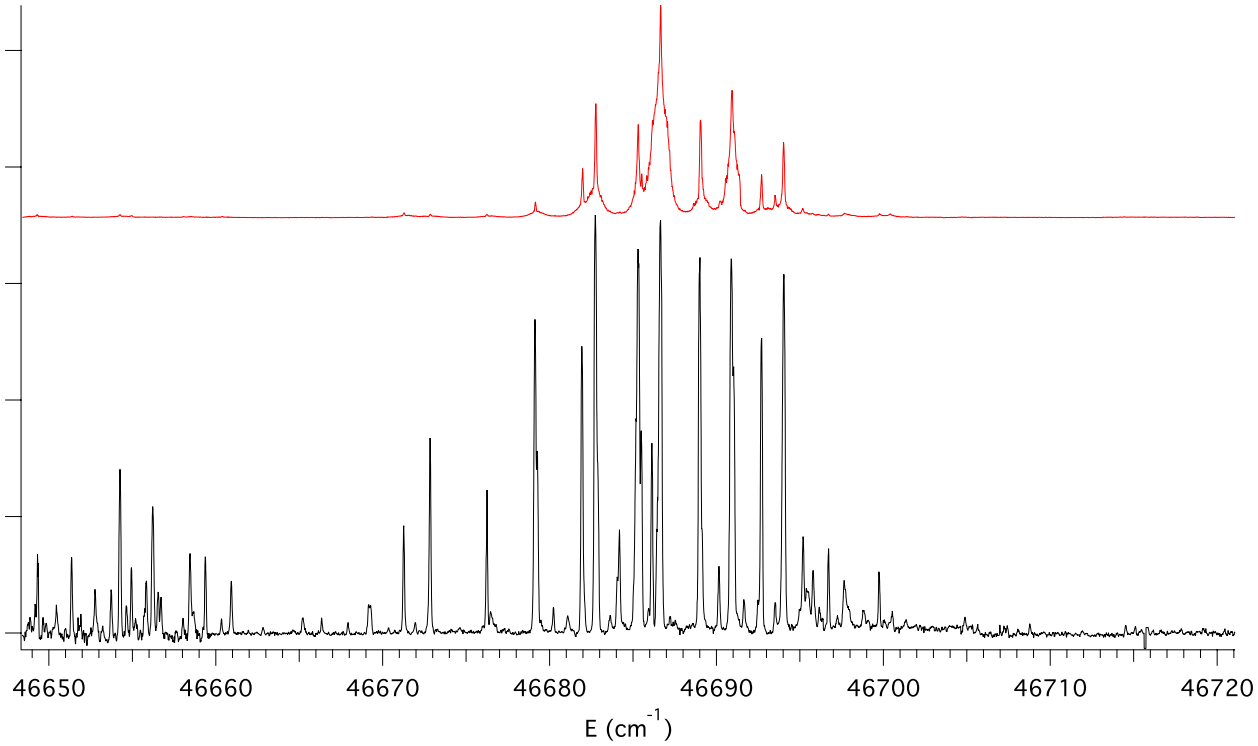

Figure 3: Comparison of new C_2H_2 LIF spectra (lower trace, black) with previous spectra (upper trace, red) in the region of the $2^1 3^3$ vibrational state. This corresponds to an increase in signal to background ratio by a factor of at least 10 for severely predissociated states and decreased linewidth by a factor of 3.

Publications supported by this project 2009–2011

[1] A. J. Merer, Z. Duan, R. W. Field, and J. K. G. Watson. Perturbations in the $4\nu_3$ level of $\tilde{A}\ ^1A_u$ state of acetylene, C_2H_2. *Canadian Journal of Physics*, 87(5):437–441, 2009.

[2] A. H. Steeves, H. A. Bechtel, A. J. Merer, N. Yamakita, S. Tsuchiya, and R. W. Field. Stretch-bend combination polyads in the $\tilde{A}\ ^1A_u$ state of acetylene, C_2H_2. *Journal of Molecular Spectroscopy*, 256(2):256–278, 2009.

[3] G. B. Park, Adam H. Steeves, Kirill Kuyanov, and Robert W. Field. Design and evaluation of a pulsed-jet chirped-pulse millimeter wave spectrometer for the 70-100 GHz region. *Journal of Chemical Physics*, 2011, submitted.

[4] Joshua H. Baraban, Annelise R. Beck, Adam H. Steeves, John F. Stanton, and Robert W. Field. Reduced Dimension DVR Study of *cis-trans* Isomerization in the S_1 State of C_2H_2. *Journal of Chemical Physics*, 2011, accepted.

[5] Anthony J. Merer, Adam H. Steeves, Joshua H. Baraban, Hans A. Bechtel, and Robert W. Field. *cis-trans* isomerism in the S_1 state of acetylene; identification of *cis*-well vibrational levels. *Journal of Chemical Physics*, 2011, submitted.

[6] Joshua H. Baraban, John F. Stanton, and Robert W. Field. Full dimensional Anharmonic Force Fields for *cis* and *trans* S_1 C_2H_2. *Journal of Chemical Physics*, 2011, in preparation.

Scanning Tunneling Microscopy Studies of Chemical Reactions on Surfaces

George Flynn, Department of Chemistry, Columbia University
Mail Stop 3109, 3000 Broadway, New York, New York 10027
gwf1@columbia.edu

Introduction:

Our work is focused on fundamental chemical events taking place on carbon surfaces[1,2] with the intent of shedding light on their role in mediating the formation of polycyclic aromatic hydrocarbons (PAHs) from small molecular precursors and the growth of soot particles.[3-7] For the past two years this effort has been focused on the chemical behavior of graphene[8] (a single graphite carbon sheet). We have now mastered the necessary preparation techniques that allow us to form graphene on insulators (silicon dioxide and mica) and metals (cobalt and copper). When compared to graphite, graphene constitutes a better laboratory model for mimicking the behavior of soot. First, the surface of graphene is not stabilized by the presence of multiple carbon sheets; second, it is relatively easy to form graphene flakes of different size on the nanoscale. For these small flakes (which are close in size to small soot particles or large PAHs) quantum confinement of electrons in the delocalized graphene aromatic π orbitals produces significant variations in electronic structure with changes in the size and shape of the nano-flakes. We have, for example, produced nano-particles of graphene by vacuum evaporating hexabenzocoronene onto the surface of a cobalt crystal followed by annealing at high temperature. The chemistry of these flakes is certain to be a sensitive function of their electronic structure. Indeed, we have already shown that graphene is more easily oxidized than graphite. In addition the mechanisms for the reaction of these two species with O_2 are quite distinct. At moderate temperatures reaction of oxygen with single sheet graphene takes place on the basal plane without the need for defects or step edges, but multi-sheet graphene and graphite react only at defect sites.

Scanning tunneling microscopy (STM) is the main probe technique that we use to study the interfacial structure and chemistry of graphene mainly because of its ability to investigate surface structure and dynamics with molecular or even atomic resolution. Scanning tunneling spectroscopy (STS), which measures the local density of quantum states over a single atom, provides information about the electronic structure of graphene and graphite. In addition we employ micro-Raman scattering to identify and distinguish among single, double and triple layered graphene samples and to assess the amount of electron or hole "doping" caused by surface adsorbates. Atomic force microscopy (AFM) is also employed to determine the large scale "flatness" of graphene on different substrates.

Results: Mechanism for Oxidation of Graphene

As noted above, we have shown that graphene on SiO_2 is oxidized at lower temperatures than either graphite or multi-layer graphene. Based on the distribution of holes etched in the graphene surface by O_2, it is clear that the mechanism for oxidizing graphene is different from that for oxidizing graphite. In particular, single sheet graphene is etched even in the absence of pit defects or step edges. The mechanism for this oxidation process, in particular the formation

of any precursor species that lead to reaction, is likely to be of importance in the oxidation of soot particles. We have performed an extensive set of experiments to identify critical aspects of this oxidation mechanism.

Using micro-Raman spectroscopy and scanning tunneling microscopy, we investigated the relationship between structural distortion and electrical hole doping (charge transfer) of graphene on a silicon dioxide substrate. Ambient STM images taken at room temperature were used to investigate annealing-induced changes in graphene morphology. To avoid contamination from resist residues, we used a shadow mask method, instead of the conventional electron beam lithography technique, to pattern electrodes on graphene. Atomically resolved images were observed on both the initial, directly deposited (exfoliated) samples, and on samples subjected to thermal annealing.

Raman spectroscopy is a sensitive, non-contact diagnostic for graphene crystalline quality and electrical doping. The Raman G band upshift from 1580 cm^{-1} is widely interpreted as a measure of carrier doping. Actually the G band can upshift due either to the application of compressive strain, or to electrical doping. Using environment-controlled in-situ Raman spectroscopy measurements, we have shown that the observed upshift in both initially exfoliated and annealed graphene is principally due to O_2 induced hole-doping rather than in-plane compressive strain.

To assess the effect of SiO_2 substrates on the annealing-induced hole doping, freestanding graphene suspended in ambient across a micro-trench in the SiO_2 was studied. The freestanding area of a double layer graphene sheet can be distinguished from the supported area in optical images of the surface. The Raman shift frequency, ω_G, of the initial exfoliated sample was the same for the freestanding region and the supported region. Following annealing at 300 ^oC in an Ar/O_2 atmosphere, however, the supported region showed a large upshift of 6±1 cm^{-1} while ω_G for the freestanding region was essentially unchanged. This result indicates that the SiO_2 substrate plays an essential role in the O_2-induced hole doping observed upon annealing. Oxygen doping does not occur for either initial or annealed freestanding graphene, which is consistent with substrate effects in carbon nanotubes and graphene.

This investigation establishes the origin of the upshift in the Raman G band as charge doping. Two independent factors control the doping: (1) the degree of graphene coupling to the substrate, and (2) exposure to oxygen and moisture. Thermal annealing induces a pronounced structural distortion due to close coupling to SiO_2 and activates the ability of diatomic oxygen to accept charge from graphene. Gas flow experiments show that dry oxygen reversibly dopes graphene; doping becomes stronger and more irreversible in the presence of moisture and over long periods of time. We believe that oxygen molecular anions are stabilized by water solvation and electrostatic binding to the silicon dioxide surface.

Present and Future Experimental Program

It should be possible to probe oxidation of graphene grown on a clean copper surface in an ultra-high vacuum chamber at temperatures ranging from 300-800 K. We have successfully grown graphene on a copper crystal using

ethylene as the precursor gas. This chemical system will provide an opportunity to test the importance of metal atoms in mediating the reactivity of graphene, and should give us some clues to the chemistry of soot particles. Interest in soot is ultimately driven by the environmental and health implications arising from its formation in combustion reactions (particularly those involving heavier, diesel fuels containing catalytic metal atoms[9-11]), which are nearly ubiquitous throughout our society.[3-7] Graphene is more tightly coupled to copper than to SiO_2, which suggests that the metal will affect the chemistry in a significant way. It is likely that copper will transfer electrons to graphene (negative doping). This will potentially open up a new mechanism for graphene oxidation. We will also investigate the chemistry of graphene on copper that has been doped with nitrogen atoms incorporated into the graphene lattice. (These samples are prepared by dosing copper at elevated temperatures with a mixture of ethylene and ammonia.) By using STM to monitor both N and C atom sites on the surface, we should be able to follow the oxidation chemistry with atomic resolution.

References

1. Li Liu, Kwang Taeg Rim, Daejin Eom, Tony Heinz, and George W. Flynn "Direct Observation of Atomic Scale Graphitic Layer Growth," Nanoletters, 8, 1872-1878 (2008)
2. Li Liu, Sunmin Ryu, Michelle R. Tomasik, Elena Stolyarova, Naeyoung Jung, Mark S. Hybertsen, Michael L. Steigerwald, Louis E. Brus, George W. Flynn, "Graphene Oxidation: Thickness-Dependent Etching and Strong Chemical Doping", Nanoletters, 8, 1965-1970 (2008)
3. J. A. Miller and G. A. Fisk, "Combustion Chemistry", Chem. & Eng. News, 65 (35), 22-46, August 31, 1987
4. Russell Whitesides, Dominik Domin, Romelia Salomon-Ferrer, William A. Lester, Jr., Michael Frenklach, "Graphene Layer Growth Chemistry: Five- and Six-Member Ring Flip Reaction", Journal of Physical Chemistry A, 112, 2125-2130 (2008)
5. Laszlo Nemes, Anna M. Keszler, Christian G. Parigger, James O. Hornkohl, Hope A. Michelsen, Vadim Stakhursky, "Spontaneous emission from the C3 radical in carbon plasma", Applied Optics, 46, 4032-4040 (2007)
6. H. A. Michelsen, M. A. Linne, B. F. Kock, M. Hofmann, B. Tribalet, C. Schulz, "Modeling laser-induced incandescence of soot: enthalpy changes during sublimation, conduction, and oxidation", Applied Physics B: Lasers and Optics, 93, 645-656 (2008)
7. H. A. Michelsen, "Derivation of a temperature-dependent accommodation coefficient for use in modeling laser-induced incandescence of soot", Applied Physics B: Lasers and Optics, 94, 103-117 (2009)
8. K. S. Novoselov, D. Jiang, F. Schedin, T. J. Booth, V. V. Khotkevich, S. V. Morozov, A. K. Geim", "Two-dimensional atomic crystals", Proc. Nat'l Acad. of Sci. of the U.S. 102, 10451-10453 (2005)
9. Kwang Taeg Rim, Mohamed Siaj, Shengxiong Xiao, Matthew Myers, Vincent D. Carpentier, Li Liu, Chaochin Su, Michael L. Steigerwald, Mark S. Hybertsen, Peter H. McBreen, George W. Flynn, and Colin Nuckolls**,**

Forming Aromatic Hemispheres on Transition Metal Surfaces, Angew. Chem. Int. Ed. 46, 7891-7895 (2007)
10. Daejin Eom, Deborah Prezzi, Kwang T. Rim, Hui Zhou, Michael Lefenfeld, Colin Nuckolls, Mark S. Hybertsen, Tony F. Heinz, and George W. Flynn, "Structure and Electronic Properties of Epitaxial Graphene on Co(0001)", Nanoletters, 9, 2844-2848 (2009)
11. R. Rosei, M. De Crescenzi, F. Sette, C. Quaresima, A. Savoia, and P. Perfetti, "Structure of graphitic carbon on Ni(111): A surface extended-energy-loss fine-structure study" Phys. Rev. B 28, 1161-1164 (1983).

DOE Publications: (2009-2011)

1. E. Stolyarova, D. Stolyarov, K. Bolotin, S. Ryu, L. Liu, M. Klima, M. Hybertsen, I. Pogorelsky, I. Pavlishin, K. Kusche, J. Hone, P. Kim, L. Brus, H. L. Stormer, V. Yakimenko, G. Flynn, "Observation of Graphene Bubbles and Effective Mass Transport Under Graphene Films", Nanoletters, 9, 332-337 (2009)
2. Daejin Eom, Deborah Prezzi, Kwang T. Rim, Hui Zhou, Michael Lefenfeld, Colin Nuckolls, Mark S. Hybertsen, Tony F. Heinz, and George W. Flynn, "Structure and Electronic Properties of Epitaxial Graphene on Co(0001)", Nanoletters, 9, 2844-2848 (2009)
3. Kwang Taeg Rim, Daejin Eom, Li Liu, Elena Stolyarova, Joan Marie Raitano, Siu-Wei Chan, Maria Flytzani-Stephanopoulos, and George W. Flynn, "Charging and Chemical Reactivity of Gold Nanoparticles and Adatoms on the (111) Surface of Single Crystal Magnetite: A Scanning Tunneling Microscopy/Spectroscopy Study", J. Phys. Chem. C, 113, 10198-10205 (2009)
4. Chun Hung Lui, Li Liu, Kin Fai Mak, George W. Flynn, and Tony F. Heinz, "Ultraflat Graphene", Nature, 462, 339-342 (2009)
5. E. Stolyarova, K. Rim, K. Douglass, D. Eom, R. Opila, T. Heinz, A. V. Teplyakov, G. W. Flynn, "STM and XPS Studies of Graphene Films Prepared by Sonication-Assisted Dispersion", accepted for publication
6. Liuyan Zhao, Kwang Taeg Rim, Hui Zhou, Rui He, Tony F. Heinz, Aron Pinczuk, George W. Flynn, Abhay N. Pasupathy, "The atomic-scale growth of monolayer graphene on single-crystal copper substrates", submitted for publication
7. L. Zhao, R. He, K. T. Rim, K. S. Kim, H. Zhou, C. Gutiérrez, S. Chockalingam, C. Arguello, T. F. Heinz, P. Kim, A. Pinczuk, G. W. Flynn, A. N. Pasupathy, "Visualizing Individual Nitrogen Dopants in Monolayer Graphene", submitted for publication
8. Kwang Taeg Rim, Daejin Eom, Siu-Wai Chan, Maria Flytzani-Stephanopoulos, and George W. Flynn, "Scanning tunneling microscopy study of water adsorption on the reduced surface of a natural single Hematite α-Fe_2O_3 crystal", in preparation

Quantitative Imaging Diagnostics for Reacting Flows

Jonathan H. Frank
Combustion Research Facility
Sandia National Laboratories
Livermore, CA 94551-0969
jhfrank@sandia.gov

Program Scope

The primary objective of this project is the development and application of quantitative laser-based imaging diagnostics for studying the interactions of fluid dynamics and chemical reactions in reacting flows. Imaging diagnostics provide temporally and spatially resolved measurements of species, temperature, and velocity distributions over a wide range of length scales. Multi-dimensional measurements are necessary to determine spatial correlations, scalar and velocity gradients, flame orientation, curvature, and connectivity. Current efforts in the Advanced Imaging Laboratory focus on planar laser-induced fluorescence and laser Rayleigh scattering techniques for probing the detailed structure of both isolated flow-flame interactions and turbulent flames. The investigation of flow-flame interactions is of fundamental importance in understanding the coupling between transport and chemistry in turbulent flames. These studies require the development of imaging diagnostic techniques to measure key species in the hydrocarbon-chemistry mechanism as well as to image rates of reaction and dissipation. Recent advances in diagnostic capabilities enable us to probe the temporal evolution of turbulent flames as well.

Recent Progress

Development of a new mixture fraction imaging technique

We are developing a new mixing diagnostic technique using a noble gas as a chemically inert tracer that can be seeded into reacting flows. Of the noble gases, krypton and xenon are the primary contenders for LIF imaging in combustion environments since they have electronic transitions that can be accessed by two-photon excitation in the UV using commercially available lasers. However, krypton has the advantage of lower cost and atomic weight. A chemically inert tracer is, by definition, a conserved scalar and is only subject to passive mixing. Mixture fraction can be determined by combining measurements of the inert tracer concentration and temperature. We demonstrated the feasibility of two-photon LIF imaging of krypton seeded into turbulent jet flames in collaboration with N. Clemens (UT Austin). Krypton was excited from the ground state to the $5p[3/2]_2$ state using 215 nm laser radiation, and the fluorescence decay to the metastable state, $5s[3/2]_2$, was detected at 760 nm. Mixture fraction and temperature measurements were performed using simultaneous imaging of krypton LIF and laser Rayleigh scattering. Single-shot krypton LIF and Rayleigh scattering images were analyzed in an iterative routine to determine mixture fraction and temperature on a pixel-by-pixel basis. Sample results are shown in Fig. 1a. Measurements of the temperature- and species-dependent quenching rates for Kr LIF are incorporated into this routine. Initial quenching rate measurements for the major combustion species in methane flames were performed in collaboration with R. Farrow and T. Settersten (Sandia). Future quenching measurements will span a wider range of temperatures and species.

We demonstrated the mixture fraction imaging technique in two turbulent jet flames: a piloted CH_4/air flame (Sandia flame D) and a $CH_4/H_2/N_2$ flame (DLR-B flame). These flames are well-documented and enabled an evaluation of krypton as a tracer in different fuel mixtures with varying degrees of differential diffusion. The resulting average radial profiles of mixture fraction and temperature for both flames agree well with results of Raman/Rayleigh scattering measurements from Sandia's Turbulent Combustion Laboratory. Fig. 1b shows a comparison of mean radial profiles for flame D.

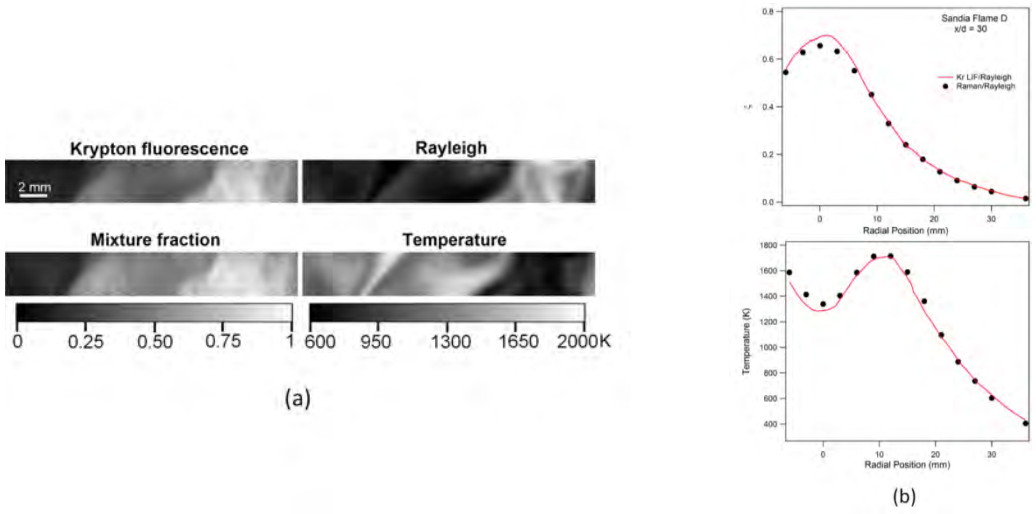

Fig. 1. (a) Single-shot two-photon krypton LIF and laser Rayleigh scattering images from Sandia flame D (top row). Resulting mixture fraction and temperature measurements (bottom row), (b) Comparisons of mean mixture fraction and temperature profiles measured using krypton LIF and laser Rayleigh scattering with previous single-point Raman/Rayleigh scattering measurements.

The use of a noble gas as a chemically inert tracer has potential applications for mixing studies in a broad range of combustion environments. Most previous mixture fraction imaging techniques have used combined measurements of chemically reactive species and temperature to construct a conserved scalar. The advantage of this new approach is that the tracer gas remains chemically inert in a wide range of conditions. We plan to refine this diagnostic technique for other flame conditions and fuel mixtures.

Effects of spatial averaging on dissipation measurements

We have studied the effects of spatial resolution on imaging measurements of dissipation rates in turbulent jet flames and non-reacting jets. Quantitative measurements of dissipation rates require detailed understanding of the effects of spatial averaging due to finite resolution. For planar imaging, the resolution within the plane of the measurement is determined by the optical transfer function of the imaging system, while the out-of-plane resolution is determined by the thickness of the laser sheet. Gradients of temperature and mixture fraction were measured using high-resolution laser Rayleigh scattering imaging. The effective resolution was then degraded by either increasing the laser sheet thickness or spatially filtering the measured signal within the imaging plane.

The effects of spatial resolution on measured power spectral densities (PSD) of axial temperature and mixture fraction gradients were studied in jet flames and non-reacting propane jets, respectively. In Fig. 2, the degradation of the PSDs in the flame caused by increasing the laser sheet thickness is compared to that resulting from reduced in-plane (radial and axial) resolution. The out-of-plane resolution has the smallest effect on the measured PSDs, and the effect of radial resolution is more pronounced. The attenuation of the PSD is far more significant when the axial resolution is reduced because this corresponds to the direction of differentiation. Similar results were obtained in the non-reacting jet experiments. We have modelled the effects of spatial averaging in the differentiated and non-differentiated directions to derive a new criterion for optimizing resolution of dissipation measurements.

Effects of equivalence ratio on extinction of turbulent premixed counterflow flames

Studies on the local perturbation of reaction rates by turbulence in premixed counterflow flames have continued in collaboration with A. Gomez and M. Smooke (Yale Univ.). We measured the effects of the hot product stoichiometry on the structure of turbulent premixed flames under conditions of stable

burning and localized extinction. A turbulent jet of lean-to-stoichiometric premixed reactants at a turbulent Reynolds number on the order of 1,000 was opposed to a stream of hot products of combustion that were generated in a preburner. The composition of the preburner products was varied while maintaining a constant temperature. The structure of the turbulent flame oxidation layer was analyzed using simultaneous CO-LIF and OH-LIF measurements. The rate of CO oxidation was reduced when the flame front approached the turbulent mixing layer of counterflowing reactants and preburner products. The local CO+OH reaction rate was readily quenched by combustion products from stoichiometric flames. In contrast, flame stability was enhanced by combustion products from lean flames. Results provide new insight into effects of stratification between combustion reactants and products, which occurs in practical combustion devices as a result of turbulent mixing.

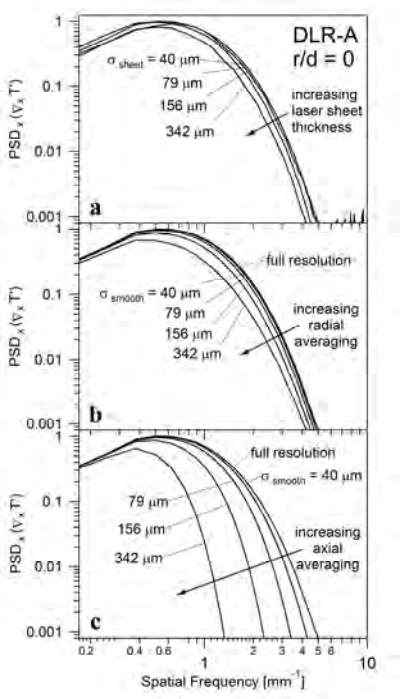

Fig. 2. Power spectral densities of axial temperature gradients for different resolution degradation in the three probe dimensions. Measurements from a turbulent jet flame (DLR-A) at x/d = 10, r/d = 0. Degradation: (a) increasing laser-sheet thickness, (b) 1-D radial smoothing, (c) 1-D axial smoothing. Spectra are normalized by their respective peak values at the full resolution.

Future Plans

The continued development of a high-repetition rate imaging facility with simultaneous scalar and velocity measurements remains an essential goal of our research plan. As new capabilities are added, we will use them to study the dynamics of flow-flame interactions in turbulent premixed, non-premixed, and stratified modes of combustion. Our efforts to build this capability at Sandia will continue to be enhanced through collaborations with other laboratories that have invested in high-repetition rate imaging equipment.

We plan to continue companion experimental and computational studies of the coupling between transport and chemistry in isolated flow-flame interactions in collaboration with J. Chen (Sandia). We are investigating the ability of different chemical mechanisms and transport models to capture the wide range of thermochemical states involved in extinction and re-ignition. Ongoing studies focus on oxygenated fuels, such as dimethyl ether.

We will continue studies of turbulent stratified combustion in which premixed flames propagate into inhomogeneous mixtures of fuel and oxidizer. Despite its practical significance, stratified combustion has been studied in much less detail than perfectly premixed or non-premixed combustion. These studies will be performed in collaboration with experimental and computational groups from Technical University of Darmstadt, Cambridge University, and Sandia.

We plan to explore new combustion diagnostic techniques using soft x-rays at the Advanced Light Source synchrotron of LBNL in collaboration with D. Osborn (Sandia) and H. Bluhm (LBNL). X-ray diagnostics promise advantages over traditional methods of probing combustion species with visible and UV radiation. First, x-ray absorption is not subject to temperature-dependent variations in Boltzmann fraction populations. Second, core-level spectroscopy can be used to probe all carbon containing molecules. Initial studies will focus on tomographic reconstruction of carbon concentration profiles from x-ray absorption measurements in steady laminar flames.

BES-Supported Publications (2009-present)

- C.S. Yoo, J.H. Chen, and J.H. Frank, "A numerical study of transient ignition and flame characteristics of diluted hydrogen versus heated air in counterflow," *Combust. Flame* **156**, 140-151 (2009).
- S. Schlachter, A.D. Elder, A. Esposito, G.S. Kaminski, J.H. Frank, L.K. van Geest, and C.F. Kaminski, "mhFLIM: Resolution of heterogeneous fluorescence decays in widefield lifetime microscopy," *Opt. Express* 17:1557-1570 (2009)
- U.D. Lee, C.S. Yoo, J.H. Chen, J.H. Frank, "Effects of H_2O and NO on extinction and re-ignition of vortex-perturbed hydrogen counterflow flames," *Proc. Combust. Inst.* **32**, 1059-1066 (2009).
- E.R. Hawkes, R. Sankaran, J.H. Chen, S.A. Kaiser, J.H. Frank, "An analysis of lower-dimensional approximations to the scalar dissipation rate using direct numerical simulations of plane jet flames," *Proc. Combust. Inst.* **32**, 1455-1463 (2009).
- W.D. Kulatilaka, J.H. Frank, T.B. Settersten, "Interference-free two-photon LIF imaging of atomic hydrogen in flames using picosecond excitation," *Proc. Combust. Inst.* **32**, 955-962 (2009).
- S.A. Kaiser and J.H. Frank, "Spatial scales of extinction and dissipation in the near field of non-premixed turbulent jet flames," *Proc. Combust. Inst.* **32**, 1639-1646 (2009).
- W. D. Kulatilaka, J. H. Frank, B. D. Patterson, and T. B. Settersten, "Analysis of 205-nm photolytic production of atomic hydrogen in methane flames," *Appl. Phys. B* **97**, 227-242 (2009).
- J.H. Frank and R. S. Barlow, "Nonpremixed turbulent combustion," in *Combustion Phenomena: Selected Mechanisms of Flame Formation, Propagation, and Extinction*, J. Jarosinski and B. Veyssiere, Eds., CRC Press, 2009, pp. 153-162.
- A.D. Elder, C.F. Kaminski, and J.H. Frank, "ϕ^2FLIM: a technique for alias-free frequency domain fluorescence lifetime imaging," *Opt. Express* **17**, 23181-23203 (2009).
- U.D. Lee, C.S. Yoo, J.H. Chen, J.H. Frank, "Effect of NO on extinction and re-ignition of vortex-perturbed hydrogen flames," *Combust. Flame* **157**, 217-229 (2010).
- J.H. Frank and S.A. Kaiser, "High-resolution imaging of turbulence structures in jet flames and non-reacting jets with laser Rayleigh scattering," *Exp. Fluids* **49**, 823-837 (2010).
- J.H. Frank, S.A. Kaiser, J.C. Oefelein, "Analysis of scalar mixing dynamics in LES using high-resolution imaging of laser Rayleigh scattering in turbulent non-reacting jets and non-premixed jet flames," *Proc. Combust. Inst.* **33**, 1373-1381 (2011).
- A.G. Hsu, V. Narayanaswamy, N.T. Clemens, J.H. Frank, "Mixture fraction imaging in turbulent non-premixed flames with two-photon LIF of krypton," *Proc. Combust. Inst.* **33**, 759-766 (2011).
- B. Böhm, J.H. Frank, A. Dreizler, "Temperature and mixing field measurements in stratified lean premixed turbulent flames," *Proc. Combust. Inst.* **33**, 1583-1590 (2011).
- A.M. Steinberg, I. Boxx, C.M. Arndt, J.H. Frank, W. Meier, "Experimental study of flame-hole re-ignition mechanism in a turbulent non-premixed jet flame using sustained multi-kHz PIV and crossed-plane OH PLIF," *Proc. Combust. Inst.* **33**, 1663-1672 (2011).
- B. Coriton, J.H. Frank, A.G. Hsu, M.D. Smooke, A. Gomez, "Effect of quenching of the oxidation layer in highly turbulent counterflow premixed flames," *Proc. Combust. Inst.* **33**, 1647-1654 (2011).
- S.A. Kaiser and J.H. Frank, "The effects of laser-sheet thickness on dissipation measurements in turbulent non-reacting jets and jet flames," *Meas. Sci. Technol.***, 22**, 045403 (2011).

MECHANISM AND DETAILED MODELING OF SOOT FORMATION

Principal Investigator: Michael Frenklach

Department of Mechanical Engineering
The University of California
Berkeley, CA 94720-1740
Phone: (510) 643-1676; E-mail: myf@me.berkeley.edu

Project Scope: Soot formation is one of the key environmental problems associated with the operation of practical combustion devices. Mechanistic understanding of the phenomenon has advanced significantly in recent years, shifting the focus of discussion from conceptual possibilities to specifics of the reaction kinetics. However, along with the success of initial models comes the realization of their shortcomings. This project focuses on fundamental aspects of physical and chemical phenomena critical to the development of predictive models of soot formation in the combustion of hydrocarbon fuels, as well as on computational techniques for the development of predictive reaction models and their economical application to CFD simulations. The work includes theoretical and numerical studies of gas-phase chemistry of gaseous soot particle precursors, soot particle surface processes, particle aggregation into fractal objects, development of economical numerical approaches to reaction kinetics, and construction of a framework for predictive models and modeling.

Recent Progress:

Patterns of Local Aromaticity in Graphene Oxyradicals (with D.Y. Zubarev, X. You, J. McClean, and W.A. Lester, Jr.)

During the past several years, we turned our attention to soot oxidation. As the first step in this direction we have examined the thermodynamic stability of critical oxygenated intermediates. The initial analysis of local electronic structure of a series of pentacene oxyradicals showed that the relative stability of linear polyaromatic hydrocarbons (PAH) can be explained by fragmentation of the delocalized π-electron system of the precursor molecule and formation of locally aromatic fragments ([9] in the publication list). During the past year, we completed investigation of relative stability of oxyradicals of two-dimensional PAH substrates ([13] in the publication list).

Two families of PAH oxyradicals were investigated using density functional theory (DFT) and the semi-empirical PM6 method. These families result from the edge oxidation of substrates that involve only zigzag edges and those that include both zigzag and armchair edges. Oxyradical stability was shown to correlate with an average harmonic oscillator measure of aromaticity (HOMA) and with the distribution of HOMA values in the molecule, as shown in the figure on the right. The results of our calculations showed that an O atom chemisorbed at the PAH edge has a non-local effect on the PAH structure and leads to distinguishable types of HOMA patterns that are common for both families of PAHs.

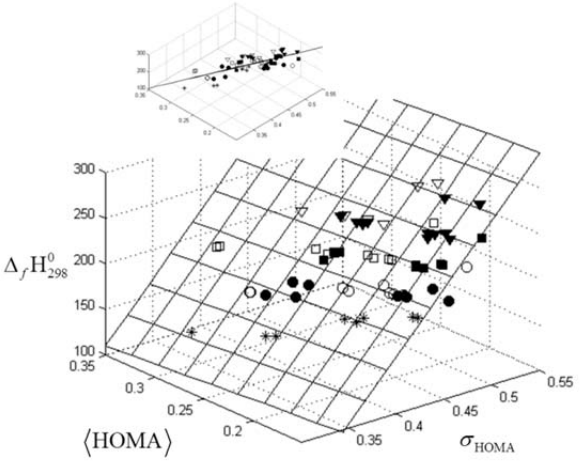

Thermal Decomposition of Pentacene Oxyradicals (with X. You, D.Y. Zubarev, and W.A. Lester, Jr.)

Oxidation of aromatic precursor molecules and soot particle surfaces is an important process. In practical combustion devices, like diesel engines, it is the oxidation of formed soot particles that determines the levels of carbon particulates in the exhaust. Following our supposition that soot particle surface can be represented on a molecular scale as a graphene edge and considering the results of oxidation studies on small-size aromatics leads to a conclusion that one of the key intermediates in the path of oxidation should be graphene-edge oxyradicals. Upon completion of the analysis of the thermodynamic stability of graphene oxyradicals, as described in the preceding section, we turned our attention to the kinetics of their decomposition.

Following our prior thermodynamics studies, we selected pentacene as a substrate and examined decomposition of its oxyradicals, those shown in the figure on the right, with the oxygen atom chemisorbed at four different positions. For comparison with literature, we also included decomposition of phenoxy, whose kinetics has been studied both experimentally and theoretically in the past.

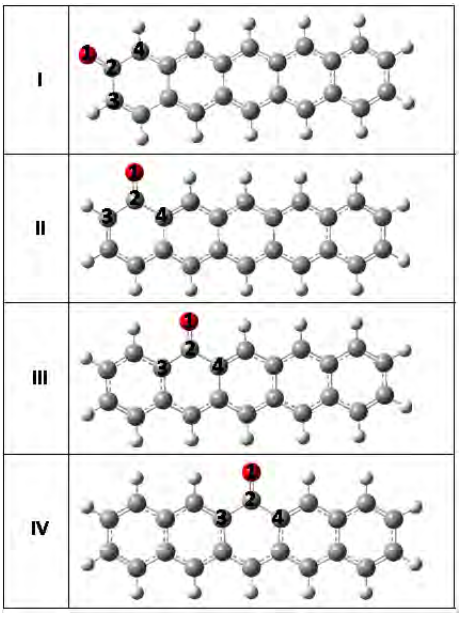

The potential energy surfaces of the decomposition reaction systems were explored using density functional theory (DFT). Specifically, geometry optimization and vibrational frequency calculations were performed for all the stationary points on the reaction pathways using the B3LYP hybrid functional and the 6-311G(d,p) basis set. Zero-point energies and vibrational frequencies were scaled by a factor of 0.96747. Through inspection of the normal modes of the corresponding imaginary frequencies, transition states were confirmed to connect the reactant and product species.

The rate coefficients of the thermally-activated reaction systems were examined using the MultiWell suite of codes. The input parameters including reaction barriers, vibrational frequencies, and moments of inertia were taken from the DFT calculations. Reaction rates were computed over a wide range of conditions, i.e., temperatures ranging from 1000 to 2500 K and pressures from 0.01 to 100 atm. For each run, 10^5 to 10^6 stochastic trials were performed to minimize statistical errors. The rate coefficient of thermal decomposition was derived from the onset of the decay of the reactant radical.

The preliminary results are as follows. Examination of potential energy surfaces revealed that the decomposition pathways of pentacene oxyradicals I and II to generate CO are very similar to that of the phenoxy radical, through a cyclization mechanism involving formation of a bicyclic intermediate followed by C-C bond cleavage and elimination of CO. In contrast, no bicyclic intermediates could be found for pentacene oxyradicals III and IV. Another possible ring-opening pathway, by breaking the C2-C3 or C2-C4 bond (the substrate bonds of the edge CO, see the figure), requires a substantially larger activation energy, thus diminishing its contribution at combustion conditions. On the basis of these results we conclude that oxyradicals III and IV are unlikely to undergo the same oxidation pathways as I and II.

Our computed rate coefficients for phenoxy agreed well with the experimental measurements. The pressure dependence of the decomposition rate of the pentacene oxyradicals was found to be negligible. Pentacene oxyradical I, with oxygen bonded to an outer ring and with free edges on both sides of the C-O bond, structurally most closely resembles the phenoxy radical. Its unimolecular decomposition rate was computed to be comparable to that of the phenoxy radical. The decomposition rate of oxyradical II, with

oxygen bonded to an outer ring and with a free edge on one side and a zigzag edge on the other side of the C-O bond, was computed to be about one order of magnitude lower than that of oxyradical I in the temperature range of 1000-2500 K. The decomposition of radicals III and IV is expected to be much slower (the analysis is in progress).

Combined with the results from the thermodynamic study, which showed that oxyradicals III and IV are significantly more stable than I and II, we conclude that oxidation of graphene zigzag edges at combustion conditions will occur preferentially at the outer rings, with the inner rings resisting oxidation.

Uncertainty-quantified analysis of complex systems: A case of Advanced Light Source flame experiments (with D.R. Yeates, W. Li, P.R. Westmoreland, T. Russi, and A. Packard)

There is an increasing need to make chemical reaction models and modeling more predictive. In a collaborative study with Phillip Westmoreland's group, we demonstrated the approach of predictive model building, Data Collaboration, with raw experimental data and a premixed laminar flame model by means of an Instrumental Model. In Data Collaboration, a data-centric approach to uncertainty quantification, model and data are equal partners. The methodology enables us to quantify what is meant by "model predicts the data".

The subject of analysis was a stoichiometric $C_2H_2/O_2/Ar$ premixed laminar flame mapped with VUV-photoionization molecular-beam mass spectrometry at the Advanced Light Source facilities of Lawrence Berkeley National Laboratory. The experimental signals were modeled with a premixed laminar flame code augmented with an Instrumental Model, designed to link raw signals to derived properties. The model was shown to be quantifiably consistent with data, and hence can be further applied to predicting properties. As specific examples, the prediction of an unmeasured property, background water vapor, was quantified and error bounds for weak-signal properties, O, OH, and C_2H_3, were computed. Bringing more data into the analysis can eliminate further assumptions and tighten model and prediction uncertainties. The impact factors produced by Data Collaboration reveal where the main effort for improving model and prediction uncertainties should be placed, which in the present case suggested improving target uncertainties.

Predictive Modeling of Hydrogen Combustion (with X. You and A. Packard)

To develop reliably predictive reaction models for complex systems requires integration of large amounts of theoretical, computational, and experimental data collected by numerous researchers and often from different disciplines. The integration entails assessment of the consistency of the data, validation of models, and quantification of uncertainties for model predictions. The problem complexity and the volume and heterogeneity of the data call for a system approach.

Process Informatics (PrIMe, http://primekinetics.org) is such a new data-centric system framework to predictive chemical reaction models and modeling. PrIMe aims at the development of a cyber-based infrastructure for organization of scientific data and applications that facilitate collaborative research in collecting, assembling, modeling, and transforming data into knowledge. PrIMe is composed of two principal constituents: a data depository and a collection of tools. Prior efforts during the past several years were devoted to building PrIMe Data Models, digitizing reaction-model and experimental data (PrIMe Warehouse), building the integrating infrastructure (PrIMe Workflow), and developing the scientific methodology of predictive modeling (Data Collaboration). During the past year, we focused on the development of tools, interfaces, and additional data models, enabling and automating the Data Collaboration methodology within the PrIMe infrastructure. The underlying scientific aim of the development is to foster a new approach to predictive modeling. As a specific platform to illustrate the ideas and methodology, we focus on a scientifically challenging problem: reliable modeling of hydrogen combustion.

Future Plans

Graphene Layer Growth and Oxidation Chemistry: We will continue exploration of reactions on graphene edges. One of the immediate goals is to investigate oxidation of PAH arm-chair sites. The work will be performed in collaboration with William Lester's group, performing DFT analysis of the reaction systems and then QMC analysis on most critical reaction steps identified in the prior DFT studies. For every reaction system, a complete set of rate coefficients will be established with master-equation solutions.

Graphene Layer Evolution: We will continue exploration of the evolution of graphene sheets through our detailed KMC approach, by inclusion of additional reaction steps as they become available and by extending the simulation conditions and constrains.

Methodology of Predictive Models and Modeling: We will continue collaborative studies with Phillip Westmoreland's group and his colleagues on the development and automation of the UQ-based framework of ALS data analysis. We will continue the efforts on building the PrIMe framework for predictive modeling of hydrogen combustion.

DOE-BES Supported Publications (2009-2011)

1. "Embedded-ring migration on graphene zigzag edge," R. Whitesides, D. Domin, W. A. Lester Jr., and M. Frenklach, *Proc. Combust. Inst.* **32**, 577 (2009).
2. "Molecular dynamics simulations of PAH dimerization," D. Wong, R. Whitesides, C. A. Schuetz and M. Frenklach, in *Combustion Generated Fine Carbon Particles* (H. Bockhorn, A. D'Anna, A. F. Sarofim, H. Wang, Eds.), Karlsruhe University Press, Karlsruhe, Germany, 2009, p. 245.
3. "Modeling particle dynamics with MOMIC," M. Frenklach, in *Modeling and Computation of Nanoparticles in* Fluid Flows, Lecture Series of van Karman Institute for Fluid Mechanics, Paper 2, 2009, http://www.rta.nato.int/Pubs/RDP.asp?RDP=RTO-EN-AVT-169.
4. "Modeling particle aggregation," M. Frenklach, in *Modeling and Computation of Nanoparticles in Fluid Flows*, Lecture Series of van Karman Institute for Fluid Mechanics, Paper 5, 2009, http://www.rta.nato.int/Pubs/RDP.asp?RDP=RTO-EN-AVT-169.
5. "Modeling nanoparticle formation," M. Frenklach and R. Whitesides, in *Modeling and Computation of Nanoparticles in Fluid Flows*, Lecture Series of van Karman Institute for Fluid Mechanics, Paper 7, 2009, http://www.rta.nato.int/Pubs/RDP.asp?RDP=RTO-EN-AVT-169.
6. "A new graphene edge surface kinetics model," R. Whitesides and M. Frenklach, *Proceedings of the 6th U.S. National Combustion Meeting*, Ann Arbor, MI, May 17-19, 2009.
7. "Time integration of chemical kinetics with computational singular perturbation and tabulation," B. Debusschere, B. Rhoads, H. Najm, Y. Marzouk, M. Valorani, D. Goussis, and M. Frenklach, Fall Meeting of the Western States Section of the Combustion Institute, Irvine, CA, October 26-27, 2009.
8. "Detailed kinetic Monte-Carlo simulations of graphene-edge growth," R. Whitesides and M. Frenklach, *J. Phys. Chem. A* **114**, 689-703 (2010), Feature Article.
9. "Local electronic structure and stability of pentacene oxyradicals," D. Y. Zubarev, N. Robertson, D. Domin, J. McClean, J. Wang, W.A. Lester, Jr., R. Whitesides, X. You, and M. Frenklach, *J. Phys. Chem. C* **114**, 5429 (2010).
10. "Extended simulations of graphene growth with updated rate coefficients," R. Whitesides, X. You, and M. Frenklach, Spring Technical Meeting, Western States Section of the Combustion Institute, Boulder, CO, March 22-23, 2010, Paper No. 10S-22.
11. "A diffusion Monte Carlo study of the O-H bond dissociation of phenol," J. Wang, D. Domin, B. Austin, D. Zubarev, J. McClean, M. Frenklach, T. Cui, and W. A. Lester, Jr., *J. Phys. Chem. A* **114**, 9832-9835 (2010).
12. "Bay-capping reactions: Kinetics and influence on graphene-edge growth," X. You, R. Whitesides, D. Zubarev, W. A. Lester, Jr., and M. Frenklach, *Proc. Combust. Inst*. **33**, 685-692 (2011).
13. "Patterns of local aromaticity in graphene oxyradicals," D. Yu. Zubarev, X. You, J. McClean, W. A. Lester, Jr., and M. Frenklach, *J. Mater. Chem.* **21**, 3404-3409 (2011).

Computer-Aided Construction of Chemical Kinetic Models

William H. Green
Department of Chemical Engineering, M.I.T.
Cambridge, MA 02139
whgreen@mit.edu

I. Program Scope

The combustion chemistry of even simple fuels can be extremely complex, involving hundreds or thousands of kinetically significant species. The most reasonable way to deal with this complexity is to use a computer not only to numerically solve the kinetic model, but also to construct the kinetic model in the first place. Because these large models contain so many numerical parameters (e.g. rate coefficients, thermochemistry) one never has sufficient data to uniquely determine them all experimentally. Instead one must work in "predictive" mode, using theoretical values for many of the numbers in the model, and as appropriate refining the most sensitive numbers through experiments. Predictive chemical kinetics is exactly what is needed for computer-aided design of combustion systems based on proposed alternative fuels, particularly for early assessment of the value and viability of proposed new fuels. Our research effort is aimed at making accurate predictive chemical kinetics practical; this is a challenging goal which necessarily includes a range of science advances. Our research spans a wide range from quantum chemical calculations on individual molecules and elementary-step reactions, through the development of improved rate/thermo estimation procedures, the creation of algorithms and software for constructing and solving the simulations, the invention of methods for model-reduction while maintaining error control, through comparisons with experiment. Many of the parameters in the models are derived from quantum chemistry, and the models are compared with experimental data measured in our lab or in collaboration with others.

II. Recent Progress

A. Methodology for Computer-Aided Kinetic Modeling

The main focus of our research continues to be the development of methodology for constructing, reducing, and solving combustion simulations. In February, 2011 we released Reaction Mechanism Generator (RMG) version 3.3, which builds a reaction mechanism valid at a set of user-specified conditions (initial composition, pressure, temperature, timescale). The new software also works for liquid-phase reactions (e.g. in fuel droplets), using a variety of methods to estimate the largest solvent effects on thermochemistry and rate coefficients.

The growing mechanism is automatically pruned (reduced) during the construction process to reduce memory usage while maintaining accuracy; this pruning now includes automatic pruning of chemically-activated reaction networks. The software automatically identifies and computes the rates of chemically-activated and other formally-direct reactions using several methods for converting the master equations into phenomenological rate coefficients. An interesting paper comparing several methods for computing phenomenological rate coefficients k(T,P) has been submitted to PCCP[15].

We have distributed the mechanism construction software to several research groups. In the past year researchers from Belgium, France, Germany, and Canada have visited our group for training in how to use the software. Several researchers from US national labs and universities are arranging similar training visits for the coming year.

We continue to make progress in automated mechanism reduction, to facilitate the use of detailed fuel chemistry models in reacting flow simulations. Our current model reduction work supported by this program is focused on clarifying the mathematical relationships between competing model-reduction methods, providing an equal basis for comparisons between different methods. This research was presented at the International Conference on Numerical Combustion in April 2011, and is now being prepared for journal publication.

We also continue to improve the chemistry solvers to make it practical to work with and test the very large chemistry models required to accurately model real fuel behavior. We have developed a strained flame solver which can handle much larger reaction mechanisms than the CHEMKIN solvers PREMIX and OPPDIFF can. With separate funding we have leveraged our model-reduction work supported by this BES grant by implementing error-controlled adaptive chemistry model-reduction into the practical engine CFD simulator KIVA. We have also ported VODE and DASAC to run efficiently on graphical processor units (GPUs).[i] The combination of adaptive chemistry and GPU solvers has increased the speed of solution of engine simulations using very large biodiesel reaction mechanism by more than 3 orders of magnitude, making it practical to run these simulations on a PC.[ii]

B. Quantum Calculations of Reaction Rates

We have focused this year on the reactions of allylic radicals, which accumulate in many combustion systems, with HO2 and O2. We presented our detailed study of allyl + HO2, an important reaction in preignition chemistry, at the International Combustion Symposium in August 2010.[12] The main product is allyloxy, so we also studied the decomposition of this radical. At the US National Combustion meeting in March 2011, we presented calculations on substituted allylic radicals plus O2 considering dozens of isomerization – dissociation channels for the unsaturated peroxyl radicals formed. The barriers for intramolecular H abstraction across the double bond were lower than literature expectations, but at combustion-relevant temperatures all the isomerizations were unimportant relative to the very fast reverse reaction back to an allylic radical + O2.[13]

C. Large Kinetic Models

We have applied the computer-aided modeling tools developed by this project to several systems, leveraging funding from other sources. We have developed detailed models of the combustion and pyrolysis chemistry of all four isomers of butanol with funding from the DOE Combustion Energy Frontier Research Center (CEFRC); this model has been extensively tested against experimental data.[iii,iv] We developed methods for on-the-fly computation of thermochemistry with Gaussian during kinetic model construction, and tested them in building a model for JP-10 combustion.[11] We have recently expanded the capability of RMG to include organosulfur compound pyrolysis.

III. Future Work

A. Methodology and Rate Estimation

Most of the difficulty in predictive kinetics has to do with estimating the thousands of rate coefficients involved. We are developing more robust group-additivity methods for making initial estimates on new systems, and extensively revising and improving the estimates for reactions of aromatics and of NOx / RNOx species.

B. Individual Reactions: Quantum Chemistry

We rely extensively on quantum chemistry calculations to improve the rate estimates. We are currently working on reactions of cyclopentadiene and cyclopentadienyl, on disproportionation reactions (in collaboration with P. Piecuch), on phenyl addition to C3 species (in collaboration with A. Mebel and R. Kaiser), and on peroxy chemistry of ketones and alchohols. We expect to do work on NOx and RONOx reactions, organosulfur reactions, and reactions of aromatics in the coming year as we expand our rate estimation database.

In the course of developing large kinetic models this year, we have identified more than 100 rate coefficients in the literature which significantly differ from the RMG estimates, indicating that either the RMG estimate or the literature values (or both) are incorrect. We have recently resolved two dozen of these discrepancies with the help of quantum chemistry. After writing up this work, we plan to address the other identified discrepancies.

C. Large Kinetic Models

We have initiated a (separately funded) collaboration with Craig Taatjes to develop models for new biofuels, including ketones and unsaturated alcohols. After we have improved the NOx / RNOx rate estimates, we will develop a detailed model for how cetane improvers affect ignition chemistry.

IV. References

i. Yu Shi, William H. Green, Hsi-Wu Wong, and Oluwayemisi O. Oluwole, "Redesigning Combustion Modeling Algorithms for the Graphics Processing Unit (GPU): Chemical Kinetic Rate Evaluation and Ordinary Differential Equation Integration", *Combustion & Flame* (2011, in press).

ii. Yu Shi, O.O. Oluwole, H.-W. Wong, & W.H. Green, "A multi-approach algorithm for enabling efficient application of very large, highly detailed reaction mechanisms in multi-dimensional HCCI engine simulations", *7th US National Technical Meeting of the Combustion Institute*, 2G08 (2011).

iii. N. Hansen, M.R. Harper, & W. H. Green, "High-Temperature Oxidation Chemistry of *n*-Butanol in Low-Pressure Premixed Flames", *7th US National Technical Meeting of the Combustion Institute*, paper 1B09 (2011).

iv. Michael R. Harper, Kevin M. Van Geem, Steven P. Pyl, Guy B. Marin, and William H. Green, "Comprehensive Reaction Mechanism for n-Butanol Pyrolysis and Combustion", *Combustion & Flame* **158**, 16-41 (2010); Erratum, *ibid.* (2011, in press)

V. Publications and submitted journal articles supported by this project 2009-2011

1. C. Franklin Goldsmith, Huzeifa Ismail, Paul R. Abel, and William H. Green, "Pressure and Temperature Dependence of the Reaction of Vinyl Radical with Alkenes II: Measured Rates and Predicted Product Distributions for Vinyl + Propene", *Proc. Combust. Inst.* **32**, 139-148 (2009).
2. M.A. Singer and W.H. Green, "Using adaptive proper orthogonal decomposition to solve the reaction-diffusion equation", *Appl. Num. Math.* **59**, 272 (2009).
3. H. Ismail, P.R. Abel, W.H. Green, A. Fahr, L. Jusinski, A. Knepp, J. Zador, G. Meloni, T. Selby, D. Osborn, and C.A. Taatjes, "Temperature-Dependent Kinetics of the Vinyl Radical (C_2H_3) Self-Reaction", *J. Phys. Chem. A* **113**, 1278-1286 (2009).
4. R.H. West, M.R. Harper, W.H. Green, "21st-Century Kinetics: Quantitative Predictions from First Principles", *Proceedings of the 8th World Congress of Chemical Engineering*, 0242 (2009).
5. Sandeep Sharma and William H. Green, "Formation of Styrene from propargyl and cyclo-pentadienyl", *Proceedings of the 6th US National Combustion meeting*, Ann Arbor, 22E3 (2009).
6. Sandeep Sharma and William H. Green, "Computed rate coefficients and product yields for C_5H_5 + CH_3 = products", *Journal of Physical Chemistry A* **113**, 8871-8882 (2009).
7. C. Franklin Goldsmith, Huzeifa Ismail, and William H. Green, "Pressure and Temperature Dependence of the Reaction of Vinyl Radical with Alkenes III: Measured Rates and Predicted Product Distributions for Vinyl + Butene", *J. Phys. Chem. A* **113**, 13357-13371 (2009).
8. Amrit Jalan, Robert Ashcraft, Richard H. West, and William H. Green, "Predicting Solvation Energies for Kinetic Modeling", *Ann. Rep.Progress of Chemistry, Section C*, **106**, 1-49 (2010).
9. Sandeep Sharma, Michael R. Harper, and William H. Green, "Modeling of 1,3-hexadiene, 2,4-hexadiene and 1,4-hexadiene doped methane flames: Flame modeling, Benzene and Styrene formation", *Combustion & Flame* **157**, 1331-1345 (2010).
10. Sandeep Sharma, Sumathy Raman, and William H. Green, "Intramolecular Hydrogen Migration in Alkylperoxy and Hydroperoxyalkylperoxy Radicals: Accurate Treatment of Hindered Rotors", *J. Phys. Chem. A* **114**, 5689-5701 (2010).
11. G.R. Magoon, W.H. Green, O.O. Oluwole, H.-W. Wong, S.E. Albo and D.K. Lewis, "Updating Our Understanding of JP-10 Decomposition Chemistry: A Detailed JP-10 Combustion Mechanism Constructed Using RMG – an Automatic Reaction Mechanism Generator", 46th AIAA/ASME/ SAE/ASEE Joint Propulsion Conference (2010); *AIAA* 2010-6825

12. C.F. Goldsmith, S.J. Klippenstein, and W.H. Green, “Theoretical rate coefficients for allyl + HO_2 and allyloxy decomposition”, *Proc. Combust. Inst.* **33**(1), 273-282 (2011).
13. J.D. Mo, E. Kosovich, H.-H. Carstensen, W.H. Green, and A.M. Dean, “Thermodynamic properties and kinetic parameters of reactions involving O_2 + substituted allylic radicals”, *7th US National Technical Meeting of the Combustion Institute*, paper 1A05 (2011).
14. R.H. West, C.F. Goldsmith, M.R. Harper, W.H. Green, L. Catoire, and N. Chaumeix, “Kinetic Modeling of Methyl Formate Oxidation”, *7th US National Technical Meeting of the Combustion Institute*, paper 1A06 (2011).
15. Joshua W. Allen, C. Franklin Goldsmith, and William H. Green, “Automatic Estimation of Pressure-Dependent Rate Coefficients” *Physical Chemistry Chemical Physics* (2011, submitted).

Quantum Dynamics of Elementary Combustion Reactions

Hua Guo (hguo@unm.edu)

Department of Chemistry and Chemical Biology, University of New Mexico

Many combustion reactions form intermediates supported by deep potential wells. One such example is the H + O_2 → HO + O reaction, which represents the bottleneck in the combustion of hydrogen and hydrocarbon fuels.[1] Much of our recent effort has been devoted to the elucidation of the reaction dynamics of this important combustion reaction, as well as several other complex-forming reactions. Our work aims at a fully quantum mechanical characterization of the reactive scattering on a highly reliable ab initio potential energy surface (PES) with as few approximations as possible. Our dynamical approach is based on the highly accurate and efficient Chebyshev propagator,[2] capable of calculating both initial state-resolved and state-to-state scattering attributes including differential cross sections.[3] Even with these state-of-the-art numerical techniques, quantum mechanical characterization of such an elementary reaction is still very challenging. Typically, a large basis/grid is needed to support the numerous quantum states in the potential well. In our wave packet approach, long propagation is also expected because of the long-lived nature of the intermediate complex. These difficulties are compounded by the barrierless reaction pathway which requires many partial waves.

To make the dynamical calculations more efficient, we have recently implemented a reactant coordinate based projection scheme,[4] which reduces the computational costs significantly without sacrificing accuracy. A distinct advantage of this approach is its ability to project out state-to-state attributes, namely the S-matrix elements, for all product channels. We have demonstrated this feature in a recent study of the NH + H' reaction, which leads to both exchange (H + NH') and abstraction (N + H_2) channels.[5] This approach was also used in some of the reactions discussed below.

We have continued our exploration of "the most important combustion reaction" (H + O_2 → HO + O), extending our earlier work by investigating the reverse reaction at the state-to-state level.[6] This reaction on the ground HO_2(X^2A") state PES proceeds via a complex-forming mechanism, evidenced by a near-symmetric angular distribution, a monotonically decaying vibrational state distribution and a highly inverted rotational state distribution for the O_2 product. Interestingly, the reaction is far from statistical, due to dynamic bottlenecks in the HO_2 well. Our quantum results confirmed an earlier observation by Miller on the same reaction.[7] Nonetheless, statistical models was, after appropriate scaling, found to reproduce the product state distributions reasonably well. This publication[6] was featured on the cover of J. Chem. Phys. (Fig. 1), and was one of the 20 most downloaded articles.

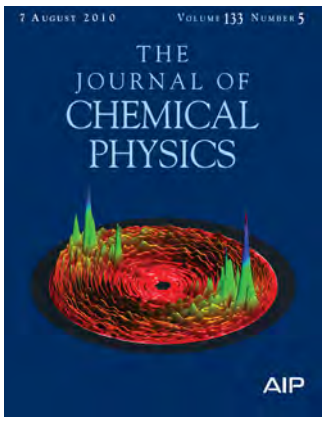

Fig. 1 Calculated differential cross section for the O + OH reaction featured on the cover of J. Chem. Phys.

We have further investigated the contribution of the first excited state of the $HO_2(A^2A')$ system to the H + O_2 reaction. This electronic state may be involved because it is adiabatically correlated to the same $O(^3P)$ + $OH(X^2\Pi)$ product channel as the ground (X^2A'') electronic state. On the other hand, its other asymptote, $H(^2S)$ + $O_2(a^1\Delta_g)$, is about 1 eV higher than its ground state counterpart, $H(^2S)$ + $O_2(X^3\Sigma^-_g)$. At high temperatures, the excited state O_2 might participate in the reaction. To determine the role played by the excited $HO_2(A^2A')$ state, a highly reliable PES for this state has recently been developed,[8] and state-to-state scattering calculations for the forward reaction have been performed.[9] Like its counterpart on the ground state HO_2, this reaction also proceeds via a complex-forming mechanism, but significant deviations from the statistical limit have been identified. It was shown that the non-statistical rotational state distribution of the OH product can be traced to a unique feature in the asymptotic PES, which exerts a torque on the departing OH product. In addition, our results suggested that the excited state O_2 does indeed contribute significantly to the H + O_2 reaction at high temperatures.

Another focus of our research has been the influence of non-adiabatic transitions on reaction dynamics. To this end, we have recently published a detailed state-to-state study of the $N(^2D)$ + H_2 reaction including the Renner-Teller coupling between the two lowest-lying electronic states of NH_2.[10] Another study in this respect is concerned with the A-band photodissociation of ammonia, which is dominated by non-adiabatic transitions to the X state of NH_3.[11] Finally, a joint theory-experiment study of the B-band non-adiabatic photodissociation of water has just been finished,[12] and for the first time the differential cross section for photodissociation of a polyatomic molecule has been calculated. As shown in Fig. 2, the agreement with the experiment of X. Yang (DICP, China) is excellent.

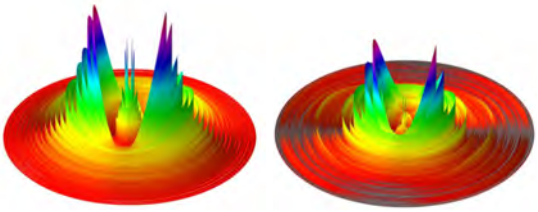

Fig. 2. Comparison of the measured (left panel) and calculated (right panel) differential cross sections of the OH(X) + H products in the photodissociation of $H_2O(B)$.

In addition to reaction dynamics, we have also been interested in spectroscopy. For example, we have used a path integral Monte Carlo method to simulate the rotational dynamics of CO_2 and N_2O in superfluid ^{4}He clusters.[13] More recently, we have computed the bending vibrational overtones in deuterated acetylene, DCCD.[14] To our surprise, the onset of localization of the cis and trans-bends of this molecule occurs much earlier than its hydrogen counterpart (HCCH),[15-16] as shown in Fig. 3. We are collaborating with Mike Kellman and Bob Field to understand this interesting isotope effect.

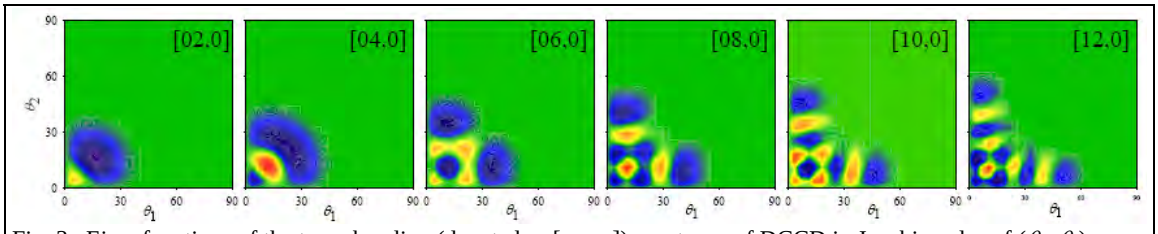

Fig. 3. Eigenfunctions of the trans-bending (denoted as [n_4, n_5]) overtones of DCCD in Jacobi angles of (θ_1, θ_2).

We have started to extend our approach to larger and more complex systems. In particular, we have finished writing our dynamic codes to describe the photodetachment of HCO_2^- and $HOCO^-$, which has been experimentally investigated by the groups of Neumark[17-18] and Continetti.[19-23] Preliminary results on the HCO_2^- photodetachment indicated the latest PES for the neutral HOCO system[24] is quantitatively inaccurate, judging from the comparison of the calculated spectrum with the measured ones. Efforts to develop a new and more reliable PES have been initiated in collaboration with Richard Dawes.

References (* indicates DOE funded work in the past year):

1. J. A. Miller, R. J. Kee and C. K. Westbrook, Annu. Rev. Phys. Chem. **41**, 345 (1990).
2. H. Guo, Rev. Comput. Chem. **25**, 285 (2007).
3. S. Y. Lin and H. Guo, Phys. Rev. A **74**, 022703 (2006).
*4. Z. Sun, H. Guo and D. H. Zhang, J. Chem. Phys **132**, 084112 (2010).
*5. Z. Li, C. Xie, B. Jiang, D. Xie, L. Liu, Z. Sun, D. H. Zhang and H. Guo, J. Chem. Phys (accepted).
*6. J. Ma, S. Y. Lin, H. Guo, Z. Sun, D. H. Zhang and D. Xie, J. Chem. Phys **133**, 054302 (2010).
7. J. A. Miller, J. Chem. Phys. **84**, 6170 (1986).
*8. A. Li, D. Xie, R. Dawes, A. W. Jasper, J. Ma and H. Guo, J. Chem. Phys **133**, 144306 (2010).
*9. J. Ma, H. Guo, A. Li, C. Xie and D. Xie, Phys. Chem. Chem. Phys. invited article for themed issue on Molecular Collision Dynamics (in press).
*10. S. Y. Lin, H. Guo, B. Jiang, S. Zhou and D. Xie, J. Phys. Chem. A **114**, 9655 (2010).
*11. W. Lai, S. Y. Lin, D. Xie and H. Guo, J. Phys. Chem. A **114**, 3121 (2010).
*12. B. Jiang, D. Xie and H. Guo, (to be published).
*13. L. Wang, D. Xie, H. Guo, H. Li, R. J. Le Roy and P. N. Roy, J. Mole. Spectrosc. invited article for the McKellar Special Issue (accepted).
*14. J. Ma, D. Xu and H. Guo, (to be published).
15. M. P. Jacobson and R. W. Field, J. Phys. Chem. **A104**, 3073 (2000).
16. D. Xu, R. Chen and H. Guo, J. Chem. Phys. **118**, 7273 (2003).
17. E. H. Kim, S. E. Bradforth, D. W. Arnold, R. B. Metz and D. M. Neumark, J. Chem. Phys. **103**, 7801 (1995).
18. E. Garand, K. Klein, J. F. Stanton, J. Zhou, T. I. Yacovitch and D. M. Neumark, J. Phys. Chem. A **114**, 1374 (2010).
19. T. G. Clements and R. E. Continetti, J. Chem. Phys. **115**, 5345 (2001).
20. A. M. Clements, R. E. Continetti and J. S. Francisco, J. Chem. Phys. **117**, 6478 (2002).
21. Z. Lu, Q. Hu, J. E. Oakman and R. E. Continetti, J. Chem. Phys **126**, 194305 (2007).
22. Z. Lu, J. E. Oakman, Q. Hu and R. E. Continetti, Mole. Phys. **106**, 595 (2008).
23. C. J. Johnson and R. E. Continetti, J. Phys. Chem. Lett. **1**, 1895 (2010).
24. M. J. Lakin, D. Troya, G. C. Schatz and L. B. Harding, J. Chem. Phys. **119**, 5848 (2003).

Gas-Phase Molecular Dynamics: High Resolution Spectroscopy and Collision Dynamics of Transient Species

Gregory E. Hall
Chemistry Department, Brookhaven National Laboratory
Upton, NY 11973-5000
gehall@bnl.gov

Program Scope

This research is carried out as part of the Gas-Phase Molecular Dynamics program in the Chemistry Department at Brookhaven National Laboratory. Chemical intermediates in the elementary gas-phase reactions involved in combustion chemistry are investigated by high resolution spectroscopic tools. Production, reaction, and energy transfer processes are investigated by transient, double resonance, polarization and saturation spectroscopies, with an emphasis on technique development and connection with theory, as well as specific molecular properties.

Recent Progress

A. Double-resonance studies of rotational energy transfer and depolarization in CH_2

The transfer of population and alignment among rotational states of CH_2 $\tilde{a}$ ($^1A_1$), driven by inelastic and elastic collisions with He, Ar, and ketene, has been investigated using an optical-optical double resonance technique. Transient frequency modulation spectroscopy with a continuous laser probes the depletion and recovery of population in a single rotational state during and after a tunable, ns pulsed laser perturbs the previously thermalized rotational distribution. With linearly polarized bleach and probe lasers, depletion and recovery signals depend on the relative laser polarizations; the probe process can independently monitor both population and alignment as the state distribution and rotational anisotropy relax due to collisions. Saturation recovery rates are found to vary non-monotonically with the energy or angular momentum of the rotational states and show and even/odd alternation in J for a series of K_a=1 rotational levels of the same nuclear spin symmetry. An elastic depolarization contribution to the alignment decay is directly observed in CH_2 + rare gas collisions, with a cross section comparable to the total inelastic cross section for low rotational states, but decreasing for states of higher angular momentum, and showing an opposite odd/even alternation to that seen in the inelastic rates. Companion theoretical studies by Ma, Alexander and Dagdigian[1] confirm and explain the observations. The theoretical studies show the alternation in total removal cross sections for even and odd J states is reversed in *ortho* and *para* nuclear spin modifications of singlet CH_2, an effect correlated with the asymmetric energy gaps to the most strongly coupled individual final states from even or odd initial states. (with postdoctoral researcher Suk-Young Lee)

B. Hyperfine signatures of singlet-triplet mixing in CH_2

Perturbations in the 7_{16} and 8_{18} mixed singlet/triplet levels of $\tilde{a}^1A_1(0,0,0)$ methylene, CH_2, have been reinvestigated by frequency-modulated sub-Doppler laser saturation spectroscopy. A single tunable cw Ti:sapphire beam is split into counterpropagating bleach and probe beams to interrogate the microsecond transient CH_2 produced from the excimer laser photolysis of ketene. The bleach beam is blocked or unblocked; the probe laser is frequency modulated. The difference spectra of demodulated

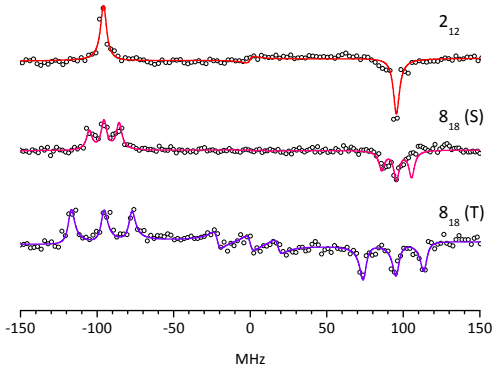

Figure 1. Sub-Doppler saturation spectra showing unresolved hyperfine structure of the (pure singlet) 2_{12} rotational state, and resolved triplet hyperfine structure of the two mixed eigenstates derived from the singlet 8_{18} rotational level and its triplet state perturber. The splitting in the mostly singlet eigenstate 8_{18}(S) is smaller than in the mostly triplet eigenstate, in direct proportion to the triplet character of the mixed states, since the splitting is dominated by the I·S (nuclear spin · electron spin) coupling. These FM spectra show matched positive and negative features, separated by the 190 MHz sideband splitting.

transient FM spectra with and without the bleach beam are shown in Figure 1, illustrating the sub-Doppler hyperfine spectra of three rotational levels of singlet CH_2. The hyperfine structure was completely resolved for both the predominantly singlet and the predominantly triplet components of these mixed rotational levels, using $\tilde{b}\ ^1B_1 - \tilde{a}\ ^1A_1$ optical transitions near 12 200 cm^{-1}. The Doppler-free saturation lines are observed with Lorentzian half-widths of 2-3 MHz, corresponding to a frequency resolution near one part in 10^8. The mixing coefficients were obtained from the observed hyperfine splittings and a two-level deperturbation model. The analysis also determines the energy separation of the unperturbed zero-order levels and the unperturbed hyperfine splittings for the triplet perturbing levels 6_{15} $\tilde{X}\ ^3B_1(0,3,0)$ and 9_{37} $\tilde{X}\ ^3B_1(0,2,0)$. The kinetics of singlet-triplet intersystem crossing in CH_2 depends on the mixing coefficients of the several most strongly perturbed "gateway" states and this measurement provides the most direct measure of the effect to date. (with postdoctoral research associate C.-H. Chang)

C. Doppler-resolved kinetics of energy transfer

We have been exploring the use of sub-Doppler saturation spectroscopy for measuring the kinetics of saturation recovery in CN to develop tools for independently characterizing the rates of rotational energy transfer, depolarization, and velocity changing collisions of ground state radicals with assorted collision partners. The same type of saturation recovery and depolarization kinetics described in section **A** above for CH_2 can be measured after the trailing edge of a rapidly chopped sub-Doppler bleach beam. Using the "one color double-resonance" method, the saturation signal can return toward zero due to a) rotationally inelastic collisions that refill the bleached velocity group of the lower bleached state, b) rotationally elastic, velocity changing collisions that refill the bleached velocity group of the lower bleached state, c) any collisions that remove the velocity group of the upper level in the bleached transition, elastic or inelastic. As we began picking apart the various components of the relaxation kinetics, we found the elastic depolarization rates to be slow compared to the rotationally inelastic rates, unlike the case for CH_2 with rare gas collision partners. We were most surprised to find that the velocity changing collisions barely contribute to the total refilling of the bleached ground state CN velocity groups, in the case of a polar collision partner, CH_3COCN, our photolytic CN precursor. To compare rotationally elastic velocity-changing collisions with rotationally inelastic cross sections, we can contrast the rates of saturation recovery following sub-Doppler vs. broad-band saturation with a chopped cw laser and a ns dye laser, respectively. In the case of broad-band saturation, we can confirm that the fractional depletion is initially independent of the probed Doppler shift – all velocity groups are uniformly bleached

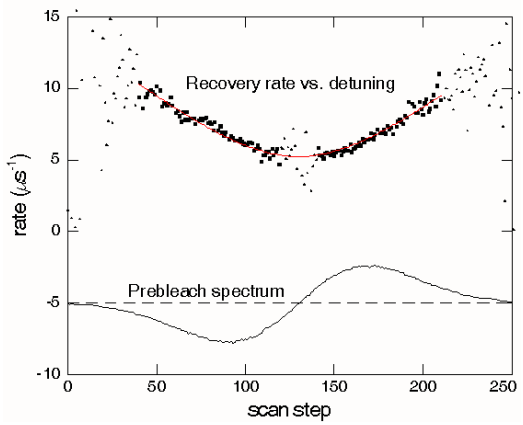

Figure 2. Saturation recovery rate vs. Doppler detuning. The observed recovery rate following broad-band bleaching of a ground state CN rotational level depends on the Doppler shift selected for kinetic measurement. The red line is a fit to the functional form k_0 sqrt($1+ax^2$) with k_0 the rate at line center and x the detuning – the same form as the average relative collision velocity when one component of the velocity of one collision partner is selected.

under power-broadened conditions. The recovery rates, however, are found to increase with probe detuning, as illustrated in Figure 2. On one hand, this is surprising, even disturbing, as it implies that the Doppler spectrum of the hole is initially thermal, in a thermal collision environment, and gradually gets "colder" as the Doppler wings of the hole relax faster than the center. Furthermore, if you measure kinetics with a narrow-band laser at line center of an isolated line, you will not measure the thermal rate coefficient. On the other hand, we shouldn't be surprised to see the rate coefficient be larger for a given process when you are selectively looking at a velocity group with higher average collision velocity. The paradox-spoiling observation is that these saturation recoveries are dominated by rotationally inelastic collisions between polar molecules, which have high efficiency at large impact parameter. These J-changing collisions can compete very effectively with velocity-randomizing collisions, which are required to maintain an uncorrelated Boltzmann velocity distribution in the presence of the perturbed rotational distribution. We should only expect these Doppler-resolved kinetic effects to be important for processes that are faster than velocity thermalization. (with postdoctoral research associate M. Hause)

Future Work

A. Fiber frequency comb enhanced FT NIR Spectroscopy.

The combination of a commercial FTIR spectrometer with a frequency comb source at the wavelength range 1500-1600 nm has been recently demonstrated[2] to offer one order of magnitude boost in sensitivity compared to conventional incoherent light sources. This advantage stems from the 'brightness' and low shot-to-shot noise of the comb sources. Our efforts are focused on increasing the comb output wavelength range to 1000-2400 nm and exploring possibilities of further improving the sensitivity of the frequency comb enhanced FT NIR Spectroscopy by employing a phase sensitive detection at the repetition rate of the mode-locked fiber ring laser. The latter also involves designing the front-end high bandwidth electronics for the commercial FTIR to improve its dynamic range.

We have built a polarization additive-pulse mode-locked fiber ring laser (frequency comb) and characterized its output power, pulse widths, line widths, mode-lock stabilities. The comb output has been amplified using a chirped-pulse Erbium fiber amplifier and broadened over one octave in a highly non-linear fiber optimized for chromatic dispersion and maximized for Kerr nonlinearities. The resulting broadened output was highly reproducible and stable, suggesting preservation of high temporal coherence. Hence, the phase-sensitive detection at the repetition rate, roughly 100 MHz, becomes possible over entire octave spanning range and could lead to the '1/f-noise' level reductions compared to conventional FTIR setup where the signal is modulated with frequencies on the order of tens of kHz.

Frequency comb enhanced FT NIR spectroscopy will be used in collaboration with the Surface Dynamics Group at BNL to probe photocatalysis at the water/semiconductor interfaces. Potential applications of this technique for problems in combustion chemistry and heavy element chemistry are being assessed as well. (with Goldhaber Research Fellow, V. Goncharov)

B. Collision dynamics

Once our laboratory move is completed, we will resume work on double resonance kinetic studies of ground-state energy and polarization transfer. Referencing the cw laser to a single frequency HeNe-stabilized cavity has been implemented and should help the frequency stability of the sub-Doppler measurements, and we intend to perform a more systematic study of rotational energy transfer and depolarization in CN (X) with different collision partners. Similar experiments in ground state HCCH will be attempted this summer. (with postdoctoral research associate C. McRaven). See abstract from my colleague T. Sears for further details.

Publications supported by this project since 2009

Sub-Doppler laser absorption spectroscopy of the $A^2\Pi_i - X^2\Sigma^+$ (1,0) band of CN: measurement of the ^{14}N hyperfine parameters in $A^2\Pi_i$ CN. M. L. Hause, G. E. Hall and T. J. Sears, *J. Molec. Spectrosc.* **253**, 122-128 (2009).

Sub-Doppler Stark spectroscopy in the *A* - *X* (1,0) band of CN. M. L. Hause, G. E. Hall, and T. J. Sears, *J. Phys. Chem. A,* **113** 13342-13346 (2009).

Spectroscopic constants of the known electronic states of lead monofluoride. C. P. McRaven, P. Sivakumar, N. E. Shafer-Ray, G. E. Hall and T. J. Sears. *J. Mol. Spectrosc.* **262**, 89 (2010).

Pseudo-continuous resonance-enhanced multiphoton ionization: application to the determination of the hyperfine constants of $^{208}Pb^{19}F$. P. Sivakumar, C. P. McRaven, P. M. Rupasinghe, T. Zh. Yang, N. E. Shafer-Ray, G. E. Hall and T. J. Sears, *Mol. Phys.* **108**, 927 (2010).

Frequency modulated circular dichroism spectroscopy: application to ICN photolysis. G. Hancock, G. Richmond, G.A.D. Ritchie, S. Taylor, M. L. Costen and G. E. Hall, *Mol. Phys.* **108**, 1083-1095 (2010).

Sub-Doppler spectroscopy of mixed state levels in CH_2. C.-H. Chang, G. E. Hall, T. J. Sears, *J. Chem. Phys.* **133**, 144310 (2010).

Transient laser absorption spectroscopy of CH_2 near 780 nm. C.-H. Chang, Z. Wang, G. E. Hall, T. J. Sears and J. Xin, *J. Molec. Spectrosc.* (2011), doi:10.1016/j.jms.2011.02.004 (in press).

CH_2 band origin at 1.20 μ. C.-H. Chang, J. Xin, T. Latsha, E. Otruba, Z. Wang, G. E. Hall, T. J. Sears and B.-C. Chang, *J. Phys. Chem. A,* (2011), doi: 10.1021/jp1115965 (in press).

The Approach to Equilibrium: Detailed Balance and the Master Equation. M. H. Alexander, G. E. Hall and P. J. Dagdigian, *J. Chem. Educ*. (submitted).

Cited References

1 L. Ma, M. H. Alexander, and P. J. Dagdigian, *J. Chem. Phys.* in press (2011).

2 J. Mandon, G. Guelachvili, and N. Picque, *Nature Photonics* 3, 99 (2009).

Flame Chemistry and Diagnostics

Nils Hansen
Combustion Research Facility, Sandia National Laboratories, Livermore, CA 94551-0969
Email: nhansen@sandia.gov

SCOPE OF THE PROGRAM

The goal of this program is to provide a rigorous basis for the elucidation of chemical mechanisms of combustion, combining experimental measurements employing state of the art combustion diagnostics with detailed kinetic modeling. The experimental program concentrates on the development and application of combustion diagnostics for measurements of key chemical species concentrations. These measurements are carried out in low-pressure, one-dimensional laminar flames and are designed to serve as benchmarks for the validation of combustion chemistry models. Comparison of experimental data to models employing detailed chemical kinetics is critical to determining important chemical pathways in combustion and in pollutant formation in combustion systems. As turbulent combustion models become increasingly sophisticated, accurate chemical mechanisms will play a larger role in computations of realistic combustion systems. Verification of detailed chemistry models against a range of precise measurements under thoroughly characterized steady conditions is necessary before such flame models can be applied with confidence in turbulent combustion calculations.

PROGRESS REPORT

Molecular Beam Mass Spectrometry at the Advanced Light Source

In collaboration with Prof. Cool of Cornell University, Prof. Kohse-Höinghaus of Bielefeld University, and Prof. Westmoreland of North Carolina State University, great progress has been made measuring low-pressure flames using molecular-beam mass spectrometry (MBMS) with synchrotron photoionization at the Advanced Light Source (ALS) of the Lawrence Berkeley National Laboratory. In the past year, different flames fueled by larger hydrocarbons species have been characterized over a wide range of stoichiometries. The main focus was on fuel-consumption and initial steps of aromatic ring formation in fuel-rich flames of the C_6H_{12} isomers 1-hexene, cyclohexane, methylcyclopentane, and 3,3-dimethyl-1-butene. The results, which have been published or have been accepted for publication during the report period, shall be discussed briefly in the following paragraphs.

Fuel-Structure Dependence of Benzene Formation Processes in Premixed Flames Fueled by C_6H_{12} Isomers: The fuel-structure dependent significance of various benzene formation pathways was analyzed using data from rich (ϕ=1.7) flames fueled by the four C_6H_{12} isomers mentioned above. While propargyl and allyl radicals dominate benzene formation in the combustion of 1-hexene, contributions from reactions involving *i*-C_4H_5 and C_5H_5 radicals were revealed in the flames of 3,3-dimethyl-1-butene

and methylcyclopentane, respectively. Close to the burner surface, successive dehydrogenation of the fuel was found to be important for the cyclohexane flame and to some smaller extent for the methylcyclopentane flame.

The Importance of Fuel Dissociation and the Propargyl + Allyl Reaction for the Formation of Benzene in a 1-Hexene Flame: A more fuel-rich flame (ϕ=2.0) of 1-hexene was used to study decomposition and benzene formation processes in more detail. To this end, quantitative mole fraction profiles of the flame species were compared with kinetic modeling results provided by the group of Prof. Westmoreland. The results indicated that 1-hexene is dominantly decomposed via unimolecular dissociation forming allyl (*a*-C_3H_5) and *n*-propyl (*n*-C_3H_7). The reaction path analysis also highlighted an outstanding contribution of the propargyl (C_3H_3) + allyl (*a*-C_3H_5) reaction to the formation of benzene. In this flame, benzene is dominantly formed through H-assisted isomerization of fulvene, which itself is almost exclusively produced by the aforementioned C_3H_3 + *a*-C_3H_5 reaction.

Multiple Benzene-Formation Paths in a Fuel-Rich Cyclohexane Flame: The chemical structure of a fuel-rich flame (ϕ=2.0) of cyclohexane and detailed modeling from Prof. Westmoreland's group was used to establish that a mixture of pathways contributes to benzene formation under these conditions. Dehydrogenation of the six-membered ring was found to be a dominant benzene formation route under these conditions, with H_2 elimination from 1,3-cyclohexadiene contributing more than cyclohexadienyl decomposition. Additional reactions make contributions, including the direct route via $2C_3H_3 \rightleftarrows$ benzene and more importantly the H-assisted isomerization of fulvene formed from *i*-C_4H_5+C_2H_2, C_3H_3+*a*-C_3H_5, and C_3H_3+C_3H_3.

Measurements of Aromatic Flame Species by Multi-Photon Ionization

A flame-sampling molecular-beam mass spectrometry (MBMS) employing photoionization with UV light has been used to detect aromatic flame constituents, such as benzene, toluene and smaller polycyclic aromatic hydrocarbons (PAH's) employing either resonant or non-resonant ionization processes. Flames fueled by acetylene, allene, propyne, propene, 1,3-butadiene, and methylcyclohexane have been studied and the data is currently being analyzed. Based on the species detected, evidence for the hydrogen abstraction acetylene addition (HACA), methyl addition/cyclization (MAC), and phenyl addition/cyclization (PAC) mechanisms was observed.

Investigating the Chemical Composition of Combustion-Generated Soot Nanoparticles

This project is led by Prof. Violi of the University of Michigan. Co-PI's and responsible for the experimental portions of this project are Dr. Michelsen and Dr. Hansen (Sandia). During the report period, a counter-flow diffusion burner system has been set-up and tested successfully. These counter-

flow flame systems will be used to study the formation of PAH's and small soot particles. Details of the planned experiments are described in the following paragraphs.

FUTURE DIRECTIONS

The chemical structure of the counter-low flames and the chemical composition of soot nanoparticles will be investigated using the flame-sampling mass spectrometer and the aerosol mass spectrometer, both installed on beamline 9.0.2 at the ALS. For the flame-chemistry experiments, all flame species, including reactions, products, and intermediates, will be extracted from these counter-flow diffusion flames by continuously withdrawing gases from within the flame using a quartz microprobe. The chemical composition is subsequently determined by mass-spectrometry. For the aerosol experiments, an ensemble of withdrawn particles will be focused into the high-vacuum region of the aerosol mass spectrometer using an aerodynamic lens system. After entering an ionization chamber, the combustion-generated particles are vaporized with a hot surface and then ionized with the tunable VUV light available at beamline 9.0.2. The thermal vaporization of soot particles on a heater tip leads to the generation of intact gas phase molecules. This phenomenon, coupled to threshold single-photon ionization with tunable VUV radiation, allows for fragment-free mass spectrometry of complex particles. For the proposed experiments, single-particle speciation is not anticipated given the sensitivity of the aerosol mass spectrometer. The experiments will thus entail averaging mass spectra collected over an extended period of time. The result will be the average composition of a particle distribution in a particular size range. Thus, the anticipated experimental results will provide spatially resolved size distributions of the combustion-generated soot particles and their molecule-specific chemical composition. The aerosol mass spectrometer at the ALS is well suited for this experiment, as it allows to specify soot particles without the uncertainties introduced by fragmentation when using other instruments and with the ability to resolve isomers. This proposed work will enhance our understanding of soot formation chemistry and will facilitate the prediction of particle-size distributions under combustion conditions.

One other key immediate task is the analysis of the large body of ALS data accumulated in the past years, which may compel further or confirmatory measurements during subsequent beam cycles. We will continue to explore isomer specific pathways of fuel-consumption and aromatic ring formation in flames fueled by C_5-C_8 species. A new reflectron time-of-light mass spectrometer has been ordered and it is expected to be delivered later this year. Throughout the next year, we will work on replacing the existing linear time-of-flight set-up of the ALS flame machine with this new instrument. This modification will lead to a significant increase in mass resolution from currently $m/\Delta m \approx 400$ to ≈ 3000. Therefore, unambiguous identifications of flame species of near-equal mass should become achievable.

In light of the recent findings regarding the fuel-consumption and benzene formation pathways in a fuel-rich 1-hexene flame, we deem it best to expand our studies to additional fuels with a similar structural feature, i.e. an allylic C-C bond. We therefore plan to study the combustion chemistry of flames fueled by 1-butene and 1-pentene. All studies employing synchrotron generated VUV photoionization will be complemented by the laser-induced fluorescence and multiphoton ionization experiments in the laser laboratory.

PUBLICATIONS ACKNOWLEDGING BES SUPPORT 2009-PRESENT

1. N. Hansen, J. A. Miller, T. Kasper, K. Kohse-Höinghaus, P. R. Westmoreland, J. Wang, T. A. Cool, "Benzene Formation in Premixed Fuel-Rich 1,3-Butadiene Flames", *Proc. Combust. Inst.*, **32,** 623-630 (2009).
2. A. Lucassen, P. Oßwald, U. Struckmeier, K. Kohse-Höinghaus, T. Kasper, N. Hansen, T. A. Cool, P. R.Westmoreland, "Species identification in a laminar premixed low-pressure flame of morpholine as a model substance for oxygenated nitrogen-containing fuels", *Proc. Combust. Inst.*, **32,** 1269-1276 (2009).
3. C. K. Westbrook, W. J. Pitz, P. R. Westmoreland, F. L. Dryer, M. Chaos, P. Oßwald, K. Kohse-Höinghaus, T. A. Cool, J. Wang, B. Yang, N. Hansen, T. Kasper, "A Detailed Chemical Kinetic Mechanism for Oxidation of Four Small Alkyl Esters in Laminar Premixed Flames", *Proc. Combust. Inst.*, **32,** 221-228 (2009).
4. N. Hansen, T. A. Cool, P. R. Westmoreland, K. Kohse-Höinghaus, "Recent Contributions of Flame-Sampling Molecular-Beam Mass Spectrometry to a Fundamental Understanding of Combustion Chemistry", *Prog. Energy Combust. Sci.*, **35,** 168-191 (2009).
5. J. Wang, M. Chaos, B. Yang, T. A. Cool, F. L. Dryer, T. Kasper, N. Hansen, P. Oßwald, K. Kohse-Höinghaus, P. R. Westmoreland, "Composition of Reaction Intermediates for Stoichiometric and Fuel-Rich Dimethyl Ether flames: Flame-Sampling Mass Spectrometry and Modeling Studies", *Phys Chem. Chem. Phys.*, **11,** 1328-1339 (2009).
6. N. Hansen, J. A. Miller, P. R. Westmoreland, T. Kasper, K. Kohse-Höinghaus, J. Wang, T. A. Cool, "Isomer-Specific Combustion Chemistry in Allene and Propyne Flames", *Combust. Flame*, **156**, 2153-2164 (2009).
7. J. Wang, B. Yang, T. A. Cool, N. Hansen, "Absolute Cross-Sections for Dissociative Photoionization of Some Small Esters", *Int. J. Mass Spectrom.*, **292,** 14-22 (2010).
8. K. Kohse-Höinghaus, P. Oßwald, T. A. Cool, T. Kasper, N. Hansen, F. Qi, C. K. Westbrook, P. R. Westmoreland, "Biofuel Combustion Chemistry: From Ethanol to Biodiesel", *Angew. Chem. Int. Ed.*, **49,** 3472-3597 (2010).
9. U. Sruckmeier, A. Lucassen, N. Hansen, T. Wada, N. Peters, K. Kohse-Höinghaus, "Demonstration of a Burner for the Investigation of Partially Premixed Low-Temperature Flames", *Combust. Flame*, **157,** 1966-1975 (2010).
10. N. Hansen, W. Li, M. E. Law, T. Kasper, P. R. Westmoreland, B. Yang, T. A. Cool, A. Lucassen, "The Importance of Fuel Dissociation and Propargyl + Allyl Association for the Formation of Benzene in Fuel-Rich 1-Hexene Flame", *Phys. Chem. Chem. Phys.*, **12,** 12112-12122 (2010).
11. N. Hansen, T. Kasper, B. Yang, T. A. Cool, W. Li, P. R. Westmoreland, P. Oßwald, K. Kohse-Hönghaus, "Fuel-Structure Dependence of Benzene Formation Processes in Premixed Flames Fueled by C_6H_{12} Isomers", *Proc. Combust. Inst.*, **33,** 585-592 (2011).
12. S. Dooley, F. L. Dryer, B. Yang, J. Wang, T. A. Cool, T. Kasper, N. Hansen, "An Experimental and Kinetic Modeling Study of Methyl Formate Low-Pressure Flames", *Combust. Flame*, **158,** 732-741 (2011).
13. B. Yang, T. A. Cool, C. K. Westbrook, N. Hansen, K. Kohse-Höinghaus, "Fuel-Specific Influences on the Composition of Reaction Intermediates in Premixed Flames of Three $C_5H_{10}O_2$ Ester Isomers", *Phys. Chem. Chem. Phys.*, in press (2011).
14. W. Li, M. E. Law, P. R. Westmoreland, T. Kasper, N. Hansen, K. Kohse-Höinghaus, "Multiple Benzene-Formation Paths in a Fuel-Rich Cyclohexane Flame", *Combust. Flame*, in press (2011).

Spectroscopy and Kinetics of Combustion Gases at High Temperatures

R. K. Hanson and C. T. Bowman
Mechanical Engineering Department, Stanford University
Stanford, CA 94305-3032
rkhanson@stanford.edu, ctbowman@stanford.edu

I. Program Scope

This program involves two complementary activities: (1) development and application of cw laser absorption methods for the measurement of concentration time-histories and fundamental spectroscopic parameters for species of interest in combustion; and (2) shock tube studies of reaction kinetics relevant to combustion.

Species currently being investigated in the spectroscopic portion of the research include C_2H_4 (at 10.5 μm), H_2O (at 2.5 μm), and CO_2 (at 2.7 μm). New efforts are also being made to study formaldehyde (CH_2O) in the UV (near 325 nm) and in the IR (near 3.4 μm), and CO (near 4.6 μm).

In parallel with these spectroscopic studies, kinetics research has advanced on several fronts. (1) Our OH diagnostic has been used to measure the rate coefficients for a series of reactions of the alkenes +OH, including ethylene, propene, butane, and 1,3-butadiene, and of the alkanes+OH including n-pentane, n-heptane, n-nonane. (2) H_2O and OH diagnostics have been used to provide improved measurements of several hydroperoxyl radical rate coefficients in the $H_2/O_2/H_2O_2/HO_2$ system, including those for the reactions $OH + HO_2 \rightarrow H_2O + O_2$ and $OH + H_2O_2 \rightarrow H_2O + HO_2$. These results, together with our earlier measurements for $H + O_2 \rightarrow OH + O$ and $H_2O_2 + M \rightarrow 2OH + M$ have been combined to form an updated H_2/O_2 reaction mechanism.

II. Recent Progress: Spectroscopy

Ethylene Detection using 10.53 micron IR Laser Absorption

Ethylene was detected [implementing the method of Pilla et al. (2010) developed earlier in our laboratory] using laser absorption of the P14 line in the (0 0 1) → (1 0 0) vibrational band of a CO_2 laser at 10.532 μm, but with reduced scatter (relative to our earlier work) achieved by utilizing IR photovoltaic detectors and better identification of the P14 line via a MIR wavemeter. An improved expression (±4%) for the cross-section over temperatures of 1050-2000 K and pressures of 1.3-3.6 atm is given by

$$\sigma = (3.9 + 80.5 \exp(-T[K]/461)\,(1.03 - 0.012\,P[atm])\ [m^2/mol]$$

Representative data are shown in Figure 1. This laser absorption diagnostic of ethylene can provide essential information regarding the reaction paths and rates of the formation of alkenes during hydrocarbon pyrolysis and oxidation. Using this diagnostic, we measured ethylene concentration time-histories behind reflected shock waves during the pyrolysis of ethylene, n-heptane and methylcyclohexane (MCH). Pyrolysis experiments for the three fuels were conducted at temperatures of 1252-1973 K and pressures of 1.9-3.2 atm, with fuel concentrations of 0.1%-1% in argon. Measured ethylene time-histories during n-heptane and MCH pyrolysis were compared to the modeled predictions of JetSurF 2.0 mechanism (Wang et al. 2010). Further details can be found in Ren et al. (2011).

II. Recent Progress: Chemical Kinetics

OH Oxidation Reactions

Because of the important role of OH oxidation reactions in combustion and ignition phenomena, we are currently reviewing the status of, and measuring, rate constants for the reactions of OH with both alkenes (important fuel decomposition products) and alkanes (major fuel surrogate components).

Representative of the alkene measurements is our recent study of the $OH + C_4H_8$ isomers. Reactions of hydroxyl (OH) radicals with 1-butene (k_1), *trans*-2-butene (k_2), and *cis*-2-butene (k_3) were studied behind reflected shock waves over the temperature range 880 K to 1341 K and at pressures near 2.2 atm. OH radicals were produced by shock-heating tert-butyl hydroperoxide, $(CH_3)_3$-CO-OH, and monitored by narrow-linewidth ring dye laser absorption of the well-characterized $R_1(5)$ line of the OH

A-X (0, 0) band near 306.7 nm. OH time-histories were modeled using a comprehensive C_5 oxidation mechanism, and rate constants for the reaction of OH with butene isomers were extracted by matching modeled and measured OH concentration time histories. This study includes the first high-temperature measurement of OH+*cis*-2-butene and extends the temperature range of the only previous high-temperature study for both 1-butene and *trans*-2-butene. Representative laser absorption data are shown in Figure 2. Further details can be found in Vasu et al. (submitted Dec. 2010).

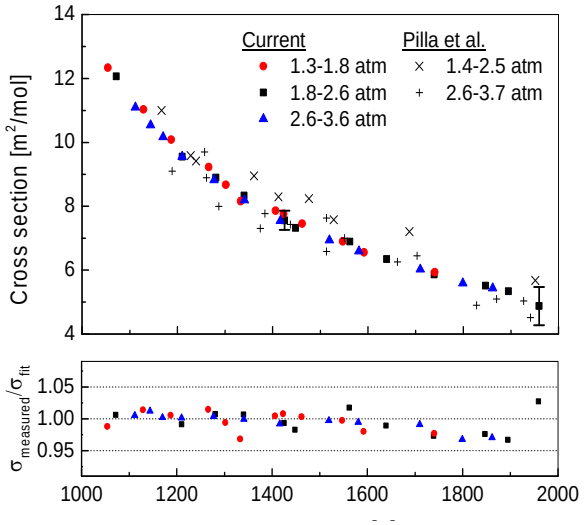

Figure 1. Ethylene cross-section (10.532 μm) at 1050-2000 K, 1.3-3.7 atm; data from Pilla et al. (2010) are also plotted for comparison.

.

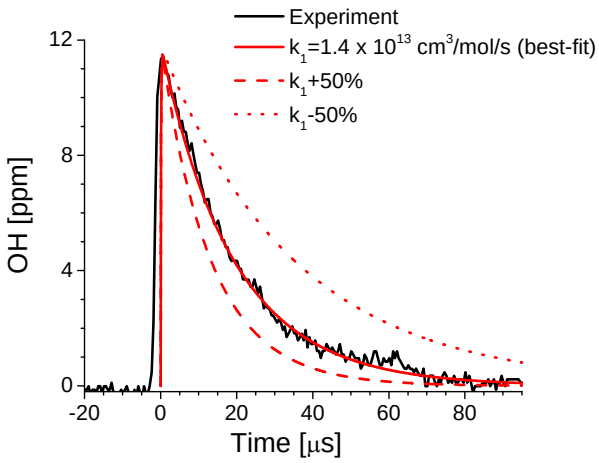

Figure 2. Example OH+1-butene (k_1) rate measurement. Initial reflected shock conditions: 1097 K, 2.12 atm, 150 ppm 1-butene, 11.8 ppm TBHP in argon. Model predictions using the best-fit predictions (k_1 = 1.4 x 10^{13} cm^3/mol/s) and 50% variation from the measured rate are also shown.

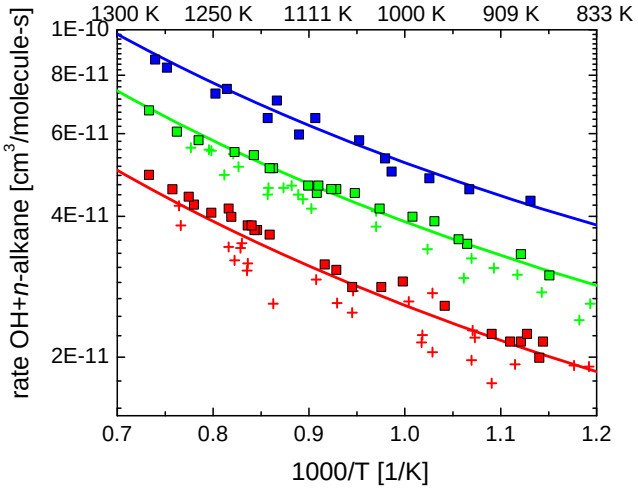

Figure 3. Arrhenius representation of the reaction rate constant data and models for OH+alkanes. Solid squares: current study; crosses; Sivarakrishnan and Michael (2009); solid lines: Kwok and Atkinson (1995); upper line, nonane; middle line, heptane; lower line, pentane.

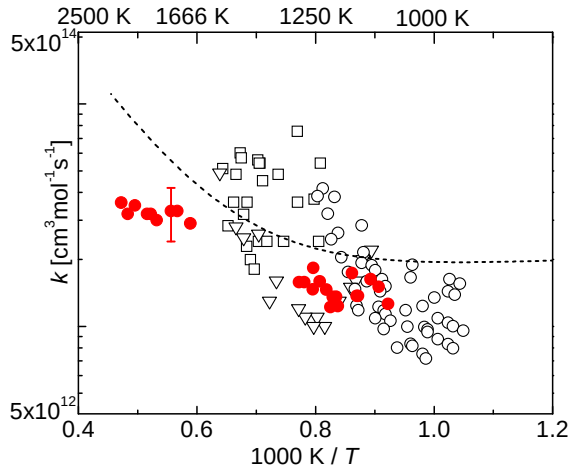

Figure 4. Arrhenius representation of reaction rate constant for $OH+H_2O=H_2O+O_2$. Solid circles: this study; open circles: Kappel et al. (2002); open squares: Srinivasan et al. (2006); open triangles: Hippler et al. (1995); dashed line: rate employed in GRI-Mech v3.0 (1999).

High-temperature measurements of the reaction rate for OH+n-alkane reactions were performed behind reflected shock waves also using tert-butyl hydroperoxide as an OH precursor and laser absorption of OH at 306 nm. Three normal alkanes were studied (n-pentane, n-heptane, and n-nonane), and the overall rate for the OH-n-alkane reaction was determined under near-pseudo-first-order conditions for temperatures from 869 K to 1364 K under pressures from 0.8 to 2.1 atm. Representative data are shown in Figure 3. The high-temperature rate measurements for OH+n-pentane and OH+n-heptane agree with the data from Sivaramakrishnan and Michael (2009) within 15% over the temperature range studied, with the current data displaying less scatter. The OH+n-nonane rate measurements are the first measurements in the literature showing the temperature dependence at high temperatures. The Structure-Reactivity Relationship of Kwok and Atkinson (1995) developed for OH+alkane reaction rates under 1000 K shows good agreement with the current data for all three normal alkanes for temperatures up to 1364 K.

Updated H_2/O_2 Reaction Mechanism

An updated H_2/O_2 reaction mechanism was developed that incorporates recent reaction rate determinations from our shock tube laboratory. These experiments used UV and IR laser absorption to monitor species time-histories and have resulted in improved high-temperature rate constants for the following reactions:

$H + O_2 \rightarrow OH + O$

$H_2O_2 + M \rightarrow 2OH + M$

$OH + H_2O_2 \rightarrow HO_2 + H_2O$

$O_2 + H_2O \rightarrow OH + HO_2$

The updated mechanism also takes advantage of the results of other recent rate constant studies, and incorporates the most current thermochemical data for OH and HO_2. The mechanism was tested (and its performance compared to that of other H_2/O_2 mechanisms) against recently reported OH and H_2O concentration time-histories in various H_2/O_2 systems, such as H_2 oxidation, H_2O_2 decomposition, and shock-heated H_2O/O_2 mixtures. In addition, the mechanism was validated against a wide range of standard H_2/O_2 kinetic targets, including ignition delay times, flow reactor species time-histories, laminar flame speeds, and burner-stabilized flame structures. These validations indicate that the updated mechanism should perform reliably over a range of reactant concentrations, stoichiometries, pressures, and temperatures from 950 to greater than 3000 K. Further details can be found in Hong et al. (2011).

Representative of these new reaction rate measurements is the new lower temperature study of $OH+HO_2 \rightarrow H_2O+O_2$ shown in Figure 3. These recent measurements used both OH and H_2O laser absorption and overlap (but with reduced uncertainties) with earlier low temperature measurements.

III. Future Work

Work to develop shock tube/laser absorption diagnostics for both CO (in the infrared) and CH_2O/formaldehyde (in the infrared and near ultraviolet) is in progress. These measurements will assist in achieving closure on the oxygen balance during oxygenate fuel pyrolysis and oxidation. Further rate constant measurements of oxidation reactions of the form OH+alkane and OH+butanol isomers are in progress as well. Investigations of the pyrolysis and oxidation of different classes of oxygenate species are planned, with work on ketones (3-pentanone) and ethers (dimethyl ether) in progress.

IV. Publications and submitted journal articles supported by this project 2009-2011

1. S. S. Vasu, L. K. Huynh, D.F. Davidson, R. K. Hanson, D. M. Golden, "Reactions of OH with Butene Isomers: Measurements of the Overall Rates and a Theoretical Study," J. Phys. Chem., submitted 12/10.

2. S. S. Vasu, Z. Hong, D. F. Davidson, R. K. Hanson, D. M. Golden, "Shock Tube/Laser Absorption Measurements of the Reaction Rates of OH with Ethylene and Propene," J. Phys. Chem. A. in press.

3. S. S. Vasu, D. F. Davidson, R. K. Hanson, "A Shock Tube Study of Syngas Ignition in Rich CO_2, Mixtures and Determination of the Ratio of the Rate of $H+O_2+CO_2 \rightarrow HO_2+CO_2$. Energy and Fuels, in press.

4. Z. Hong, D. F. Davidson, R. K. Hanson, "An Improved H_2/O_2 Mechanism based on Recent Shock Tube/Laser Absorption Measurements," Combustion and Flame **138**, 633-644 (2011).

5. R. K. Hanson, "Applications of Quantitative Laser Sensors to Kinetics, Propulsion and Practical Energy Systems," Proc. Combust. Inst. **33**, 1-40 (2011).

6. K.-Y. Lam, Z. Hong, D. F. Davidson, R. K. Hanson, "Shock Tube Ignition Delay Time Measurements in Propane/O_2/Argon Mixtures at Near-Constant-Volume Conditions," Proc. Combust. Inst. **33**, 251-258 (2011).

7. Z. Hong, D. F. Davidson, E. A. Barbour, R. K. Hanson, "A New Shock Tube Study of the $H+O_2 \rightarrow OH+O$ Reaction Rate using Tunable Diode Laser Absorption near 2.5 μm," Proc. Combust. Inst. **33**, 309-316 (2011).

8. Z. Hong, D. F. Davidson, R. K. Hanson, "A New Shock Tube Study of the Reactions $OH + H_2O_2 \rightarrow H_2O + HO_2$ and $H_2O_2 + M \rightarrow 2OH + M$ using Simultaneous Laser Absorption of H_2O and OH," Journal of Chemical Physics A **114**, 5718-5727 (2010).

9. Z. Hong, S. S. Vasu, D.F. Davidson, R. K. Hanson, "Experimental Study of the Ratio of $OH+HO_2 \rightarrow H_2O+O_2$ at High Temperatures using the Reverse Reaction," J. Phys. Chem. A **114**, 5520-5525 (2010).

10. D. F. Davidson, S. C. Ranganath, K.-Y. Lam, M. Liaw, Z. Hong, R. K. Hanson, "Ignition Delay Time Measurements of Normal Alkanes and Simple Oxygenates," J. Prop. Power **26**, 280-287 (2010).

11. S. S. Vasu, J. Zador, D. F. Davidson, R. K. Hanson, D. M. Golden, J. A. Miller, "High-temperature Measurement and a Theoretical Study of the Reaction of OH with 1-3 Butadiene," J. Chem. Phys. A **114**, 8312-8318 (2010).

12. S. S. Vasu, Ph.D. Thesis "Measurements of Ignition Times, OH Time-Histories, and reaction rates in Jet Fuel and Surrogate Oxidation Systems" Stanford University, August 2010.

13. Z. Hong, Ph.D. Thesis "An Improved Hydrogen/Oxygen Mechanism Based on Shock Tube/Laser Absorption Measurements," Stanford University, November 2010.

14. D. F. Davidson, R. K. Hanson, "Recent Advances in Shock Tube/Laser Diagnostic Methods for Improved Chemical Kinetics Measurements," Shock Waves **19**, 271-283 (2009).

15. G.A Pang, D. F. Davidson, R. K. Hanson, "Experimental Study and Modeling of Shock Tube Ignition Delay Times for Hydrogen-Oxygen-Argon Mixtures at Low Temperatures," Proc. Combust. Inst. **32**, 477-484 (2009).

16. R .D. Cook, D. F. Davidson, R. K. Hanson, "High-Temperature Shock Tube Measurements of Dimethyl Ether Decomposition and the Reaction of Dimethyl Ether with OH, J. Phys. Chemistry **113**, 9974-9980 (2009).

17. Z. Hong, G. A. Pang, S. S. Vasu, D. F. Davidson, R. K. Hanson, "The Use of Driver Inserts to Reduce Facility Effects behind Reflected Shock Waves," Shock Waves **19**, 113-123 (2009).

18. W. Ren, D. F. Davidson, R. K. Hanson, Shock Tube Measurements of Ethylene Concentration Time-histories during Ethylene, n-Heptane and methylcyclohexane Pyrolysis," 7th U.S. National Combustion Meeting, Atlanta, March 2011.

19. K.-Y. Lam, Z. Hong, S. W. Durrstein, D. F. Davidson, R. K. Hanson, C. Schulz, "Shock Tube Measurements of Ignition Delay Times and OH and H_2O Species Time-histories in 3-pentanone/O_2/Ar Mixtures" submitted to 7th Int. Conf. on Chemical Kinetics, MIT, July 2011.

Theoretical Studies of Potential Energy Surfaces*

Lawrence B. Harding
Chemical Sciences and Engineering Division
Argonne National Laboratory, Argonne, IL 60439
harding@anl.gov

Program Scope

The goal of this program is to calculate accurate potential energy surfaces for both reactive and non-reactive systems. Our approach is to use state-of-the-art electronic structure methods (CASPT2, MR-CI, CCSD(T), etc.) to characterize multi-dimensional potential energy surfaces. Depending on the nature of the problem, the calculations may focus on local regions of a potential surface (for example, the vicinity of a minimum or saddle point), or may cover the surface globally. A second aspect of this program is the development of techniques to fit multi-dimensional potential surfaces to convenient, global, analytic functions that can then be used in dynamics calculations.

Recent Progress

Roaming Radical Mechanisms: The existence of roaming radical mechanisms for the decomposition of formaldehyde and acetaldehyde is well established. We have recently reported theoretical evidence for the existence of roaming radical mechanisms in the decomposition of all alkanes larger than ethane. The calculations demonstrate that these reactions are controlled by a combination of covalent and long-range, dispersion forces with the covalent forces being most important for smaller molecules and the dispersion forces becoming dominant as the size of the molecule increases. A key new aspect of this study is an orbital overlap analysis of the reaction paths for these reactions. It is this overlap analysis that allows one to distinguish between reactions controlled primarily by covalent forces and those controlled by long-range dispersion forces. A novel feature of the reactions controlled by covalent forces is that one of the radical centers involved becomes inverted during the course of the reaction. This inversion induces a phase change in the radical orbital making the reaction Woodward-Hoffman allowed. The additional finding of Woodward-Hoffman forbidden or dispersion controlled pathways for larger alkanes suggests that roaming radical mechanisms should play an important role in the decomposition of much larger hydrocarbons.

A second new aspect of our work on roaming radical mechanisms concerns the roaming pathways in the decomposition of alkenes. A roaming-type saddle point for the decomposition of propene has been found in which there is a partial fragmentation forming nascent methyl and vinyl radicals followed by a disproportionation between the nascent radicals to make methane and acetylene. An unexpected feature of the IRC associated with this saddle point is that both the methyl radical and the vinyl radical invert before the final disproportionation. The methyl inversion is driven by the Woodward-Hoffman orbital phase argument mentioned above. The vinyl inversion makes it possible for the methyl to abstract the nearer, cis hydrogen from the vinyl radical.

A third new aspect of our work on roaming radical mechanisms concerns the possibility of isomerizations occurring via roaming mechanisms. This can happen when one of the nascent radical fragments is a resonance stabilized radical. Resonance stabilized radicals have multiple radical sites and thus two nascent radicals can begin to separate, reorient, and then recombine at a different radical site. A Woodward-Hoffman, orbital overlap analysis suggests that this will not be very favorable if the roaming radical is a hydrogen atom but could be favorable if the roaming radical is a methyl or any other radical having a p-type radical orbital. We have found roaming-type saddle points for the isomerization of methylallene to 1-butyne lying ~3 kcal/mol below the energy of separated methyl and propargyl radicals, and for the isomerization of the head-to-head propargyl dimer to the head-to tail dimer, also lying ~3 kcal/mol below the energy of two separated propargyl radicals.

Multi-State effects in OH Abstraction Reactions: The potential surfaces for abstraction reactions involving OH radicals are often complicated by the near-degeneracy of the two components of the OH, $^2\Pi$ state in the vicinity of the transition state. For example, in Figure 1 we show the energies of the key stationary points (reactants, reactant-complex, saddle point, product-complex and products) for the reaction $OH+H_2O_2 \rightarrow H_2O+HO_2$. For each of these stationary points we also show the energies of the first excited electronic state. The two electronic states differ by the orientations of the OH singly-occupied and doubly-occupied p orbitals relative to the HOOH fragment. For the reactant complex, the doubly occupied, OH, p orbital points toward an HOOH hydrogen, forming a hydrogen-bonded complex. For the saddle point it is the singly-occupied, OH, p orbital that is pointing towards this hydrogen. This switch implies a strong mixing between these two states as we move from the reactant complex to the saddle point. In a collaboration with Stephen Klippenstein, we have found that this interaction between these two electronic states results in an artifactual roughness of the surface in the vicinity of the saddle point when treated at the CASPT2 level. This in turn results in saddle point, harmonic frequencies that are too high and a TST rate that is too low. Preliminary results suggest that a computationally tractable solution to this problem is the use of a multi-state, CASPT2 approach[1]. In Figure 2 we compare the results of TST calculations using both conventional, single-state, CASPT2 (SS-CASPT2) and multi-state, CASPT2 (MS-CASPT2) to the results of a number of previous experimental studies, including the recent work of Hong et al[2]. The TST calculations using SS-CASPT2 are found to underestimate the observed rate by up to a factor of 10 while the MS-CASPT2 results agree with experiment to within a factor of two except at the lowest temperatures where tunneling is expected to dominate and more accurate tunneling treatments (beyond a simple one dimensional Eckart treatment) may be required.

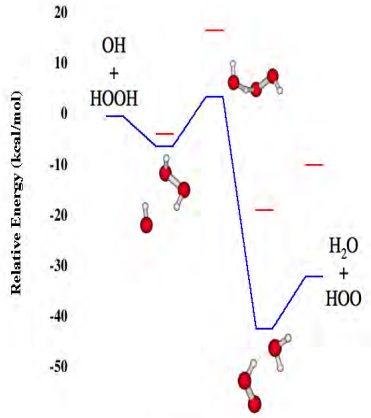

Figure 1

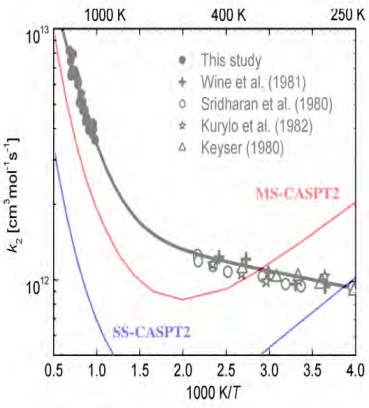

Figure 2

Future Plans

We plan to continue our studies of multi-state effects in OH abstraction reactions including the reaction $OH+HO_2 \rightarrow H_2O+O_2$. Combustion mechanisms have shown a high sensitivity to this reaction but there is considerable uncertainty in the rate of this reaction. We also plan to continue our studies of roaming radical pathways in hydrocarbons, ethers and peroxides.

Acknowledgement: This work was performed under the auspices of the Office of Basic Energy Sciences, Division of Chemical Sciences, Geosciences and Biosciences, U.S. Department of Energy, under Contract DE-AC02-06CH11357.

References:

(1) J. Finley, P. A. Malmqvist, B. O. Roos and L. Serrano-Andres, Chem. Phys. Letts. **288**, 299 (1998)
(2) Z. Hong, R. D. Cook, D. F. Davidson, and R. K. Hanson, J. Phys. Chem. A **114**, 5718 (2010)

PUBLICATIONS (2009 - Present):

Kinetics of the H + NCO Reaction
S. J. Klippenstein and L. B. Harding
32nd Symposium (International) on Combustion **32**, 149-155(2009)

Theoretical Rate Coefficients for the Reaction of Methyl Radical with Hydroperoxyl Radical and for Methylhydroperoxide Decomposition
A. W. Jasper, S. J. Klippenstein and L. B. Harding
32nd Symposium (International) on Combustion **32**, 279-286(2009)

A Crossed-Molecular Beam Study on the Formation of the Exotic Cyanoethynyl Radical in Titan's Atmosphere
X. Gu, R. I. Kaiser, A. M. Mebel, V. V. Kislov, S. J. Klippenstein, L. B. Harding, M. C. Liang, and Y. L. Yung, Astrophysical Journal **701**, 1797-1803 (2009)

The Thermal Decomposition of NH_2OH and Subsequent Reactions: Ab Initio Transition State Theory and Reflected Shock Tube Experiments
S. J. Klippenstein, L. B. Harding, B. Ruscic, R. Sivaramakrishnan, N. K. Srinivasan, M.-C. Su, and J. V. Michael, J. Phys. Chem. A. **113**, 10241-10259 (2009)

Shock Tube and Theory Investigation of Cyclohexane Decomposition
J. H. Kiefer, K. Gupte, L. B. Harding and S. J. Klippenstein
J. Phys. Chem. A. **113**, 13570-13583 (2009)

Roaming Radical Kinetics in the Decomposition of Acetaldehyde
L. B. Harding, Y. Georgievskii and S.J. Klippenstein, J. Phys. Chem. A. **114**, 765-777 (2010)

Reactions Between Resonance Stabilized Radicals: Propargyl+Allyl
J. A. Miller, S. J. Klippenstein, L. B. Harding, Y. Georgievskii, W. D. Allen, and A. C. Simmonett J. Phys. Chem. A **114**, 4881-4890 (2010)

The Effect of Spin-Orbit Splitting on the Association Kinetics of Barrierless Halogen Atom–Hydrocarbon Radical Reactions
A. W. Jasper, S. J. Klippenstein and L. B. Harding, J. Phys. Chem. A **114**, 5759-5768 (2010)

Experimental and Theoretical Investigation of the Self-Reaction of Phenyl Radicals
R. S. Tranter, S. J. Klippenstein, L. B. Harding, B. R. Giri, X. Yang and J. H. Kiefer J. Phys. Chem. A **114**, 8240-8261 (2010)

Theoretical Validation of Chemical Kinetic Mechanisms: Combustion of Methanol
R. T. Skodje, A. S. Tomlin, S. J. Klippenstein, L. B. Harding and M. J. Davis J. Phys. Chem. A **114**, 8286-8301 (2010)

Rate Constants for the Thermal Decomposition of Ethanol and its Bimolecular Reaction with OH and D: Reflected Shock Tube and Theoretical Studies
R. Sivaramakrishnan, M.-C. Su, J. V. Michael, S. J. Klippenstein, L. B. Harding and B. Ruscic J. Phys. Chem. A **114**, 9425-9439 (2010)

Roaming Radical Pathways in the Decomposition of Alkanes
L. B. Harding and S. J. Klippenstein, J. Phys. Chem. Letters **1**, 3016-3020 (2010)

Uncertainty Driven Theoretical Kinetics Studies for CH_3OH Ignition: HO_2+CH_3OH and O_2+CH_3OH
S. J. Klippenstein, L. B. Harding, M. J. Davis, A. S. Tomlin, R. T. Skodje 33nd Symposium (International) on Combustion, **33**, 351-357 (2011)

The Role of NNH in NO Formation and Control
S. J. Klippenstein, L. B. Harding, P. Glarborg, J. A. Miller Combustion and Flame, **158**, 774-489 (2011)

Roaming Radicals in the Thermal Decomposition of Dimethyl Ether: Experiment and Theory
R. Sivaramakrishnan, J. V. Michael, A. F. Wagner, R. Dawes, A. W. Jasper, L. B. Harding, Y. Georgievskii, S. J. Klippenstein, Combustion and Flame, **158**, 618-632 (2011)

Shock Tube and Theoretical Studies on the Thermal Decomposition of Propane: Evidence for a Roaming Radical Channel
R. Sivaramakrishnan, M.-C. Su, J. V. Michael, L. B. Harding, S. J. Klippenstein J. Phys. Chem. A (in press)

Near-threshold H/D Exchange in CD_3CHO Photodissociation
B. R. Heazlewood, A. T. Maccarone, D. U. Andrews, D. L. Osborn, L. B. Harding, S. J. Klippenstein, M. J. T. Jordan, and S. H. Kable, Nature Chemistry (accepted)

CHEMICAL ACCURACY FROM AB INITIO MOLECULAR ORBITAL CALCULATIONS

Martin Head-Gordon
Department of Chemistry, University of California, Berkeley, and,
Chemical Sciences Division, Lawrence Berkeley National Laboratory,
Berkeley, CA 94720.
mhg@cchem.berkeley.edu

1. Scope of Project.

Short-lived reactive radicals and intermediate reaction complexes play central roles in combustion, interstellar and atmospheric chemistry. Due to their transient nature, such molecules are challenging to study experimentally, and our knowledge of their structure, properties and reactivity is consequently quite limited. To expand this knowledge, we develop new theoretical methods for reliable computer-based prediction of the properties of such species [9]. We apply our methods, as well as existing theoretical approaches, to study prototype radical reactions, often in collaboration with experimental efforts. These studies help to deepen understanding of the role of reactive intermediates in diverse areas of chemistry. They also sometimes reveal frontiers where new theoretical developments are needed in order to permit better calculations in the future.

2. Summary of Recent Major Accomplishments.

2.1 Improved density functionals.

We have been interested in the use of range-separation to reduce self-interaction, and have developed the ωB97 family of functionals, that yield a reduction of roughly 2/3 in self-interaction errors, relative to e.g B3LYP. The combination of range separation with the use of double-hybrid construction yielded a functional that we have termed ωB97X-2 [14], which is probably our most accurate to date. It is an interesting and open question as to whether the form of range separation used so far is optimal, as more general constructions can be found [9].

2.2 Wave-function methods for excited states of large molecules.

SOS-CIS(D0): For excited states, we recently developed the quasidegenerate scaled opposite spin (SOS) doubles correction to single excitation CI. The cost of SOS-CIS(D0) [4,12] scales only 4^{th} order with molecular size, versus 5^{th} order for conventional perturbation methods such as CIS(D). It is self-interaction free, and charge-transfer excited states are correctly described. Both energies and analytical gradients [4] are available. Numerical tests of accuracy [12] suggest that it is comparable to more computationally expensive methods such as CC2.

RAS-2SF: Based on the double spin-flip (SF) approach (co-developed with Anna Krylov [1]), we have defined a new restricted active space (RAS) SF method [13] that is (i) spin-complete, (ii) size-consistent (iii) variational (iv) multistate, (v) has amplitudes whose number scale no worse than single excitations with molecule size, and (v) is exact for 4 strongly correlated electrons. RAS-2SF can be applied to quite large molecules – eg.

[20]. RAS-2SF appears to be a viable and inexpensive replacement for CASSCF in many problems, which can also remove the problem of state-averaging.

2.3 Optimizing orbitals with low-order perturbation theory.

Second order Moller-Plesset (MP2) theory can perform very poorly for radicals because of spin-contamination. For instance, the conjugated radical, phenalenyl, C13H9, (), exhibits $\langle S^2 \rangle > 2.0$ rather than 0.75. This problem can be resolved by optimizing the orbitals in the presence of 2^{nd} order electron correlation, an approach we call O2. Furthermore, O2 potential energy curves that are smoother than standard MP2 [6]. MP2 forces and dipole moments are discontinuous when orbitals change from restricted to unrestricted, while O2 is continuous. Indeed, the MP2 effective density matrices can be non-n-representable (i.e. unphysical) while those for O2 are not [6]. This suggests that orbital optimized double hybrid density functionals should be developed, as existing double hybrids have the same weaknesses as MP2.

2.4 Pairing methods for strong electron correlations.

To treat large molecules that have strong electron correlations (e.g. singlet biradicaloids), we have been developing generalized valence bond coupled cluster methods, which systematically approximate CASSCF. Perfect pairing is the starting point: exact for one pair, and extensive. The next well-defined level is the perfect quadruples (PQ) model [2], which is exact for two pairs (matches CASSCF) and extensive. It is a subset of valence space CCSDTQ, in which only the quadratic number of excitations necessary for exactness for 2 pairs are retained. This is followed the perfect hextuples (PH) model, which is exact for 3 pairs of electrons, and still scales computationally with only the 5^{th} power of molecule size [18]. PH appears to be an excellent approximation to CASSCF for computational organic chemistry. We have also begun to explore dynamical correlation corrections to the PQ and PH models [23], and have also made progress on the challenging problem of orbital optimization for these active space methods [16].

2.5 Valence bond methods for strong electron correlations.

Instead of approximating the CASSCF limit for treating strong correlations, another, relatively unexplored possibility is to approximate the spin-coupled valence bond limit (also exponentially expensive). We have made exciting recent progress on this problem, yielding a new approximate valence bond method that can break any number of chemical bonds with only a quadratic number of spin-coupling variables, maintaining extensivity, and spin-purity [3]. It still remains to treat the remaining essentially dynamical correlations, and we have started to develop a multireference density functional theory framework [10] towards this goal – it requires the reference system to be partially interacting rather than non-interacting as in Kohn-Sham DFT.

2.6 Fundamental studies of chemical bonding.

We have developed a simple and potentially broadly useful method for computational evaluation of metal oxidation states [15]. We have also gained insight into the origin of the generation of small amounts of electricity from the oxidation of CO to CO2 on a Pt thin-film catalyst – a nonadiabatic effect we show is associated with electron transfer from CO2(δ–) to the surface as the nascent product linearizes after crossing the barrier to

reaction between CO(ads) + O(ads) [7]. Other applications to biradicaloid [27] and tetraradicaloid [20] molecules have recently been completed.

3. Summary of Research Plans.

- Development of range-separated density functionals using the new "2 error function" separator.
- Efficient implementation and possibly further extension of the CC-VB model.
- Dynamic correlation corrections to the PQ and PH models using perturbation theory.
- Density-functional approaches to augmenting the CC-VB method
- New studies of the properties of reactive radicals and radical reactions.

4. Publications from DOE Sponsored Work, 2009-present.

[1] "Double spin-flip approach within equation-of-motion coupled cluster and configuration interaction formalisms: Theory, implementation and examples" D. Casanova, L.V. Slipchenko, A.I. Krylov, and M. Head-Gordon, J. Chem. Phys. 130, 044103 (2009).

[2] "The perfect quadruples model for electron correlation in a valence active space", J.A. Parkhill, K.V. Lawler, and M. Head-Gordon, J. Chem. Phys. 130, 084101 (2009)

[3] "Tractable spin-pure methods for bond-breaking: Local many-electron spin-vector sets and an approximate valence bond model", D.W. Small and M. Head-Gordon, J. Chem. Phys 130, 084103 (2009).

[4] "Quartic-scaling analytical gradient of quasidegenerate scaled opposite spin second order perturbation corrections to single excitation configuration interaction", Y.M. Rhee and M. Head-Gordon, J. Chem. Theor. Comput. 5, 1224-1236 (2009).

[5] "The numerical condition of electron correlation theories when only active pairs of electrons are spin-unrestricted", K.V. Lawler, J.A. Parkhill, and M. Head-Gordon, J. Chem. Phys. 130, 184113 (2009) (7 pages)

[6] "Violations of N-representability from spin-unrestricted orbitals in Møller-Plesset perturbation theory and related double-hybrid density functional theory", W. Kurlancheek and M. Head-Gordon, Mol. Phys. 107, 1223-1232 (2009).

[7] "Chemistry of fast electrons", S.N. Maximoff and M. Head-Gordon, Proc. Natl. Acad. Sci. USA 106, 11461-11465 (2009).

[8] "Improving approximate optimized effective potentials by imposing exact conditions: Theory and application to electronic statics and dynamics", Y. Kurzweil and M. Head-Gordon, Phys. Rev. A 80, 012509 (2009).

[9] "The exchange energy of a uniform electron gas experiencing a new, flexible range separation", J.A. Parkhill, J.-D. Chai, A.D. Dutoi and M. Head-Gordon, Chem. Phys. Lett. 478, 283-286 (2009).

[10] "Analysis of multi-configuration density functional theory methods: Theory and model application to bond-breaking", Y. Kurzweil, K.V. Lawler and M. Head-Gordon, Mol. Phys. 107, 2103-2110 (2009).

[11] "Hartree-Fock solutions as a quasidiabatic basis for non-orthogonal configuration interaction", A.J.W. Thom and M. Head-Gordon, J. Chem. Phys. 131, 124113 (2009).

[12] "Performance of quasidegenerate scaled opposite spin perturbation corrections to single excitation configuration interaction for excited state structures and excitation energies with application to the Stokes shift of 9-methyl-9,10-dihydro-9-silaphenanthrene", Y.M. Rhee, D. Casanova, and M. Head-Gordon, J. Phys. Chem. A 113, 10564-76 (2009).

[13] "Restricted active space spin-flip configuration interaction approach: Theory, implementation and examples" D. Casanova and M. Head-Gordon, Phys. Chem. Chem. Phys. 11, 9779-9790 (2009).

[14] “Long-range corrected double hybrid density functionals”, J.-D. Chai and M. Head-Gordon, J. Chem. Phys. 131, 174105 (2009) (13 pages).
[15] “LOBA: A localized orbital bonding analysis to calculate oxidation states, with application to a model water oxidation catalyst”, A.J.W. Thom, E. Sundstrom, and M. Head-Gordon, Phys. Chem. Chem. Phys. 11, 11297-11304 (2009)
[16] “Orbitals that are unrestricted in active pairs for generalized valence bond coupled cluster methods”, K.V. Lawler, D.W. Small and M. Head-Gordon J. Phys. Chem. A 114, 2930-2938 (2010).
[17] “A Sparse Framework for the Derivation and Implementation of Fermion Algebra”, J.A. Parkhill and M. Head-Gordon, Mol. Phys. 108, 513-522 (2010).
[18] “A tractable and accurate model for static electron correlations: The perfect hextuples model”, J.A. Parkhill, and M. Head-Gordon, J. Chem. Phys. 133, 024103 (2010) (10 pages).
[19] “Ab initio calculations on the electronically excited states of small helium clusters”, K.D. Closser and M. Head-Gordon, J. Phys. Chem. A 114, 8023-8032 (2010).
[20] “Theoretical study of substituted PBPB dimers: Structural analysis, tetraradical character and excited states”, F. Bell, D. Casanova and M. Head-Gordon, J. Am. Chem. Soc. 132, 11314–11322 (2010)
[21] “An Additive Long-range Potential to Correct for the Charge-transfer Failure of Time-dependent Density Functional Theory”, A. Dreuw, J. Plotner, M. Wormit, M. Head-Gordon, and A.D. Dutoi, Z. Phys. Chem. 224, 311-324 (2010)
[22] “Modeling the charge transfer between alkali metals and polycyclic aromatic hydrocarbons using electronic structure methods”, T. Baker and M. Head-Gordon, J. Phys. Chem. A 114, 10326-10333 (2010).
[23] “A truncation hierarchy of coupled cluster models of strongly-correlated systems based on perfect-pairing references: the single plus doubles models”, J.A. Parkhill and M. Head-Gordon, J. Chem. Phys. 133, 124102 (2010)
[24] “Ab initio molecular dynamics with dual-basis methods”, R.P. Steele, M. Head-Gordon and J.C. Tully, J. Phys. Chem. 114, 11853-11860 (2010)
[25] “The higher-order singular value decomposition in quantum chemistry”, F. Bell, D.S. Lambrecht and M. Head-Gordon, Mol. Phys. 108, 2759-2774 (2010).
[26] “A parallel implementation of the analytic nuclear gradient for time-dependent density functional theory within the Tamm-Dancoff approximation”, F.-L. Liu, Z. Gan, Y. Shao, C.-P. Hsu, A. Dreuw, M. Head-Gordon, B.T. Miller, B.R. Brooks, J.-G. Yu, T.R. Furlani and J. Kong, Mol. Phys. 108, 2791-2800 (2010).
[27] “Intermediate-Valence Tautomerism in Decamethylytterbocene Complexes of Methyl-Substituted Bipyridines”, C. Booth, D. Kazhdan, E. Werkema, M. Walter, W. Lukens, E. Bauer, Y.-J. Hu, L. Maron, O. Eisenstein, M. Head-Gordon, R. Andersen, J. Am. Chem. Soc. 132, 17537-17549 (2010).
[28] “Fast Sparse Cholesky Decomposition and Inversion using Nested Dissection Matrix Reordering”, K. Brandhorst and M. Head-Gordon, J. Chem. Theor. Comput. 7, 351-368 (2011).
[29] “A new fitting metric for resolution of the identity second-order Møller-Plesset perturbation theory”, D.S. Lambrecht, K. Brandhorst, W.H. Miller, and M. Head-Gordon J. Phys. Chem. A 115, 2794-2801 (2011).

Laser Studies of Combustion Chemistry

John F. Hershberger

Department of Chemistry and Biochemistry
North Dakota State University
NDSU Dept. 2735, PO Box 6050
Fargo, ND 58108-6050
john.hershberger@ndsu.edu

Time-resolved infrared diode laser absorption and laser-induced fluorescence spectroscopy are used in our laboratory to study the kinetics and product channel dynamics of chemical reactions of importance in the gas-phase combustion chemistry of nitrogen-containing species. This program is aimed at improving the kinetic database of reactions crucial to the modeling of NO_x control strategies such as Thermal de-NO_x, RAPRENO$_x$, and NO-reburning. The emphasis in our study is the quantitative measurement of both total rate constants and product branching ratios.

NCCO Kinetics

We have successfully detected the NCCO radical using high-resolution infrared absorption spectroscopy for the first time. NCCO is formed by the photolysis of methyl cyanoformate or ethyl cyanoformate:

$$CH_3OC(O)CN \rightarrow NCCO + CH_3O \quad (1)$$
$$C_2H_5OC(O)CN \rightarrow NCCO + C_2H_5O \quad (2)$$

As described in last year's report, we have found several infrared transient absorption signals attributable to the NCCO radical in the 1887-1890 cm^{-1} range, in good agreement with high level ab initio calculations.[1] We have studied the kinetics of NCCO with O_2, NO, and NO_2. We are currently finishing the NO_2 studies, and also investigating whether NCCO reacts with hydrocarbons.

For NCCO + O_2, several product channels are possible:

$$NCCO + O_2 \rightarrow NCC(O)OO \quad (3a)$$
$$\rightarrow NCO + CO_2 \quad (3b)$$
$$\rightarrow 2\ CO + NO \quad (3c)$$

We find a slow, slightly pressure-dependent rate constant of k_3 (298 K) = (5.2 ± 0.3) × 10^{-13} cm^3 molecule^{-1} s^{-1} at 2 Torr pressure of N_2. Our result is in good agreement with the one previous kinetic study which used mass spectrometric

detection.[2] Channel (3a), the NCC(O)OO adduct, which we cannot spectroscopically detect, appears to be the major product channel in this reaction, but we estimate a branching ratio into (3b) of $\varphi_{3b} = 0.28 \pm 0.06$ at 3.2 Torr total pressure. This is in qualitative agreement with a recent ab initio calculation[3] which predicted that both (3a) and (3b) may be present. Channel (3c) is unimportant, with $\varphi_{3c} < 0.03$.

For NCCO with NO, possible product channels include:

$$\begin{aligned} NCCO + NO &\rightarrow CO_2 + NCN && (4a)\\ &\rightarrow NCO + NCO && (4b)\\ &\rightarrow CO + NCNO && (4c)\\ &\rightarrow NCC(NO)O && (4d) \end{aligned}$$

This reaction also displays pressure-dependent kinetics:
k_4 (298 K) = (3.2-27.1) × 10^{-13} cm^3 $molecule^{-1}$ s^{-1} over the total pressure range 3.0-25.0 Torr. This result suggests that channel (4d) is important. In fact, we only detect extremely small yields of CO and CO_2 in this reaction, suggesting that φ_{4a}, φ_{4b}, and φ_{4c} are all less than 0.02.

We have also calculated critical points on both the triplet and singlet potential energy surfaces of this reaction. We find that all pathways to product channels (4a), (4b), and (4c) involve high energy barriers, and are therefore inaccessible at moderate temperatures. In summary, both experiment and theory are in agreement that this reaction is dominated by collisional stabilization of the NCC(NO)O adduct, channel (4d).

For NCCO + NO_2, possible product channels include:

$$\begin{aligned} NCCO + NO_2 &\rightarrow CO_2 + CN + NO && (5a)\\ NCCO + NO_2 &\rightarrow NCO + NO + CO && (5b)\\ NCCO + NO_2 &\rightarrow N_2O + 2\ CO && (5c)\\ NCCO + NO_2 &\rightarrow CO_2 + CO + N_2 && (5d) \end{aligned}$$

Work on this reaction is still in progress. We find a rate constant of $(2.1\pm0.1)\times10^{-11}$ cm^3 $molecule^{-1}$ s^{-1} at 298 K and ~1.0 Torr total pressure, substantially faster than NCCO+NO or NCCO + O_2. Ab initio calculations suggest a complicated potential energy surfaces, with many loosely-bound intermediate structures, but channel (5a) appears to be the most likely product channel. Experimental probes of the product distributions are currently underway. One complication is that CN produced in the photolysis reacts quickly with NO_2, producing some of the same products. We are investigating the possibility of using a hydrocarbon to quickly remove CN radicals without removing NCCO. In order for this to work, NCCO must not react with hydrocarbons. We have measured an upper limit of ~5×10^{-15} cm^3 $molecule^{-1}$

s^{-1} for the rate constant of the NCCO + C_2H_4 reaction, suggesting that C_2H_4 can remove CN radicals without affecting NCCO.

CN + CS_2

We have studied the reaction of CN with CS_2, which has not previously been reported in the literature. We used 266-nm photolysis of ICN, along with transient infrared detection of CN radicals.

We find a highly pressure dependent rate constant at 298 K of:

$k = (7.1 \pm 0.2 - 41.9 \pm 2.9) \times 10^{-12}$ cm^3 $molecule^{-1}$ s^{-1}
over the pressure range 2 – 40 Torr.

Ab initio calculations (at the CCSD(T)/6-311++G(d,p)//B3LYP/6-311++G(d,p) level), show a barrierless addition to bent N-C-S-C-S adducts, or addition through a 3.4 kcal/mole barrier to a T-shaped N-C-CS_2 adduct. The bent adduct can dissociate to NCS + CS products, which are nearly thermoneutral with respect to reactants: at the CCSD(T)/6-311++G(d,p)//B3LYP/6-311++G(d,p) level, NCS + CS is lower in energy than the reactants by 0.4 kcal/mole, but at the CCSD(T)/6-31G(d,p)//CCSD(T)/6-31G(d,p) level, using B3LYP only for zero-point energy corrections, we find NCS + CS to be 2.5 kcal/mole higher than reactants. In any case, the experimental observation of a pressure dependence suggests that collisional stabilization of the adducts dominates this reaction.

CN + SO_2

We have studied this reaction using similar techniques to that described above for CN + CS_2. We find no measurable reaction, with an upper limit of $k<3.1\times10^{-14}$ cm^3 $molecule^{-1}$ s^{-1} at 298 K. This is in disagreement with the one previous reported value[4] (4.40×10^{-12} cm^3 $molecule^{-1}$ s^{-1}, based on LIF measurements); a surprising discrepancy, considering that these measurements are fairly straightforward. We do not have a perfect explanation for this, but note that it is much easier to have an experimental rate constant be erroneously high than erroneously low. We have also performed ab initio calculations, which show that although formation of NCO + SO products is nearly thermoneutral, the likely path through a bent O-S-O-C-N adduct has a substantial entrance barrier of 8.4 kcal/mole. Formation of a T-shaped N-C-SO_2 adduct has a ~10 kcal/mole barrier. In summary, our calculations appear to support our observation of a very slow reaction.

HCNO Kinetics

Last year's report demonstrated an upper limit of $<2\times10^{-13}$ cm^3 molecule^{-1} s^{-1} for the 298 K rate constant of the Cl + HCNO reaction. Further work in the past year has lowered this upper limit to $k <3.5\times10^{-15}$ cm^3 molecule^{-1} s^{-1}, verifying that fulminic acid is unreactive towards chlorine (and probably other halogen atoms as well). Characterization of the potential energy surface by ab initio methods is underway.

References

1. A.C. Simmonett, F.A. Evangelista, W.D. Allen, H.F. Schaefer III, J. Chem. Phys. 127, 14306 (2007).
2. T. Imamura, N. Washida, Int. J. Chem. Kinet. 33, 440 (2001).
3. Y. Tang, R. Wang, B. Wang, J. Phys. Chem. 112, 5295 (2008).
4. T.A. Titarchuk and J.B. Halpern, Chem. Phys. Lett. 232, 192 (1995).

Publications acknowledging DOE support (2009-present)

1. "A Re-investigation of the Branching Ratio of the CN + O_2 Reaction", W. Feng and J.F. Hershberger, J. Phys. Chem. A 113, 3523 (2009).
2. "Infrared Diode Laser Study of the Kinetics of the NCCO + O_2 Reaction", W. Feng and J.F. Hershberger, Chem. Phys. Lett. 488, 140 (2010).
3. "Kinetics and Mechanism of the NCCO + NO Reaction", W. Feng and J.F. Hershberger, J. Phys. Chem. A 114, 6843 (2010).
4. "Kinetics of the CN + CS_2 and CN + SO_2 Reactions", W. Feng and J.F. Hershberger, J. Phys. Chem. A 115, 286 (2011).

Breakthrough Design and Implementation of Electronic and Vibrational Many-Body Theories

So Hirata (principal investigator: DE-FG02-11ER16211; formerly DE-FG02-04ER15621)
Department of Chemistry, University of Illinois at Urbana-Champaign,
600 South Mathews Avenue, Urbana, IL 61801
sohirata@illinois.edu

Program Scope

Predictive chemical computing requires hierarchical many-body methods of increasing accuracy for both electrons and vibrations. Such hierarchies are established, at least conceptually, as configuration-interaction (CI), many-body perturbation (MP), and coupled-cluster (CC) methods, which all converge at the exact limit with increasing rank of a hierarchical series. These methods can generate results of which the convergence with respect to various parameters of calculations can be demonstrated and which can thus be predictive in the absence of experimental information.

The wide use of the hierarchical electronic and vibrational many-body methods has, however, been hindered (1) by the immense cost of *executing* the calculations with these methods and, furthermore, the non-physical rapid increase of the cost with increasing molecular size, (2) by the complexity and cost of *developing* some of the high-rank members of these methods, and (3) by the slow convergence of electronic energies and wave functions with respect to one-electron basis set sizes, which further drives up the cost of execution.

The overarching goal of our research is to address all three difficulties for electrons and vibrations in small molecules in the gas phase as well as in solids and molecules in condensed phases. We have eradicated the second difficulty for electrons by developing a computerized symbolic algebra system that completely automates the mathematical derivations of electron-correlation methods and their implementation. For vibrations, an assortment of vibrational many-body methods has been implemented in the general-order algorithm that allows us to include anharmonicity and vibrational mode-mode couplings to any desired extent. We have also addressed the third difficulty by departing from the conventional Gaussian basis sets and introduce a new hierarchy of converging electron-correlation methods with completely flexible but rational (e.g., satisfying asymptotic decay and cusp conditions) basis functions such as numerical basis functions on interlocking multicenter quadrature grids and explicit r_{12} (inter-electronic distance) dependent basis functions.

Our current research focus is to address the first difficulty and to make the hierarchical electronic and vibrational many-body methods applicable to solids.

Recent Progress

We have made significant progress in the fundamental as well as computational aspects of the electronic and vibrational many-body theories for solids. For the anharmonic vibrational problem, we have laid out a complete framework of size-consistent many-body theories encompassing the vibrational self-consistent field (VSCF), vibrational MP (VMP), and vibrational CC (VCC) methods. We have also implemented a size-consistent version of VSCF for molecules. For the electron-correlation problem, we have derived a number of diagrammatic and algebraic theorems for the "size-consistent design" of electronic structure methods. In this relation, we have also addressed more fundamental physical question as to why energy is extensive and statistical thermodynamics works in chemistry. We have found a proof of the extensivity of energy for electrically neutral, perfect crystal, which is alternative to and more accessible and chemical than Fefferman's original proof. The details are summarized below.

Since the 31st Annual Combustion Research Meeting, 8 peer-reviewed papers[5–12] including one mini-review[7] have been published and one invited Feature Article[23] is being reviewed. In total, 23 publications[1–23] (including one submitted) have resulted from this grant in 2009–2011. During the same period, the PI was an invited speaker at 15 international and domestic conferences (including one as a plenary speaker and one as an award lecturer) and gave 12 invited talks at 9 universities and one national laboratory. The PI was appointed as a Professor at University of Illinois at Urbana-Champaign and an Alumni Research Scholar in 2010 as well as a member of the editorial boards of *The Journal of Chemical Physics* and *International Journal of Quantum*

Chemistry in 2011. A graduate student partially supported by this grant, Murat Keçeli, received a University Block Grant Fellowship and another student, Olaseni Sode, received a Roger Adams Fellowship and a GAANN Fellowship.

First-principles theories for anharmonic lattice vibrations (Hirata, Keçeli and Yagi).[11] VSCF and other anharmonic vibrational methods based on it contain numerous contributions that do not exhibit physically correct size dependence. The correct size dependence is extensivity for zero-point energies and intensivity for transition energies. We have made size-consistent generalizations of VSCF, VMP, and VCC for anharmonic lattice vibrations in solids and presented their formalisms. The size dependence of the methods has been determined by inspecting the asymptotic functional dependence of various quantities entering their formalisms on the number (K) of wave vector sampling points in the Brillouin zone (BZ). Our analysis has revealed that VSCF for an infinite periodic system in normal coordinates has numerous terms that have nonphysical size dependence and vanish in the bulk limit. We have identified and eliminated these terms to arrive at the most compact and explicitly size-consistent equations taking a quartic force field (QFF) as an example of the potential energy surface (PES). This size-consistent VSCF with a QFF, termed *q*VSCF, has no contributions from cubic force constants in the zero-point or transition frequencies with its effective one-mode potential being harmonic and containing a subset of quartic force constants. The *q*VSCF method also provides a way to evaluate an anharmonic correction to the lattice structure due to cubic force constants of a certain type. We have also defined size-consistent VMP and VCC with a QFF in the size-consistent *q*VSCF reference. These methods (*q*VMP and *q*VCC) account for anharmonic effects on the frequencies due to all cubic and quartic force constants. We have also given an algebraic proof of the lack of size consistency in vibrational truncated CI. All of these methods can be readily extended to a higher-order truncated Taylor expansion of a PES, but not to a grid representation of a PES or *n*-mode coupling approximation to a PES.

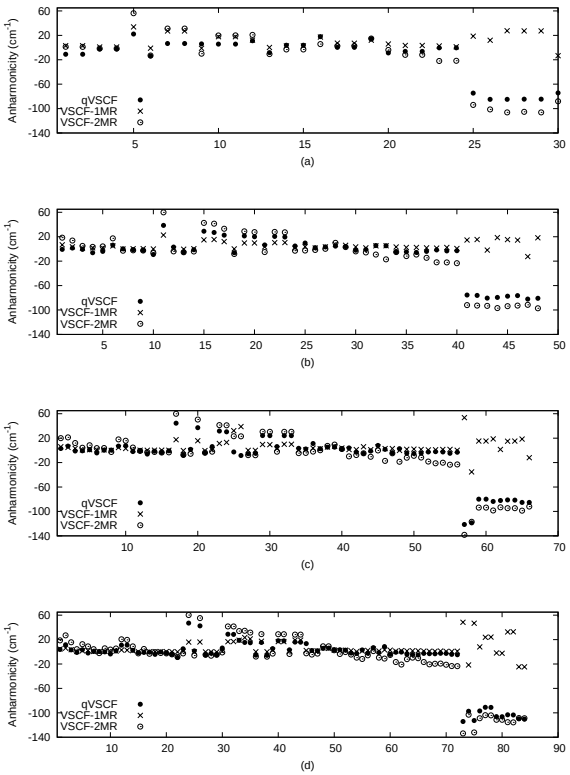

Figure 1. Frequencies of (a) C_6H_6, (a) $C_{10}H_8$, (a) $C_{14}H_{10}$, and (a) $C_{18}H_{12}$ calculated by VSCF with one- (1MR) and two-mode coupling (2MR) approximation to QFF and *q*VSCF.

A computer implementation of size-consistent VSCF (Keçeli and Hirata). We have developed algorithms of the *q*VSCF method and implemented them initially for molecules along with the conventional VSCF method. The *q*VSCF algorithm is considerably simpler with only two types of integrals (both analytically evaluated in harmonic-oscillator basis functions) and two types of force constants involved instead of four and nine types of integrals and force constants. The *q*VSCF method, unlike VSCF, also does not need any diagonalization step while it is still based on iterative achievement of a self-consistent field. Because of this simplification, *q*VSCF is faster than VSCF by more than two orders of magnitude in our implementations (the size dependence of the cost is the same). Owing to the lack of all cubic and some quartic force constants in the formalism of *q*VSCF, it does not capture as much anharmonic effects as VSCF does for small molecules. However, for larger molecules such as C_6H_6, $C_{10}H_8$, $C_{14}H_{10}$, and $C_{18}H_{12}$, the differences between *q*VSCF and VSCF become insignificant (see **Figure 1**) because the former eliminates all nonphysical, vanishing contributions from the formalism of the latter.

Anharmonic vibrational frequencies of polyethylene and polyacetylene (Keçeli and Hirata).[8,10] We have reported the frequencies of the infrared- and/or Raman-active vibrations of polyethylene and polyacetylene at the "double *ab initio*" level, namely, using the PES obtained by *ab initio* MP2 crystal orbital (CO) theory for the polymers and by solving the vibrational problem with the *ab initio* VSCF, VCI, and VMP methods.

The issue of size-consistency has been avoided by using the so-called Γ approximation, which amounts to including only the BZ-center modes in the expansion of the wave function. We have shown that accounting for both electron correlation and anharmonicity is essential in achieving good agreement (the mean and maximum absolute deviations less than 50 and 90 cm^{-1}, respectively) between theory and experiment. The corresponding values in the calculations including only one of those effects are in excess of 120 and 300 cm^{-1}, respectively. The VCI calculations also reproduce the frequency separation and intensity ratio of the Fermi doublets in polyethylene.

Thermodynamic limit of energy density and size-consistent design (Hirata and Ohnishi).[23] Why is energy extensive? Why is an application of statistical thermodynamics to chemistry valid? It has taken 40 years for the finest mathematicians to complete the proof of the extensivity of energy or, equivalently, the existence of thermodynamic (infinite-volume) limit of energy density. We have found an alternative, more accessible proof of the extensivity of energy for electrically neutral, metallic and nonmetallic crystals by establishing the same for its individual energy components, namely, the kinetic, Coulomb, exchange, and correlation energies. On this basis, we have derived several diagrammatic and algebraic theorems for the size-consistent design of electronic and vibrational many-body methods. Our findings are summarized as follows: The significance of the distinct use of the intermediate and standard normalization for extensive and intensive operator amplitudes, respectively; The extensive and intensive diagram theorems, which serve as the foolproof criteria for determining size consistency of a method for extensive and intensive quantities; The extensive-intensive operator consistency theorem, which stipulates the precise balance between the determinant spaces reached by extensive and intensive operators in a size-consistent excited-state method.

Fast CC singles and doubles for extended systems (Keçeli and Hirata).[8] The modulo-*n* scheme, introduced earlier in this research program, has been used in conjunction with the CC singles and doubles (CCSD) and third-order MP (MP3) methods for one-dimensional, infinitely extended, periodic systems. By downsampling uniformly the wave vectors in BZ integrations, this scheme accelerates these accurate but expensive correlation-energy calculations by two to three orders of magnitude while incurring negligible errors in their total and relative energies. The CCSD and MP3 methods have been applied to the PES of polyethylene in its anharmonic frequency calculations.

Hybrid CC and MP for extended systems (Ohnishi and Hirata). In small-gap semiconductors and metals, the MP methods are expected to work poorly in evaluating correlation effects involving energy bands near Fermi level. On the Fermi surface of a metal, in fact, the denominators in the MP expressions can vanish and the corresponding MP contributions may diverge (although the total MP energies do not). We have thus combined CC and MP methods for these small-gap semiconductors and metals. We apply CCD, which may be more robust for degenerate or quasi-degenerate energy levels, to calculate the correlation contributions that involve energy bands that are near Fermi level, while we use MP2 to the remainder of the correlation effects. This hybrid CC/MP scheme has been introduced by Nooijen and studied subsequently by Bochevarov and Sherrill for molecules, but we have applied it for the first time to solids. This has required us to redefine the intermediate tensors and contraction orders of molecular integrals and excitation amplitudes in CCD to achieve maximum efficiency.

Future Plans

With the understanding of the structure of wave functions in solids and size-consistent design principles of electronic and vibrational methods revealed in this funding cycle, we plan to develop the electronic and vibrational many-body methods for solids that exploit this knowledge into efficient computer programs. Our primary focus of the methodological developments is on (1) the quantitative theories and algorithms for the electronic structures of metals (that go beyond density-functional approximations), (2) the quantitative theories and algorithms for the anharmonic vibrational effects on the lattice constants as well as frequencies of solids, (3) the finite-temperature formalisms (for both electrons and vibrations), and (4) the quantitative theories of superconductivity. Our interest for application lies in molecular crystals such as ice and molecular liquid such as water. We can already routinely apply MP2 and CCSD to proton-ordered phases of ice, but we hope to extend these calculations to proton-disordered phases, liquid water, chemical reactions and excitations in aqueous phases, etc. To achieve this, we are incorporating parallelism in the algorithm and the application of static pressure.

Publications of DOE Sponsored Research (2009–Present)

Book chapters

1. S. Hirata, O. Sode, M. Keçeli, and T. Shimazaki, "Electron correlation in solids: Delocalized and localized orbital approaches," a chapter in *Accurate Condensed-Phase Quantum Chemistry* edited by F. Manby, p.129–161 (CRC Press, Boca Raton, 2010).
2. S. Hirata, T. Shiozaki, E. F. Valeev, and M. Nooijen, "Eclectic electron-correlation methods," a chapter in *Recent Progress in Coupled-Cluster Methods: Theory and Application* edited by P. Carsky, J. Paldus, and J. Pittner, p.191–217 (Springer, Dordrecht, 2010).
3. S. Hirata, P.-D. Fan, M. Head-Gordon, M. Kamiya, M. Keçeli, T. J. Lee, T. Shiozaki, J. Szczepanski, M. Vala, E. F. Valeev, and K. Yagi, "Computational interstellar chemistry," a chapter in *Recent Advances in Spectroscopy: Astrophysical, Theoretical and Experimental Perspective* edited by R. K. Chaudhuri, R. K. Mekkaden, M. V. Raveendran, A. S. Narayanan, p.21–30 (Springer-Verlag, Berlin, 2010).
4. T. Shiozaki, E. F. Valeev, and S. Hirata, "Explicitly correlated coupled-cluster methods," a chapter in *Annual Reports of Computational Chemistry, Vol. 5* edited by G. Tschumper, p.131–148 (2009).

Refereed articles (reviews and perspectives in bold letters)

5. D. G. Patel, Y.-Y. Ohnishi, Y. Yang, S.-H. Eom, R. T. Farley, K. R. Graham, J. Xue, S. Hirata, K. S. Schanze, and J. R. Reynolds, *Journal of Polymer Science Part B: Polymer Physics* (in press, 2011), "Conjugated polymers for pure UV light emission: Poly(*meta*-phenylenes)."
6. I. Grabowski, V. Lotrich, and S. Hirata, *Molecular Physics* [QTP Special Issue] **108**, 3313-3322 (2010), "Ab initio DFT–the seamless connection between WFT and DFT."
7. **S. Hirata, *Molecular Physics* [QTP Special Issue] 108, 3113–3124 (2010), "Bridging quantum chemistry and solid-state physics."**
8. M. Keçeli and S. Hirata, *Physical Review B* **82**, 115107 (2010) (6 pages), "Fast coupled-cluster singles and doubles for extended systems: Application to the anharmonic vibrational frequencies of polyethylene in the Γ approximation."
9. O. Sode and S. Hirata, *The Journal of Physical Chemistry A* [Klaus Ruedenberg Special Issue] **114**, 8873–8877 (2010), "Second-order many-body perturbation study of solid hydrogen fluoride."
10. M. Keçeli, S. Hirata, and K. Yagi, *The Journal of Chemical Physics* **133**, 034110 (2010) (6 pages), "First-principles calculations on anharmonic vibrational frequencies of polyethylene and polyacetylene in the Γ approximation."
11. S. Hirata, M. Keçeli, and K. Yagi, *The Journal of Chemical Physics* **133**, 034109 (2010) (14 pages), "First-principles theories for anharmonic lattice vibrations."
12. Y.-Y. Ohnishi and S. Hirata, *The Journal of Chemical Physics* **133**, 034106 (2010) (8 pages), "Logarithm second-order many-body perturbation method for extended systems."
13. T. Shiozaki and S. Hirata, *The Journal of Chemical Physics* (*Communications*) **132**, 151101 (2010) (4 pages), "Explicitly correlated second-order Møller–Plesset perturbation method for extended systems."
14. S. Hirata, E. B. Miller, Y.-Y. Ohnishi, and K. Yagi, *The Journal of Physical Chemistry A* [Russell M. Pitzer Special Issue] **113**, 12461–12469 (2009), "On the validity of the Born–Oppenheimer separation and the accuracy of diagonal corrections in anharmonic molecular vibrations."
15. **S. Hirata, *Physical Chemistry Chemical Physics* [an invited Perspective Article] 11, 8397–8412 (2009), "Quantum chemistry of macromolecules and solids."**
16. S. Hirata and T. Shimazaki, *Physical Review B* **80**, 085118 (2009) (7 pages), "Fast second-order many-body perturbation method for extended systems."
17. T. Shiozaki, E. F. Valeev, and S. Hirata, *The Journal of Chemical Physics* **131**, 044118 (2009) (12 pages), "Explicitly correlated combined coupled-cluster and perturbation methods."
18. T. Shimazaki and S. Hirata, *International Journal of Quantum Chemistry* [Frank E. Harris Special Issue] **109**, 2953–2959 (2009), "On the Brillouin-zone integrations in second-order many-body perturbation calculations for extended systems of one-dimensional periodicity"
19. K. Yagi, H. Karasawa, S. Hirata, and K. Hirao, *ChemPhysChem* (*Communications*) **10**, 1442–1444 (2009), "First-principles quantum vibrational simulations of the guanine-cytosine base pair."
20. M. Keçeli, T. Shiozaki, K. Yagi, and S. Hirata, *Molecular Physics* [Henry F. Schaefer III Special Issue] **107**, 1283–1301 (2009), "Anharmonic vibrational frequencies and vibrationally-averaged structures of key species in hydrocarbon combustion: HCO^+, HCO, HNO, HOO, HOO^-, CH_3^+, and CH_3."
21. O. Sode, M. Keçeli, S. Hirata, and K. Yagi, *International Journal of Quantum Chemistry* [Kimihiko Hirao Special Issue] **109**, 1928–1938 (2009), "Coupled-cluster and many-body perturbation study of energies, structures, and phonon dispersions of solid hydrogen fluoride."
22. T. Shiozaki, M. Kamiya, S. Hirata, and E. F. Valeev,*The Journal of Chemical Physics* **130**, 054101 (2009) (10 pages), "Higher-order explicitly correlated coupled-cluster methods."

Submitted articles (reviews and perspectives in bold letters)

23. **S. Hirata, *Theoretical Chemistry Accounts* [an invited Feature Article] (2011), "Size consistency."**

Generalized Van Vleck Variant of Multireference Perturbation Theory

Mark R. Hoffmann
University of North Dakota
Chemistry Department
Grand Forks, ND 58202-9024
Email: mhoffmann@chem.und.edu

I. Project Scope

There remains a need to develop new, cutting edge theoretical and computational electronic structure methods to support the study of complex potential energy surfaces (PESs). While standard methods of computational chemistry are usually adequate for studying the ground electronic states of molecular species near their equilibrium geometries, reaction intermediates, transition states and excited states generally require advanced methods that take into account their multiconfigurational nature. Multireference (MRPT) and quasidegenerate (QDPT) perturbation theories have been demonstrated to be efficient and effective for the description of electron correlation in essentially arbitrarily complex molecules. Recent work demonstrated that the mathematically robust and physically correct structures in our MRPT, called Generalized van Vleck Perturbation Theory (GVVPT), are amenable to highly efficient algorithms. Specifically, second- and third-order approximations of GVVPT (i.e., GVVPT2 and GVVPT3) utilize routines in common with our highly efficient macroconfiguration-based, configuration-driven MRCISD[1]. Consequently, theoretical and computational development can proceed by first addressing the structurally simpler equivalent CI problem. Chemical problems that are not addressed readily by other theoretical methods become accessible to MRPT or QDPT: problems such as the descriptions of large regions of excited electronic state PESs of polyatomics, especially when the characters of the excited states are doubly excited relative to the ground state, and the characterizations of multiple PESs of the same symmetry in close proximity. Within the scope of this grant, we intend to apply these theoretical techniques to combustion-relevant Group 15 oxides, and to develop their descriptions of derivative and spin-orbit nonadiabatic couplings.

II. Recent Progress

A. GVVPT2 Molecular Derivatives and Nonadiabatic Coupling Terms. The fully variational Lagrangian functional formalism, first introduced to quantum chemistry by Helgaker and Jørgensen,[2] was used to construct analytical formulas for GVVPT2 and MRCISD molecular gradients and nonadiabatic coupling terms. Under this approach, a Lagrangian is formed from the constraint functions $\mathbf{e}(\mathbf{x}, \boldsymbol{\lambda}(\mathbf{x}))$, which determine the nonvariational electronic structure parameters $\boldsymbol{\lambda}(\mathbf{x})$ that influence the electronic energy, and a suitable function $g(\mathbf{x})$ which has a geometry gradient that corresponds to either the GVVPT2 (or MRCISD) molecular gradient or the GVVPT2 (or MRCISD) nonadiabatic coupling terms

$$\mathscr{L}\big(\mathbf{x},\boldsymbol{\lambda}(\mathbf{x}),\boldsymbol{\eta}(\mathbf{x})\big) = g\big(\mathbf{x},\boldsymbol{\lambda}(\mathbf{x})\big) + \big\langle \boldsymbol{\eta}(\mathbf{x}) \big| \mathbf{e}\big(\mathbf{x},\boldsymbol{\eta}(\mathbf{x})\big)\big\rangle \tag{1}$$

It can be shown that when the Lagrangian is stationary with respect to both the electronic structure parameters and the Lagrange multipliers $\boldsymbol{\eta}(\mathbf{x})$ which multiply the constraint functions,

$$\frac{\partial \mathscr{L}}{\partial \lambda_i} = 0 \qquad \frac{\partial \mathscr{L}}{\partial \eta_j} = 0\,, \tag{2}$$

the explicit geometry derivatives of the Lagrangian will be equal to the molecular derivatives of the electronic energy (or equal to the nonadiabatic coupling terms); i.e.,

$$\frac{\partial \mathscr{L}}{\partial x_a} = \frac{dg}{dx_a} \quad ; \tag{3}$$

i.e. the geometry derivatives of the nonvariational electronic structure parameters of the electronic energy are not required. There is some flexibility in the definition of the Lagrangian for GVVPT2 and MRCISD, primarily because of redundancies associated with the underlying MCSCF. The choice that we made is

very convenient in that: it does not impose any restrictions on the choice of the weights within the SA-MCSCF orbital optimization; and it accounts for the restrictions on the variations of the MCSCF CI coefficients through the Lagrange multipliers (thereby avoiding the necessity of introducing state rotation operators within the MCSCF space).

A common set of constraint functions was determined, which can be used in each of the Lagrangians. Appropriate $g(\mathbf{x})$ functions were also identified for each Lagrangian and details are given in Ref. 3 and in a paper that we recently submitted to *J. Chem. Phys*. Because the standard GVVPT2 wave functions are not orthogonal to 2nd order in $\mathbf{X}_{QP}$, obtaining GVVPT2 nonadiabatic coupling terms of sufficient accuracy required beginning from the GVVPT3 nonadiabatic coupling terms and removing all 3rd and higher order $\mathbf{X}_{QP}$ corrections.

The implementation of the formulas that were derived for the GVVPT2 and MRCISD analytic gradients and nonadiabatic coupling terms efficiently evaluate the nuclear derivatives and the electronic structure derivatives of the $g(\mathbf{x})$ function, by rewriting the formulas for those derivatives in terms of a common set of one- and two- particle density matrices that only need to be evaluated once. Once the matrices are calculated they can be quickly used to determine all of the derivatives of $g(\mathbf{x})$. The time that is required to evaluate those density matrices is approximately the same as the CPU time of the electronic energy calculation.

B.1. NO Dimer. The nitric oxide dimer $(NO)_2$ poses both experimental and theoretical challenges and has attracted much attention over the years. In its ground ($\widetilde{X}\,^1A_1$) state, the dimer has planar C_{2v} symmetry and is formed by the pairing of two π^* orbitals of NO, leading to a weak (D_0 = 710±10 cm^{-1}) but covalent N-N bond. While the ground state properties of the dimer, including its equilibrium geometry, dipole moment, and fundamental frequencies, are experimentally, but not theoretically, well characterized, there are neither definitive experimental electronic excitation energies nor predictions of excited state properties. Of particular interest to our studies are the excited states that correlate with the lowest excited asymptote NO($X\,^2\Pi$) + NO($a\,^4\Pi$). All previous studies neglected the existence of the states that correlate to that asymptote and the influence they have on the dynamics of the NO dimer.

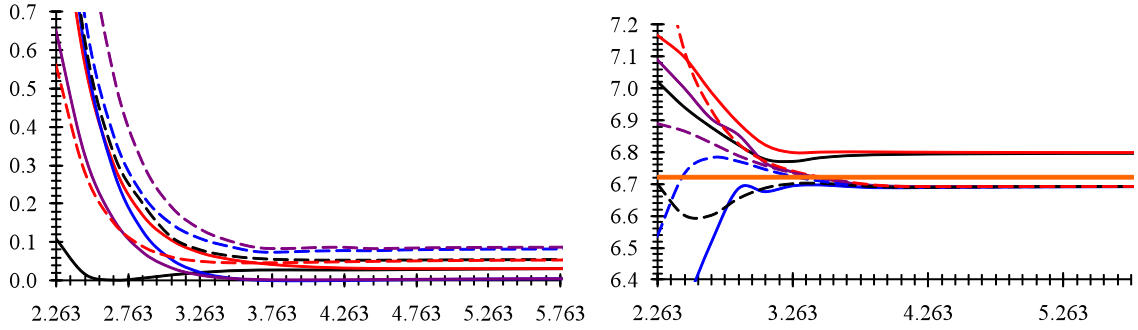

Fig. 1. $(NO)_2 \rightarrow NO\ (X\,^2\Pi) + NO\ (X\,^2\Pi)$ (*left*) and $(NO)_2 \rightarrow NO\ (X\,^2\Pi) + NO\ (a\,^4\Pi)$ (*right*) dissociation curves. Energy is in eV and *N-N* distance in Ångstroms. Singlet states are represented by solid lines for the lowest dissociation limit; dashed lines are used for the triplet states. The ordering of states in the *left* figure at 2.863 is: $1\,^1A_1$; $1\,^1B_1$; $1\,^3B_1$; $1\,^1A_2$; $2\,^1A_1$; $1\,^3A_2$; $1\,^3B_2$; $2\,^3B_2$. The ordering of states in the *right* figure at 2.563 is: $2\,^3A_2$; $2\,^3B_1$; $3\,^3B_2$; $4\,^3B_2$; $1\,^3A_1$; $3\,^3A_2$; $3\,^3B_1$; $2\,^3A_1$. The horizontal line in the *right* figure displays the value for the NO ($X\,^2\Pi$) → NO ($a\,^4\Pi$) vertical exciation exciation energy that was calculated at the MRCISD level of theory.

In order to obtain reliable potential energy surfaces for several of the low-lying excited states GVVPT2 calculations were performed. The calculations were performed on the 8 lowest electronic ($1,2\,^1A_1$, $1\,^1A_2$, $1\,^3A_2$, $1\,^1B_1$, $1\,^3B_1$, $1,2\,^3B_2$) states that correlate with the ground NO($X\,^2\Pi$) + NO($X\,^2\Pi$) asymptote and 8 additional triplet states ($1,2\,^3A_1$, $2,3\,^3A_2$, $2,3\,^3B_1$, $3,4\,^3B_2$) that correlate to the NO($X\,^2\Pi$) + NO($a\,^4\Pi$) asymptote. The active space that was used accounts for the π–π^* and π^*–Rydberg excitations that contribute to the dominant configurations of the two lowest NO + NO dissociation limits of the dimer.

The *aug-cc-p*VTZ basis set was used in the calculations in order to provide an accurate description of the Rydberg orbitals.

These curves demonstrate that the GVVPT2 method predicts a fairly accurate value for the ground state R_{NN} bond length and determines reliable asymptotic excitation energies for each of the excited states. The curves also show that, while none of the excited states that correspond to the lowest energy dissociation limit possess any minima, some of the states that correspond to the NO ($X\ ^2\Pi$) + NO ($a\ ^4\Pi$) dissociation limit possess quasibound structures.

B.2. Arsenic Oxides. GVVPT2 calculations were performed to determine the relative stabilities of the smaller arsenic oxides (AsO, AsO_2, and AsO_3) that could potentially be formed during the combustion of coal. GVVPT2 geometry optimizations and frequency calculations were performed on AsO using the *cc-p*VTZ basis set and two different active spaces, an 8 orbital,7 electron complete active space [(8:7)-CAS] and a (6:7)-CAS. The bond lengths and the harmonic and anharmonic frequencies that were calculated were compared to the experimentally measured values (see Table I). The results of that comparison confirm that the GVVPT2 method is capable of accurately modeling the behavior of the smaller arsenic oxides.

Table I. Bond Lengths and Vibrational Frequencies of AsO

Method	R_{AsO}(Å)	ω_e(cm^{-1})	$\omega_e x_e$(cm^{-1})	α_e(cm^{-1})	B_e(cm^{-1})
GVVPT2(6|7)/*cc-p*VTZ	1.630	982.9	5.3	0.4815	0.003273
GVVPT2(8|7)/*cc-p*VTZ	1.641	954.6	5.1	0.4747	0.003277
Exp. $X\ ^2\Pi$	1.624	966.5	4.88	0.4840	0.003299

Geometry optimizations for the lowest $^2A_1$, $^2A_2$, $^2B_1$, and $^2B_2$ states of AsO_2 and AsO_3 indicate that the ground electronic states of AsO_2 and AsO_3 have $^2A_1$ and $^2B_2$ symmetry, respectively. O ($X\ ^3P$) + O ($X\ ^3P$), As ($X\ ^4S$) + O ($X\ ^3P$), As ($X\ ^4S$) + O_2 ($X\ ^3\Sigma^-$), and AsO_2 ($X\ ^2A_1$) + O ($X\ ^3P$) dissociation calculations suggest that as the oxidation of the arsenic oxides increase, the stability of the oxides also increase (see Table II). GVVPT3 calculations confirm that result.

Table II. Relative Stabilities of AsO, AsO_2, and AsO_3

Oxidation Reaction	GVVPT2	GVVPT3
As ($X\ ^4S$) + $\frac{1}{2}$ O_2 ($X\ ^3\Sigma^-$) → AsO ($X\ ^2\Pi$)	-48.6	-49.6
AsO ($X\ ^2\Pi$)+ $\frac{1}{2}$ O_2 ($X\ ^3\Sigma^-$) → AsO_2 ($X\ ^2A_1$)	-50.7	-48.9
AsO_2 ($X\ ^2A_1$) + $\frac{1}{2}$ O_2 ($X\ ^3\Sigma^-$) → AsO_3 ($X\ ^2B_2$)	-14.5	---

Preliminary GVVPT2 and B3LYP calculations have also been performed to identify the geometries and relative energies of the As_2O_3 and As_2O_5 oxides. Those calculations suggest that the lowest energy isomers for As_2O_3 and As_2O_5 have the structure and geometric parameters shown in Fig. 2. Higher energy isomers have been identified for As_2O_3, however, there is qualitative disagreement between the minima that were obtained for the GVVPT2 and B3LYP levels of theory. Additional calculations are being run to understand the origin of those differences.

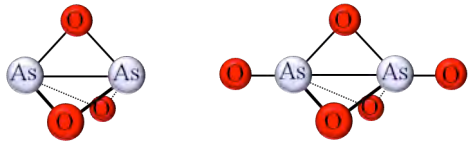

Figure 2. Lowest energy isomers As_2O_3 and As_2O_5 that were optimized using B3LYP/6-31G*. The R_{AsO} and R_{AsAs} bond lengths of As_2O_3 were determined to be 1.846 Å and 2.392 Å (NB: GVVPT2(15|18)/*cc-p*VDZ gives 1.883 Å and 2.504 Å). For As_2O_5, the R_{AsO} (*terminal*), R_{AsO} (*bridging*), and R_{AsAs} bond lengths were 1.607 Å, 1.836 Å, and 2.330 Å, respectively.

B.3. Antimony Oxides. Preliminary calculations have been performed on SbO to investigate whether GVVPT2 can reliably predict the behavior of the antimony oxides. From those calculations, it was observed that accurate excitation energies and R_{SbO} bond lengths could be obtained for the first three states of the molecule (see Table III). The calculations also predict a dissociation energy for the ground state that is close to the upper limit for the energy that was determined experimentally. GVVPT2 optimizations are currently being performed for the SbO_2, SbO_3, and larger antimony oxides to determine the geometries and relative energies of those compounds.

Table III. Thermodynamic Constants for the Three Lowest States of SbO

Method	SbO ($X\ ^2\Pi$)			SbO ($a\ ^4\Pi$)			SbO ($A\ ^2\Pi$)		
	T_e(Å)	R_{SbO}(Å)	$D_e(eV)$	T_e(Å)	R_{SbO}(Å)	$D_e(eV)$	T_e(Å)	R_{SbO}(Å)	$D_e(eV)$
GVVPT2	0.00	1.840	4.22	2.01	2.045	2.21	2.48	2.048	2.48
MRCISD	0.00	1.836	3.5-3.6	1.80	2.067	---	2.32	2.066	---
Exp.	0.00	~1.826	$\leq$ 4.29	2.00	---	---	2.45	---	---

III. Future Work

We expect continued progress in both the advancement of derivative methods for GVVPT and in applications to primarily Group 15 and 16 oxides. In regard to nonadiabatic coupling, work will focus on optimizing the computer code for MRCISD wave functions and to obtain a pilot implementation for the corresponding algorithm for GVVPT2. We expect to make quick progress on the GVVPT2 nonadiabatic coupling, since there are many common elements with MRCISD. Attention during the preceding year was on derivatives, but the upcoming year will see resumption of work on relativistic corrections in GVVPT2. With use of the in-house configuration-driven UGA code, spin-orbit coupling matrix elements in MRCISD, for both true SOCI and primary space CI, will be pursued next. Although the initial study of the $(NO)_2$ potential energy surfaces for all singlet and triplet states that correlate to the lowest two dissociation limits is complete at the GVVPT2 level, some questions will need to be addressed by more accurate methods of electronic structure theory. The eventual study of dynamics on the NO+NO surface, with inclusion of nuclear derivative and spin-orbit nonadiabatic coupling, is expected.

IV. References

[1] W. Jiang, Y. G. Khait, and M. R. Hoffmann, J. Phys. Chem. A **113**, 4374 (2009).

[2] T. Helgaker and P. Jørgensen, Adv. Quantum Chem. **19**, 183 (1988); Theor. Chim. Acta **75**, 111 (1989).

[3] Y. G. Khait, D. P. Theis, and M. R. Hoffmann, Mol. Phys. **108**, 2703 (2010).

V. Publications and Submitted Journal Articles Supported by this Project 2009-2011

M. R. Hoffmann, D. Datta, S. Das, D. Mukherjee, A. Szabados, Z. Rolik, and P. R. Surjan, Comparative study of multireference perturbation theories for ground and excited states, *J. Chem. Phys.* **131**, 204104 (2009).

D. P. Theis, Y. G. Khait, S. Pal, and M. R. Hoffmann, Molecular dipole moments using the GVVPT2 variant of multireference perturbation theory, *Chem. Phys. Lett.* **487**, 116 (2010).

Y. G. Khait, D. Theis, and M. R. Hoffmann, Lagrangian approach for geometrical derivatives and nonadiabatic coupling terms in MRCISD, *Mol. Phys.* **2010**, *108, 2703-2716.*

E. S. Olson, A. Azenkeng, J. D. Laumb, R. R. Jensen, S. A. Benson, and M. R. Hoffmann, New Developments in the theory and modeling of mercury oxidation and binding on activated carbons in flue gas, *Fuel. Process. Technol.* **2009**, *90*, 1360-1363.

T. J. Dudley, J. J. Howard, and M. R. Hoffmann, Generalized Van Vleck Perturbation Theory Study of Chlorine Monoxide, *AIP Conference Proceedings (in press).*

Y. E. Bongfen Mbote, Y. G. Khait, C. Hardel, and M. R. Hoffmann, Multireference Generalized Van Vleck Perturbation Theory (GVVPT2) Study of the NCO + HCNO Reaction: Insight into Intermediates, *J. Phys. Chem. A* **2010**, *114*, 8831-8836.

Theoretical Kinetics and Non-Born–Oppenheimer Molecular Dynamics

Ahren W. Jasper
Combustion Research Facility, Sandia National Laboratories
Livermore, CA 94551-0969
ajasper@sandia.gov

I. Program Scope

The goal of this project is the development and validation of theoretical methods for obtaining quantitative rate coefficients for elementary reactions and for elucidating reaction mechanisms. An accurate and complete first principles theoretical description is the goal for small to moderate sized systems, and more approximate methods are being developed for larger and more complex systems. This work involves quantum chemistry, transition state theory, master equation, and molecular dynamics calculations. We are extending the applicability of the theoretical models to a broader range of systems, including non-Born–Oppenheimer (NBO) processes, which involve coupled electronic states, and pressure dependent reactions. This program benefits from interactions with experimentalists at the CRF and elsewhere who provide data with which to test the theoretical methods. In turn, theoretical insights gained using the validated models are useful for interpreting data obtained under less straightforward experimental conditions. The combined experimental/theoretical results are more accurate over a broader range of temperature and pressures than would be obtained otherwise.

II. Recent Progress

A. Theoretical Chemical Kinetics

In collaboration with Argonne experimentalists (Michael, Sivaramakrishnan) and theorists (Klippenstein, Harding, Wagner), the importance of roaming to molecular products in the thermal decomposition of dimethyl ether was studied. A strategy for obtaining analytic six dimensional interaction potentials for roaming radicals was developed and applied in reduced dimensional trajectory calculations of the roaming branching fraction. Roaming was identified as a minor channel both theoretically and experimentally, although the theory underpredicted the measured molecular branching fractions (2% vs 19 ± 7%).

We have conducted several combined experimental/theoretical studies of decomposition kinetics in collaboration with Tranter. Dioxane decomposition was studied theoretically using a combination of single reference and multireference quantum chemistry calculations. Four low-energy ring opening pathways were found, and three of these involve a concerted H-atom transfer across the ring as it opens. For each of the concerted pathways, related stepwise pathways were found with weakly-bound diradical intermediates. The major immediate products of dioxane ring opening are $CH_2CHOCH_2CH_2OH$ and $CH_3CH_2OCH_2CHO$, which subsequently decompose at the central bond to radical and molecular products.

In coordination with efforts of the Princeton Combustion EFRC (J. A. Miller) and the Argonne-Sandia Consortium on High Pressure Combustion Chemistry, we have continued our development of methods for parametrizing energy transfer models using classical trajectories. In one study, energy transfer in CH_4 was studied for eight baths (He, Ne, Ar, Kr, H_2, N_2, CO, CH_4), which required generalizing our previously described strategy to handle molecular baths. A detailed study of the predictive accuracy of direct dynamics and commonly employed approximate potential energy surfaces was carried out. For simple interaction potentials (e.g., CH_4 + He), the separable pairwise approach and the use of parameterized Buckingham potentials were shown to be very accurate. For

more complicated interaction potentials, this approximation can introduce errors of up to 40% in the predicted energy transfer averages. An efficient scheme for calculating energy transfer parameters for multiple temperatures simultaneously was developed. Parameter-free rate coefficients obtained via master equation calculations using the calculated energy transfer properties, as well as ab initio and transition state theory calculations, are within a factor of two of experimental rates for CH_4 decomposition several baths. These studies suggest that the treatment of vibrational anharmonicity may be the dominant source of error in many low pressure unimolecular rate calculations.

B. Non-Born–Oppenheimer Molecular Dynamics Simulations

Detailed descriptions of our most accurate and well-validated multistate NBO trajectory methods have been given in a recent book chapter. This chapter complements the release of our direct trajectory code DiNT (http://www.sandia.gov/~ajasper/dint/), which has been interfaced with the Gaussian and Molpro quantum chemistry packages. This work is conducted in collaboration with Truhlar.

C. Quantum Chemistry

In collaboration with Richard Dawes (at Missouri University of Science and Technology and while he was at Sandia as a postdoctoral researcher), the interpolated moving least squares (IMLS) method for fitting analytic potential energy surfaces to automatically grown ab initio data was developed, and several applications were made.

Several three atom systems were studied. Vibrational states of the S_2 state of CDF were calculated on an IMLS surface generated from dynamically weighted state averaged MRCI+Q/CBS ab initio data. Good agreement with the experimental measurements of Reid (Marquette) and Kable (Sydney) was obtained, confirming the spectroscopic accuracy of the theoretical procedures. In collaboration with Camden (Tennessee), hyperthermal O + HCl collisions were studied on global IMLS potential energy surfaces for the ground and first excited electronic states. The two states predict different branching ratios to the OCl and OH products, and this observation was rationalized in terms of differences in the attractive potential near the H atom of the reactant diatom. With Guo, the first excited state of HO_2 was studied using high level quantum chemistry, IMLS fits, and wave packet dynamics.

Several rigid body interaction potentials were developed. With Carrington (Queen's University, Ontario), the van der Waals interaction of the N_2O dimer was characterized using a series of high level quantum chemistry calculations. Sensitivities of the quantum chemistry calculations to the choice of basis set, complete basis set extrapolation scheme, and treatment of electron correlation were considered in detail. The resulting fitted four-dimensional IMLS surface was used in rovibrational energy level and tunneling lifetime calculations. The results of these calculations are in good agreement with available experimental results. As discussed above, general schemes for obtaining IMLS fits for radical–radical interaction potentials were developed and applied to study roaming in dimethyl ether decomposition.

III. Future Work

A. Theoretical Chemical Kinetics

We will continue to use established theoretical kinetics techniques to make quantitative predictions for important elementary combustion reactions. Several applications are underway, including a collaboration with Tranter studying the importance of roaming reactions in the decompositions of organoiodides. In another collaboration (Klippenstein and Osborn), we are studying the phenyl + propargyl reaction. With Hansen, we are studying reactions relevant to C_6H_{12} flame chemistry.

More generally, we are developing new transition state theory strategies for systems that are currently not well described by statistical theories. For example, barrierless abstraction reactions pose challenges to current theories. For these reactions variable reaction coordinate TST is appropriate for characterizing the kinetics at low temperatures, but the assumptions involved in this approach are not suitable at higher temperatures where the reacting fragments are significantly distorted from their isolated geometries at the important dynamical bottlenecks. A two transition state approach will be applied to study these systems.

We will continue to develop our trajectory-based method for studying energy transfer. We will compute fully ab initio (i.e., parameter-free) rate coefficients for a series of small hydrocarbon molecules and radicals. In addition to providing improved theoretical kinetics for pressure dependent reactions involving these species, the proposed systematic studies of energy transfer will be used to guide the development of simple models and predictive rules for parameterizing collisional energy transfer models in master equation calculations. These studies also enable validation of improved strategies for handling other sources of error, such as vibrational anharmonicity and intramolecular vibrational energy redistribution.

In other work, the experimentally observed enhanced energy transfer in C_2H_2 for internal energies above the acetylene–vinylidene isomerization threshold will be studied.

B. Non-Born–Oppenheimer Molecular Dynamics Simulations

A major component of future work will involve the application of our validated NBO molecular dynamics (MD) methods to polyatomic systems, including: (1) The photodissociation of vinyl halides, which will be useful for interpreting the experimental results of Osborn and others. (2) Intersystem crossing in spin-orbit coupled systems formed from the addition of oxygen atoms to hydrocarbons. (3) Direct NBO MD simulations of the photodissociation of H + HO_2 reaction, including characterization of intersystem crossing pathways to form H_2O + $O(^3P)$.

To complement our previous study of the energetic effect of spin-orbit coupling discussed above, we will study the dynamical effect of spin-orbit coupling using NBO MD. Transition state theory allows for the efficient computation of accurate rate coefficients as long as the so-called "transmission coefficient" is close to unity or can be calculated. The transmission coefficient may deviate from unity for three reasons: (1) tunneling through potential barriers, (2) single surface recrossing at the dividing surface, and (3) electronically nonadiabatic surface switches. Methods exist for reliably estimating the magnitudes of the first two effects, but only approximate methods exist for treating the third. We will use direct NBO MD simulations to compute electronically nonadiabatic transmission coefficients for the CH_3 + F, Cl, and Br reactions.

With Truhlar, the photochemistry of anisole will be studied using quantum chemistry and NBO MD calculations.

C. Quantum Chemistry

An important practical bottleneck for performing NBO MD simulations is the need for inexpensive and accurate potential energy surfaces and their couplings. Two strategies will be pursued for obtaining potential energy surfaces in the NBO MD simulations. Direct dynamics methods will be developed based on single reference methods (DFT, MP2, etc) for spin-orbit coupled systems and multireference methods (CASPT2, etc) for other systems.

Semiautomated surface fitting strategies will also be implemented. One project will involve developing general strategies for automatically generating analytic potential energy surfaces for reactive systems. Schemes for modeling the coupling between the electronic surfaces will also be developed.

V. Publications and submitted journal articles supported by this project 2009-2011

1. A. W. Jasper and J. A. Miller, "Theoretical unimolecular kinetics for $CH_4 + M \rightarrow CH_3 + H + M$ in eight baths, M = He, Ne, Ar, Kr, H_2, CO, N_2, and CH_4," J. Phys. Chem. A, submitted.
2. X.-G. Wang, T. Carrington, Jr., R. Dawes, A. W. Jasper, "The vibration–rotation–tunneling spectrum of the polar and T-shaped-N-in isomers of $(NNO)_2$," J. Mol. Spectrosc., in press.
3. A. W. Jasper and D. G. Truhlar, "Non-Born–Oppenheimer molecular dynamics for conical intersections, avoided crossings, and weak interactions," in *Conical Intersections: Theory, Computation, and Experiment*, edited by W. Domcke, D. R. Yarkony, and H. Koppel (World Scientific, 2011), in press.
4. R. Sivaramakrishnan, J. V. Michael, A. F. Wagner, R. Dawes, A. W. Jasper, L. B. Harding, Y. Georgievskii, and S. J. Klippenstein, "Roaming radicals in the thermal decomposition of dimethyl ether: Experiment and theory," Combust. Flame 158, 618 (2011).
5. X. Yang, A. W. Jasper, B. R. Giri, J. H. Kiefer, and R. S. Tranter, "A shock tube and theoretical study on the pyrolysis of 1,4-dioxane," Phys. Chem. Chem. Phys. 13, 3686 (2011).
6. A. Li, D. Xie, R. Dawes, A. W. Jasper, J. Ma, and H. Guo, "Global potential energy surface, vibrational spectrum, and reaction dynamics of the first excited ($A\ ^2A'$) state of HO_2," J. Chem. Phys. 133, 144306 (2010).
7. R. Dawes, X.-G. Wang, A. W. Jasper, T. Carrington, Jr., "Nitrous oxide dimer: A new potential energy surface and rovibrational spectrum of the nonpolar isomer," J. Chem. Phys. 133, 134304 (2010).
8. A. J. Binder, R. Dawes, A. W. Jasper, J. P. Camden, "The role of excited electronic states in hypervelocity collisions: Enhancement of the $O(^3P)$+HCl → OCl+H reaction channel," J. Phys. Chem. Lett. 1, 2940 (2010).
9. A. W. Jasper, S. J. Klippenstein, and L. B. Harding, "The effect of spin-orbit splitting on the association kinetics of barrierless halogen atom–hydrocarbon radical reactions," J. Phys. Chem. A 114, 5759 (2010).
10. R. Dawes, A. W. Jasper, C. Tao, C. Richmond, C. Mukarakate, S. H. Kable, and S. A. Reid, "Theoretical and experimental spectroscopy of the S_2 state of CHF and CDF: Dynamically weighted multireference configuration interaction calculations for high-lying electronic states," J. Phys. Chem. Lett. 1, 641 (2010).
11. J. Zádor, A. W. Jasper, and J. A. Miller, "The reaction between propene and hydroxyl," Phys. Chem. Chem. Phys. 11, 11040 (2009).
12. X. Yang, A. W. Jasper, J. H. Kiefer, and R. S. Tranter, "The dissociation of diacetyl: A shock tube and theoretical study," J. Phys. Chem. A 113, 8318 (2009).
13. D. Bomhommeau, R. Valero, D. G. Truhlar, and A. W. Jasper, "Coupled-surface investigation of the photodissociation of $NH_3(\tilde{A})$: Effect of exciting the symmetric and antisymmetric stretching modes," J. Chem. Phys. 130, 234303 (2009).
14. A. W. Jasper and J. A. Miller, "Collisional energy transfer in unimolecular reactions: Direct classical trajectories for $CH_4 \rightleftarrows CH_3 + H$ in Helium," J. Phys. Chem. A 113, 5612 (2009).
15. A. W. Jasper, S. J. Klippenstein, and L. B. Harding, "Theoretical rate coefficients for the reaction of methyl radical with hydroperoxyl radical and for methylhydroperoxide decomposition," Proc. Combust. Inst. 32, 279 (2009).

Probing the Reaction Dynamics of Hydrogen-Deficient Hydrocarbon Molecules and Radical Intermediates via Crossed Molecular Beams

Ralf I. Kaiser
Department of Chemistry, University of Hawai'i at Manoa, Honolulu, HI 96822
ralfk@hawaii.edu

1. Program Scope

The major goals of this project are to explore experimentally in crossed molecular beams experiments the reaction dynamics and potential energy surfaces (PESs) of hydrocarbon molecules and their corresponding radical species which are relevant to combustion processes. The reactions are initiated under single collision conditions by crossing two supersonic reactant beams containing radicals and/or closed shell species under a well-defined collision energy and intersection angle. By recording angular-resolved time of flight (TOF) spectra, we obtain information on the reaction products, intermediates involved, on branching ratios for competing reaction channels, on the energetics of the reaction(s), and on the underlying reaction mechanisms. These data are of crucial importance to understand the formation of carbonaceous nanostructures as well as of polycyclic aromatic hydrocarbons and their hydrogen deficient precursors in combustion flames.

2. Recent Progress

2.1. Formation and Unimolecular Decomposition of Resonantly Stabilized Free Radicals

The formation of polycyclic aromatic hydrocarbons (PAHs) and related species such as their partially hydrogenated and dehydrogenated counterparts has been the subject of investigation by the combustion community for over four decades. Here, the formation of PAHs and soot particles is thought to be linked and to proceed stepwise involving resonantly stabilized hydrocarbon radicals, such as the C_{2v} symmetric propargyl radical (H_2CCCH), in which the unpaired electron is delocalized and spread out over three carbon atoms in the molecule. The delocalization of the unpaired electron results in a number of resonant electronic structures of comparable importance. Owing to the delocalization, resonantly stabilized free hydrocarbon radicals (RSFRs) are more stable than ordinary radicals. Consequently RSFRs can reach high concentrations in flames. These high concentrations make them important reactants to be involved in the formation of soot and PAHs. Here, we report on studies involving the propargyl radical (H_2CCCH; hereafter: C_3H_3) [2.1.1.] as well as the next higher members of this series: the 2,4-pentadiynyl-1 radical ($H_2CCCCCH$; hereafter: C_5H_3) [2.1.2.] together with its isomers.

2.1.1. The Propargyl Radical (H_2CCCH) and its Isomers (C_3H_3)

We carried out the crossed molecular beam reaction of ground state methylidyne radicals, $CH(X^2\Pi)$, with acetylene, $C_2H_2(X^1\Sigma_g^+)$, at a nominal collision energy of 16.8 $kJmol^{-1}$. Under single collision conditions, we identified ***both*** the atomic and molecular hydrogen loss pathways forming C_3H_2 and C_3H isomers, respectively (Figures 1-3). A detailed analysis of the experimental data suggested the formation of c-C_3H_2 (31.5 ± 5.0 %), HCCCH/H_2CCC (59.5 ± 5.0 %), and l-HCCC (9.0 ± 2.0 %). The reaction proceeded indirectly via complex formation and involved the unimolecular decomposition of long-lived propargyl radicals to form l-HCCC plus molecular hydrogen and HCCCH/H_2CCC plus atomic hydrogen. The formation of c-C_3H_2 was suggested to be produced via unimolecular decomposition of the cyclopropenyl radical, which in turn could be accessed via addition of the methylidyne radical to both carbon atoms of the acetylene molecule or after an initial addition to only one acetylenic carbon atom via ring closure. This investigation brings us closer to unraveling of the reaction of important combustion radicals –

methylidyne – and the connected unimolecular decomposition of chemically activated propargyl radicals. - We also expanded these experimental studies to the CD + C_2H_2 and CH + C_2D_2 systems to assign the position of the atomic hydrogen versus deuterium loss. The data analysis of the CD + C_2H_2 system is in the final stages (fits are complete, branching ratios to be calculated). Utilizing the power of partially deuteration of the reactant, we observed a total of 6 reactive scattering channels leading to c-C_3HD + H / l-C_3HD + H (m/z = 39), c-C_3H_2 + D, l-C_3H_2 + D, l-C_3D + H_2 (m/z = 38), and l-C_3H + HD (m/z = 37). – The data analysis of the CH + C_2D_2 system is in its final stages.

2.1.2. The 2,4-Pentadiynyl-1 Radical ($H_2CCCCCH$) and its Isomers (C_5H_3)

We investigated the reaction dynamics of ground state carbon atoms, C(^3P_j), with vinylacetylene at two collision energies of 18.8 mol^{-1} and 26.4 kJ mol^{-1} employing the crossed molecular beam technique leading to two resonantly stabilized free radicals. The reaction was found to be governed by indirect scattering dynamics and to proceed without an entrance barrier through a long lived collision complex to reach the products, *n*- and *i*-C_5H_3 isomers, i.e. $H_2CCCCCH$ and HCCCHCCH, via tight exit transition states. The reaction pathway taken is dependent on whether the carbon atom attacks the π electron density of the double or triple bond, both routes have been compared to the reactions of atomic carbon with ethylene and acetylene (Figure 4). Electronic structure/statistical theory calculations determined the product branching ratio to be 2:3 between the *n*- and *i*-C_5H_3 isomers.

2.2. Formation of PAHs – Reaction Dynamics of the Phenyl Radical (C_6H_5)

In year II, we also started untangling the reaction dynamics of phenyl radicals with selected hydrocarbon molecules accessing the C_9H_x (x=8,10) and $C_{10}H_x$ (x=6,8,10) PESs and, hence, the formation of bicyclic aromatic (like) species holding the *indene* and *naphthalene* carbon skeletons at low collision energies (< 80 $kJmol^{-1}$) under single collision conditions. This is achieved by crossing supersonic beams of phenyl radicals with allene (H_2CCCH_2), methylacetylene (CH_3CCH), and propylene ($CH_3C_2H_3$) (indene core) as well as diacetylene (HCCCCH), vinylacetylene ($HCCC_2H_3$), and 1,3-butadiene ($C_2H_3C_2H_3$) and its isomers (naphthalene core). Since our previous phenyl radical reactions showed that at elevated collision energies, ring cyclization processes do not take place, studies are conducted at collision energies less than 80 $kJmol^{-1}$. By reducing the collision energy, the life time of the intermediate(s) will be prolonged; this will increase the possibilities of ring closure processes and hence the formation of indene and naphthalene cores. The formation of individual PAH (like) molecules has never been studied under single collision conditions in a crossed beams setup to date. From these results we expect to extract generalized reaction mechanisms and gain fundamental insights into how phenyl radical reactions with unsaturated hydrocarbon molecules lead to bicyclic PAH-cores such as of *naphthalene* and *indene* and their acyclic isomers.

We finalized crossed beam reactions of the phenyl radical – generated via photolysis of helium-seeded chlorobenzene at 193 nm – with six hydrocarbons: allene, methylacetylene, and propylene (formation of indene core) as well as diacetylene, vinylacetylene, and 1,3-butadiene (formation of naphthalene core) together with their (partially) deuterated counterparts. The data analysis of the vinylacetylene and allene/methylacetylene is complete depicting for the first time the formation of naphthalene and indene, respectively, under single collision conditions. In collaboration with Profs. Mebel (FIU) and Green (MIT) we are conducting electronic structure calculations and incorporate the results in flame models.

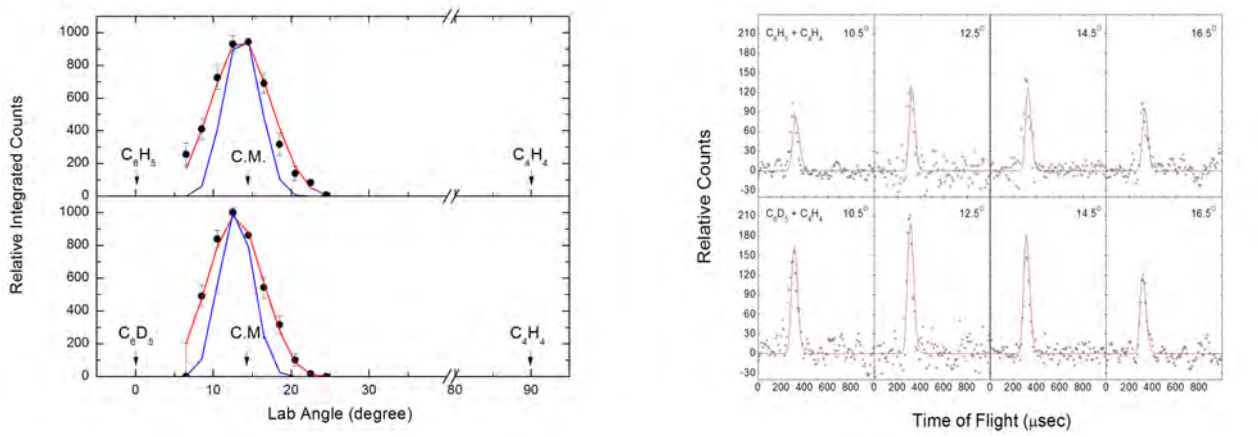

Figure 1: Left: Laboratory angular distributions of ions recorded at mass to charge ratios (m/z) of 128 ($C_{12}H_8^+$) and 133 ($C_{12}H_3D_5^+$) in the reactions of vinylacetylene with the phenyl (top) and D5-phenyl radicals at a collision energy of ~48 kJmol^{-1}. The black circles represent the experimental data, the red lines the fit for the channel yielding the naphthalene molecule plus atomic hydrogen. For comparison, the unacceptable fits of the laboratory data with the reaction channel leading to the thermodynamically less stable acyclic isomers are overlaid in blue. Right: Time of flight spectra recorded at mass to charge ratios (m/z) of 128 ($C_{12}H_8^+$) and 133 ($C_{12}H_3D_5^+$) in the reactions of vinylacetylene with the phenyl (top) and D5-phenyl radicals.

2.3. PAH Species – A Photoionization Study at the ALS

To yield further insights on the formation of PAHs under combustion relevant conditions (pressure, temperature, reactant molecules), we commissioned in collaboration with Musa Ahmed (LBNL) at the Chemical Dynamics Beamline a high temperature 'chemical reactor'. A' directed synthesis' of the PAHs is performed *in situ* in a supersonic molecular beam through reaction of pyrolytically generated phenyl radicals (C_6H_5) with hydrocarbons inside a heated silicon carbide tube ('chemical reactor'). The PAHs together with their acyclic isomers formed are then photoionized by vacuum ultraviolet (VUV) light from the Advanced Light Source at various photon energies from 7.5 to 12 eV to record photoionization efficiency (PIE) curves. Based on known PIE curves of the individual PAHs and their acyclic isomers, the recorded PIE curves are then simulated theoretically to extract the nature of the products formed and their branching ratios over a range of combustion-relevant reaction vessel temperatures (1,000-2,000 K) and pressures (few 100 Torr to a few 1,000 Torr). By selecting the reactants, allene (H_2CCCH_2), methylacetylene (CH_3CCH), propylene ($CH_3C_2H_3$), diacetylene (HCCCCH), vinyl-acetylene ($HCCC_2H_3$), and 1,3-butadiene ($C_2H_3C_2H_3$), these studies access the important C_9H_x (x=8,10) and $C_{10}H_x$ (x=6,8,10) potential energy surfaces (PESs), among them are the crucial combustion intermediates with indene and naphthalene cores. To date, no experiment has been conducted in which an individual PAH (like) species is formed via a gas phase reaction under well-defined conditions in a high temperature chemical reactor. A preliminary data analysis of photoionization efficiency curves derived from ions of mass-to-charge ratio, m/z, of 116 ($C_9H_8^+$) utilizing allene (purple) and methylacetylene (green) as seed and reactant gases with the phenyl radical. The onsets of the PIE curves agree very well with the adiabatic ionization energy of the aromatic indene molecule.

3. Future Plans

In year III, we are planning to expand our studies in the following directions: i) to utilize the crossed beam reaction of ground state carbon atoms with the vinyl radical to experimentally access the C_3H_3 potential energy surface and to elucidate the chemical dynamics – in comparison with the CH + C_2H_2 system studied earlier in our group – of the formation of C_3H_2 and C_3H isomers, ii) to finalize the reactive scattering experiments and data analysis of the phenyl radical reactions at low collision energies forming PAHs with naphthalene and indene cores, and iii) to continue the photoionization studies at the ALS yielding PAHs in our newly developed chemical reactor.

4. Acknowledgements

This work was supported by US Department of Energy (Basic Energy Sciences; DE-FG02-03-ER15411).

5. Publications Acknowledging DE-FG02-03-ER15411 (2009-2011)

1. X. Gu, F. Zhang, R.I. Kaiser, *A Crossed Molecular Beam Study of the Phenyl Radical Reaction with 1,3-Butadiene and its Deuterated Isotopomers.* JPCA 113, 998-1006 (2009).

2. X. Gu, R.I. Kaiser, *Reaction Dynamics of Phenyl Radicals in Extreme Environments - A Crossed Molecular Beam Study*. Acc. Chem. Res. 42, 290-302 (2009).

3. X. Gu, F Zhang, R.I. Kaiser, V.V. Kislov, A.M. Mebel, *Reaction Dynamics of the Phenyl Radical with 1,2-Butadiene*. CPL 474, 51-56 (2009).

4. R.I. Kaiser, F. Zhang, X. Gu, V.V. Kislov, A.M. Mebel, *Reaction Dynamics of the Phenyl Radical (C_6H_5) with 1-Butyne ($HCCC_2H_5$) and 2-Butyne (CH_3CCCH_3).* CPL 481, 46-53 (2009).

5. R.I. Kaiser, A.M. Mebel, O. Kostko, M. Ahmed. *On the Ionization Potentials of C_4H_3 Isomers.* CPL 485, 281-285 (2010).

6. R.I. Kaiser, *Reaction Dynamics of Carbon-Centered Radicals in Extreme Environments Studied by the Crossed Molecular Beams Technique.* in: Carbon–Centered Radicals: Structure, Dynamics and Reactivity. Malcolm D. E. Forbes, Editor, Wiley, p. 221-248 (2010).

7. F. Zhang, B. Jones, P. Maksyutenko, R. I. Kaiser, C. Chin, V.V. Kislov A.M. Mebel, *Formation of the Phenyl Radical [$C_6H_5(X^2A_1)$] under Single Collision Conditions – A Crossed Molecular Beam and Ab Initio Study*. JACS 132, 2672-2683 (2010).

8. O. Kostko, J. Zhou, B.J. Sun, J.S. Lie, A.H.H. Chang, R.I. Kaiser, M. Ahmed, *Determination of ionization energies of C_nN (n=3-14) clusters: Vacuum-ultraviolet (VUV) photoionization experiments and theoretical calculations,* ApJ 717, 674-682 (2010).

9. P. Maksyutenko, F. Zhang, X. Gu, R.I. Kaiser, *A Crossed Molecular Beam Study on the Reaction of Methylidyne Radicals [$CH(X^2\Pi)$] with Acetylene [$C_2H_2(X^1\Sigma_g^+)$] – Competing C_3H_2 + H and C_3H + H_2 Channels.* PCCP 13, 240-252 (2011).

10. D.S.N. Parker, F. Zhang, Y. Seol Kim, R. I. Kaiser, A.M. Mebel. *On the Formation of the Resonantly Stabilized C_5H_3 Radicals - A Crossed Beam and Ab Initio Study of the Reaction of Ground State Carbon Atoms with Vinylacetylene.* JPCA 115, 593-601 (2011).

DYNAMICAL ANALYSIS OF HIGHLY EXCITED MOLECULAR SPECTRA

Michael E. Kellman
Department of Chemistry, University of Oregon, Eugene, OR 97403

kellman@uoregon.edu

PROGRAM SCOPE:

The highly excited vibration-rotation dynamics of small molecular species, including those approaching the threshold of reaction, are crucial to understanding fundamental processes important for combustion. The goal of our program is to develop theoretical tools to analyze spectra and dynamics of these highly excited systems. A constant theme is the use of effective spectroscopic fitting Hamiltonians to make the link between experimental data and theoretical dynamical analysis. We emphasize particularly the role of bifurcations and the "birth of new modes in bifurcations from the low energy normal modes". We use bifurcation analysis of semiclassical versions of the effective Hamiltonians used by spectroscopists to fit complex experimental spectra. Observable phenomena associated with bifurcations such as changes in spectral patterns have been predicted and observed. A developing focus is systems approaching and undergoing chemical reactivity, including intramolecular (isomerization) reactions.

RECENT PROGRESS AND FUTURE PLANS: The progress described below is in collaboration with postdoctoral associates Vivian Tyng and George Barnes. Our current research is pursuing two main directions.

CRITICAL POINTS BIFURCATION ANALYSIS OF EFFECTIVE SPECTROSCOPIC HAMILTONIANS.

We are performing a critical points bifurcation analysis for the first time for a rotation-vibration effective Hamiltonian, using a recent spectroscopic Hamiltonian for CO_2 fit to experimental data. There have been some theoretical dynamics studies of rotation-vibration problems, mostly on model systems, but in real systems with high excitation of both vibrations and rotations, little connection has been made of nonlinear theory with either computation or experiment. Our path to connecting experiment and theory in purely vibrational problems has been to use effective spectroscopic fitting Hamiltonians. A great deal of progress using the critical points analysis has been made on purely vibrational problems. However, to our knowledge no analysis has ever been performed on the effective Hamiltonian of a real molecular rotation-vibration system, probably in part because of the greater essential complexity of the problem. This rotation-vibration bifurcation problem of even a linear triatomic involves an unprecedented degree of complexity in the critical points approach. It has been a real question whether it can be carried out and whether it will be possible to get intelligible information. The basic problem is that all previous applications of the critical points method have involved effectively at most 1 or 2 nontrivial degrees of freedom (DOF), whereas rotation-vibration problems involve 3 DOF or more.

We are now successfully completing the critical points analysis of rotation-vibration dynamics of CO_2 on the effective Hamiltonian fit to experimental data. The analysis gives relatively simple, intelligible dynamics, comparable to but significantly extending what has been obtained with pure vibrational dynamics. At J = 0 there is only the bifurcation tree of normal modes and Fermi resonance modes. Then, as J increases, we find a principal "Coriolis mode" that bifurcates out of one of the Fermi resonance modes at very low J, with further finer branching of the tree into Coriolis modes with increasing J.

Considerable work remains to be done in the physical interpretation of the results of the critical points analysis. What is the physical nature of the rotation-vibration motion in the new bifurcation rotation-vibration "modes" of the molecule? A good starting point is the standard picture of the rotation-vibration motion of a symmetric top. In the new Coriolis modes of CO_2 determined in the bifurcation analysis, things will be somewhat but not altogether different from the symmetric top; and also with some similarities to the asymmetric top. In the critical points Coriolis modes, the molecule "locks" into certain configurations that involve combinations of the zero-order vibrational angle variables. The full motion of the molecule separates into a resonant periodic vibration (due to the combined effects of Fermi and Coriolis couplings); and a periodic precession-like rotational motion. In the body-fixed frame, the resonant periodic vibration involves the four vibrational modes including vibrational angular momentum and, unlike the pure Fermi resonance problem, the antisymmetric stretch. We hope that animations will dramatically simplify the visualization, following the example of our animations of the new bending modes born in bifurcations of acetylene.

POLYAD BREAKING GENERALIZED EFFECTIVE HAMILTONIANS.

A recent emphasis of our work is systems in which the standard spectroscopic polyad approximation breaks down. This involves a significant extension of the standard effective spectroscopic fitting Hamiltonian. The Hamiltonian used in virtually all existing spectral fits invokes an approximate conserved quantity known as the polyad or total quantum number. Recently we demonstrated [1] in a model system that a generalized effective Hamiltonian can successfully describe the polyad breaking by successively adding a small number of additional resonance couplings to the standard polyad effective Hamiltonian. The system of Ref. [1] was a pair of coupled anharmonic oscillators, each of which monotonically approaches a dissociation limit.

In the next step, recently initiated with two papers [8,9], we are concerned with a far more difficult question of principle: whether it is possible to construct an effective Hamiltonian to encompass multiple potential energy minima, especially in a system that does not have two simple uncoupled modes as a zero-order limit. An example is a molecule that shifts between two isomeric forms, each possessing its own potential minimum. We are investigating this problem using an example from combustion reaction systems. One of the most important elementary combustion species is the hydroperoxyl radical HO_2. In its equilibrium configuration it has a bent H—O—O

structure. At very high energies the system can make transitions over a saddle in which the H atom is situated symmetrically above the O—O in an isosceles triangle. In our current work we are concerned with this isomerization pathway. At still higher energies, the molecule can assume a linear form, and at even higher energies, it can dissociate into either HO + O or O_2 + H.

We have devised a simplified model for HO_2 based on a high level ab initio potential energy surface of Guo and coworkers. Our model includes two vibrational coordinates, which may be designated as bend and O—H stretch modes. That is, we remove the O—O coordinate, taking a slice of the full-dimensional potential surface. The resulting potential encompasses both the lowest isomerization pathway and the lowest dissociation channel of the system, so that unlike the system of Ref.[1], it does not have two simple uncoupled modes as a zero-order limit -- a significant generalization of constraints beyond allowing for existence of multiple wells. The resulting model potential, shown below, has similar features to the full three dimensional PES.

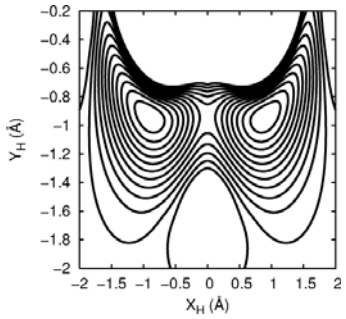

Fig. 1. Plot of the model potential energy surface with contours representing 2000 cm^{-1}equipotential lines. The O—O bond length is fixed to the equilibrium value. The oxygen atoms are symmetrically placed on the x-axis about zero.

In order to test the generalized spectroscopic fitting Hamiltonian, we obtain a set of essentially exact vibrational levels from the model potential and use these as "data". These levels result from a discrete variable representation (DVR) calculation.

In Refs. [8,9] we show that spectroscopic fitting Hamiltonians are capable of reproducing large scale vibrational structure above the isomerization barrier. Good fits for below barrier states are obtained from just a diagonal Hamiltonian, but there is a severe breakdown above the barrier. Two resonances, the 2:1 and 3:1, are necessary to describe the pertinent physical features of the system and hence a polyad-breaking Hamiltonian is required. We further illustrate, through the use of approximate wave functions, that inclusion of additional coupling terms yield physically unrealistic results despite an improved agreement with the exact energy levels. Insight into the dynamical nature of isomerization is also gained through classical trajectories. Contrary to physical intuition the bend mode is not the initial "reaction mode," but rather isomerization requires excitation in both the stretch and bend modes. The dynamics reveals a Farey tree formed between the 2:1 and 3:1 resonances with the prominent 5:2 (2:1+3:1) feature

effectively dividing the tree into portions. The 3:1 portion is associated with isomerization while the 2:1 portion leads to "localization" and perhaps dissociation at higher energies than those considered in this work. Simple single resonance models analyzed on polyad phase spheres are able to account in a qualitative way for the spectral, periodic orbit, and wave function patterns that we observe.

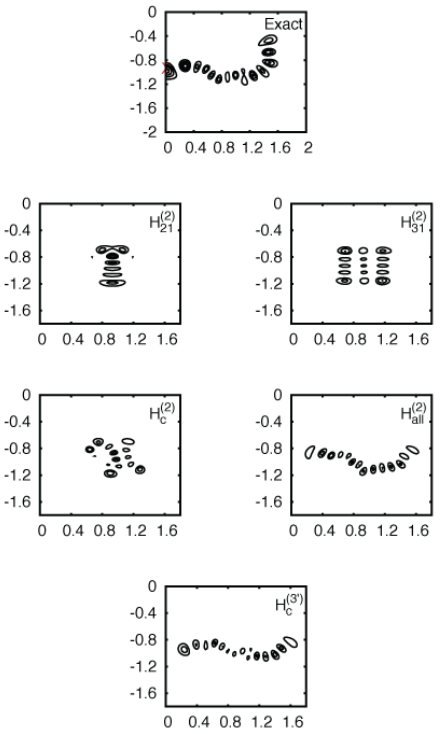

Fig. 2. A comparison of squared wave functions from various Hamiltonians for an isomerizing state. The best comparison is between the Exact state from the PES, top; and our best polyad-breaking effective Hamiltonian, bottom. In contrast, polyad Hamiltonians and some polyad-breaking Hamiltonians (middle panels) can give poor results.

Recent publications related to DOE supported research:

1. A. Chakraborty and M.E. Kellman, "Effective Hamiltonian for Chaotic Coupled Oscillators", J. Chem. Phys. (Communication) 129, 171104 (2008).

2. V. Tyng and M.E. Kellman, "Catastrophe Map and the Role of Individual Resonances in C_2H_2 Bending Dynamics", J. Chem. Phys. 130, 144311, 1-14 (2009).

3. V. Tyng and M.E. Kellman "Critical Points Bifurcation Analysis of High-ı Bending Dynamics in Acetylene", J. Chem. Phys. 131, 244111, 1-11 (2009).

4. V. Tyng and M.E. Kellman, "Spectral Intensity Patterns and Vibrational Phase Space Structure", J. Phys. Chem. A 113, 13246–13250 (2009).

5. V. Tyng and M.E. Kellman, "The Bifurcation Phase Diagram For C_2H_2 Bending Dynamics Has A Tetracritical Point With Spectral Patterns But No Monodromy", submitted to J. Phys. Chem. A.

6. S. Yang and M.E. Kellman, "Resonance induced spectral tuning", Phys. Rev. A. 81, 062512 (2010).

7. V. Tyng and M.E. Kellman, "The Bifurcation Phase Diagram For C_2H_2 Bending Dynamics Has A Tetracritical Point With Spectral Patterns", J. Phys. Chem. A . 114, 9825–9831 (2010).

8. G. L. Barnes and M.E. Kellman, "Effective Spectroscopic Hamiltonian for Multiple Minima with Above Barrier Motion: Isomerization in HO_2", J. Chem. Phys. 133, 101105 (2010).

9. G.L. Barnes and M.E. Kellman, "Detailed Analysis of Polyad-Breaking Spectroscopic Hamiltonians for Multiple Minima with Above Barrier Motion: Isomerization in HO_2", J. Chem. Phys. 134, 074108 (2011).

Theory and Modeling of Small Scale Processes in Turbulent Flow

Alan R. Kerstein
Combustion Research Facility
Sandia National Laboratories
Livermore, CA 94551-0969
Email: arkerst@sandia.gov

PROJECT SCOPE

New, broadly applicable conceptual frameworks for computational modeling of turbulent combustion and related turbulent multi-physics environments appear roughly once in a generation. The most widely used existing frameworks, Reynolds averaged Navier-Stokes (RANS) and large-eddy simulation (LES), are very capable tools that have yielded fundamental insights as well as many results of practical importance. Additional valuable contributions from these methods can be expected in the foreseeable future, but concurrently, technological and associated scientific challenges raised by new energy conversion approaches are becoming increasingly difficult to address using these methods.

The reason for this is the increasing sophistication of energy-conversion approaches designed to meet ever more stringent efficiency and environmental-impact requirements, and the resulting dependence of combustor performance on subtle details of chemistry-turbulence coupling. This coupling typically occurs at scales not resolved by RANS or LES, so it is represented by sub-grid parameterizations that are problematic with respect to both their representation of the coupling and the exchange of information between the sub-grid and mesh-resolved flow states.

This project focuses on the development of an alternative turbulent combustion modeling framework whose foundation is an economical yet faithful representation of the small scale phenomena. This small scale treatment is the building block for construction of the large scale flow advancement scheme. Thus, instead of appending a sub-grid combustion model to a coarse-grained flow solver originally intended for a different purpose, the entire framework is designed from the bottom (in the sense of small scales) up to be well suited for combustion applications. The two key elements of this approach are the small scale treatment and the coupling of its instantiations in order to obtain the large scale flow advancement. These are described next.

The typical sub-grid parameterization advances the small scale processes in a state space of thermo-chemical variables, representing the reacting flow locally either as a probability distribution of possible thermo-chemical states [A] or as a one-to-one relation between the thermo-chemical state and some reduced variable such as mixture fraction [B]. In this project, a sub-grid spatial coordinate is introduced in order to capture the coupling of diffusive fluxes driven by spatially resolved property gradients to combustion chemistry and turbulent motions. Cost considerations mandate a minimal approach, hence a one-dimensional (1D) formulation. This requires a representation of turbulent motions in 1D, which is achieved by applying instantaneous maps to selected sub-regions of the 1D domain, where each map is the analog of a turbulent eddy. A map formulation has been developed that, in concert with diffusive and chemical advancement, captures the relevant couplings with unprecedented fidelity relative to the computational cost of the method.

Two map-based 1D formulations have been developed, the Linear-Eddy Model (LEM), which

predicts mixing and chemical reactions under prescribed flow conditions but does not predict the flow *per se*, and subsequently, One-Dimensional Turbulence (ODT), a predictive simulation of turbulent flow as well as mixing and chemical reactions within it.

ODT is a complete enough flow representation so that the coupled array of ODT domains can in principle simulate 3D turbulent flow with no coarse-grained advancement of the 3D momentum equation. Owing to the modeling at the small scales, which are represented in 1D, details of the domain coupling involve trade-offs that have motivated the formulation of several coupling strategies, as described in the sections that follow.

RECENT PROGRESS

While model development efforts presently focus on the aforementioned ODT-based 3D reacting flow solver, stand-alone applications of LEM and ODT are continuing. A previous [2] LEM study of the transition to detonation in supernovae by the nuclear burning of carbon has been extended by examining the role of the slower-burning oxygen flame that trails the carbon flame. It was found that preconditioning of the fuel by carbon burning could result in a regime of oxygen burning that provides a previously unsuspected alternate pathway to supernova detonation [7].

Double-diffusive convection is a mixing phenomenon with implications ranging from supernova precursor evolution to the exchange of heat and carbon dioxide between the deep ocean and the surface layer. It is a dynamical consequence of differential molecular diffusion, and hence is a paradigm of differential molecular diffusion effects in combustion. Namely, in water that is stably stratified with respect to salt concentration but unstably stratified with respect to temperature, the difference between salt and temperature diffusivities induces molecular transport leading to locally unstable layers in an overall stable configuration. This generates turbulent convective layers separated by thin stable interfaces.

For use in ongoing combustion studies, an ODT formulation has been developed that uses an adaptive mesh to resolve the internal structure of thin flames in turbulence. To evaluate the performance of the new algorithm in an analogous but simpler context, it was used to simulate double-diffusive convection. Greatly improved performance relative to uniform-mesh implementation was demonstrated. In addition, the parameter study that was performed yielded agreement with the limited experimental data that is available and enabled the development of algebraic correlations describing the transport of heat and salt over a wide range of the relevant parameter space [8].

Shear-driven stably stratified turbulence is another useful test case because it also exhibits layering with thin interfaces and other sporadic localized phenomena. For this case, ODT simulations again confirmed the good performance of the new algorithm. Also, the wide range of parameter space that ODT can affordably explore enabled the demonstration that a previously reported heat-flux correlation omitted significant parameter dependences. This led to a synthesis of theoretical concepts resulting in an improved correlation [9].

Coupling of 1D domains to capture 3D motions is subject to two artifacts, numerical diffusion and the placement of dissimilar fluid parcels in direct contact. The choice of coupling method affects the relative importance of these artifacts. The first artifact has more impact on scalar mixing, while the second has more impact on flow advancement. Therefore the preferred coupling method could turn out to be problem dependent. It is also possible to couple the chemical species and the flow variables in different ways.

A particular approach among these possibilities has been implemented and was initially applied to homogeneous decaying turbulence [4]. This is an incompressible formulation that uses pressure projection to enforce solenoidal flow. It couples domains in a way that introduces the first but not the second artifact. In a step toward reacting-flow applications (see the next section) the numerical implementation was recently generalized for application to inhomogeneous incompressible flow.

Four such flows have been simulated: confined channel flow, open channel flow, flow in a square duct, and flow in a lid-driven cavity. Evaluation of the results is ongoing, but all flow properties examined thus far indicate that this formulation achieves its objective of capturing large scale flow behavior while providing the affordable small scale fidelity that has been demonstrated previously using stand-alone ODT simulations.

Open channel flow, with a no-slip lower wall and a free-slip upper surface, is a key test case. Near the upper surface, the flow is effectively 2D and therefore develops the large-scale vortical motions that result from vortex alignment in 2D turbulence. The simulations reproduce the statistical signatures of this behavior.

Square duct flow is also an important test because it develops secondary circulations through spontaneous symmetry breaking. The simulations reproduce this behavior.

FUTURE WORK

Ongoing ODT comparisons to DNS simulations of various turbulent combustion regimes will continue. A key goal is to determine whether inferences based on the DNS cases are valid under more turbulent conditions or with more detailed kinetic mechanisms than can be run affordably in DNS. One DNS target case is a planar Bunsen methane-air flame in which the co-flow consists of combustion products at an equivalence ratio different from the reactant flow. Another target case is DNS of soot-radiation-turbulence interactions in an ethylene flame.

Some of the most useful data for validation of hydrocarbon combustion mechanisms is from plug-flow reactor and jet-stirred reactor studies. These configurations are subject to significant mixing delays that have not been adequately characterized or taken into account when interpreting the measurements. ODT simulations representing idealizations of these experiments will be used to estimate the possible contribution of mixing delays to the uncertainty of chemical rate parameters inferred from the measurements.

In collaboration with astrophysicists at the Univ. of Minnesota, ODT will be used to simulate the multi-phase reacting flow in the crust of a neutron star. The crust contains several hundred dynamically relevant species, some of which crystallize and fall, and then possibly melt due to nuclear reactions. This process, which is not yet well understood, is believed to promote the occurrence of nova explosions.

Development of ODT-based 3D simulation tools will continue. Incompressible-flow results described in the previous section lay the groundwork for extension of the method described there to reacting flows.

Several considerations indicate that more than one approach should be pursued. As noted, the preferred domain-coupling method is likely to be problem dependent. Also, there are several

strategies for generalizing from incompressible flow to incorporate combustion-induced thermal expansion and other dilatation mechanisms. Presently a pseudo-compressible approach [C] appears to be advantageous, though it requires careful implementation for combustion applications. Pressure projection is a coarse-grained 3D operation whose outcome is communicated down-scale to the ODT-resolved flow field. Pseudo-compressible advancement avoids this potentially problematic down-scale coupling.

Initial target applications for the reacting-flow extension of ODT-based 3D simulation include flame-wall interaction and flame stabilization in recirculating flow. For non-reacting flow, it is anticipated that the method will have diverse applications to heat transfer due to the feasibility of discriminating thermal and viscous wall layers on a time-resolved basis and of resolving flow-thermal couplings such as temperature-dependent viscosity (which is important in combustion).

REFERENCES

A. S. B. Pope, *Prog. Energy Combust. Sci.* **11**, 119 (1985).
B. N. Peters, *Proc. Combust. Inst.* **21**, 1231 (1986).
C. E. F. Toro, Riemann Solvers and Numerical Methods for Fluid Dynamics: A Practical Introduction (Springer, Berlin, 2009).

PUBLICATIONS SINCE 2009

1. A. R. Kerstein, "One-Dimensional Turbulence: Stochastic Simulation of Multi-Scale Dynamics," *Lect. Notes Phys.* **756**, 291 (2009).
2. S. E. Woosley, A. R. Kerstein, V. Sankaran, A. J. Aspden, and F. Roepke, "Type Ia Supernova: Calculations of Turbulent Flames Using the Linear Eddy Model," *Astrophys. J.* **704**, 255 (2009).
3. J. R. Schmidt, J. O. L. Wendt, and A. R. Kerstein, "Non-equilibrium Wall Deposition of Inertial Particles in Turbulent Flow," *J. Stat. Phys.* **137**, 233 (2009).
4. R. C. Schmidt, A. R. Kerstein, and R. J. McDermott, "ODTLES: A Multi-Scale Model for 3D Turbulent Flow Based on One-Dimensional Turbulence Modeling," *Comput. Methods Appl. Mech. Engrg.* **199,** 865 (2010).
5. A. J. Ricks, J. C. Hewson, A. R. Kerstein, J. P. Gore, S. R. Tieszen, and Wm. T. Ashurst, "A Spatially Developing One-Dimensional Turbulence (ODT) Study of Soot and Enthalpy Evolution in Meter-Scale Buoyant Turbulent Flames," *Combust. Sci. Tech.* **182**, 60 (2010).
6. N. Punati, J. C. Sutherland, A. R. Kerstein , E. R. Hawkes, and J. H. Chen, "An Evaluation of the One-Dimensional Turbulence Model: Comparison with Direct Numerical Simulations of CO/H2 Jets with Extinction and Reignition," *Proc. Combust. Inst.* **33**, 1515 (2011).
7. S. E. Woosley, A. R. Kerstein, and A. J. Aspden, "Flames in Type Ia Supernova: Deflagration-Detonation Transition in the Oxygen Burning Flame," *Astrophys. J.* (in press).
8. E. Gonzalez-Juez, A. R. Kerstein, and D. O. Lignell, "Fluxes across Double-Diffusive Interfaces: A One-Dimensional-Turbulence Study," *J. Fluid Mech.* (in press).
9. E. Gonzalez-Juez, A. R. Kerstein, and L. H. Shih, "Vertical Mixing in Homogeneous Sheared Stratified Turbulence: A One-Dimensional-Turbulence Study," *Phys. Fluids* (in press).

Picosecond Nonlinear Optical Diagnostics

Christopher J. Kliewer (PI) and Thomas B. Settersten (Contributor)
Combustion Research Facility, Sandia National Laboratories
P.O. Box 969, MS 9055
Livermore, CA 94551-0969
cjkliew@sandia.gov

Program Scope

This program focuses on the development of innovative laser-based techniques for measuring temperature and concentrations of important combustion species as well as the investigation of fundamental physical and chemical processes that directly affect quantitative application of these techniques. Our development efforts focus on laser-induced fluorescence (LIF) and crossed-beam approaches such as time-resolved nonlinear wave-mixing. A critical aspect of our research includes the study of fundamental spectroscopy, energy transfer, and photochemical processes. This aspect of the research is essential to the development of accurate models and quantitative application of techniques to the complex environments encountered in combustion systems. Many of these investigations use custom-built tunable picosecond (ps) lasers, which enable efficient nonlinear excitation, provide high temporal resolution for pump/probe studies of collisional processes, and are amenable to detailed physical models of laser-molecule interactions.

Recent Progress

Direct measurement of pure-rotational Raman collisional broadening coefficients by time-domain coherence dephasing measurements: Coherent anti-Stokes Raman spectroscopy (CARS) has been extensively developed over the past 30 years as a nonintrusive probe of temperature and major species concentrations in combustion environments. By fitting the signal spectrum, the gas-phase temperature can be calculated, as both the relative line intensities and the Raman linewidths are highly temperature dependent. One of the difficulties in the quantitative interpretation of CARS signal is its sensitivity to the *J*-dependent Raman linewidths. In nanosecond-based CARS the signal intensity for a specific Raman transition scales as $1/\gamma^2$ where γ is the Raman linewidth. The Raman linewidth for a given molecular transition is sensitive to the temperature, pressure, and the molecule's collision partner(s). Both experimental and theoretical work over the past decades therefore has been dedicated to the measurement and modeling of rotational and rovibrational Raman linewidths for combustion-relevant species such as N_2, O_2, CO, CO_2, H_2O and small fuel molecules. N_2 is the most commonly probed molecule in CARS measurements as it is present in high concentration in all air-breathing combustion processes. High-resolution data have been used to construct phenomenological linewidth models, such as the modified exponential gap (MEG) model[1], to extrapolate the high-resolution data set to arbitrary temperature.

In our laboratory, we have developed a technique for measuring coherence decays directly in the time-domain. This is accomplished by preparing pure-rotational coherences in the probed molecules and then delaying the probe pulse in time. By tracking the signal decay as a function of probe delay, the coherence dephasing rate is measured directly in the time domain. This is made possible by the use of picosecond laser pulses as the exponential time constant for signal decay in N_2 collisional dephasing at room temperature and atmospheric pressure is about 60 ps. The frequency-domain Raman linewidth can thus be calculated from the time-domain dephasing data. We have found that our time-domain measurements agree well with reported high-resolution inverse Raman spectroscopy (IRS) data[2] on the Raman linewidth for N2 self-broadening, as shown in Figure 1a. The slight increase in linewidth at low-*J* in our data is because of the anisotropic broadening present in S-branch pure-rotational transitions, while the IRS data measured the Q-branch linewidth, demonstrating the utility of this technique for highly accurate and rapid linewidth determination. In collaboration with Per-Erik Bengtsson from Lund University we have collected a substantial coherence decay data set for various mixtures of N_2 and H_2 from 295K – 1500K. It has previously been shown that taking account of the $N_2 - H_2$ line-broadening coefficient is quite important for accurate thermometry in rich

flames.[3] This data is being used to develop a Raman linewidth model for use with pure-rotational CARS in flames with significant H_2 concentrations, such as diffusion flames.

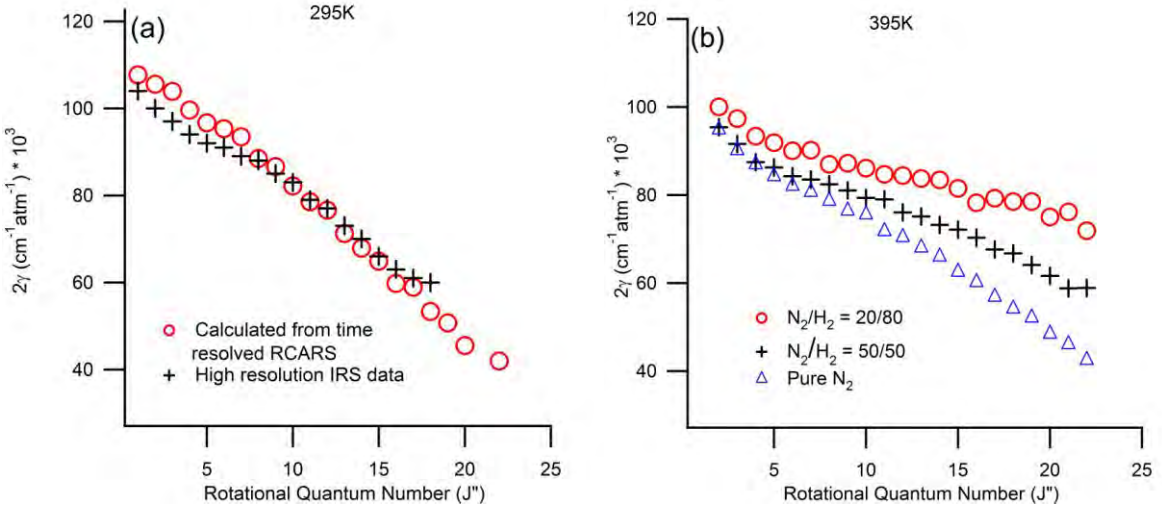

Figure 1. Panel (a) displays room temperature N_2 Raman linewidths calculated from time-domain coherence decay measurements (red) compared with high resolution IRS data from the literature[2] (black). Panel (b) shows linewidths calculated from time-resolved coherence decays at 395K for three N_2/H_2 ratios.

1D ps-RCARS imaging: We have recently developed the technique of 1-dimensional picosecond pure-rotational CARS imaging and demonstrated its precision and accuracy as a combustion diagnostic for temperature and major species concentrations.[4] Because only moderate pulse energies are required to excite coherences with picosecond pulses, it is feasible to implement a CARS imaging configuration. In this case, the pump, Stokes, and probe laser beams are formed into sheets that intersect along a line. The signal from the 1-D probe volume is relay-imaged onto the spectrometer slit, dispersed, and the spatially resolved CARS spectra detected with a 2-D CCD array. Initial imaging experiments employed time-delayed probing to eliminate fuel interference in a rich propane jet flame, enabling 1-D imaging along a 9-mm line through the flame. Spectra were fitted to produce a 1-D map of temperature and relative O_2/N_2 concentration. With our current laser energies, we have shown this 1D imaging technique capable of single-shot imaging of N_2 at temperatures up to ~1200K, and shot-averaged imaging in flames at ~2100K. At room temperature, 1D images of up to 12 mm were acquired.

High-spatial-resolution 1D RCARS imaging: A disadvantage of the standard BOXCARS phase-matching scheme employed in our initial 1D RCARS imaging experiments is the lack of spatial resolution in the probe volume along the beam-propagation dimension. The length of the probed volume in this dimension is termed the "interaction length". Most of our CARS measurements have resulted in interaction lengths of 2-3 mm, and this is common within the CARS community. In many situations higher resolution is required to avoid spatially averaging over important combustion features. The interaction length can be reduced by using a large-angle phase matching configuration. However, CARS signal intensity decreases quadratically as the interaction length is reduced. Thus, a reduction in interaction length from 2 mm to 200 μm would correspond to a 100-fold decrease in CARS signal intensity. I have developed a novel 1D imaging phase-matching configuration to address these problems, depicted in Figure 2. The pump and Stokes pulses are not stretched into sheets, but instead are counter-propagated and focused to ~150 μm symmetrically. The phase-matching condition for the wavelengths used then requires the narrowband probe to intersect this excited coherence at 33º to the Stokes beam (Figure 2). This configuration has two major advantages. First, the probe crosses the pump and Stokes pulses at such a steep angle the interaction length is reduced to < 200 μm,

corresponding to an order of magnitude increase in spatial resolution. Second, the corresponding loss in CARS signal is mitigated by the fact that both the pump and Stokes beams are focused to a point (150 μm) as opposed to sheets (~12000 μm) in this geometry thereby greatly increasing the irradiance of the coherence preparation pulses. In simple measurements of room air, the new high-spatial-resolution technique yielded a 1D image 2 cm in length with an order of magnitude greater spatial resolution and a factor of 10 increase in signal intensity.

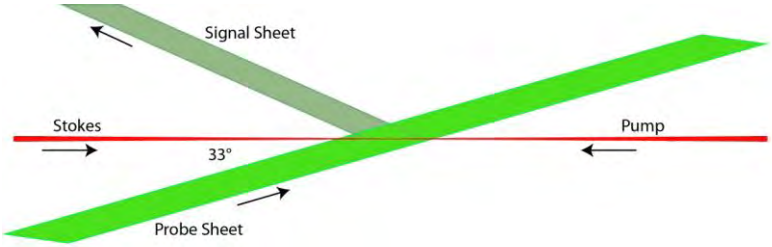

Figure 2. Top-down view of the high-spatial-resolution phase matching scheme for 1D ps-RCARS imaging.

Model Development for Time-Domain CARS: The collisional dephasing which occurs during the time-interval between the driving of a Raman coherence and the probing of that coherence in probe-delayed CARS causes significant shifts in the signal spectral envelope because of the *J*-dependent dephasing which occurs. Thus, a frequency domain code for fitting time-domain CARS spectra is not sufficient. We have developed a time-domain CARS model to explicitly account for the evolution of the CARS polarization during the time interval between the pump and Stokes pulses and the probe pulse. The model has been validated against time-domain coherence measurements in N_2 at 295K, and was shown to accurately calculate CARS spectra for probe-delayed measurements. The model treats the broadband pulse by assuming Gaussian noise statistics and allows us to explore the affect of a range of broadband driving fields from transform-limited (fs pump pulses) to noise-dominated (such as is found in our ps broadband dye laser).

Future Work

Validation of the time-domain CARS model: We will continue to develop the time-domain CARS code for use in the general CARS community. This will require further model-validation experiments. We plan to explore how the CARS signal intensity depends on Raman linewidth for ultrafast pulses (ps and fs pulses). At atmospheric pressure, ns CARS signal intensity depends on the Raman linewidth as $1/\gamma^2$ where γ is the linewidth. However, the average time between molecular collisions at room temperature and atmospheric pressure is on the order of picoseconds. As the probe pulse gets shorter in time, the CARS signal intensity will become less linewidth dependent, eventually approaching a linewidth-independent signal intensity if the probe pulse is shorter than collision times. The time-dependent collisional dynamics involved here must be more fully understood, especially as ps-CARS and fs-CARS are to be applied at elevated pressures. We plan to build a high-pressure, high-temperature cell which will allow us to vary the average number of molecular collisions for a given pulse-length to clarify these issues.

Linewidth measurements for various combustion-relevant colliders: We have shown that the technique of coherence decay measurement for pure-rotational CARS (RCARS) yields highly accurate Raman linewidth measurements. There exists a significant lack of data in the literature regarding the dependence of N_2 Raman linewidth on collision partner for pure-rotational CARS, especially for fuel-colliders. In collaboration with Per-Erik Bengtsson of Lund University, Sweden, we plan to carry out a series of experiments collecting N_2 Raman linewidth data as a function of collision partner to refine the CARS linewidth models used in the community. This will increase the accuracy of CARS

measurements in diffusion flames, for example, where N_2 collisions are dominated by N_2-fuel interactions on the interior side of the flame front. Perhaps the most powerful aspect of this technique is the capability to measure the *total* Raman broadening coefficient *in-situ*. In this manner, with no *a priori* knowledge of the flame composition, N_2 concentration, or temperature, the exact Raman linewidth can be determined at any given point in a flame, negating the need for a linewidth model altogether. We plan to perform experiments on sooting flames, building on collaboration with Hope A. Michelsen at Sandia, to improve the accuracy of temperature and species concentration profiles for standard sooting flames (Santoro burner and McKenna burner) used in LII modeling.

Energy transfer studies for quantitative Kr imaging: We are developing a predictive model for collisional quenching of Kr 5p $^2[3/2]_2$ in collaboration with Jonathan Frank. This work will contribute to development of a new mixture-fraction diagnostic technique using Kr two-photon LIF. Because the natural radiative lifetime of this excited state is only 27 ns and collisions at even modest pressures (< 10 Torr) of strongly quenching species reduce the effective fluorescence lifetime to a few ns, excitation by standard dye lasers (10-ns pulses) is not sufficient for accurate time-resolved studies, and excitation with picosecond (ps) laser pulses is necessitated.

References

1. M. L. Koszykowski, L. A. Rahn, R. E. Palmer, M. E.Coltrin, *J. Chem. Phys.* **91** (1987) 41–46.
2. L. A. Rahn, R. Palmer, *J. Opt. Soc. Am. B* **3** (1986)
3. A. Bohlin, F. Vestin, P. Joubert, J. Bonamy, P.E. Bengtsson, *J. Raman Spec.* **40** (2009) 788
4. C. J. Kliewer, Y. Gao, T. Seeger, B. D. Patterson, R. L. Farrow, and T. B. Settersten, *Appl. Opt.* **50**, in press (2011)

Publications and submitted journal articles supported by this project (2009-present)

1. C. J. Kliewer, Y. Gao, T. Seeger, B. D. Patterson, R. L. Farrow, and T. B. Settersten, "Quantitative one-dimensional imaging using picosecond dual-broadband pure-rotational CARS" *Appl. Opt.* **50**, in press (2011).
2. C. J. Kliewer, T. Seeger, Y. Gao, J. Kiefer, B. D. Patterson, and T. B. Settersten, "Picosecond time-resolved pure-rotational coherent anti-Stokes Raman spectroscopy in sooting flames," *Proc. Comb. Instit.* **33**, 831 (2011).
3. T. Seeger, J. Kiefer, Y. Gao, B. D. Patterson, C. J. Kliewer, and T. B. Settersten, "Suppression of Raman-resonant interferences in rotational CARS using time-delayed picosecond probe pulses," *Opt. Lett.* **35**, 2040 (2010).
4. T. Seeger, J. Kiefer, A. Leipertz, B. D. Patterson, C. J. Kliewer, and T. B. Settersten, "Picosecond time-resolved pure-rotational coherent anti-Stokes Raman spectroscopy for N2 thermometry," *Opt. Lett.* **34**, 3755 (2009).
5. W. D. Kulatilaka, J. H. Frank, and T. B. Settersten, "Interference-free two-photon LIF imaging of atomic hydrogen in flames using picosecond excitation," *Proc. Comb. Instit.* **32**, 955 (2009).
6. R. W. Schefer, W. D. Kulatilaka, B. D. Patterson, and T. B. Settersten, "Visible emission of hydrogen flames," *Combust. Flame* **156**, 1234 (2009).
7. X. Chen, T. B. Settersten, and A. P. Kouzov, "State- and time-resolved rotational relaxation signatures in two-color resonant four-wave mixing spectra," *J. Raman Spectrosc.* **40**, 847 (2009).
8. W. D. Kulatilaka, J. H. Frank, B. D. Patterson, and T. B. Settersten, "Analysis of 205-nm photolytic production of atomic hydrogen in methane flames," *Appl. Phys. B* **97**, 227 (2009).
9. A. K. Patnaik, S. Roy, J. R. Gord, R. P. Lucht, and T. B. Settersten, "Effects of collisions on electronic-resonance-enhanced coherent anti-Stokes Raman scattering of nitric oxide," *J. Chem. Phys.* **130**, 214304 (2009).
10. T. B. Settersten, B. D. Patterson, and C. D. Carter, "Collisional quenching of NO $A^2\sum^+(\upsilon' = 0)$ between 125 and 294 K," *J. Chem. Phys.* **130**, 204302 (2009).
11. T. B. Settersten, B. D. Patterson, and W. H. Humphries, IV, "Radiative lifetimes of NO $A^2\sum^+(\upsilon' = 0,1,2)$ and the electronic transition moment of the $A^2\sum^+$ - X $^2\Pi$ system," *J. Chem. Phys.* **131**, 104309 (2009)

ARGONNE-SANDIA CONSORTIUM ON HIGH-PRESSURE COMBUSTION CHEMISTRY

Stephen J. Klippenstein (PI), Michael J. Davis, Lawrence B. Harding, Joe V. Michael, James A. Miller, Branko Ruscic, Raghu Sivaramakrishnan, Robert S. Tranter

Chemical Sciences and Engineering Division, Argonne National Laboratory, Argonne, IL, 60439
sjk@anl.gov

Craig A. Taatjes (PI), Ahren W. Jasper, David L. Osborn, Leonid Sheps, Judit Zádor

Combustion Research Facility, Mail Stop 9055, Sandia National Laboratories
Livermore, CA 94551-0969
cataatj@sandia.gov

Program Scope

The goal of this project is to explore the fundamental effects of high pressure on the chemical kinetics of combustion and to use that knowledge in the development of accurate models for combustion chemistry at the high pressures of current and future engines. Such accurate chemical models will aid in the effective use of novel alternative fuels, in the development of advanced engine designs, and in the reduction of pollutants. We design and implement novel experiments, theory, and modeling to probe high-pressure combustion kinetics from elementary reactions, to submechanisms, to flames. The work focuses on integrating modeling, experiment, and theory (MET) through feedback loops at all levels of chemical complexity. We are developing and testing the methodology for propane, n-heptane, and 1-butanol as key prototype fuels, and will extend this approach to a general fundamental theory of pressure effects. The consortium expands and enhances collaborations between Argonne's Dynamics in the Gas Phase Group and the Combustion Chemistry Group in Sandia's Combustion Research Facility and also interacts closely with the Princeton-led Combustion Energy Frontier Research Center (CEFRC).

Recent Progress

High pressure, miniature high repetition rate shock tube (HRRST). A high pressure, miniature HRRST has been designed and built as part of a suite of new experimental devices intended for probing the challenging problems of pre-ignition chemistry and particle formation at elevated temperatures and pressures. The HRRST is intended to be coupled to a VUV time-of-flight mass spectrometer (TOF-MS) at the Chemical Dynamics beam line of the Advanced Light Source, an electron impact ionization (EI) TOF-MS at Argonne, and a time resolved small angle X-ray scattering detector (TR-SAXS) at the Advanced Photon Source. The shock tube is intended to run at a repetition rate of 4-10 Hz (required for efficient use of beam facilities), reflected shock temperatures as low as 700 K, and reflected shock pressures up to 100 bar. The high repetition rates are achieved by use of a pulsed valve for the driver section and novel vent valves in the driven section that allow efficient evacuation and filling of the shock tube.

The solenoid actuated driver valve was obtained from Oak Ridge National Laboratory and has been tested for repeatability and reliability of operation. Two prototypes of the pneumatically actuated vent valve have been built and tested to ensure that sufficiently rapid opening/closing times could be obtained, Fig. 1. Following the successful initial tests of the

driver and vent valves a prototype of the full miniature shock tube has been constructed, Fig. 1, and initial tests have begun. Currently, the apparatus is operated manually, however, we anticipate moving to fully automated operation shortly. All the necessary data acquisition and control hardware is in place and software is in the final debugging stages. In the initial tests shock waves were successfully generated in argon with helium driver with quite good repeatability and reproducibility. Reflected shock temperatures >3000 K were achieved with reflected shock pressures of approximately 1 bar. While these pressures are low they simply represent the results of conservative initial tests.

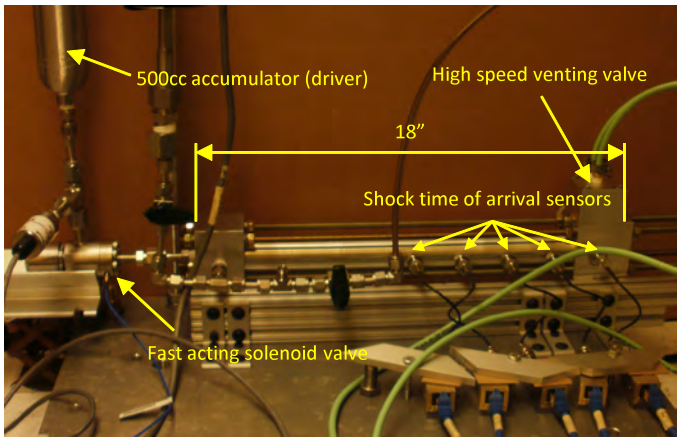

Fig. 1: Prototype of the high pressure, miniature, high repetition rate shock tube.

High Pressure Multiplexed Photoionization Mass Spectrometry (HP-MPIMS). The first-generation HP-MPIMS reactor, constructed with Laboratory Directed Research and Development funds at Sandia, has been tested and interfaced with the existing MPIMS apparatus of Taatjes and Osborn. Initial experiments were performed at Lawrence Berkeley Lab's Advanced Light Source, yielding the first HP-MPIMS data on propyl radical oxidation. These data, collected over a limited pressure and temperature range (up to 2 atm and 600 K, respectively), are consistent with the recently described propyl radical oxidation mechanism.[1] At these experimental conditions the product distributions are determined largely by propyl peroxy (RO_2) radical stabilization and the subsequent RO_2 + RO_2 chemistry. The MPIMS results complement other experimental strategies, such as OH laser-induced fluorescence detection. These initial experiments, still in progress, pave the way for multiplexed isomer-resolved kinetic measurements of many other important combustion reactions at elevated pressures.

C_2H_5OH Modeling: Global Uncertainty and C_2H_5OH + HO_2. We have developed a detailed model for the combustion of ethanol and methanol. The developed model was validated against a variety of speciation measurements in atmospheric and high-pressure flow reactors, jet stirred reactors, and low-pressure flames, ignition delay measurements from shock tubes, and laminar burning velocity measurements. Our modeling results coupled with global sensitivity analyses indicate that high pressure ignition delays (>5 atm) and high pressure measurements of ethanol concentrations in reactors (6-12 atm) are sensitive primarily to the total rate constants for C_2H_5OH + $HO_2 \rightarrow$ products (1). CH_3CHO and C_2H_4 (which

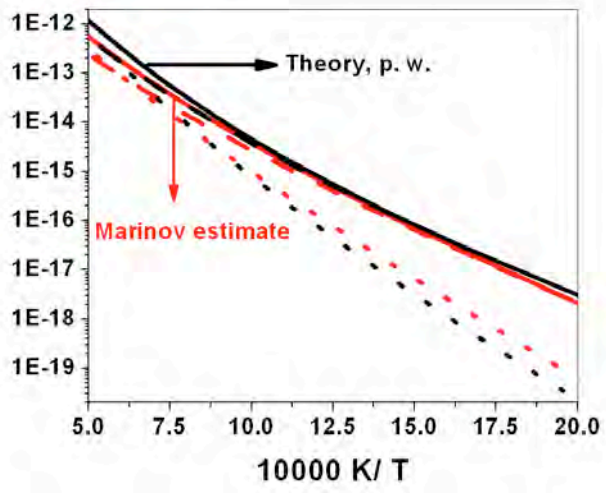

Fig. 2: Rate constants for 1 (solid line), 1a (dashed line), 1b (dotted line).

represent the primary intermediates) speciation measurements at high pressure are also particularly sensitive to the branching between $CH_3CHOH + H_2O_2$ (1a) and $CH_2CH_2OH + H_2O_2$ (1b).

There are no prior direct experimental measurements or theoretical predictions for the rate constants for reaction 1. We have used RCCSD(T)/∞//B3LYP/6-311++G(d,p) calculations to characterize the energetics for the various channels in reaction (1). Transition state theory predictions for k_{1a} and k_{1b} (cf. Fig. 2), which are expected to be accurate to within a factor of 2-3, are in surprisingly good agreement with the empirical estimates of Marinov.[2] These predictions offer an increased measure of confidence when validating our detailed model for ethanol combustion.

$C_4H_9O + O_2$. The reactions of hydroxybutyl radicals with O_2 were studied quantum chemically at the RQCISD(T)/CBS//B3LYP/6-311++G(d,p) level. All four hydroxybutyl radicals that can be formed by H-abstraction from 1-butanol were considered: ($CH_3CH_2CH_2CHOH$, α-R), ($CH_3CH_2CHCH_2OH$, β-R), ($CH_3CHCH_2CH_2OH$, γ-R) and ($CH_2CH_2CH_2CH_2OH$, δ-R). The hydroxybutyl radicals react with O_2 to form the corresponding hydroxybutylperoxy (RO_2) radicals. For these species, both direct HO_2 elimination *via* five-membered cyclic transition states and isomerization *via* intramolecular H-abstraction to hydroperoxyalkyl (QOOH) radicals were taken into account. For the QOOH species, C-O bond fission reactions producing HO_2 + alkene/aldehyde, formation of OH radicals + cyclic ethers, as well as C-C bond fission channels were considered.

The α-R + O_2 reaction predominantly yields HO_2 + butanal *via* direct HO_2 elimination from α-RO_2, in close analogy with the results of Zádor *et al.*[3] for the analogous α-hydroxyethyl + O_2 reaction. For the β, γ, and δ-hydroxybutyl radicals the $RO_2 \rightarrow$ QOOH isomerization saddle points are comparable in energy to those for direct HO_2 elimination. The presence of the alcoholic OH group in 1-butanol opens up new pathways not present for alkyl radicals, which can lead to OH formation by C-C bond fission of the QOOH species rather than formation of cyclic ethers. For the hydroxybutyl + O_2 reactions, this has been experimentally suggested by detection of stable products from Cl-initiated 1-butanol oxidation using time-resolved synchrotron photoionization mass spectrometry (see Taatjes abstract).

Propane Decomposition. We have studied the decomposition of propane with both shock tube experiments and ab initio transition state theory-based master equation calculations. The theoretical and experimental results are in remarkably good agreement, yielding a well validated model for the temperature and pressure dependent kinetics. Furthermore, the combined analysis provides strong evidence for a minor contribution from a $CH_4 + C_2H_4$ channel arising from a roaming radical mechanism.

Future Directions

Propane Combustion. We are continuing to work on the development of an accurate mechanism for the combustion of propane at high-pressures over a range of temperatures. The pressure and temperature range of the existing HP-MPIMS reactor will be extended up to 10 bar and 1000 K and a greater range of conditions will be sampled for propyl radical oxidation. Further experiments on propane oxidation reactions are scheduled at the ALS in May and June of 2011. Theoretical kinetics predictions will be obtained for the following reactions: C_3H_7 decomposition, $C_3H_8 + O_2$, $C_3H_8 + HO_2$, and $C_3H_7 + HO_2$. The propyl decomposition study will include a priori estimates of the energy transfer parameters as well as a detailed analysis of the rovibrational properties. Modeling predictions from the mechanism will be compared with the

experimental results and global uncertainty analyses will be used in conjunction with theoretical kinetics studies to improve the mechanism.

Butanol Combustion. We also plan to continue with studies related to the combustion of butanol. The potential energy surface generated for the $C_4H_9O + O_2$ reactions will be used to obtain transition state theory based master equation predictions for the kinetics. These calculations will quantitatively assess the relative importance of the various channels. HP-MPIMS data will be used together with OH production measurements and computational efforts to validate and improve mechanisms for butanol combustion, such as that being developed under the auspices of the Princeton-led CEFRC.

HP-MPIMS Developments. We will use the extensive benchmark measurements made with the existing reactor to design and build a second-generation HP-MPIMS apparatus. The largest potential for improvement lies in better product detection efficiency and optimizing the sampling geometry out of the reactor. High-pressure MPIMS experiments suffer from "signal dilution": with increase in bath gas pressures the reactive species represent a smaller mole fraction of the sample mixture. An improved second-generation reactor will move photoionization to a higher-density region of the sampling expansion, dramatically boosting experimental signal and thus extending the available range of sample pressures. In addition (with the help of R. Tranter), we will re-design the sampling nozzle to optimize the fluid dynamics of the reaction mixture, minimize wall effects, and achieve a more homogeneous reactive environment.

Theory Developments. We continue to work at improving the accuracy of our theoretical predictions via the detailed study of energy transfer, anharmonicity, and angular momentum conservation; which are intimately related. We also continue our work on understanding the radical-complex mechanism, focusing initially on the $CH_3 + O_2$ reaction, where we have made substantial progress in predicting the standard high pressure limit rate coefficients.

References

[1] H. F. Huang, D. J. Merthe, J. Zádor, L. E. Jusinski, and C. A. Taatjes, *Proc. Comb. Inst.*, **33**, 293 (2011)].

[2] N. M. Marinov, *Int. J. Chem. Kin*. **31**, 183 (1999).

[3] J. Zádor, R. X. Fernandes, Y. Georgievskii, G. Meloni, C. A. Taatjes and J. A. Miller, *Proc. Combust. Inst.*, **32**, 271 (2009).

DOE Supported Publications, 2009-Present

1. **Theoretical Rate Coefficients for Allyl + HO_2 and Allyloxy Decomposition**, C. F. Goldsmith, S. J. Klippenstein, and W. H. Green, *Proc. Comb. Inst.*, **33,** 273-282 (2011).
2. **Role of Peroxy Chemistry in the High Pressure Ignition of *n*-Butanol - Experiments and Detailed Kinetic Modelling**, S. Vranckx, K. A. Heufer, C. Lee, H. Olivier, L. Schill, W. A. Kopp, K. Leonhard, C. A. Taatjes, R. X. Fernandes, *Combust. Flame*, in press, doi:10.1016/j.combustflame.2010.12.028 (2011).
3. **Shock Tube and Theoretical Studies on the Thermal Decomposition of Propane: Evidence for a Roaming Radical Channel,** R. Sivaramakrishnan, M.-C. Su, J. V. Michael, S. J. Klippenstein, L. B. Harding, and B. Ruscic, *J. Phys. Chem. A,* in press (2011).
4. **Theoretical Unimolecular Kinetics for $CH_4 + M \rightarrow CH_3 + H + M$ in Eight Baths, M = He, Ne, Ar, Kr, H_2, CO, N_2, and CH_4**, A. W. Jasper and J. A. Miller, *J. Phys. Chem. A*, submitted.

THEORETICAL CHEMICAL KINETICS

Stephen J. Klippenstein
Chemical Sciences and Engineering Division
Argonne National Laboratory
Argonne, IL, 60439
sjk@anl.gov

Program Scope

The focus of this program is the theoretical estimation of the kinetics of elementary reactions of importance in combustion chemistry. The research involves a combination of *ab initio* quantum chemistry, variational transition state theory (TST), classical trajectories, and master equation simulations. The emphasis of our current applications is on reactions that are of importance in (i) soot formation, (ii) hydrocarbon oxidation, or (iii) NO_x chemistry. We are also interested in a detailed understanding of the limits of validity of and, where feasible, improvements in the accuracy of specific implementations of transition state theory. Detailed comparisons with experiment and with other theoretical methods are used to explore and improve the predictive properties of the transition state theory models. Dynamics simulations are performed as a means for testing the statistical assumptions, for exploring reaction mechanisms, and for generating theoretical estimates where statistical predictions are clearly inadequate. Master equation simulations are used to study the pressure dependence of the kinetics and to obtain phenomenological rate coefficients for use in kinetic modeling.

Recent Progress

Nitrogen Chemistry

The NNH species is believed to play a key role in NO formation and control. Unfortunately, due to its metastable nature, there is essentially no direct experimental information regarding the kinetics of NNH. Prior models for the thermal $DeNO_x$ process have indicated a key competition between NNH dissociation and the reaction of NNH with O_2. Furthermore, the reaction of NNH with O has been suggested to provide a high temperature pathway for NO formation in the NNH mechanism. In collaboration with Peter Glarborg, Jim Miller, and Larry Harding we have obtained ab initio transition state theory based master equation predictions for the kinetics of the NNH + O_2 and NNH + O reactions. Furthermore, prior theoretical predictions for the lifetime of NNH were analyzed and the NH_2 + O_2, NH + NO, and NNO + H reactions were studied. For the barrierless reactions, large active space multi-reference electronic structure methods were employed in conjunction with the variable reaction coordinate transition state theory approach. For the NNH + O reaction, an analytic transitional mode potential was formulated and the branching between the three addition products was also studied with trajectory simulations. For the reactions where experimental data is available, (i.e., the NO + NH and NNO + H reactions) the predictions were in good agreement with experiment.

The inclusion of these predictions in an update to the chemical kinetic model of Miller and Glarborg yields modeling results for the thermal $DeNO_x$ process that satisfactorily reproduce a wide range of experimental data. The model predictions were directly compared with experimental observations of the NO, NO_2, and NNO profiles as a function of O_2 concentration

and with or without H_2 additions. Interestingly, the chain branching is now mainly restricted by the small value of the branching fraction to NNH + OH for the NH_2 + NO reaction, rather than by subsequent reactions of NNH with O_2. Meanwhile, the predictions suggest a more limited role for the high temperature NNH mechanism.

Hydrocarbon Oxidation

A recent experimental study of Kable and coworkers on the photodissociation of CD_3CHO provides a unique test for statistical theories. In particular, the observed branching between HCO and DCO formation is determined by the effective fluxes for the pathways that lead to these two products. The HCO products are formed by simple CC bond fission, while the DCO products arise from a sequence of isomerizations (which leads to scrambling of the H and D atoms) followed again by CC bond fission. The branching is determined by the ratio of the CC bond fission transition state number of states to that arising from the sequence of transition states encountered in the isomerizations. Interestingly, the density of states for the complex factors out of the transition state theory analysis for the branching ratio. Thus, the experimental results provide a strong test of the transition state numbers of states. Our transition state theory based master equation predictions for this branching, which are an extension of our earlier predictions of the dissociation rate, are in good agreement with the experimental observations, differing by only 30%.

In collaboration with Joe Michael, Raghu Sivaramakrishnan, M.-C. Su, Larry Harding and Branko Ruscic we have studied the thermal decomposition of ethanol and the reaction of ethanol with OH and H/D. The experimental analysis yielded observed temperature and pressure dependent rate constants for the formation of $C_2H_4 + H_2O$, $CH_3 + CH_2OH$, and $C_2H_5 + OH$. The theoretical analysis provided an adequate description of these measurements for an average downwards energy transfer represented as $125\ (T/300)^{0.85}\ cm^{-1}$. Notably, similar energy transfer expressions, with prefactors ranging from 100 to 150 cm^{-1}, provide satisfactory models for the dissociations of acetaldehyde, ethane, dimethyl ether, and propane. The a priori theoretical predictions for the abstractions reactions by H and OH were in good agreement with the high temperature experimental data (1000 K and higher), differing by about 30 % or less. However, comparisons with measurements at lower temperatures suggest that the theoretical barrier heights are slightly too small.

A joint theory (Wagner, Dawes, Jasper, Harding, Georgievskii) experiment (Sivaramakrishnan, Michael) study of the dissociation of CH_3OCH_3 examined the contribution from the roaming radical mechanism for this species. The experimental observations indicate that a significant fraction (0.19 +/- 0.07) of the reaction produces products other than H atoms. The theoretical analysis shows that these products cannot arise from traditional tight transition state processes. An analytic potential energy surface for the transitional modes was developed with the interpolated moving least squares method. Reduced dimensional trajectory simulations employing this potential do indicate some roaming trajectories, but yield a smaller branching fraction of only ~0.02. The predictions for the temperature and pressure dependence of the decomposition rate constants yield a satisfactory reproduction of both the present and earlier experimental observations.

Future Directions

We will continue our studies of aromatic ring formation, hydrocarbon oxidation, and NO_x chemistry. Our work with Tranter (Argonne) on the self-reaction of phenyl radicals has suggested the importance of benzyne radicals to the PAH growth process. Thus, we are initiating some studies of the kinetics of these radicals. We have made preliminary theoretical predictions for the self-reaction of *o*-C_6H_4.

We continue to collaborate with Jim Miller on the study of various soot related reactions. We are in the process of studying the reaction of propargyl with OH, which may provide an important oxidative loss channel for this key resonantly stabilized radical. We also intend to study the reaction of vinyl radical with 1,3 butadiene, which may provide an important ring formation pathway in ethylene flames. Both of these studies will involve complicated multiple well *ab initio* transition state theory based master equation calculations.

The H2/O2 mechanism is central to all of combustion chemistry. Thus, we are planning to study a number of the reactions in the H2/O2 mechanism with high levels of theory.

DOE Supported Publications, 2009-Present

1. **A Shock Tube and Theory Study of the Dissociation of Acetone and Subsequent Recombination of Methyl Radicals**, S. Saxena, J. H. Kiefer, and S. J. Klippenstein, *Proc. Comb. Inst.*, **32**, 123-130 (2009).
2. **Kinetics of the H + NCO Reaction**, S. J. Klippenstein and L. B. Harding, *Proc. Comb. Inst.*, **32**, 149-155 (2009).
3. **Theoretical Rate Coefficients for the Reaction of Methyl Radical with Hydroperoxyl Radical and for Methylhydroperoxide Decomposition**, A. W. Jasper, S. J. Klippenstein, and L. B. Harding, *Proc. Comb. Inst.*, **32**, 279-286 (2009).
4. **Detailed Balance in Multiple-Well Chemical Reactions**, J. A. Miller, S. J. Klippenstein, S. H. Robertson, M. J. Pilling, and N. J. B. Green, *Phys. Chem. Chem. Phys*., **11**, 1128-1137 (2009).
5. **A Crossed Molecular Beams Study on the Formation of the Exotic Cyanoethynyl Radical in Titan's Atmosphere,** X. Gu, R. I. Kaiser, A. M. Mebel, V. V. Kislov, S. J. Klippenstein, L. B. Harding, M. C. Liang, Y. L. Yung, *Astrophysical J.,* **701,** 1797-1803 (2009).
6. **The Thermal Decomposition of NH_2OH and Subsequent Reactions: Ab Initio Transition State Theory and Reflected Shock Tube Experiments,** S. J. Klippenstein, L. B. Harding, B. Ruscic, R. Sivaramakrishnan, N. K. Srinivasan, M.-C. Su, and J. V. Michael, *J. Phys. Chem. A*, **113**, 10241-10259 (2009).
7. **Shock Tube and Theory Investigation of Cyclohexane and 1-Hexene Decomposition,** J. H. Kiefer, K. S. Gupte, L. B. Harding, and S. J. Klippenstein, *J. Phys. Chem. A*, **113,** 13750-13583 (2009).
8. **On the Temperature Dependence of Two Key Interstellar Reactions of H_3^+: $O(^3P) + H_3^+$ and $CO + H_3^+$,** S. J. Klippenstein, Y. Georgievskii, and B. J. McCall, *J. Phys. Chem. A*, **114,** 278-290 (2010).
9. **Direct Observation of Roaming Radicals in the Thermal Decomposition of Acetaldehyde,** R. Sivaramakrishnan, J. V. Michael, and S. J. Klippenstein, *J. Phys. Chem. A*, **114,** 755-764 (2010).

10. **Roaming Radical Kinetics in the Decomposition of Acetaldehyde,** L. B. Harding, Y.Georgievskii, and S. J. Klippenstein, *J. Phys. Chem. A*, **114,** 765-777 (2010).
11. **Reactions between Resonance Stabilized Radicals: Propargyl + Allyl**, J. A. Miller, S. J. Klippenstein, Y. Georgievskii, L. B. Harding, W. D. Allen, and A. C. Simmonett, *J. Phys. Chem. A*, **114,** 4881-4890 (2010).
12. **D-Atom Products in Predissociation of CD_2CD_2OH from the 202-215 nm Photodissociation of 2-bromoethanol**, L. W. Edwards, M. Ryazanov, H. Reisler, and S. J. Klippenstein, *J. Phys. Chem. A*, **114,** 5453-5461 (2010).
13. **The Effect of Spin-Orbit Splitting on the Association Kinetics of Barrierless Halogen-Atom-Hydrocarbon Radical Reactions,** A. W. Jasper, S. J. Klippenstein, and L. B. Harding, *J. Phys. Chem. A*, **114,** 5759-5768 (2010).
14. **Formation of CH_2NH and NH_3 in Titan's Upper Atmosphere**, R. V. Yelle, V. Vuitton, P. Lavvas, S. J. Klippenstein, M. Smith, S. Horst, and J. Cui, *Faraday Discussions*, **147**, 31-49 (2010).
15. **An Experimental and Theoretical Investigation of the Self-Reaction of Phenyl Radicals**, R. S. Tranter, S. J. Klippenstein, L. B. Harding, B. R. Giri, X. Yang, and J. H. Kiefer, *J. Phys. Chem. A*, **114,** 8240-8261 (2010).
16. **Theoretical Validation of Chemical Kinetic Mechanisms: Combustion of Methanol**, R. T. Skodje, A. S. Tomlin, S. J. Klippenstein, L. B. Harding, and M. J. Davis**,** *J. Phys. Chem. A*, **114** 8286-8301 (2010).
17. **Exploring the Role of PAHs in the Formation of Soot: Pyrene Dimerization**, H. Sabbah, L. Biennier, S. J. Klippenstein, I. R. Sims, and B. R. Rowe, *J. Phys. Chem. Lett.*, **1**, 2962-2967 (2010).
18. **Rate Constants for The Thermal Decomposition of Ethanol and its Bimolecular Reactions with OH and D: Reflected Shock Tube and Theoretical Studies**, R. Sivaramakrishnan, M.-C. Su, J. V. Michael, S. J. Klippenstein, L. B. Harding, and B. Ruscic, *J. Phys. Chem. A*, **114,** 9425-9439 (2010).
19. **Roaming Radical Pathways for the Decomposition of Alkanes**, L. B. Harding and S. J. Klippenstein, *J. Phys. Chem. Lett.*, **1**, 3016-3020 (2010).
20. **Uncertainty Driven Theoretical Kinetics Studies for CH_3OH Ignition: HO_2 + CH_3OH and O_2 + CH_3OH**, S. J. Klippenstein, L. B. Harding, M. J. Davis, A. S. Tomlin, and R. T. Skodje, *Proc. Comb. Inst.*, **33**, 351-357 (2011).
21. **Ab Initio Kinetics for the Decomposition of Monomethylhydrazine (CH_3NHNH_2)**, P. Zhang, S. J. Klippenstein, H. Sun, and C. K. Law, *Proc. Comb. Inst.*, **33,** 425-432 (2011).
22. **Roaming Radicals in the Thermal Decomposition of Dimethyl Ether: Experiment and Theory,** R. Sivaramakrishnan, J. V. Michael, A. F. Wagner, R. Dawes, A. W. Jasper, L. B. Harding, Y. Georgievskii, and S. J. Klippenstein, *Comb. Flame*, **158**, 618-632 (2011).
23. **The Role of NNH in NO Formation and Control**, S. J. Klippenstein, L. B. Harding, P. Glarborg, and J. A. Miller, *Comb. Flame*, **158,** 774-789 (2011).
24. **Near-Threshold H/D Exchange in CD_3CHO Photodissociation** B. R. Heazlewood, A. T. Maccarone, D. U. Andrews, D. L. Osborn, L. B. Harding, S. J. Klippenstein, M. J. T. Jordan, and S. H. Kable, *Nature Chem.*, accepted (2011).
25. **Insights into the Role of PAH Condensation in Haze Formation in Jupiter's Atmosphere,** L. Biennier, H. Sabbah, V. Chandrasekaran, S. J. Klippenstein, I. R. Sims, and B. R. Rowe, *Astronomy and Astrophysics*, accepted (2011).

Theoretical modeling of spin-forbidden channels in combustion reactions

Anna I. Krylov
Department of Chemistry, University of Southern California,
Los Angeles, CA 90089-0482
krylov@usc.edu

1 Scope of the project

The goal of our research is to develop predictive theoretical methods, which can provide crucial quantitative data (e.g., rate constants, branching ratios, heats of formation), identify new channels and refine reaction mechanisms. Specifically, we are developing tools for computational studies of spin-forbidden and non-adiabatic pathways of reactions relevant to combustion, and applying these tools to study electronic structure and reactions of open-shell and electronically excited species involved in these processes.

2 Summary of recent major accomplishments

During the past year, we conducted several computational studies of open-shell and electronically excited species. The common theme in these studies is interactions between states of different character and intersections between the corresponding potential energy surfaces (PESs). We also continued to develop computational methods for modeling electronic structure and spectroscopy of open-shell species. The DOE support is acknowledged in nine publications.[1–9] The previous year DOE-supported publications are Refs. 1, 2. Some of the recent results are highlighted below. The following students and postdocs have been supported by this grant during 2010: Lucas Koziol, Vadim Mozhaiskii, Dr. Tomasz Kuś, Dr. Arik Landau, Dr. Liang Tao, and Dr. Eugene Kamarchik.

2.1 Roaming dynamics of 2-hydroxy-ethyl radical

In collaboration with Prof. Hanna Reisler's and Joel Bowman's group, we investigated dynamics of energetic CH_2CH_2OH radicals.[1] Our calculations identified a previously unexplored channel leading to the production of vinyl and water via a roaming mechanism (see Fig. 1). The trajectory calculations suggest that the roaming pathway constitutes a minor (a few percent) but robust channel of the overall C_2H_4OH dissociation. Hydrogen can be abstracted from either carbon, which can be verified by deuteration experiments.

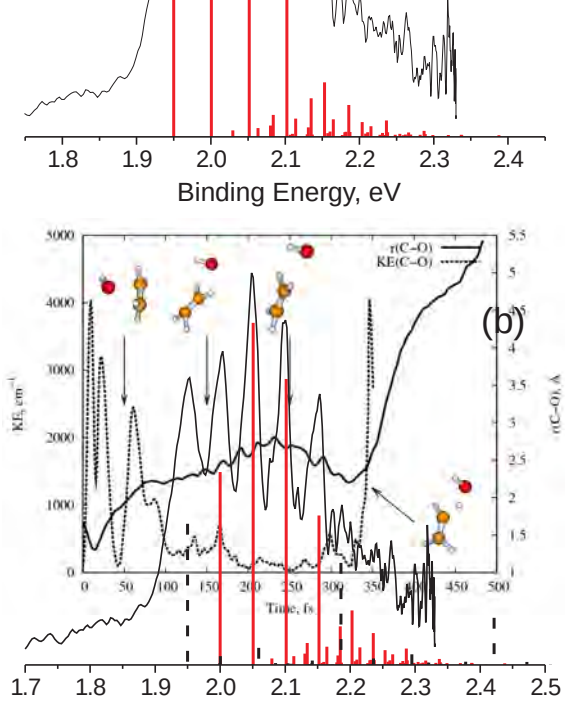

Figure 1: Kinetic energy in the C-O bond stretch and $r(\mathrm{C}-\mathrm{O})$ bond length during a water loss event. Until $t = 0$ fs the OH fragment undergoes normal oscillations for about 10 ps. From $t = 50$ fs to $t = 300$ fs the OH fragment begins to move away and enters a region of increased $r(\mathrm{C}-\mathrm{O})$ bond length and decreased vibrational kinetic energy until at $t = 350$ fs the OH abstracts a hydrogen from the same carbon from which it dissociated to m water + vinyl.

2.2 Oxyallyl diradical

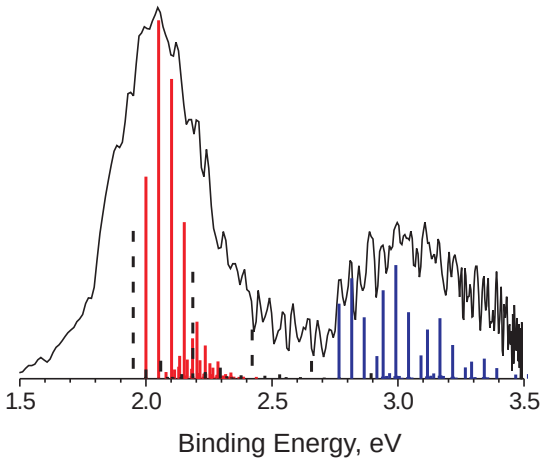

Figure 2: The calculated and experimental photoelectron spectrum of the OXA anion. Solid red bars, dashed black, and solid blue bars denote the progressions in the triplet $^3B_2$, singlet $^1A_1$ and triplet $^3B_1$ bands, respectively. Solid black lines are the experimental photoelectron spectra measured with 355 nm laser.

In collaboration with Prof. Andrei Sanov, we investigated electronic structure of the oxyallyl (OXA) diradical and the anion using high-level *ab initio* methods. Our best estimates of the adiabatic energy differences between the anion $^2A_2$ and the neutral $^3B_2$ and $^3B_1$ states are: 1.94 and 2.73 eV, respectively. We found that the $^1A_1$ state lies above $^3B_2$ vertically, but geometric relaxation brings it below the triplet. The two-dimensional scan of the singlet $^1A_1$ PES reveals that there is no minimum corresponding to a singlet diradical structure. Thus, singlet OXA undergoes prompt barrierless ring closure. However, a flat shape of the PES results in the resonance trapping in the Franck-Condon region giving rise to the experimentally observable features in the photoelectron spectrum. By performing reduced-dimensionality wave-packet calculations, we estimated that the wave packet lingers in the Franck-Condon region for about 170 fs, which corresponds to the spectral line broadening of about 200 cm^{-1}. We also computed the photodetachment spectrum and compared it with experimental data (Fig. 2). Our calculations lend strong support to the reported assignment of the photodetachment spectra of the OXA anion.

3 Using charge stabilization method in EOM-DIP calculations

We employed (Kuś, Krylov, manuscript in preparation) the charge stabilization method to stabilize unstable dianion reference functions (see Fig. 3) that spoil the numeric performance of equation-of-motion (EOM-DIP) limiting applications of this method. We found that reliable EOM-DIP excitation energies can be computed using a stabilized resonance wave function instead of the lowest energy solution corresponding to the neutral + free electron(s) state of the system. Singlet-triplet energy gaps of selected diradicals shown in Table 1 demonstrate the performance. DIP is particularly suitable for oxygen-containing diradicals.

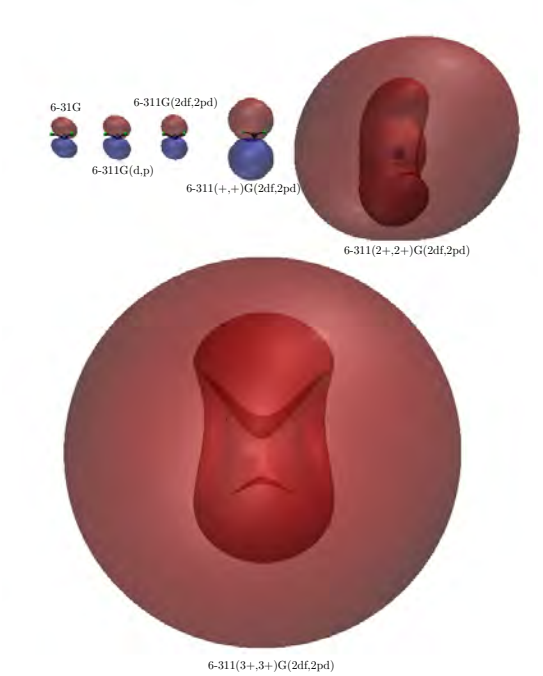

Figure 3: The shape of the HOMO of CH_2^{-2} in different basis sets. The orbitals are visualized using a contour value enclosing 70% of the electron density. The HOMO of the unstable dianion reference state becomes increasingly diffuse in its attempt to detach to extra electrons spoiling the quality of the DIP wave functions. Applying stabilizing potential increases the detachment energy of the reference converting it to a bound state suitable for the DIP expansion. Note that in small bases the dianion reference behaves as a stable bound state.

Table 1: Errors (eV) in the ST gaps computed by the DIP method stabilized by the charged cage. The errors are computed as $E_{DIP} - E_{ref}$, where E_{ref} is the SF value computed without the stabilized potential and in the same basis set (augmented triple-zeta quality).

system	C_{stab}	DIP/not stabilized	DIP/stabilized
CH_2	10.0	-7.84	-0.18
o-benzyne	10.2	-3.49	-0.22
m-benzyne	10.4	-1.55	-0.15
NH	10.6	-10.60	-0.07
TMM		-0.45	-0.02

4 Current developments and future plans

Currently, we are pursuing modeling of electronic structure and dynamics of several radicals relevant to combustion. In collaboration with Profs. Hanna Reisler and Joel Bowman, we are investigating spectroscopy and dissociation dynamics of CH_2OH. In collaboration with Prof. Hai Wang, we are applying SF-DFT to characterize different pathways in combustion of aromatic hydrocarbons. We are also developing complex-scaled EOM-CC for treating resonance states and photoionization cross sections.

References

[1] E. Kamarchik, L. Koziol, H. Reisler, J.M. Bowman, and A.I. Krylov, A roaming pathway leads to unexpected water+vinyl products in C_2H_4OH dissociation, J. Phys. Chem. Lett. **1** (2010).

[2] V. Mozhayskiy, D.J. Goebbert, L. Velarde, A. Sanov, and A.I. Krylov, Electronic structure and spectroscopy of oxyallyl: A theoretical study, J. Phys. Chem. A **114**, 6935 (2010).

[3] H. Reisler and A.I. Krylov, Interacting Rydberg and valence states in radicals and molecules: Experimental and theoretical studies, Int. Rev. Phys. Chem. **28**, 267 (2009).

[4] I. Fedorov, L. Koziol, A.K. Mollner, A.I. Krylov, and H. Reisler, Multiphoton ionization and dissociation of diazirine: A theoretical and experimental study, J. Phys. Chem. A **113**, 7412 (2009).

[5] L. Koziol, V. Mozhayskiy, B.J. Braams, J.M. Bowman, and A.I. Krylov, Ab initio calculation of the photoelectron spectra of the hydroxycarbene diradicals, J. Phys. Chem. A **113**, 7802 (2009).

[6] C.M. Oana and A.I. Krylov, Cross sections and photoelectron angular distributions in photodetachment from negative ions using equation-of-motion coupled-cluster Dyson orbitals, J. Chem. Phys. **131**, 124114 (2009).

[7] C.A. Taatjes, D.L. Osborn, T.M. Selby, G. Meloni, A.J. Trevitt, E. Epifanovsky, A.I. Krylov, B. Sirjean, E. Dames, and H. Wang, Products of the benzene + $O(^3P)$ reaction, J. Phys. Chem. A **114**, 3355 (2010).

[8] E. Kamarchik, O. Kostko, J.M. Bowman, M. Ahmed, and A.I. Krylov, Spectroscopic signatures of proton transfer dynamics in the water dimer cation, J. Chem. Phys. **132**, 194311 (2010).

[9] B. Karpichev, L. Koziol, K. Diri, H. Reisler, and A.I. Krylov, Electronically excited and ionized states of the CH_2CH_2OH radical: A theoretical study, J. Chem. Phys. **132**, 114308 (2010).

SYNCHROTRON STUDIES OF COMBUSTION RADICAL REACTIONS AND AEROSOL CHEMISTRY

Stephen R. Leone, Kevin Wilson, Fabien Goulay, Jordy Bouwman, Theodora Nah, and Musahid Ahmed

Departments of Chemistry and Physics and Lawrence Berkeley National Laboratory
University of California, Berkeley, California 94720
(510) 643-5467 srl@berkeley.edu

Scope of the Project

Combustion is a complex process involving short-lived radical species, highly excited states, kinetics, transport processes, heterogeneous chemistry on aerosols such as organic liquid nanoparticles and soot, fluid dynamics, and energy transfer. Vacuum ultraviolet (VUV) light from the Chemical Dynamics Beamline of the Advanced Light Source (ALS) provides a powerful tool to selectively detect reaction products of carbon-based radical species (e.g. C_2H, CH, C_3H_3, C_5H_5 …) with hydrocarbons by photoionization mass spectrometry. The multiplexed photoionization mass spectrometer apparatus at the ALS was jointly constructed with David Osborn and Craig Taatjes of the Sandia Combustion Research Facility. Products from key combustion reactions can now be detected and branching ratios estimated. Detailed measurements of microscopic reaction pathways result in considerable information to aid in the understanding of combustion processes. In addition, an aerosol apparatus coupled with photoionization mass spectrometry is used to study aerosol heterogeneous chemistry. This endeavor explores aerosol particulate species chemistries, such as in fuel sprays, their production in combustion, and impact on the environment.

C_2H + pyridine

The gas phase reaction of the ethynyl radical (C_2H) with pyridine (C_5H_5N) is studied at temperatures of 295 K and 375 K using a multiplexed photoionization mass spectrometer coupled to tunable VUV synchrotron radiation. The ethynyl radical is formed by 193 nm laser photolysis of CF_3CCH. The major reaction product is 3-ethynylpyridine (80±20%) with an upper limit for the production of 2-ethynylpyridine of 20%. Because of the presence of C_2H radicals in combustion flames, the reaction can play a role in molecular growth processes involving pyridine, such as in the combustion of coal and coal-derived fuels. The reaction of the C_2H radical with pyridine is likely to play a role in the formation of polycyclic nitrogen heterocycles (PANH), which are soot precursors in incomplete combustion processes.

CH + pyrrole

The products of the gas phase reaction of the ground state methylidyne radical CH ($X^2\Pi$) with pyrrole (C_4H_5N) is studied at 295 K and 363 K [Soorkia et al., PCCP, 2010]. The CH radicals are produced by laser multiphoton photolysis of bromoform ($CHBr_3$) at 248 nm. A signal at m/z = 79 (C_5H_5N) is identified as the main reaction product formed by CH addition to pyrrole followed by H-elimination. The photoionization efficiency curve unambiguously identifies m/z = 79 as pyridine. With deuterated methylidyne radicals (CD), the product mass peak is shifted by +1 mass unit, consistent with the formation of C_5H_4DN and identified as deuterated pyridine. Within detection limits, there is no evidence that the intermediate addition complex undergoes hydrogen scrambling. The results are consistent with a reaction mechanism that proceeds *via* the direct CH cycloaddition or insertion into the five-member pyrrole ring. The carbon ring expansion is followed by elimination of the H atom from the nitrogen to form the resonance stabilized pyridine molecule. The N-H bond of the secondary amine in pyrrole is weaker than any of the C-H bonds in pyrrole, providing a thermodynamic driving force for this selective outcome and the lack of randomization of the H atoms in the adduct.

CH + benzene

Benzene is purportedly central to soot formation in many combustion systems, and the fate of its reaction with the CH radical impacts possible soot-forming pathways. The reaction is also of

particular significance as the addition of CH to benzene forms an intermediate of the formula C_7H_7 that could implicate the benzyl radical or cycloheptatrienyl radical. The high exothermicities of CH + hydrocarbon reactions are interesting and informative high-energy probes of the relevant potential energy surfaces. Photoionization mass spectra of the species involved in the CH + benzene reaction reveals a dominant product at the C_7H_6 mass corresponding to CH addition followed by H elimination. The photoionization vs. energy plot of this mass channel has a signal onset and general morphology that is consistent with fulvenallene (c-C_5H_4-CCH_2). This product is a ring-contracted species that has recently been predicted to be the dominant benzyl radical thermal decomposition product [see da Silva, et al., JPC A, 2010]. Further studies are currently underway to elucidate the mechanism of the CH + benzene reaction.

CH + acetaldehyde

Aldehydes are very important intermediates in the combustion of hydrocarbons and are recognized to promote combustion processes, acetaldehyde being the most effective of these promoters. In homogeneous charge compression ignition (HCCI) engines the addition of aldehyde enhances the ignition process by promoting the preflame reaction of the main natural fuel region. Studying the chemistry of aldehydes with carbon radicals present in combustion environments will improve our understanding of the role of these molecules in combustion chemistry. The products of the reaction of the CH radical with acetaldehyde are detected at room temperature. Several reaction channels are detected in the experiments here, resulting from: direct hydrogen abstraction, CH insertion and CH addition. Direct abstraction of the hydrogen atom on the carbonyl group produces the acetyl radical. Insertion of the CH radical to the C-H bond of the methyl group of the acetaldehyde followed by CH_3-elimination leads to the formation of a ketene. Addition of the CH radical onto the π-electron system of the carbonyl forms a cyclic adduct that is likely to further dissociate to form C_3H_4O isomers and an H atom. Photoionization efficiency curves demonstrate that methylketene, acrolein and cyclopropanone are the main C_3H_4O reaction products. By using, deuterium substituted CH radicals and acetaldehyde molecules it is possible to gain very detailed information about the reaction mechanism. Following CH addition to acetaldehyde, acrolein is formed by loss of a hydrogen atom from the methyl group while all the other C_3H_4O isomers are formed by loss of the H atom from the CH radical. Such a level of understanding of the reaction mechanism allows the prediction of the reaction products of CH reactions with larger molecules containing a carbonyl group.

Heterogeneous Chemistry – reactions of squalane with Cl in the absence/presence of oxygen

An important process in complex combustion reactions are possible heterogeneous reactions between sprayed fuel droplets, or fuel and oil on cylinder walls, and reactive gas-phase radicals or molecules. While heterogeneous reactions with spray droplets is not likely to change the models of combustion, the role of fuel films and oils on cylinder walls is implicated in stochastic variations in engine ignition. Compared to the gas phase, there are potentially more highly coupled reactions between reactants, products, and intermediates occurring in the particle phase or gas-liquid phase. A simple atomic radical, Cl, is used to understand the reaction mechanism initiated *via* a heterogeneous H abstraction reaction by a gas phase radical at the surface of a sub-micron droplet of squalane. In the absence of O_2, chlorinated reaction products are formed and radical chain chemistry is observed, propagated by the $R\cdot + Cl_2 \rightarrow RCl + Cl\cdot$ reaction in the particle phase. Effective reactive uptake coefficients vary from 0.8 to 3.5, corresponding to radical chain propagation lengths of 1.4 and 6.4, respectively. The magnitude of the effective uptake coefficient is found to be approximately proportional to the [Cl_2] in the flow reactor. Molecular oxygen competes with molecular chlorine for reaction with R· and replaces the chain propagation mechanism by a terminating reaction through the formation of stable oxygenated products. Adding as much as 20% O_2 to the reaction effectively shuts off the chain cycling reaction, producing oxygenated products and decreasing the uptake coefficient to a diffusion-corrected value of 0.65±0.07. Additionally, the chemical evolution of the particle follows a sequential oxidation mechanism. Under these conditions the Cl initiated oxidation of the particle

is nearly identical to that found for the OH + squalane reaction albeit ~2.2 times faster, due to the larger initial reactive uptake coefficient of Cl atoms compared to OH.

Heterogeneous Chemistry–reactivity of aerosols composed of unsaturated molecules

Oleic acid, linoleic acid, linolenic acid, and squalene, containing 1, 2, 3, and 6 C=C double bonds, respectively, are investigated to explore the reactivity of droplets composed of unsaturated molecules. These molecules are similar in structure to the long chain alkyl (methyl, ethyl, or propyl) esters found in biodiesel and are reasonable model systems to begin to examine the fundamental heterogeneous reactions between hydrocarbon droplets and gas phase radicals and molecules. A closed shell molecule, Cl_2, is found to react with these droplets despite the fact that analogous reactions in the gas phase occur very slowly or not at all at room temperature. The rates of these heterogeneous reactions are higher for the compounds containing more unsaturated reaction sites. For example, squalene (6 C=C double bonds) reacts with Cl_2 more rapidly than oleic acid (1 C=C double bond). From the chemical evolution of the particle phase, it is found that one Cl atom replaces one H atom for each reaction. Efforts are underway to construct a detailed heterogeneous reaction mechanism.

Cl radicals are also used to probe the heterogeneous reactivity of gas phase radicals with C=C double bonds in hydrocarbon droplets. These studies are designed to examine how hydrogen abstraction reactions compete with radical addition when C=C double bonds are present. Very large effective uptake coefficients are observed and depend upon $[O_2]$ in the reactor as well as the number of unsaturated sites in the organic droplets. Effective uptake coefficients are 1.7 – 4.2, 14 – 47, and 50 – 130 for oleic acid, linolenic acid, and squalene, respectively, at $[O_2]$ from 0 to 20%. The effective uptake coefficient of Cl with squalene droplets increases from 50 to 95 when the chlorine molecule concentration increases from 4 ppm to 12 ppm in the absence of O_2. Effective uptake coefficients much larger than 1 are clear indications of chain reaction chemistry, which has the net effect of making the reaction rate 100 times faster than the Cl atom collision frequency. Efforts are currently underway to develop a detailed molecular understanding of these heterogeneously initiated chain reactions.

A new class of investigations has been initiated to study heterogeneous OH + alkene reactions. Squalene ($C_{30}H_{50}$) is a branched alkene that has 6 double bonds, and 8 primary, 16 secondary and 6 tertiary carbon atoms, making it an ideal proxy to represent the different kinds of reactive carbon sites typically found on hydrocarbon surfaces. The free radical reaction of liquid squalene particles by OH radicals is measured using H_2O_2 as a photolytic precursor of OH. Kinetic measurements find that the uptake coefficient for OH on squalene particles in the presence of O_2 is significantly larger than unity, indicating the existence of a chain propagating mechanism that produces peroxy and alkoxy radical intermediates and regenerates OH radicals within the particle, thus accelerating the rate of particle oxidation. The extent of secondary chemistry can be controlled by the concentrations of oxygen and hydrogen peroxide in the system. In addition, the uptake coefficient is inversely proportional to the concentration of OH, signaling a chain termination step that competes with the chain propagation steps. Based on the masses of the observed oxidation products, alcohols and carbonyls are formed during the heterogeneous oxidation process.

Future plans

New studies will focus on additional gas phase radical-molecule reactions. In particular, we are examining the trends of insertion reactions compared to cycloaddition reactions of the CH radical. Products of the reaction of CH with cyclopentadiene (c-C_5H_6) and indene (C_9H_8) will be investigated to determine the influence of resonance-stabilized intermediates on the final product branching fractions of the reaction. The reaction of small hydrocarbon radicals with oxygenated molecules, such as ketones and alcohols, will be studied to further understand the chemistry occurring in the combustion of biomass related fuels. Also, radical reaction/heterogeneous chemistry on carbonaceous soot particles has yet to be explored at the level of detail that is now

possible by using aerosol generation and introduction instruments, flow tube reactors, and mass spectrometric detection tools. By preparing fresh soot particles in a flame and immediately introducing them into a flow tube system, we will study their reactivity and products with radicals, such as Cl atoms or C_2H radicals. The formation of larger PAH molecules that partition to the particle phase, produced by the reaction of hydrocarbon radicals with naphthalene and higher aromatic ring compounds, species present in oil shales, will be investigated using the VUV photoionization aerosol mass spectrometer. Since PAH molecules have low ionization energies, they are readily identified by both their mass spectra and ionization energy. The oxidation of PAHs is a heterogeneous process that competes with the formation of soot. Oxidation reactions take place on the surfaces of soot particles and decrease the mass of PAHs and soot material through the formation of CO and CO_2. The main oxidation reactants are with OH radicals (under fuel-rich conditions) and O_2 (under fuel-lean conditions). Experiments will be carried out to determine the mechanisms by which these oxidants react with heterogeneous phase PAHs. These studies will shed light on how different types of combustion particulate emissions also evolve in the atmosphere.

Recent Publications Citing DOE Support (2009-2011)

C.-L. Liu, J. D. Smith, D. L. Che, M. Ahmed, S. R. Leone, and K. R. Wilson, "The direct observation of secondary radical chain chemistry in the heterogeneous reaction of chlorine atoms with submicron squalane droplets," Phys. Chem. Chem. Phys. DOI:10.1039/C1CP20236G, in press (2011).

S. R. Leone, M. Ahmed, and K. R. Wilson, "Chemical dynamics, molecular energetics, and kinetics at the synchrotron," Phys. Chem. Chem. Phys. **12**, 6564 (2010).

S. Soorkia, A. J. Trevitt, T. M. Selby, D. L. Osborn, C. A. Taatjes, K. R. Wilson and S. R. Leone, "Reaction of the C_2H radical with 1-butyne (C_4H_6): low-temperature kinetics and isomer-specific product detection," J. Phys. Chem. A **114**, 3340 (2010).

S. Soorkia, C. A. Taatjes, D. L. Osborn, T. M. Selby, A. J. Trevitt, K. R. Wilson and S. R. Leone, "Direct detection of pyridine formation by the reaction of CH (CD) with pyrrole: a ring expansion reaction," Phys. Chem. Chem. Phys. **12**, 8750 (2010).

A. J. Trevitt, F. Goulay, C. A. Taatjes, D. L. Osborn, and S. R. Leone, "Reactions of the CN radical with benzene and toluene: product detection and low temperature kinetics," J. Phys. Chem. A. **114**, 1749 (2010).

R. I. Kaiser, A. Mebel, O. Kostko and M. Ahmed, "On the ionization energies of C_4H_3 Isomers," Chem. Phys. Lett. **485**, 281 (2010)

R. I. Kaiser, B. J. Sun, H. M. Lin, A. H. H. Chang, A. Mebel, O. Kostko and M. Ahmed "An experimental and theoretical study on the ionization energies of polyynes (H-$(CC)_n$-H; n = 1 - 9)," Astrophys. J. **719**, 1884 (2010).

O. Kostko, J. Zhou, A. Chang, B. J. Sun, J. S. Lie, A. H. H. Chang, R. I. Kaiser and M. Ahmed "Determination of ionization energies of C_nN (n=3-12) clusters: Vacuum-ultraviolet (VUV) photoionization experiments and theoretical calculations," Astrophys. J. **717**, 674 (2010)

F. Goulay, A. J. Trevitt, G. Meloni, T. M. Selby, D. L. Osborn, C. A. Taatjes, L. Vereeken, and S. R. Leone, "Cyclic versus linear isomers produced by reaction of the methylidyne radical (CH) with small unsaturated hydrocarbons," J. Am. Chem. Soc. **131**, 993 (2009).

A. J. Trevitt, F. Goulay, G. Meloni, D. L. Osborn, C. A. Taatjes, and S. R. Leone, "Isomer-specific product detection of CN radical reactions with ethene and propene by tunable VUV photoionization mass spectrometry," Int. J. Mass. Spectrom. **280**, 113 (2009)

J. D. Smith, J. H. Kroll, C. D. Cappa, D. L. Che, C. L. Liu, M. Ahmed, S. R. Leone, D. R. Worsnop, and K. R. Wilson, "The heterogeneous reaction of hydroxyl radicals with sub-micron squalane particles: a model system for understanding the oxidative aging of ambient aerosols," Atmos. Chem. Phys. **9**, 3209 (2009)

D. L. Che, J. D. Smith, S. R. Leone, M. Ahmed and K. R. Wilson, "Quantifying the reactive uptake of OH by organic aerosols in a continuous flow stirred tank reactor," Phys. Chem. Chem. Phys. **11**, 7885 (2009)

Intermolecular Interactions of Hydroxyl Radicals on Reactive Potential Energy Surfaces

Marsha I. Lester
Department of Chemistry, University of Pennsylvania
Philadelphia, PA 19103-6323
milester@sas.upenn.edu

I. Program Scope

Hydroxyl radicals are important in combustion and atmospheric environments, where they are often detected by laser-induced fluorescence (LIF) on the $A^2\Sigma^+$ - $X\ ^2\Pi$ band system. However, collision partners known to quench electronically excited OH $A^2\Sigma^+$ radicals are ubiquitous in these environments. Thus, great effort has been made to quantify the rates and/or cross sections for collisional quenching, so that its effects on LIF signals may be taken into account to allow an accurate determination of OH concentrations. Despite extensive kinetic measurements, fundamental questions remain regarding the fate of the collisionally quenched molecules and the ***mechanism*** by which these nonadiabatic processes occur. The experimental work carried out under DOE-BES funding in the Lester laboratory is aimed at understanding the fundamental chemical dynamics governing quenching of OH $A^2\Sigma^+$ by molecular partners (M = H_2, O_2, N_2, CO, CO_2, H_2O) of significance in combustion environments.

II. Recent Progress

A. Collisional quenching of OH $A^2\Sigma^+$ by H_2 and its isotopic variants

Additional key information on the mechanism for quenching can be obtained by identification of the main products from quenching and their quantum state distributions. For the OH $A^2\Sigma^+ + H_2$ system, there are two highly exoergic outcomes of collisional quenching. These are nonreactive quenching,

$$OH\ A^2\Sigma^+ + H_2 \rightarrow OH\ X^2\Pi + H_2 \qquad \Delta E = -4.02\ eV$$

which produces OH and H_2 products in their ground electronic states, and reactive quenching

$$OH\ A^2\Sigma^+ + H_2 \rightarrow H_2O + H \qquad \Delta E = -4.72\ eV$$

Both processes are predicted to occur via nonadiabatic passage through a seam of conical intersection (CI), which occurs when the O-side of OH points toward H_2, that couples the electronically exited and ground state potential energy surfaces.

Our recent studies on the OH + H_2 system (and isotopic variants) focused on the outcome from the nonreactive quenching process by examining the internal energy distribution of the OH $X^2\Pi$ products as well as the branching between nonreactive (12%) and reactive (88%) quenching channels.[1-4] The dynamical outcomes can be connected directly with properties of the potential energy surfaces in the vicinity of the CI: Specifically, <u>efficient quenching</u> arises from a barrierless downhill path in HO – H_2 orientations to a region of strong coupling between the lowest potentials of $^2A'$ symmetry.[5] The <u>highly rotationally excited OH $X^2\Pi$ products</u> results from steep angular gradients that place a substantial torque on the OH moiety upon approach and exit from the CI region.[1] The <u>branching</u> between nonreactive and reactive quenching reflects the topography of the CI in the tilt of the cone.[5-6] The experimental studies have been complemented recently by the first dynamical calculations,[4, 7-10] which provide important insights on the evolution of the HO – H_2 system through the conical intersection region.

1. OD $X^2\Pi$ products from nonreactive quenching

Stimulated by the recent calculations of quenching dynamics in the OH $A^2\Sigma^+ + H_2$ system, we have carried out experimental studies of the nonreactive and reactive outcomes for the isotopic variant OD $A^2\Sigma^+ + H_2$.[4, 11] This isotopic substitution changes the nuclear motions as the system evolves from

reactants through the conical intersection region to products, but not the underlying electronic potential energy surfaces that give rise to reactive and nonreactive quenching.

Specifically, experimental results shown in Fig. 1 reveal a rotational distribution for the most populated v''=0 level that peaks at N''~21 with an average rotational energy of 4600 cm^{-1}. Complementary trajectory calculations of the post quenching dynamics by Bowman and coworkers show even more rotational excitation and a slightly warmer vibrational distribution for the OD $X^2\Pi$ products. Experimental branching fraction measurements reveal that nonreactive quenching accounts for less than 20% of the quenching outcomes, while trajectory calculations within a "diabatic" model predict that 12% of the products arise from nonreactive quenching with the dominant contribution from reactive quenching. Experiments show a selectivity for the $\Pi(A')$ Λ-doublet component, indicating strong alignment of the half-filled pπ orbital in the OD rotation plane. There is no evidence of OH $X^2\Pi$ products from exchange reaction in experimental or theoretical studies.

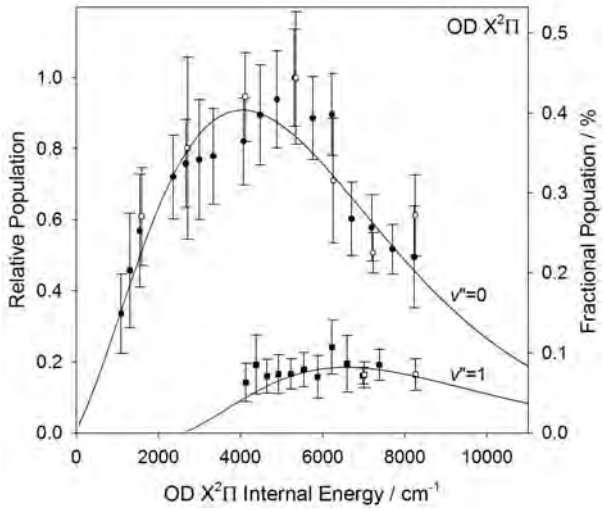

Fig. 1 Significant rotational excitation of OD $X^2\Pi$ (v'', N'') products arising from quenching of OD $A^2\Sigma^+$ by H_2.

The OD $X^2\Pi$ products from nonreactive quenching are released with an additional ~6 quanta of rotational angular momentum on average (experiment) than the OH $X^2\Pi$ products from OH $A^2\Sigma^+ + H_2$.[3] Nevertheless, the rotational energy distributions observed experimentally for the hydroxyl radical products from quenching of OH $A^2\Sigma^+$ and OD $A^2\Sigma^+$ by H_2 are remarkably similar, both indicating that 14% of the available energy is deposited into product rotation. Theory shows a greater increase in the degree of rotational excitation of products for OD compared to OH ($\Delta N''$~8-10) and an increase in the average rotational energy of the products upon deuteration. Both experimental and theoretical results suggest a small increase in the branching fraction for nonreactive quenching upon quenching of OD compared to OH with H_2.

2. Insights on reactive quenching from isotope specific studies

In current work, we are investigating the reactive quenching channel for O**D** $A^2\Sigma^+ + \mathbf{H_2}$ to examine the kinetic energy release and relative abundance of **H**- and **D**-atom products arising from the corresponding abstraction- and insertion-like mechanisms.

$$\text{O}\mathbf{D}\ A^2\Sigma^+ + \mathbf{H_2} \rightarrow \text{HOD} + \mathbf{H}\ \text{(abstraction)}$$
$$\rightarrow \text{H}_2\text{O} + \mathbf{D}\ \text{(insertion)}$$

The branching between these two reactive quenching processes is a place where experiment[12] and quasiclassical trajectory calculations of the post quenching dynamics[7-8] differ considerably for O**H** $A^2\Sigma^+ + \mathbf{D_2}$, and thus we considered reinvestigation of these processes with a different isotopic combination to be essential for validating our earlier results and unraveling the origin of the discrepancy. Theory predicts that insertion is a very minor channel (1%), while prior experiments had shown that insertion accounts for nearly 40% of the products. Indeed, our latest experiments using two-photon Doppler spectroscopy of the H- and D-atom products from reactive quenching of O**D** $A^2\Sigma^+$ by $\mathbf{H_2}$, depicted in Fig. 2, show a significant contribution of D-atom products (25%) from an insertion-like process.[11] The branching between these two different reaction channels surely reflects the forces at play as the HO-H_2 system evolves through the CI region.

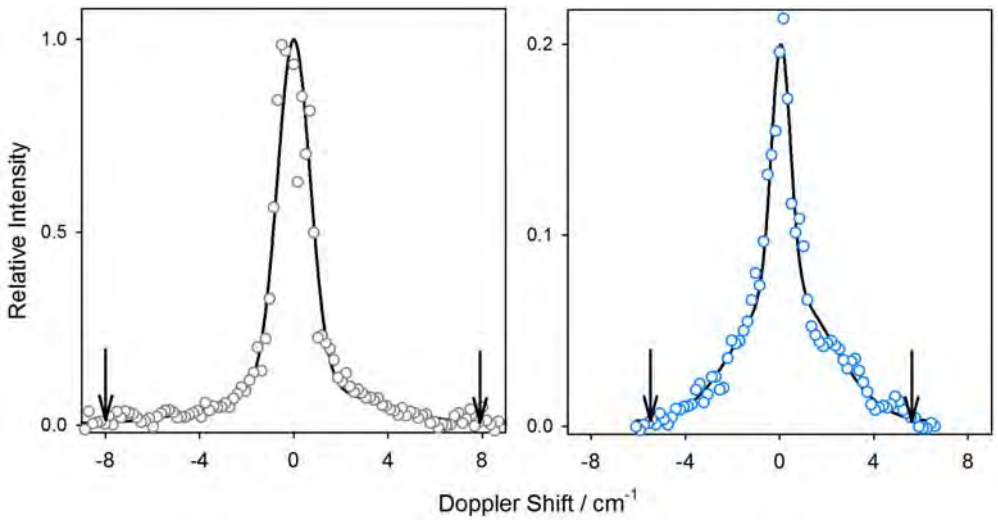

Fig. 2 Doppler profiles of H-atoms (left) and D-atoms (right) from abstraction and insertion channels resulting from reactive quenching of OD $A^2\Sigma^+$ by H_2. Arrows show maximum Doppler shifts based on available energy.

The product translational energy distributions $P(E_T)$ for the abstraction (**H**-atom) and insertion-like (**D**-atom) processes following reactive quenching of O**D** $A^2\Sigma^+$ by $\mathbf{H_2}$ are deduced directly from the Doppler profiles (Fig. 2) using a new robust analysis method. The **H**-atom profile is strongly peaked at line center with a smaller broad contribution, corresponding to a highly peaked $P(E_T)$ distribution at low translational energy (below 0.5 eV) with a tail extending to the energetic limit. By contrast, the **D**-atom profile has a larger contribution in the wings. The corresponding $P(E_T)$ distribution for the insertion-like process has the majority of the distribution at higher translational energy with a distinctive secondary peak at ~1.8 eV and only a small peak at low translational energy. Information is simultaneously obtained on the corresponding internal energy distribution of the 'hot' HOD or H_2O co-fragments, which are produced with most of the 4.7 eV of available energy. Reanalysis of prior experimental results from this laboratory at low collision energies (0.005 eV) with different isotopic combinations,[12-13] are consistent with the latest results. A broader $P(E_T)$ distribution peaked at 0.6 eV was observed for **D**-atom products of the abstraction channel for O**H** $A^2\Sigma^+ + \mathbf{D_2}$ at higher collision energies (0.16 eV) in crossed molecular beam scattering experiments by Davis and coworkers.[14] We suspect that this difference may reflect a strong collision energy dependence in the quenching dynamics.

B. Collisional quenching of OH $A^2\Sigma^+$ by O_2

A comprehensive quantum state distribution has also been measured for the OH $X^2\Pi$ products from quenching OH $A^2\Sigma^+$ (v'=0, N'=0) by O_2.[15] OH products are formed predominantly in v''=0 with less population in v''=1 and none detected in v''=2. With O_2 as the collision partner, the ground-state OH $X^2\Pi$ products are generated with a significant degree of rotational excitation, peaking at N'' ~ 17 with ~4800 cm^{-1} of rotational energy on average; no fine-structure effects are observed. Branching fraction measurements reveal that 40(1)% of the products are OH $X^2\Pi$ (v''=0, 1) and indicate that reactive quenching is significant. Energetically accessible reactive channels include

$$\begin{aligned} \text{OH } A^2\Sigma^+ + O_2\ X^3\Sigma_g^- &\rightarrow HO_2\ X^2A'' + O\ (^3P_J) \qquad \Delta E = -1.69 \text{ eV} \\ &\rightarrow HO_2\ A^2A' + O\ (^3P_J) \qquad \Delta E = -0.82 \text{ eV} \\ &\rightarrow O_3\ X^1A_1 + H\ (^2S) \qquad \Delta E = -0.68 \text{ eV} \end{aligned}$$

We have carried out preliminary studies of the H-atom products from the H + O_3 reactive quenching channel by characterizing the H-atom Doppler profiles. The initial H-atom profiles can be characterized a Gaussian lineshape with 2.6 cm^{-1} FWHM, indicating an average kinetic energy release to products of 0.25 eV. The Doppler profile indicates that 65% of the available energy results in internal excitation of O_3.

III. Future Plans

In the next three years, our planned research will focus on the ***outcomes*** of collisional quenching of electronically excited OH $A^2\Sigma^+$ radicals. Specifically, the experimental studies will examine reactive quenching processes that generate chemically distinct products as well as nonreactive quenching processes that return OH $A^2\Sigma^+$ radicals to their ground $X^2\Pi$ electronic state, the latter with an emphasis on the energy transferred to the collision partner. The observed product state distributions from reactive and nonreactive quenching processes will be used to identify the forces acting on the nuclei as the system switches from the electronically excited to ground state potential energy surface. The systems investigated and experimental methods utilized will be expanded to include velocity map imaging to probe previously unobserved outcomes of collisional quenching. Finally, collaborations will be developed with theoretical groups to obtain a comprehensive model for quenching consistent with kinetic rate measurements, product branching ratios, quantum state distributions, and kinetic energy release.

IV. References

1. P. A. Cleary, L. P. Dempsey, C. Murray, M. I. Lester, J. Kłos and M. H. Alexander, J. Chem. Phys. **126**, 204316 (2007).
2. L. P. Dempsey, C. Murray and M. I. Lester, J. Chem. Phys. **127**, 151101 (2007).
3. L. P. Dempsey, C. Murray, P. A. Cleary and M. I. Lester, Phys. Chem. Chem. Phys. **10**, 1424-32 (2008).
4. J. H. Lehman, L. P. Dempsey, M. I. Lester, B. Fu, E. Kamarchik and J. M. Bowman, J. Chem. Phys. **133**, 164307 (2010).
5. B. C. Hoffman and D. R. Yarkony, J. Chem. Phys. **113**, 10091-9 (2000).
6. L. P. Dempsey, T. D. Sechler, C. Murray, M. I. Lester and S. Matsika, J. Chem. Phys. **130**, 104307 (2009).
7. E. Kamarchik, B. N. Fu and J. M. Bowman, J. Chem. Phys. **132**, 091102 (2010).
8. B. Fu, E. Kamarchik and J. M. Bowman, J. Chem. Phys. **133**, 164306 (2010).
9. P.-Y. Zhang, R.-F. Lu, T.-S. Chu and K.-L. Han, J. Phys. Chem. A **114**, 6565-8 (2010).
10. P.-Y. Zhang, R.-F. Lu, T.-S. Chu and K.-L. Han, J. Chem. Phys. **133**, 174316 (2010).
11. J. H. Lehman, M. I. Lester, J. Bertrand and T. A. Stephenson, manuscript in preparation (2011).
12. M. W. Todd, D. T. Anderson and M. I. Lester, J. Phys. Chem. A **105**, 10031-6 (2001).
13. D. T. Anderson, M. W. Todd and M. I. Lester, J. Chem. Phys. **110**, 11117-20 (1999).
14. M. Ortiz-Suárez, M. F. Witinski and H. F. Davis, J. Chem. Phys. **124**, 201106 (2006).
15. L. P. Dempsey, T. D. Sechler, C. Murray and M. I. Lester, J. Phys. Chem. A **113**, 6851-8 (2009).

V. Publications supported by this project 2009-2011

1. L. P. Dempsey, T. D. Sechler, C. Murray, M. I. Lester, and S. Matsika, "State-resolved distribution of OH $X^2\Pi$ products arising from electronic quenching of OH $A^2\Sigma^+$ by N_2", *J. Chem. Phys.* **130**, 104307 (2009).
2. L. P. Dempsey, T. D. Sechler, C. Murray and M. I. Lester, "Quantum state distribution of the OH $X^2\Pi$ products from collisional quenching of OH $A^2\Sigma^+$ by O_2 and CO_2", *J. Phys. Chem. A* **113**, 6851-6858 (2009).
3. T. D. Sechler, L. P. Dempsey, and M. I. Lester, "State-to-state vibrational energy transfer in OH $A^2\Sigma^+$ with N_2", *J. Phys. Chem. A* **113**, 8845-8851 (2009).
4. P. Soloveichik, B. A. O'Donnell, M. I. Lester, A. B. McCoy, and J. S. Francisco, "Infrared spectrum and stability of the H_2O-HO complex: Experiment and theory", *J. Phys. Chem. A* **114**, 1529-1538 (2010).
5. J. H. Lehman, L. P. Dempsey, M. I. Lester, B. Fu, E. Kamarchik, and J. M. Bowman, "Collisional quenching of OD $A^2\Sigma^+$ by H_2: Experimental and theoretical studies of the state-resolved OD $X^2\Pi$ product distribution and branching fraction", *J. Chem. Phys.* **133**, 164307 (2010).

Theoretical Studies of Molecular Systems

William A. Lester, Jr.
Chemical Sciences Division
Ernest Orlando Lawrence Berkeley National Laboratory and
Kenneth S. Pitzer Center for Theoretical Chemistry
Department of Chemistry, University of California, Berkeley
Berkeley, California 94720-1460
walester@lbl.gov

Program Scope

This research program is directed at extending fundamental knowledge of atoms and molecules. The approach combines the use of ab initio basis set methods and the quantum Monte Carlo (QMC) method to describe the electronic structure and energetics of systems of primarily combustion interest.

Recent Progress

a) Bay-capping reactions: Kinetics and influence on graphene-edge growth

A capping reaction was found in a recent study to cause curvature in graphene edges and affect their growth rates. This reaction is initiated by acetylene addition to an armchair-like graphene radical site containing an embedded five-member ring. In this work, a combination of quantum-chemical calculations and reaction rate analysis was employed to explore the elementary steps of bay-capping reactions and to derive their rate coefficients. To evaluate the influence of the embedded five-member ring on six-member ring cyclization, the energetics and reaction rates of capping an embedded five-member ring were compared with those of capping a graphene armchair site. Detailed kinetic Monte Carlo simulations were performed to model evolution of graphene edges at conditions typical of soot growth and to examine the influence of the newly-derived rate coefficients.

b) Patterns of local aromaticity in graphene oxyradicals

Two families of polyaromatic hydrocarbon (PAH) oxyradicals were investigated using density functional theory (DFT) and the semi-empirical PM6 method. These families result from the edge

oxidation of substrates that involve only zigzag edges and those that include both zigzag and armchair edges. Oxyradical stability is shown to correlate with local aromatic character of six-atom rings characterized by the harmonic oscillator measure of aromaticity (HOMA) and with the distribution of HOMA values in molecules. It was demonstrated, that oxidation at the edge has a non-local effect on the structure of PAHs and leads to distinguishable types of HOMA patterns that are common for both families of PAHs.

c) Edge versus interior in the chemical bonding and magnetism of zigzag edged triangular graphene molecules

Ab initio density functional theory calculations show that in zigzag-edged triangular graphene molecules the CC bond lengths fall into three distinct groups: core, apex, and edge, irrespective of whether the molecular center is a single atom or a C-6-ring. The core, with a geometry that approximates infinite graphene, extends to the penultimate triangular row of carbon atoms, except in the vicinity of an apex. Impressed on the core bonds starting at the center is a small increasing length oscillation. The perimeter CC bonds joined at the apex are the shortest in the molecule. The edge carbon atoms are separated from interior atoms by the longest bonds in the molecule. The spin density localized primarily on edge (not apex) carbons with attached hydrogen (A-sublattice) is likely the highest attainable in any graphene molecule. The CC bonds in the high spin section of the edges are uniform in length and longer than perimeter CC bonds in the zigzag edged linear acenes, hexangulenes, annulenes, and benzene. This is attributed to the large number of edge localized nonbonding molecular orbitals (NBMOs) that sequester pi-charge making it unavailable for bonding.

d) Intramolecular competition in the photodissociation of C3D3 radicals at 248 and 193 nm

Motivated by recent experimental work, a theoretical study of the photodissociation of perdeuterated propargyl (D2CCD) and propynyl (D3CCC) radicals has been carried out, focusing on the C-C bond cleavage and D2 loss channels. High-level ab initio calculations were carried out, and RRKM rate constants were calculated for isomerization and dissociation pathways. The resulting reaction barriers, microcanonical rate constants and product branching ratios are consistent with the experimental findings, supporting the overall mechanism of internal conversion followed by statistical dissociation on the ground state surface. We found loose transition states and very low exit barriers for two of the C-C bond cleavage channels and an additional CD2 + CCD channel, which had not been reported previously. Our results probe the extent of propargyl and propynyl isomerization prior to dissociation at 248 and 193 nm and deliver a comprehensive picture of all ongoing molecular

dynamics.

Future Plans

We shall continue investigation of electronic structure of pristine and chemically modified graphenes in collaboration with Michael Frenklach's group. Computational results obtained using semi-empirical methods and density functional theory will be augmented by QMC studies of the most critical reaction steps. Frenklach's group will determine a complete set of rate coefficients for every reaction system.

QMC methodology will be applied to simulate X-ray absorption spectra of carbonaceous systems as a combustion diagnostic tool. We shall also investigate applicability of QMC methods to studies of energy transport in molecular systems.

DoE Supported Publications (2009-2011)

1. R. Olivares-Amaya, R. Salomon-Ferrer, W. A. Lester, Jr., C. Amador-Bedolla, "Creating a GUI for Zori, a Quantum Monte Carlo Program," Computing in Science & Engineering, **11**, 41-47 (2009)
2. R. Whitesides, D. Domin, R. Salomon-Ferrer, W. A. Lester, Jr., M. Frenklach, "Embedded-ring migration on graphene zigzag edge," Proc. Combust. Inst. **32**, 577-583 (2009)
3. W. A. Lester, Jr., L. Mitas, B. Hammond, "Quantum Monte Carlo for atoms, molecules and solids ," Chem. Phys. Lett. **478**, 1-10 (2009)
4. D. Yu. Zubarev, N. Robertson, D. Domin, J. McClean, J. Wang, W. A. Lester, Jr., R. Whitesides, X. You, M. Frenklach, "Polyaromatic hydrocarbon ovyradical stability," J. At. Mol. Sci. **1**, 48-53 (2010).
5. W. A. Lester, Jr. "Quantum Monte Carlo for Electronic Structure," in Practical Aspects of Computational Chemistry, J. Leszczynski and M. K. Shukla, Eds., Springer, pp. 315-325 (2010).
6. D. Yu. Zubarev, D. Domin, W. A. Lester, Jr., "Quantitative Characteristics of Qualitative Localized Bonding Patterns," J. Phys. Chem. A **114**, 3074–3079 (2010)
7. D. Yu. Zubarev, N. Robertson, D. Domin, J. McClean, J. Wang, W. A. Lester, Jr., R. Whitesides, X. You, M. Frenklach, "Local Electronic Structure and Stability of Pentacene Oxyradicals," J. Phys. Chem. C **114**, 5429-5437 (2010)
8. M. R. Philpott, S. Vukovic, Y. Kawazoe, W. A. Lester, Jr., "Edge versus interior in the chemical bonding and magnetism of zigzag edged triangular graphene molecules," J. Chem. Phys. **133**, 044708 (2010)

9. J. Wang, D. Yu. Zubarev, M. R. Philpott, S. Vukovic, W. A. Lester, Jr., T. Cui, Y. Kawazoe, “Onset of diradical character in small nanosized graphene patches,” Phys. Chem. Chem. Phys. **12**, 9839-9844 (2010)

10. J. Wang, D. Domin, B. Austin, D. Yu. Zubarev, J. McClean, M. Frenklach, T. Cui, W. A. Lester, Jr., “A Diffusion Monte Carlo Study of the O-H Bond Dissociation of Phenol,” J. Phys. Chem. A **114**, 9832-9835 (2010)

11. L. Castiglioni, S. Vukovic, P. E. Crider, W. A. Lester, D. M. Neumark, “Intramolecular competition in the photodissociation of C3D3 radicals at 248 and 193 nm,” Phys. Chem. Chem. Phys. **12**, 10714-10722 (2010)

12. D. Yu. Zubarev, X. You, J. McClean, W. A. Lester, Jr., M. Frenklach, “Patterns of local aromaticity in graphene oxyradicals,” J. Mater. Chem. **21**, 3404-3409 (2011)

13. X. You, R. Whitesides, D. Yu. Zubarev, W. A. Lester, Jr., M. Frenklach, “Bay-capping reactions: Kinetics and influence on graphene-edge growth,” Proc. Combust. Inst. **33**, 685-692 (2011)

Development of Kinetics for Soot Oxidation at High Pressures Under Fuel-Lean Conditions

JoAnn S. Lighty
Department of Chemical Engineering, University of Utah, jlighty@utah.edu
Randall Vander Wal
Dept. of Energy and Mineral Engineering, Pennsylvania State University, ruv12@psu.edu

Project Scope

The focus of the proposed research is to develop kinetic models for soot oxidation with the hope of developing a validated, predictive, multi-scale, combustion model to optimize the design and operation of evolving fuels in advanced engines for transportation applications. The work focuses on the relatively unstudied area of the fundamental mechanisms for soot oxidation. The objectives include understanding of the kinetics of soot oxidation by O_2 under high pressure which will require: 1) development of intrinsic kinetics for the surface oxidation, which takes into account the dependence of reactivity upon nanostructure and 2) evolution of nanostructure and its impact upon oxidation rate and 3) inclusion of internal surface area development and possible fragmentation resulting from pore development and/or surface oxidation. These objectives will be explored for a variety of pure fuel components and surrogate fuels.

The project is a joint effort between the Univ. of Utah (UU) and Pennsylvania State Univ. (Penn State). Work at the UU focuses on experimental studies using a two-stage burner and a high-pressure TGA. Currently experiments in the two-state burner are being conducted using a jet-fuel surrogate and at atmospheric pressure. Data at higher pressures will be taken using a high pressure TGA. Penn State will provide HRTEM images and guidance in the fringe analysis algorithms and parameter quantification for the images.

Recent Progress

Fuel Components

The work will investigate both oxygenated and jet fuels. Currently, the plan is to focus on pure components of diesels and jet fuels as well as simplified surrogates to study synergies between components. As a start, n-dodecane was chosen as a Fischer Tropsch fuel. A surrogate for jet fuel will be a simple mixture of m-xylene and n-dodecane, a mixture which has been used in a current study. In the future, n-dodecane with the addition of butanol will be used for an oxygenated diesel.

Oxidation Studies

Two experimental systems will be used. A two-stage burner will be used for scoping studies while a high pressure TGA will help investigate the effects of pressure on the nanostructure development under oxidation conditions. In the two-stage burner [1], soot is formed in the first burner, passes through a mixing zone where additional air is added depending upon the equivalence ratio. The soot then passes to a second burner where the soot is oxidized under both fuel rich and fuel lean conditions. This system is at ambient pressure and will be used as a first step to look at fuel effects and structure. To determine the amount of oxidation, samples are taken from the exhaust and passed to a SMPS, capable of detecting sizes down to 3 nm [2]. Details on sampling can be found in [2]. A commercial vaporizer (Mesoscopic Devices) coupled with a flow control system, will be used to feed liquid fuels.

Two-stage burner studies have been conducted for pure m-xylene and n-dodecane and a mixture of m-xylene/dodecane (10/90 by volume). The first burner was run under equivalence ratios of 1.7 (C/O =

0.65), 2.11 (C/O ratio = .697) and 2.15 (C/O ratio = .697) for m-xylene/air, m-xylene/n-dodecane/air and n-dodecane/air premixed flames respectively, while the overall equivalence ratio was 0.8 and 1.14 for each flame. TEM samples were taken as a function of the height above the second burner using a thermophoretic probe. A TEM grid holder was attached to a piston and compressed air at 60 psig was used to quickly insert the TEM grid (200 Mesh) into the flame [3]. TEM grids taken at 2.5 mm above the second burner surface were sent to Penn State and the results of the image analysis are described below.

Preliminary TGA studies were performed with soot from the m-xylene and n-dodecane (10/90) mixture surrogate. The mixture was combusted under heavily-sooting conditions, C/O=0.83, in a flat flame premixed burner. Soot was captured on a water-cooled stabilization plate placed 5 cm above the burner surface. The collected soot was crushed into a powder. The soot was oxidized using a Cahn TherMax 500 high pressure TGA. A 10 mg soot sample was placed in a quartz crucible (18 mm diameter and 20 mm height). The crucible was suspended from a ceramic coil attached to a microbalance. An inert material (blasting zirconium silicate beads 0.125-0.250 mm diameter) was used in all of the runs to minimize thermal and mass transfer effects by decreasing the stagnant atmosphere between the surface of the soot and the entrance of the container. Isothermal tests were completed at 500°C to 700°C, with increments of 50 ^{0}C. Atmospheric pressure and gas flow rates at 0.55 l/min were used to develop experimental protocol.

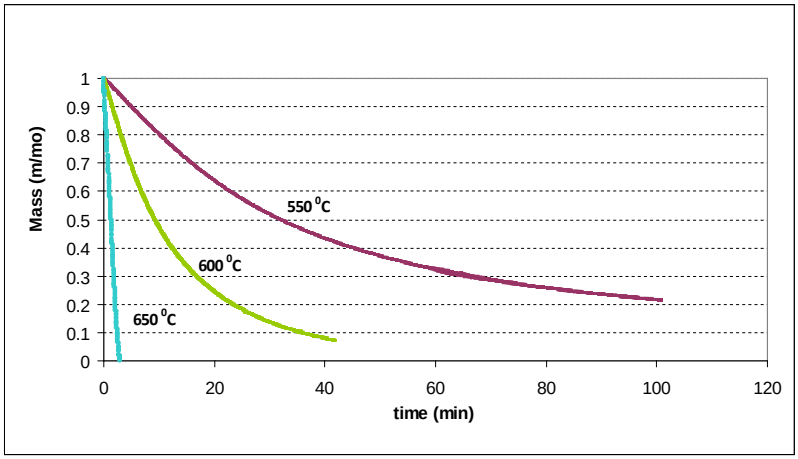

Based on the change in mass as a function of time, numerical analysis was performed to extract the rate constants (kc) at each temperature. Figure 1 shows the mass-loss data for three different temperatures.

Figure 1. Mass versus time data from TGA at isothermal conditions.

Rate constants were obtained for multiple isothermal experiments at various temperatures and then used to obtain the activation energy (E) and frequency factor (A) using a ln kc versus 1/T plot (Figure 2). The activation energy was found to be approx. 170 kJ/mol, the same order of magnitude as other published values for the activation energy of uncatalyzed soot oxidation [4].

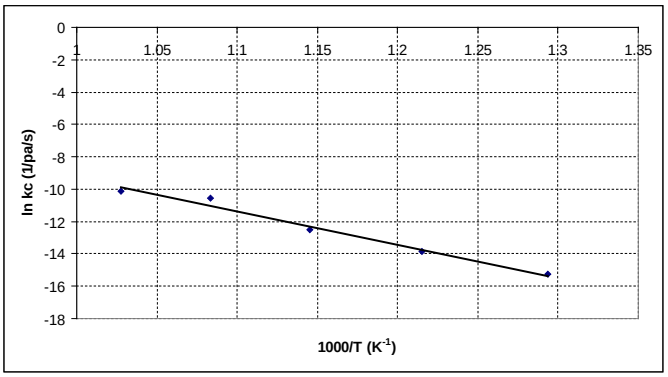

Figure 2. Plot of kc versus inverse temperature.

HR-TEM and Fringe Analysis

Representative images for the two soots for each fuel component of the surrogate jet fuel blend are shown in Figure 3. Both fuels separately yield the same nanostructure, termed "fullerenic", somewhat surprisingly given the different molecular structures.

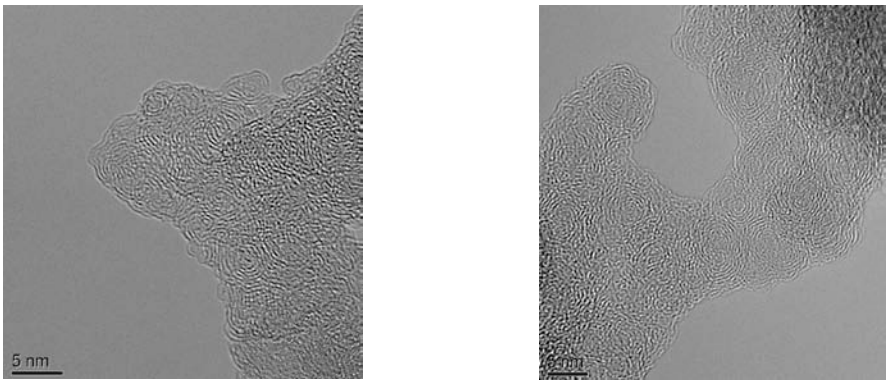

Figure 3. HRTEM from n-dodecane (left) and m-xylene (right).

Image processing algorithms have been developed at Penn State for quantifying the carbon lamella segments displayed in the HRTEM images. Various statistical quantities such as lamella length, tortuosity and separation distance can be extracted and quantified with results summarized in the form of histograms, as illustrated in Figure 4, quantifying the lamella length. The algorithm development and validation have been documented elsewhere [5-7]. Highlighting the similarity of lamella length distributions for these two different soots is the difference plot in Figure 5; it was obtained by subtracting the two lamella length distributions for each fuel component. It shows differences of only a few percent, well within normal variation.

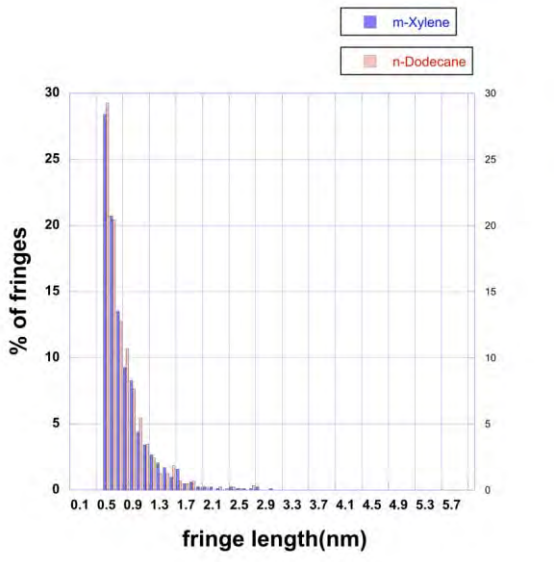

Figure 4. Distributions of carbon lamella from the soots of each fuel (m-xylene and n-dodecane).

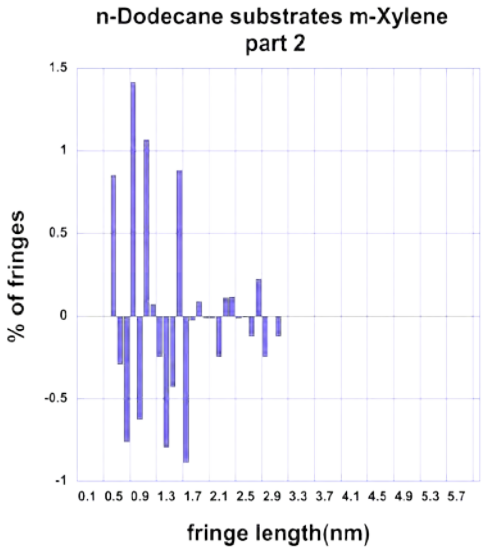

Figure 5. Difference plot of the lengths from histograms of carbon lamella lengths.

In contrast to the similar soot nanostructure observed for soots produced from the two fuels separately, their mixture leads to soot with a graphitic nanostructure as shown in Figure 6. Though the differences

are starkly seen by comparison of the respective HRTEM images, or respective lamella length distributions, the difference plot in Figure 7 highlights the length differences between the lamella length distributions of the separate fuel component(s) and that of the combined mixture.

These results suggest that the gas-phase chemistry associated with the fuel mixture is dramatically different than that associated with each individual fuel component of the surrogate jet fuel mixture. The synergistic chemistry leading to a loss of the fullerenic nanostructure and the rise of graphitic nanostructure is currently under investigation. Associated chemical models are being tested.

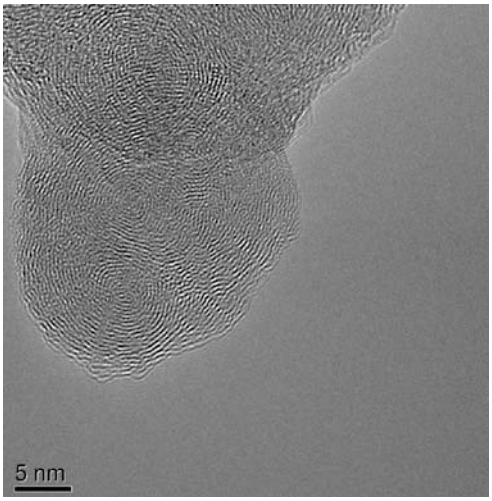

Figure 6. HRTEM image of soot from the blended fuel mixture.

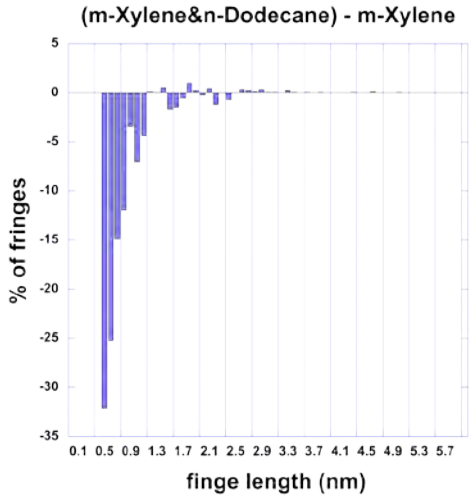

Figure 7. Difference plot of the histograms of carbon lamella lengths between the fuel component and blend.

Future Plans

Future work will continue to explore the operation of the TGA under atmospheric conditions with an extension to higher pressures. If there are no differences due to pressure, then we will continue to use the two-stage burner for the studies. The oxygenated fuel will also be investigated in the two-state burner to complement the surrogate jet fuel studies.

For the HR-TEMs, we are now investigating the formation conditions for the differences between the pure components and the mixture. We are concentrating on predictions of PAHs from the first burner to decipher possible changes between components and looking at additional images taken at the 2nd burner surface, prior to oxidation.

References

1. C. J. Merrill. University of Utah, Salt Lake City, M.S. Thesis 2005.
2. C. A. Echavarria; A. F. Sarofim; J. S. Lighty; A. D'Anna, *Proceedings of the Combustion Institute,* 2009, 32, 705-711.
3. R. A. Dobbins; C. M. Megaridis, *Langmuir 3,* 1987, 254-259.
4. G.A. Stratakis, A.M. Stamatelos. *Combustion and Flame*, 132, 2003, 157-169.
5. R. L. Vander Wal, et al., *J. Nanoparticle Research* 6, 2004, 555-568.
6. R. L. Vander Wal, et al., *Appl. Spectrosc.*, 58, 2004, 230-237.
7. K. Yehliu, R. L. Vander Wal and A. L. Boehman, *Combustion and Flame* (*in press*).

Advanced Nonlinear Optical Methods for Quantitative Measurements in Flames

Robert P. Lucht
School of Mechanical Engineering, Purdue University
West Lafayette, IN 47907-2088
Lucht@purdue.edu

I. Program Scope

Nonlinear optical techniques such as laser-induced polarization spectroscopy (PS), resonant wave mixing (RWM), and electronic-resonance-enhanced (ERE) coherent anti-Stokes Raman scattering (CARS) are techniques that show great promise for sensitive measurements of transient gas-phase species, and diagnostic applications of these techniques are being pursued actively at laboratories throughout the world. We have continued our fundamental theoretical and experimental investigations of these techniques. We have also initiated both theoretical and experimental efforts to investigate the potential of femtosecond (fs) laser systems for sensitive and accurate measurements in gas-phase media. Our initial efforts have been focused on fs CARS, although the systems will be useful for a wide range of future diagnostic techniques involving two-photon transitions.

The objective of this research program is to develop and test strategies for quantitative concentration and temperature measurements using nonlinear optical techniques in flames and plasmas. We are investigating the physics of these processes by direct numerical integration (DNI) of the time-dependent density matrix equations for the resonant interaction. Significantly fewer restrictive assumptions are required using this DNI approach compared with the assumptions required to obtain analytical solutions. Inclusion of the Zeeman state structure of degenerate levels has enabled us to investigate the physics of PS and of polarization effects in DFWM and ERE CARS. We are concentrating on the accurate simulation of two-photon processes, including Raman transitions, where numerous intermediate electronic levels contribute to the two-photon transition strength. The DNI numerical methods can be extended to the calculation of the interaction of laser pulses as short as 50 fs simply by decreasing the integration time step (for pulses shorter than this the rotating wave approximation will no longer be valid and the density matrix equations will need to include terms that are negligible for longer pulses).

During the last year we continued our numerical simulations of ERE CARS spectroscopy of nitric oxide (NO). We have incorporated an effective intermediate electronic level in our calculations to account for the effects of the numerous intermediate electronic levels for the $A^2\Sigma^+$-$X^2\Pi$ two-photon resonances. We also continued a detailed investigation of ERE CARS spectroscopy of nitric oxide, concentrating on a DNI analysis of saturation effects in the ERE CARS process, and we further developed a DNI model for broadband Stokes, single-pulse ERE CARS measurements. During the last year we predicted saturation behavior in ERE CARS of NO that shows striking similarity to electromagnetically induced transparency (EIT) effects for single-photon resonances.

We have continued detailed DNI analysis of the fs CARS process for gas-phase N_2. We have demonstrated the acquisition of single-shot fs CARS signals from flames using a chirped-pulse- probe (CPP) following excitation of the Raman coherence using nearly Fourier-transform-limited pump and Stokes pulses. We have developed analytical techniques and numerical codes for the accurate an rapid determination of temperature from CPP fs CARS signals, and we continue to work on improving and optimizing these codes. We also purchased last year a new Coherent ultrafast system; the system was installed last fall.

We have continued our development and application of injection-seeded optical parametric sources for high-resolution spectroscopy. In particular, we have now developed and are operating a system of two injection-seeded optical parametric generators (OPGs) coupled with pulsed dye amplifiers (PDAa) for the generation of pulsed, tunable, single-axial-mode laser radiation at 486 nm

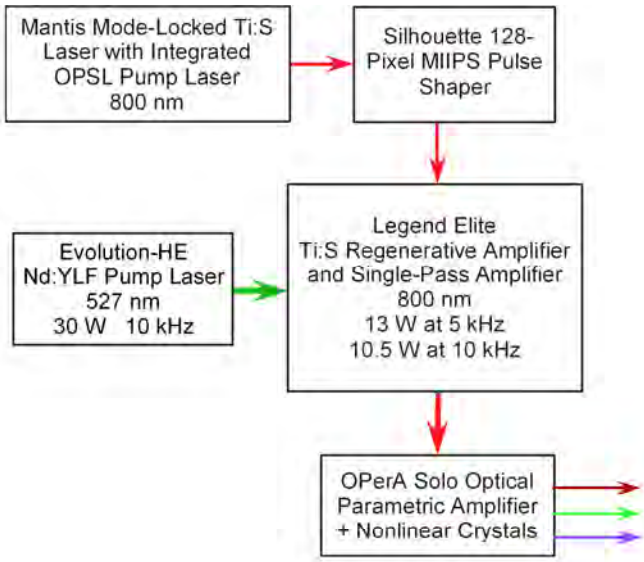

Figure 1. Coherent ultrafast laser system for femtosecond CARS measurements in the Applied Laser Spectroscopy Laboratory.

and 656 nm. This system will be used for six-wave mixing (6WM) and polarization spectroscopy (PS) studies of atomic hydrogen.

II. Recent Progress

A. Femtosecond CARS Calculations and Experiments

Fs CARS offers several major potential advantages compared with nanosecond (ns) CARS; i.e., CARS as usually performed with nanosecond pump and Stokes lasers. These potential advantages include an elimination of collisional effects in the generation of the signal and the capability of performing real-time temperature and species measurements at data rates of 1 kHz or greater as compared to 10-50 Hz for ns CARS. During the past year single-laser-shot temperature measurements at a data rate of 1 kHz were performed in a gas cells, in near-adiabatic laminar flames and in a turbulent Bunsen burner flame [P2,P4,P6,P8]. The measurements were performed using a laser system at Wright-Patterson Air Force Base in collaboration with Drs. Sukesh Roy and James R. Gord.

During the last year we purchased a new Coherent ultrafast laser system with significantly enhanced repetition rate and pulse energy. A schematic diagram of the new laser system is shown in Fig. 1. The new laser system is currently installed in the Applied Laser Spectroscopy Laboratory at Purdue University. The system is being operated at 5 kHz and the pulse energy for the fundamental beam at 800 nm is 2.6 mJ. The fundamental pulse width is 60 fs and the pulse is Fourier-transform-limited to within a few percent. The fundamental beam will be used as the probe beam for the next set of chirped-pulse-probe (CPP) fs CARS experiments as shown in Fig. 2. The greatly increased pulse energy of the chirped-pulse-probe beam resulting from this should result in a significant increase in the signal-to-noise ratio of the single-pulse measurements. We have also begun to explore methods for quantitative single-pulse concentration measurements and the use of polarization suppression of the nonresonant background.

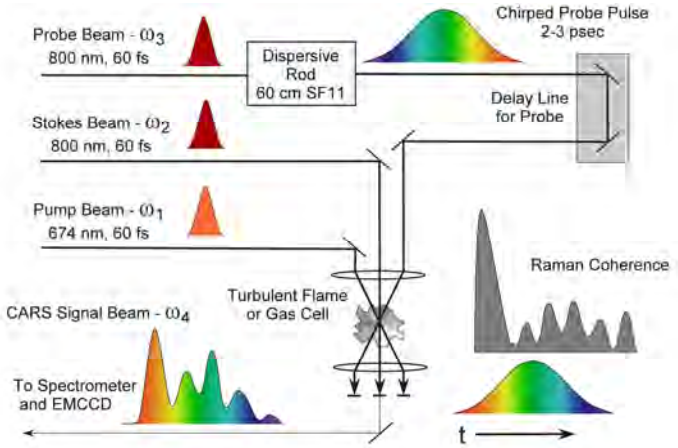

Figure 2. Schematic diagram of CPP fs CARS experiment.

The physics of the CPP fs CARS process was previously analyzed using a time-dependent density matrix analysis. The time-dependent density matrix equations for the fs CARS process were formulated and manipulated into a form suitable for solution by direct numerical integration (DNI). The temporal shapes of the pump, Stokes, and probe laser pulses are specified as an input to the DNI calculations. Based on these numerical results, a much faster

fitting code was developed to generate synthetic CPP fs CARS spectra. The parameters in the fitting code were varied to obtain the best fit theoretical spectrum for a given experimental spectrum, and temperature was determined as one of the best-fit parameters. This code is described in detail in publication P8.

B. Electronic-Resonance-Enhanced CARS Spectroscopy of Nitric Oxide

We continue to investigate the physics and explore the diagnostic potential of ERE CARS for measurements of NO [P3, P5]. The primary motivation for the work is to determine whether ERE CARS can be used to measure NO in high-pressure environments, where LIF measurements are very difficult because of interfering LIF signals from species such as O_2, H_2O, and CO_2. ERE CARS is inherently more selective because of the requirement for both electronic and Raman resonance for signal generation. The inclusion of the AC Stark effect in the ERE CARS code was necessary to obtain good agreement between theory and experiment. We have completed a detailed investigation of saturation effects in narrowband, scanning NO ERE CARS spectroscopy. The coupling of saturation effects for the Raman transition and the ultraviolet probe transition is quite complex and was investigated in detail. The effect of a strong probe on the Raman coherence for weak Raman pumping is shown in Fig. 1. Raman levels E and G are coupled by the pump and Stokes lasers, and levels E and S are coupled by the ultraviolet probe beam. For the weak probe beam, the normalized population of upper Raman level E increases from an equilibrium value of 10^{-4} to a peak value of almost 10^{-2}, as shown in Fig. 1a. As the probe intensity increases, however, the Raman excitation is suppressed, until in Fig. 1d we see that the combined population of levels E and S actually decreases during the laser interaction and population is driven back into ground Raman level G.

We have also continued our development of a DNI model for single-shot, broadband Stokes ERE CARS. We have also incorporated the AC Stark effect in the broadband Stokes ERE CARS code. At this point the effect of the ac Stark effect on the detection limit for broadband Stokes ERE CARS is not clear. It may actually act to increase signals by sweeping neighboring probe transitions into resonance with the probe laser during the ERE CARS interaction. The broadband Stokes ERE CARS system is currently being used for measurements in atmospheric pressure counterflow flames and in the near future will be used to measure NO profiles in high-pressure counterflow flames.

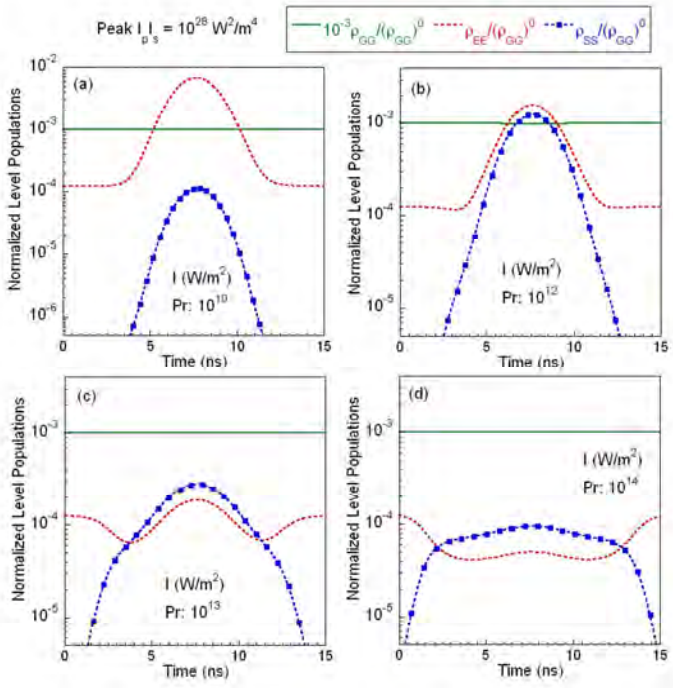

Figure3. Energy level diagram for the AC Stark shifting of the probe level in NO ERE CARS.

C. Six-Wave Mixing: Experiments and Modeling Efforts

We are continuing our collaborative efforts with Dr. Thomas B. Settersten at Sandia's Combustion Research facility on six-wave mixing (6WM) spectroscopy and polarization spectroscopy of atomic hydrogen. The DNI computer code for the calculation of 6WM and PS signals from atomic hydrogen was significantly modified to incorporate all of the different possible photon mixing

processes that can potentially contribute to both the 6WM and PS signals. The modeling of collisional processes in atomic hydrogen has also been modified to account for coherence transfer as well as population transfer.

We have developed a new apparatus for the atomic hydrogen experiments featuring OPGs seeded at 1320 nm and 774 nm with signal outputs at 486 nm and 656 nm, respectively. The signals beams from the OPGs are amplified using PDAs [P1], and the 486-nm beam is then frequency-doubled to 243 nm for two-photon excitation of the 1S-2S resonance. The 656-nm beam will be used to probe the 2S-3P transition.

III. Future Work

We will perform fs CARS experiments in our laboratory using the new Coherent ultrafast laser system. This system is significantly more powerful and capable than the system at WPAFB that has been used for CPP fs CARS measurements to date. Our studies of polarization suppression and concentration measurements using CPP fs CARS will continue. We plan to pursue further theoretical and experimental investigations of the ERE CARS process for species such as NO, OH, and CH, especially at higher pressures where collisional narrowing may result in significant improvement in the detection limits. The DNI code for single-pulse, broadband Stokes ERE CARS will be used to further explore the physics of the single-pulse ERE CARS process. The EIT-like behavior of the ERE CARS saturation process is of significant interest. Our investigation of the physics of two-photon, two-color PS and 6WM measurements of atomic hydrogen will continue in collaboration with Tom Settersten at Sandia. We have developed a new experimental appartus for these measurements featuring simultaneous operation of two injection-seeded OPG/PDA systems. We will use the systems for two-color PS and 6WM measurements of atomic hydrogen and, later, for other species including atomic oxygen. In the fall of 2011 we will be moving all of our experimental facilities into a new 2800-square-foot laboratory in the new Gatewood Wing of the Mechanical Engineering Building.

IV. Refereed publications and submitted journal articles supported by this project 2009-2011

1. A. H. Bhuiyan, D. R. Richardson, S. V. Naik, and R. P. Lucht, "Development of an Injection-Seeded Optical Parametric Generator/Pulsed Dye Amplifier System for High-Resolution Spectroscopy," Appl. Phys. B **94**, 559-567 (2009).
2. S. Roy, D. R. Richardson, P. J. Kinnius, R. P. Lucht, and J. R. Gord, "Effects of N_2-CO Polarization Beating on Femtosecond Coherent Anti-Stokes Raman Scattering (CARS) Spectroscopy of N_2," Appl. Phys. Lett. **94**, Article No. 144101 (2009).
3. A. K. Patnaik, S. Roy, R. P. Lucht, J. R. Gord and T. B. Settersten, "Effects of Collisions on Electronic-Resonance-Enhanced Coherent Anti-Stokes Raman Scattering of Nitric oxide," J. Chem. Phys. **130**, Article No. 214304 (2009).
4. S. Roy, D. R. Richardson, W. D. Kulatilaka, R. P. Lucht, and J. R. Gord, "Gas-Phase Thermometry at 1-kHz Using Femtosecond Coherent Anti-Stokes Raman Scattering (fs-CARS) Spectroscopy," Opt. Lett. **34**, 3857-3859(2009).
5. N. Chai, R. P. Lucht, W. D. Kulatilaka, S. Roy, and J. R. Gord, "Electronic-Resonance-Enhanced Coherent Anti-Stokes Raman Scattering Spectroscopy of Nitric Oxide: Nonperturbative Time-Dependent Modeling and Saturation Effect," J. Chem. Phys. **133**, Article Number 084310 (2010).
6. D. R. Richardson, R. P. Lucht, S. Roy, W. D. Kulatilaka, and J. R. Gord, "Single-Laser-Shot Femtosecond Coherent Anti-Stokes Raman Scattering Thermometry at 1000 Hz in a Driven H_2-Air Flame," Proc. Combust. Inst. **33**, 839-845 (2011).
7. S. Roy, R. P. Lucht, and J. R. Gord, "Orientation and Alignment Dynamics During Generation of Laser-Induced Polarization Spectroscopy (LIPS) Signal," JOSA B **28**, 208-219 (2011).
8. D. R. Richardson, R. P. Lucht, S. Roy, W. D. Kulatilaka, and J. R. Gord, "Theoretical Modeling of Single-Laser-Shot, Chirped-Probe Pulse Femtosecond Coherent Anti-Stokes Raman Scattering Thermometry," Applied Physics B, accepted for publication (2011).

Time-Resolved Infrared Absorption Studies of Radical Reactions

R. G. Macdonald
Chemistry Division
Argonne National Laboratory
Argonne, IL 60439
Email: rgmacdonald@anl.gov

Background

Information about the dynamics of radical-radical reactions is sparse. However, these processes are important in combustion being either chain propagating or terminating steps as well as potentially producing new molecular species. For almost all radical-radical reactions, multiple product channels are possible, and the determination of product channels will be a central focus of this experimental effort. In the current experiments, both transient species are produced by excimer laser photolysis of suitable photolytes, and if possible, two species are detected simultaneously using different continuous-wave laser sources operating in the red, near infrared and infrared spectral regions. This approach allows for the direct determination of the second-order rate constant under any concentration conditions if the appropriate absorption cross sections have been measured. The time dependence of individual ro-vibrational states of the reactants and/or products is followed by frequency- and time-resolved absorption spectroscopy. The simultaneous detection of multiple species ensures that species concentration profiles can be normalized to a common set of reaction conditions. In order to determine branching ratios and second-order rate constants, it is necessary to measure state-specific absorption coefficients and transition moments of radicals. These measurements play an important role in this experimental study.

Recent Results

The recently acquired continuous wave infrared OPO laser has been up-graded to operate in a dual cavity configuration. The pump YAG laser and idler wave (IR output) are now in resonance and the tuning range of the YAG pump wavelength is now imprinted onto the desired infrared output. This extends the mode hop free tuning range from 400 MHz up to 9 GHz, and significantly improves the tuning of the infrared output radiation to the peak of the desired transition, with only modest sacrifice in wavelength stability. Further improvements have been made to the data acquisition systems and now signals from both near infrared and infrared probe lasers are sampled simultaneously with 14 and 16-22 bit AD digitizers, respectively. This enables the direct detection of the initial DC level of both laser systems for an accurate determination of I_0, and the detection of small changes in absorbance without interference from bit resolution noise.

The NH_3 inlet port to the reaction chamber has been redesigned to facilitate mixing of small amounts of NH_3 at higher chamber pressure. With the extended tuning range of the infrared laser, the steady state concentration of NH_3 can now be measured directly using infrared absorption.

$NH_2(X^2B_1) + OH(X^2\Pi)$.

The NH_2 radical is an important intermediate in both the production of NO_X in combustion processes and the removal of NO_X from combustion exhaust gases. The

removal processes are based on the addition of NH_3, $(HOCN)_3$ or $(NH_2)_2CO$ to the gas stream, resulting in the Thermal DeNO_X, RAPRENO_X and NO_XOUT treatment processes, respectively. A key reaction in these processes is the NH_2 + NO reaction. The NH_2 radical also plays a key role in the pyrolysis of NH_3 and other environments where nitrogen chemistry is important. However, in spite of its importance, the chemistry of the NH_2 radical, especially in reactions with other transient species, has not been widely studied.

Experiments have been completed at room temperature and low pressure on the study on the NH_2 + OH radical-radical reaction system. The OH radical possess electronic angular momentum so that the singlet and triplet spin manifolds now have A′ and A″ electronic symmetry in planar geometry. There are several possible product channels:

$$\begin{aligned} NH_2 + OH &\rightarrow NH_3 + O(^3P) && \Delta H_{0,r} = -49.5 \text{ kJ mole}^{-1} && (1a)\\ &\rightarrow H_2O + NH(X^3\Sigma^-) && = -106 \text{ kJ mole}^{-1} && (1b)\\ &\rightarrow H_2 + HNO(X^1A') && = -124 \text{ kJ mole}^{-1} && (1c)\\ &\xrightarrow{M} NH_2OH(X^1A') && = -258 \text{ kJ mole}^{-1}. && (1d) \end{aligned}$$

S. J. Klippenstein *et al.* J. Phys. Chem. A **113,** 10241 (2009), have conducted high temperature shock tube studies of the NH2 + OH reaction and provided detailed theoretical estimates for many radical-radical and radical-molecule reactions pertaining to this system. For the NH_2 + OH reaction, the theoretical prediction was that channel 2b would dominate at 300 K with a rate constant of 1.6×10^{-11} cm^3 $molecules^{-1}$ s^{-1}.

The NH_2 radical was produced by 193 nm photolysis of NH_3 and monitored by time-resolved high-resolution absorption spectroscopy on the $^12_{21} \leftarrow {}^13_{31}$ rotational transition of the $(070)A^2A_1 \leftarrow (000)X^2B_1$ band near 675 nm. The OH radical was produced by the 193 nm photolysis of N_2O to create $O(^1D)$ atoms and the subsequent reaction of $O(^1D)$ with H_2O to give OH. Multiple infrared species were monitored using time-resolved high-resolution infrared absorption spectroscopy on rotational transitions of fundamental vibrational transitions assessable to the tuning range of the OPO laser system. The temporal dependences of the NH_2 radical and one of the infrared absorbing species were recorded simultaneously. The absorption coefficient for the NH_2 radical transition was characterized by the measured direct loss of NH_3. Both NH and HNO were detected in these experiments but only under conditions of high N_2O concentration. These species were produced in the interfering reaction of NH_2 + $O(^3P)$ reaction. The $O(^3P)$ atoms were produced in the quenching of $O(^1D)$ by N_2O and carrier gas. Neither species was detected under conditions where the expected $O(^3P)$ concentration was < 5×10^{10} molecules cm^{-3}. Attempts were made to observe NH_2OH but were unsuccessful.

As mentioned, NH_3 was monitored in these experiments but no influence of channel 1a was detectable on the NH_3 profiles. This and the lack of signals from either NH or HNO suggest that channel 1d is the major product channel at 295 K. To suppress the production of $O(^3P)$, the experiments were conducted in mixtures of He and H_2O with small amounts of N_2O. In separate experiments, the self-recombination rate constant for NH_2 in He was found to be much smaller than that for H_2O. The results of these measurements are summarized in Figure 1.

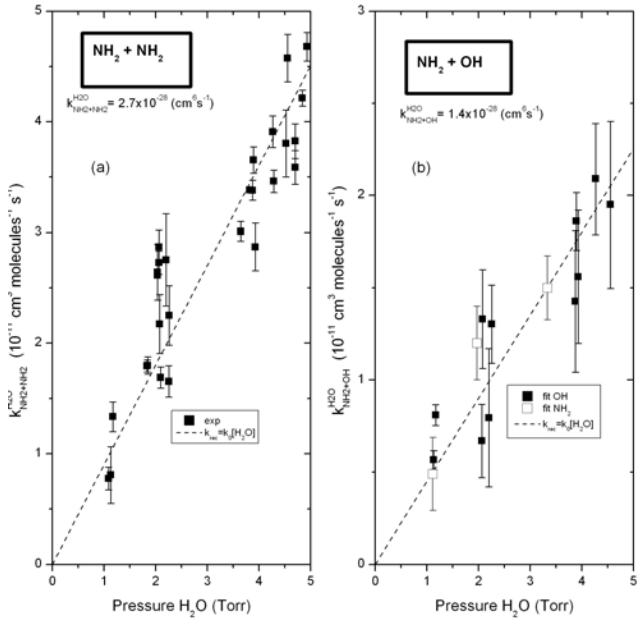

Figure 1a shows the results for the determination of the rate constant for the NH_2 + NH_2 reaction with H_2O as third body. The dotted line is a least squares fit to the data forced through the origin. The slope of this line gives the self-recombination rate constant for NH_2 to be 2.7×10^{-28} cm^6 $molecules^{-2}$ s^{-1} in H_2O. The small influence of He has been subtracted. Figure 1b shows the same except for the NH_2 + OH reaction. The rate constant for reaction 1d was found to be 1.4×10^{-28} cm^6 $molecules^{-2}$ s^{-1} in H_2O/He mixtures.

Figure 1. The results for the NH_2+ NH_2 and NH_2 + OH reaction.

$NH_2(X^2B_1)$ + $NH_2(X^2B_1)$ Recombination

The NH_2 + NH_2 reaction is an ideal system to study the influence of different third bodies on a simple radical-radical recombination reaction. The theoretical calculations of Klippenstein *et al* show that near 300 K bimolecular rate processes make little contribution to the removal process; furthermore, these workers have calculated the low and high pressure limits for this system. The reaction system is quite straightforward:

$$NH_3 \xrightarrow{193\,nm} NH_2 + H$$

$$NH_2 + NH_2 \xrightarrow{M} N_2H_4 \qquad \Delta H_{0,r} = -267.5 \text{ kJ mole}^{-1}. \qquad (2)$$

As already mentioned, both NH_2 and NH_3 are monitored simultaneously following the photolysis laser pulse. The loss of NH_3 provides a direct measure of the NH_2 radical concentration. With the extended mode hop free tuning range of the new dual cavity OPO laser, it is straightforward to determine the NH_3 concentration by recording on and of line laser intensity. The Doppler width of the NH_2 transition is over a factor of four times larger than the infrared NH_3 transition. Thus, it is possible to increase the pressure range of the experiments by about a factor of four without pressure broadening effects being important because the NH_2 line shape is still a Doppler profile.

At pressures greater than 10 Torr, the NH_3 temporal profiles were sensitive to the recombination rate reaction:

$$NH_2 + H \rightarrow NH_3 \qquad \Delta H_{0,r} = 444.5 \text{ kJ mole}^{-1}, \qquad (3)$$

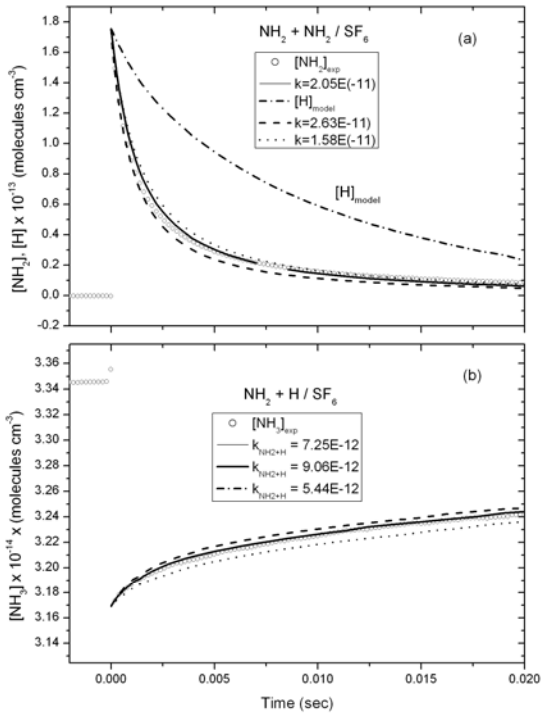

Figure 2. Determination of k_2 and k_3 in SF_6.

The recombination rate constants for both reaction 2 and 3 could be determined by analysis of both the NH_3 and NH_2 profiles. An example of these measurements is shown in Figure 2 with SF_6 as the third body. Figure 2 shows the simultaneous determination of the removal of NH_2 by both reactions 2 and 3 at a pressure of 15.5 Torr of SF_6. Note that both the NH_2 and NH_3 profiles are recorded with high signal-to-noise enabling reasonable extraction of the appropriate rate constant for the data analysis. The experimental data is given by the open circles. The NH_2 profile was fit to determine k_2 for a fixed value of k_3 and the NH_3 profile was fit to determine k_3 with k_3 fixed at the optimum value. The solid line provides the best fit to the data set after several iterations. The dash-dot line is the calculated model profile for the H atom temporal concentration profile. The major removal process for H atoms is loss by diffusion. However, the NH_3 profile, shown in Figure 2b, is only sensitive to reaction 3 for the first few milliseconds, and hence, not sensitive to the diffusion rate constant for the H atoms, a calculated quantity. The dotted and dash lines show the model NH_2 concentration profile for a +25% and -25% variation in k_2. Figure 2b shows the same for the determination of k_3.

Work is progressing on extending these measurements to other third bodies as well as extending the pressure range of previous measurements of k_2 and k_3 in Ar, N_2, and CF_4.

Publications 2009-present.

Determination of the rate constants for the radical-radical reactions $NH_2(X^2B_1)$ + $NH(3^2\Sigma^-)$ and $NH_2(X^2B_1)$ + $H(^2S)$ at 293 K.
-Mi-Kyung Bahng and R. G. Macdonald
J. Phys. Chem. A **113,** 2415-2423 (2009).

Theoretical studies of chemical reactions related to the formation and growth of polycyclic aromatic hydrocarbons and molecular properties of their key intermediates

Alexander M. Mebel
Department of Chemistry and Biochemistry, Florida International University
Miami, Florida 33199. E-mail: mebela@fiu.edu

Program Scope

Because of the great environmental and health effects of polycyclic aromatic hydrocarbons (PAH) and their importance in different applications of combustion technology, there is a strong need for better understanding of the reaction pathways leading to ecologically hazardous PAH and soot in combustion flames. Chemical mechanisms of PAH formation and growth are complex as the critical elementary reactions are convoluted and involve multiple interconnected isomers as products and/or intermediates. To understand, describe, and model these reactions in combustion engines, one needs to establish their energetics, to determine rate constants, to identify reaction products and their branching ratios under various conditions, and to assign reaction intermediates. Complementary to experimental studies of these data, it is crucial to carefully investigate potential energy surfaces (PES) of these reactions. In this project, we continue theoretical studies of the reactions of PAH formation and growth using highly-accurate ab initio molecular orbital (CCST(T)/CBS, G3, G4, and explicitly correlated methods) and density functional calculations of PESs and statistical (TST and RRKM/Master Equation) computations of absolute rate constants and product branching ratios. The underlying theme of the current project period concerns the reactions of phenyl and cyclopentadienyl radical, which are able to produce the smallest PAH and CP-PAH molecules, naphthalene and indene, respectively. In addition, we investigate a variety of oxidation reactions competing with the PAH growth. We also continue studies of the reactions of the carbon atom and dicarbon with unsaturated hydrocarbons leading to the production of reasonance stabilized free radicals (RSFR), playing an important role in the formation of the first aromatic ring and in the PAH growth. Our primary objectives include (i) to unravel reaction mechanisms through detailed, accurate, and reliable calculations of pertinent PESs; (ii) to compute rate constants for individual reaction steps and total absolute reaction rate constants and product branching ratios depending on reaction conditions, such as collision energy or temperature and pressure; (iii) to characterize molecular, energetic, and spectroscopic parameters of various possible reaction intermediates and products including their enthalpies of formation, geometric structure, vibrational frequencies and rotational constants, as well as photoionization and photoexcitation spectra.

Recent Progress

Reactions of vinylacetylene with $C(^3P)$ and $C_2(^1\Sigma_g^+/^3\Pi_u)$. CCSD(T)/CBS//B3LYP/6-311G** calculations were performed to investigate the potential energy surfaces and mechanism of the reactions of vinylacetylene with carbon atoms and dicarbon molecules followed by kinetic RRKM calculations of the reaction rate constants and product branching ratios at various collision energies. The theoretical studies were performed in collaboration with Ralf Kaiser's group who studied these reactions in crossed molecular beams experiments. The results for $C_4H_4 + C(^3P)$ showed that the reaction can proceed by barrierless addition of the carbon atom to either triple or double C-C bond in vinylacetylene to form initial three-member ring adducts **i1** and **i3** on the

triplet C_5H_4 PES. Next, the carbon atoms inserts into the attacked C-C bond giving rise to the chain isomers $HCCCCHCH_2$ (**i2**) and $HCCCHCCH_2$ (**i4**). Both **i2** and **i4** can lose a hydrogen atom to form the resonance stabilized *i*-C_5H_3 radical ($HCCCCCH_2$); alternatively, **i4** can also dissociate to *n*-C_5H_3 (HCCCHCCH). Other possible reaction pathways include H migration in **i4** to form HCCCHCHCH (**i5**), which in turn can decompose to *n*-C_5H_3 + H or HCCCH (^{3}B) + C_2H_2. The calculated exothermicities of the *i*-C_5H_3 + H, *n*-C_5H_3 + H, and HCCCH + C_2H_2 product channels of the C_4H_4 + C(^{3}P) reaction are 50.7, 49.2, and 53.8 kcal/mol, respectively. The computed product branching ratios, 3:2 between the *i*- and *n*-C_5H_3 isomers, appeared to be nearly independent of the collision energy and only less than 1% of the HCCCH + C_2H_2 products can be formed. The theoretical results were in agreement with the crossed molecular beams experiment, in which the reaction was found to be governed by indirect scattering dynamics and to proceed without an entrance barrier through a long-lived collision complex to reach the products, *i*- and *n*-C_5H_3 isomers via tight exit transition states.

In the C_4H_4 + $C_2(^1\Sigma_g^+)$ reaction occurring on the singlet C_6H_4 PES, dicarbon can add to both triple and double C-C bonds of vinylacetylene to form initial three-member ring adducts without a barrier. The triple-bond C_2 addition is followed by isomerization to a four-member ring intermediate, which in turn ring-opens to the chain $HCCCCCHCH_2$ structure, completing the formal C_2 insertion into the C≡C bond. The chain intermediate can then split the non-terminal H atom and produce the $HCCCCCCH_2$ resonance stabilized radical. The double-bond C_2 addition is followed by a six-member ring closure followed by ring reopening to the chain $HCCCHCCCH_2$ intermediate, decomposing to $HCCCCCCH_2$ + H at the final reaction step. Pathways leading to the *ortho*, *meta*, and *para* benzyne isomers are also open and the benzynes can eliminate an atomic hydrogen to form tridehydrobenzenes. According to the results of RRKM calculations, the major product of the C_4H_4 + $C_2(^1\Sigma_g^+)$ reaction is expected to be $HCCCCCCH_2$ (90-91%), followed by C_4H_2 + C_2H_2 (7-8%), and 1,2,3-tridehydrobenzene (~1%). The C_4H_4 + $C_2(^3\Pi_u)$ reaction taking place on the triplet C_6H_4 surface also proceeds without an entrance barrier and leads to the formation of chain and six-member ring C_6H_4 intermediates. The triplet C_6H_4 species then decompose by H eliminations producing the $HCCCCCCH_2$ radical or tridehydrobenzenes. If the triplet dicarbon adds to the CH_2 end of vinylacetylene, the computed branching ratios are 96% for $HCCCCCCH_2$ and 4% for 1,2,4-tridehydrobenzene. All other modes of $C_2(^3\Pi_u)$ addition result in almost exclusive production of the linear C_6H_3 product. The reactions of vinylacetylene with dicarbon are thus concluded to mostly produce the linear C_6H_3 RSFR together with small amounts of tridehydrobenzenes and diacetylene + acetylene.

Reaction of phenyl radical with propylene. We employed G3(MP2,CC)//B3LYP/6-311G** calculations to investigate the C_9H_{11} PES in relation to the C_6H_5 + C_3H_6 reaction as a potential source of indane and, eventually, indene in combustion flames. Various reaction channels were considered including direct H abstraction to form benzene + C_3H_5 and additions of phenyl radical to propylene producing different C_9H_{11} adducts, which can isomerize and/or dissociate at the ensuing reaction steps. The direct H abstraction by phenyl radical can occur from the CH_3, CH, and CH_2 groups in propylene to form CH_2CHCH_2, CH_3CCH_2, and CH_3CHCH via the barriers of 3.6, 6.3, and 8.2 kcal/mol. Alternatively, C_6H_5 can add to the terminal C atom of the CH_2 group or to the central carbon of propylene overcoming lower barriers of 1.5 and 2.7 kcal/mol, respectively, and resulting in the intermediates $C_6H_5CH_2CHCH_3$ (**i2**) and $C_6H_5C(H)(CH_2)CH_3$ (**i1**). The most favorable decomposition channel of **i2** is calculated to be H elimination from the terminal CH_3 group producing $C_6H_5CH_2CHCH_2$, 1-phenyl-2-propene, with

the overall exothermicity of 3.2 kcal/mol relative to the C_6H_5 + C_3H_6 reactants. The preferential dissociation pathway of **i1** is a loss of the CH_3 group producing styrene, where the $C_6H_5C_2H_3$ + CH_3 products are exothermic by 16.7 kcal/mol. A pathway leading to the formation of indane + H has been also found but it appeared to involve a higher-barrier H migration step followed by a five-member ring closure and H elimination. In collaboration with William Green's group at MIT, the results of the ab initio calculations of the PES were utilized in RRKM/TST calculations of reaction rate constants and product branching ratios at various temperatures relevant to combustion as well as at single-collision conditions relevant to the crossed molecular beams experiment on the C_6H_5 + C_3H_6 reaction conducted by Ralf Kaiser's group. According to our calculations, the major products of the C_6H_5 + C_3H_6 reaction at typical combustion temperatures include benzene and products of hydrogen abstraction from C_3H_6, such as CH_2CHCH_2, CH_3CCH_2, and CH_3CHCH, followed by products of phenyl radical addition to C_3H_6, including $C_6H_5C_3H_5$ and $C_6H_5C_2H_3$, formed after H and CH_3 eliminations from the initial C_9H_{11} adducts. The reaction pathway leading to indane C_9H_{10} appeared to be unlikely due to a high critical barrier. However, this finding does not rule out the formation of indene precursors following the C_6H_5 + C_3H_6 addition reaction because they can be easily produced by secondary reactions involving the $C_6H_5C_3H_5$ products, i.e. hydrogen abstractions from the ring or the side chain followed by a closure of the five-membered ring. For example, direct H abstraction from the vicinal CH_2 group in the $C_6H_5CH_2CHCH_2$ primary product by an H radical gives chemically activated $C_6H_5CHCHCH_2$ radical (exothermic by 20.6 kcal/mol) via a barrier of 4.9 kcal/mol. Next, this radical can ring-close overcoming a 31.3 kcal/mol barrier and then undergo an H loss from a C atom common for the six- and five-member rings producing indene. We have studied all possible direct H abstraction reactions from the C_9H_{10} primary products of C_6H_5 + C_3H_6 and subsequent transformations on the C_9H_9 PES and found that the channels leading to the indene production are preferable. Thus, the conversion of the six-member-ring-side-chain C_9H_{10} molecules produced in the phenyl + propylene reaction to indene precursors can be effectively catalyzed by free H radicals. Further RRKM-ME calculations are now underway to evaluate temperature and pressure dependent rate constants and relative product yields in the primary C_6H_5 + C_3H_6 and secondary C_9H_{10} + H reactions.

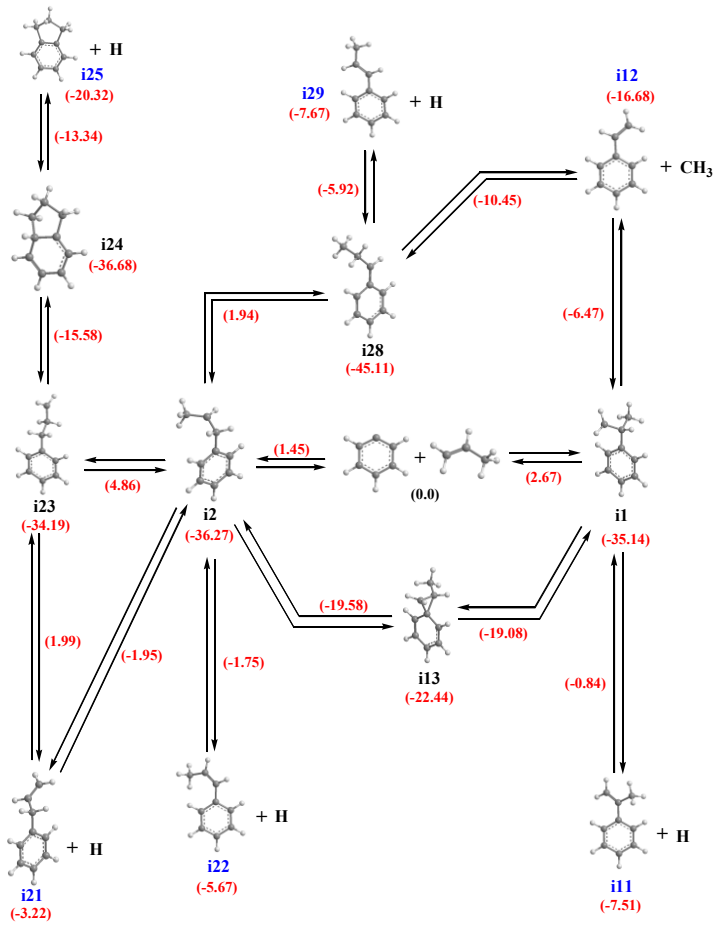

Figure 1. Potential energy diagram for various addition channels in the C_6H_5 + C_3H_6 reaction calculated at the G3(MP2,CC)//B3LYP/6-311G** level of theory. The numbers in parentheses are relative energies in kcal/mol.

Future Plans

Ab initio calculations are currently ongoing for the potential energy surface of the reaction of phenyl radical with vinylacetylene, which is likely to produce naphthalene as one of the major products. Once the PES for $C_6H_5 + C_4H_4$ is compiled, it will be utilized for RRKM calculations of product branching ratios under single-collision conditions to complement cross molecular beams experiments on this reaction by Ralf Kaiser's group. Also, multichannel-multiwell RRKM-ME calculations will be performed to predict the absolute reaction rate constants and relative product yields in the $C_6H_5 + C_4H_4$ reaction under combustion conditions, at different temperatures and pressures. This study will be performed in collaboration with William Green's group, who plans to include the results into kinetic models of PAH formation and growth in real flames. We plan to continue our theoretical kinetics studies of the $C_{10}H_x$ and $C_{10}H_x^+$ (x = 8-12) systems (naphthalene, hydronaphthyl radicals, dihydronaphthalenes, trihydronaphthyl radicals, tetrahydronaphthalenes, and the corresponding cations), in order to evaluate thermal rate constants for the reactions of H and H_2 addition/elimination. This work will be carried out to complement spectroscopic studies by Timothy Zwier's group. In collaboration with Stephen Klippenstein, we intend to complete multichannel-multiwell RRKM-ME calculations for the $C_6H_5 + O_2$ reaction and to move eventually to the reaction of oxidation of naphthyl radical, $C_{10}H_7 + O_2$, for which our ab initio calculations of the PES are now nearly finished.

DOE/BES sponsored publications (2009-2011)

1. Gu X., Zhang F., Kaiser R.I., Kislov V.V., Mebel A.M., "Reaction dynamics of the phenyl radical with 1,2-butadiene", Chem. Phys. Lett., 2009, 474, 51-56.
2. Mebel A.M., Kislov V.V., "Can the $C_5H_5 + C_5H_5 \rightarrow C_{10}H_{10} \rightarrow C_{10}H_9 + H$ / $C_{10}H_8 + H_2$ reaction produce naphthalene? An ab initio/RRKM study", J. Phys. Chem. A, 2009, 113, 9825-9833.
3. Zhou W., Mebel A.M., Li X.-Y., "An ab initio/Rice-Ramsperger-Kassel-Marcus study of the reactions of propenols with OH. Mechanism and Kinetics", J. Phys. Chem. A, 2009, 113, 10667-10677.
4. Kaiser R.I., Zhang F., Gu X., Kislov V.V., Mebel A.M., "Reaction dynamics of the phenyl radical (C_6H_5) with 1-butyne ($HCCC_2H_5$) and 2-butyne (CH_3CCCH_3)", Chem. Phys. Lett., 2009, 481, 46-53.
5. Kaiser R.I., Mebel A.M., Kostko O., Ahmed M., "On the Ionization Energies of C_4H_3 Isomers", Chem. Phys. Lett., 2010, 485, 281-285.
6. Zhang F., Jones B., Maksyutenko P., Kaiser R.I., Chin C., Kislov V.V., Mebel A.M., "Formation of the Phenyl Radical [$C_6H_5(X^2A_1)$] under Single Collision Conditions – A Crossed Molecular Beam and Ab Initio Study", J. Am. Chem. Soc., 2010, 132, 2672-2683.
7. Sebree J.A., Kislov V.V., Mebel A.M., Zwier T.S., "Spectroscopic and Thermochemical Consequences of site-specific H-atom addition to Naphthalene", J. Phys. Chem. A, 2010, 114, 6255–6262.
8. Kislov V.V., Mebel A.M., "Ab Initio/RRKM-ME Study on the Mechanism and Kinetics of the Reaction of Phenyl Radical with 1,2-Butadiene", J. Phys. Chem. A, 2010, 114, 7682-7692.
9. Sebree J.A., Kislov V.V., Mebel A.M., Zwier T.S., "Isomer Specific Spectroscopy of $C_{10}H_n$, n = 8-12: Exploring Pathways to Naphthalene in Titan's Atmosphere", Faraday Disc., 2010, 147, 231-249.
10. Parker D.S.N., Zhang F., Kim, Y.S. Kaiser R.I., Mebel A.M., "On the Formation of Resonantly Stabilized C_5H_3 Radicals -A Crossed Beam and Ab Initio Study of the Reaction of Ground State Carbon Atoms with Vinylacetylene", J. Phys. Chem. A, 2011, 115, 593-601.

FLASH PHOTOLYSIS-SHOCK TUBE STUDIES

Joe V. Michael

Gas Phase Chemical Dynamics Group, Chemistry Division
Argonne National Laboratory, Argonne, IL 60439
E-mail: jmichael@anl.gov

The scope of the program is to measure, with the ANL flash photolysis reflected shock tube technique, high-temperature thermal rate constants for use in high-temperature combustion. This year we have concentrated on reactions where H(or D) is either a reactant or product using H/D-atom atomic resonance absorption spectrometry (ARAS) as the detection technique.[1,2]

Rate constants for the reactions of D with C_2H_6 and C_3H_8 have been measured in reflected shock wave experiments over the temperature range, 1100 – 1300 K. D-atoms are detected using ultra-sensitive atomic resonance absorption spectrometry (ARAS). The measured D-atom profiles are sensitive to only the thermal dissociation of the D-atom source molecule, C_2D_5I, and to the title reactions. Since this dissociation has previously been studied in this laboratory,[3] the profiles at long times allow for direct determinations of the bimolecular rate constants for

$$D + C_2H_6 \rightarrow C_2H_5 + HD \qquad (1)$$

$$D + C_3H_8 \rightarrow C_3H_7 + HD \qquad (2)$$

Rate constant measurements of the protonated reactions have previously been carried out, but no measurements above 1000 K have been reported because the product radicals, C_2H_5 and C_3H_7, thermally dissociate giving H-atoms back again. Use of D-atoms eliminates this complication. The results can be expressed in Arrhenius form as

$$k_1 = 9.83 \times 10^{-10} \exp(-6475\ K/T)$$

$$k_2 = 2.54 \times 10^{-9} \exp(-6133\ K/T)$$

We have compared the present data to the related all protonated work[4] and have carried out theoretical analyses to predict both rate constants and the magnitude of isotope effect. In the high-T range, the isotope effects are found to be <10%. Hence, both the protonated and the present deuterated data sets can be used together to evaluate the temperature dependence over an extended range that includes combustion conditions.

In the past, we reported experimental estimates on branching fractions from a roaming radical reaction in acetaldehyde.[5] This process is ubiquitous and probably occurs in all thermal dissociations where two radicals are products. From H-atom yields in acetaldehyde, 0.22 to 0.25 of the initially formed HCO- and CH_3-radicals roam and subsequently abstract forming the molecular products, CO and CH_4. Additional studies on dimethyl ether[6] and propane[7] are now complete. The measured rate constants for dimethyl ether are in adequate agreement with earlier investigations. The observed

branching to the roaming products, $CH_4 + H_2CO$, was 0.19 ± 0.07 and there is some evidence that the fraction increases with decreasing temperature but decreases with increasing pressure. These trends are seen in the theoretical treatment even though the predicted branching ratio at ~1400 K is about a factor of ten lower than experimentally observed. The rate constants measured for propane are also in agreement with earlier studies. Branching ratios to the roaming products, $CH_4 + C_2H_4$, were small but observable being 0.10 ± 0.08. We consider this to be evidence for roaming. Theoretical estimates of overall rate constants are also in good agreement with the present data.

Following our recent work on benzyl dissociation,[8] we have initiated studies on o-xylyl-radical chemistry since xylyl-radicals play a dominant role in the overall combustion chemistry of xylene, an important aromatic surrogate molecule in real fuels. Consequently, experimental studies have been carried out using the ANL flash photolysis shock tube on o-xylylbromide ($o\text{-}CH_3C_6H_4CH_2Br$) decomposition. Br-ARAS experiments used with the shock tube confirm that at high-T (>1200 K) o-xylyl radicals ($o\text{-}CH_3C_6H_4CH_2$) are generated instantaneously. The high sensitivity H-atom ARAS detection technique has been subsequently used to obtain quantitative measurements of the H-atom yields and rate coefficients, for o-xylyl decomposition. These H-ARAS experiments span a temperature range, 1267-1597 K, and pressure range, 0.3-1.0 atm. The results from these studies and comparisons to earlier studies are discussed in terms of two processes.

$$\text{o-xylyl} \rightarrow \text{H} + \text{o-xylylene} \quad (3)$$

$$\text{o-xylyl} \rightarrow \text{non-H-atom channel} \quad (4)$$

Figure 1 shows a typical H-atom profile for the conditions shown in the caption. It is obvious that the long time yield of [H] is only about one third of that for [o-xylylBr] depletion suggesting that there is a non-H-atom dissociation channel accompanying one that gives [H]. Figure 2 shows the H-atom sensitivity to a many step chemical model that includes H-atom abstractions from o-xylene and the radical. These are the only two secondary reactions that show slight senstitivity, with the profile being completely dominated by reactions (3) and (4). This allows rate constants and branching ratios to be determined using psuedo-first-order analysis.

The overall rate constants for radical decomposition in first-order is:

$$k_{total} = 1.313 \times 10^{10} \exp(-21789\ \text{K/T})\ \text{s}^{-1}\ (1267\text{-}1597\ \text{K and } 0.3\text{-}1.0\ \text{atm})$$

No discernible pressure dependence was noted over the temperature range of the present experiments. Branching ratios, k_3/k_{total}, varied from 0.10 to 0.45 with increasing temperature.

This work was supported by the U. S. Department of Energy, Office of Basic Energy Sciences, Division of Chemical Sciences, Geosciences, and Biosciences, under Contract No. DE-AC02-06CH11357.

References

[1]S.S. Kumaran, J.J. Carroll, and J.V. Michael, Proc. Combust. Inst. **27**, 125 (1998).
[2] Mielke, S.L.; Peterson, K.A.; Schwenke, D.W.; Garrett, B.C.; Truhlar, D.G.; Michael, J.V.; Su, M-C.; Sutherland, J.W., Phys. Rev. Lett. **91**, 063201 (2003).
[3]M.-C. Su and J.V. Michael, Proc. Combust. Inst. **29**, 1219 (2002)**.**
[4]D.L. Baulch et al., J. Phys. Chem. Ref. Data **34**, 757 (2005).
[5] R. Sivaramakrishnan, J.V. Michael, and S.J. Klippenstein, J. Phys. Chem. A **114**, 755-764 (2010).
[6] R. Sivaramakrishnan, J.V. Michael, A.F. Wagner, R. Dawes, A.W. Jasper, L.B. Harding, Y. Georgievskii, and S.J. Klippenstein, Combust. and Flame **158**, 618-632 (2011).
[7] R. Sivaramakrishnan, M.-C. Su, J.V. Michael, S.J. Klippenstein, L.B. Harding, and B. Ruscic, J. Phys. Chem. A, in press.
[8] R. Sivaramakrishnan, M.-C. Su, and J.V. Michael, Proc. Combust. Inst. **33**, 243-250 (2010).

PUBLICATIONS FROM DOE SPONSORED WORK FROM 2009-2010.

- *High Temperature Rate Constants for OH + Alkanes*, R. Sivaramakrishnan, N.K. Srinivasan, M.-C. Su, and J.V. Michael, Proc. Combust. Inst. **32**, 107-114 (2009).

- *Shock Tube Measurements of High Temperature Rate Constants for OH with Cyclo-alkanes and Methyl-cycloalkanes*, R. Sivaramakrishnan and J.V. Michael, Combust. and Flame **156**, 1126-1134 (2009).

- *Rate Constants for OH with Selected Large Alkanes: Shock Tube Measurements and an Improved Group Scheme*, R. Sivaramakrishnan and J.V. Michael, J. Phys. Chem. A **113**, 5047-5060 (2009).

- *Thermal Decomposition of NH_2OH and Subsequent Reactions: Ab Initio Transition State Theory and Reflected Shock Tube Experiments,* S.J. Klippenstein, L.B. Harding, B. Ruscic, R. Sivaramakrishnan, N.K. Srinivasan, M.-C. Su, and J.V. Michael, *J. Phys. Chem. A*, **113**, 10241–10259 (2009).

- *The Direct Observation of Roaming Radicals in the Thermal Decomposition of Acetaldehyde*, R. Sivaramakrishnan, J.V. Michael, and S.J. Klippenstein, J. Phys. Chem. A **114**, 755-764 (2010).

- *The Thermal Decomposition of Ethanol and its Bimolecular Reactions with OH and D: Reflected Shock Tube and Theoretical Studies*, R. Sivaramakrishnan, M.-C. Su, J.V. Michael, S.J. Klippenstein, L.B. Harding,and B. Ruscic, *J. Phys. Chem. A* **114**, 9425-9439 (2010).

- *H- and D-atom Formation from the Pyrolysis of $C_6H_5CH_2Br$ and $C_6H_5CD_2Br$: Implications for High-Temperature Benzyl Decomposition*, R. Sivaramakrishnan, M.-C. Su, and J.V. Michael, Proc. Combust. Inst. **33**, 243-250 (2010).

- *Pyrolysis of $C_6D_5CH_3$: Rate Constants and Branching Ratios in the High Temperature Thermal Decomposition of Toluene*, R. Sivaramakrishnan and J.V. Michael, Proc. Combust. Inst. **33**, 225-232 (2010).

- *Shock Tube and Theoretical Studies on the Thermal Decomposition of Propane: Evidence for a Roaming Radical Channel*, R. Sivaramakrishnan, M.-C. Su, J.V. Michael, S.J. Klippenstein, L.B. Harding, and B. Ruscic, J. Phys. Chem. A, ASAP article, doi: dx.doi.org/10.1021/jp2006205

- *Roaming Radicals in the Thermal Decomposition of Dimethyl Ether: Experiment and Theory*, R. Sivaramakrishnan, J.V. Michael, A.F. Wagner, R. Dawes, A.W. Jasper, L.B. Harding, Y. Georgievskii, and S.J. Klippenstein, Combust. and Flame **158**, 618-632 (2011).

- The Thermal Decomposition of o-Xylyl Radicals using H-ARAS, R. Sivaramakrishnan and J.V. Michael, in preparation.

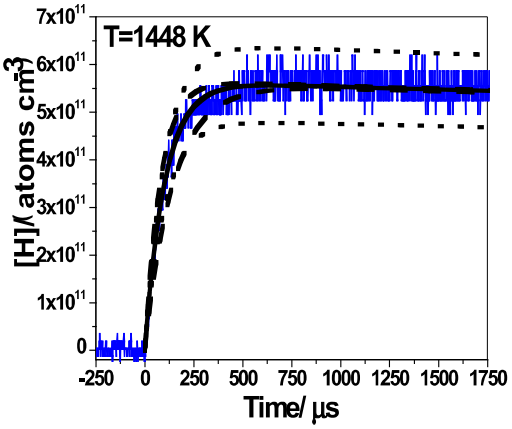

Fig. 1: [H] profile at 1448 K. Solid line – fit using the mechanism in Table S1 with k_{total} = 9500 s^{-1} and BR_H = 0.35, dashed lines – k_{total} ± 30% with BR_H = 0.35, dotted lines – BR_H ± 0.05 with k_{total} = 9500 s^{-1}. The conditions for the experiment are P_1 = 15.94 Torr, M_s = 2.401, ρ_5 = 2.937 x 10^{18} molecules cm^{-3}, $[o\text{-}XylylBr]_0$ = 1.649 x 10^{12} molecules cm^{-3}.

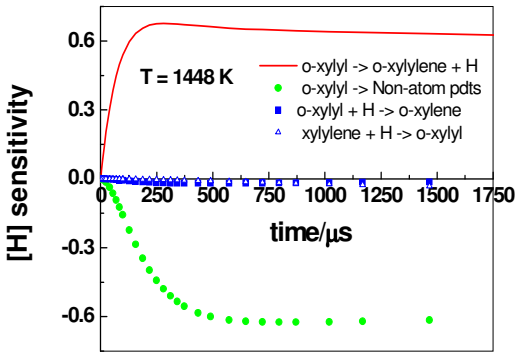

Fig. 2. Sensitivity analysis for Fig. 1 [H] profile.

Particle Diagnostics Development

H. A. Michelsen
Sandia National Labs, MS 9055, P. O. Box 969, Livermore, CA 94551
hamiche@sandia.gov

I. Program Scope

Combustion processes often produce solid carbon particles, i.e., soot. These particles may be oxidized to form gas-phase species or released into the exhaust stream, where they can be coated with liquid coatings. These coatings can be comprised of any of a number of components, including unburned fuel, lube oil, sulfuric acid, water, and other combustion by-products.[1,2] The research program described here focuses on the development of optical diagnostics for soot particles in combustion environments and combustion exhaust plumes. The goal of this work is *in situ* measurements of volume fraction, size, composition, and morphology of combustion-generated particles with fast time response and high sensitivity. Measurement techniques are targeted for studies of soot formation and evolution and must be versatile enough to probe particles throughout their entire life cycle. Techniques are being developed for detection and characterization of particles in combustion environments from incipient particles that are 2-20 nm in diameter and composed of condensed large organic species to mature soot particles composed of aggregates of carbonaceous primary particles resembling polycrystalline graphite. Diagnostics are also being developed for characterization of inhomogeneous exhaust particles.

II. Recent Progress

Our work has focused on developing a detailed understanding of the chemical and physical mechanisms that influence the applicability of laser-based techniques for soot detection under a wide range of conditions. In recent work, for instance, we have investigated the optical properties of soot in a flame. Using a combination of laser-induced incandescence (LII), extinction, and particle temperature measurements from spectrally and temporally resolved radiative emission, we have studied the wavelength and temperature dependence of the scattering and absorption cross-sections of soot.[3] We have used these results in a model that describes the energy- and mass-balance equations for laser-heated soot and compared the model predictions of time-resolved incandescence signals and particle temperatures to observed LII and temperature temporal profiles. We have also built a particle-beam chamber for focusing and coating soot particles and measuring their optical properties under controlled conditions. We have used this chamber to measure LII of flame-generated soot under low-pressure conditions.[4]

A. High-Vacuum Time-Resolved Laser-Induced Incandescence

LII is used extensively to characterize soot in various combustion environments.[5,6] This technique generally involves heating soot with a pulsed laser and recording the resulting blackbody emission. The intensity of the incandescence is used to measure the soot volume fraction, and the decay rate of the LII signal after the laser pulse provides information about the primary-particle size of the soot aggregate. The temporal evolution of the LII signal depends strongly on the laser spatial and temporal profiles, temporal and spectral response of the detection system, and surrounding gas-phase environment. Although LII is a promising technique for characterizing and quantifying soot, reliable application under a wide range of combustion environments requires a better understanding of experimental factors that influence the signal and the underlying physical mechanisms involved in signal generation.

Models have been developed to reproduce and predict the temporal profile of soot emission over a wide range of laser fluences.[7] These models solve the mass- and energy-balance equations during and after the laser pulse by considering the most important physical and chemical processes expected to occur during LII, including laser absorption, radiative and conductive cooling, sublimation, non-thermal ablation, phase-changes, and surface chemistry. Predictions from these models have been compared with experimental LII profiles from soot generated in diffusion and premixed flames. Models have also been developed to predict the LII signal evolution under more extreme environments, such as very dense media,[8] high-pressure environments,[9] and high-vacuum conditions.[10] Nevertheless, large uncertainties in predicting LII signals still remain. The most significant of these uncertainties stem from an incomplete understanding of mass-loss processes, conductive cooling, and temperature and wavelength dependencies

of the soot optical properties. The development of LII as a quantitative tool for soot characterization requires a better understanding of these phenomena. Narrowing these uncertainties will require careful studies of LII data obtained under broad and very well controlled experimental conditions.

We used an ethylene diffusion flame combined with an aerodynamic lens system to measure time-resolved LII profiles at pressures of ~3 x 10^{-6} torr. A schematic diagram of the experimental setup is shown in Fig. 1. We irradiated the particle beam emanating from the aerodynamic lens with a pulsed 532-nm laser over a range of laser fluences spanning from 0.06 to 0.50 J/cm^2. We recorded LII temporal profiles under vacuum for a time period as long as 3 μs after the laser pulse with sub-nanosecond time resolution. In this work we established proper flame operating conditions by monitoring the effects of fuel and air co-flow volumetric flow rates on vacuum LII signal.

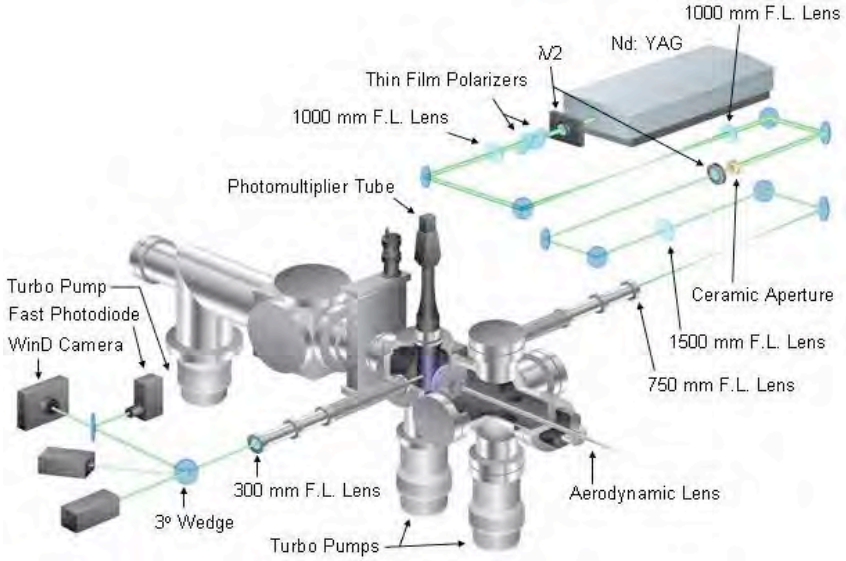

Figure 1. Schematic diagram of the experimental setup.

Figure 2 shows the temporal evolution of LII signal during the laser pulse for four laser fluences. The absolute timing of the laser pulse relative to the LII profiles has not been measured directly and was approximated with an uncertainty of 2-3 ns. It is expected that sublimation is not a dominant process at the lowest laser fluence and that the laser energy absorbed by the particle simply raises the temperature of the soot, yielding an increase in LII signal. Radiative cooling occurring during the laser pulse is negligible compared to laser absorption; thus, the particle temperature and LII temporal profile are both at a maximum at the end of the laser pulse. The position of the laser profile relative to the LII profiles is determined by matching the maximum of the integrated laser pulse to the LII temporal maximum observed at the lowest laser fluence (0.06 J/cm^2).

At higher fluences (Fig. 2) the LII signal starts to decay before the end of the laser pulse. The fast LII signal decay observed at 0.17 J/cm^2 and 0.27 J/cm^2 is characteristic of fast mass-loss processes similarly observed at atmospheric conditions. At atmospheric flame conditions soot particles will reach sublimation temperatures during the laser pulse, leading to the formation of C, C_2, or C_3 species in the surrounding gas phase. Laser-induced incandescence signal is extremely sensitive to mass loss during the laser pulse because the intensity of the emitted light is approximately proportional to the volume (i.e., mass) of the soot primary particle. Similar fast mass-loss processes will likely occur under vacuum. During the laser pulse other forms of fast mass loss, such as laser ablation, can occur.

Figure 3 displays peak vacuum LII signal and peak LII signal from an atmospheric flame as a function of laser fluence over the entire experimental fluence range studied here. The error bars for the flame data represent 1-σ standard deviation about the mean, whereas the errors for the vacuum data represent the 18.2% deviation, which represents long-term drift in the soot source. The flame and vacuum data are normalized to unity at 0.2 J/cm^2 in Fig. 3. Under vacuum conditions and at fluences below 0.10 J/cm^2 the peak LII signal increases nearly linearly with increasing fluence. A similar increase in the peak LII signal is observed when recording LII data in an ethylene flame and is attributed to an increase of the maximum soot temperature during the laser pulse. The onset and rise of LII signals under vacuum conditions occur at fluences ~0.03 J/cm^2 higher than observed in the ethylene flame data. This difference between the vacuum and atmospheric flame data is likely due to the large difference in initial soot

temperature (~1660 K in the flame, compared to 300 K in the vacuum chamber), with the colder vacuum soot requiring more laser energy to induce observable incandescence emission.

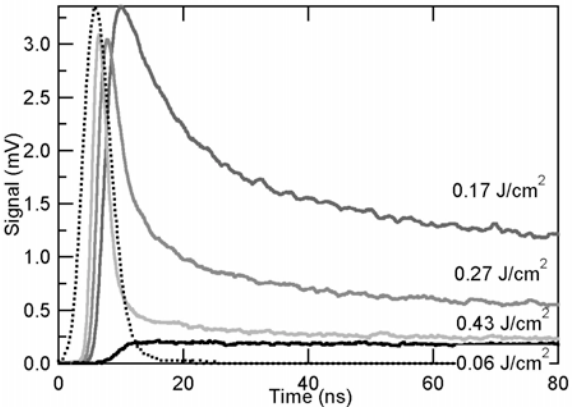

Figure 2. Vacuum LII temporal profiles at selected laser fluences. LII temporal profiles (solid lines) are shown for four laser fluences, as labeled. The laser temporal profile is represented by a dotted line and is displayed in arbitrary units.

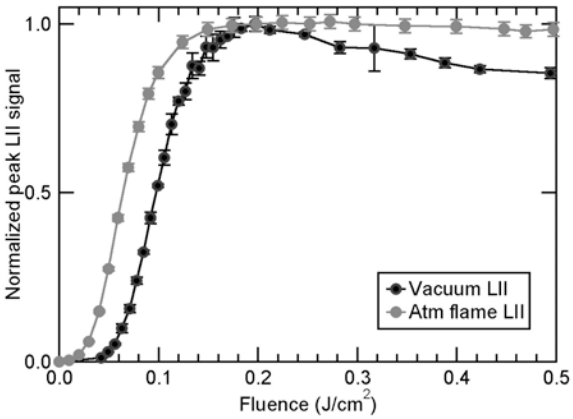

Figure 3. Fluence dependence of the peak LII. The peak of the temporal profile of the vacuum LII (black) is shown as a function of fluence in comparison to the maximum of the temporal profile of LII measured in a flame at atmospheric pressure and a temperature of ~1660K (gray). Error bars for the flame data represent 1-σ standard deviation about the mean; error bars for the vacuum data represent the 18.2% deviation observed for the LII stability.

The peak vacuum LII signal decreases gradually after reaching a maximum at ~0.2 J/cm^2, whereas the peak LII is nearly independent of fluence at these fluences in the atmospheric flame. Based on particle temperatures observed following laser heating of particles in flames at atmospheric pressure, plateaus in the peak LII signal imply that the soot temperature is approximately 4400 to 4500 K.[11] These temperatures correspond to the sublimation threshold for C and C_2 from graphite at atmospheric pressure. Above the sublimation threshold the energy absorbed by the particles vaporizes the soot without any increase of temperature. The absolute value of the maximum soot temperature is likely to be greatly dependent on the surrounding pressure. These results will provide a good case for testing LII models. We are currently collecting grids for imaging the particles by transmission electron microscopy (TEM) and collecting multicolor LII in order to determine the temperature evolution of the particles during laser heating in vacuum. We will then use these results to test our LII model.

III. Future Work

Current work builds on these results and extends them to combustion-generated particles with inorganic and organic coatings representative of particles found in exhaust plumes. In order to simulate exhaust-plume particulates, we have modified our flow-tube system to allow controlled deposition of a coating with low volatility on flame-generated soot. The thickness of the coating can be varied, and the particles collected for analysis by TEM and near-edge X-ray absorption fine structure (NEXAFS) spectroscopy. Coatings investigated to date have been selected for diagnostic development for diesel exhaust and include sulfuric acid, heptamethylnonane, and oleic acid. These experiments are currently limited by our inability to determine the mass loading of particle coatings. Developing an understanding of the cause and magnitude of the effects of coatings will require characterization of the particle coatings. Coating the particles increases the mean aggregate size as measured by a scanning mobility particle sizer (SMPS), but measurements of mobility diameter provided by the SMPS do not provide a quantitative measure of the volatile coating fraction either by volume or by mass. In order to measure the volatile fraction, we will build a chamber that includes a temperature-controlled oscillating crystal microbalance for differential mass measurements on coated and evaporatively dried particles.

We have also recently started a project led by Prof. Angela Viola to develop a validated predictive multiscale model to describe the chemical composition of soot nanoparticles in premixed and diffusion flames. This project closely couples experimental investigations of soot precursors and incipient

particle characteristics with the development of a predictive model for the chemical composition of soot nanoparticles. The co-investigators on the project are Profs. Angela Violi (University of Michigan) and Bernhard Schlegel (Wayne State University) for model development and Drs. Hope Michelsen (Sandia), Nils Hansen (Sandia), and Kevin Wilson (LBNL ALS) for experimental investigations.

Experimental and modeling studies will be carried out for several low- and atmospheric pressure flames fueled by the hydrocarbons of interest. A new counter-flow burner and sampling probe has been designed and built for this project. Polycyclic aromatic hydrocarbons (PAHs) and small soot particles will be extracted from the counter-flow flames via a microprobe. The flames will vary from lean to rich conditions in order to cover a wide range of practical conditions. The composition of incipient particles will be measured using the aerosol mass spectrometer developed by Kevin Wilson and coworkers at the ALS. The corresponding particle size distributions will be measured using an SMPS. Angela Violi and coworkers will use the experimental results in the development and validation of a predictive multiscale soot model.

IV. References

1. Kittelson, D. B. *J. Aerosol Sci.* **1998**, *29*, 575.
2. Lighty, J. S.; Veranth, J. M.; Sarofim, A. F. *J. Air Waste Manage. Assoc.* **2000**, *50*, 1565.
3. Michelsen, H. A.; Schrader, P. E.; Goulay, F. *Carbon* **2010**, *48*, 2175.
4. Headrick, J. M., Goulay, F., Schrader, P. E., and Michelsen, H. A. *Appl. Phys. B* **2011**, in press.
5. Santoro, R. J.; Shaddix, C. R. Laser-Induced Incandescence. In *Applied Combustion Diagnostics*; Kohse-Höinghaus, K., Jeffries, J. B., Eds.; Taylor & Francis: New York, NY, 2002.
6. Schulz, C.; Kock, B. F.; Hofmann, M.; Michelsen, H. A.; Will, S.; Bougie, B.; Suntz, R.; Smallwood, G. J. *Appl. Phys. B* **2006**, *83*, 333.
7. Michelsen, H. A.; Liu, F.; Kock, B.; Bladh, H.; Boiarciuc, A.; Charwath, M.; Dreier, T.; Hadef, R.; Hofmann, M.; Reimann, J.; Will, S.; Bengtsson, P.-E.; Bockhorn, H.; Foucher, F.; Geigle, K. P.; Mounaïm-Rousselle, C.; Schulz, C.; Stirn, R.; Tribalet, B.; Suntz, R. *Appl. Phys. B* **2007**, *87*, 503.
8. Chen, L. H.; Garo, A; Cen, K.; Grehan, G. *Appl. Phys. B* **2007**, *87*, 739.
9. Hofmann, M.; Kock, F.; Dreier, T.; Jander, H.; Schulz, C. *Appl. Phys. B* **2008**, *90*, 629.
10. Liu, F.; Daun, K. J.; Beyer, V.; Smallwood, G. J.; Greenhalgh, D. A. *Appl. Phys. B* **2007**, *87*, 179.
11. Goulay, F; Schrader, P. E.; Michelsen, H. A. *Appl. Phys. B* **2010**, *100*, 655.

V. Publications and submitted journal articles supported by this project 2009-2011

1. J. M. Headrick, F. Goulay, P. E. Schrader, and H. A. Michelsen, " High-vacuum time-resolved laser-induced incandescence of flame-generated soot", *Appl. Phys. B*, in press (2011).
2. H. A. Michelsen, P. E. Schrader, and F. Goulay, "Wavelength and temperature dependences of the absorption and scattering cross sections of soot", *Carbon* **48**, 2175-2191 (2010).
3. F. Goulay, P. E. Schrader, and H. A. Michelsen, "Effect of the wavelength dependence of the emissivity on inferred soot temperatures measured by spectrally resolved laser-induced incandescence", *Appl. Phys. B* **100**, 655-663 (2010).
4. F. Goulay, L. Nemes, P. E. Schrader, and H. A. Michelsen, "Spontaneous emission from $C_2(d^3\Pi_g)$ and $C_3(A^1\Pi_u)$ during laser irradiation of soot particles", *Mol. Phys.* **108**, 1013-1025 (2010).
5. F. Goulay, P. E. Schrader, and H. A. Michelsen, "The effects of pulsed laser injection seeding and triggering on the temporal behavior and magnitude of laser-induced incandescence from soot", *Appl. Phys. B* **96(4)**, 613-621 (2009).
6. H. A. Michelsen, "Derivation of a temperature-dependent accommodation coefficient for use in modeling laser-induced incandescence of soot", *Appl. Phys. B* **94**, 103-117 (2009).
7. F. Goulay, P. E. Schrader, and H. A. Michelsen, "A dataset for validation of models of laser-induced incandescence from soot; Temporal profiles of LII signal and particle temperature", *Appl. Phys. B*, submitted (2009).
8. F. Goulay, P. E. Schrader, L. Nemes, M. A. Dansson, and H. A. Michelsen, "Photochemical interferences for laser-induced incandescence of flame-generated soot", *Proc. Comb. Inst.* **32**, 963-970 (2009).

Detection and Characterization of Free Radicals Relevant to Combustion Processes

Terry A. Miller
Laser Spectroscopy Facility, Department of Chemistry
The Ohio State University, Columbus OH 43210, email: tamiller@chemistry.ohio-state.edu

1 Program Scope

Combustion processes have been studied for many years, but the chemistry is very complex and yet to be fully understood. Modern computer codes for its modeling typically employ hundreds of reaction steps with a comparable number of chemical intermediates. The predictions of such models are obviously limited by the dynamical and mechanistic data that are input. Spectroscopic identifications and diagnostics for the chemical intermediates in the reaction mechanisms constitute an important experimental benchmark for the models, as well as providing molecular parameters that are "gold standards" against which quantum chemistry computations of molecular properties may be judged. Our recent work has emphasized the spectroscopy of reactive organic peroxy radicals which are known to be key intermediates in combustion reactions.

2 Recent Progress

Our earlier cavity ringdown spectroscopic (CRDS) studies mainly involved the $\widetilde{A}$ - $\widetilde{X}$ absorptions of simple alkyl peroxy radicals. Our recent work has extended these studies towards unsaturated and hydroxy-substituted peroxies. Last year we reported the $\widetilde{A}$ - $\widetilde{X}$ absorption spectra of the β-hydroxy ethyl peroxy radical (β-HEP) which is an important intermediate in the oxidation of ethanol and represents a model system for the OH-initiated oxidation of atmospherically important olefins, such as ethylene, isoprene, and terpenes. We have now extended this work to include the first observation of the corresponding spectrum of β-hydroxy propyl peroxy radical (β-HPP). This brings us one step closer to identifying the spectra of hydroxy peroxy derivatives of such key atmospheric species as butadiene and isoprene.

Unsaturated hydrocarbon radicals are significant as precursors to polycyclic aromatic hydrocarbons and soot; understanding reaction mechanisms which contribute to their removal, such as peroxy formation, is fundamentally important in combustion chemistry. The cyclopentadiene moiety appears in the structure of coal and other fuels and the cyclopentadienyl group is ubiquitous in large aromatic molecules. The cylopentadienyl radical has been suggested as a possible intermediate in the early stages of soot formation. We recently obtained the $\widetilde{A} - \widetilde{X}$ absorption spectrum of the cyclopentadienyl peroxy radical and are presently completing its analysis.

Another recent focus of our research has involved obtaining quantitative concentration measurements from the spectra of organic peroxy radicals. Monitoring the concentration of these species in complex chemical environments requires the selectivity of the $\widetilde{A} - \widetilde{X}$ transition. We have developed an experimental method for cross-section determination which utilizes only absorption measurements in a dual wavelength (2λ-CRDS) spectrometer. Previously we have demonstrated the utility of this approach by reporting the peak absorption cross-section for the ethyl peroxy radical. This cross-section permits a quantitative concentration determination of ethyl peroxy radicals, from the $\widetilde{A} - \widetilde{X}$ absorption spectrum, but is rigorous only for the experimental conditions of room temperature and ≈300 torr pressure of air. We have now performed a significantly more detailed investigation of the absorption spectrum of ethyl peroxy and from the measured cross-section derived an experimental value for the electronic transition moment. With this result, one can predict the peak cross-section, and correspondingly concentrations, for a variety of experimental conditions.

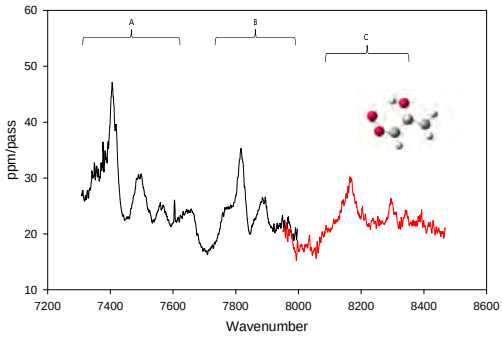

Figure 1: CRDS spectra of β-HPP radical obtained from photolysis of 1-iodo-propan-2-ol, followed by O_2 reaction. Frequency regions labeled A, B, and C denote the origin, C-O-O bend, and O-O stretch band regions of the spectrum. The black and red traces (CD version) are independent scans with different CRDS mirror sets.

2.1 β-Hydroxy Propyl Peroxy Radical

The CRDS $\widetilde{A} - \widetilde{X}$ electronic spectrum of the β-HPP radical is shown in Fig. 1. To produce this spectrum we synthesized an iodo precursor by addition of HI to propylene oxide which is expected to produce predominately 1-iodo-propan-2-ol, as confirmed by NMR. Photolysis of 1-iodo-propan-2-ol in the presence of O_2 should yield β-HPP and we attribute the observed spectrum entirely to this isomer. Similar spectra with poorer signal/noise were observed following Cl attack on propanol in the presence of O_2.

The β-HPP radical should have at least 16 stable conformers. However quantum chemical calculations that predict the Boltzmann distribution among the conformers and their $\widetilde{A} - \widetilde{X}$ oscillator strengths indicate that the observed spectrum should be dominated by the $G_1G_2G_3T_4$ conformer depicted in Fig. 1. This conformer is stabilized by intramolecular H-bonding, as is the corresponding conformer of β-HEP, which is mainly responsible for its previously reported $\widetilde{A} - \widetilde{X}$ spectrum. Analysis of the spectrum in Fig. 1 is on-going. However as indicated in the figure the typical peroxy radical bands, an origin, C-O-O bend, and O-O stretch, appear to be present.

2.2 Cyclopentadienyl Peroxy Radical

In addition to the open-chain unsaturated hydrocarbon radicals, such as allyl and propargyl radicals whose spectra we have reported, there obviously exist cyclic species. The prototypical unsaturated cyclic hydrocarbon species are phenyl and cyclopentadienyl radicals. Their self or cross reactions can lead to larger polycyclic aromatic hydrocarbons and ultimately soot formation which can at least partially be interdicted by peroxy radical formation.

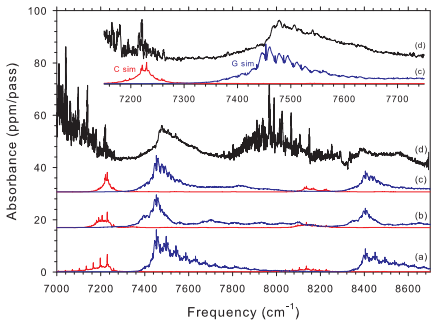

Figure 2: CRDS spectrum of the $\widetilde{A} - \widetilde{X}$ transition of cyclopentadienyl peroxy, in comparison with simulations of the G (blue) and C (red) conformers (CD version). In the simulations the OOCH torsion vibration is treated (a) using a harmonic oscillator model, (b) solving the vibrational Schrödinger equation for the B3LYP/cc-pVDZ surfaces shown in Fig. 4, and (c) for the B3LYP surfaces, but with the $\widetilde{X}$ state surface interpolated onto the G2 energy at OOCH = 0°. Trace (d) is the experimental spectrum. In the inset, the experimental spectrum is compared with the simulation (c) in the band origin region (7150-7750 cm^{-1}).

Previously we reported the spectrum of phenyl peroxy, and we have now turned our attention to cyclopentadienyl. A survey spectrum resulting from the 193 nm photolysis of cyclopentadiene monomer produced by thermal cracking of commercially available dicyclopentadiene is shown in Fig. 2. The broader absorption features in the spectrum are assigned to cyclopentadienyl peroxy, $C_5H_5O_2$, radical, produced by 3-body reaction of photolytically generated C_5H_5 with O_2 and N_2 present in the cell. Two series of sharp lines in the 7000-7250 cm^{-1} and 7800-8300 cm^{-1} regions are assigned to the $\widetilde{A} - \widetilde{X}$ system of the HO_2 radical. HO_2 is expected to be formed by the addition of photolytically generated H to O_2. It is also possible that HO_2 is generated from unimolecular decay of the peroxy adduct. Our experiment does not allow us to distinguish between HO_2 formed from these possible routes.

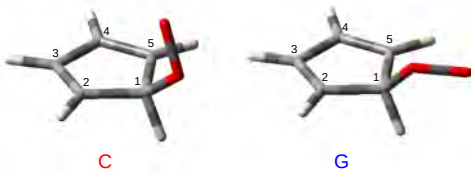

Figure 3: Conformers of cyclopentadienyl peroxy. The C/G labels correspond to OOCH dihedral angles of 180°/±51°, respectively, where the *gauche* conformer exists as an enantiomeric pair.

Results of electronic structure calculations performed on the cyclopentadienyl peroxy system are shown in Table 1, where conformer degeneracies, relative energies, T_{00} values, Boltzmann weights, and $\widetilde{A} - \widetilde{X}$ oscillator strengths are listed. We located two conformers of cyclopentadienyl peroxy as potential energy minima; these are labeled 'C' and 'G' and are distinguished by ∠OOCH dihedral angles of 180° and ±51°, respectively (Fig. 3). The cyclopentadienyl moiety is not strongly perturbed by the peroxy functionality and is nearly flat. The G2 and B3LYP levels of theory predict similar T_{00} values for the two conformers. Both levels also place the G conformer lower in energy than the C in the $\widetilde{X}$ state, but the difference between the two calculations here is notable, as manifested by the relative Boltzmann weights. The oscillator strengths are similar to those calculated for other organic peroxy radicals, with both saturated and unsaturated R groups.

We have computed harmonic vibrational frequencies for the conformers of cyclopentadienyl peroxy in both the $\widetilde{X}$ and $\widetilde{A}$ electronic states. Since peroxy torsion vibrations are typically anharmonic, we performed a scan (see Fig. 4) of the OOCH dihedral angle at the B3LYP level in order to shed light on the potential energy surface and energy level structure arising from this low frequency vibration. These potentials have been used to calculate the torsional vibrations by directly solving the Schrödinger equation.

The OOCH torsion curves for cyclopentadienyl peroxy are similar in many respects to OOCH or OOCC potentials obtained for other peroxy radicals, such as methyl, allyl, and propargyl (acetylenic isomer) peroxies. As in those cases, the barriers separating the conformers are lower in the $\widetilde{X}$ state than in the $\widetilde{A}$ state. However,

Table 1: Degeneracies (g), calculated relative energies (E) and origin frequencies (T_{00}, cm^{-1}), Boltzmann weights (w), $\tilde{A} - \tilde{X}$ oscillator strengths (f-values), and relative intensities (I) for conformers of cyclopentadienyl peroxy radical predicted by the indicated methods. Relative energies have been ZPE corrected. Relative intensities are given as products of Boltzmann weights calculated from G2 energies and UCIS oscillator strengths multiplied by 10^5.

		B3LYP[a]				G2				UCIS[b]	Expt.	
Conformer	g	E		T_{00}	w	E		T_{00}	w	$10^5 f$	I	T_{00}
		$\widetilde{X}$	$\widetilde{A}$			$\widetilde{X}$	$\widetilde{A}$					
C	1	0	7231	7231	1.00	0	7230	7230	1.00	6.08	6.1	7218
G	2	-455	7106	7560	17.97	-221	7231	7453	5.83	3.03	17.7	7479

[a] aug-cc-pVTZ basis [b] 6-31G(d) basis

there is a difference between the $\tilde{X}$ state torsional potential of cyclopentadienyl peroxy and those computed for some of the other peroxies. Allyl peroxy (C_2 conformers) and acetylenic propargyl peroxy possess very low barriers (<200 cm^{-1}) separating their C_s-symmetric T conformers from the enantiomeric G conformer minima, but the barriers separating the G conformer enantiomers from one another are larger (1953 and 825 cm^{-1} for G_1C_2 allyl and acetylenic-G propargyl peroxies, respectively, at the B3LYP/cc-pVDZ level). For cyclopentadienyl peroxy the situation is reversed: the computed barrier separating the enantiomers of the G conformer is only 138 cm^{-1}, compared with 904 cm^{-1} for the G/C barrier. In all three cases the low barriers occur at geometries in which the peroxy moiety is in an eclipsed arrangement with respect to a hydrogen atom, while the high barriers occur at geometries in which the peroxy fragment is eclipsed with respect to a carbon atom of the R group. The OOCH potential of cyclohexyl peroxy reveals the same trend.

In Fig. 2 the experimental spectrum is shown in comparison with several simulations. As the Figure shows the spectrum is dominated by the G conformer of $C_5H_5O_2$ with the origin and O-O stretch bands being readily identifiable. In addition there is evidence for the same bands of the C conformer, albeit considerably weaker.

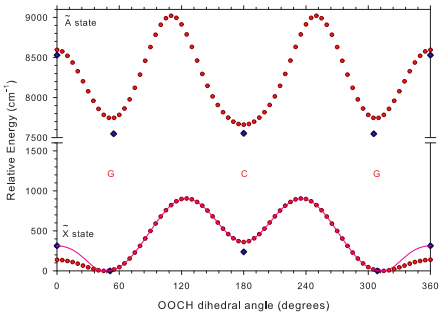

Figure 4: Potential energy curves obtained along the ∠OOCH dihedral angle coordinate for the $\tilde{X}$ and $\tilde{A}$ states of cyclopentadienyl peroxy. Points shown as circles (•) were obtained from relaxed potential energy scans performed at the B3LYP/cc-pVDZ level. Points shown as diamonds (◇) correspond to G2 electronic energies obtained for selected stationary point geometries. The solid curve corresponds to the $\tilde{X}$ state B3LYP surface which has been interpolated to fit the G2 energy at the G→G′ barrier (OOCH = 0°). See text for details.

2.3 Absorption Cross-sections and Transition Dipole Moment

To obtain quantitative concentration measurements under a variety of experimental conditions requires knowledge of the transition dipole moment (TDM) responsible for the molecule's spectrum. In principle the TDM can be obtained from the peak absorption cross-section, σ_p, measured under a given set of conditions. The origin frequency of the $\tilde{X} \leftarrow \tilde{A}$ transition of peroxy radicals is sensitive to conformational structure but for $C_2H_5O_2$ and many other cases, only the G conformer contributes significantly to the absorption spectrum near its peak, ν_p. Under these circumstances, the relationship between σ_p, ν_p and $|\mu_e^G|$ can be written as

$$|\mu_e^G|^2 = \frac{\sigma_p}{\nu_p} \frac{3hc}{8\pi^3} \frac{Q(T)}{A_p} \tag{1}$$

where μ_e^G is the TDM of the $\widetilde{A}-\widetilde{X}$ transition of the G conformer of $C_2H_5O_2$. $Q(T)$ is the total partition function and $A_p = A(\nu_p)$ is the peak value of the absorption profile $A(\nu)$ as a function of frequency ν. Both $Q(T)$ and A_p depend on the energy level structure of the $\tilde{X}$ state. A_p is computed as the sum of the normalized profiles of individual rotational lines weighted by their Boltzmann, Franck-Condon and Honl-London factors and hence also requires knowledge about the $\tilde{A}$ state as well as the orientation of the TDM with respect to the principal axes of the molecule. Given appropriate molecular parameters the function A_p is straightforward to calculate but appears quite complex given that the observed spectra are congested due to many thermally populated levels and the resulting overlap of numerous rovibronic bands in the vicinity of the peak frequency.

To obtain the energies of the vibrational levels with total $v < 3$ quanta of excitation in both electronic states we performed anharmonic calculations at UB3LYP/aug-cc-pVTZ level of theory. Additionally, the energies of levels with $v \geq 3$ quanta in the lowest frequency CCOO torsional mode were derived from the solution of the Schrödinger equation for the potential energy cut along the CCOO torsion coordinate for both electronic states. The value of $Q(T)$ has been calculated using a weakly anharmonic approximation for all modes, and by substituting a direct summation for the CCOO torsion. Both methods yield consistent (within 4%) values of

Table 2: Calculated values of the TDM using the indicated levels of theory. The geometry optimization was performed using UMP2(full)/6-31G(d) calculations.

Method	UCIS/ 6-31G(d)	UCIS/ aug-cc-pVTZ	EOM-CCSD/ 6-31G(d)	EOM-CCSD/ aug-cc-pVTZ	Exp
10^2 $\lvert\mu_e^G\rvert$ Debye	2.61	2.04	3.43	2.80	2.06(7)

$Q(T)$.

The absorption profile $A(\nu)$, has been calculated using the values of the rotational constants and orientation of the dipole moment obtained from high-resolution free-jet studies of $C_2H_5O_2$. Various vibrational hot bands are included in $A(\nu)$ weighted by their Boltzmann fraction calculated as discussed above for $Q(T)$. Fig. 5 compares the resulting simulation with the experimental spectrum.

The resulting preliminary value of the transition dipole is given in Table 2. This experimental value is compared with quantum chemical calculations in which the molecular geometry is optimized at the UMP2(full)/6-31G(d) level and the TDM is calculated with various combinations of levels of theory and basis sets. The calculated values of $|\mu_e^G|$ vary significantly, but they are generally consistent with the experimental value.

3 Future Directions

Efforts will continue to obtain the spectra of, and thereby provide diagnostics for, other important peroxy radicals. In this respect, obtaining spectra of the hydroxy peroxy radicals derived from unsaturated hydrocarbons are of key importance for both combustion and atmospheric chemistry. For example we aim to synthesize a photolysis precursor to produce the γ-hydroxy propyl peroxy radical as this isomer is preferentially produced by OH attack on propene. We then plan to investigate the hydroxy peroxy derivatives of the key dienes, butadiene and isoprene.

An area of interest closely related to the hydroxy alkyl peroxy radicals is their alkoxy peroxide isomers, ·OROOH. Structurally these radicals are similar to the extremely elusive ·QOOH species that is critically important for chain branching in low temperature combustion. In terms of detection the alkoxy functionality, RO· , represents a much more favorable spectroscopic chromophore than does Q· .

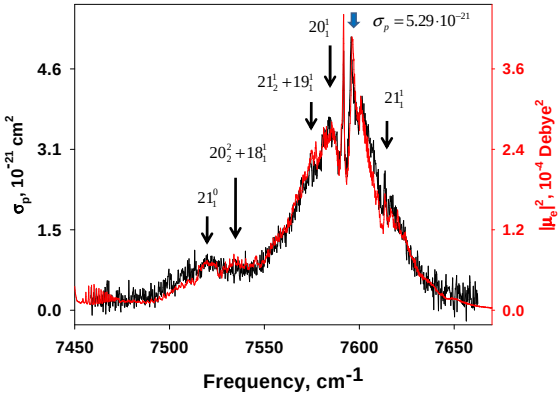

Figure 5: Origin band region of $\tilde{A} - \tilde{X}$ transition of G $C_2H_5O_2$. Blue arrow marks $A(\nu_p)$. Red trace (CD version) represents simulation while back trace is experimental. The position of some vibronic bands are labeled.

Now that the work on $C_2H_5O_2$ is complete, we can proceed to use the 2λ-CRDS apparatus to measure the cross-sections and TDMs for other peroxy species. In addition we can begin to compare $\tilde{A} - \tilde{X}$ and $\tilde{B} - \tilde{X}$ alkyl peroxy cross-sections.

Publications Supported by DOE (2009-2010)

[1] "Observation of the $\tilde{A} - \tilde{X}$ Electronic Transitions of Cyclopentyl and Cyclohexyl Peroxy Radicals Via Cavity Ringdown Spectroscopy," P. S. Thomas, R. Chhantyal-Pun, and T. A. Miller, *J. Phys. Chem. A* **114**, 218 (2010).

[2] "The $\tilde{A} - \tilde{X}$ Absorption of Vinoxy Radical Revisited: Normal and Herzberg-Teller Bands Observed Via Cavity Ringdown Spectroscopy," P. S. Thomas, R. Chhantyal-Pun, N. D. Kline, and T. A. Miller, *J. Chem. Phys.* **132**, 114302 (2010).

[3] "Cavity Ringdown Spectroscopy of the NIR $\tilde{A} - \tilde{X}$ Electronic Transition of Allyl Peroxy Radical (H_2C=CH-CH_2OO·)," P. S. Thomas and T. A. Miller, *Chem. Phys. Lett.* **491**, 123 (2010).

[4] "Observation of the $\tilde{A} - \tilde{X}$ Electronic Transition of the β-Hydroxyethylperoxy Radical," R. Chhantyal-Pun, N. D. Kline, P. S. Thomas, and T. A. Miller, *J. Phys. Chem. Lett.* **1**, 1846 (2010).

[5] "Measurement of the Absolute Absorption Cross Sections of the $\tilde{A} \leftarrow \tilde{X}$ Transition in Organic Peroxy Radicals by Dual Wavelength Cavity-Ringdown Spectroscopy," D. Melnik, R. Chhantyal-Pun, and T. A. Miller, *J. Phys. Chem. A* **114**, 11583 (2010).

[6] "Cavity Ringdown Spectroscopy of Peroxy Radicals: The $\tilde{A} - \tilde{X}$ Absorption of Propargyl Peroxy (H-C=C-CH_2OO·)," P. S. Thomas, N. D. Kline, and T. A. Miller, *J. Phys. Chem. A* **114**, 12437 (2010).

Reaction Dynamics in Polyatomic Molecular Systems

William H. Miller

Department of Chemistry, University of California, and
Chemical Sciences Division, Lawrence Berkeley National Laboratory
Berkeley, California 94720-1460
millerwh@berkeley.edu

I. Program Scope or Definition

The goal of this program is the development of theoretical methods and models for describing the dynamics of chemical reactions, with specific interest for application to polyatomic molecular systems of special interest and relevance. There is interest in developing the most rigorous possible theoretical approaches and also in more approximate treatments that are more readily applicable to complex systems.

II. Recent Progress

Research efforts are being focused on the problem of how to add quantum mechanical effects to the classical molecular dynamics (MD) simulations that are now so ubiquitously applied to all types of dynamical processes in complex molecular systems, e.g., chemical reactions in clusters, nano-structures, molecules on or in solids, bio-molecular systems, etc. Semiclassical (SC) theory — since it is based on the classical trajectories of the molecular system — is a natural way to approach the problem, and one knows from much work[1] in the early 1970's that SC theory describes *all* quantum effects in molecular dynamics at least qualitatively, and typically quite quantitatively; the primary challenge is thus to develop methods for implementing it for large molecular systems. In this regard, the 'initial value representation'[2] (IVR) of SC theory has emerged as the most useful starting point since it replaces the non-linear boundary value problem of earlier SC approaches by a Monte Carlo average over the initial conditions of classical trajectories, a procedure more amenable to systems with many degrees of freedom.[3]

Several technical advances in the basic SC-IVR methodology have been accomplished over the last year, the most important of which has been to show how a *time-dependent sampling function* can by used in Monte Carlo calculations for SC-IVR time correlation functions.[4] Thus a quantum time correlation function of the form

$$C_{\mathrm{QM}}(t) = tr\left[\hat{A}e^{i\hat{H}t/\hbar}\hat{B}e^{-i\hat{H}t/\hbar}\right] \quad , \tag{1}$$

is given in classical mechanics by a phase space average over the initial conditions of classical trajectories

$$C_{\mathrm{CL}}(t) = (2\pi\hbar)^{-F}\int d\mathbf{q}_0\, d\mathbf{p}_0\, A_{\mathrm{CL}}(\mathbf{p}_0,\mathbf{q}_0)B_{\mathrm{CL}}(\mathbf{p}_t,\mathbf{q}_t) \quad , \tag{2}$$

where $(\mathbf{p}_t,\mathbf{q}_t)$ are the momenta and coordinates at time t that evolve from the initial phase point $(\mathbf{p}_0,\mathbf{q}_0)$. This classical expression is typically evaluated by Metropolis Monte Carlo, where the initial conditions are sampled from the function $A_{\rm CL}(\mathbf{p}_0,\mathbf{q}_0)$ (or its absolute value if $A_{\rm CL}$ is not a positive function). The SC-IVR expression for the correlation function involves a *double* phase space average, over two sets of initial conditions (because of the two time evolution operators in the quantum expression, Eq. 1),

$$C_{\rm SC}(t) = (2\pi\hbar)^{-2N}\int d\mathbf{q}_0\, d\mathbf{p}_0 \int d\mathbf{q}'_0\, d\mathbf{p}'_0\, C_t(\mathbf{p}_0,\mathbf{q}_0) C_t(\mathbf{p}'_0,\mathbf{q}'_0)^* \times e^{i[S_t(\mathbf{p}_0,\mathbf{q}_0)-S_t(\mathbf{p}'_0,\mathbf{q}'_0)]/\hbar}\langle \mathbf{p}_0\mathbf{q}_0|\hat{A}|\mathbf{p}'_0\mathbf{q}'_0\rangle\langle \mathbf{p}'_t\mathbf{q}'_t|\hat{B}|\mathbf{p}_t\mathbf{q}_t\rangle \quad , \tag{3}$$

where S_t is the classical action for each trajectory and C_t a pre-exponential factor involving elements of the monodromy matrix (derivatives of the coordinates and momenta at time t with respect to their initial values).

To date, most evaluations of this full double phase space integral have used Monte Carlo methods with the importance sampling function being analogous to that used in the classical case, namely

$$\rho_{MC}(\mathbf{p}_0,\mathbf{q}_0,\mathbf{p}'_0,\mathbf{q}'_0) \propto \left|\langle \mathbf{p}_0\mathbf{q}_0|\hat{A}|\mathbf{p}'_0\mathbf{q}'_0\rangle\right| \quad . \tag{4}$$

However this has proved to be quite inefficient,[5,6] typically requiring orders of magnitude more Monte Carlo passes (and thus classical trajectories) than needed for convergence of the classical calculation (though the results of such SC-IVR calculations have invariably been excellent). The reason for this is not primarily the increased dimensionality of the double phase space average, but rather because the two time-evolved phase points, $(\mathbf{p}_t,\mathbf{q}_t)$ and $(\mathbf{p}'_t,\mathbf{q}'_t)$, will in general not be close to one another (particularly so the longer the time t), making the matrix element of operator $\hat{B}$, $\langle \mathbf{p}'_t\mathbf{q}'_t|\hat{B}|\mathbf{p}_t\mathbf{q}_t\rangle$, negligibly small. I.e., most pairs of initial phase points do not contribute to the double phase space integral, *only those for which the two time-evolved phase points are not too far from each other.* (Think of the classic two-slit problem: the contribution is from trajectories that *start* at the source, i.e., close together, and *end* at the same location, i.e., close together.) Such considerations have thus suggested that one include in the importance sampling function a factor that requires the two final phase points to be in the vicinity of one another. This could be the magnitude of their overlap, $\left|\langle \mathbf{p}'_t\mathbf{q}'_t|\mathbf{p}_t\mathbf{q}_t\rangle\right|$, or simply the matrix element of operator $\hat{B}$ itself. Thus the importance sampling function that we have proposed is

$$\rho_{MC}(\mathbf{p}_0,\mathbf{q}_0,\mathbf{p}'_0,\mathbf{q}'_0) \propto \left|\langle \mathbf{p}_0\mathbf{q}_0|\hat{A}|\mathbf{p}'_0\mathbf{q}'_0\rangle\langle \mathbf{p}'_t\mathbf{q}'_t|\hat{B}|\mathbf{p}_t\mathbf{q}_t\rangle\right| \quad . \tag{5}$$

If operators $\hat{A}$ and $\hat{B}$ are well-behaved, this will sample initial conditions for which the initial *and* final phase points for the two trajectories are not too distant from one another. This will also greatly ameliorate the phase cancellation problem for the Monte Carlo integration since the phase of the integrand that survives is only that which *should* survive. It is also significant that we choose to omit the pre-exponential factors in Eq. 3 from the sampling function of Eq. 5, so

that these need be evaluated only for the trajectories that are selected by the usual Metropolis procedure, and not for those that are rejected.

Applications[4] of this time-dependent sampling approach to a variety of examples have shown that the number of trajectories needed to converge the IVR space averages is drastically reduced (by a factor of 10^2 to 10^3) from that needed with the sampling function based only on initial conditions [Eq. 4], and is in fact comparable to the number needed for the classical calculation.

III. Future Plans

A particularly interesting application of SC-IVR approaches is to electronically non-adiabatic processes, as has been discussed in a recent review.[7] More recent work[8] has utilized an even more ambitious 'classical model for electronic degrees of freedom', namely the classical model developed by Miller and White[9] for a general second-quantized many-electron Hamiltonian. Application of this approach is extremely successful in describing electron transmission by a molecular junction between two electrodes, suggesting a variety of extensions. It is expected that this will be the focus of activity for at least the next year.

References

1. For reviews, see W. H. Miller, Adv. Chem. Phys. **25**, 69-177 (1974); **30**, 77-136 (1975).
2. W. H. Miller, J. Chem. Phys. **53**, 1949-1959 (1970).
3. For reviews, see (a) W. H. Miller, J. Phys. Chem. A **105**, 2942-2955 (2001); (b) W. H. Miller, Proceedings of the National Academy of Sciences, **102**, 6660-6664 (2005); (c) W. H. Miller, J. Chem. Phys. **125**, 132305.1-8 (2006).
4. See DOE Publication 13 below.
5. X. Sun and W. H. Miller, J. Chem. Phys., **117**, 5522-5528 (2002).
6. N. Ananth, Ph.D. thesis, University of California, Berkeley (2007), LBL-#886E.
7. W. H. Miller, J. Phys. Chem. **113**, 1405-1415 (2009).
8. See DOE Publication 12 below.
9. W. H. Miller and K. A. White, J. Chem. Phys. **84**, 5059-5066 (1986).

IV. 2009 - 2011 (to date) DOE Publications

1. W. H. Miller, "Electronically non-adiabatic dynamics via semiclassical initial value methods," J. Phys. Chem. **113**, 1405-1415 (2009).
2. G. Tao and W. H. Miller, "Semiclassical description of vibrational quantum coherence in a 3d I_2Ar_n ($n \leq 6$) cluster: A forward-backward initial value implementation," J. Chem. Phys. **130**, 184108.1-7 (2009).
3. J. Liu and W. H. Miller, A simple model for the treatment of imaginary frequencies in chemical reaction rates and molecular liquids, J. Chem. Phys. **131**, 074113.1-19 (2009).
4. J. Liu, W. H. Miller, F. Paesani, W. Zhang and D. A. Case, Quantum dynamical effects in liquid water: A semiclassical study on the diffusion and the infrared absorption spectrum, J. Chem. Phys. **131**, 164509.1-12 (2009).
5. G. Tao and W. H. Miller, Gaussian approximation for the structure function in semiclassical forward-backward initial value representations of time correlation functions, J. Chem. Phys. **131**, 224107.1-8 (2009).

6. G. Tao and W. H. Miller, Semiclassical description of electronic excitation population transfer in a model photosynthetic system, J. Phys. Chem. Lett. **1**, 891-894 (2010).
7. A. L. Kaledin, C. W. McCurdy, W. H. Miller, A semiclassical correction for quantum mechanical energy levels, J. Chem. Phys. **133**, 054101.1-6 (2010).
8. D. Lambrecht, K. Brandhorst, W. H. Miller, C. W. McCurdy, and M. Head-Gordon, A kinetic energy fitting metric for resolution of the identity second-order Möller-Plesset perturbation theory, J. Phys. Chem. A **115**, 2794-2801 (2011).
9. J. Liu and W. H. Miller, An approach for generating trajectory-based dynamics which conserves the canonical distribution in the phase space formulation of quantum mechanics. I. Theories, J. Chem. Phys. **134**, 104101.1-14 (2011).
10. J. Liu and W. H. Miller, An approach for generating trajectory-based dynamics which conserves the canonical distribution in the phase space formulation of quantum mechanics. II. Thermal Correlation Functions, J. Chem. Phys. **134**, 104102.1-19 (2011).
11. J. Liu, Two more approaches for generating trajectory-based dynamics which conserves the canonical distribution in the phase space formulation of quantum mechanics, J. Chem. Phys. (submitted).
12. D. W. H. Swenson, T. Levy, G. Cohen, E. Rabani and W. H. Miller, Application of a semiclassical model for the second-quantized many-electron Hamiltonian to nonequilibrium quantum transport: The resonant level model, J. Chem. Phys. (submitted).
13. G. Tao and W. H. Miller, Time-dependent importance sampling in semiclassical initial value representation calculations for time correlation functions, J. Chem. Phys. (submitted).

Dynamics of Activated Molecules

Amy S. Mullin
Department of Chemistry and Biochemistry, University of Maryland
College Park, MD 20742
mullin@umd.edu

I. Program Scope

The focus of my DOE-funded research program is to investigate collisional energy transfer of molecules with large amounts of internal energy. Collisional energy transfer is ubiquitous in gas-phase chemistry and relaxation of activated molecules through collisions competes directly with chemical reactions, thereby impacting overall reaction rates and branching ratios. However there are substantial challenges to making detailed experimental measurements of molecular energy transfer at energies that are relevant to chemistry under combustion conditions. High energy molecules contain extremely large densities of states, are of transient nature and have poorly understood interactions with other molecules. Currently, there are no first-principle theories of collisional energy transfer and the lack of fundamental knowledge often results in cursory and insufficient treatments in reactive models. A goal of my research is to gain new insights into the microscopic details of relatively large complex molecules at high energy as they undergo quenching collisions and redistribute their energy.

We use state-resolved transient IR absorption to characterize the energy transfer pathways that are responsible for the collisional cooling of high energy molecules. To overcome the inherent difficulties in developing a molecular level understanding of collisions involving high energy molecules, we use high-resolution IR probing to measure population changes in small collision partners that undergo collisions with the high energy molecules. Using this technique, we have performed in-depth spectroscopic studies that provide a greater understanding of high energy molecules and their collisional energy transfer.

II. Recent Progress

A. Measuring full energy transfer distributions for collisions of highly excited molecules

In the past several years, we have made important progress in developing the capability to measure the outcome of small ΔE collisions for states of the bath gas that are thermally populated prior to collisions with high energy molecules. This development represents an important breakthrough as it allows us to investigate for the first time the dynamics that are associated with so-called "weak" collisions. The terms "weak" and "strong" are qualitative descriptors that refer to collisions leading to small-ΔE and large-ΔE energy transfer, based historically on Hinschelwood's strong collision assumption. Strong collisions account for approximately 10% of all collisions and have been studied using transient IR probing for a number of years. The ability to interrogate the dynamics associated with the other 90% of collisions represents an important breakthrough.

We characterize the outcome of weak collisions by measuring nascent Doppler-broadened line profiles using transient IR absorption for bath molecules in low energy rotational states. These measurements involve the simultaneous appearance and depletion of population of low-J states that change due to collisions with high energy molecules. The data are fit to double Gaussian profiles (that account for positive going appearance and negative going depletion absorption signals). This analysis yields population and rate information for individual bath states and gives direct information about the nascent state-resolved collision dynamics for the full range of elastic and inelastic collisions. Because our measurements are sensitive to changes in quantum state and/or velocity vector, our data also measure the outcome of elastic collisions. So far, we have focused on nascent products generated from single collisions, but this approach could be applied to mapping out how energy distributions in the bath molecule evolve under higher pressure conditions.

Collisions that induce small exchanges of energy make up the vast majority of energy transfer events but they are difficult to distinguish from the ambient background population in low-J states at 300 K.

Parallel energy transfer processes that excite bath vibrational states (V-to-V energy transfer) interfere with high-resolution absorption measurements by moving population into upper states of the IR probe transitions. If this is the case, it is impossible to sort out how state-specific energy flow pathways contribute to the overall absorption signals. We overcome this problem by judiciously choosing probe transitions that have negligible cross sections for V-to-V energy transfer. For CO_2 probing, we use $00^00 \rightarrow 10^01$ transitions near λ=2.7 μm. The 10^01 state of CO_2 is of sufficiently high energy that it is not excited in single collisions with high energy molecules. For HOD, DCl and HCl probing, direct collisional excitation of the bath stretching modes are not observed and single quantum probe transitions are used to measure weak collisions.

B. Collisional quenching with CO_2: energy-dependence and donor dependence

During the recent funding cycle, we completed experimental measurements for two studies on the full energy transfer distributions for collisions between highly vibrationally excited molecules and CO_2. In one study we measured how the distribution of scattered molecules depends on the initial energy of the vibrationally excited molecules, in this case pyrazine with E=327000 and 37900 cm^{-1}). In the second study, we measured how the distribution of scattered molecules depends on the structure of the vibrationally excited molecules. For this study, we measured the outcome of collisional relaxation for 2-methylpyridine, 2,6-dimethylpyridine and 3,5-dimethylpyridine with E~38500 cm^{-1}. The key results from these studies were presented in the progress report of the previous year. Two manuscripts are in preparation.

III. Collisions of high energy molecules with HCl

We have continued our study on the inelastic collisions of highly excited molecules with HCl as the energy accepting bath molecule. In previous studies, we have measured the full distribution of scattered DCl molecules from collisions with pyrazine E=37900 cm^{-1}. We found that the DCl (v=0) product distributions for rotation and translation are markedly narrower than those observed for collisions with CO_2, yet broader than for HOD collisions, as shown in Fig. 1. For the three bath molecules studied (DCl, CO_2 and HOD), the final average translational energy increases with final rotational state. The bath-specific translational energy profiles show distinct behavior when plotted as a function of rotational energy, but coalesce when plotted as a function of rotational quantum state, suggesting that angular momentum changes play a controlling role in the relaxation process. The HCl studies are designed to test how the rotational energy structure of the energy-accepting bath molecule affects the energy exchange dynamics in collisions of highly excited molecules while nominally having the same intermolecular potential. The B constant (B=10.59 cm^{-1}) of HCl is approximately two times larger than for DCl (B=5.39 cm^{-1}), leading to a sparser rotational energy ladder for the energy acceptor.

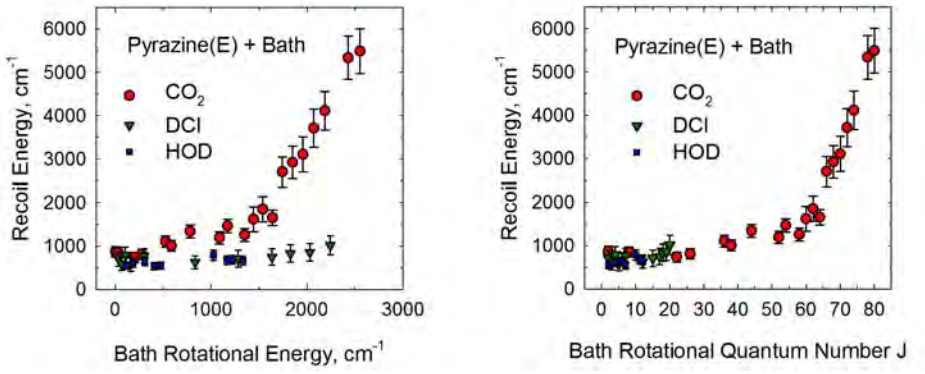

Fig. 1. Nascent translational and rotational energy distributions for CO_2, DCl and HOD following collisions with pyrazine(E). HOD data: Havey et al, J Phys Chem A 111, 13321-13329 (2007); DCl data [ref 2]; CO_2 data [ref 4].

For studies on HCl scattering, we perform transient IR measurements using P-branch transitions of the (0→1) vibrational fundamental at λ=3.3 μm. The IR light source is a lead salt diode laser with temperature

control from circulating compressed helium. Transient signals for HCl/pyrazine(E) collisions are shown in Fig. 2 for the J=0 and J=7 states of HCl. The J=0 state is dominated by population depletion at the center frequency of the probe transition, while the J=7 state shows overall appearance.

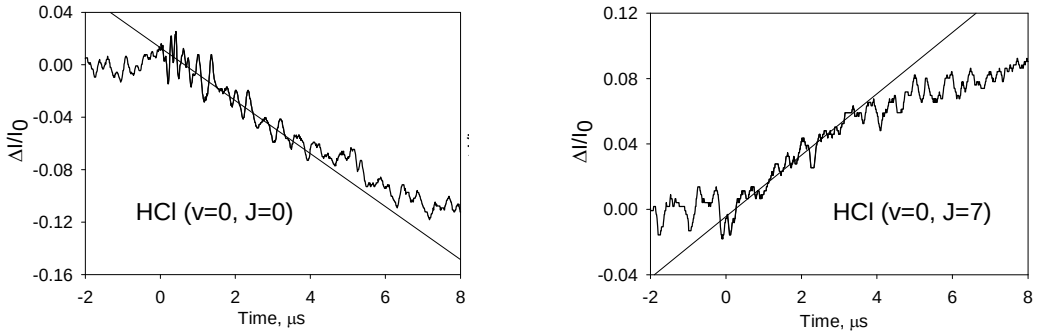

Fig. 2. Transient absorption signals for scattered HCl molecules resulting from collisions of pyrazine(E) with HCl, where E=38000 cm^{-1}. The J=0 states show population loss at the center probe frequency, while J=7 shows overall appearance.

We have measured transient line profiles for several individual rotational states of HCl with J between 0 and 7. Doppler-broadened line profiles at t=1 μs are shown in Fig. 3 for the J=0 and J=7 states. The depletion profile for HCl J=0 has a line width corresponding to a translational temperature of T_{dep}=213 K. This result is slightly lower than the initial ambient cell temperature (300 K) and is similar to depletion temperatures seen for DCl. The HCl J=7 line profile is broadened relative to 300 K and has a translational temperature of T_{app}=1430 K. It is noteworthy that we have yet to observe symmetric appearance peaks for the low-J states of HCl, such as those observed for DCl, CO_2 and HOD. It is likely that our current set up is near the limit of our ability to measure these events, given the unstable mode quality of our diode lasers in this spectral region. Nevertheless, the data we have collected so far provide a glimpse of how the rotational ladder of the bath molecule affects the recoil energy from collisions. Fig. 4 compares the product recoil energy for several rotational states of HCl and DCl. We find that the HCl molecules in J=7 are scattered with more translational energy than DCl in nearby states.

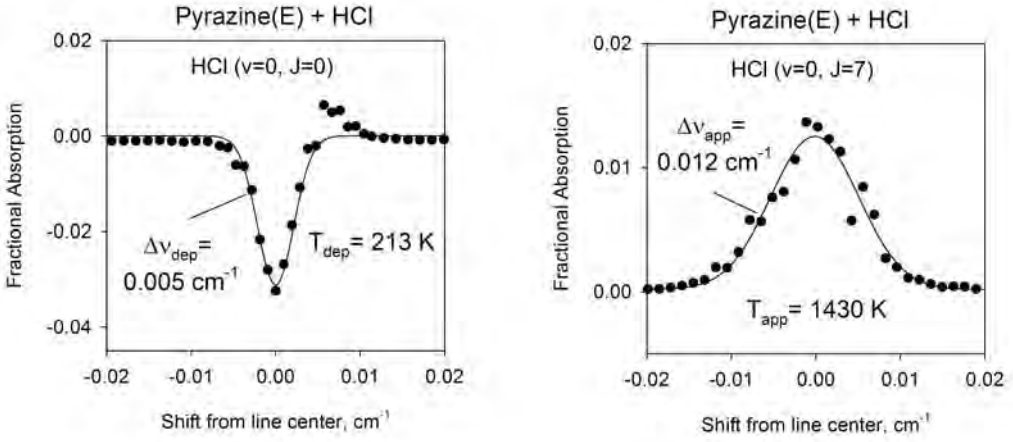

Fig. 3. Nascent Doppler broadened line profiles for HCl measured 1 μs following pyrazine excitation at 266 nm at a total pressure of 20 mTorr. The J=0 state shows primarily depletion of population with a translational temperature slightly below the initial cell temperature of 300 K. For the J=7 state, population appearance is observed from collisions with pyrazine(E). The appearance line profile corresponds to a translational temperature of 1430 K.

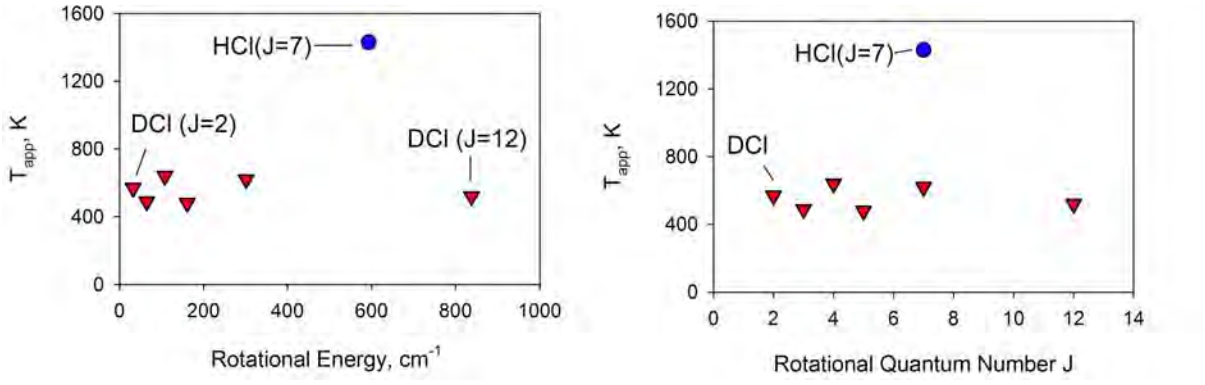

Fig. 4. State-specific recoil energies of HCl and DCl following collisions with pyrazine(E=37,900 cm^{-1}). Preliminary data for HCl shows that recoil velocities for HCl are substantially larger than for DCl with comparable energy and rotational quantum number.

III. Future Work

Our immediate plans are to replace the lead salt diode laser with a high resolution mid-IR OPO that is tunable from λ=2.5 to 3.9 μm. The OPO provides higher power, greater intensity stability and broader tenability than our λ=3.3 μm diode laser. Our goal is to complete the HCl experiments and then turn our attention to collisions of high energy molecules with methane.

IV. Publications supported by this project 2008-2011

1. L. Yuan, J. Du and A. S. Mullin, "State resolved strong collisions of vibrationally excited azulene (E= 20,100 and 38,500 cm^{-1}) with CO_2," J. Chem. Phys. 129, 014303/1-11 (2008).
2. J. Du, L. Yuan, S. Hsieh, F. Lin and A. S. Mullin, "Energy transfer dynamics of weak and strong collisions between vibrationally excited pyrazine (E=37900 cm^{-1}) + DCl," J. Phys. Chem. A 112, 9396-9404 (2008).
3. D. K. Havey, Q. Liu and A. S. Mullin, "Energy transfer dynamics in the presence of preferential hydrogen bonding: Collisions of highly vibrationally excited pyridine-h_5, -d_5, and -f_5 with water," J. Phys. Chem. A 112, 9509-9515 (2008).
4. Q. Liu, D. K. Havey, Z. Li and A. S. Mullin, "Effects of alkylation on deviations from Lennard-Jones collision rates for highly excited aromatic molecules: Collisions of methylated pyridines with HOD" J. Phys. Chem. A 113, 4387-4396 (2009).
5. D. K. Havey, J. Du and A. S. Mullin, Full state-resolved energy gain profiles of CO2 (J=2-80) from collisions with highly vibrationally excited molecules. I. Relaxation of pyrazine (E=37900 cm^{-1})" J. Phys. Chem. A 114, 1569-80 (2010).

Upcoming publications

6. J. Du, N. A. Sassin, D. K. Havey, K. Hsu and A. S. Mullin, "Full energy gain profiles of CO_2 from collisions with highly vibrationally excited molecules. II. Energy dependent pyrazine (E=32700 and 37900 cm^{-1}) relaxation" in preparation.
7. J. Du, D. K. Havey, S. W. Teitelbaum and A. S. Mullin, "Full energy gain profiles of CO_2 from collisions with highly vibrationally excited molecules. III. 2-Methylpyridine, 2,6-dimethylpyridine and 3,5-dimethylpyridine (E~38500 cm^{-1}) relaxation" in preparation.

Reacting Flow Modeling with Detailed Chemical Kinetics

Habib N. Najm

Sandia National Laboratories
P.O. Box 969, MS 9051, Livermore, CA 94551
hnnajm@sandia.gov

I. Program Scope

The goal of this research program is to improve our fundamental understanding of reacting flow, thereby advancing the state of the art in predictive modeling of combustion. The work involves: (1) Using computations to investigate the structure and dynamics of flames using detailed chemical kinetics; (2) Developing techniques for analysis of multidimensional reacting flow; (3) Developing numerical methods for the efficient solution of reacting flow systems of equations with detailed kinetics and transport; (4) Developing massively parallel codes for computing large scale reacting flow with detailed kinetics; and (5) Developing numerical methods for uncertainty quantification in reacting flow computations, including methods for the construction of uncertain chemical models from experimental data.

II. Recent Progress

A. Reacting Flow Computations, Analysis, and Model Reduction

We have completed the analysis of an n-heptane edge flame structure using Computational Singular Perturbation (CSP). Extending our previous work on methane-air edge flames, we performed a detailed computation of an n-heptane-air edge flame established in a mixing layer. The numerical model involved a detailed reaction mechanism of 560 species and 2538 reversible reactions, including the low-temperature chemistry of this reference fuel. The analysis involved identification of important reactions leading to heat-release and the main fuel-consumption pathways in different regions of the triple flame. CSP was used to construct reaction networks in the premixed branches and the diffusion flame by analyzing importance indices of the species involved. These reaction networks showed the main pathways from the fuel to the main combustion products and identified the species that can be considered as fuel in the diffusion flame which is established between the premixed branches. CSP was also used to study explosive modes in the triple flame. These modes have a positive real eigenvalue and involve processes which move the chemical system away from a manifold. Two regions of explosive behavior could be identified. The first one occurs in the reaction zone of the premixed branches at temperatures between 1200-1800K, the second explosive region was found in the cold preheat zone of the premixed flame branches at temperatures between 600-800K. By analyzing participation indices of these modes, reactions could be identified which support the explosive behavior. Finally, the accuracy of a skeletal mechanism of 66 species was assessed and we found good agreement in the main properties and major species concentrations of the edge flame. The skeletal mechanism was used to study the influence of increasing the equivalence ratio in the fuel stream.

We have also concluded the implementation of changes to the low-Mach number reacting flow solver to enable axisymmetric flow configurations. It was necessary to implement a new solver for the pressure field. The pressure solver involves the solution of a Poisson equation with constant coefficients. We use the HYPRE library to efficiently solve the resulting system of linear equations in a scalable way on massively parallel computers. This new pressure solver can also be used for the rectangular 2D flow configurations, increasing the parallel efficiency of the code. Several test cases have shown the stability and efficiency of the implementation. Self-convergence studies were carried out for freely propagating flame fronts and for the interaction of a Hill's spherical vortex with a flame front. Second order spatial convergence was confirmed. Further code validation and verification are currently underway.

We have also continued exploring the performance of our MPI/OpenMP low Mach number flow solver in rectangular coordinates. The goal is to gain an understanding of factors that control parallel efficiency in strong scalability studies for large numbers of processors. As a test case, we used the n-heptane/air edge flame computations, involving 560 species and a modest grid size of 512×512 cells. The code was instrumented to provide detailed information about time spent in each of its sections. We found that most of the computational work occurs in the time-advancement of the species concentrations due to the chemical source terms which amounts to

approximately 70% of the total time. The analysis shows that most of the loss of parallel efficiency occurs in this part of the code. The load balancer which aims to spread this load evenly among all processors produces a larger variance in loads as the number of processors increases. The main reason is found to be the discrete nature of the partitioning which becomes more important as the size of partitions decreases. The situation was found to be improved by considering larger computational domains. A test case using 1024 times 1024 cells showed a parallel efficiency of 71% using 16384 cores compared to the base case using 1024 cores. (w/J. Prager)

In the context of high-order adaptive mesh refinement (AMR), we completed the transition from the Grace to the Chombo library in our AMR code. Results obtained with the Chombo library for canonical advection-diffusion and advection-diffusion-reaction configurations were matched with the corresponding results obtained with the Grace library. We have further validated the hybrid numerical construction, i.e. uniform mesh for momentum advance coupled with AMR for scalar transport, through comparisons with results obtained from high-resolution uniform simulations. These results, corresponding to a flame-vortex pair configuration, showed that it is sufficient to solve for momentum on a uniform mesh only while the AMR hierarchy is only needed to capture the inner flame structure. These tests also showed that computational expense for AMR simulations compared to equivalent uniform runs is directly related to the relative size of the refined area. For 2-level AMR runs with 5-30% of the area being refined, the CPU time is 17-37% of the equivalent uniform mesh simulation. CPU time tests for simulations involving more refinement levels are in progress. After the transition to Chombo was complete we commenced parallel scalability tests. Current simulations performed using GRI-Mech 3.0 to model methane chemistry show a "strong" parallel efficiency of about 60% when increasing the number of processors from 16 to 256. We have identified several avenues to improve the efficiency. These include increasing the computational domain size, and improving handling of transport and thermodynamical properties at the interfaces between computational mesh blocks. We will implement these changes in the near future. (w/C. Safta and J. Ray)

An in-depth analysis was performed of the accuracy and efficiency of the CSP integrator with tabulation on the ignition of homogeneous H_2–air and CH_4–air mixtures. For both systems, tables were constructed that store CSP information from states extracted from detailed chemistry simulations over a range of initial conditions. The table data structure relies on *k*d-trees, which allow storing CSP information from states that are arbitrarily located in the chemical configuration space, thereby removing the need for a pre-defined partitioning or meshing of this high-dimensional space. Data retrieval employs efficient nearest-neighbor look-ups in the reduced dimensional space of the non-radical species. To test the CSP integrator with and without tabulation, it was used in the simulation of 1000 H_2–air ignition cases and 100 CH_4–air ignition cases, all randomly sampled from the range of initial conditions that the CSP tables were constructed on. Comparison with detailed chemistry simulations using an implicit solver for stiff ODE systems (CVODE) showed excellent accuracy for the CSP integrator: deviations were observed on the order of one thousandth of a percent in the predicted ignition times in H_2–air, and on the order of a hundredth of a percent in the predicted ignition times in CH_4–air. In terms of CPU time usage, the CSP integrator with tabulation was up to 6 times faster than regular CSP (without tabulation) in the H_2–air ignition cases, and up to 10 times faster than regular CSP in the CH_4–air cases. In comparison with detailed chemistry simulations, CSP with tabulation was at best two times slower in the H_2 cases, but up to 40% faster in the CH_4 cases. These results show the potential for tabulation to dramatically improve the computational performance of the CSP integrator. Moreover, this potential is larger for fuels with more complex chemistries as they tend to be more stiff and therefore benefit more from stiffness reduction. The approach therefore holds the promise of being more computationally efficient than direct integration of the detailed reaction mechanism with stiff ODE solvers, as is already apparent in the CH_4 results. (w/B. Debusschere)

B. Uncertainty Quantification in Reacting Flow

A significant challenge with Uncertainty Quantification (UQ) in chemical systems is that the uncertainties in chemical kinetic model parameters are not well known. Even when error bars are available on reaction rate parameters such as the pre-exponential Arrhenius rate constant A, or activation energy E, based on published experimental measurements, there is typically no information available on the joint probability density function (PDF) representing the uncertainty in (A,E). We have found in previous work that the choice of correlation among these parameters can have a drastic effect on the predicted uncertainties in the results. The joint density can in principle be reconstructed with the raw data from the original experiments, but that is rarely available. Accordingly, we have been working on a procedure for inferring these densities based on available information, in the absence of data, namely a Data Free Inference (DFI) procedure. This procedure employs Bayesian inference, and involves two nested Markov Chain Monte Carlo (MCMC) chains, one on data sets, and another on the parameters. It estimates

the joint posterior PDF on the parameters as a pooled posterior resulting from inference with a large number of possible data sets all of which are consistent with the *available* information. We have established its convergence towards the true posterior in simple model problems involving single/double exponential decay functions.

We recently demonstrated this algorithm in the context of a chemical system. We used synthetic ignition-time data for methane-air ignition at 1 atm over a range of initial temperature, produced using GRImech3.0 with added noise. This data was then used to calibrate a global single-step irreversible methane reaction model, thereby inferring a joint posterior on the two model parameters (A, E). Extracting from this posterior the nominal parameter values and the marginal (5%, 95%) bounds, we then applied DFI to discover this posterior without using the data. We presume knowledge of the fit model, the range of the initial temperature used in the fitting, the nominal parameter values, and their bounds. Because of the nested 2-chain structure of the algorithm, computational expense of the forward model is of concern. We used a Legendre-Uniform polynomial chaos surrogate for the forward model, employing a non-intrusive quadrature construction over the space of initial temperature and (A, E), and a fast robust adaptive MCMC algorithm on the inner chain. The results were very successful in discovering the proper shape and correlation structure of the posterior PDF with even a short 1000-long data chain. Tests with a 5000-long data chain exhibited a pooled posterior that nearly overlays the reference posterior. Tests with longer chains are in progress in order to adequately quantify the convergence behavior towards the correct posterior in the ignition context. (w./R. Berry, C. Safta, K. Sargsyan and B. Debusschere)

III. Future Plans

A. Reacting Flow Computations, Analysis, and Model Reduction

We will continue our development of advanced massively parallel reacting flow algorithms and codes. Our axisymmetric code is in place, with confirmed second-order accuracy. Present activity is focused on verification of the solution using the method of manufactured solutions. Once this is confirmed, we will begin comparisons to axisymmetric flame cases where experimental data is available in the published literature, and from J. Frank at Sandia-CRF.

With 71% strong scalability parallel efficiency demonstrated on 16384 cores, for detailed nHeptane-air kinetic models, and the bottlenecks having been found to be primarily load-balancing due to the relatively small number of computational cells per core and inadvertent resulting imbalances, it is clear that going to larger computational domains, beyond 1024^2, will further increase the parallel efficiency. We are moving in this direction at present, expanding domain size beyond an edge-flame geometry, towards a laminar jet flame context. Going forward, our goal is to explore the limits of performance and scalability for $O(10^5)$ cores on larger domains.

Having completed our detailed analysis of both methane and nHeptane edge flames, we have been more recently focusing on computations of jet flames. At present, we have ongoing methane-air laminar jet flame computations in a 6 cm long domain. Having established the steady-state solution, we are proceeding towards time-unsteady computations. We will explore lifted methane-air jet flame dynamics, focusing on flame interaction with shear layer vorticity. We will study this system for a range of variation of the composition of the shear-layer streams.

Ongoing research on the CSP integrator with tabulation involves rigorous assessment of the accuracy of this integrator approach, specifically focusing on the accuracy of the CSP approach by itself, and the additional approximations introduced by the tabulation. The findings will inform the selection of integrator parameters such as time step factors and optimal table density. Further, a scaling study will be performed to study the performance of this approach for homogeneous mixture ignition problems involving more complex chemistries such as n-heptane and iso-octane. The CSP integrator approach will further be extended to reacting flow simulations, with the goal of replacing operator split schemes in the longer term. Starting with FY11, this ongoing and future research on the CSP integrator with tabulation will be the subject of a separate BES research project, under a new BES PI, Bert Debusschere, pending succesful review of the research proposal.

B. Uncertainty Quantification in Reacting Flow

Given our recent advances in the UQ area, particularly involving development and demonstration of a range of computational tools and libraries, including general UQ toolkit capabilities for intrusive/non-intrusive manipulations, Bayesian inference for parameter estimation, a flexible thermochemistry (TChem) toolkit, and particularly

DFI, we are ready to move towards building the uncertain input space for a simple chemical kinetic model.

Future progress in UQ for chemical systems will involve foremost DFI-construction of the joint PDF of kinetic and thermodynamic parameters, before proceeding to forward-propagation of uncertainty. Having demonstrated the use of DFI on a single chemical reaction, we will next proceed towards its application in earnest on a H_2-O_2 chemical kinetic model. Typical elementary reaction H_2-O_2 models involve $\sim$9 species, and 19 reactions. We will closely inspect each reaction in the model, identifying which experiments/computations were employed in determining its rate constants' nominal values and bounds, and understanding what fitting/analysis was done. We will then develop code to redo this fitting with data sets that are proposed, and evaluated, using DFI. Particular attention will be focused on dependencies among reactions, in terms of the fitting process for each associated experiment/analysis. This will provide a dependence tree among a set of fitting operators, which would provide, via DFI, a joint PDF on the full set of parameters. We will pursue this for both kinetic rates and thermodynamic parameters in the model. Progress along this path will hit numerous challenges resulting from missing information on the specification of fitting models in the literature. Innovative remedies will be necessary, potentially employing maximum entropy methods.

Once the uncertain input space of this H_2-O_2 model is properly constructed, *i.e.* a joint parametric PDF has been constructed using DFI, following steps will focus on forward propagation of this uncertainty. This model has $\sim$60 uncertain parameters. In order to propagate uncertainty forward in such a high-dimensional setting, a very large number of non-intrusive samples will be necessary, even when using sparse-quadrature methods available in our UQ toolkit. This is the familiar curse of dimensionality. We will address this challenge in various ways. First, we will pursue adaptive anisotropic sparse-quadrature constructions that minimize the number of requisite samples for a given accuracy in non-intrusive forward UQ. Second, we will employ low order forward UQ computations in order to identify important parameters in a global sensitivity analysis context. Finally, with the reduced dimensionality of the important set of parameters, we will conduct high-order forward UQ studies in order to assign accurate uncertainties on model predictions.

We will also explore the utility of compressive sensing methods for forward UQ. These methods employ random samples, as opposed to deterministic sparse-quadrature samples, but they can attain superior performance, with much reduction in the number of samples for a given target accuracy, when the underlying problem exhibits a sufficiently high degree of sparsity. Compressive sensing methods have been demonstrated for non-intrusive forward UQ in heat-transfer problems, but have yet to be examined in chemical systems.

IV. BES-Supported Published/In-Press Publications [2009-2011]

[1] Prager, J., Najm, H., Valorani, M., and Goussis, D., Structure of n-Heptane/Air Triple Flames in Partially-Premixed Mixing Layers, *Combustion and Flame* (2011) in press.

[2] Sonday, B.E., Berry, R.D., Najm, H.N., and Debusschere, B.J., Stochastic Eigenvalue Analysis, *SIAM J. Sci. Comp.* (2011) in press.

[3] Najm, H.N., Uncertainty Quantification in Fluid Flow, in *Turbulent Combustion Modeling: Advances, New Trends and Perspectives* (T. Echekki and N. Mastorakos, Eds.), Springer-Verlag, Berlin,, 2011, , pp. 381–407.

[4] Ray, J., Armstrong, R., Safta, C., Debusschere, B.J., Allan, B.A., and Najm, H.N., Computational frameworks for advanced combustion simulations, in *Turbulent Combustion Modeling: Advances, New Trends and Perspectives* (T. Echekki and N. Mastorakos, Eds.), Springer-Verlag, Berlin,, 2011, , pp. 409–437.

[5] Najm, H.N., Valorani, M., Goussis, D.A., and Prager, J., Analysis of Methane-Air Edge Flame Structure, *Combustion Theory and Modelling*, 14(2):257–294 (2010).

[6] Safta, C., Ray, J., and Najm, H.N., A High-Order Low-Mach Number AMR Construction for Chemically Reacting Flows, *J. Comput. Phys.*, 229(24):9299–9322 (2010).

[7] Najm, H.N., Debusschere, B.J., Marzouk, Y.M., Widmer, S., and Le Maître, O.P., Uncertainty Quantification in Chemical Systems, *Int. J. Num. Meth. Eng.*, 80:789–814 (2009).

[8] Marzouk, Y. M., and Najm, H. N., Dimensionality reduction and polynomial chaos acceleration of Bayesian inference in inverse problems, *Journal of Computational Physics*, 228(6):1862–1902 (2009).

[9] Valorani, M., and Paolucci, S., The *G-Scheme*: A framework for multi-scale adaptive model reduction, *Journal of Computational Physics*, 228:4665–4701 (2009).

[10] Najm, H.N., Uncertainty Quantification and Polynomial Chaos Techniques in Computational Fluid Dynamics, *Annual Review of Fluid Mechanics*, 41(1):35–52 (2009).

Spectroscopy, Kinetics and Dynamics of Combustion Radicals

David J. Nesbitt
JILA, University of Colorado and National Institute of Standards and Technology, and Department of Chemistry and Biochemistry, University of Colorado, Boulder, Colorado

Spectroscopy, kinetics and dynamics of jet cooled hydrocarbon transients relevant to the DOE combustion mission have been explored, taking synergistic advantage of i) high resolution IR lasers, ii) slit discharge sources for efficient production of supersonically cold radicals, and iii) long path length detection with direct absorption sensitivities (10^{-7}/root Hz) near the quantum shot noise limit (10^7 radicals/cm^3/quantum state). With such a hybrid approach, targeted radical transients can be "synthesized" by electron dissociative attachment with commercially available alkyl halide precursors. This yields remarkably high concentrations (under favorable conditions up to 10^{16} radials/cm^3) at pressures characteristic of combustion conditions, and yet rapidly cools the radicals (T ≈10-20K) into a small number of quantum states in slit supersonic expansion environment. In conjunction with the powerful generality of tunable IR laser absorption methods over the 3-10 μm fingerprint region, this unique approach offers prospects for first time spectral study of many critical combustion species. A few selected highlights from work over the past year are summarized below.

I. Spectroscopic Studies of Rovibronic Coupling Dynamics in C_2H Radical

The ethynyl radical (C_2H) is known to be an important reactive intermediate in both combustion chemistry here on earth and in the chemistry occurring in the interstellar medium. Specifically, it has been postulated to play a role in the formation of polycyclic aromatic hydrocarbons (PAHs) in both environments. One postulated mechanism for the formation of PAHs in combustion involves the reaction of free radical intermediates, such as phenyl radical (C_6H_5), with small unsaturated hydrocarbons like C_2H_2 and C_2H. PAH formation is likely a precursor to soot formation, which remains a poorly understood byproduct of many combustion processes. A similar nucleation process has been postulated in interstellar space chemistry, involving C_2H reacting with other unsaturated small molecules to form PAHs and then further reactions of PAHs leading to formation of solid particulates. A reaction mechanism of this type has been considered to contribute to the haze formation observed in the atmosphere of Titan.

What makes C_2H particularly interesting from a unimolecular perspective is the presence of low lying electronically excited states, in which the quantum states due to vibrations of the C_2H framework are imbedded and can lead to anomalously strong vibronic mixing To explore these non-adiabatic effects, we have undertaken a spectroscopic reinvestigation of C_2H under sub-Doppler conditions of the slit jet apparatus.[1,2] Specifically, jet-cooled C_2H radicals are produced by adiabatically expanding a mixture of ~0.04% acetylene in a 70:30 neon-helium buffer gas through a pulsed slit-jet (operated at 19 Hz, with approximately a 1 ms pulse duration),

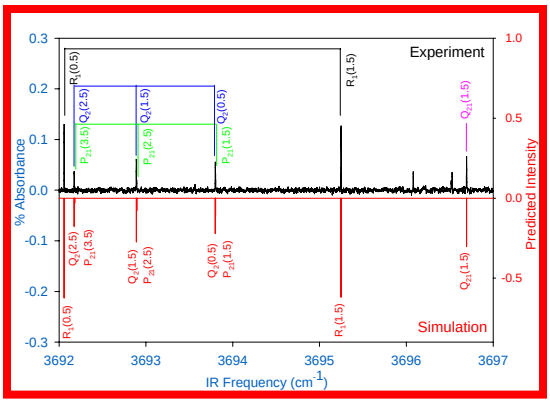

and striking a discharge to form radicals by electron associative detachment. Optimum discharge conditions included 450 V for 0.2 A of current, along with a 50 kHz square wave modulation of the discharge to utilize lock-in detection in order to enhance those signals that are produced by the discharge. The efficiency of C_2H formation from HCCH in the discharge is not high, with the slit-jet cooled discharge source yielding peak absorbances as low as 0.01% on the weakest lines and as high as 0.4% on the strongest lines for the C_2H $^2\Pi$-$^2\Sigma^+$ band reported here. However, at typical rms sensitivity levels of 0.003% in a 10 kHz bandwidth, this still translates into signal to noise ratios > 50:1 on the strongest lines, as shown in the sample data above.

Exploiting these sub-Doppler jet cooled methods, high resolution infrared spectra for four $^2\Pi$-$^2\Sigma^+$ bands of jet-cooled ethynyl radical (i.e. C_2H) in the gas phase have been observed and analyzed. The combination of i) slit-jet cooling ($T_{rot} \approx 12$ K) and ii) sub-Doppler resolution (≈ 60 MHz) permits satellite branches in each $^2\Pi$-$^2\Sigma^+$ band to be observed and resolved for the first time, as well as helps identify a systematic parity misassignment from previous studies. The observed lines in each band are least squares fit to a Hamiltonian model containing rotational, spin-rotational, spin-orbit, and lambda-doubling contributions for the $^2\Pi$ state, from which we report revised excited state constants and band origins for the observed bands. Three of the four bands fit extremely well within a conventional $^2\Pi$ model (i.e. $\sigma < 20$ MHz), while one band exhibits a local perturbation due to an avoided crossing with a near resonant dark state. Vibronic assignments are given for the observed bands, with the dark state clearly identified as a highly excited stretch and bending overtone level $\tilde{X}$ $(1,2^2,0)$ by comparison with high level *ab initio* efforts by Carter and coworkers.[3]

Of special dynamical interest is the degree of vibronic coupling between the electronically excited A($^2\Pi$) state and highly excited vibrational states in the ground state of this radical, which is clearly responsible for the rich unexpected complexity observed in the near IR spectrum. This coupling is particularly well exemplified in the shifts in line positions as well as the appearance of "dark" transitions in the spectrum to states where the oscillator strength comes solely from the vibronic mixing. To explore this further, a high resolution infrared spectrum of the origin band region near 3600 cm^{-1} of jet-cooled ethynyl radical (C_2H) has been explored and analyzed in detail, which exhibits a very strong and parity specific local perturbation in the excited spin orbit F_2 $^2\Pi_{1/2}$ state. Based on the revised parity assignments of the corresponding levels, the perturbing state can be unambiguously determined to be of $^2\Sigma^+$ vibrational symmetry, and thus must be coupled to the A($^2\Pi$) state by local rotational Coriolis interactions. By incorporating this Σ-Π Coriolis coupling into the unperturbed Hamiltonian model (containing only rotational, spin-rotational, spin-orbit, and lambda-doubling contributions), we are able to fit the observed $^2\Pi$-$^2\Sigma^+$ origin band to a standard deviation of 15 MHz, i.e. essentially the experimental limit. In addition, the coupling is sufficiently strong to permit observation of *pairs of transitions* out of the same lower state to upper states mixed by the vibronic interaction. By virtue of the high frequency precision, these data permitted a direct

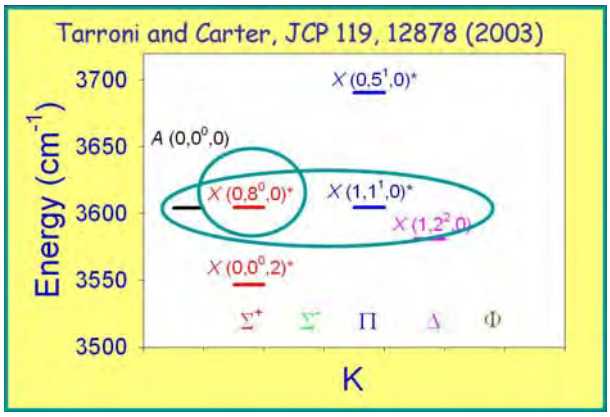

determination of the band origin (ν_{pert}) and rotational constant (B_{pert}) for the perturbing "dark" $^2\Sigma^+$ state. Furthermore, since the vibrational density of states is still relatively modest in a small triatomic such as C_2H at 3600 cm^{-1}, one can attempt a rather novel identification of the vibrational dark state by rigorous comparison with high quality predictions of Tarroni and Carter. As shown in the accompanying figure, the results indicate the source of strong vibronic coupling to be unambiguously between a fortuitous near resonant "avoided crossing" between the F_2 $^2\Pi_{1/2}$ state and the high overtone $^2\Sigma^+$ $(0,8^0,0)$ state with 8 quanta of CH bending excitation. By way of further confirmation, the rotational constants observed from the high resolution analysis are also in excellent agreement with the UV dispersed fluorescence studies of Hsu *et al.*.[4]

II. Slit Jet IR Spectroscopy of Isotopically Substituted Methyl Radical

Methyl radical is a critical transient radical species in the combustion of essentially all hydrocarbon fuels, which has provided motivation for numerous spectroscopic studies of the in-plane and out-of-plane vibrational degrees of freedom. In particular, the breaking of rotational symmetry in this radical by partial H/D isotopic substitution in species such as CH_2D permits one to investigate the unimolecular coupling dynamics in much greater detail by localizing the CD vs CH vibrational motion and thereby lowering the effective symmetry from D_{3h} to C_{2v}. To help explore these dynamical effects in this important radical species, we have obtained first high resolution sub-Doppler spectroscopy of CH_2D radical via infrared absorption spectra in the symmetric/ antisymmetric C-H stretching region.for isotopically substituted CH_2D methyl radical.[5] These isotopic studies are feasible in the slit discharge due to i) high density radical generation via dissociative electron attachment to CH_2DI, ii) low rotational temperatures from supersonic cooling, iii) long absorption path length along the slit jet axes, and iv) near shot noise limited absorption sensitivity on a dual beam single mode difference frequency laser spectrometer.

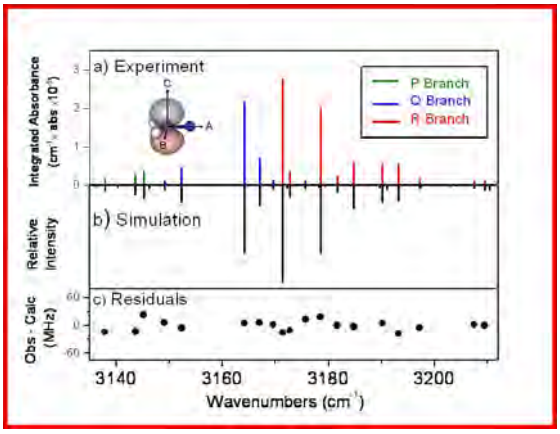

The spectral structure is rovibrationally fully resolved and can be fit to a Watson asymmetric top Hamiltonian to yield rotational/centrifugal constants and vibrational band origins. An asymmetric top stick spectrum for the observed rotational lines of CH_2D is shown in the accompanying figure, along with residuals from a least squares fit simulation. In addition, the transverse velocity distribution along the laser probe direction is collisionally quenched in the slit jet expansion, thus yielding sub-Doppler resolution of spin-rotation structure and even partial resolution of nuclear hyperfine structure for each rovibrational line. Global least-squares fits to the lineshapes provide additional information on spin-rotation and nuclear hyperfine constants, which both complement and clarify previous FTIR studies of CH_2D in the out of plane bending region. Analysis of the band origins for all known vibrational modes in the isotopomeric CH_mD_{3-m} series with a harmonically coupled anharmonic oscillator model Hamiltonian now provides a quantitative framework for describing the in-plane stretching dynamics in this fundamental combustion radical. Furthermore, symmetry breaking allows the molecule to

have a weak but non-vanishing dipole moment, which based on the current high resolution IR data will enable further study of this radical via microwave/mm wave spectroscopy.

III. Intermolecular Spectroscopy of Combustion Products: H_2/D_2+H_2O

A first principles description of combustion processes requires a detailed understanding of state-to-state collisional energy transfer dynamics, which in turn requires high quality multidimensional intra- and intermolecular potential energy surfaces for reactants and products, benchmarked against high quality experimental data. As progress in this direction, we have recently initiated a collaborative exploration of H_2 + H_2O interactions by a synergistic combination of i) ab initio calculations, ii) exact multidimensional quantum dynamics and comparing with iii) high resolution direct absorption spectroscopy of the corresponding H_2-H_2O and D_2-H_2O complexes.[6,7] Specifically, jet cooled H_2O-H_2 and H_2O-D_2 complexes are formed by pulsed supersonic expansion through a slit valve and detected via direct absorption of high resolution IR light in the 6.2 μm region corresponding to ν_2 bending of the H_2O chromophore. The stagnation gas is formed by passing a mixture of H_2 (99.999%) or D_2 (> 99%) and "first run" Ne (70/30 Ne/He) at 260 kPa through a distilled H_2O bubbler at 273 K. Absolute frequencies are determined from $H_2{}^{17}O$ and $H_2{}^{18}O$ transitions measured also in the slit jet expansion, which are readily observable in natural isotopic abundance. Rotational structure for each of the H_2O-H_2 and H_2O-D_2 complexes are observed, which can be unambiguously assigned to progressions in the K_a=0-0 and 1-1 manifolds arising from overall rotation and large amplitude internal rotor motion in the complex. A 5D intermolecular potential for H_2O-D_2 is obtained from the state-of-the art 9D *ab initio* potential surface of Valiron *et al* by averaging over the ground state vibrational wave functions of H_2O and H_2/D_2. On this potential, we calculate the bound rovibrational levels for total angular momentum J = 0 to 3, based on a coupled free rotor basis for the hindered internal rotations (with permutation/inversion symmetry associated with the para/ortho (p/o) nature of both H_2O and H_2/D_2), and a discrete variable representation in the intermolecular distance R. Agreement between experiment and theory proves to be remarkably quantitative (< 0.1% in B_{rot}), providing an extremely promising isotopically invariant test of the H_2 + H_2O potential energy surface from a rigorous first principles perspective.

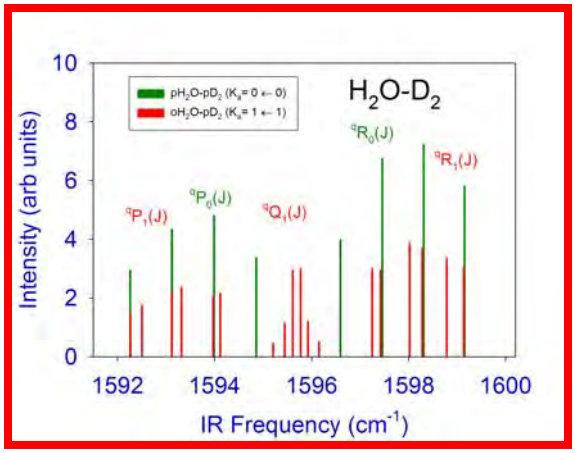

1 **E. N. Sharp-Williams, M. A. Roberts, and D. J. Nesbitt, *J. Chem. Phys.* 134 (6).**
2 **E. N. Sharp-Williams, M. A. Roberts, and D. J. Nesbitt, *Phys. Chem. Chem. Phys.* (submitted).**
3 **R. Tarroni and S. Carter, *J. Chem. Phys.* 119, 12878 (2003).**
4 **Y.-C. Hsu, Y.-J. Shiu, and C.-M. Lin, 103, 5919 (1995).**
5 **M. A. Roberts, C. Savage, and D. J. Nesbitt, (in preparation).**
6 **A. van der Avoird and D. J. Nesbitt, *J. Chem. Phys.* 134 (4).**
7 **A. van der Avoird, Y. Scribano, A. Faure, M. J. Weida, J. R. Fair, and D. J. Nesbitt, *Chem. Phys.* (submitted).**

Radical Photochemistry and Photophysics

Daniel M. Neumark
Chemical Sciences Division
Lawrence Berkeley National Laboratory
Berkeley, CA 94720
email: dneumark@berkeley.edu

Program Scope:

Our research program is focused on fundamental aspects of radical photochemistry and photophysics, with particular emphasis on radicals that play an important role in the combustion of hydrocarbons. Radicals are generated from neutral or anionic precursors and photodissociated in the ultraviolet. We then determine which fragmentation channels occur and measure the photofragment translational energy and angular distributions for each channel. These measurements address the following central issues. First, they yield the primary photochemistry for a particular radical as a function of excitation energy. While many photodissociation experiments provide extremely sensitive probes of particular products (i.e. Rydberg tagging to detect H atoms), our experiments incorporate more universal detection schemes that are sensitive to all or most photofragmentation channels. Secondly, measurements of the product translational energy distributions provide considerable insight into the dissociation mechanism following photoexcitation and how this mechanism might vary with excitation energy. For example, very different translational energy distributions are expected if dissociation occurs on an excited state surface as opposed to internal conversion (IC) to the ground state followed by statistical decay. The relative importance of these two limiting mechanisms is a sensitive probe of the conical intersections that govern the dynamics of electronically excited polyatomic molecules. Moreover, results for radicals that decay from the ground state can be directly compared to experiments in which the thermal decomposition rates and products of radicals are determined, since in both cases internal energy tends to be randomized prior to dissociation. Finally, photodissociation experiments can provide direct measures of bond dissociation energies in free radicals, information that is critical in developing kinetic mechanisms for complex combustion processes in which radicals serve as key intermediates.

The radical photodissociation experiments are carried out on two instruments with complementary capabilities: a fast beam photofragment translational spectroscopy apparatus, and a molecular beam photodissociation instrument. In the fast beam experiment, radicals are generated by laser photodetachment of a fast (8–10 keV) beam of mass-selected negative ions. The radicals are then photodissociated by a second laser, and the photofragments are collected with high efficiency. We can measure the total dissociation signal as a function of excitation wavelength, thereby mapping out the photofragment yield spectrum of the radical. In addition, at fixed wavelengths, photofragment coincidence imaging yields the position and arrival times for all photofragments from each photodissociation event, from which the photofragment translational energy and angular distribution are obtained for each mass channel. In the molecular beam experiments, radicals are generated by either photolysis or pyrolysis of a stable precursor and then photodissociated at either 248 or 193 nm. Photofragments are detected and analyzed using a rotating mass spectrometer with electron impact ionization. The choice of

experiment for a particular radical depends on whether it can be generated more easily by photodetachment or by photolysis/pyrolysis. Also, compared to the fast beam experiment, the molecular beam instrument is more suitable for radicals that dissociate via loss of H atoms.

Recent Results and Future Plans:

The reaction dynamics of small hydrocarbon radicals are of great interest owing to their important role in combustion, planetary atmospheres and interstellar clouds. The chemistry of these systems is often governed by the dynamics of a few key radical species, one of which is the propargyl (H_2CCCH) radical. This species is the most stable of all C_3H_3 isomers and its self-reaction is believed to form the first benzene ring in the combustion of hydrocarbons. Subsequent reactions of propargyl radicals with benzene lead to polycyclic aromatic hydrocarbons (PAH) and ultimately soot. We previously carried out experimental studies of the UV photodissociation of propargyl and the higher energy propynyl isomer (H_3CCC) in complementary studies on our molecular beam and fast beam instruments. Motivated by this work, we performed a theoretical study of the photodissociation of perdeuterated propargyl (D_2CCD) and propynyl (D_3CCC) radicals has been carried out, focusing on the C-C bond cleavage and D_2 loss channels. High-level *ab initio* calculations were carried out, and RRKM rate constants were calculated for isomerization and dissociation pathways. The resulting reaction barriers, microcanonical rate constants and product branching ratios were consistent with the experimental findings, supporting the overall mechanism of internal conversion followed by statistical dissociation on the ground state surface. We found loose transition states and very low exit barriers for two of the C-C bond cleavage channels and an additional CD_2 + CCD channel, which had not been reported previously. Our results probed the extent of propargyl and propynyl isomerization prior to dissociation at 248 and 193 nm and delivered a comprehensive picture of all ongoing molecular dynamics. Specifically, we found that at 248 nm excitation, the isomerization of propynyl to propargyl is faster than propynyl dissociation, so that the photodissociation dynamics of the two isomers are similar. In contrast, at 193 nm, propynyl dissociation via C-C bond cleavage competes effectively with isomerization to propargyl, resulting in quite different dynamics of the two isomers.

The phenyl radical, *c*-C_6H_5, plays a central part in the combustion chemistry of aromatic hydrocarbons. Its formation from the bimolecular reaction of smaller aliphatic species has been proposed to be the rate-limiting step in the production of larger aromatic molecules. The phenyl radical is an intermediate in the thermal decomposition of benzene, so its bimolecular reactivity and unimolecular decay kinetics are of considerable interest in formulating a complete mechanism for this process. Motivated by these considerations, photofragment translational spectroscopy (PTS) was used to study the photodissociation dynamics of the phenyl radical at 248 and 193 nm. At 248 nm, the only dissociation products observed were from H atom loss, attributed primarily to H + *o*-C_6H_4 (*ortho*-benzyne). The observed translational energy distribution was consistent with statistical decay on the ground state surface. At 193 nm, dissociation to H + C_6H_4 and C_4H_3 + C_2H_2 was observed. The C_6H_4 fragment can be either *o*-C_6H_4 or *l*-C_6H_4 resulting from decyclization of the phenyl ring. The C_4H_3 + C_2H_2 products dominate over the two H loss channels. Attempts to reproduce the observed branching ratio by assuming ground state dynamics were unsuccessful . However, these calculations assumed that the C_4H_3 fragment was *n*-C_4H_3, and better agreement would be expected if the lower energy *i*-C_4H_3 + C_2H_2 channel were included.

The photodissociation dynamics of the *t*-butyl radical (*t*-C_4H_9) were investigated using photofragment translational spectroscopy. The *t*-butyl radical was produced from flash pyrolysis of azo-*tert*-butane and dissociated at 248 nm. Two distinct channels of approximately equal importance were identified: dissociation to H + 2-methylpropene, and CH_3 + dimethylcarbene. Neither the translational energy distributions that describe these two channels nor the product branching ratio were consistent with statistical dissociation on the ground state. On the ground state potential energy surface, H atom loss is expected to be a nearly barrierless process, while the P(E_T) reveals products with large translational energy. The P(E_T) distribution for the methyl loss channel extends to a maximum of 27 kcal/mol and is attributed to the formation of dimethylcarbene, rather than isomerization followed by dissociation to propene. The branching ratio was determined to be 1.1±0.3, indicating approximately equal branching between the two channels, whereas H atom loss would be expected to dominate if a statistical mechanism were operative. Hence, it appears that the photodissociation of *t*-butyl is either a non-statistical process on the ground state or involves dissociation on an excited state for one or both channels; the CH_3 loss channel in particular appears to be an excited state process.

Future plans on the fast beam instrument are focused on investigating three-body dissociation in free radicals. With this in mind, the photodissociation of gas-phase I_2Br^- was investigated using fast beam photofragment translational spectroscopy. Anions were photodissociated from 300 to 270 nm (4.13 - 4.59 eV) and the recoiling photofragments were detected in coincidence by a time- and position-sensitive detector. Both two- and three-body channels were observed throughout the energy range probed. Analysis of the two-body dissociation showed evidence for four distinct channels: $Br^- + I_2$, $I^- + IBr$, $Br + I_2^-$, and $I + IBr^-$. In three-body dissociation, $Br(^2P_{3/2}) + I(^2P_{3/2}) + I^-$ and $Br^- + I(^2P_{3/2}) + I(^2P_{3/2})$ are produced primarily from a concerted decay mechanism. A sequential decay mechanism was also observed and attributed to $Br^-(^1S) + I_2(B^3\Pi_{0u}^+)$ followed by predissociation of $I_2(B)$. Our two-body photofragment translational energy distributions [*P(E_T)* distributions] suggest that I_2, I_2^-, IBr, and IBr^- are formed in highly vibrationally excited states, in accordance results on other trihalides. We obtain bond dissociation energies and the heat of formation of I_2Br^- from our three-body *P(E_T)* distributions, and extract detailed information on the three-body dissociation mechanism by means of Dalitz plots. These experiments provide a basis for comparison of the photodissociation dynamics of the extensively studied triiodide anion and a non-centrosymmetric analog.

Publications:

S. J. Goncher, D. T. Moore, N. E. Sveum, and D. M. Neumark. "Photofragment Translational Spectroscopy of Propargyl Radicals at 248nm." J. Chem Phys. 128, 114303 (2008).

P. E. Crider, L. Castiglioni, K. K. Kautzman, and D. M. Neumark. "Photodissociation of the Propargyl and Propynyl (C_3D_3) Radicals at 248 nm and 193 nm." J. Chem Phys. 130, 044310 (2009).

W. A. Donald, R. D. Leib, M. Demireva, B. Negru, D. M. Neumark, and E. R. Williams. "Weighing' Photons with Mass Spectrometry: Effects of Water on Ion Fluorescence." J. Am. Chem. Soc. 132, 6904, (2010).

B. Negru, S. J. Goncher, A. L. Brunsvold, G. M. P. Just, D. Park, and D. M. Neumark. "Photodissociation Dynamics of the Phenyl Radical Via Photofragment Translational Spectroscopy." J. Chem. Phys. 133, 074302 (2010).

L. Castiglioni, S. Vukovic, P. E. Crider, W. A. Lester, and D. M. Neumark. "Intramolecular Competition in the Photodissociation of C_3D_3 Radicals at 248 and 193 nm." Phys. Chem. Chem. Phys. 12, 10714-10722, (2010).

W. A. Donald, R. D. Leib, M. Demireva, B. Negru, D. M. Neumark, and E. R. Williams. "Average Sequential Water Molecule Binding Enthalpies of $M(H_2O)_{19-124}^{2+}$ (M=Co, Fe, Mn, and Cu) Measured with Ultraviolet Photodissociation at 193 and 248nm." J. Phys. Chem. A. 115, 2, (2011).

B. Negru, G. M. P. Just, D. Park, and D. M. Neumark. "Photodissociation Dynamics of the *t*-butyl Radical Via Photofragment Translational Spectroscopy at 248 nm." Phys. Chem. Chem. Phys. (in press).

P. E. Crider, A. W. Harrison, D. M. Neumark. "Two-and Three-body Photodissociation Dynamics of Diiodobromide (I_2Br^-) Anion." J. Chem. Phys. (in press).

Determination of Accurate Energetic Database for Combustion Chemistry by High-Resolution Photoionization and Photoelectron Methods

C. Y. Ng

Department of Chemistry, University of California, Davis, California 95616
E-mail Address: cyng@chem.ucdavis.edu

I. Program Scope:

The main goal of this research program is to obtain accurate thermochemical data, such as ionization energies (IEs), 0 K dissociative photoionization thresholds or appearance energies (AEs), 0 K bond dissociation energies (D_0's), and 0 K heats of formation ($\Delta H°_{f0}$'s) for small and medium sizes molecular species and their ions of relevance to combustion chemistry. Accurate thermochemical data determined by high-resolution photoionization and photoelectron studies for selected polyatomic neutrals and their ions are also useful for benchmarking the next generation of *ab initio* quantum computational procedures.

II. Recent Progress:

Sulfur monoxide (SO) and its cation (SO^+) are species of great chemical and astrophysical importance. The spin-orbit coupling constant (A) of $SO^+(X^2\Pi_{1/2,3/2})$ obtained by different experimental and theoretical methods are found to fall in the range of 330 – 371 cm^{-1}, and is in need of further improvement. We have completed a high-resolution VUV laser pulsed field ionization-photoelectron (VUV-PFI-PE) study of SO prepared by a photodissociation supersonic radical beam source.[1] In addition to yielding more precise A and IE[$SO^+(X^2\Pi_{1/2,3/2})$] values, this study has shown that the UV photodissociation radical beam source is capable of producing cold radicals with sufficiently high intensities for photoionization studies.

In this experiment, the 193 nm laser photodissociation of SO_2 was employed for the preparation of cold SO radicals. The precursor SO_2 was introduced into the beam source chamber in the form of a pulsed supersonic beam of SO_2 seeded in He. The 193nm laser was focused at the SO_2/He jet at the nozzle tip to induce photodissociation of SO_2. The SO radicals thus formed at this high pressure region of the supersonic jet undergo further collisions, resulting in the cooling of the rovibrational populations of SO. The supersonically cooled SO beam then passes through a conical skimmer before intersecting with the VUV laser beam at the photoexcitation/photoioionization (PE/PI) region.

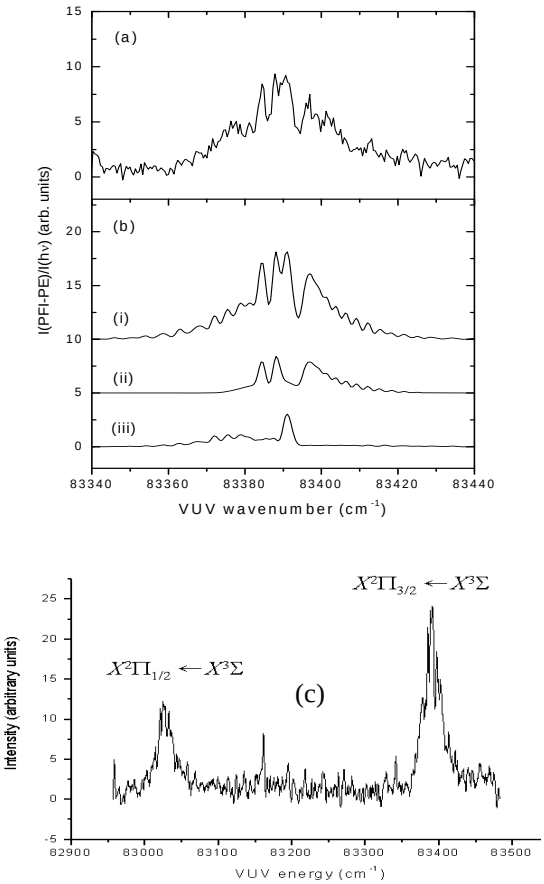

Fig. 1. (a) The VUV-PFI-PE spectrum for the $SO^+(X^2\Pi_{3/2})$ origin band. (b) Simulated spectrum (i curve) and contributions (ii and iii curves) from the $\Delta J^+ = \pm 1.5$ (ii curve) and ± 2.5 (iii curve) branches. (c) The VUV-PFI-PE spectrum covering the $SO^+(X^2\Pi_{1/2,3/2})$ origin bands.[1]

Nascent SO($X^3\Sigma$; v) radicals produced by the 193 nm photoionization of SO_2 are known to have a vibrational distribution with the major populations in SO(v=0-2). Considering that vibrational relaxation is inefficient under the present supersonic expansion conditions, the SO beam is expected to have a significant population in these excited vibrational states. Since cold SO(v=0) radicals have the highest kinetic energies, we found that the key to perform photoionization sampling of cold SO radicals is to adjust the delay of firing the VUV laser with respect to the application of 193 nm photodissociation laser to time the arrival of cold SO($X^3\Sigma$; v=0) radicals at the PE/PI regions.

We show in Fig. 1(a) the VUV-PFI-PE spectrum for the $SO^+(X^2\prod_{3/2})$ origin band. Figure 1(b) depicts the simulation spectrum (i curve) along with the contributions from the $\Delta J^+ = \pm 0.5$ (ii curve) and $\Delta J^+ = \pm 1.5, \pm 2.5$ (iii curve) rotational branches. The VUV-PFI-PE spectrum that covers both the $SO^+(X^2\prod_{3/2})$ and $SO^+(X^2\prod_{1/2})$ origin bands is shown in Fig. 1(c). On the basis of the simulation, we have obtained highly precise values for the A (365.36 ± 0.12 cm^{-1}) and the IEs (10.2945 ± 0.0002 and 10.3398 ± 0.0002 eV for the formation of $SO^+(X^2\Pi_{1/2}; v^+=0)$ and $SO^+(X^2\Pi_{3/2}; v^+=0)$], respectively. The ratio of the intensity of the PFI-PE bands for $SO^+(X^2\prod_{1/2})$ to that for $SO^+(^2\prod_{3/2})$ is measured to be ½.

III. Ongoing experiments and Future Plans

A. High-resolution near threshold photo-electron-imaging measurements

We have recently implemented the VUV photoelectron imaging (VUV-PEI) technique with the ion-imaging apparatus by adding appropriate μ-metal shields to the velocity-mapped ion-imaging apparatus.[2] We found that this method can provide an energy resolution close to that achieved in VUV-PFI-PE measurements if the VUV photoionization energy is set near the photoelectron band of interest.

Further to this development, we have successfully established the VUV laser threshold photoelectron imaging (VUV-TPEI) technique for high-resolution TPE measurements, achieving an electron energy resolution of 2 cm^{-1} (FWHM). The TPE measurements are made by gating the TPE signal imaged at the center of the imaging detector. Figure 2 compares the VUV-TPE imaging (VUV-TPEI) spectrum (upper curve) thus obtained with the VUV-PFI-PE spectrum (lower curve) of C_6H_5Cl in the energy range of 9.06-9.48 eV. The energy resolution for the VUV-PFI-PE measurement has been measured to be 1.5-2.0 cm^{-1} (FWHM). Since the FWHMs of all the VUV-TPEI bands are nearly identical to those of the corresponding VUV-PFI-PE bands, we conclude that the energy resolution achieved in this VUV-TPEI measurement is 2 cm^{-1} (FWHM).

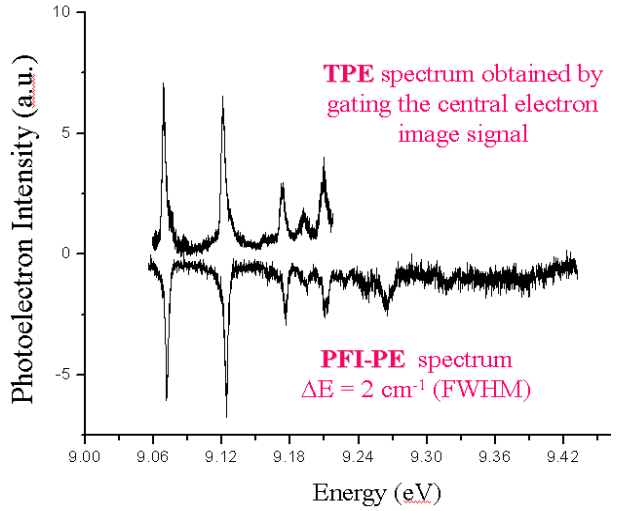

Figure 2. Comparison of the VUV-TPEI spectrum (upper spectrum) with the VUV-PFI-PE spectrum (lower spectrum), showing that the resolution achieved for the VUV-TPE-EI measurement is close to 2 cm^{-1} (FWHM) observed in VUV-PFI-PE measurements.[2]

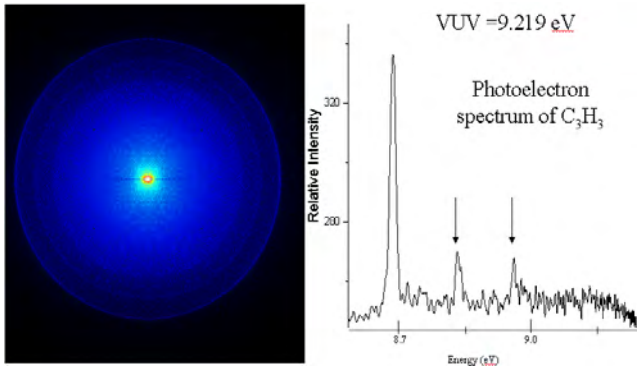

Figure 3. Photoelectron image and the VUV-PEI spectrum of propargyl radical (C_3H_3) derived from the e-image. The new features resolved in the energy region of 8.7-9.0 eV have not been observed previously.[3]

B. VUV-PEI and VUV-TPEI measurements of radicals

The VUV-TPEI method is significantly more sensitive than the VUV-PFI-PE technique because a high extraction field (100 V/cm) can be used in the e-imaging measurements, such that essentially all photoelectrons are collected. The high sensitivity makes VUV-TPEI a promising method for high-resolution photoelectron measurements of radicals, where the radical intensity is usually weak. Up to the present, nearly all PFI-PE studies of radicals have been limited to the origin band because the PFI-PE technique lacks the sensitivity for scanning over of a broad VUV energy range. It is hopeful that the VUV-PEI and VUV-TPEI approach would allow the high-resolution measurements of excited photoelectronic bands of radical species.

We have recently succeeded in performing VUV laser PEI and TPEI measurements on propargyl radical (C_3H_3). In this experiment, C_3H_3 radicals were prepared by the supersonic radical beam source based on 193 nm photodissociation of C_3H_3Cl. Figure 3 depicts the photoelectron-image of C_3H_3 (left panel) observed at the VUV photoionization energy of 9.219 eV along with the VUV-PEI spectrum derived from this image (right panel). By changing the VUV photoionization energies, we have identified vibrational bands for $C_3H_3^+$ at 876.6, 1126.6, 1737, 2102.5, and 4122 cm^{-1}. These observed vibrational bands include the 2 weak photoelectron bands (marked by arrows) in Fig. 3. A hot band at -663 cm^{-1} has also been observed for C_3H_3.

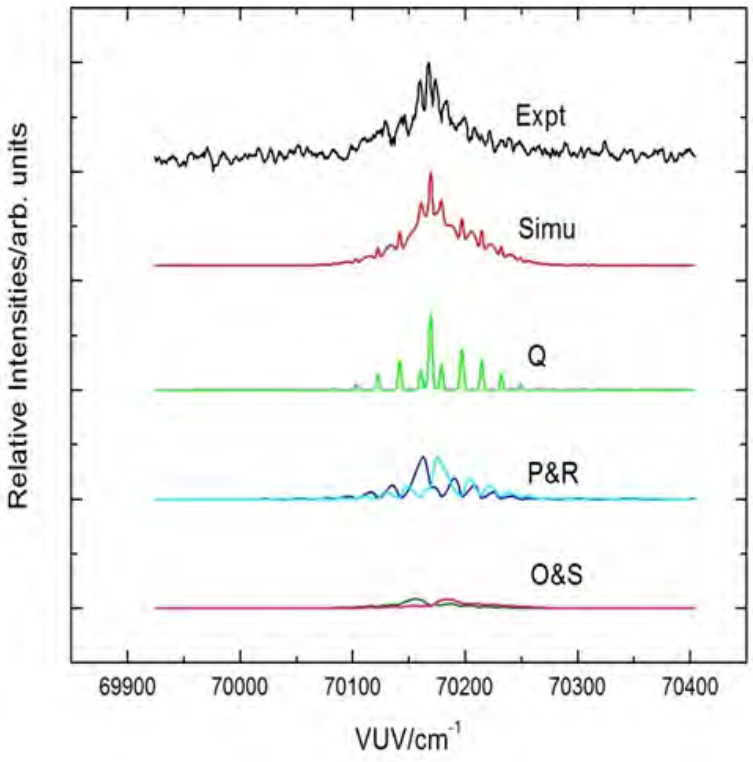

Figure 4. Top curve: VUV-TPEI spectrum of propargyl radical (C_3H_3) obtained by gating the central signal of the e-image in the VUV range of 8.60-9.22 eV. The spectrum marked as Simu is the best simulated spectrum (see the text). The lower curves are the simulated contributions by the Q, P, R, O, and S-branches.[3]

The VUV-TPEI spectrum for the origin band of $C_3H_3^+$ measured with an energy resolution of 3 cm^{-1} (FWHM) is shown as the top (black) spectrum in Fig. 4.[3] To our knowledge, this is the first successful application of this technique for high-resolution photo-electron spectroscopic study of radicals or photofragments. The simulated (brown) spectrum confirms that the sharp fine structures observed in the VUV-TPEI spectrum are originated from rotational structures of the Q-branch (green spectrum). The contributions of the P, R, Q and S-branches are mostly responsible for the broader profile of the VUV-TPEI spectrum. Based on spectral simulation, we have determined the IE(C_3H_3) = 70199.7±3.0 cm^{-1} (8.7037 ±0.0004 eV), which is more than 30 meV higher than the literature value of 8.67 eV, and is in agreement with the result of 8.70 eV obtained in a recent synchrotron based[4] TPE study. The VUV-TPEI measurements of excited photoelectron bands of C_3H_3 are in progress.

We are making progress in PIE, PFI-PE, and VUV-TPE-EI measurements on other aromatic radicals, such as phenyl (C_6H_5) and phenoxyl (C_6H_5O) radicals. These experiments represent collaborative projects between our group and the groups of Dr. Xu Zhang (Jet propulsion Laboratory, NASA), and Prof.

Barney Eillison (University of Colorado, Boulder). Using the IR-VUV-photoion technique developed in our laboratory,[5] we also plan to examine the vibrational bands for neutral C_3H_3 and C_3H_5.

References:

1. C.-S. Lam, H. Wang, Y. Xu, K.-Chung Lau,[b)] and C. Y. Ng, *J. Chem. Phys*. revised.
2. L. Yang, H. Gao, C. S. Lam, and Y. Xu, *Rev. Sci. Instrum.*, to be submitted.
3. L.Yang, H. Gao, and Y. Xu, *J. Chem. Phys.*, to be submitted.
4. T. Schubler *et al.*, *Phys. Chem. Chem. Phys.*, **7,** 819-825 (2005).
5. See Publication 1 of Section IV.

IV. Publications of DOE sponsored research (2009-present)

1. C. Y. Ng, "Spectroscopy and Dynamics of Neutrals and Ions by high-resolution infrared-vacuum ultraviolet photoionization and photoelectron methods", in "*Frontiers of Molecular Spectroscopy*", edited by Jaan Laane (Elsvier Science and Technology, 2009) Chap. 19, page 659-691.
2. B. Reed, C.-S. Lam, Y.-C. Chang, X. Xing, and C. Y. Ng, "A high-resolution photoionization study of ^{56}Fe using vacuum ultraviolet laser", *Astrophys. J.*, **693**, 940 (2009).
3. Y.-C. Chang, C.-S. Lam, B. Reed, K.-C. Lau, H. T. Liou, and C. Y. Ng, "Rovibronically selected and resolved two-color laser photoionization and photoelectron study of the iron carbide cation", *J. Phys. Chem.* A (invited), **113**, 4242 (2009).
4. Qing-Zhu Yin, Xiaoyu Shi, Cheuk-Yiu Ng, Comment on "Experimental Test of Self-Shielding in Vacuum Ultraviolet Photodissociation of CO", *Science*, 324, 1516-c (2009).
5. K.-C. Lau, Y.-C. Chang, C.-S. Lam, and C. Y. Ng, "High-level *ab initio* predictions of the ionization energy, bond dissociation energies and heats of formations for Iron carbide (FeC) and its cation (FeC^+)", *J. Phys. Chem.* A (invited), **113**, 14321 (2009).
6. Y.-C. Chang, X. Shi, K.-C. Lau, Q. Yin, and C. Y. Ng, "Rovibronically selected and resolved two-color laser photoionization and photoelectron study of the nickel carbide cation", *J. Chem. Phys*. **133**, 054310 (2010).
7. K.-C. Lau, Y.-C. Chang, X. Shi, and C. Y. Ng, "High-level *ab initio* predictions of the ionization energy, bond dissociation energies and heats of formations for nickel carbide (NiC) and its cation (NiC^+)", *J. Chem. Phys*. **133**, 114304 (2010).
8. C.-S. Lam, H. Wang, Y. Xu, K.-Chung Lau,[b)] and C. Y. Ng, "A Vacuum-Ultraviolet Laser Pulsed Field Ionization-Photoelectron Study of Sulfur Monoxide (SO) and its Cation (SO^+)", *J. Chem. Phys*., revised.
9. L. Yang, H. Gao, C. S. Lam, and Y. Xu, "High-resolution VUV laser photoelectron imaging and threshold photoelectron imaging methods", *Rev. Sci. Instrum.*, to be submitted.
10. H. Gao, L. Yang, and Y. Xu, "High-resolution vacuum ultraviolet laser threshold photoelectron imaging study of propargyl radical (C_3H_3)", *J. Chem. Phys.*, to be submitted.

Large Eddy Simulation of Turbulence-Chemistry Interactions in Reacting Multiphase Flows

Joseph C. Oefelein

Combustion Research Facility, Sandia National Laboratories
Livermore, CA 94551-0969 (oefelei@sandia.gov)

Program Scope

Application of the Large Eddy Simulation (LES) technique within the Diagnostics and Reacting Flows program at the CRF was initiated with two primary objectives. The first is to establish a set of high-fidelity computational benchmarks that identically match the geometry (i.e., experimental test section and burner) and operating conditions of selected experimental target flames. The second is to establish a scientific foundation for advanced model development. The goal is to provide a direct one-to-one correspondence between measured and modeled results at conditions unattainable using the Direct Numerical Simulation (DNS) technique by performing a series of detailed simulations that progressively incorporate the fully coupled dynamic behavior of reacting flows with detailed chemistry and realistic levels of turbulence. Our focal point is the series of flames that have been studied as part of the Experimental Reacting Flow Research program in collaboration with Rob Barlow and Jonathan Frank (see related abstracts). This represents a direct extension of joint activities being pursued as part of the International Workshop on Measurement and Computation of Turbulent Nonpremixed Flames organized by Barlow *et al.* (www.ca.sandia.gov/TNF).

Recent Progress

Recently, our primary goals have been to: 1) continue to develop our theoretical-numerical capabilities in LES through application of advanced subgrid-scale (SGS) models, 2) maximize the benefits of high performance computing through close collaboration with key DOE Office of Science computational facilities, and 3) continue to establish key links between DOE basic and applied research programs. All of the cases considered involve direct coupling with key target experiments and the common objective of establishing a one-to-one correspondence with these experiments while adhering to the strictest accuracy requirements for LES. These requirements include treatment of complex geometries, use of clean numerics with non-dissipative spatial stencils and no artificial dissipation terms, high-quality grids, and science-based SGS models that are designed specifically for high-resolution applications.

Over the past several years we have been successful in linking our LES activities under the BES program to various applied programs, both within the DOE and elsewhere. Figure 1 shows an example of the synergy established with the DOE Advanced Engine Combustion program. This program is funded by the Office of Vehicle Technologies (OVT), with emphasis placed on development of high-pressure, low-temperature combustion concepts for internal combustion engines. A subset of turbulent flames being studied as part of the BES program are shown on the left. A subset of experiments associated with the Advanced Engine Combustion program are shown on the right. Objectives and milestones for both projects are aimed at establishing high-fidelity computational benchmarks that identically match the geometry and operating conditions of key target experiments using a single unified theoretical-numerical framework. The projects are complementary in that BES funded research provides the basic science foundation for advanced model

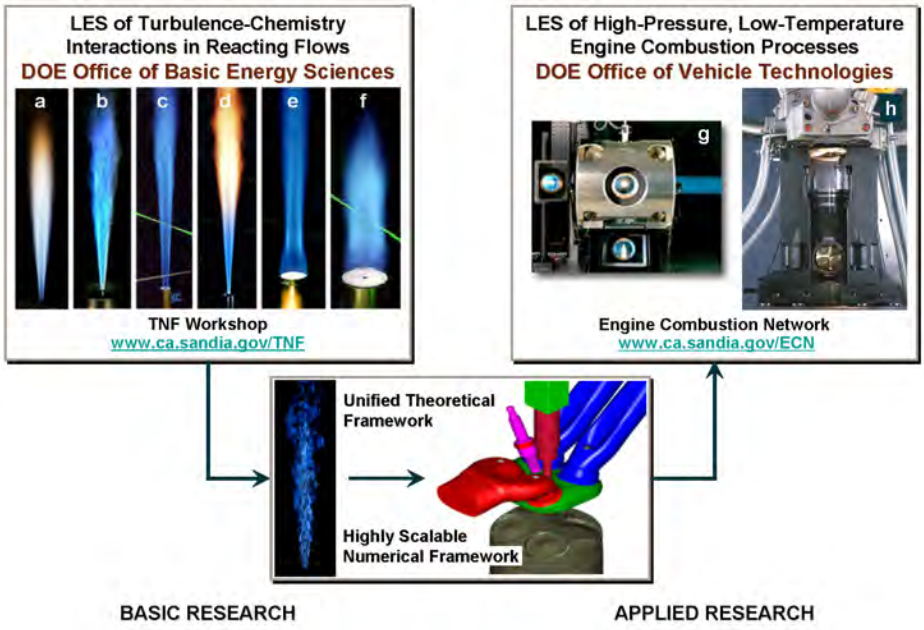

Figure 1: Advanced capabilities in LES provide a synergistic link between basic and applied research programs. A subset of turbulent flames associated with the BES Experimental Reacting Flow Research program are shown on the left (a,b: Simple jet flames, c,d: Piloted jet flames, e: Bluff-body; f: Bluff-body with swirl). A subset of experiments associated with the OVT Advanced Engine Combustion program are shown on the right (g: Constant-volume Diesel combustion facility, h: Typical single-cylinder optically accessible internal combustion engine).

development. OVT funded research provides the applied component for development of advanced engine concepts. This combination of projects directly addresses targeted research areas identified as part of the BES sponsored workshop entitled *Basic Research Needs for Clean and Efficient Combustion of 21st Century Transportation Fuels*, and more recent activities aimed at program development in *Predictive Simulations of Internal Combustion Engines* (PreSISE). Our approach applies to any propulsion and power device.

Our efforts to combine state-of-the-art LES, experiments, and High Performance Computing (HPC) over the past several years has catalyzed significant growth and collaborative opportunities. Much of this growth has been facilitated by first establishing the *Computational Combustion and Chemistry Laboratory*, and subsequently the *Combustion Research and Computational Visualization* (CRCV) facility in 2010. These dedicated resources provide a significant production level computing capability for routine calculations, and also serve as staging platforms for more efficient use of large-scale computing facilities such as the Lawrence Berkeley National Laboratory, National Energy Research Scientific Computing Center (www.nersc.gov); and the Oak Ridge National Laboratory, National Center for Computational Science (www.nccs.gov). Using these platforms in concert with grants such as the Innovative and Novel Computational Impact on Theory and Experiment (www.sc.doe.gov/ascr/INCITE) has enabled access to the full hierarchy of computing resources needed for state-of-the-art combustion simulations. From 2008 to present, the LES effort has been among the new projects awarded under the INCITE program. Our most recent grant for 2011-2013 is entitled *High-Fidelity Simulations for Advanced Engine Combustion Research.*

Using the hierarchy of HPC resources described above to its full potential requires the development of specialized massively-parallel flow solvers that can be easily ported to a variety of platforms and scale efficiently on $\mathcal{O}(10^5)$ processing cores (and beyond). From this perspective, the approach described above has been enabled through a unique theoretical-numerical framework developed over the last nineteen years called RAPTOR. Unlike conventional LES solvers, RAPTOR is a massively-parallel DNS solver that has been designed specifically for application of LES to turbulent, chemically reacting, multiphase flows in complex geometries. In the most general case it solves the fully coupled conservation equations of mass,

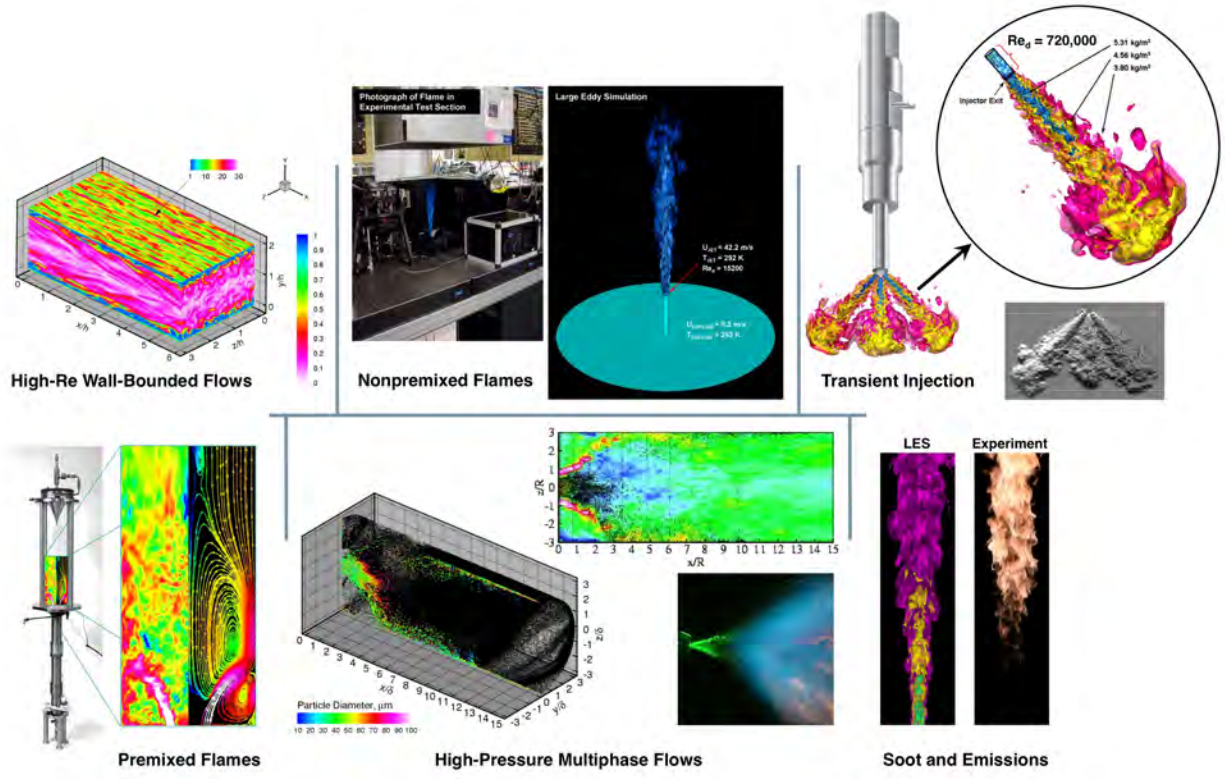

Figure 2: RAPTOR has been validated for a wide range of turbulent reacting multiphase flows.

momentum, total-energy, and species for a chemically reacting system. It also accounts for real gas/liquid phenomena, detailed thermodynamics, and detailed transport in multicomponent (or mixture averaged) systems. This framework has been optimized to provide excellent parallel scalability using a distributed multiblock domain decomposition with a generalized connectivity scheme. Distributed-memory message-passing is performed using MPI and the Single-Program–Multiple-Data (SPMD) model. It accommodates complex geometries and time varying meshes while maintaining the high accuracy attributes of structured spatial stencils. The numerical framework has been ported to a variety of major platforms and provides highly efficient coarse- and fine-grain (i.e., weak and strong) scalability attributes. Over the current period, we continue to perform a combination of validation and performance studies to anchor the accuracy and computational efficiency of the code. A set of sample results are shown in Fig. 2.

In 2009, RAPTOR was selected as one of the application codes to be evaluated under the DOE Office of Advanced Scientific Computing Research (ASCR) annual *Joule Metric on Computational Effectiveness*. A key element of this program was to evaluate the existing baseline performance of the code and demonstrate that it could scale linearly on DOE capability-class computers. To achieve this goal, a series of weak scaling studies were performed to demonstrate the combined computational effectiveness of the ORNL NCCS Cray-XT platform (Jaguar) and RAPTOR. The first step toward measuring the performance was defining a realistic model problem that was representative of actual production simulations. For this study we chose the turbulent nonpremixed $CH_4/H_2/N_2$ jet flame known as the DLR-A configuration. A photograph of this flame is shown in Fig. 1b, and also in Fig. 2 at center with a corresponding LES solution. Using this configuration, we successfully demonstrated that the code scaled linearly well beyond 100,000 processor cores for extremely fine-grain problems. Collaborative activities such as this have now anchored RAPTOR as a capability-class flow solver and set the stage for future improvements that coincide with the evolution of HPC hardware. Details related to this activity can be found in a recent report by Kothe *et al*.

Future Work

Using the framework described above, we continue to investigate several new modeling approaches. One employs a stochastic reconstruction methodology that treats detailed chemistry directly within the LES formalism. This model is science-based in that it facilitates direct treatment of turbulence-chemistry interactions and multiple-scalar mixing in a manner consistent with the application of DNS. Others employ tabulated combustion closures based on either the Linear Eddy Model or flamelet concept. With this, it is clear that quality assessment and uncertainty quantification techniques for LES must be further developed to make meaningful progress in model development. Addressing these issues will be a priority in future studies.

BES Sponsored Publications (2009–Present)

1. J. C. Oefelein and G. Lacaze. Low temperature injection dynamics and turbulent flame structure in high-pressure supercritical flows. *Proceedings of the 23rd International Colloquium on the Dynamics of Explosions and Reactive Systems*, July 24-29 2011. Irvine, California.
2. R. N. Dahms, L. M. Pickett, and J. C. Oefelein. A dense fluid approximation for the simulation of diesel fuel injection processes. *Proceedings of the 23rd Annual Conference on Liquid Atomization and Spray Systems*, May 15-18 2011. Ventura, California.
3. B. Hu, M. P. Musculus, and J. C. Oefelein. Large eddy simulation of scalar mixing and entrainment during the decelerating phase of a transient turbulent jet. *Physics of Fluids*, 2011. Submitted.
4. G. Lacaze and J. C. Oefelein. A tabulated chemistry model for turbulent nonpremixed flames at high-pressure supercritical conditions. *Combustion and Flame*, 2011. Submitted.
5. A. M. Kempf, B. J. Geurts, and J. C. Oefelein. Error analysis of large eddy simulation of the turbulent non-premixed Sydney bluff-body flame. *Combustion and Flame*, 2011. Submitted.
6. J. H. Frank, S. A. Kaiser, and J. C. Oefelein. Analysis of scalar mixing dynamics in LES using high-resolution imaging of laser Rayleigh scattering in turbulent non-reacting jets and non-premixed jet flames. *Proceedings of the Combustion Institute*, 33:1373–1381, 2011.
7. V. Sick, D. Reuss, C. Rutland, D. Haworth, J. Oefelein, J. Janicka, T.-W. Kuo, X. Yang, and M. Freitag. A common engine platform for LES development and validation. *IFP Workshop on Large Eddy Simulation for Internal Combustion Flows*, November 18-19 2010. Ruell-Malmaison, France.
8. C. R. Shaddix, J. Zhang, R. W. Schefer, J. J. Doom, J. C. Oefelein, S. Kook, L. M. Pickett, and H. Wang. Understanding and predicting soot generation in turbulent nonpremixed jet flames. Technical Report SAND2010-7178, Sandia National Laboratories, 2010.
9. J. C. Oefelein. A staggered dual-time all-Mach-number algorithm for LES of reacting flows. *CERFACS Colloquium on Multiphysics and Unsteady Simulations for Aeronautical Flows*, September 27-29 2010. Toulouse, France.
10. B. Hu, M. P. Musculus, and J. C. Oefelein. Large eddy simulation of a transient gas jet with emphasis on entrainment during deceleration. *SAE World Congress, Paper 2010-01-1133*, April 13-15 2010. Detroit, Michigan.
11. D. Kothe, K. Roche, R. Kendall, M. Adams, S. Ahern, C.-S. Chang, H. Childs, E. D'Azevedo, K. Evans, T. Evans, J. Hack, S. Klasky, S.-H. Ku, J. Oefelein, D. Pugmire, J. Rosinski, R. Sankaran, and P. Worley. FY 2009 Annual report of joule software metric SC GG 3.1/2.5.2, improve computational science capabilities. Technical Report ORNL/TM-2009/322, Oak Ridge National Laboratory, December 2009.
12. J. C. Oefelein and R. Sankaran. Large eddy simulation of turbulence-chemistry interactions in reacting flows: Experiences on the ORNL NCCS Cray-XT platforms (Jaguar). *Proceedings of the 21st International Conference on Parallel Computational Fluid Dynamics*, May 18-22 2009. Moffett Field, California.
13. J. C. Oefelein, J. H. Chen, and R. Sankaran. High-fidelity simulations for clean and efficient combustion of alternative fuels. *Journal of Physics*, 180:1–5, 2009. DOI 10.1088/1742-6596/180/1/012033.
14. J. H. Frank, S. A. Kaiser, and J. C. Oefelein. Coupling imaging measurements and LES of dissipation structures in turbulent nonreacting jets and nonpremixed jet flames. *Proceedings of the 6th Joint Meeting of the US Sections of the Combustion Institute, Paper 32D1*, May 17-20 2009. Ann Arbor, Michigan.
15. J. H. Frank, S. A. Kaiser, and J. C. Oefelein. Coupling imaging diagnostics and large eddy simulation in turbulent nonreacting jets and nonpremixed jet flames. *Proceedings of the 4th European Combustion Meeting*, April 14-17 2009. Vienna, Austria.
16. V. Sankaran, T. G. Drozda, and J. C. Oefelein. A tabulated closure for turbulent nonpremixed combustion based on the linear eddy model. *Proceedings of the Combustion Institute*, 32:1571–1578, 2009.

KINETICS AND DYNAMICS OF COMBUSTION CHEMISTRY

David L. Osborn
Combustion Research Facility, Mail Stop 9055
Sandia National Laboratories
Livermore, CA 94551-0969
Telephone: (925) 294-4622
Email: dlosbor@sandia.gov

PROGRAM SCOPE

The goal of this program is to elucidate mechanisms of elementary combustion reactions through the use of multiplexed optical spectroscopy and mass spectrometry. We developed a technique known as time-resolved multiplexed photoionization mass spectrometry (MPIMS), which is used to sensitively and selectively probe unimolecular and bimolecular reactions. This work is in collaboration with Craig Taatjes and many scientists from other institutions in the US and abroad. The Sandia-designed MPIMS instrument utilizes tunable vacuum ultraviolet light from the Advanced Light Source synchrotron at Lawrence Berkeley National Laboratory for sensitive, isomer-specific ionization of reactant and product molecules in chemical reactions.

As a complementary approach, we utilize time-resolved Fourier transform spectroscopy (TR-FTS) to probe multiple reactants and products with broad spectral coverage (> 1000 cm^{-1}), moderate spectral resolution (0.1 cm^{-1}), and a wide range of temporal resolution (ns – ms). The inherently multiplexed nature of TR-FTS makes it possible to simultaneously measure product branching ratios, internal energy distributions, energy transfer, and spectroscopy of radical intermediates. Together with total rate coefficients, this additional information provides further constraints upon and insights into the potential energy surfaces that control chemical reactivity. Because of its broadband nature, the TR-FTS technique provides a global view of chemical reactions and energy transfer processes that would be difficult to achieve with narrow-band, laser-based detection techniques.

RECENT PROGRESS

Isomer-resolved mass spectrometry

The multiplexed chemical kinetics photoionization mass spectrometer operates both at Sandia National Laboratories (using a discharge lamp to create VUV radiation), and at the Chemical Dynamics Beamline of the Advanced Light Source (ALS) synchrotron of LBNL. The chemical reactor is based on the Gutman design,[1] which allows the study of photodissociation and bimolecular reactions at pressures of 1 – 10 Torr and temperatures of 300 – 1000 K.

While the study of chemical kinetics using PIMS is well-established, this apparatus has two unique features that make it especially powerful for chemical kinetics. First, the widely tunable, intense VUV radiation from the ALS enables isomer-specific ionization of product species. As an example, we have studied the isomer-resolved products of the CN radical with benzene and toluene, measuring the branching ratios of the product isomers.

The second unique feature is the high repetition rate mass spectrometer that allows us to take snapshots of the complete chemical composition in our reactor as a function of time. Leveraging designs from the analytical chemistry community, we have built an orthogonal acceleration time-of-flight mass spectrometer (OA-TOF), compatible with continuous ionization sources. Although the OA-TOF approach does not have 100% duty cycle, the duty cycle is as high as possible for a time-of-flight system, operating at a repetition rate of 50 kHz. In return, mass resolution of $m/\Delta m \sim 1600$ has been achieved using a simple linear (i.e., not reflectron) approach. This mass resolution has already been used to separate $HCCO^+$ from $C_3H_5^+$ (both nominally mass 41) and will be increasingly valuable in separating other $O \leftrightarrow CH_4$ substitutions in larger hydrocarbons (e.g., acetone vs. butane, ketene vs. propene) in the chemistry of hydrocarbon oxidation. The increase in mass resolution by more than a factor of 10 compared to our original design has been accompanied with greater reliability and increased sensitivity (due to the lack of beam-defining slits in OA-TOF).

The $C_5H_5 + C_5H_5$ self reaction

The cyclopentadienyl radical (*c*-C_5H_5) is an exceptionally stable, resonance stabilized free radical that has been implicated in molecular weight growth chemistry as a potential route, via its self reaction, to the 2-ring aromatic compound naphthalene ($C_{10}H_8$). Melius and coworkers[2] proposed the so-called spiran mechanism for this transformation, which was investigated more recently by Kislov and Mebel,[3] who also propose pathways to two other $C_{10}H_8$ isomers: azulene 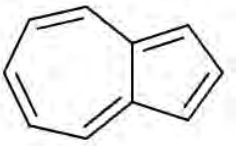 and fulvalene 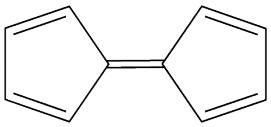

When two cyclopentadienyl radicals combine, the initial adduct is almost certainly the formation of a fairly weak C-C bond (~ 52 kcal/mol) between the two five member rings to form 9,10-dihydrofulvalene (DHF). This weakness of this bond arises because the resonance stabilization in both *c*-C_5H_5 reactants is lost when DHF is formed. We have studied the recombination of cyclopentadienyl radicals at a total density of 1.3×10^{17} molecules cm^{-3} over a temperature range of 300 – 800K. At all temperatures we observe strong signals from $C_{10}H_{10}$, but the photoionization efficiency curve of this mass cannot be explained by considering only the initial adduct, DHF. It appears there is substantial isomerization of the intial adduct, even at 300K, via H atom migration, to form other isomers of $C_{10}H_{10}$.

We also observe $C_{10}H_9$ and $C_{10}H_8$ species, but these signals are more than an order of magnitude weaker than $C_{10}H_{10}$ at low temperature. The concentration of the intermediate $C_{10}H_9$ increases substantially from 500K to 800K, and again appears to comprise multiple isomers. $C_{10}H_8$ is observed, but is a very small signal even at 800K.

It has also been suggested[4] that the formation of naphthalene and indene (C_9H_8) in cyclopentadiene pyrolysis results from the reaction of cyclopentadienyl radical with cyclopentadiene

$$c\text{-}C_5H_5 + c\text{-}C_5H_6 \rightarrow C_{10}H_{11} \rightarrow \text{products}$$

The cyclopentadienyl radical self reaction has no entrance barrier, whereas the c-C_5H_5 + c-C_5H_6 reaction has an 8.2 kcal/mol entrance barrier.[5] Therefore, at least at low temperatures, the radical + closed shell reaction should be strongly disfavored, allowing the study of c-C_5H_5 + c-C_5H_5. Even at the highest temperature of this preliminary study, we see no evidence of the $C_{10}H_{11}$ species that would be indicative of the radical + closed-shell reaction.

The CH_3 + c-C_5H_5 reaction

Because of the high concentration of methyl radicals in rich flames, the reaction

$$CH_3 + c\text{-}C_5H_5 \rightarrow C_6H_8 \rightarrow C_6H_7 + H \rightarrow C_6H_6 + H_2$$

has also been proposed as a ring expansion pathway leading to benzene.[6,7] Most recently, Sharma and Green have done a detailed theoretical study of the rate coefficiencts and product yields for this reaction.[8] Their calculations (at 900K and above) show that the product yield is dominated by formation of the methyl-cyclopentadienyl radical (c-C_5H_4-CH_3) + H.

Our initial data on this reaction spans the temperature range from 300 – 1000 K. We photolyze CH_3I and c-C_5H_6 at 248 nm to produce the two radicals, with an excess of methyl radicals. Although there is only one initial C_6H_8 adduct that can be formed (methyl cyclopentadiene), the barriers to 1,2 and 1,3 H atom shifts around the ring are calculated to be well below reactants, and the ionization energies of the three distinct isomers so formed are sufficiently separated that we should be able to resolved these species. Our preliminary results are consistent with extensive isomerization of the initial adduct essentially independent of temperature, based on the PIE curves of C_6H_8. These findings are consistent with the predictions of Sharma and Green, who find this equilibration to be fast at temperatures as low as 900K. Our results suggest this equilibration is rapid even at 300K.

Future Directions

Using TR-FTS, we will continue to investigate photodissociation reactions that show evidence for roaming dynamics. Following on the recent work of Suits and coworkers[9] on acetone photodissociation, we plan to study production of C_2H_6 in this system.

A new modification of the MPIMS apparatus is the creation of a low temperature flow tube accessing the temperature range 230 – 300 K. This improvement will allow us to access a much broader range of reciprocal temperature space, providing more stringent tests of global mechanisms in combustion reactions.

BES-sponsored publications, 2009 – present

1) "Near-threshold H/D exchange in CD_3CHO photodissociation," B. R. Heazlewood, A. T. Maccarone, D. U. Andrews, D. L. Osborn, L. B. Harding, S. J. Klippenstein, M. J. T. Jordan, and S. H. Kable, Nature Chemistry (2011) *accepted for publication*
2) "Infrared emission following photolysis of methylisothiocyanate and methylthiocyanate," E. A. Wade, J. L. Pore, and D. L. Osborn, J. Phys. Chem. A (2011) *accepted for publication*
3) "Reactions of the CN radical with benzene and toluene: product detection and low temperature kinetics," A. J. Trevitt, F. Goulay, C. A. Taatjes, D. L. Osborn, and S. R. Leone, J. Phys. Chem. A **114**, 1749 (2010).
4) "Reaction of the C_2H radical with 1-butyne (C_4H_6): Low temperature kinetics and isomer-specific product detection," S. Soorkia, A. J. Trevitt, T. M. Selby, D. L. Osborn, C. A. Taajtes, K. R. Wilson, and S. R. Leone, J. Phys. Chem. A **114**, 3340 (2010).
5) "Products of the benzene + $O(^3P)$ reaction," C. A. Taatjes, D. L. Osborn, T. M. Selby, G. Meloni, A. J. Trevitt, E. Epifanovsky, A. Krylov, B. Sirjean, E. Dames, and H. Wang, J. Phys. Chem. A **114**, 3355 (2010).
6) "Direct detection of pyridine formation by the reaction of CH (CD) with pyrrole: a ring expansion reaction," S. Soorkia, C. A. Taatjes, D. L. Osborn, T. M. Selby, A. J. Trevitt, K. R. Wilson, and S. R. Leone, Phys. Chem. Chem. Phys. (accepted, 2010).
7) "Isomer-selective study of the OH initiated oxidation of isoprene in the presence of O_2 and NO: I. The minor inner OH-addition channel" E. E Greenwald, B. Ghosh, K. C. Anderson, K. S. Dooley, P. Zou, T. M. Selby, D. L. Osborn, G. Meloni, C. A. Taatjes, F. Goulay, and S. W. North, J. Phys. Chem. A **114**, 904 (2009).
8) "Cyclic versus linear isomers produced by reaction of the methylidyne radical (CH) with small unsaturated hydrocarbons" F. Goulay, A. J. Trevitt, G. Meloni, T. M. Selby, D. L. Osborn, C. A. Taatjes, L. Vereecken, and S. R. Leone, Journal of the American Chemical Society **131**, 993 (2009).
9) "Temperature-Dependent Kinetics of the Vinyl Radical (C_2H_3) Self-Reaction," H. Ismail, P. Abel, W. Green, A. Fahr, L Jusinski, A. Knepp, J. Zádor, G. Meloni, T. M. Selby, D. L. Osborn, C. A. Taatjes, Journal of Physical Chemistry A **113**, 1278 (2009).
10) "Isomer-specific product detection of CN radical reactions with ethene and propene by tunable VUV photoionization mass spectrometry," A. J. Trevitt, F. Goulay, G. Meloni, D. L. Osborn, C. A. Taatjes, and S. R. Leone, International Journal of Mass Spectrometry **208**, 113 (2009).

References

[1] I. R. Slagle and D. Gutman, *J. Am. Chem. Soc.* **107**, 5342 (1985).
[2] C. F. Melius, M. E. Colvin, N. M. Marinov, W. J. Pitz, and S. M. Senkan, Proc. Int. Symp. Combust. **26**, 685 (1996).
[3] V. V. Kislov and A. M. Mebel, J. Phys. Chem. A. **111**, 9532 (2007).
[4] D. Wang, A. Violi, D. H. Kim, and J. A. Mullholland, J. Phys. Chem. A **110**, 4719 (2006).
[5] V. V. Kislov and A. M. Mebel, J. Phys. Chem. A **112**, 700 (2008).
[6] A. Lamprecth, B. Atakan, and K. Kohse-Hoinghaus, *Proc. Combust Inst.* **28**, 1817 (2000)
[7] A. Lifshitz, C. Tamburu, A. Suslensky, and F. Dubnikova, *Proc. Combust. Inst.* **30**, 1039 (2005).
[8] S. Sharma and W. H. Green, *J. Phys. Chem. A* **113**, 8871 (2009).
[9] V. Goncharov, N. Herath, and A. G. Suits, *J. Phys. Chem. A* **112**, 9423 (2008).

Theoretical Studies of the Combustion Reactions of Asphaltene Model Compounds

Carol A. Parish
Department of Chemistry, University of Richmond
Richmond, VA 23173
cparish@richmond.edu

I. Program Scope

We seek to utilize theoretical methods to understand the gas phase structures and energies of the combustion and pyrolysis reactions of the molecular constituents of asphaltenes contained in oil sand and oil shale. Asphaltenes represent an untapped source of hydrocarbon fuels in North America; however, information about the molecular nature of these deposits has only recently become available.[1] Theoretical and experimental evidence suggests that asphaltenes are composed of molecules that contain 4-10 fused ring cores, with alkyl chain arms extending from the core. Sulfur and nitrogen may also be present.[2] Very little is known about the reaction pathways of these heteroaromatic species.

II. Summary of Recent Accomplishments related to the project

A. Pyrolysis Mechanism of Thiophene and Methylthiophene in Asphaltenes

The pyrolysis mechanisms of thiophene in asphaltenes have been investigated theoretically using density functional and *ab initio* quantum chemical techniques. All of the possible reaction pathways were explored using B3LYP, MP2 and CBS-QB3 models. A comparison of the calculated heats of reaction with the available experimental values indicates that the CBS-QB3 level of theory is quantitatively reliable for calculating the energetic reaction paths of the title reactions. The pyrolysis process is initiated via four different types of hydrogen migrations. According to the reaction barrier heights, the dominant 1,2-H shift mechanism involves two competitive product channels, namely, C_2H_2 + CH_2CS and CS + CH_3CCH. The minor channels include the formation of CS + CH_2CCH_2, H_2S + C_4H_2, HCS + CH_2CCH, CS + CH_2CHCH, H + C_4H_3S and HS + C_4H_3. The methyl substitution effect was investigated with the pyrolysis of 2-methylthiophene and 3-methylthiophene. The energetics of such systems were very similar to that for unsubstituted thiophene, suggesting that thiophene alkylation may not play a significant role in the pyrolysis of asphaltene compounds.

B. Mechanistic Study of the 2-Thienylmethyl + HO_2 radical reaction

The *ab initio* potential energy surface for the reaction of the 2-thienylmethyl radical with the HO_2 radical has been presented. Sixteen product channels were explored via either addition/elimination or direct hydrogen abstraction mechanisms. The association paths of the two radical reactants are barrierless with the formation of three adducts, as distinguished by the radical centers of the 2-thienylmethyl radical. The addition is exothermic by 37 ~ 55 kcal mol^{-1} and these excess energies are available to promote further decomposition or rearrangement of the adducts, leading to nascent products such as H, OH, H_2O, CH_2O. The formation of OH via a simple OO bond fission might be the dominant channel in view of the barrier heights and exothermicities. Moreover, direct hydrogen abstraction may take place on

both the singlet and triplet surfaces, forming molecular oxygen. The barrier for singlet abstraction is around 10 kcal/mol while that for triplet is essentially zero with respect to the initial reactants. The mechanisms are compared to the analogous 2-furanylmethyl + HO_2 reaction and the benzyl + HO_2 reaction.

III. Future Work

Work is currently underway to characterize the singlet and triplet combustion surfaces of methyl thiophene reaction with triplet oxygen; in particular we are investigating a hydrogen abstraction and ring opening pathway. We are also pursuing a complete characterization of the singlet and triplet surfaces of the electrocyclization reaction of (Z)-hexa-1,3,5-triene leading to *p*-benzyne and the excited states of 2,5 didehydrothiopehene.

IV. References

1. Mullins, O. C.; Sheu, E. Y.; Hammami, A.; Marshall, A. G. Asphaltenes, Heavy Oils and Petroleomics; Springer: New York, 2007.
2. Ruiz-Morales, Y.; Wu, X.; Mullins, O. C. *Energy and Fuels* **2007**, *21*, 944-952.

V. Recent publications and journal articles (undergraduate co-authors underlined).

1. "Pyrolysis Mechanisms of Thiophene and Methylthiophene in Asphaltenes," Xinli Song and Carol Parish,* *Journal of Physical Chemistry A* **2011**, *115*, 2882-2891.
2. "Oligonucleotide Incorporation and Base Pair Stability of 9-deaza-2'-deoxyguanosine," Michelle L. Hamm*, Anna J. Parker, Jennifer L. Carman, Tyler W. E. Steele, and Carol A. Parish,* *Journal of Organic Chemistry* **2010**, *75*, 5661-5669.

The Dynamics of Large-Amplitude Motion in Energized Molecules

David S. Perry, Principal Investigator
Department of Chemistry, The University of Akron
Akron OH 44325-3601
DPerry@UAkron.edu

I. Program Scope

Chemical reactions, by definition, involve large-amplitude nuclear motion along the reaction coordinate that serves to distinguish reactants from products. Some reactions, such as roaming reactions and reactions proceeding through a loose transition state, involve more than one large-amplitude degree of freedom. In principle, the exact quantum nuclear dynamics may be calculated, but such calculations are limited by practical considerations to a few degrees of freedom. Thus in systems larger than 3 or 4 atoms, one must define the active degrees of freedom and separate them in some way from the other degrees of freedom. In this project, we use large-amplitude motion in bound systems as a model of reaction coordinates to investigate the coupling of large-amplitude degrees of freedom to other nuclear degrees of freedom. This allows us to use the precision and power of high-resolution molecular spectroscopy to probe the specific coupling mechanisms involved, and to explore the limits of approximate means of separating the degrees of freedom, such as the adiabatic approximation. In addition to cavity ringdown experiments and calculations at the University of Akron, experimental work on this project involves collaboration with Brooks Pate's group at the University of Virginia (CCPT-FTMW-IR). A collaboration with Michel Herman of the Université Libre de Bruxelles probes the rotationally dependent vibrational dynamics of acetylene.

II. Recent Progress

II.1. Spectroscopy and Intramolecular Coupling in the CH Stretch Region of Methanol

Infrared spectra of jet-cooled CH_3OD and CH_3OH in the OD and CH stretch regions [4, 5, 6] are observed by coherence-converted population transfer Fourier transform microwave-infrared (CCPT-FTMW-IR) spectroscopy (E torsional species only) and by slit-jet single resonance spectroscopy (both A and E torsional species, CH_3OH only). The analysis of ν_3 symmetric CH stretch region (2750 -2900 cm^{-1}) [5] is now extended to higher frequency (2900-3020 cm^{-1}) [6].

The overall observed spectra contain 17 interacting vibrational bands for CH_3OD and 28 for CH_3OH. The sign and magnitude of the torsional tunneling splittings are deduced for three CH stretch fundamentals (ν_2, ν_3, ν_9) of both molecules and are compared to a model calculation and to *ab initio* theory. The number and distribution of observed vibrational bands indicate that the CH stretch bright states couple first to doorway states that are binary combinations of bending modes. In the parts of the spectrum where doorway states are present, the observed density of coupled states is comparable to the total density of vibrational states in the molecule, but where there are no doorway states, only the CH stretch fundamentals are observed.

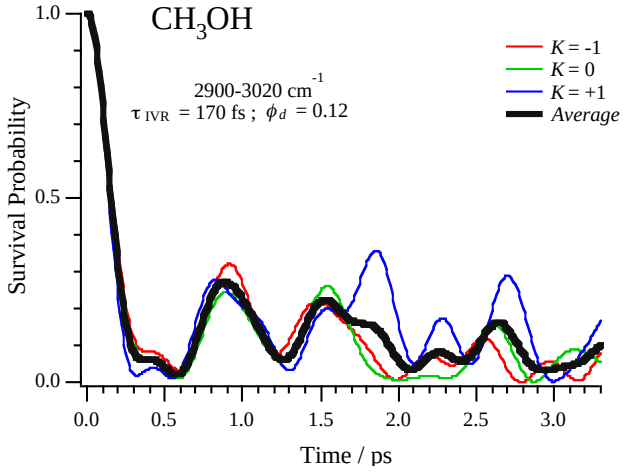

Fig. 1. Computed survival probability of the bright state following a coherent excitation of the indicated section of CH_3OH spectrum.

A time-dependent interpretation of the present FTMW-IR spectra (Fig. 1) indicates a fast (~200 fs) initial decay of the bright state followed by a second, slower redistribution (about 1 to 3 ps). A third timescale, beyond the range of the time axis in Fig. 1, is evident in slower (10 - 12 ps) recurrences that decay over several 10's of ps. The qualitative agreement of the two fastest timescales with the time-dependent experiments of Iwaki and Dlott provides further support for the similarity of the fastest vibrational relaxation processes in the liquid and gas phases. At long times (> 5 ps), the processes in the two phases necessarily differ because of energy transfer to solvent molecules in the liquid phase.

II.2. Two-Dimensional Large-Amplitude Motion

The two-dimensional torsion-inversion potential energy surfaces of methylamine, protonated methanol, and ethyl radical have been investigated with partially optimized *ab initio* calculations [2]. All three molecules belong to the G_{12} molecular symmetry group and each has six equivalent minima. CH_3NH_2 has a high barrier to inversion (~1950 cm^{-1}), whereas in $CH_3OH_2^+$ the barrier is lower (~875 cm^{-1}). In $CH_3CH_2^{\cdot}$, there is no barrier to inversion. The torsional barriers in these systems are about 704, 400, and 21 cm^{-1} respectively. The computed torsion-inversion surfaces were fit to a function of the form (Fig. 2),

$$V(\alpha,\tau) = \sum_{n=0}^{4}\sum_{m=0}^{12} V_{m,3n}\tau^m \cos(3n\alpha), \quad (1)$$

where α, is the torsional angle, τ is the inversion angle, and $m+n$ = even. Even though the three surfaces are quite different (Fig. 2(a)), we find that the torsion-inversion coupling is similar in strength (Fig. 2(b)). The dominant torsion-inversion coupling term in all three cases has the form, $V_{1,3}\tau\cos 3\alpha$, with $V_{1,3}$ in the range 280 to 450 cm^{-1}.

The 2-dimensional quantum torsion-inversion dynamics were solved for these three systems using a Hamiltonian based on these *ab initio* surfaces and including the dependence of the reduced masses on the inversion coordinates. The manifolds of torsion-inversion energy levels are compared to the available experimental and theoretical data. The patterns of the tunneling splitings vary systematically as the inversion and torsional barriers go from low to high in the sequence, $CH_3CH_2^{\bullet}$, $CH_3OH_2^+$ and CH_3NH_2.

The synthesis these results, together with previous work on methanol, nitromethane, and hydrogen peroxide [1], indicates that the coupling terms, whether torsion-vibration or torsion-inversion, have typical values that vary by less than a factor of two in a range of systems where the barriers to torsion or inversion vary by orders of magnitude.

Methylamine is the focus of our experimental effort on these six-well G_{12} systems. Results to date include high-resolution slit-jet spectra of the ν_{11} asymmetric CH stretch (2965-3005 cm^{-1}) and the first FTMW-IR spectra in the ν_3 symmetric CH stretch

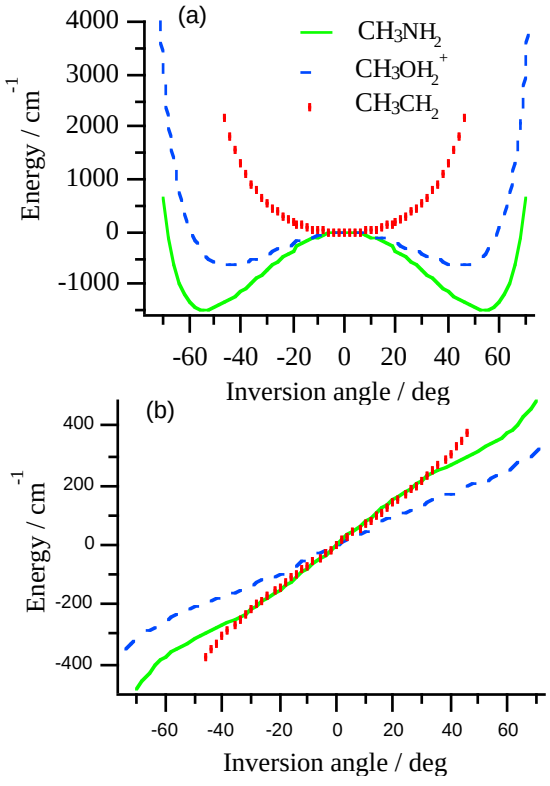

Fig. 2. *Ab initio* results at the CCSD(T)/6-311++G(3df,2p)//MP2/6-311++G(3df,2p) level on three CH_3XH_2 molecules. (a) The torsionally invariant part ($V_{m,0}$ terms) of the fitted potentials. (b) The cos3α part of the torsion-inversion coupling ($V_{m,3}$ terms).

region (Fig. 2). Whereas there is a single vibrational band in the ν_{11} region, Fig. 3 shows four distinct vibrational bands in the ν_3 region. This behavior is qualitatively similar to what we have observed in methanol (Section II.1. above). The extra bands in the ν_3 region likely result from interactions with bending combinations that serve as IVR "doorway" states. The pattern of the torsion and inversion tunneling splittings in the ν_{11} band is qialitatively different from the ground state and contains information about the coupling the upper state vibrations to the large-amplitude degrees of freedom.

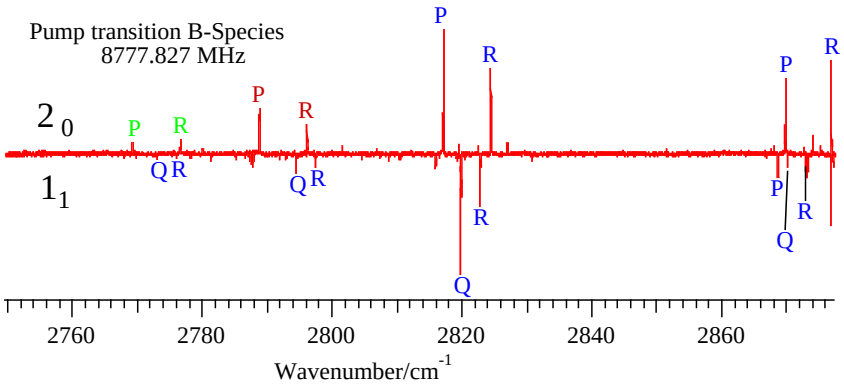

Fig. 3. Rotationally selected infrared spectrum of methylamine obtained at the University of Virginia with the coherence-converted population transfer Fourier transform microwave infrared technique (CCPT-FTMW-IR or FTMW-IR). The selected rotational states are $J_K = 2_0$ and 1_1 for the upward and downward pointing lines respectively.

II.3. Rotational Dependence of the Intramolecular Dynamics in Acetylene

The rotation-vibration Hamiltonian of acetylene is known in detail up to 13,000 cm^{-1} in the electronic ground state and allows the calculation of time-dependent dynamics for postulated excitations of certain bright states [3]. The spectroscopic Hamiltonian, derived by Michel Herman's group, includes four types of off-diagonal interactions: vibrational *l*-resonances, rotational *l*-resonances, anharmonic coupling, and Coriolis coupling. At high energies, hundreds of states may be coupled in each polyad and the rate and extent of intramolecular vibrational redistribution (IVR) increases substantially with rotational excitation. As each coupling mechanism becomes active, a hierarchical, sequential flow of probability through the different regions of phase space occurs on timescales ranging from 20 fs to 10 ps. As the energy is increased from one polyad to the next, the dynamics of similar bright states are similar; however, the dynamics depend critically on the nature of the bright state excited within a given polyad. The rotationally-mediated dynamics of the local CH stretch, the local bender and counter-rotator bright states are qualitatively similar to their normal mode counterparts.

Three different measures of phase space exploration are examined including the participation number, Gruebele's dispersion, and the Shannon entropy. The timescales for phase space exploration span the range from 20 fs to 10 ps. The volume of phase space explored by the dynamics increases with energy and the rotational quantum number, *J*, reaching about 90% of the (GOE) statistical limit at 12,000 cm^{-1} and $J = 100$. At low and intermediate *J*, the extent of phase space exploration is reduced for the local bender and counter-rotator bright

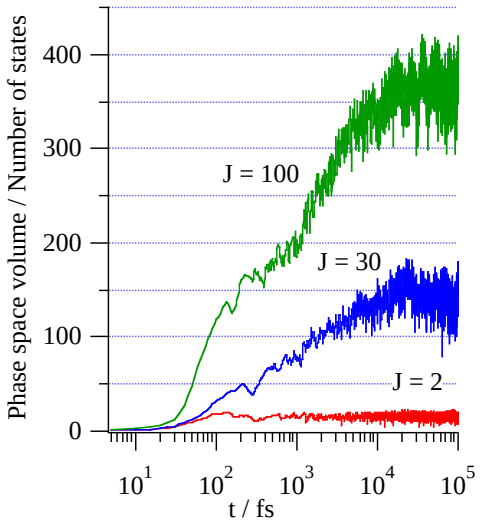

Fig. 4. Calculated volume of phase space explored for acetylene as a function of time following a coherent excitation of the bending vibration $\{v_4, v_5\} = \{14, 2\}$ at a total energy near 10,000 cm^{-1}.

states as compared to their normal mode counterparts. However, the phase space exploration of the local mode CH stretch state is similar to that of the corresponding normal mode vibration. These calculations shed light on the applicability of the energy randomization assumption that is at the heart of the Rice-Rampsberger-Kassel-Marcus (RRKM) theory of unimolecular reactions.

III. Future Plans

The CCPT-FTMW-IR experiments at the University of Virginia will focus on the CH stretch region of CH_3NH_2, with possible extensions to the NH stretches and torsional combinations. A high frequency microwave capability is being developed to access the R(0) lines of CH_3OH and CH_3NH_2 (44 – 49 GHz region), which will allow access to different nuclear spin species. The quantum nuclear dynamics calculations on $CH_3CH_2^{\bullet}$, $CH_3OH_2^+$ and CH_3NH_2 will be extended to 5 dimensions include the three CH stretches. The acetylene work will be written for publication.

IV. Publications from this Project, 2009-2011

[1] David S. Perry, The Adiabatic Approximation as a Diagnostic Tool for Torsion-Vibration Dynamics, *J. Mol. Spectrosc*. **257**(1), 1-10, 2009 (feature article), http://dx.doi.org/10.1016/j.jms.2009.05.002.

[2] Ram S Bhatta, Amy Gao, David S Perry, A comparative ab initio study of torsion-inversion coupling in CH_3NH_2, $CH_3OH_2^+$ and CH_3CH_2, *J. Mol. Struct.: THEOCHEM*, **941**, 22-29, 2009, http://dx.doi.org/10.1016/j.theochem.2009.10.033.

[3] David Perry, Anthony Miller, B. Amyay, A. Fayt and M. Herman, Vibration–rotation alchemy in acetylene ($^{12}C_2H_2$), X $^1\Sigma_g^+$ at low vibrational excitation: From high resolution spectroscopy to fast intramolecular dynamics (invited article), *Mol. Phys*. **108**, 1115-1132, 2010, http://dx.doi.org/10.1080/00268971003660874.

[4] Sylvestre Twagirayezu; David S. Perry, PhD; Justin L Neill; Matt T Muckle, Coherence-converted population transfer FTMW-IR double resonance spectroscopy of CH_3OD in the OD -stretch region, *J. Mol. Spectrosc*., **262**, 65-68 (2010), http://dx.doi.org/10.1016/j.jms.2010.05.003.

[5] Sylvestre Twagirayezu, Trocia N. Clasp, David S. Perry, Justin L. Neill, Matt T. Muckle, Brooks H. Pate, Vibrational coupling pathways in methanol as revealed by coherence-converted population transfer FTMW-IR double resonance spectroscopy, *J. Phys. Chem. A*, **114**, 6818-6828 (2010), http://dx.doi.org/10.1021/jp1019735.

[6] Sylvestre Twagirayezu, David S. Perry, Justin L. Neill, Matt T. Muckle, Brooks H. Pate, Coherence-converted population transfer FTMW-IR double resonance spectroscopy of CH_3OD in the asymmetric CH-Stretch Region, Sylvestre Twagirayezu, David S. Perry, Justin L. Neill, Matt T. Muckle, Brooks H. Pate, Bull. Am. Phys. Soc., Mar. 2010, P27.3, http://meetings.aps.org/link/BAPS.2010.MAR.P27.3.

New Single- and Multi-Reference Coupled-Cluster Methods for High Accuracy Calculations of Ground and Excited States

Piotr Piecuch
Department of Chemistry, Michigan State University
East Lansing, MI 48824
piecuch@chemistry.msu.edu

I. Program Scope

This research program focuses on the development and applications of new generations of *ab initio* electronic structure methods and computer codes, exploiting the exponential coupled-cluster (CC) wave function ansatz, which can provide an accurate description of chemical reaction pathways, radicals, biradicals, potential energy surfaces (PESs), properties other than energy, and electronic excitations in molecular species. The goal is to design and apply affordable computational methods that enable precise modeling of molecular processes and properties relevant to combustion, catalysis, light harvesting, photochemistry, and photobiology. Among the most promising methods developed in this program are (i) the renormalized CC and equation-of-motion CC (EOMCC) approaches, and the low-order scaling, local correlation extensions of the conventional and renormalized CC methods to larger molecular systems involving hundreds of correlated electrons, (ii) the active-space CC and EOMCC methods, and (iii) the genuine multi-reference CC (MRCC) theories. The main focus is on methods that can balance high accuracy with the relative ease of use and relatively low computer costs compared to other quantum-chemistry approaches that aim at similar accuracies, so that one can study chemical processes and phenomena involving complex molecular problems with dozens or hundreds of non-hydrogen atoms, in addition to the more traditional smaller systems. The renormalized CC methods and their open-shell, local correlation, and excited-state generalizations extend the standard single-reference theories to multi-reference situations created by radicals, biradicals, bond breaking, and two-electron excitations with an ease of a black-box calculation that can be performed by non-experts. The active-space CC and EOMCC approaches, and their open-shell generalizations via the electron attached (EA) and ionized (IP) theories as well as the genuine MRCC methods have the flexibility that enables accurate *ab initio* calculations for all kinds of closed- and open-shell electronic states, with manageable computer costs, including systems characterized by strong electronic near-degeneracies that cannot be handled by single-reference approaches. All methods pursued in this program can effectively utilize modern multi-node computer architectures and are well suited for pursuing novel coding strategies, such as the automated and parallel computer implementations. They address two main challenges of electronic structure theory, which are (i) the development of practical and systematically improvable computational schemes that can provide a balanced and accurate description of closed- and open-shell systems, and the rapidly changing electron correlation effects along reaction coordinates and in electronic excitations, and (ii) the development of algorithms that can reduce prohibitive costs of traditional high-accuracy *ab initio* calculations by orders of magnitude by directly attacking the scaling laws that define the dependence of computer costs on the system size. Methods developed in this program are shared with the community by incorporating them in the GAMESS package.

II. Recent Progress (2009-2011)

We have extended the left-eigenstate, completely renormalized (CR) CC method with singles, doubles, and non-iterative triples [CR-CC(2,3)] to excited states of open-shell systems [6] (see [16] for an overview). The resulting CR-EOMCC(2,3) approach [6] and its rigorously size-intensive modification, termed δ-CR-EOMCC(2,3) [15,17], correct the EOMCCSD energies for the effect of triple excitations using the non-iterative N^7 steps similar to those used in CCSD(T) and CR-CC(2,3), offering great improvements in the EOMCCSD results [4,6,13,15,17]. The CR-EOMCC(2,3) and δ-CR-EOMCC(2,3) codes, using the computationally efficient expressions from [6], have been incorporated in the GAMESS package as a standard option (CCTYP=CR-EOML). The open-shell CR-EOMCC(2,3) approach utilizing the ROHF reference provides great improvements in the EOMCCSD results for doublet and quartet states of radicals and other open-shell species, particularly for the excited states dominated

by two-electron processes, where errors in the excitation energies obtained with EOMCCSD often exceed 1 eV, as shown for CH, CNC, C_2N, N_3, and NCO [4,6]. The same applies to other applications of the CR-EOMCC(2,3) theory, including the low-lying singlet and triplet states of biradical species, such as methylene, where the CR-EOMCC(2,3) results for the adiabatic excitation and total energies extrapolated to the complete basis set limit, including states dominated by two-electron transitions, are in perfect agreement with the converged Quantum Monte Carlo and the available experimental data, eliminating, in particular, large errors in the EOMCCSD results [13]. We have continued applying the CR-CC/EOMCC methods to important chemical and spectroscopic problems [3,4,6,10,12,13,15,17]. In addition to the above examples, the CR-CC(2,3)+Q method was used to provide the new best estimates of the stationary point energetics for the cycloadditions of ozone to ethyne and ethane [3]. We also used the size-intensive δ-CR-EOMCC(2,3) approach to examine the small shifts in the $\pi\rightarrow\pi^*$ excitation energy of the cis-7-hydroxyquinoline (cis-7HQ) chromophore induced by hydrogen bonding with small molecules, on the order of 500-2000 cm^{-1}, along with the corresponding excitation energies, on the order of 30,000 cm^{-1}, obtained in the frozen-density embedding theory (FDET) and supermolecular time-dependent density functional theory (TDDFT) calculations, and in experiment [15,17]. By considering eight complexes of cis-7HQ with up to three small hydrogen-bonded molecules, we demonstrated that the spectral shifts resulting from the FDET calculations employing nonrelaxed environment densities and their δ-CR-EOMCC(2,3) counterparts are in excellent agreement with one another and experiment (to within 100 cm^{-1} or 15 % on average), whereas the analogous shifts obtained in the supermolecular TDDFT calculations do not agree with the δ-CR-EOMCC(2,3) data, producing large errors (39% on average). The δ-CR-EOMCC(2,3) excitation energies match the experimental ones to within a few hundred cm^{-1}. We used the δ-CR-EOMCC(2,3) results as a way to benchmark FDET and supermolecular TDDFT, and to examine formal and practical problems facing DFT-based methods.

We have developed the local correlation CCSD, CCSD(T), and CR-CC(2,3) approaches, and their multi-level extensions, which enable one to combine different CC or CC and non-CC (e.g., MP2) approaches, and which exist under the common term of 'cluster-in-molecule' (CIM) methods [1,8-11]. The resulting CIM-CCSD, CIM-CCSD(T), and CIM-CR-CC(2,3) methods, and their CIM-MP*n* analogs use orthonormal localized orbitals and enable high-accuracy calculations for systems with hundreds of correlated electrons and thousands of basis functions. Our CIM-CC and CIM-MP2 codes [1,8-11], which we have incorporated in the GAMESS package (the official release expected within the next few months), are characterized by the linear scaling of the CPU time with the system size when a single-level CIM-CC or CIM-MP2 approach is used, memory requirements that do not grow with the size of the system, coarse-grain parallelism, which can be further enhanced by the fine-grain parallelism of each CIM subsystem calculation, and the purely non-iterative character of the local triples and other perturbative corrections to correlation energy. They enable one to mix different theory levels in a variety of different ways. One such way is to combine some affordable, relatively lower-order, canonical *ab initio* calculation, such as canonical MP2 or CCSD, with a local CIM approach to handle higher-order correlation effects, such as the triples corrections of CCSD(T) and CR-CC(2,3) [1,8,9]. Another possibility is represented by the intrinsically multi-level local correlation theories exploiting the CIM framework that combine the high-level CC methods, such as CR-CC(2,3), to treat, for example, the reactive part of a large molecular system with the lower-order *ab initio* (e.g., MP2) scheme(s) to handle the chemically inactive regions without splitting it into *ad hoc* fragments and saturating dangling bonds [10]. If the reactive region treated by CC has a fixed size and the system is grown by adding MP2 regions, the size dependence of the costs of multi-level CIM-CC/MP2 computations is close to none. By comparing the canonical and CIM-CC results for alkanes and water clusters of varying size, we demonstrated that CIM-CCSD, CIM-CCSD(T), and CIM-CR-CC(2,3) recover the corresponding CC correlation energies to within 0.1 % or so, while offering savings in the computer effort by orders of magnitude [1,8,9,11]. By examining bond breaking in alkanes and low-energy structures of the $(H_2O)_n$ clusters, we showed that the CIM-CC methods accurately reproduce the relative energetics of the canonical CC calculations [1,8,9]. We applied CIM-CR-CC(2,3), combined with the embedded cluster QM/MM method

called SIMOMM, to the etching and diffusion of atomic oxygen on the Si(100) surface, obtaining highly accurate information about the activation barriers and energetics characterizing these processes [12]. Thanks to the use of the CIM-CC methodology, we could perform the CR-CC(2,3) calculations converged to the canonical limit via a sequence of the CIM-CR-CC(2,3) calculations with the increasingly tight criteria for the design of CIM subsystems for clusters as large as $Si_{15}H_{16}O$ [12]. The results of multi-level CIM-CC/MP2 calculations for bond breaking in large alkanes and the reactions between the bis(2,4,4-trimethylpentyl)dithiophosphinic acid and water or water dimer (important for nuclear waste management) are outstanding [10]. We have recently completed the unprecedented calculations for the Co-C bond dissociation in the Im-[Co^{III}corrin]-Me^{+} model of methylcobalamin (the B12 cofactor; 58 atoms). Our local CIM-CR-CC(2,3) method combined with canonical CCSD or MP2 allowed us to produce the entire Co-C bond breaking curve and the dissociation energy of 39-40 kcal/mol. Experiment gives 37±3 or 36±4 kcal/mol, and DFT approaches give values between 6 and 41 kcal/mol. These results will be discussed in the next annual report. We have also worked toward improvements in the CIM-CC methodology that are particularly relevant for large weakly bound molecular clusters, where the relative energies between different structures on the PES are on the order of a few kcal/mol and where one has to use basis sets with diffuse functions, obtaining excellent results [11].

We have continued our earlier work on extending the active-space CC and EOMCC theories, reviewed in [14], to ground and excited states of radicals and other valence systems by combining them with the EA/IP EOMCC methodology [4,14,18]. We demonstrated an overall excellent performance, in terms of accuracy and computational efficiency, of the active-space EA-EOMCCSD(3p2h) and IP-EOMCCSD(3h2p) approaches in calculations of the excitation energies in CH, CNC, C_2N, N_3, and NCO, where some of the low-lying excited states have a significant multi-reference character, causing problems to EOMCCSD, EA-EOMCCSD(2p1h), and IP-EOMCCSD(2h1p) [4,6,14,18]. We showed that the active-space EA/IP EOMCC schemes, which use small subsets of higher-than-2p1h and 2h1p excitations, reproduce the results of their parent methods, where all such excitations are included, while requiring a computational effort similar to CCSD. This applies to excitation energies [4,6,14,18] and ground- and excited-state geometries [18]. Some of the results are puzzling though and require further study. For example, although the full and active space EA-EOMCCSD(3p-2h) calculations for the CNC and C_2N molecules greatly improve the EA-EOMCCSD(2p-1h) excitation energies, some differences with experiment remain in spite of the use of complete basis set extrapolations, indicating that either one needs 4p-3h excitations or that the experimental data are uncertain [18]. The EA-EOMCCSD(2p1h), IP-EOMCCSD(2h1p), and full and active-space EA-EOMCCSD(3p2h) and IP-EOMCCSD(3h2p) codes have been incorporated in the official GAMESS distribution (CCTYP=EA-EOM2, EA-EOM3A, IP-EOM2, IP-EOM3A). We also applied the method of moments of CC equations to the generalized MRCC formalism representing the continuous transition between the state-specific Brillouin-Wigner-type and state-universal Rayleigh-Schrödinger-type MRCC theories, and derived the novel formula for the non-iterative corrections to the corresponding MRCC energies that recover the exact energies in the general model space case [5]. As in the past, we continued applying the CC methods to nuclei [2,7].

III. Immediate Future Plans (2011/2012)

- Work on the open-shell extensions of the local single- and multi-level CIM-CC approaches.
- Development of the PES extrapolation procedure based on the concept of correlation energy scaling that uses lower-order methods to calculate correlation energy scaling factors for high-level calculations.
- Development of the active-space doubly electron attached (DEA) and ionized (DIP) EOMCC methods.
- Development of a new hybrid CC scheme combining the active-space CC methods to describe the non-dynamic and most of the dynamic electron correlation effects with the CR-CC approaches to describe missing correlations. The preliminary results for the PESs along bond breaking coordinates, based on combining the active-space CCSDt approach with CR-CC(2,3), are highly promising, providing the agreement with full CCSDT on the order of tiny fractions of a millihartree.
- New studies of radical and biradical reactions, and molecular electronic spectra. The systems being studied right now are the elusive $HOOO \rightarrow O_2$+OH reaction, the electronic spectrum of azulene, where recent experiments revealed the existence of strongly correlated states that have not been seen in earlier

calculations, and the electronic excitations in the copper tetrachloride and tetrabromide dianions that require the inclusion of relativity, along with the higher-order electron correlation effects.

IV. Publications and submitted journal articles supported by this project (2009-2011)

1. W. Li, P. Piecuch, and J.R. Gour, "Local Correlation Calculations Using Standard and Renormalized Coupled-Cluster Methods," in: *Theory and Applications of Computational Chemistry - 2008*, AIP Conference Proceedings, Vol. 1102, edited by D.-Q. Wei and X.-J. Wang (American Institute of Physics, Melville, NY, 2009), pp. 68-113.
2. R. Roth, J.R. Gour, and P. Piecuch, "Ab Initio Coupled-Cluster and Configuration Interaction Calculations for ^{16}O Using V_{UCOM}," *Phys. Rev. C* **79**, 054325-1 - 054325-19 (2009).
3. Y. Zhao, O. Tishchenko, J.R. Gour, W. Li, J.J. Lutz, P. Piecuch, and D.G. Truhlar, "Thermochemical Kinetics for Multireference Systems: Addition Reactions of Ozone," *J. Phys. Chem. A* **113**, 5786-5799 (2009).
4. M. Ehara, J.R. Gour, and P. Piecuch, "Low-Lying Valence Excited States of CNC, C_2N, N_3, and NCO Studied Using the Electron-Attached and Ionized Symmetry-Adapted-Cluster Configuration-Interaction and Equation-of-Motion Coupled-Cluster Methodologies," *Mol. Phys.* **107**, 871-880 (2009).
5. J. Pittner and P. Piecuch, "Method of Moments for the Continuous Transition Between the Brillouin-Wigner-Type and Rayleigh-Schrödinger-Type Multireference Coupled Cluster Theories," *Mol. Phys.* **107**, 1209-1221 (2009).
6. P. Piecuch, J.R. Gour, and M. Włoch, "Left-Eigenstate Completely Renormalized Equation-of-Motion Coupled-Cluster Methods: Review of Key Concepts, Extension to Excited States of Open-Shell Systems, and Comparison with Electron-Attached and Ionized Approaches," *Int. J. Quantum Chem.* **109**, 3268-3304 (2009).
7. R. Roth, J.R. Gour, and P. Piecuch, "Center-of-Mass Problem in Truncated Configuration Interaction and Coupled-Cluster Calculations," *Phys. Lett. B* **679**, 334-339 (2009).
8. W. Li, J.R. Gour, P. Piecuch, and S. Li, "Local Correlation Calculations Using Standard and Renormalized Coupled-Cluster Approaches," *J. Chem. Phys.* **131**, 114109-1 - 114109-30 (2009).
9. W. Li, P. Piecuch, and J.R. Gour, "Linear Scaling Local Correlation Extensions of the Standard and Renormalized Coupled-Cluster Methods," in: *Progress in Theoretical Chemistry and Physics*, Vol. 19, edited by P. Piecuch, J. Maruani, G. Delgado-Barrio, and S. Wilson (Springer, Dordrecht, 2009), pp. 131-195.
10. W. Li and P. Piecuch, "Multi-level Extension of the Cluster-In-Molecule Local Correlation Methodology: Merging Coupled-Cluster and Møller-Plesset Perturbation Theories," *J. Phys. Chem. A* **114**, 6721-6727 (2010).
11. W. Li and P. Piecuch, "Improved Design of Orbital Domains within the Cluster-in-Molecule Local Correlation Framework: Single-Environment Cluster-in-Molecule Ansatz and its Application to Local Coupled-Cluster Approach with Singles and Doubles," *J. Phys. Chem. A* **114**, 8644-8657 (2010).
12. P. Arora, W. Li, P. Piecuch, J.W. Evans, M. Albao, and M.S. Gordon, "Diffusion of Atomic Oxygen on the Si(100) Surface," *J. Phys. Chem. C* **114**, 12649-12658 (2010).
13. J.R. Gour, P. Piecuch, and M. Włoch, "Comparison of the Completely Renormalized Equation-of-Motion Coupled-Cluster and Quantum Monte Carlo Results for the Low-Lying Electronic States of Methylene," *Mol. Phys.* **108**, 2633-2646 (2010).
14. P. Piecuch, "Active-space coupled-cluster methods," *Mol. Phys.* **108**, 2987-3015 (2010).
15. G. Fradelos, J.J. Lutz, T.A. Wesołowski, P. Piecuch, and M. Włoch, "Embedding vs Supermolecular Strategies in Evaluating the Hydrogen-Bonding-Induced Shifts of Excitation Energies," *J. Chem. Theory Comput.*, submitted (2011); in minor revision.
16. P. Piecuch, M. Włoch, J.R. Gour, W. Li, and J.J. Lutz, "Dealing with Chemical Reaction Pathways and Electronic Excitations in Molecular Systems via Renormalized and Active-Space Coupled-Cluster Methods," in: *Proceedings of the International Conference on Computational Methods in Science and Engineering 2010 (ICCMSE 2010)*, AIP Conference Proceedings, Vol. XXX, edited by T.E. Simos and G. Maroulis, (American Institute of Physics, Melville, NY, 2011), pp. XX-XXX; in press.
17. G. Fradelos, J.J. Lutz, T.A. Wesołowski, P. Piecuch, and M. Włoch, "Shifts in Excitation Energies Induced by Hydrogen Bonding: A Comparison of the Embedding and Supermolecular Time-Dependent Density Functional Theory Calculations with the Equation-of-Motion Coupled-Cluster Results," in: *Progress in Theoretical Chemistry and Physics*, Vol. XXX, edited by P.E. Hoggan, E. Brändas, J. Maruani, G. Delgado-Barrio, and P. Piecuch (Springer, Dordrecht, 2011), pp. XX-XXX.
18. J.A. Hansen, P. Piecuch, J.J. Lutz, and J.R. Gour, "Geometries and Adiabatic Excitation Energies of the Low-Lying Valence States of CNC, C_2N, N_3, and NCO Studied with the Electron-Attached and Ionized Equation-of-Motion Coupled-Cluster Methodologies," *Physica Scripta*, submitted (2011).

Kinetic Modeling of Combustion Chemistry

W.J. Pitz and C. K. Westbrook
Physical and Life Sciences Directorate
Lawrence Livermore National Laboratory
Livermore, CA 94550
pitz1@llnl.gov

I. Program Scope

We develop chemical kinetic reaction mechanisms to describe the combustion of hydrocarbon and related fuels. These mechanisms are validated through comparisons between computed and experiments in carefully controlled laboratory-scale facilities including laminar flames, shock tubes, stirred reactors and rapid compression machines, then used to understand more complex combustion phenomena in practical engines and other combustion systems. Chemical systems and fuels are chosen for analysis because they represent practical fuels used in transportation and other energy devices. We do try to anticipate kinetic modeling needs of the DOE combustion community, so other researchers can have useful reaction mechanisms to use in their programs. Our resulting kinetic mechanisms are routinely available on the LLNL web page at http://www-pls.llnl.gov/?url=science_and_technology-combustion and provide a valuable service to the combustion community.

II. Recent Progress

A. Chemical kinetic modeling of transportation primary reference fuels

Primary reference fuels (PRF) provide a convenient way to rank the autoignition properties of transportation fuels. In spark-ignition (SI) engines, the autoignition property of concern is the fuel's tendency to knock, and this is represented as an Octane Number (ON). The PRFs for ON are n-heptane and iso-octane; our group developed the most widely used kinetic models for these fuels about ten years ago, and we have carried out extended revisions and improvements of these mechanisms during the past year [9]. Recently, we published the first detailed chemical kinetic reaction mechanisms for the two PRFs for diesel combustion, n-hexadecane (n-$C_{16}H_{34}$) [2] and 2,2,4,4,6,8,8-heptamethyl nonane [3], which has the similar overall formula (i-$C_{16}H_{34}$). Validation of these kinetic models was difficult, due to a small number of available experimental studies, but the mechanisms provide results in very good agreement with those available experiments. We also used the kinetic models to address the chemical factors responsible for variations in the diesel Cetane Number (CN) which is used to rate the ignition properties of different diesel fuels [7]. In addition to providing a convenient modeling tool to study the combustion properties of the reference fuels, these models contribute a great deal towards the goal of defining surrogate fuel mixtures for studying gasoline, diesel fuel and aviation fuels.

A third major effort during the past year has been the development of a large family of detailed kinetic reaction mechanisms for the 2-methyl alkanes [12] from 2-methyl heptane (2-C_8H_{18}) through 2-methyl nonadecane (2-$C_{20}H_{42}$). These fuels provide a large fraction of the components in fuels made via the Fischer-Tropsch process, as well as a significant fraction of other transportation fuels and therefore are also valuable for building surrogate fuels.

The key to understanding, modeling and predicting the combustion of these families of fuels lies in the differences between the strength and location within each fuel molecule of primary, secondary, and tertiary C-H bonds. Also important are the relative ring strain energy barriers to RO_2 isomerization reactions within each fuel molecule, and relative addition/dissociation energies of molecular oxygen at different C atom sites.

B. Chemical kinetic modeling of biofuels

During the past two years, we have extended our kinetic modeling capabilities to model the reactions in large methyl ester fuels which are the primary components of biodiesel fuels [4,8,11]. In the United States, the most common biodiesel fuel is made from soybean oil, and in Europe most biodiesel fuel is made from canola/rapeseed oil. Both of these fuels consist almost entirely of the same five methyl esters, methyl palmitate, methyl stearate, methyl oleate, methyl linoleate and methyl linolenate.

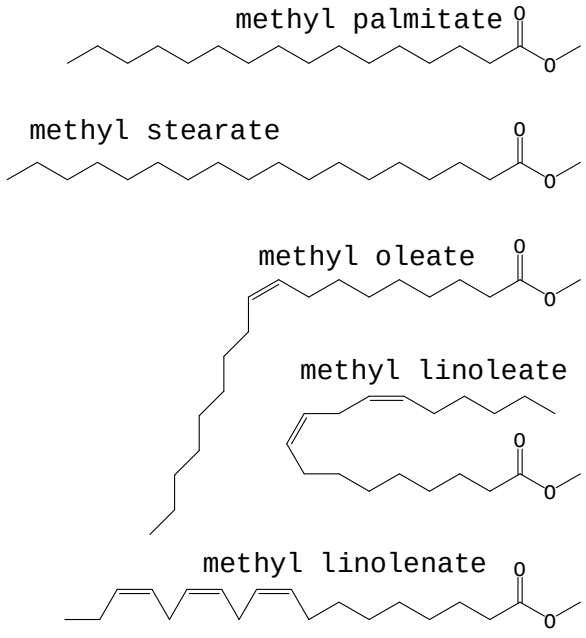

Overall, the kinetics of combustion of these large methyl esters is quite similar to that of the large n-alkanes, but modified by the presence of the methyl ester moiety at one end of the molecule. Two of these biodiesel molecules have saturated carbon chains, but the other three components have one, two or three C=C double bonds in the chain, and these provide important differences in rates of alkylperoxy radical isomerization reactions at low temperatures. In particular, we have found [10,13] that the presence of a double bond strongly inhibits RO_2 isomerization reactions across the double bond, thereby reducing the rate of low temperature fuel oxidation, with strong influences on the CN and ON observed for such fuels. The double bond provides allylic and vinylic C-H bonds in the carbon chain, in contrast with the saturated chains in n-alkanes and in methyl palmitate and methyl stearate. The allylic C-H bonds provide favored sites for H atom abstraction within the unsaturated biodiesel molecules, but the adjacent double bond makes it virtually impossible for RO_2 isomerization in the direction of the double bond. Two factors are responsible for these effects, including the fact that the O_2 bond at the allylic site is quite weak, so the RO_2 species has a short lifetime, and the enhanced electron density at the double bond also inhibits reactions over this moiety. Theoretical analysis of these problems is needed to refine our understanding of these processes. Our kinetic modeling shows how the relative amounts of low temperature reactivity of the methyl stearate, oleate, linoleate and linolenate decrease quite dramatically as C=C double bonds are added, which explains how their CN values decline from 101 to 59 to 38 to 23.

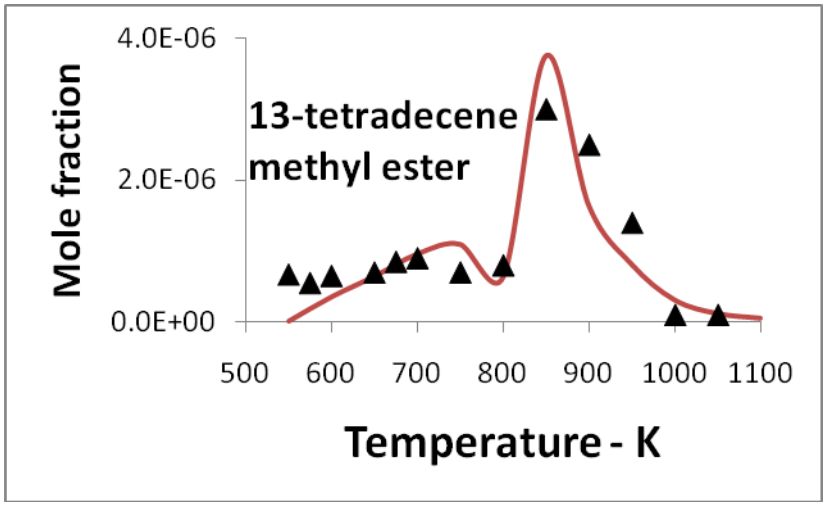

Comparison between experimental results (triangles) and computed values for an unsaturated methyl ester intermediate in JSR oxidation of methyl palmitate [11].

We are also developing kinetic models for biofuels intended to displace gasoline as fuels in spark-ignition engines. Most of these smaller fuel molecules consist of alcohols, particularly ethanol, n-butanol and iso-pentanol, and we have developed new kinetic mechanisms for all of these fuels [5]. In addition, studies of small methyl and ethyl ester fuels have been carried out in collaboration with experimental projects elsewhere [6]; this work provides an independent opportunity to explore the kinetic features of the ester moiety, somewhat independent of the alkyl chain in the molecule.

Taken as a whole, our recent work on kinetic modeling of large petrochemical fuels and biofuels combines the influences of molecular structure, differences between types of C-H bonds, and the presence of C=C double bonds to explain a considerable range of kinetic phenomena about combustion of practical fuels.

III. Future Work

The lack of an extended body of experimental validation data for both the small-molecule and large-molecule fuels for which we have built kinetic mechanisms is a serious problem. As new experiments have appeared, most recently for the large n-alkanes and large 2-methyl alkanes, our mechanisms have demonstrated remarkable agreement with the new measurements, and the minor differences have enabled us to refine our models.

In terms of fuel studies, we are working to apply the biodiesel models to a wide variety of additional fuel types. It is very interesting to note that biodiesel fuels are produced from oils of many types in addition to the most common soybeans and canola beans. These additional sources of biodiesel fuels include sunflower, safflower, olive, linseed, palm, cottonseed, and jatropha oils, as well as beef tallow and other animal fats, all of which biodiesel fuel mixtures made primarily of the same five methyl esters as soy and rapeseed biodiesel fuels. Therefore, our kinetic mechanism for the soy and rapeseed biodiesel fuels are also, without further modification, appropriate mechanisms for all these other types of biodiesel fuels, and we are carrying out computational studies of all of those biofuels. Again, the lack of careful laboratory experiments for any of these biodiesel fuels, with either integrated data such as flame speeds or ignition delay times, and especially for experiments in which species-specific data are measured, are almost entirely lacking. Even practical data, such as measured values for CN for these fuels, have unacceptably large variations and are effectively unavailable.

We are continually refining existing kinetic mechanisms, as new theoretical studies make this possible. New studies of RO_2 and O_2QOOH isomerization reactions, which we know are the keys to low temperature combustion rates and product distributions, are still now sufficiently understood, and we are

allied with other groups who are addressing these reaction pathways. Our studies of detailed oxidation of olefins have shown that reactions of alkenyl radicals, especially resonantly stabilized such radicals, are poorly understood and need attention in order for us to incorporate them reliably in kinetic mechanisms. We are also extending our applications of large molecule fuels into engine studies, carried out by collaborators who do such experiments.

IV. References and Journal articles supported by this project 2009-2011

1. M.A. Oehlschlaeger, J. Steinberg, C.K. Westbrook. and W.J. Pitz, "The Autoignition of iso-Cetane at High to Moderate Temperatures and Elevated Pressures: Shock Tube Experiments and Kinetic Modeling", Combust. Flame **156**, 2165-2172 (2009).
2. C.K. Westbrook, W.J.Pitz, O.Herbinet, H.J. Curran and E.J. Silke, "A Comprehensive Detailed Chemical Kinetic Reaction Mechanism for Combustion of n-Alkane Hydrocarbons From n-Octane to n-Hexadecane", Combust. Flame **156**, 181-199 (2009).
3. E.J. Silke, W.J. Pitz, C.K. Westbrook, M. Sjoberg and J.E. Dec, "Understanding the Chemical Effects of Increased Boost Pressure under HCCI Conditions", SAE Int. J. Fuels Lubric. **1**, 12-25 (2009).
4. O. Herbinet, W.J. Pitz, and C.K. Westbrook, "Detailed Chemical Kinetic Mechanism for the Oxidation of Biodiesel Fuels Blend Surrogate", Combust. Flame **157**, 893-908 (2010).
5. P.S. Veloo, Y.L. Wang, F.N. Egolfopoulos and C.K. Westbrook, "A comparative experimental and computational study of methanol, ethanol, and *n*-butanol flames", Combust. Flame **157**, 1989-2004 (2010).
6. K. Kohse-Hoinghaus, P. Oswald, T.A. Cool, T. Kasper, N. Hansen, F. Qi, C.K. Westbrook and P.R.Westmoreland, "Biofuel Combustion Chemistry: From Ethanol to Biodiesel", Angew. Chem. Int. Ed. **49**, 3572-3597 (2010).
7. C.K. Westbrook, W.J. Pitz, M. Mehl and H.J. Curran, "Detailed chemical kinetic reaction mechanisms for primary reference fuels for diesel cetane number and spark-ignition octane number", Proc. Combust. Inst. **33**, 185-192 (2011).
8. C.V. Naik, C.K. Westbrook, O. Herbinet, W.J. Pitz, and M. Mehl, "Detailed chemical kinetic reaction mechanism for biodiesel components methyl stearate and methyl oleate", Proc. Combust. Inst. **33**, 383-389 (2011).
9. M. Mehl, W.J. Pitz, C.K. Westbrook, and H.J. Curran, "Kinetic modeling of gasoline surrogate components and mixtures under engine conditions", Proc. Combust. Inst. **33**, 193-200 (2011).
10. M. Mehl, W.J. Pitz, C.K. Westbrook, K. Yasunaga, C. Conroy, and H.J. Curran, "Autoignition behavior of unsaturated hydrocarbons in the low and high temperature ranges", Proc. Combust. Inst. **33**, 201-208 (2011).
11. C.K. Westbrook, C.V. Naik, O.Herbinet, W.J.Pitz, M. Mehl, S.M. Sarathy and H.J. Curran, "Detailed chemical kinetic reaction mechanisms for soy and rapeseed biodiesel fuels", Combust. Flame in press (2011).
12. S.M.Sarathy, C.Yeung, C.K.Westbrook, W.J.Pitz, M.Mehl and M.J.Thomson, "An experimental and kinetic modeling study of n-octane and 2-methyl heptane in an opposed-flow diffusion flame", Combust. Flame in press (2011).
13. M.Mehl, G. Vanhove, W.J. Pitz and E. Ranzi, "Oxidation and combustion of the n-hexene isomers: A wide range kinetic modeling study", Combust. Flame 155, 756-772 (2008).
14. W. J. Pitz and C. J. Mueller, "Recent progress in the development of diesel surrogate fuels," *Progress in Energy and Combustion Science* In Press, (2010)
15. Z. Tian, W. J. Pitz, R. Fournet, P.-A. Glaude and F. Battin-Leclerc, "A detailed kinetic modeling study of toluene oxidation in a premixed laminar flame," Proceedings of the Combustion Institute, 2010, in press. DOI: 10.1016/j.proci.2010.06.063
16. S. M. Sarathy, M. J. Thomson, W. J. Pitz and T. Lu, "An Experimental and Kinetic Modeling Study of Methyl Decanoate Combustion," Proceedings of the Combustion Institute, 2010, http://dx.doi.org/10.1016/j.proci.2010.06.058.

INVESTIGATION OF NON-PREMIXED TURBULENT COMBUSTION

Grant: DE-FG02-90ER14128

Stephen B. Pope
Sibley School of Mechanical & Aerospace Engineering
Cornell University
Ithaca, NY 14853
s.b.pope@cornell.edu

1 Scope of the Research Program

The focus of the current work is on the development of computational approaches which allow our detailed knowledge of the chemical kinetics of combustion to be applied to the modeling and simulation of combustion devices. In the past year, the work has been focused on combining strategies for the accurate and efficient implementation of combustion chemistry in modeling and simulation of turbulent combustion. As described more fully in the next Section, the methodologies used are: rate-controlled constrained equilibrium (RCCE) for the dimension-reduction of the combustion chemistry; a greedy algorithm with local improvement (GALI) for the selection of "good" constrained species; and *in situ* adaptive tabulation (ISAT).

2 Recent Progress

The principal research results from this program are described in the publications listed in Section 4. The following subsections detail the progress made in the computationally-efficient implementation of combustion chemistry.

2.1 Efficient Implementation of Combustion Chemistry

Detailed mechanisms of real fuels may contain hundreds or thousands of species and thousands of reactions [1]. Incorporating such detailed chemistry in combustion calculations is prohibitive. Among the various efforts put into reducing the computational cost of representing chemistry, the three main widely used approaches include: (1) *mechanism reduction* to reduce the number of species and reactions involved [2, 3]; (2) *dimension-reduction* to represent chemistry using a reduced number of variables [4, 5]; and (3) *tabulation* to significantly reduce the cost of expensive evaluations of the reaction mappings involving ODE integrations [6]. In recent times, combined methodologies have also been developed, wherein reduced reaction mechanisms or dimension-reduction methods are used in conjunction with tabulation [7].

In this work we present results with a new combined dimension reduction (using RCCE [4]) and tabulation (using ISAT [6]) methodology. In this combined approach a specified set of represented (constrained) species is used as constraints to perform dimension-reduction. The specification of good constraints is crucial for the accuracy of dimension-reduction and we have recently developed a new automated *Greedy Algorithm with Local Improvement* (GALI) [8, 9] for selecting good represented species. In this study we present quantitative results using the combined ISAT-RCCE-GALI approach and compare its accuracy and efficiency to detailed and reduced mechanisms.

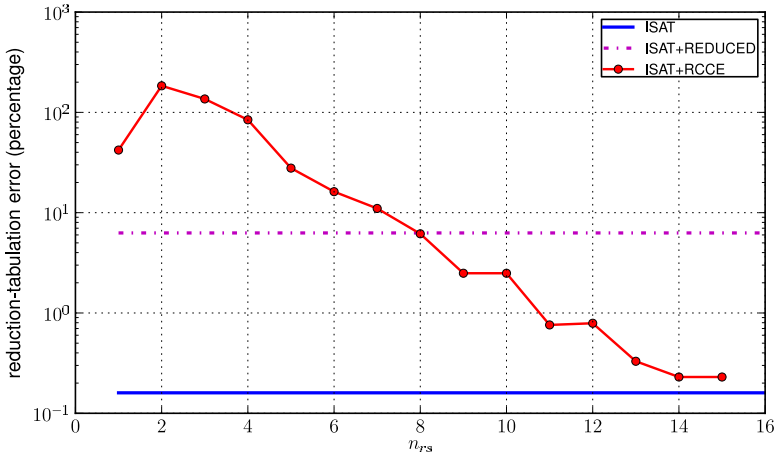

Figure 1: Error incurred using various methods of representing chemistry. The error is computed by considering 10^5 compositions and their reaction mappings (computed using ODE integration) obtained from a PaSR run involving methane/air premixed combustion with chemistry represented using the 31-species GRI-Mech 1.2 detailed mechanism.

The combined methodology has been extensively tested using the partially-stirred reactor (PaSR) for the methane/air premixed combustion. The PaSR has two inflowing streams: one premixed stream of methane/air mixture at $600\,K$ and a pilot stream of equilibrium products of the stoichiometric methane/air mixture. Other important parameters involved are: number of particles, $N_P = 100$; residence time, $\tau_{res} = 10\,ms$; mixing time, $\tau_{mix} = 1\,ms$; pairing time, $\tau_{pair} = 1\,ms$; and reaction time step, $\Delta t = 0.033\,ms$. An ISAT error tolerance of $\epsilon_{tol} = 10^{-5}$ is used.

In this study, we compare the accuracy and efficiency of the following three methodologies for representing methane chemistry:

1. ISAT: using ISAT directly to tabulate chemistry with the 31-species GRI-Mech 1.2 detailed mechanism (without any dimension reduction)
2. ISAT+REDUCED: using ISAT to tabulate chemistry with the 16-species ARM1 reduced mechanism
3. ISAT+RCCE: using the combined ISAT-RCCE reduction-tabulation algorithm with n_{rs} number of represented species selected using GALI

2.2 Results

The primary quantity of interest is the accuracy of the *reaction mapping* (i.e., the species composition after the reaction time-step Δt) obtained using the aforementioned methodologies. We compute the error involved in these three methods by considering the error in the reaction mapping obtained using these methods relative to a direct evaluation using ODE integration with the detailed mechanism. The reaction mappings obtained using an ODE integrator (we use DDASAC [10] in this work) typically involve very small errors (relative to these methods) and hence can be deemed accurate. We refer to the error involved in these methods as the *reduction-tabulation* error, which for a direct use of ISAT with a detailed mechanism reduces to simply *tabulation* error (as there is no reduction involved). The errors computed for the aforementioned three methodologies of representing chemistry are shown in Figure 1. We see that the tabulation error is about 0.1%, and the error using the reduced mechanism is about 6%. However, the combined ISAT-RCCE-GALI yields less than 6% error with just 8 species and less than 1% error with just 11 or more species.

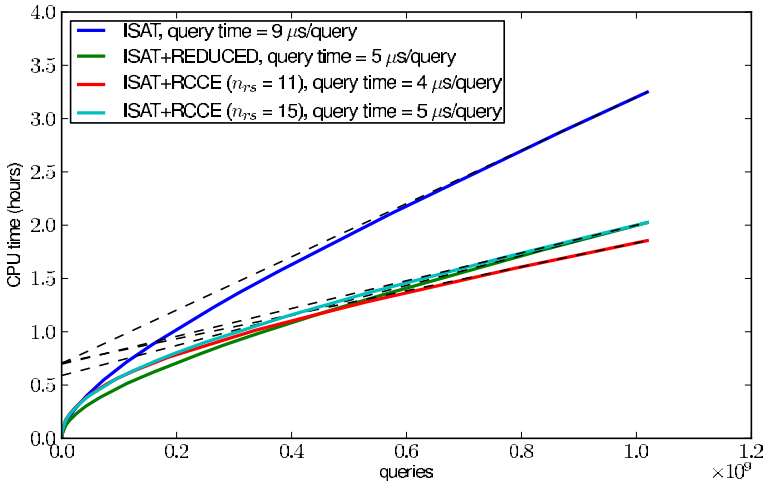

Figure 2: ISAT query time for a PaSR run (with over 10^9 queries) involving methane/air premixed combustion. The slope of the linear extrapolation (dashed-line) gives the query time and the y-intercept gives an estimate of the ISAT build time for each case. The CPU time is computed by performing (serial) runs on the TACC Ranger cluster.

We also compare the performance of ISAT within these three methods. To gauge the performance of ISAT when used with a particular method, we perform a long duration PaSR run involving over 10^9 queries and gather ISAT CPU time statistics. We then compute the following two quantities: (i) *build time*: this is the time taken to add to and to build the table. It is the total time less the time spent retrieving; and (ii) *query time*: this is the average time taken per query after the ISAT table has been fully built with very few adds or grows being performed in the table. These quantities have been computed in Figure 2, and we see that the build-time using all the three methodologies is comparable (about 1 hour), however the query time with ISAT-RCCE is only about 4 μs compared to 5 and 10 μs with the reduced and detailed mechanisms, respectively.

2.3 Conclusions

Based on the results presented here, we can conclude that the ISAT-RCCE-GALI methodology:

1. achieves the same level of accuracy as the detailed and reduced mechanisms with relatively fewer represented species;
2. is computationally efficient providing significant speedup relative to the detailed mechanism;
3. reduces the total number of scalars that need be carried in reactive flow simulations.

This combined dimension-reduction and tabulation strategy can also be used with the ICE-PIC [5] dimension-reduction method.

3 Future Plans

The focus of the work in the next year is on a new "mesh free" implementation of molecular diffusion and mixing in LES/PDF. The combination of large-eddy simulation (LES) and probability density function (PDF) methods is an attractive approach to simulating turbulent combustion: the large scales are explicitly represented in LES, and the effects of the small scales are comprehensively described by the PDF approach. Viswanathan, Wang & Pope (2010) developed a "particle/mesh" implementation of molecular diffusion and mixing, including differential diffusion. Preliminary

research suggests that a different "mesh free" implementation is possible, and that it has distinct advantages in terms of accuracy and computational efficiency. Research will be performed to develop, implement and evaluate this new implementation.

4 Publications from DOE Research 2009-2011

1. D.C. Haworth and S.B. Pope (2011) "Transported Probability Density Function and Filtered Density Function Methods," in *Turbulent Combustion Modeling: Advances, New Trends and Perspectives*, eds. T. Echekki, E. Mastorakos, Springer.

2. V. Hiremath, Z. Ren and S.B. Pope (2010) "A Greedy Algorithm for Species Selection in Dimension Reduction of Combustion Chemistry," Combustion Theory and Modelling, **14**, 619–652.

3. V. Hiremath, Z. Ren and S.B. Pope (2011) "Combined Dimension Reduction and Tabulation Strategy using ISAT-RCCE-GALI for the Efficient Implementation of Combustion Chemistry", Combustion and Flame (submitted).

4. S.B. Pope (2011) "Simple models of turbulent flows", Physics of Fluids **23**, 011301.

5. Z. Ren, G.M. Goldin, V. Hiremath and S.B. Pope (2010) "Reduced description of reactive flows with tabulated chemistry", Combustion Theory and Modelling (to be published).

6. Z. Ren and S.B. Pope (2009) "Sensitivity calculations in PDF modelling of turbulent flames," Proceedings of the Combustion Institute, **32**, 1629–1637.

7. S. Viswanathan, H. Wang and S.B. Pope (2010) "Numerical implementation of mixing and molecular transport in LES/PDF studies of turbulent reacting flows", Journal of Computational Physics, (submitted).

References

[1] C. K. Westbrook, W. J. Pitz, O. Herbinet, H. J. Curran, E. J. Silke, Combust. Flame 156 (2009) 181-199.

[2] T. Lu, C. K. Law, Proc. Combust. Inst. 30 (2005) 1333-1341.

[3] T. Nagy, T. Turanyi, Combustion and Flame 156 (2009) 417-428.

[4] J.C. Keck, Prog. Energy Combust. Sci. 16 (1990) 125-154.

[5] Z. Ren, S.B. Pope, A. Vladimirsky, J.M. Guckenheimer, J. Chem. Phys. 124 (2006) 114111.

[6] L. Lu, S.B. Pope, J. Comput. Phys. 228 (2009) 361-386.

[7] Z. Ren, V. Hiremath, S. B. Pope, 6th US National Combustion Meeting (2009).

[8] V. Hiremath, Z. Ren, S. B. Pope, Combustion Theory and Modelling 14(5) (2010) 619-652.

[9] V. Hiremath, Z. Ren, S. B. Pope, Combustion and Flame (submitted).

[10] M. Caracotsios, W. E. Stewart, Computers & Chemical Engineering 9 (1985) 359-365.

OPTICAL PROBES OF ATOMIC AND MOLECULAR DECAY PROCESSES

S.T. Pratt
Building 200, B-125
Argonne National Laboratory
9700 South Cass Avenue
Argonne, Illinois 60439
E-mail: stpratt@anl.gov

PROJECT SCOPE

Molecular photoionization and photodissociation dynamics can provide considerable insight into how energy and angular momentum flow among the electronic, vibrational, and rotational degrees of freedom in isolated, highly energized molecules. This project involves the study of these dynamics in small polyatomic molecules, with an emphasis on understanding the mechanisms of intramolecular energy flow and determining how these mechanisms influence decay rates and product branching ratios. It is also aimed at understanding how internal energy can influence photoionization cross sections and dissociative ionization processes. The experimental approach combines double-resonance laser techniques, which are used to prepare selected highly excited species, with mass spectrometry, photoion- and photoelectron-imaging, and high-resolution photoelectron spectroscopy, which are used to characterize the decay of the selected species.

RECENT PROGRESS

Photoionization studies and absolute photoionization cross sections

I am continuing to use ion imaging, vuv single-photon ionization, and resonant multiphoton ionization to probe the photodissociation dynamics of small polyatomic molecules, and to characterize the photoionization dynamics of combustion-relevant species. One aspect of this work is to determine absolute photoionization cross sections of radicals by photodissociating the appropriate precursor and photoionizing both fragment species. Knowledge of the photoionization cross section of one of the species then allows the determination of the cross section for the other. Last year, the photodissociation of acetaldehyde to CH_3 + HCO, along with the known photoionization cross section of CH_3, were used to determine the photoionization cross section of HCO, an important combustion radical. These results have now been published. As discussed last year, the very small photoionization cross section of HCO near threshold can be understood in terms of the atomic d character of the HOMO, and the non-penetrating nature of the f-wave continuum. Our analysis indicates that the cross section should increase substantially a few eV about the ionization threshold. Unfortunately, at these higher energies the dissociative ionization of HCO becomes energetically possible.

A new photoion and photoelectron imaging spectrometer was completed and tested by recording one- and two-color photoelectron spectra of atomic Xe and the van der Waals dimer, Xe_2. Two-color ionization resulting in low photoelectron energies produced very high (<5 meV) electron energy resolution almost immediately. These high resolution photoelectron spectra and angular distributions not only provided new information on the Rydberg states of Xe_2, but also resulted in a considerable refinement in the potential curve of one of the low-lying excited states of Xe_2^+. The ability to record high-resolution photoelectron spectra of Xe_2, a minor component in the molecular beam, supports the belief that photoelectron spectroscopy of cold free radicals produced in the expansion will also be possible. One of the improvements in the apparatus is that there is optical access to the molecular beam source, allowing the use of photodissociation and other techniques to produce reactive species. A second set of experiments is underway to characterize the effect of external electric fields on photoelectron imaging experiments, particularly photoelectron angular distributions. In general, photoelectron imaging experiments are performed with linearly polarized light with polarization parallel to the face of the detector and perpendicular to the time-of-flight axis. Reconstruction algorithms make use of the fact that the photoelectron angular distributions are cylindrically symmetric about the polarization axis. (Slice imaging techniques avoid this restriction, but have not yet been implemented in photoelectron imaging

owing to the very short flight times of the electrons.) In particular, most photoelectron imaging experiments to date have been performed with not insignificant electric fields used to define the potentials in the imaging lens. Because this field is perpendicular to the polarization axis, it breaks the cylindrical symmetry of the system, and could potentially compromise the reconstruction. To characterize this effect, we are performing studies of the photoionization of Xe as a function of electric field. In particular, by focusing on relatively high Rydberg states, we can characterize the angular distribution of individual Stark states and determine how they change with the magnitude of the field. Analysis of the data is currently in progress.

Femtosecond photoelectron spectroscopy
Work continued on the analysis of data from my 2008 and 2009 visits to the laboratory of Valerie Blanchet at the CNRS in Toulouse, France. This work focused on the photodissociation of methyl iodide via the B state. Our first paper on this work discussed the photoelectron spectra of the fragments, and was published in 2010. A second paper focusing on the product branching ratios was finished and submitted late in 2010. One of the most interesting results of this work is the observation of different photofragment angular distributions for the CH_3 and I fragments, providing clear evidence for significant alignment of the CH_3 product. The detailed analysis of this alignment is currently underway.

Dissociative recombination of small polyatomic ions
In collaboration with Christian Jungen, I have continued to work on theoretical models of vibrational autoionization and, in particular, dissociative recombination. Dissociative recombination involves the capture of an electron by a positive ion followed by dissociation to neutral fragments - often these fragments are atomic or molecular radicals. Dissociative recombination is important in low temperature plasmas, planetary atmospheres, astrochemistry, and diverters plasmas in tokamak reactors. It may play a role in enhancing ignition in plasma-assisted combustion, and is likely one of the initial recombination processes producing radicals during the neutralization of plasmas produced in spark ignition. Two mechanisms exist for dissociative recombination, corresponding to direct capture of an electron into a dissociative state of the neutral, and indirect capture of the electron into a temporarily bound Rydberg state, which then predissociates before re-ionization can occur. One such process involves capture into vibrationally excited Rydberg states, a process that is the reverse of vibrational autoionization. It turns out that this indirect vibrational capture mechanism is important in many hydrocarbon ions. Last year, we showed that our models for vibrational autoionization could be used to calculate the capture cross sections and rates for the dissociative recombination of H_3^+ and HCO^+. This work indicated that Jahn-Teller and Renner-Teller active vibrations were often responsible for the indirect capture mechanism. More recently, we have shown that the experimental cross section for a significant number of small molecular ions show evidence for these same mechanisms. In particular, the cross sections for many small polyatomic ions such as H_3O^+, NH_4^+, CH_3^+, and CH_5^+ show significant drops at the threshold for excitation of the fundamental of one of the vibrational levels of the ion, and this vibration is typically Renner-Teller or Jahn-Teller active. It also appears that some larger hydrocarbon ions show signs of the same kinds of processes, even though the interaction is no longer a true Jahn-Teller interaction.

Photoionization with hard x-rays
In the Fall of 2009, I participated in two sets of experiments performed during the first block of user time at the Linac Coherent Light Source at SLAC National Accelerator Laboratory, the world's first hard x-ray free-electron laser. Much of the data from these experiments was analyzed and published over the past year. The first set of experiments were led by Argonne's Atomic, Molecular, and Optical Physics Group, while the second set was led by Western Michigan University; both sets of experiments involved large collaborations involving multiple institutions, most notably Lawrence Berkeley Laboratory, Ohio State University, and Stanford University. The photon energy for these experiments was tunable between 800 and 2000 eV, and the pulse duration was tunable between 4 and 280 fs. Initial experiments were performed on atomic Ne, while subsequent experiments were performed on the molecules N_2, CO, H_2S, and SF_6. In some instances, the absorption of the first photon led to the ejection of a 1s electron, followed

by Auger decay to fill the hole - that is, the events observed with conventional x-ray sources. However, the high intensity of this source made sequential K-shell absorption quite routine. Thus, subsequent absorption of additional photons and Auger decay led to the stripping of all of the atom's or molecule's electrons. In some cases, however, two 1s electrons were ejected before Auger decay occured, resulting in "hollow" atoms or molecules. Both the photoelectrons and Auger electrons associated with these states have unique signatures. In double K-hole production in a molecule such as N_2, the second hole can either be produced on the same atom as the first hole, or on the opposite atom. This situation leads to a number of interesting issues with respect to screening of the nuclear charges, chemical shifts, etc. While definitive evidence for the double core-hole process on two sites was not found, clear evidence for the double core hole single-site process was observed. These results represent the first steps in the new world of hard x-ray FELs, and will likely have implications for single-shot diffraction and imaging studies. Owing to the novelty of this world's first x-ray FEL, these new results have already produced three significant publications.

FUTURE PLANS

We plan on continuing our studies of the photodissociation and photoionization of combustion-relevant radicals by using ion-imaging techniques, vacuum-ultraviolet single-photon ionization, and resonant multiphoton ionization techniques. We will continue to determine absolute photoionization cross sections of selected radicals. Potential targets include: the phenoxyl radical, C_6H_5O, which can be produced in conjunction with CH_3 by the photodissociation of anisole; CH_2CH_2OH, which can be produced in conjunction with I by the photodissociation of 2-iodoethanol, and vinoxy radicals, which can be produced in conjunction with CH_2CH_2OH by the photodissociation of ethylene glycol vinyl ether. Given the popularity of frequency tripling the third harmonic output of YAG lasers to produce 118 nm (10.486 eV) light, we are considering measuring a number of additional radical cross sections at this photon energy.

Photoionization cross sections of stable species are also important for quantitative studies based on photoionization mass spectrometry, and an understanding of the systematics of these cross sections is important. David Osborn has brought to our attention the extremely large photoionization cross section of 2-butyne at threshold, which is approximately 2.5 times larger than that for propyne or acetylene. This very large cross section can be understood in terms of a shape resonance that occurs at threshold in 2-butyne, but only at higher energies in propyne and acetylene. Robert Lucchese has performed theoretical calculations that show just this effect. We will use photoelectron imaging spectroscopy to characterize this shape resonance more fully. In particular, we are planning to use single-photon ionization, direct two-photon ionization, and two-color, two-photon resonant, three photon ionization to characterize the threshold region of 2-butyne. If successful, the two-color studies should allow the selection of different intermediate vibrational levels, which will in turn allow a more detailed characterization of how the shape resonance depends on the geometry of the molecule. Following these studies of 2-butyne, we will also attempt two-color studies of the C_3H_4 isomers propyne and allene, as well as of the propargyl radical. All of these systems are expected to show shape resonances relatively close to threshold.

I will continue to collaborate with Christian Jungen on theoretical models of vibrational autoionization and dissociative recombination in polyatomic molecules. In the coming year, we will begin working on extending our studies of the Jahn-Teller effect to include quadratic interactions. We will also work to apply our results to other systems such as NH_4^+ and CH_3^+.

This work was supported by the U.S. Department of Energy, Office of Science, Office of Basic Energy Sciences, Division of Chemical Sciences, Geosciences, and Biological Sciences under contract No. DE-AC02-06CH11357.

DOE-SPONSORED PUBLICATIONS SINCE 2009

1. Ch. Jungen and S. T. Pratt
JAHN-TELLER INTERACTIONS IN THE DISSOCIATIVE RECOMBINATION OF H_3^+

Phys. Rev. Lett. **102**, 023201 (2009).
2. S. T. Pratt
HIGH-RESOLUTION VALENCE-SHELL PHOTOIONIZATION
in *Handbook of High-Resolution Spectroscopies*, edited by M. Quack and F. Merkt (Wiley, New York, XXXX). (in press).
3. V. A. Shubert, M. Rednic, and S. T. Pratt
PHOTODISSOCIATION OF I-C_3H_7I WITHIN THE A BAND AND ANISOTROPY-BASED DECOMPOSITION OF THE TRANSLATIONAL ENERGY DISTRIBUTIONS
J. Chem. Phys. **130**, 134306 (2009).
4. V. A. Shubert, M. Rednic, and S. T. Pratt
PHOTODISSOCIATION OF 2-IODOETHANOL WITHIN THE A BAND
J. Phys. Chem. A **113**, 9057-9064 (2009).
5. V. A. Shubert, M. Rednic, and S. T. Pratt
PREDISSOCIATION AND DISSOCIATIVE IONIZATION OF RYDBERG STATES OF Xe_2 AND THE PHOTODISSOCIATION OF Xe_2^+
J. Chem. Phys. **132**, 124108 (2010).
6. N Thiré, R. Cireasa, V. Blanchet, and S. T. Pratt
TIME-RESOLVED PHOTOELECTRON SPECTROSCOPY OF THE CH_3I B ^{1}E 6s [2] STATE
Phys. Chem. Chem. Phys. 12, 15644-15652 (2010).
7. L. Young, E. P. Kanter, B. Krässig, Y. Li, A. M. March, S. T. Pratt, R. Santra, S. H. Southworth, N. Rohringer, L. F. DiMauro, G. Doumy, C. A. Roedig, N. Berrah, L. Fang, M. Hoener, P. H. Bucksbaum, J. P. Cryan, S. Ghimire, J. M. Glownia, D. A. Reis, J. D. Bozek, C. Bostedt, M. Messerschmidt
FEMTOSECOND ELECTRONIC DAMAGE BY ULTRAINTENSE X-RAYS
Nature **466**, 56-61 (2010).
8. V. A. Shubert and S. T. Pratt
PHOTODISSOCIATION OF ACETALDEHYDE AND THE ABSOLUTE PHOTOIONIZATION CROSS SECTION OF HCO
J. Phys. Chem. A **114**, 11238 (2010).
9. M. Hoener, L. Fang, O. Kornilov, O. Gessner, S.T. Pratt, M. Gühr, E.P. Kanter, C. Blaga, C. Bostedt, J.D. Bozek, P.H. Bucksbaum, C. Buth, M. Chen, R. Coffee, J. Cryan, L. DiMauro, M. Glownia, E. Hosler, E. Kukk, S.R. Leone, B. McFarland, M. Messerschmidt, B. Murphy, V. Petrovic, D. Rolles, and N. Berrah
ULTRA-INTENSE X-RAY INDUCED IONIZATION, DISSOCIATION, AND FRUSTRATED ABSORPTION IN MOLECULAR NITROGEN
Phys. Rev. Lett. **104**, 253002 (2010).
10. L. Fang, M. Hoener, O. Gessner, F. Tarantelli, S.T. Pratt, O. Kornilov, C. Buth, M. Gühr, E. P. Kanter, C. Bostedt, J.D. Bozek, P.H. Bucksbaum, M. Chen, R. Coffee, J. Cryan, J.M. Glownia, E. Kukk, S. R. Leone, and N. Berrah
DOUBLE CORE HOLE PRODUCTION IN N_2: BEATING THE AUGER CLOCK
Phys. Rev. Lett. **105**, 083005 (2010).
11. Ch. Jungen and S. T. Pratt
LOW-ENERGY DISSOCIATIVE RECOMBINATION IN SMALL POLYATOMIC MOLECULES
J. Chem. Phys. **133**, 214302 (2010).
12. S. T. Pratt and Ch. Jungen
DISSOCIATIVE RECOMBINATION OF SMALL POLYATOMIC MOLECULES
J. Phys. Conf. Ser. (in press).
13. V. A. Shubert and S. T. Pratt
PHOTOELECTRON IMAGING OF SEVERAL 5d AND 6p RYDBERG STATES Xe_2 AND IMPROVING THE Xe_2^+ I(1/2g) POTENTIAL
J. Chem. Phys. **134**, 044315 (2011).

Photoinitiated Reactions of Radicals and Diradicals in Molecular Beams

Hanna Reisler
Department of Chemistry, University of Southern California
Los Angeles, CA 90089-0482
reisler@usc.edu

Program Scope

Open shell species such as radicals and diradicals are central to reactive processes in combustion and environmental chemistry. Our program is concerned with photoinitiated reactions of hydroxyalkyl radicals and carbenes. The goal is to investigate the detailed dynamics of dissociation of free radicals and diradicals for which multiple pathways including molecular rearrangements compete, and compare them with high level calculations. Studies include unimolecular reactions on the ground state as well as photodissociation dynamics on excited Rydberg and valence states that involve multiple potential energy surfaces. The photodissociation of triplet methylene, the prototypical carbene, exhibits several conical intersections and the experiments will be compared with high-level electronic structure calculations. The detailed measurements on simple systems will serve as benchmarks for homologous series.

Recent Progress

1. A roaming pathway leading to unexpected water + vinyl products in CH_2CH_2OH dissociation

In our experiments on the vibrational predissociation of CD_2CD_2OH we always observed a significant ion signal from the vinyl radical, CD_2CD. As the barrier to dissociation to $CD_2CD + H_2O$ was much higher than the available energy, we collaborated with Anna Krylov and Joel Bowman in search for an explanation. Molecular dynamics calculations of the unimolecular dissociation of rovibrationally excited C_2H_4OH radicals were carried out using a full-dimensional potential energy surface (PES). Quasiclassical trajectories were initiated on the surface using microcanonical sampling at a total energy similar to that of the experiments. The trajectories revealed a roaming channel leading to the formation of water after an initially frustrated dissociation to $OH + C_2H_4$. Even though direct water production is energetically inaccessible, the roaming pathway finds a lower-energy route via frustrated dissociation to hydroxyl that makes water + vinyl production feasible. The roaming channel is minor (only a few percent) but it is robust. The mechanism of the roaming pathway is analyzed in terms of the geometrical proximity of the transition states leading to OH loss and internal abstraction, as well as the partitioning of energy among the vibrational modes in the radical and products necessary to overcome the small barrier in the $OH + C_2H_4$ reaction.

2. Slice imaging of H photofragments from CH_2OH dissociation

In order to determine rovibrational state distributions of products in photoinitiated dissociation of radicals, we replaced the existing TOF detection system in our experimental arrangement with slice imaging. In incorporating slice imaging, the primary design goal was to obtain sliced velocity map imaging (VMI) of hydrogen fragments. Because of budgetary constraints, cost-saving solutions were implemented and two of those were: (i) a custom-built 5 ns high voltage gating pulser, which made the slice imaging of hydrogen fragments possible; and (ii) a cheap, easy to use camera with sufficient resolution and sensitivity for imaging. Since slicing is achieved by fast time gating of the MCP, the ion optics must provide sufficient TOF dispersion of the ions with respect to the initial velocity component along the TOF axis. The reduction in electric fields required for dispersion sufficient for slice imaging of the light hydrogen ions leads to an increase in image size. This, in turn, requires either larger detectors,

which are expensive and more difficult to gate fast, or a reduction in the total TOF length, which reduces mass resolution. Therefore, an ion-optics system that reduces image size without increasing the voltage was designed. In addition, the imaging arrangement had to fit into our existing "radical machine" with minimal modifications and allow using our existing MCP detector (dia. ~ 40 mm).

Our design, which is based on previous ones with modifications in the ion optics, satisfies both TOF and velocity map focusing. Numerical simulations show that the achievable range of magnification with the traditional VMI ion optics is small and comes at the expense of deterioration in resolution. Therefore, an additional cylindrical einzel lens was added to the drift tube to improve control of image size, while maintaining desired *temporal* characteristics. We achieved fivefold variation in magnification with kinetic energy resolution of 0.8- 2%. With an effective gating pulse halfwidth of ~ 5 ns (convolution of ionization laser pulse, detector gating pulse, and jitters), the TOF dispersion for the maximum detectable kinetic energy should be ~ 50 ns. With our design, slicing conditions are achieved for hydrogen ions with initial kinetic energies from a fraction of an electronvolt to several electronvolts. Taking into account the size constraints of our instrument and ion-optics design parameters, the accelerator assembly was built as a stack of 14 equally spaced electrodes. Adjustment of the effective lengths of the two regions of different electric fields required for VMI is achieved by voltage division among the electrodes.

The high-voltage pulser was developed in collaboration with Dr. A. Kuthi from the Pulsed Power Laboratory at USC and NOVEM Co. The pulser is a 3-stage magnetic pulse compressor with a diode opening switch in the final stage. It is based on a simpler model described in ref. 1. The pulse has a Gaussian-like shape, a width of $\leq$ 5 ns FWHM, and an adjustable amplitude > 2 kV. The jitter is < 1 ns and the drift is ~ 1 ns during several hours of operation.

Imaging data are recorded using a 1.3 Mpix CMOS camera with FireWire interface (PixeLink PL-B741F). The camera can record up to 26 frames per second (externally triggered) with a resolution up to 1280x1024 pixels. The software we have developed includes an option of obtaining velocity resolved action spectra by scanning the laser wavelength while monitoring only fragments with selected velocities. This helps identify different precursors that can give rise to the same product.

Test results for O^+ and H^+ ions from photodissociation of O_2, HBr and H_2S were in excellent agreement with the simulations – within 1% in velocity scale. This allows us to use parameters obtained from simulations for different experiments, and choose the best operation conditions without the need for tedious experimental calibrations for each case. Our first results for CH_2OH dissociation demonstrate a better than order of magnitude improvement in sensitivity and energy resolution for H photofragments compared with the core-sampling TOF method we used before. Below we present preliminary results that demonstrate the capability of the slice imaging arrangement for our ongoing experiments.

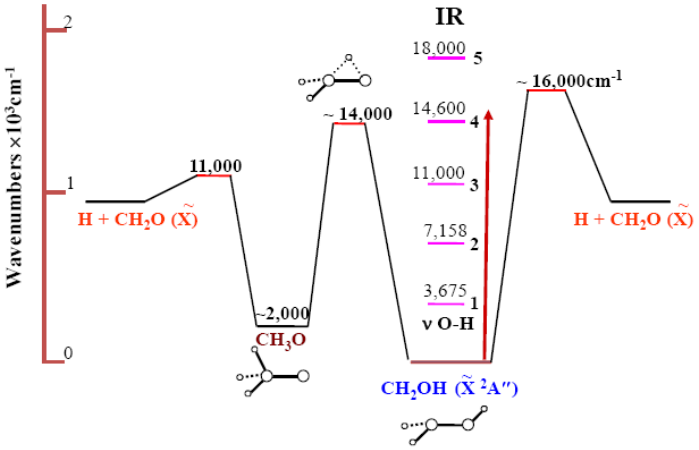

Fig. 1. Energetics of ground state dissociation and isomerization of CH_2OH. Note the lower barrier to dissociation in CH_3O than in CH_2OH and the comparable barriers to O-H bond fission and isomerization in CH_2OH.

One of the nicest results of our previous studies of CH_2OH was the observation of overtone-induced vibrational predissociation *via tunneling*.[2] What is special here is that the excited O-H stretch is the bond that breaks; i.e. overtone excitation is in the reaction coordinate. We hoped that the existence of a barrier in $CH_2OH \rightarrow CH_2O + H$ (Fig. 1) would render sufficient local-mode character to the OH vibration to enable high overtone excitation. We indeed observed the production of H atoms via tunneling upon excitation to $4\nu_{OH}$; however, we could not study the dynamics of predissociation because the H-photofragment TOF detection method did not have the resolution needed to reveal structures in the velocity distribution. As demonstrated below, it is now possible to obtain energy distributions of the CH_2O co-fragment by taking sliced images of H^+.

Our goal is to examine the role of $CH_2OH \leftrightarrow CH_3O$ isomerization in predissociation on the ground PES. As it requires less energy for CH_2OH to dissociate via the methoxy route, the isomerization barrier height and shape (calculated at ~14,000 cm^{-1} from the CH_2OH side) are of crucial importance. Although the energetically favored pathway for CH_2OH decomposition appears to be isomerization, excitation of the O-H stretch deposits the energy in the wrong coordinate.

In the first test of the new arrangement, CH_2OH was excited to the region of the $4\nu_{OH}$ overtone, and the excitation wavelength was varied while detecting H atoms (by 1+1' REMPI via the Lyman-α transition), and recording sliced images (Fig. 2). We discovered that in addition to the $4\nu_{OH}$ overtone reported previously,[2] there was a smaller feature, shifted by ~ 60 cm^{-1} to the blue, which was revealed only in the present, high S/N experiments. Our preliminary analysis suggests that the two peaks arise from an accidental resonance between the $4\nu_{OH}$ and the $3\nu_{OH}$ $+1\nu_{CH\text{-}asym}$ levels. We also obtained good velocity resolution in the sliced images of H-fragments. The resolution achieved for H slicing may not be as high as for heavier particles, which can be time-stretched to a greater extent, but it is sufficient to resolve the vibrational structure in the formaldehyde co-fragment (Fig. 2). While the largest feature corresponds, as expected, to CH_2O in the ground vibrational state, skeletal motions (but not CH stretching) are also excited. Analysis of the results is in progress, as well as experiments with CD_2OH to explore the role of isomerization.

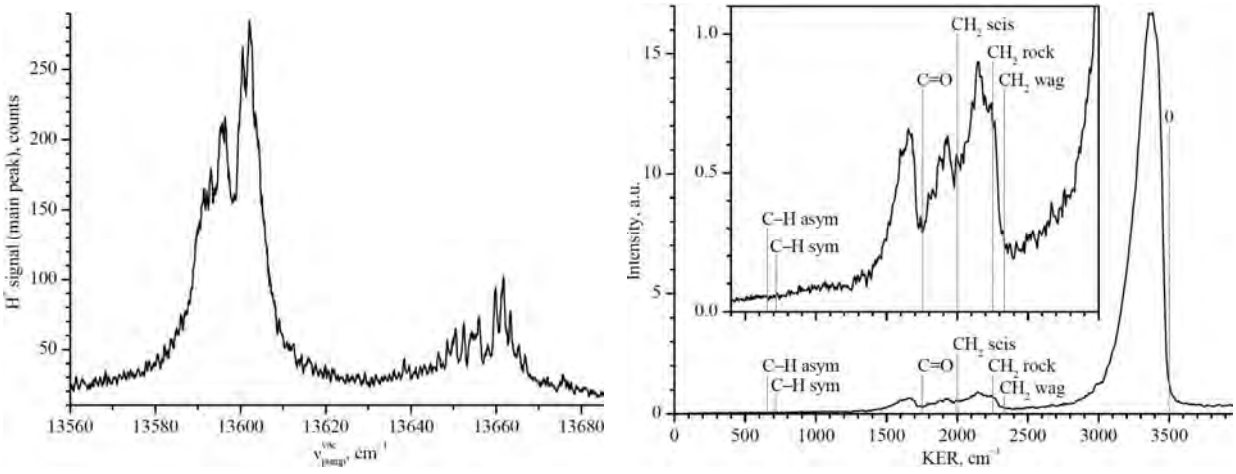

Fig. 2. (Left) H-Photofragment yield spectrum of CH_2OH recorded in the region of $4\nu_{OH}$. (Right) Kinetic energy release (KER) obtained from a sliced image of H-photofragments recorded following ~13,600 cm^{-1} excitation. The time stretching of the ion cloud was 48 ns. The inset shows an enhanced view of the low energy region, which demonstrates the good S/N and vibrational resolution in the CH_2O co-fragment. The widths of the features in the KER reflect the extent of rotational excitation in the co-fragment (~150 K).

Similarly, we achieved vibrational resolution when detecting H atoms from photodissociation of CH_2OH from the 3s Rydberg state. The preliminary results shown in Fig. 3 reveal excitation in the CO

stretch and maybe also in other skeletal modes. These results will be analyzed in terms of the conical intersections identified by Yarkony.[3]

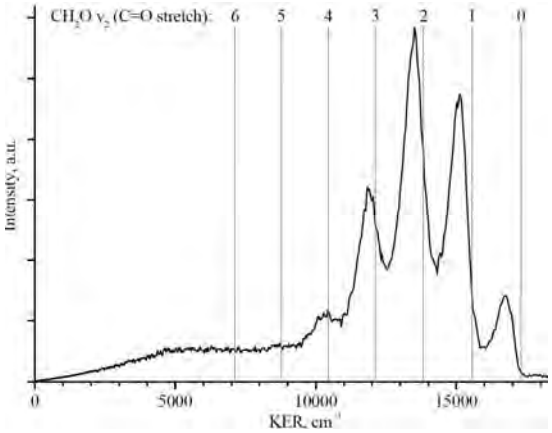

Fig. 3. Kinetic energy release in CH_2OH photodissociation from 3s obtained from a sliced-image of H photofragment with 364.7 nm excitation (unpublished). The time stretching was 47 ns. The resolution is the same as that in the traditional VMI after Abel transformation, but the noise level in the sliced image is much lower, so the feature at ~ 10,400 cm^{-1}, for example, can be clearly discerned.

References

1. A. Kuthi, P. Gabrielsson, M. R. Behrend, P. T. Vernier, M. A. Gundersen, IEEE Trans. Plasma Sci. 33: 1192-1197 (2005).

2. Wei, J., Karpichev, B., and Reisler, H., J. Chem. Phys. 125 (2006): 34303, 8 p.

3. B. C. Hoffman and D. R. Yarkony, J. Chem. Phys. 116:8300-8306 (2002); D. R. Yarkony, J. Chem. Phys. 122:084316, 1-7 (2005).

Future Work

Our next goals are to study the vibrational predissociation of CH_2OH and its deuterated isotopologs on the ground and excited states and the photodissociation of triplet methylene using REMPI and slice imaging. Methylene is being produced efficiently by pyrolysis of diazirine. We will also continue working with our theory collaborators (Krylov, Bowman) to fully characterize the potential energy surface of CH_2OH on the ground state at energies above the isomerization and dissociation barriers.

Publications, 2009-2011

1. Fedorov, I., Koziol, L., Mollner A. K., Krylov, A. I., and Reisler H, "Multiphoton ionization and dissociation of diazirine: A theoretical and experimental study" J. Phys. Chem. A 113 (2009): 7412-7421.

2. Reisler, H and Krylov, A.I. "Interacting Rydberg and valence states in radicals and molecules: Experimental and theoretical studies", Int. Rev. Phys. Chem. 28 (2009): 267-308.

3. B. Karpichev, L. Koziol, K. Diri, H. Reisler and A. I. Krylov, "Electronically excited and ionized states of the CH_2CH_2OH radical: A theoretical study", J. Chem. Phys. 132 (2010): 114308.

4. L.W. Edwards, M. Ryazanov, H. Reisler and S. J. Klippenstein, **"**D-atom products in predissociation of CD_2CD_2OH from the 202-215 nm photodissociation of 2-bromoethanol", J. Phys. Chem. A 114 (2010): 5453–5461.

5. Kamarchik, E.; Koziol, L.; Reisler, H.; Bowman, J. M.; Krylov, A. I., "Unexpected Roaming Pathway Leading to Water plus Vinyl Products in C_2H_4OH Dissociation." J. Phys. Chem. Lett. **1** (2010): 3058-3065.

Electronic Structure, Molecular Bonding and Potential Energy Surfaces

Klaus Ruedenberg
Ames Laboratory USDOE, Iowa State University, Ames, Iowa, 50011
ruedenberg@iastate.edu

Resolution of long-range contributions to the potential energy curve of chemically bonded atoms in terms of multipole, induction and dispersion interactions. An ab-initio super-molecule approach

Between atoms that form a covalent bond at short range, attractive interactions exist from the long range regime through a transition region into the short range regime, creating intricate mixtures in the transition region. We have examined this problem for the $^1\Sigma_g$ ground state of the F_2 molecule using the super-molecule approach which, in contrast to the asymptotic approach, permits a non-empirical ab-initio analysis over the full range. A physical elucidation was achieved by resolving the total potential energy curve V(R) as the sum of the curve $V_o(R)$, generated by including only non-dynamic (≡ static ≡ strong) correlations, and the additional contributions $V_{corr}(R)$ arising from the dynamic correlations:

$$V(R) = V_o(R) + V_{corr}(R)$$

For both parts of the energy, very close approximations to the complete basis set limits of the full configuration interaction were determined.

From about 4 Å on out, the *strongly correlated part* of the wave function assumes the form

$$V_o = + C_Q/R^5 + C_I/R^8, \qquad \text{with} \quad C_Q = 2.66014 \text{ au}, \qquad C_I = 9.46173 \text{ au},$$

the mean-absolute deviation between the LHS and the RHS of this equation being 1×10^{-9} hartree between 5.5 and 12Å. The value of C_Q was calculated as $6\Theta^2$, with $\Theta = 0.66585$ au being the calculated quadrupole moment of the fluorine atom. This term represents the electrostatic interaction between the quadrupoles of the two F atoms, which is repulsive because, as a consequence of the $^1\Sigma_g$ symmetry, both quadrupoles are lined up parallel to the inter-nuclear axis and hence to each other.

The coefficient C_I was obtained by a LMSQ fit of C_I/R^8 to the values $[V_o(R) - 6\Theta^2/R^5]$ between 5.6 and 12 Å. This (more than two orders of magnitude smaller) term represents the induction interaction, as shown by the following calculation. Since the electric field exerted by the quadrupole Θ of one fluorine atom on the other fluorine atom is $3\Theta/R^4$, asymptotic perturbation theory yields for the coefficient C_I the expression $2\times\frac{1}{2}\times\alpha\times(3\Theta)^2$, where α is the zz-dipole polarizability of the fluorine atom. The latter was calculated as 2.22136 au, yielding $2\times\frac{1}{2}\times\alpha\times(3\Theta)^2 = 8.8637$ au, close to the fitted value 9.46 au quoted above.

The transition of $V_o(R)$ from this *long-range repulsive electrostatic* regime to the *attractive covalent short-range* regime occurs between 4 and 3 Å. Coming from large distances, the positive V_o curve reaches a maximum at about 3 Å, descending at shorter distances and turning from positive to negative at about 2.5Å as the covalent forces take over due to increasing atomic orbital overlap.

From about 4.6 Å on out, the *dynamic correlation* contribution to the potential energy curve assumes the form

$$V_{corr} = -C_6/R^6 - C_8/R^8, \quad \text{with} \quad C_6 = 8.954 \text{ au}, \quad C_8 = 146.018 \text{ au}$$

the mean-absolute deviation between the LHS and the RHS of this equation being 3×10^{-9} hartree between 5.5 and 12Å. The coefficients C_6 and C_8 were obtained by LMSQ fitting of $R^6V_{corr}(R)$ to R^{-2}. Independent recent asymptotic calculations of these dispersion coefficients by other authors with different methods gave values between 8.4 and 9.5 au for C_6, and 146.8 to 150.7 au for C_8. It is therefore apparent that, in the long-range region, $V_{corr}(R)$ becomes the dispersion interaction. It may be noted that the $(1/R^8)$ term of the dispersion energy is 15 times stronger than the $(1/R^8)$ term arising from the induction.

At large distances the quadrupole-quadrupole repulsion $[\sim1/R^5]$ prevails over the dispersion attraction $[\sim(1/R^6)]$. Towards shorter distances, the dynamic correlation becomes stronger while the non-dynamic repulsion becomes weaker (see above) so that at about 3.5Å the dynamic correlation prevails, turning the total potential energy curve V(R) from being repulsive to being attractive. The total potential energy curve has therefore a maximum (a "bump") of about 4×10^{-8} hartree at about 4 Å.

From 2.5Å towards shorter distances the non-dynamic curve is attractive as well, as mentioned above, but the dynamic correlation contribution steadily increases relative to the non-dynamic correlation contribution until, at the equilibrium distance (1.41Å), about 32 mh of the total binding energy of 62 mh arise from the dynamic correlations whereas the strongly correlated part of the wave function contributes only 30 mh, even though the covalent overlap forces dominate the strongly correlated part at this point.

This first super-molecule analysis shows that it is possible to resolve the transition to the long-range potential energy curve in terms of the various discussed contributions without any semi-empirical terms, such as damping factors. However, it should be noted that, since the non-dynamic $V_o(R)$ curve dissociates into the *SCF wave functions of the atoms, with the pz orbital being non-equivalent to the px and py orbitals, it is this atomic wave function* that must be used in the calculation of the quadrupole moment and the polarizability of the atom in order to obtain values that yield the correct fit to the super-molecule ab-initio curve. This is in contrast to the conventional asymptotic approaches where the atomic multipole moments and polarizabilities are attributed to atomic wave functions that include dynamical correlations. An analysis of this difference in interpretation may yield some insight.

The actual physical potential energy curve suffers from a further complication. From about 3 Å on outward, several Π states lie *below* the discussed $^1\Sigma_g^+$ state because, in contrast to the latter, they have *attractive quadrupole interactions* in the $V_o(R)$ term. The resulting curve crossings presumably entail non-adiabatic interactions for the nuclear motions, complicating the spectroscopic deduction of the dissociation energy.

Publications in 2008, 2009, 2010

Intrinsic Local Constituents of Molecular Electronic Wave Functions. I. Exact Representation of the Density Matrix through Chemically Deformed and Oriented Atomic Minimal Basis Orbitals.

J. Ivanic, G. J. Atchity and K. Ruedenberg,

Theor. Chem. 120, 281-294 (2008).

Intrinsic Local Constituents of Molecular Electronic Wave Functions. II. Electronic Structure Analyses in terms of Intrinsic Oriented Quasi-Atomic Molecular Orbitals for the Molecules FOOH, $H_2BH_2BH_2$, H_2CO and the Isomerization HNO $\rightarrow$ NOH.

J. Ivanic and K. Ruedenberg,
Theor. Chem. Acc, 120, 295-305 (2008).

Correlation Energy and Dispersion Interaction in the Ab Initio Potential Energy Curve of the Neon Dimer.

Laimutis Bytautas and Klaus Ruedenberg
J. Chem. Phys., 128, 214308, 1-12 (2008).

A-Priori Identification of Configurational Deadwood.

Laimutis Bytautas and Klaus Ruedenberg
Chem. Phys., 356, 64-75 (2009)

Physical Understanding through Variational Reasoning: Electron Sharing and Covalent Bonding.

K. Ruedenberg and M.W. Schmidt,
J. Phys. Chem., 113, 1954-1968 (2009)

Ab Initio Potential Energy Curve of F_2. IV. Transition from the Covalent to the van der Waals Regime. Competition between Multipolar and Correlation Forces.

L. Bytautas and K. Ruedenberg,
J. Chem. Phys., 130, 204101, 1-14 (2009)

Accurate ab initio potential energy curve of O_2. I. Non-relativistic full CI valence correlation by the CEEIS method.

L. Bytautas and K. Ruedenberg,
J. Chem. Phys. 132, 074109, 1-10 (2010)

Accurate ab initio potential energy curve of O_2. II. Core-valence correlations, relativistic contributions and vibration-rotation spectrum.

L. Bytautas, N. Matsunaga , K. Ruedenberg,
J. Chem. Phys. 132, 074307, 1-15 (2010)

The range of electron correlation between localized molecular orbitals. A full configuration interaction analysis for the NCCN molecule.

L. Bytautas and K. Ruedenberg,
J. Phys. Chem. 114, 8601–8612 (2010)

Electronic structure analysis of the ground state potential energy curve of Be_2.

M.W. Schmidt, J. Ivanic, K. Ruedenberg,
J. Phys. Chem. 114, 8687-8696 (2010)

Analysis of the bonding patterns in the valence isoelectronic series O_3, S_3, SO_2 and OS_2 in terms of oriented quasi-atomic molecular orbitals.

V.A. Glezakou, S.T. Elbert, S. S. Xantheas, K. Ruedenberg,
J. Phys. Chem. 114, 8923–8931 (2010)

Toward a Physical Understanding of Electron-Sharing Two-Center Bonds. II.
A Pseudo-Potential Based Approach.

T. Bitter, S.G. Wang, K. Ruedenberg, W.H.E. Schwarz,
Theor. Chem Acc., 127, 237-257 (2010)

Active Thermochemical Tables – Progress Report

Branko Ruscic
Chemical Sciences and Engineering Division, Argonne National Laboratory,
9700 South Cass Avenue, Argonne, IL 60439
ruscic@anl.gov

Program Scope

The *spiritus movens* of this program is the need to provide the scientific community with accurate and reliable thermochemical information on chemical species that are relevant in combustion, or play prominent roles in the associated post–combustion environmental chemistry, thus contributing to the comprehension of the underlying chemical reactions and/or providing reliable benchmark values for development and testing of state–of–the–art theoretical approaches. Thermochemistry is one of the essential underpinning scientific blocks that is enabling DOE to successfully interpret, analyze, model, and optimize energy–producing chemical reactions and thus fulfill its mission, and is, as such, a long–term component of the DOE BES research program. The current focus of this program is on bringing substantial innovations to the field of thermochemistry through the development of new tools and methodologies, and utilizing these new approaches to systematically advance the quality and quantity of available thermochemical data relevant to energy–producing processes. In order to accomplish the stated goals, this program has undertaken the development of a novel approach that is centered on the idea of analyzing and optimally utilizing the knowledge content of thermochemically relevant measurements. The aim of these developments is not only to produce *the best currently possible* thermochemical parameters for the targeted chemical species, but also to allow *efficient updates with new knowledge*, properly propagating its consequences through all affected chemical species, as well as to provide *critical tests of new experimental or theoretical data*, and, when possible, to develop *pointers to future determinations that will most efficiently improve the thermochemical knowledge base*. The effort of this program is synergistically coordinated with related experimental and theoretical efforts within the Argonne Chemical Dynamics Group to provide a broad perspective of this area of science.

Recent Progress

Development of Active Thermochemical Tables and the Core (Argonne) Thermochemical Network

Our primary activity over the past year was the continuation of the development and deployment of Active Thermochemical Tables (ATcT). ATcT are a new paradigm of how to develop accurate, reliable, and internally consistent thermochemical values for stable, reactive, and transient chemical species by utilizing to the fullest all available experimental measurements as well as state–of–the art theoretical data. Originally driven by the lack of adequate tools and the inability to process the necessary amount of information, intertwined dependencies that underpin virtually all thermochemistry were historically considered to be an intractable complication, leading to the adoption of a simplified sequential approach to thermochemistry (A begets B, which begets C, etc). In spite of the fact that both speed and bandwidth of information–processing capabilities increased exponentially with time, the intrinsic property of thermochemistry of having massive interdependencies was for many decades simply ignored in favor of the sequential approach. The success of ATcT is rooted in readdressing the original problem by expressing the underlying interdependencies as a network of relationships that is amenable to explicit and comprehensive mathematical and statistical manipulation. This does not merely transform an intractable problem into a tractable one, but it effectively metamorphoses the original nuisance into a valuable asset that is largely responsible for the quantum leap in the quality and reliability of the resulting ATcT thermochemical values. The ability to produce reliable high–quality thermochemical parameters has triggered an exceptionally broad interest in the chemical community (including two different IUPAC Task Groups), making it effectively the archetype of thermochemistry for the 21st century. Traditional

sequential thermochemistry utilizes the available information in an inherently incomplete manner, is prone to cumulative errors, and results in tabulations that are encumbered by a hidden maze of progenitor–progeny relationships and thus cannot be updated with new knowledge without introducing serious inconsistencies across the other existing values. As opposed to this, ATcT operate on the underlying Thermochemical Network (TN), which explicitly carries the available thermochemically–relevant determinations and thus allows statistical scrutiny and manipulation of the intricate manifold of relationships characterizing thermochemistry. The end result of this scrutiny is the extraction of the best possible thermochemical values for all chemical species described by the TN, based on optimal use of all the available knowledge, hence making conventional tabulations of thermochemical values obsolete.

The ATcT effort has two essential fronts: the development of the ATcT software and the development of the Thermochemical Network, which, once analyzed and solved by ATcT, produces new thermochemical knowledge. While the ATcT software kernel is well–rounded and adequate for most current tasks involving the TN analysis and solution, needs for additional capabilities related to finer details of the partition function–related properties (*vide infra*) have recently arisen. Rather than engaging in major modifications of the current ATcT kernel, these needs are currently addressed by developing a number of separate software tools. Thus, adding to the library of previously developed external tools that enable us to more effectively use the information stored in the covariance matrix computed by ATcT as part of solving the TN, we have developed a sequence of tools that compute the reduced moment of inertia of an internal rotor (including unsymmetrical tops), find the energy levels of the hindered rotor potential (either by solving the underlying Mathieu equation in a conventional way, or by using a DVR approach), and compute the thermochemical contributions of a hindered rotor by direct level counting; a sequence of tools that compute various corrections to the partition function due to centrifugal distortion, anharmonicity, rotation–vibration interaction, Darling–Dennison resonances, Fermi resonances, etc.; a tool that uses the empirically determined heat capacities of substances in condensed phases to compute the related entropy and enthalpy increment; a tool that helps us derive the real–to–ideal (and vice versa) correction to vaporization enthalpies using 2^{nd} (and 3^{rd}, if available) virial coefficients; etc.

The cardinal TN from which ATcT derives new thermochemical insights is the Core (Argonne) Thermochemical Network, C(A)TN. The overreaching goal is to create a TN that describes in the best possible manner the thermochemistry of all radicals and stable species relevant to combustion. C(A)TN currently encompasses nearly a thousand chemical species of C/H/O/N/Hal composition, intertwined by nearly 14,000 thermochemically–relevant determinations. The C(A)TN is now large enough to allow us to concentrate on groups of key chemical species that are spanned by reasonably complete dependency manifolds and capable of producing thermochemistry that has converged toward a stable value, and to undertake the effort of bringing the thermochemistry of such species to a 'release–quality' level. As we were attempting to finalize the thermochemistry of the first batch of these species by honing the targeted sections of C(A)TN and inspecting and resolving residual inconsistencies, it became manifest that in a number of cases the constraint in achieving the 'final' converged values is not any longer in the information content of the TN, but, rather, in the quality of the externally given partition–function related properties. Namely, thus far the ATcT approach has been mostly focusing on finding and resolving inconsistencies between thermochemically–relevant determinations expressed in the TN, while the partition–function properties (such as isobaric heat capacity, entropy, and enthalpy increment) were either adopted from other sources (such as the meticulous compilation of CODATA and of Gurvich et al.) or, when such information was not available, computed on the fly using the RRHO approach and the best available spectroscopic constants. However, as improvements in the TN led to increased accuracy of the ATcT thermochemistry, it gradually became evident that RRHO function are in many cases not entirely adequate because of non–negligible corrections due to anharmonicity, centrifugal effects, rotation–vibration interaction, etc. Similarly, it also became evident that some of the existing partition functions from CODATA or from Gurvich et al. (including those that ostensibly incorporated nearly all imaginable corrections) need to be refurbished with new spectroscopic knowledge that has become available since

they were constructed. These issues motivated the development of the tools mentioned earlier in this abstract. We are currently in the process of using these tools to improve the partition function properties of small species of O/H, C/H, C/O, C/H/O, N/H, and N/O composition.

In a separate effort, we have completed the ATcT analysis that provides accurate ATcT thermochemistry for phenyl radical and its positive and negative ions. This effort was conducted in collaboration with Tom Baer (UNC), who carried out at UNC and at the Swiss Light Source accurate photoionization ion–electron coincidence measurements of the dissociative ionization thresholds from several monosubstituted benzenes. This joint ATcT and PEPICO study exhibits a high degree of synergism, and clarifies not only the so far rather uncertain thermochemistry of phenyl (where historic values of the enthalpies of formation differ by several times the declared uncertainties) and its ionization energy (the knowledge of which affects attempts to monitor combustion processes via photoionization mass spectrometric sampling), but it also provides accurate and validated thermochemistry of benzene itself and monohalosubstituted benzenes. The published study, featured on the Dec. 23, 2010 cover of J. Phys. Chem. A (see Figure 1), also provides advanced preliminary values for the thermochemistry of atoms relevant in combustion, accurate values of which are needed by electronic structure computational efforts that use computed TAEs to produce theoretical enthalpies of formation.

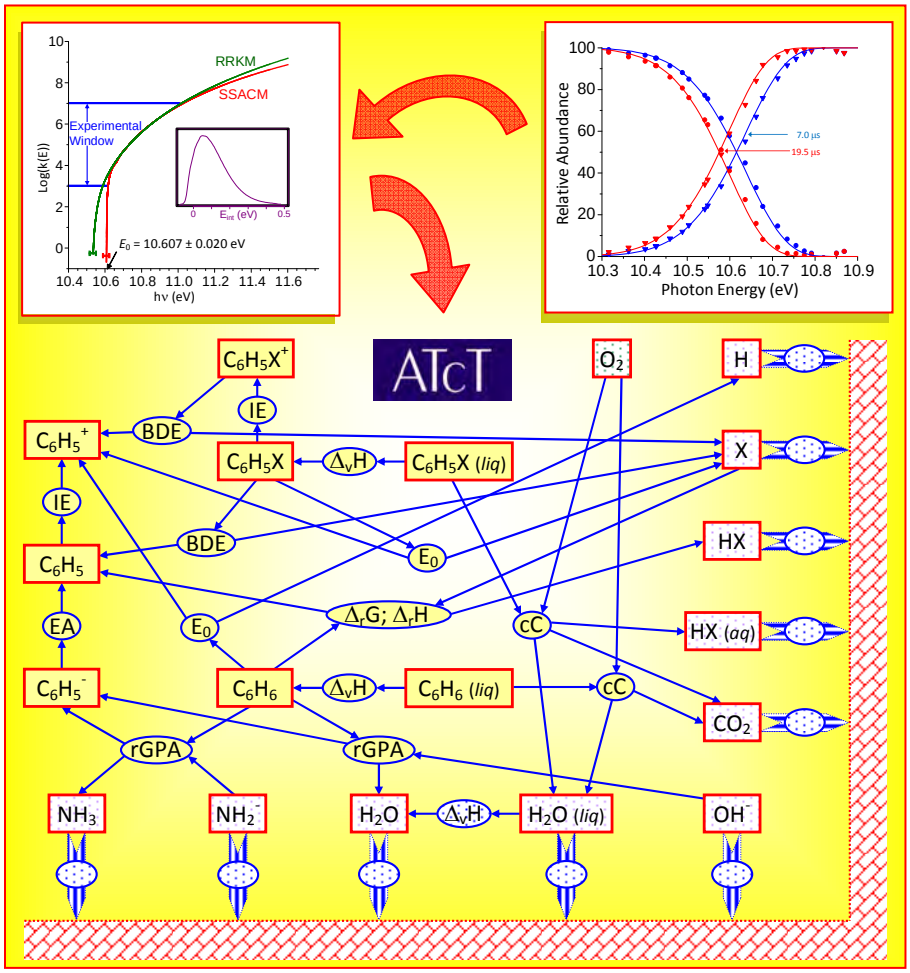

Figure 1. Synergism between accurate photoionization measurements (TPEPICO breakdown diagram, upper right, and extraction of the dissociation threshold by statistical unimolecular decay rate theory, upper left) and the Active Thermochemical Tables approach (a section of the underlying Thermochemical Network, center and bottom) produces the best currently available thermochemistry of phenyl, its ions, benzene, and monohalobenzenes.

One of the recent accomplishments of the ATcT project was the launch of the ATcT website (http://ATcT.anl.gov) in May/June 2010. The website is still under development, and its public face is currently transiting from the initial alpha version to a beta version. The website is based on a series of html/JavaScript templates that we have recently developed, and while for the initial alpha version these templates were filled–in manually, the beta version that we are currently developing will include partial

automation. The goal is to ultimately develop a website that will be (re)generated entirely automatically by a post–processing step implemented as an associated ATcT tool.

Future Plans

Future plans of this program pivot around further developments and expansive use of Active Thermochemical Tables, providing accurate thermochemistry, and driving targeted theoretical and laboratory experimental investigation of radicals and transient species that are intimately related to combustion processes. The most pressing task for the forthcoming period is to continue the effort toward finalizing and disseminating the ATcT results. A necessary prerequisite is to coerce the related thermochemistry to converge to a stable, "release quality" value, and we intend to continue expanding the number of species that belong to this category. Another prerequisite is the continuation of the current effort on designing and producing an entirely computer–generated ATcT web site that will be populated by "release quality" results automatically by a suitable post–processing step in ATcT. Besides full automation with archival capability, an additional desideratum for the website is the automatic inclusion of sufficient background information to document the pedigree for every recommended value, providing credit to the actual original (experimental and/or theoretical) determination(s) that are responsible for the final ATcT value.

This work is supported by the U.S. Department of Energy, Office of Basic Energy Sciences, Division of Chemical Sciences, Geosciences, and Biosciences, under Contract No. DE–AC02–06CH11357.

Publications resulting from DOE sponsored research (2008 – present)

- *HEAT: High Accuracy Extrapolated ab initio Thermochemistry. III. Additional Improvements and Overview*, M. E. Harding, J. Vazquez, B. Ruscic, A. K. Wilson, J. Gauss, and J. F. Stanton, *J. Chem. Phys.* **128**, 114111/1-15 (2008).
- *Accurate ab initio Computation of Thermochemical Data for C_3H_x (x = 0,...,4) Species*, J. Aguilera–Iparraguirre, A. D. Boese, W. Klopper, and B. Ruscic, *Chem. Phys.* **346**, 56-68 (2008).
- *Atomization Energies from Coupled-Cluster Calculations Augmented with Explicitly-Correlated Perturbation Theory*, W. Klopper, B. Ruscic, D. P. Tew, F. A. Bischoff, and S. Wolfsegger, *Chem. Phys.* **356**, 14-24 (2009).
- *Is HO_2^+ a Detectable Interstellar Molecule?*, S. L. Widicus Weaver, D. E. Woon, B. Ruscic, and B. J. McCall, *Astrophys. J.* **697**, 601-609 (2009).
- *Thermal Decomposition of NH_2OH and Subsequent Reactions: Ab Initio Transition State Theory and Reflected Shock Tube Experiments*, S. J. Klippenstein, L. B. Harding, B. Ruscic, R. Sivaramakrishnan, N. K. Srinivasan, M.-C. Su, and J. V. Michael, *J. Phys. Chem. A* **113**, 10241-10259 (2009).
- *Rate Constants for the Thermal Decomposition of Ethanol and Its Bimolecular Reactions with OH and D: Reflected Shock Tube and Theoretical Studies*, R. Sivaramakrishnan, M.-C. Su, J. V. Michael, S. J. Klippenstein, L. B. Harding, and B. Ruscic, *J. Phys. Chem. A* **114**, 9425-9439 (2010).
- *The Heats of Formation of C_6H_5, $C_6H_5^+$, and C_6H_5NO by TPEPICO and Active Thermochemical Tables Analysis*, W. R. Stevens, B. Ruscic, and T. Baer, *J. Phys. Chem A* **114**, 13134–13145 (2010).
- *Shock Tube and Theoretical Studies on the Thermal Decomposition of Propane: Evidence for a Roaming Radical Channel*, R. Sivaramakrishnan, M.-C. Su, J. V. Michael, S. J. Klippenstein, L. B. Harding, and B. Ruscic, *J. Phys. Chem. A* **115**, *in press* (2011).
- *Inhibition of Hydrogen Oxidation by HBr and Br_2*, P. Glarborg, P. Marshall, B. Ruscic, A. Burcat, E. Goos, A. Cuoci, A. Frassoldati, T. Faravelli, and G. Dixon-Lewis, *m/s in finishing stages of completion.*

Gas-Phase Molecular Dynamics: High Resolution Spectroscopy and Collision Dynamics of Transient Species

Trevor J. Sears
Department of Chemistry, Brookhaven National Laboratory
Upton, NY 11973-5000
sears@bnl.gov

Program Scope

This research is carried out as part of the Gas-Phase Molecular Dynamics program in the Chemistry Department at Brookhaven National Laboratory. High-resolution spectroscopy, augmented by theoretical and computational methods, is used to investigate the structure and collision dynamics of chemical intermediates in the elementary gas-phase reactions involved in combustion chemistry. Applications and methods development are equally important experimental components of this work.

I. Recent Progress

A. New spectroscopy of singlet CH_2

The origin band in the $\tilde{b}\ ^1B_1 - \tilde{a}\ ^1A_1$ transition of CH_2 near 1.2 μm has been recorded at Doppler-limited resolution using diode laser transient absorption spectroscopy. The assignments of rotational transitions terminating in upper state levels with K_a = 0 and 1, were confirmed by ground state combination differences and extensive optical-optical double resonance experiments. The assigned lines are embedded in a surprisingly dense spectral region, which includes strong hot band, $\tilde{b}\,(0,1,0)\ K_a$=0 — $\tilde{a}\,(0,1,0)\ K_a$=1 subband lines. Here, (v_1, v_2, v_3) are the vibrational quantum numbers of the level. Combination or overtone transitions in the $\tilde{a}^1A_1$ state likely responsible for the majority of unassigned transitions in this region. From measured line intensities and an estimate of the concentration of CH_2 in the sample, we find the transition moment for the $0_{00} \leftarrow 1_{10}$ transition in the $\tilde{b}^1B_1(0,0,0)^0 - \tilde{a}^1A_1(0,0,0)^1$ sub-band is 0.005(1) D[2].

Prominent $\tilde{b}^1B_1(0,1,0)^0 - \tilde{a}^1A_1(0,1,0)^1$ (the superscript is the K_a value of the level) hot band lines were observed in the same spectral region. Comparison of the intensities of corresponding rotational transitions in the two bands suggests the hot band has an intrinsic strength approximately 28 times larger than the origin band. Perturbations of the excited state K_a= 0 and 1 levels were observed and were analyzed. The new measurements will lead to improved future theoretical modeling and calculations of the Renner-Teller effect between the $\tilde{a}$ and $\tilde{b}$ states in CH_2.

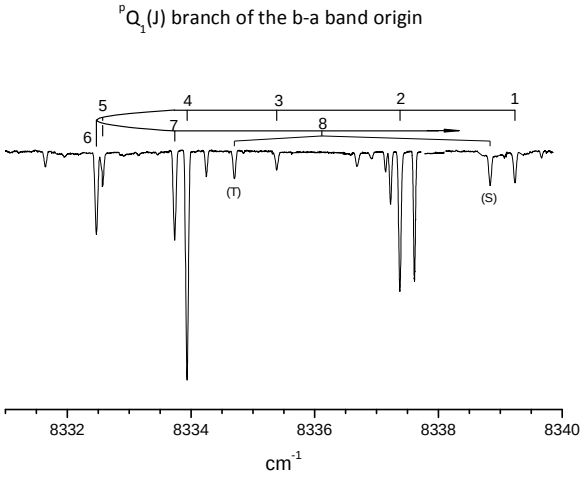

Figure 1. Part of the *b-a* system origin band of CH_2 showing the *Q*-branch of the K_a=0-1 sub-band, with *J*-assignments. The 8_{18} level is split by a known, previously characterized, interaction with the 9_{37} level in (020) of the triplet ground state of the molecule.

Bands in the CH_2 $\tilde{b}\ ^1B_1 - \tilde{a}\ ^1A_1$ transition between 12500 – 13000 cm^{-1} were recorded at Doppler-limited resolution using a transient frequency-modulation (FM) laser absorption spectrometer. Although the $\tilde{b}\ ^1B_1 - \tilde{a}\ ^1A_1$ spectrum of CH_2 has been extensively studied, this region had not been investigated since the work of Herzberg and Johns in 1966. Rotational levels in 7 upper vibronic states: $\tilde{a}(0,11,0)^{1,3}$, $\tilde{a}(2,6,0)^1$, $\tilde{b}(0,2,0)^4$, $\tilde{b}(1,1,0)^{1,2}$, and $\tilde{b}(0,3,0)^1$ were assigned with the assistance of optical-optical double resonance (OODR) and ground state combination differences. Perturbations due to rotation-vibration coupling, anharmonic couplings, ℓ – resonance, as well as the Renner-Teller effect were identified as the sources of the irregular rotational patterns observed in the $\tilde{b}\,(0,3,0)^1$, $\tilde{b}\,(1,1,0)^1$, and

$\tilde{a}(0,11,0)^3$ vibronic levels, and detailed patterns of perturbations were clearly separated. The extensive use of OODR to label the lower state rotational levels permitted a larger percentage of observed lines to be assigned in this region than even in the origin band spectrum described above, despite the much lower density of background levels at the longer wavelengths.

B. Double resonance and sub-Doppler studies of radical collision dynamics

Rotational energy transfer within the $\tilde{a}$ state of CH_2 and between rotational levels of CN has been studied by saturation recovery and saturation transfer double resonance kinetic spectroscopy, as reported last year. We have extended the measurements to Doppler-resolved collisions using sub-Doppler spectroscopic techniques and have designed and constructed an improved stabilization method for a high resolution Ti:sapphire laser. These aspects are discussed in more detail in G. Hall's abstract elsewhere.

C. Spectroscopy with comb-stabilized extended cavity diode lasers

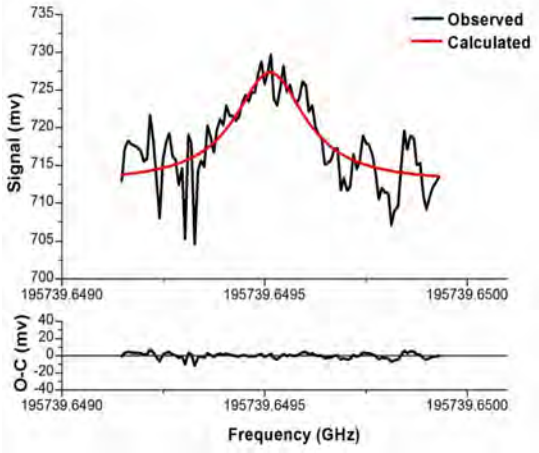

Figure 2. Sub Doppler saturation dip spectrum of the P(11) line of the $\nu_1 + \nu_3$ band of C_2H_2. The fitted linewidth is 105(2) kHz (HWHM) and the line center is at 195 739.6495135(80) GHz.

As described last year, our sub-Doppler measurements of spectral lines are limited by the accuracy and precision associated with wavelength standards normally used to calibrate spectra. The best measurements using wavelength standards and stabilized cavities reach accuracies of the order of 1 part in 10^8. Figure 2 shows a result obtained using a frequency comb to stabilize an extended cavity diode laser (ECDL) that is in turn used to measure a saturation dip in a single line of the acetylene $\nu_1 + \nu_3$ band. The line position is measured to an accuracy of 2.5 parts in 10^{12}. These $\nu_1 + \nu_3$ combination band lines in acetylene near 1.5μm were previously adopted as a secondary frequency standard, and our measurement agrees to within the published uncertainty of the standard frequency.

The exquisite accuracy of this spectrometer is not only of use for precision measurements of narrow spectral lines, but can be used to improve the measurement of the shapes and widths of broad features. We have demonstrated this in work on pressure broadening of the same transition shown in figure 2. Broadening, shift and narrowing parameters were determined at 296 K. For the most appropriate, hard-collision, model in units of cm^{-1}/atm, we find 0.146317(27), 0.047271(104), –0.0070819(22) for the acetylene self-broadening, narrowing and shift, and 0.081129(35), 0.022940(74), and –0.0088913(25) respectively, for the nitrogen broadening parameters. The uncertainties are expressed as one standard deviation (in parenthesis) in units of the last digit reported. These parameters are 2–3 orders of magnitude more precise than those reported in any previous measurements. Similar analyses of the experimental data using soft collision and simple Voigt lineshape models were made for comparison. Measurements with helium as the collision partner are potentially simpler to model, and very recent measurements have shown a positive pressure induced shift for low J lines. Published measurements have never reported a measurement of the small shifts produced on collisions with He atoms. Other frequency comb work at BNL is described in G. Hall's abstract for this meeting.

D. Spectroscopy and photophysics of aromatic species

Vibrational structure of the S_1-S_0 electronic band of phenylacetylene (PA) has been recorded by 1+1 resonance-enhanced multiphoton ionization (REMPI), accompanied by slow electron velocity mapping imaging photoelectron spectroscopy at each resonant vibrational band. Assignments of the S_1 vibrations (up to 2000 cm^{-1} above the band origin) were based upon relative intensities of the vibronic bands calculated by complete second-order vibronic coupling, vibration-rotation (Coriolis and Birss) coupling calculations, and the vibrational structure of the S_1 resonant photoelectron spectra. Although this is an

allowed electronic transition, the relative intensities of the a_1 bands are often largely determined by vibronic coupling rather than simple Franck-Condon factors, and second-order coupling is substantial. Non-symmetric vibrations have intensities obtained through either vibronic or Coriolis coupling and calculations have been instrumental in discriminating between alternate possibilities in the assignments. Strong vibronic effects are expected to be present in spectra of most mono-substituted benzenes, and the calculations presented here show that theoretical treatments based upon electronic structure calculations will generally be useful in the analysis of their spectra. Cavity ring-down absorption spectroscopy of jet cooled PA was also performed as a check of the relative intensities measured in the REMPI experiments and analysis of these data is in progress.

II. Future Work

A. Precision spectroscopy and dynamics

Time resolved measurements designed to investigate the relative efficiencies *J*-changing and velocity-changing collisions, both of which contribute to the pressure broadening of spectroscopic line shapes are planned. Following previous work on collisional dynamics in CH_2, we will monitor specific rotational levels of C_2H_2 using an extended cavity diode laser, optionally locked to the frequency comb, and transfer population from this or another ground state level using a ns pulsed dye laser tuned to an allowed transition in the well known C_2H_2 $\tilde{A} - \tilde{X}$ system near 240 nm. The transmitted diode laser power will probe the time-dependent behavior of the population hole as it is collisionally equilibrated. Use of a high resolution (pulse amplified c.w.) laser system will even permit the monitoring of the velocity re-equilibration as a particular velocity group in the sample is depleted. These measurements will provide new insights into the function describing the intermolecular potential and the various contributions leading to pressure broadening and dephasing in gaseous systems.

Continued ultra-high resolution spectroscopy efforts using comb-stabilized single frequency lasers will target improved saturation dip measurements. As a spin-off from our work on building fiber-laser combs, we have demonstrated seeded amplification of a sample of light from an ECDL in a length of diode-pumped Er-doped fiber. This exciting development provides 60-100 mW of comb-stabilized laser power in a single stage of amplification from a few hundred μw of seed power, which will make saturation spectroscopy experiments possible without the complication of the resonant cavity absorption cell needed for the saturation dip measurement described above. We will characterize the linewidth of the amplified light in experiments during the next few months, followed by new precision spectroscopy measurements. Other work will investigate to use of comb-locked simple distributed feed-back diode lasers.

All these developments will be applied to both new Doppler and sub-Doppler resolved measurements of the spectroscopy and dynamics of transient species. Additionally, in collaboration with Prof. Neil Shafer-Ray, (Oklahoma) we plan to make ultra high precision measurements of the $\tilde{X}_2 - \tilde{X}_1$ transition in a slit-jet cooled sample of diatomic PbF, which lies near 1.2 μm. This DOE EPSCoR funded project is directed toward investigating parity violation effects in small molecules containing a heavy atom.

III. Publications supported by this project since 2009

Sub-Doppler laser absorption spectroscopy of the $A^2\Pi_i - X^2\Sigma^+$ (1,0) band of CN: measurement of the ^{14}N hyperfine parameters in $A^2\Pi_i$ CN. M. L. Hause, G. E. Hall and T. J. Sears, *J. Molec. Spectrosc.* **253**, 122-128 (2009).

Sub-Doppler Stark spectroscopy in the *A* - *X* (1,0) band of CN. M. L. Hause, G. E. Hall, and T. J. Sears, *J. Phys. Chem. A*, **113** 13342-13346 (2009).

The halocarbenes: model systems for understanding the spectroscopy and dynamics of carbenes. S. H. Kable, S. A. Reid and T. J. Sears, *Int. Revs. Phys. Chem.* **28** 435-480 (2009).

Pseudo-continuous resonance-enhanced multiphoton ionization: application to the determination of the hyperfine constants of $^{208}Pb^{19}F$. P. Sivakumar, C. P. McRaven, P. M. Rupasinghe, T. Zh. Yang, N. E. Shafer-Ray, G. E. Hall and T. J. Sears, *Mol. Phys.* **108**, 927-935 (2010).

Spectroscopic constants of the known electronic states of lead monofluoride, C.P. McRaven, P. Sivakumar, N.E. Shafer-Ray, Gregory E. Hall and Trevor J. Sears, J. *Molec. Spectrosc.* **262**, 89–92 (2010).

Effect of laser injection seeder on rotationally resolved spectra of benzonitrile, H.-F. Xu, P. M. Johnson and T. J. Sears, *Chin. Phys. Lett.* **27**, 083301(3) (2010).

Vibronic analysis of the $S_1 - S_0$ transition of phenyl acetylene using photoelectron imaging and spectral intensities derived from electronic structure calculations, C.-H. Chang, G. Lopez, T. J. Sears and P. M. Johnson, *J. Phys. Chem. A* **114**, 8262-8270 (2010).

Sub-Doppler spectroscopy of mixed state levels in CH_2, C. -H. Chang, G. E. Hall and T. J. Sears, *J. Chem. Phys.* **133**, 144310(6) (2010).

The CH_2 $\tilde{b}\,^1B_1 - \tilde{a}\,^1A_1$ band origin at 1.20μm, C.-H. Chang, J. Xin, T. Latsha, E. Otruba, Z. Wang, G. E. Hall and T. J. Sears, *J. Phys. Chem. A*, http://pubs.acs.org/articlesonrequest/AOR-nNx9NnP5TBfzvspaHGKN

Transient laser absorption spectroscopy of CH_2 near 780 nm, C.-H. Chang, Z. Wang, G. E. Hall, T. J. Sears and J. Xin, *J. Molec. Spectrosc.* http://dx.doi.org/10.1016/j/jms.2011.02.004

Frequency comb-referenced measurements of self- and nitrogen-broadening in the $\nu_1 + \nu_3$ band of acetylene, C. P. McRaven, M. J. Cich, G. V. Lopez, T. J. Sears, D. Hurtmans and A. W. Mantz, *J. Molec. Spectrosc.* http://dx.doi.org/10.1016/j/jms.2011.02.016

Precision spectroscopy of the $^{207}Pb^{19}F$ molecule: implications for measurement of P-odd and T-odd effects, L. D. Alphei, J.-U Grabow, A. N. Petrov, R. Mawhorter, B. Murphy, A. Baum, T. J. Sears, T. Zh. Yang, P. M. Rupasinghe, C. P. McRaven and N. E. Shafer-Ray, *Phys. Rev. A.* (accepted, Feb 2011).

Precise characterization of the ground X_1 state of $^{206}Pb^{19}F$, $^{207}Pb^{19}F$ and $^{208}Pb^{19}F$, R. Mawhorter, B. Murphy, A. Baum, T. J. Sears, T. Zh. Yang, P. M. Rupasinghe, C. P. McRaven, N. E. Shafer-Ray, L. D. Alphei and J.-U. Grabow, *Phys. Rev. A.* (submitted, Mar 2011).

Theoretical Studies of Potential Energy Surfaces and Computational Methods

Ron Shepard
Chemical Sciences and Engineering Division,
Argonne National Laboratory, Argonne, IL 60439
[email: shepard@tcg.anl.gov]

Program Scope: This project involves the development, implementation, and application of theoretical methods for the calculation and characterization of potential energy surfaces (PES) involving molecular species that occur in hydrocarbon combustion. These potential energy surfaces require an accurate and balanced treatment of reactants, intermediates, and products. This difficult challenge is met with general multiconfiguration self-consistent field (MCSCF) and multireference single- and double-excitation configuration interaction (MR-SDCI) methods. In contrast to the more common single-reference electronic structure methods, this approach is capable of describing accurately molecular systems that are highly distorted away from their equilibrium geometries, including reactant, fragment, and transition-state geometries, and of describing regions of the potential surface that are associated with electronic wave functions of widely varying nature. The MCSCF reference wave functions are designed to be sufficiently flexible to describe qualitatively the changes in the electronic structure over the broad range of molecular geometries of interest. The necessary mixing of ionic, covalent, and Rydberg contributions, along with the appropriate treatment of the different electron-spin components (e.g. closed shell, high-spin open-shell, low-spin open shell, radical, diradical, etc.) of the wave functions are treated correctly at this level. Further treatment of electron correlation effects is included using large-scale multireference CI wave functions, particularly including the single and double excitations relative to the MCSCF reference space. This leads to the most flexible and accurate large-scale MR-SDCI wave functions that have been used to date in global PES studies.

Recent Progress: ELECTRONIC STRUCTURE CODE MAINTENANCE, DEVELOPMENT, AND APPLICATIONS: A major component of this project is the development and maintenance of the COLUMBUS Program System. The COLUMBUS Program System computes MCSCF and MR-SDCI wave functions, MR-ACPF (averaged coupled-pair functional) energies, MR-AQCC (averaged quadratic coupled cluster) energies, spin-orbit CI energies, analytic energy gradients, and nonadiabatic coupling. Geometry optimizations to equilibrium and saddle-point structures can be done automatically for both ground and excited electronic states. The COLUMBUS Program System is maintained and developed collaboratively with several researchers including Isaiah Shavitt (University of Illinois), Russell M. Pitzer (Ohio State University), Thomas Mueller (Central Institute for Applied Mathematics, Juelich, Germany), and Hans Lischka (University of Vienna, Austria). The nonadiabatic coupling and geometry optimizations for conical intersections is done in collaboration with David R. Yarkony (Johns Hopkins University). The distributed development effort and software coordination uses an svn repository of source code. The parallel sections of the code are based on the single-program multiple-data (SPMD) programming model with explicit

This work was performed under the auspices of the Office of Basic Energy Sciences, Division of Chemical Sciences, Geosciences, and Biosciences, U.S. Department of Energy, under contract number DE-AC02-06CH11357.

message passing using the portable MPI library, and the portable Global Array Library (distributed from PNNL) is used for data distribution. The next major release of the COLUMBUS codes will begin to incorporate the newer language features of F90 and later. This will facilitate future development and maintenance effort.

GRAPHICALLY CONTRACTED FUNCTION METHOD: We have recently developed a novel expansion basis for electronic wave functions [*J. Phys. Chem. A* **109**, 11629 (2005)]. In this approach, the wave function is written as a linear combination of *graphically contracted functions* (GCFs), and each GCF in turn is formally equivalent to a linear combination of configuration state functions (CSFs) that comprise an underlying linear expansion space of dimension N_{csf}. The CSF coefficients that define the GCFs are nonlinear functions of a smaller number of variables $N_{\varphi} \ll N_{\mathrm{csf}}$. GCF expansions with 10 to 20 basis functions can approach the full-CI PES to within chemical accuracy (1 kcal/mole or better) [*Int. J. Quantum Chem.* **107**, 3203 (2007)]. The method is formulated in terms of spin-eigenfunctions using the Graphical Unitary Group Approach (GUGA) of Shavitt, and consequently it does not suffer from spin contamination or spin instability.

Our new method is characterized by several important features. First, open-shell spin-eigenfunctions are included in the wave function expansions. This allows our new method to be used for the reactions that are important to combustion chemistry (i.e. involving radicals and other open-shell electronic states) without introducing spin contamination. Second, we place no intrinsic restrictions on the orbital occupations, so our GCFs are not restricted to only geminals or to other preselected molecular fragments, and there are no artificial excitation-level or occupation restrictions with respect to a reference function or reference space. Third, we use linear combinations of N_{GCF} basis functions rather than a single expansion term. This allows our method to be used for both ground and excited electronic states, the increased wave function flexibility leads to more accurate wave functions, and it will allow the computation of transition moments, nonadiabatic coupling, and other properties that at present can only be computed reliably with MCSCF and MRCI approaches.

Efficient procedures to compute hamiltonian matrix elements and reduced one- and two-particle density matrices for this nonlinear expansion have been developed [*J. Phys. Chem. A* **110**, 8880 (2006)]. The effort required to construct an individual hamiltonian matrix element between two GCFs $H_{PQ} = \langle P | \hat{H} | Q \rangle$ scales as $\mathcal{O}(\omega n^4)$ for a wave function expanded in n molecular orbitals. The prefactor ω depends on the complexity of the underlying Shavitt Graph and scales between N^0 and N^2 for N electrons. The corresponding metric matrix element $S_{PQ}=\langle P | Q \rangle$ requires effort that scales as $\mathcal{O}(\omega n)$, the one-particle transition density $\mathbf{D}^{MN}$ requires $\mathcal{O}(\omega n^2)$ effort, the two-particle density $\mathbf{d}^{MN}$ requires $\mathcal{O}(\omega n^4)$ effort. There is no component of the effort or storage for matrix element computation or wave function optimization that scales as N_{csf}. This feature allows very large wave functions to be employed, much larger than would be possible with any of the traditional electronic structure methods. Timings with our initial implementation of this method are very promising. A hamiltonian matrix element involving GCFs corresponding to an underlying linear expansion space with dimension $N_{\mathrm{csf}} \approx 5.5 \cdot 10^{24}$ requires only 10 to 15 seconds on a typical laptop or desktop computer. The computation of this same matrix element would require over a million times the age of the universe

using traditional full-CI technology. Timings for the computation of spin density matrices for expansions as large as $N_{csf} \approx 10^{200}$ were presented in last year's abstract.

The minimization of the GCF energy with respect to the variational parameters is a difficult nonlinear optimization problem. A previous algorithm to compute optimization gradients of these nonlinear parameters, called arc factors, required $\mathcal{O}(\omega n^5)$ effort. This resulted in a focus on optimization methods that require relatively few gradients compared to the number of function evaluations. In the past year, an efficient recursive algorithm has been implemented to compute these optimization gradients with only $\mathcal{O}(\omega n^4)$ effort, a dramatic improvement over the previous algorithm, particularly for larger orbital basis sets [*Int. J. Quantum Chem.* **110**, 2938 (2010)]. This is a recursive algorithm that closely models the construction of the one- and two-particle reduced density matrices and of Hamiltonian matrix elements. With the new algorithm, the effort to compute a gradient is about three times that required to compute an energy expectation value for a given set of arc factors; thus the energy and gradient have the same scaling behavior with increasing molecule size, N_{GCF} dimension, and orbital basis size.

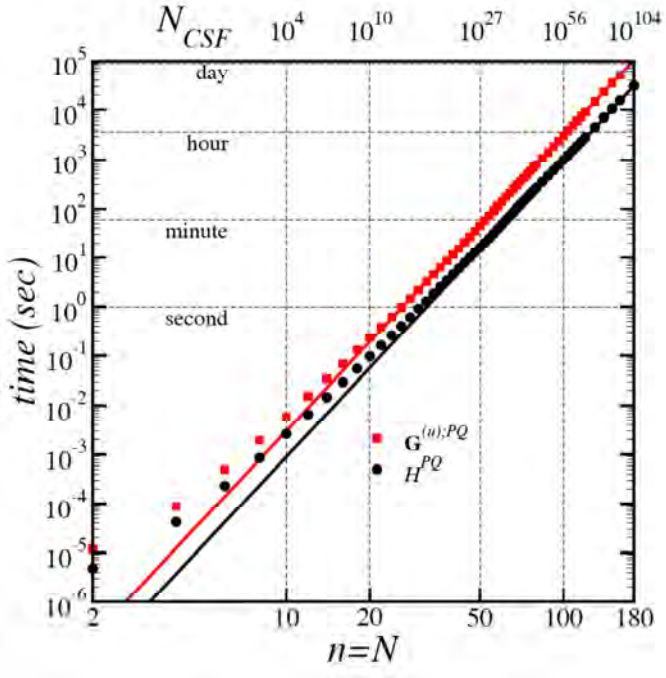

Fig. 1. Time required to compute the Hamiltonian matrix element H_{PQ} (circles) and $\mathbf{G}^{(u)PQ}$ matrix (squares) for all orbital levels u=1…n. Calculations are performed for a sequence of singlet wave functions with n=N. The number of electrons N ranges from 2 to 180, and the corresponding number of CSFs is indicated on the upper axis. The solid lines indicate monomial fits of the form $f(n)=\alpha n^6$, where the scalar factor is adjusted to fit the large-N data. Note that the H_{PQ} and $\mathbf{G}^{(u)PQ}$ curves are parallel for large systems.

The optimization gradients are computed from intermediate arrays called orbital level Hamiltonian matrices denoted $\mathbf{G}^{(u)PQ}$. As the initial calculations were performed with the new algorithm, it was observed that the memory space required to hold these arrays was a limiting factor for larger orbital basis sets. The largest calculation that could be performed was n=120 and $N_{csf} \approx 10^{73}$. However, these orbital level Hamiltonian matrices become very sparse for larger orbital basis sets, so the actual number of nonzero matrix elements is only a small fraction of the total memory that was used to store these arrays. As a result of this observation, a new storage scheme was developed in which only the nonzero elements are stored [*Mol. Phys.* **108**, 2717 (2010)]. This not only allows calculations on larger systems (up to n=180, $N_{csf} \approx 10^{104}$), but the memory requirements are so negligible that the calculations remain largely in cache memory,

eliminating some of the large timing variations of the previous version which were due to cache thrashing. Fig. 1 shows timings for this new implementation on a single core of a desktop computer. It may be seen that the ratio of gradient time to H_{PQ} construction time is relatively constant and well-behaved over the entire range of calculations.

Future Plans: GCF METHOD: Our applications have so far used single-headed Shavitt graphs appropriate for describing individual molecular states with a given number of electrons, with a particular spin state, and that belong to a particular irrep. We will generalize this in several respects. First, we will introduce state averaging over individual irreps and state averaging over multiple irreps. This will allow the nonlinear arc factor parameters to be optimized for several electronic states simultaneously rather than for individual electronic states. For the multiple irrep case, this will allow the computation of several molecular states with essentially no additional effort over single-irrep calculations. Next, we will employ multiheaded Shavitt graphs in the state-averaging procedure. This will allow the computation of hamiltonian matrix elements corresponding to states with different numbers of electrons, different spin values, and different irreps simultaneously with only a relatively small increase in effort over the current single-state approach.

The GCF code has now been placed in a development branch of the COLUMBUS svn repository. In this way the code is now available for a wider range of inspection and scrutiny. We hope to develop a robust implementation and incorporate the GCF method into the standard distribution version of COLUMBUS for even wider use over the next year.

Publications:

"Computation of Determinant Expansion Coefficients Within the Graphically Contracted Function Method", G. Gidofalvi and R. Shepard, *J. Comp. Chem.* **30**, 2414 (2009).

"The Evaluation of Spin-Density Matrices Within the Graphically Contracted Function Method", G. Gidofalvi and R. Shepard, *Int. J. Quantum Chem.* **109**, 3552 (2009).

"Evaluation of the Spin-Orbit Interaction Within the Graphically Contracted Function Method", S. R. Brozell and R. Shepard, *J. Phys. Chem. A* **113**, 12741 (2009).

"An Efficient Recursive Algorithm to Compute Wave Function Optimization Gradients for the Graphically Contracted Function Method", R. Shepard, G. Gidofalvi and P. D. Hovland, *Int. J. Quantum Chem.* **110**, 2938-2948 (2010).

"Exploiting Sparsity in the Graphically Contracted Function Configuration Interaction Method," G. Gidofalvi and R. Shepard, *Mol. Phys.* **108**, 2717-2724 (2010).

"COLUMBUS–A Program System for Advanced Multireference Theory Calculations," H. Lischka, T. Müller, P. G. Szalay, I. Shavitt, R. M. Pitzer, R. Shepard, *WIREs Comput. Mol. Sci.* **1**, 191, (2011).

"Computational and Methodological Elements for Nonadiabatic Trajectory Dynamics Simulations of Molecules," M. Barbatti, R. Shepard, and H. Lischka, in "Conical Intersections: Theory, Computation and Experiment", W. Domcke, D.R. Yarkony and H. Köppel, Eds., *Advanced Series in Physical Chemistry*, **17** (World Scientific, Singapore, 2011) (*in press*).

Mechanisms and Models for Combustion Simulations

Raghu Sivaramakrishnan
Chemical Dynamics Group, Chemical Sciences & Engineering Division
Argonne National Laboratory, Argonne, IL 60439
raghu@anl.gov

I. Program Scope

Mechanisms describing the combustion chemistry of even simple fuels can be complex involving a myriad of unimolecular and bimolecular elementary steps. The primary scope of this program is to develop and validate detailed chemical kinetics mechanisms and models for use in simulations for combustion.

The kinetics models will be developed on the basis of a consistent framework incorporating theoretical predictions, experimental measurements, and evaluations of elementary reaction rate coefficients, with feedback loops between them. The detailed models will subsequently be used for simulations of data from reactors, shock-tubes, rapid compression machines, and flames with the aim of validating the mechanistic and kinetic aspects of these models over practical combustion regimes.

II. Recent Progress

A. The combustion chemistry of prototype small alcohols - Methanol and Ethanol

Alcohols such as butanol and iso-pentanol are potential candidates for the next generation of biofuels derived from renewable sources. These larger alcohols have been shown to possess superior physical and chemical properties in comparison to ethanol that enable their usage as neat fuels in modern engines [1,2]. It is quite evident that a systematic approach to model the combustion of these alcohols should start with the simpler prototypical alcohols, methanol and ethanol.

We have assembled a detailed chemical kinetic model for ethanol combustion in a hierarchical fashion which of course incorporates the methanol sub-mechanism. With ethanol being a widely used renewable fuel, its combustion chemistry has been the subject of intense scrutiny since the 1990 Clean Air Act Amendments [3] required oxygenated components in gasoline refinery streams. There is a rich body of literature studies on ethanol combustion and these are summarized in the modeling studies of Marinov [4] and Li et al. [5]. Initiation in ethanol combustion is primarily through the C-C bond fission leading to CH_3 and CH_2OH, except in the case of ethanol-air mixtures in which case a competing initiation channel may be $C_2H_5OH + O_2$. For the lab-scale experiments simulated in this work, C-C bond fission is the only initiation channel. Our recent studies on the thermal decomposition kinetics of C_2H_5OH as part of a collaboratory effort between Michael, Harding, Klippenstein, and Ruscic [6] provides good estimates for the rate constants and branching ratios for the two major thermal decomposition channels, dehydration and C-C bond fission, at high temperatures with C-O bond fission contributing <5% under typical combustion conditions (T<2000 K, P<100 bars). The primary propagation routes in ethanol involve H-atom abstractions by OH, H, O, HO_2, and CH_3. Fuel consumption and ignition at intermediate temperatures (<1400 K) and pressure < 5 atm are sensitive to abstraction by OH simply because their rates are larger by as much as a factor of 2-4, with the next competing abstractions by H and O. Of course in a higher pressure/lower temperature environment with increasing availability of HO_2 through $H + O_2 (+M) \rightarrow HO_2 (+M)$, abstraction by HO_2 dominates fuel consumption.

In collaboration with Michael Davis (Argonne) we have initiated global sensitivity analyses of our ethanol model for a variety of reactor modules that sample stable species or characterize ignition. These analyses have highlighted that R (C_2H_5OH, CH_3OH, CH_3CHO etc.) + HO_2 not only dominates fuel consumption but that fuel consumption, intermediates formation and ignition in a high-pressure, low-temperature environment are also very sensitive to the rates for this class of reactions. We have performed ab-initio/transition state theory calculations to systematically characterize these H-atom abstraction reactions by HO_2 (particularly from ethanol and acetaldehyde) in our model. Our model for ethanol

combustion incorporates 53 species and 340 reactions and we believe that with our modeling and theory based estimates and the available literature kinetics data, the primary reactions in the ethanol and methanol sub-mechanisms are now reasonably well characterized.

Our modeling results indicate large uncertainties in rate coefficients for reactions important to CH_3CHO (primary intermediate in ethanol) consumption at combustion temperatures. We have also incorporated reactions that lead to vinyl alcohol, an intermediate produced in substantial amounts in ethanol flames [7]. Unlike a variety of hydrocarbon flames where the alkene + OH is the dominant enol source [7], the hydroxyalkyl radicals (ex. α-hydroxyethyl in ethanol) produced from H-atom abstractions represent a direct source for enol formation in alcohols. Large uncertainties reside in mechanistic routes and rate coefficients for vinyl alcohol consumption. We hope to resolve these remaining discrepancies using our model simulations, global sensitivity analyses in collaboration with Michael Davis (Argonne) and Dingyu Zhou and Rex T. Skodje (Univ. of Colorado-Boulder) and ab-initio/TST based predictions.

The assembled chemical kinetic model was tested against species profiles in flow reactors, jet stirred reactors, and laminar premixed flames. The model was also tested against ignition delay measurements behind shock waves and laminar flame speeds. Figures 1-4 represent predictions made by the assembled model against speciation data in reactors and flames and ignition delay measurements in shock tubes for ethanol combustion. The model is able to capture well the fuel decay, intermediates and products formation, and global combustion parameters such as ignition delay and flame speeds, over a wide range of conditions, 0.05 – 12 atm and temperatures 750 – 1700 K. The quality of the model predictions with the updated model used in the present work is of comparable if not better quality with literature models for ethanol combustion despite the significant differences between the rate constants and branching ratios used for the dominant initiation and propagation steps.

B. Toluene combustion

Toluene, the simplest alkyl-substituted aromatic species, is a major component in gasoline and diesel (5-25 % by volume) and represents a model aromatic surrogate species for these fuels. It also represents the simplest realistic surrogate to probe soot precursor mechanisms involving aromatic fuels. While significant progress has been made in the past few years towards understanding some of the important elementary steps in toluene combustion, the detailed modeling of toluene combustion poses several challenges from mechanistic aspects. Building on our experience from earlier modeling and experimental studies [8-12] we have assembled a detailed mechanism for toluene combustion. The present modeling effort incorporates updated mechanistic routes and fall-off considerations in the primary decomposition steps in toluene [11], benzyl [12], and phenyl [13], which appears to be lacking in recent modeling efforts in toluene combustion. The preliminary model predictions are in reasonable agreement with speciation data in shock tubes and flow reactors and ignition measurements in shock tubes.

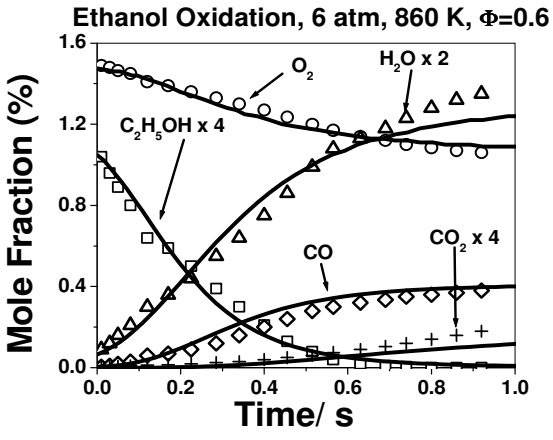

Figure 1: Flow reactor speciation data, Li et al.[5] Symbols-Data, Lines-Model, p.w, time shifted.

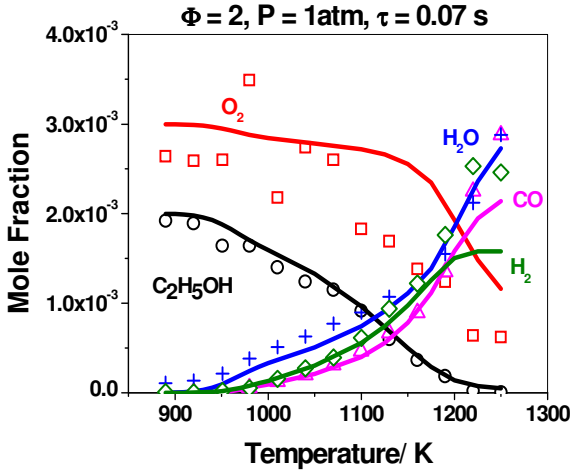

Figure 2: Jet stirred reactor speciation data, Leplat et al.[14] Symbols-Data, Lines-Model, p.w.

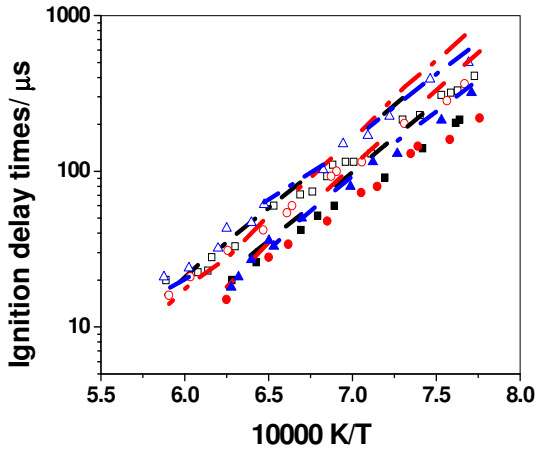

Figure 3: Ignition delay measurements, Natarajan and Bhaskaran[15], Open Symbols-Data 1atm, Dashed dot lines-Model, p. w., Closed symbols-Data 2 atm, Dashed Line-Model., Red – Phi=0.5, Black-Phi=1, Blue-Phi=2.

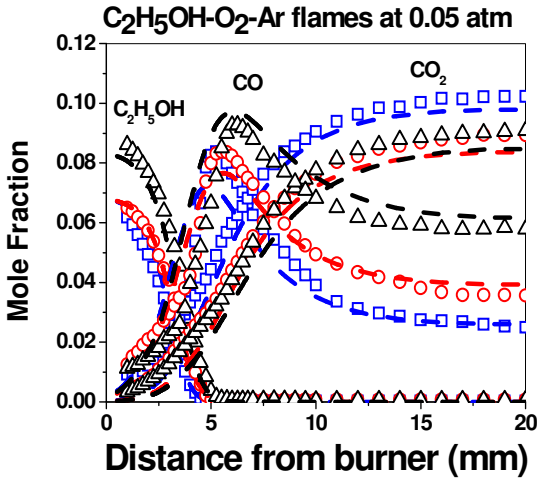

Figure 4: Laminar flame speciation data, Leplat et al.[14] Symbols-Data, Lines-Model, p.w.; Blue – Phi=0.75, Red-Phi=1, Black-Phi=1.25.

III. Future work

We plan to complete our small alcohol (C_1-C_2) combustion modeling and theoretical studies and use this experience to focus on developing models in a systematic approach for C_3-C_4 alcohols. Our modeling studies on toluene combustion are in progress and we propose to use global sensitivity analyses (in collaboration with Michael Davis) to guide model development and validation. We also propose to characterize theoretically H-atom abstractions by H and OH from small methylesters in a systematic manner. These abstractions represent dominant fuel consumption routes in methylesters. Furthermore ignition delays are sensitive to the rate coefficients for these abstractions. There are no high-temperature experiments and reliable theoretical predictions for the rates for these reactions [16]. Consequently we propose to initiate a collaborative effort with Joe Michael (experiments) to characterize the reactions of OH and H with four small methylesters (methyl formate, methyl acetate, methyl propionate, and methyl butanoate). The experiments will provide high-T measurements of the total rate constants. These measurements, in combination with the theoretical predictions for the total rate constants and branching ratios to various abstraction channels, will allow group estimates to be made for individual primary and secondary abstractions in methylesters. These groups can then be reliably extrapolated to larger methylesters that are better representative components of biodiesel.

IV. References

1. K. Kohse-Höinghaus, P. Osswald, T. A. Cool, T. Kasper, N. Hansen, F. Qi, C. K. Westbrook, P. R. Westmoreland, Angew. Chem. Int. Ed. **49** 3572 (2010).
2. S. Atsumi, T. Hanai, J.C. Liao, Nature **451** 86-U13 (2008).
3. www.epa.gov/air/caa/
4. N. M. Marinov, Int. J. Chem. Kin. **31**, 183 (1999).
5. J. Li, A. Kazakov, M. Chaos, F. L. Dryer, 5th US Combustion Meeting, Paper C26, (2007).
6. R. Sivaramakrishnan, M.-C. Su, J. V. Michael, S. J. Klippenstein, L. B. Harding, and B. Ruscic, J. Phys. Chem. A, **114**, 9425 (2010).
7. C. A. Taatjes, N. Hansen, J. A. Miller, T. A. Cool, J. Wang, P. R. Westmoreland, M. E. Law, T. Kasper, K.Kohse-Hoinghaus, J. Phys. Chem. A, **110**, 3254 (2006).
8. R. Sivaramakrishnan, R. S. Tranter, K. Brezinsky, Proc. Combust. Inst. **30**, 1165 (2005).

9. R. Sivaramakrishnan, R. S. Tranter, K. Brezinsky, J. Phys. Chem. A **110**, 9388 (2006).
10. R. Sivaramakrishnan, R. S. Tranter, K. Brezinsky, J. Phys. Chem. A **110**, 9399 (2006).
11. R. Sivaramakrishnan, J. V. Michael, Proc. Combust. Inst. **33,** 225 (2011) and references therein.
12. R. Sivaramakrishnan, M.–C. Su, J. V. Michael, Proc. Combust. Inst. **33**, 243 (2011) and references therein.
13. R. S. Tranter, S. J. Klippenstein, L. B. Harding, B R. Giri, X. Yang, J. H. Kiefer, J. Phys. Chem. A **114**, 8240 (2010).
14. N. Leplat, P. Dagaut, C.Togbe, J. Vandooren, Combust. and Flame, **158**, 705 (2011).
15. K. Natarajan, K. A. Bhaskaran, 13th International Symposium on Shock Waves 834 (1981).
16. http://kinetics.nist.gov

V. Journal articles supported by this project 2009-2011

1. R. Sivaramakrishnan, N. K. Srinivasan, M.-C. Su and J. V. Michael, "High Temperature Rate Constants for OH + Alkanes," Proc. Combust. Inst. **32**, 107-114 (2009).
2. R. Sivaramakrishnan and J. V. Michael, "Shock tube measurements of high temperature rate constants for OH with cyclo-alkanes and methyl-cyclo-alkanes," Combust. and Flame **156**, 1126-1134 (2009).
3. R. Sivaramakrishnan and J. V. Michael, "Rate constants for OH with selected large alkanes: Shock-tube measurements and an improved group scheme," J. Phys. Chem. A **113**, 5047-5060 (2009).
4. S. J. Klippenstein, L. B. Harding, B. Ruscic, R. Sivaramakrishnan, N. K. Srinivasan, M.-C. Su and J. V. Michael, "The thermal decomposition of NH_2OH and subsequent reactions: Ab initio Transition State Theory and reflected shock tube experiments," J. Phys. Chem. A **113**, 10241-10259 (2009).
5. R. Sivaramakrishnan, J. V. Michael and S. J. Klippenstein, "The direct observation of roaming radicals in the thermal decomposition of acetaldehyde," J. Phys. Chem. A **114**, 755-764 (2010).
6. R. Sivaramakrishnan, M.-C. Su, J. V. Michael, S. J. Klippenstein, L. B. Harding, and B. Ruscic, "Rate constants for the thermal decomposition of ethanol and its bimolecular reactions with OH and D: Reflected shock tube and theoretical studies" J. Phys. Chem. A **114**, 9425-9439 (2010).
7. R. Sivaramakrishnan, M.-C. Su, and J. V. Michael, "H- and D-atom formation from the pyrolysis of $C_6H_5CH_2Br$ and $C_6H_5CD_2Br$: Implications for high-temperature benzyl decomposition," Proc. Combust. Inst. **33**, 243-250 (2011).
8. R. Sivaramakrishnan and J. V. Michael, "Pyrolysis of $C_6D_5CH_3$: Rate constants and branching ratios in the high temperature thermal decomposition of toluene," Proc. Combust. Inst. **33**, 225-232 (2011).
9. R. Sivaramakrishnan, J. V. Michael, A. F. Wagner, R. Dawes, A. W. Jasper, L. B. Harding, Y. Georgievskii and S. J. Klippenstein, "Roaming radicals in the thermal decomposition of dimethyl ether: Experiment and theory," Combust. and Flame **158**, 618-632 (2011).
10. R. Sivaramakrishnan, M.-C. Su, J. V. Michael, S. J. Klippenstein, L. B. Harding and B. Ruscic, "Shock tube and theoretical studies on the thermal decomposition of propane: Evidence for a roaming radical channel," ASAP article, J. Phys. Chem. A, **115** (2011), dx.doi.org/10.1021/jp2006205

Other Publications supported by this project 2009-2011

1. R. Sivaramakrishnan, D. Y. Zhou, R. T. Skodje and M. J. Davis, "A comprehensive mechanism for ethanol combustion" Paper 3A03, 7th National Technical Meeting of the Combustion Institute, Atlanta, GA, Mar 20-23, 2011.
2. R. Sivaramakrishnan and J. V. Michael, "The thermal decomposition of o-xylyl radicals" Paper 2B03, 7th National Technical Meeting of the Combustion Institute, Atlanta, GA, Mar 20-23, 2011.

COMPUTATIONAL AND EXPERIMENTAL STUDY OF LAMINAR FLAMES

M. D. Smooke and M. B. Long
Department of Mechanical Engineering
Yale University
New Haven, CT 06520
mitchell.smooke@yale.edu

Program Scope

Our research has centered on an investigation of the effects of complex chemistry and detailed transport on the structure and extinction of hydrocarbon flames in coflowing axisymmetric configurations. We have pursued both computational and experimental aspects of the research in parallel. The computational work has focused on the application of accurate and efficient numerical methods for the solution of the boundary value problems describing the various reacting systems. Detailed experimental measurements were performed on axisymmetric coflow flames using two-dimensional imaging techniques. Spontaneous Raman scattering and laser-induced fluorescence were used to measure the temperature, and major and minor species profiles. Laser-induced incandescence (LII) has been used to measure soot volume fractions and particle sizes. A new approach to optical pyrometry has been developed to measure temperatures where the other techniques fail due to the presence of soot. Our goal has been to obtain a more fundamental understanding of the important fluid dynamic and chemical interactions in these flames so that this information can be used effectively in combustion modeling.

Recent Progress

Parallel Computing Methodology

Three different parallel implementations of a fully implicit, Newton-based, elliptic PDE solver have been developed and described. The three methods differ in their choices of whether to communicate quantities that are needed in each subdomain's halo region, or to recalculate those quantities locally. In conjunction with two types of domain decomposition, the three implementations have been applied to the test problem of an axisymmetric laminar coflow ethylene/air diffusion flame. In the "ideal" test case of one core per CPU and balanced-grid calculations all three methods compute the flame accurately with efficiencies of 75% to 90%. If multi-core calculations are considered, the parallelization efficiency inevitably drops because of the shared use of computational resources. However, when a faster network (20-Gbit/s Infiniband) is used, high scalability can still be obtained by substituting the calculation of chemical and transport quantities in the halo regions with appropriate message passing. The proposed implicit approach is particularly efficient for large mechanisms, for which it benefits both from high parallelization efficiencies and from unconstrained numerical stability (because of the fully implicit nature of the solver). In particular, results for a scalability test with five mechanisms (using box decomposition) have been generated which illustrate that the parallelization efficiency increases with the number of species even on a coarse grid (91×82 points) with 128 processes (see Figure 1). The results suggest that the proposed Newton-based communication intensive approach may also be applicable to larger scale problems that use a small chemical mechanism but very large computational grids. These parallel computational methods will enable the multidimensional study of flames having very complex fuel molecules, as well as the re-examination of simpler-fuel flames via chemical mechanisms that can have much greater detail than before.

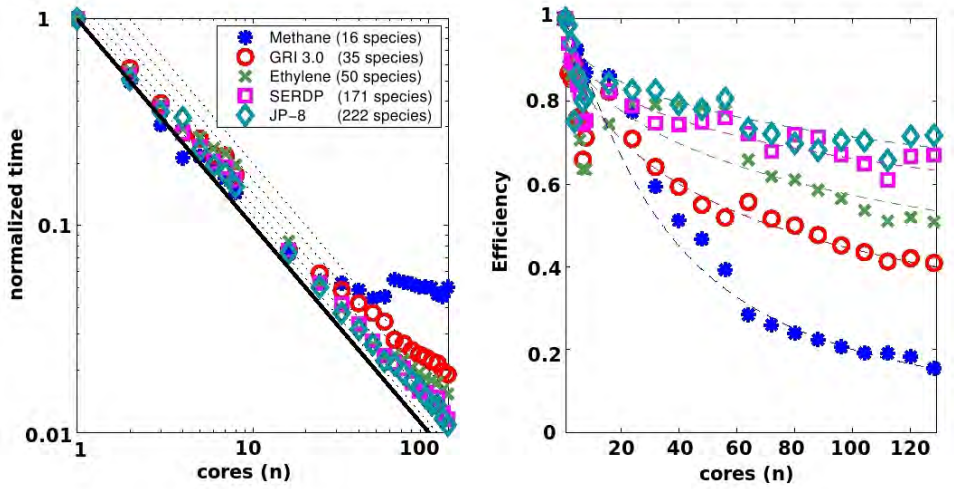

Figure 1. Scalability of the algorithm using multiple cores per node, box decomposition, and a 20-Gbit/s Infiniband network connection, comparing different chemical mechanisms and fuel molecules on an identical burner geometry. The left-hand plot shows the normalized computational time; the thick dark line represents the perfectly scalable limit while the dashed lines represent decreasing efficiencies of 90%, 80%, 70%, 60%, and 50%. In the right-hand plot, the parallelization efficiency is shown as a function of the number of processes, and the dashed line is a smooth interpolation to represent graphically the general trend of the data.

Time-Varying Flames:

The extension of the low order implicit solver to model time-dependent chemically reacting flows is hindered by the presence of large artificial diffusion, in particular from the first-order upwind discretizations of the convective terms in the governing equations. As in the steady-state problem, this can be reduced through grid refinement. In a time-evolving flow, however, node clustering must be adjusted dynamically to follow the movement of flow structures such as vortices. Otherwise, during some stages of the computations, important flow nonuniformities may penetrate regions of the domain having insufficient grid resolution and experience a significant amount of artificial diffusion, thus spuriously altering the flow dynamics. As an alternative approach, high order discretization schemes with negligible numerical diffusion can be used for flame computations.

We are applying high order compact spatial discretizations in a fully implicit framework that avoid these problems, and offer many advantages over other current approaches to solving reacting flow problems. Compact schemes are well suited to the simulation of time-dependent flows with complicated structures due to their excellent resolution characteristics [1,2]. Their integration into an efficient Newton-based flame code is an extremely challenging problem requiring research in modern iterative linear algebra solvers and preconditioning, novel storage/retrieval methodologies, fast Jacobian matrix algorithms, and domain decomposition methods. The necessity of implementing all these numerical techniques on message-passing parallel architectures only compounds the difficulty. However, an operation count/cost estimate indicates that the use of compact spatial discretizations with implicit time stepping may be able to reduce overall computation times by upwards of two orders of magnitude compared to other numerical methods commonly employed in detailed-chemistry combustion simulations [3].

Soot Measurements in a Series of Time-Varying Flames

Because the study of sooting time-varying flames are computationally intensive it is important to determine which flow conditions are best suited for study. For this reason, an effort to map out

the parameter space of sooting tendencies for various fuel dilutions and forcing levels was carried out experimentally. A fast, interline transfer camera (Cooke Sensicam) was used to acquire 1-ms exposure, phase-locked, images at 10 phases of sooting flames forced at 20 Hz. Soot luminosity images over a range of dilution levels were taken separately through two interference filters at 488 nm (blue) and at 633 nm (red). The luminosity images were Abel inverted to produce radial profiles of detected soot luminosity [4]. By calibration of the detector's spectral response and absolute sensitivity, the soot luminosity images can be used to determine both the soot temperature and volume fraction [5]. Measurements were taken for a series of fuel dilutions (28%, 30%, 32%, 35% and 40% C_2H_4 in N_2, respectively) and for a range of fuel flow modulations (20%, 30%, 40% and 50%). Figure 2 shows the soot volume fraction for different forcing levels in the 35% C_2H_4 flame. The quantitative results from this exploration will be used to guide further studies both computationally and experimentally.

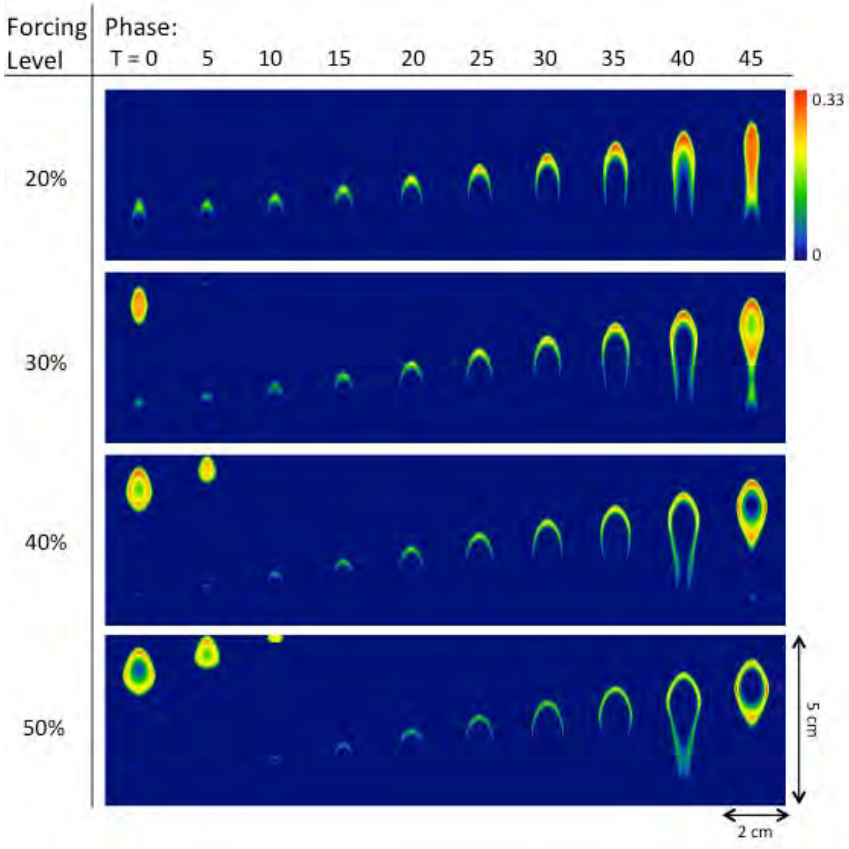

Figure 2. Soot volume fractions for a series of 35% C_2H_4 time-varying flames, for a range of forcing levels (20%, 30%, 40% and 50%). All images are shown on the same color scale (in ppm).

Future Plans

During the next year we will continue our study of time varying flames with the goal of fully implementing higher order compact-based methods. We plan to study both sooting and nonsooting hydrocarbon flames. Experimentally, we plan to add minor species measurements (*OH*, *CH* and *NO*) with laser- induced fluorescence to complete the characterization of species in these time-varying flames. Further, we will perform phase-resolved PIV measurements of the velocity profiles within the flames and, using the same techniques that we have developed for the steady sooting flames, we will perform phase-averaged measurements to characterize the soot in the time-varying flames.

References

1. S.K. Lele, “Compact Finite Difference Schemes with Spectral-Like Resolution,” J. Comput. Phys., 103, 16–42, 1992.
2. R.V. Wilson, A.O. Demuren, and M. Carpenter, “Higher-Order Compact Schemes for Numerical Simulation of Incompressible Flows, Part II: Applications,” Numer. Heat Transfer, Part B, 39, 231–255, 2001.
3. M. Noskov, Ph.D. Thesis, Yale University, 2004.
4. B. C. Connelly, Ph.D. Thesis, Yale University, 2009.
5. P. B. Kuhn, B. Ma, B. C. Connelly, M. D. Smooke, and M. B. Long, “Soot and Thin-filament Pyrometry Using a Color Digital Camera,” *Proceedings of the Combustion Insitute*, **33**, 2011.

DOE Sponsored Publications since 2009

1. B. C. Connelly, B. A. V. Bennett, M. D. Smooke, M. B. Long, “A Paradigm Shift in the Interaction of Experiments and Computations in Combustion Research,” *Proceedings of the Combustion Institute*, **32**, (2009).
2. B. C. Connelly, M. B. Long, M. D. Smooke, R. J. Hall and M. B. Colket, “Computational and Experimental Investigation of the Interaction of Soot and NOx in Coflow Diffusion Flames,” *Proceedings of the Combustion Institute*, **32**, (2009).
3. S. B. Dworkin, M. D. Smooke and V. Giovangigli, “The Impact of Detailed Multicomponent Transport and Thermal Diffusion Effects on Soot Formation in Ethylene/Air Flames,” *Proceedings of the Combustion Institute*, **32**, (2009).
4. J. H. Miller, B. McAndrew, M. P. Puccio, S. B. Dworkin, A. M. Schaffer, B. C. Connelly, M. B. Long and M. D. Smooke, “Measurements and Calculations of Formaldehyde Concentrations in a Methane/N2/Air, Non-Premixed Flames," *Proceedings of the Combustion Institute*, **32**, (2009).
5. B. A. V. Bennett, C. S. McEnally, L. D. Pfefferle, M. D. Smooke and M. B. Colket, “Computational and Experimental Study of the Effects of Adding Dimethyl Ether and Ethanol to Nonpremixed Ethylene/Air Flames,” *Comb. and Flame*, **156**, (2009).
6. H. Bufferand, L. Tosatto, B. La Mantia, M. D. Smooke and A. Gomez, “The Structure of Methane Counterflow Diffusion Flames Perturbed by Trace Amounts of Either JP-8 or a Six-Component Surrogate,” accepted for publication *Comb. and Flame*, **156**, (2009).
7. S. B. Dworkin, J. A. Cooke, B. A. V. Bennett, B. C. Connelly, M. B. Long, M. D. Smooke, R. J. Hall and M. B. Colket, “Distributed-Memory Parallel Computation of a Forced, Time-Dependent, Sooting, Ethylene/Air Coflow Diffusion Flame," *Comb. Theory and Modelling*, **13**, (2009).
8. M. Sanchez-Sanz, B. A. V. Bennett, M. D. Smooke and A. Linan, “Influence of Strouhal Number on Pulsating Methane/Air Coflow Jet Diffusion Flames,” **14**, *Comb. Theory and Modelling*, (2010).
9. R. B. Dobbins and M. D. Smooke, “A Fully Implicit Compact Finite Difference Method for the Numerical Solution of Unsteady Laminar Flames,” *Flow, Turb. and Comb.*, **85**, (2010).
10. P. B. Kuhn, B. Ma, B. C. Connelly, M. D. Smooke, and M. B. Long, “Soot and Thin-filament Pyrometry Using a Color Digital Camera,” *Proceedings of the Combustion Insitute*, **33**, 2011.
11. L. Tosatto, B. A. V. Bennett and M. D. Smooke, “A Flux-Based Directed Relation Graph Method for the On-the-Fly Reduction of Chemical Mechanisms,” to appear *Comb. and Flame*, (2011).
12. L Tosatto, B. A. V. Bennett and M. D. Smooke, “Parallelization strategies for an Implicit Newton-based Reactive Flow Solver,” to appear *Comb. Theory and Modelling*, (2011).

Quantum Chemistry of Radicals and Reactive Intermediates

John F. Stanton
Institute for Theoretical Chemistry
University of Texas
Austin, TX 78712

Scope of Research

My research group works in the area of theoretical chemical physics, especially on the properties and chemistry of organic radicals and other reactive intermediates. This research follows a number of paths, including first-principles calculations of bond energies and other thermochemical information (as well as development of methodology for such calcualtions), methods for the simulation and analysis of molecular spectroscopy, especially relevant to those experiments that can be used to glean thermochemical information, and the development of *ab initio* methods needed for the accurate treatment of transient organic molecules.

Summary of recent major accomplishments

We have investigated the thermochemistry of three fundamental and relatively stable organic radicals: vinyl, allyl and vinoxy; all of these being important in combustion. These calculations, which use the so-called HEAT protocol for thermochemistry, are the most accurate to date for these systems. The HEAT approach was designed to be as accurate as possible without making sacrifices for range of application. As a result, the approach was originally only applied to very small molecules and atoms. However, significant computational advances made in the parallelization of our CFOUR set of computer programs have allowed the required and very large calculations to be run for "large" molecules such as vinoxy, as well as (see below) hydrocarbons with as many as *seventeen* atoms. For the three important organic radicals mentioned above, the calculated values of $\Delta_f H^o(0K)$ evaluated at the HEAT-345(Q) level of theory are: 301.2 (vinyl), 179.4 (allyl) and 22.8 (vinoxy) kJ mol^{-1}, with corresponding 298 K values of 297.7, 168.7 and 16.7 kJ mol^{-11}.

In addition, we have begun work on a collaboration with W.D. Allen (Georgia) in which we aim to establish - by high-level HEAT and focal-point calculations - the enthalpies of formation of a group of compounds that serve as a basis set of sorts for a paradigm of computational thermochemistry using what are called hypohomodesmotic reactions[2]. In a hypohomodesmotic reaction (a class which represents a subset of isodesmic - bond types conserved reactions) involving hydrocarbons (to which this effort is restricted), the number of isopentyl, methyl, methylene and acetylenic carbons is also conserved. It transpires that the formation of *any* hydrocarbon can be written in terms of a hypohomodesmotic reaction involving the molecule of interest and eleven "synthons", none of which is larger than neopentane (the aforementioned seventeen-atom molecule). Consequently, if the enthalpies of formation for these "synthons" are known either *via* pure theory or Ruscic's ATcT approach, the enthalpy of formation of other - perhaps much larger - hydrocarbons can be computed at lower levels of theory that exploit the cancellation of basis set and correlation effects that are associated with reactions involving transformations between similar chemical species. At present, we have completed HEAT-345(Q) calculations on methane, ethane, acetylene, and ethylene; the remainder of the compounds are largely done, the latter effort involving one of the largest CCSD(T) and perhaps the largest CCSDT calculation performed to date (on neopentane). It is anticipated that all of these results will be completed by the end of the calendar year, paving the way for rapid new advances in our knowledge of hydrocarbon thermochemistry.

Also in the area of thermochemistry, we have carried out a study on the photoionization of formic acid in collaboration with T. Baer, an effort that was mapped out at a previous contractor's meeting at Airlie. In this work, we find both experimental and theoretical evidence for an unusual barrier for hydrogen loss from

[1] D.P. Tabor, M.E. Harding and J.F. Stanton, in preparation.
[2] S.E. Wheeler, K.N. Houk, P.R. Schleyer and W.D. Allen *J. Amer. Chem. Soc.* 131, 2547 (2009).

the formic acid cation. This barrier, which had previously complicated the analysis of the experimental data, is accurately predicted by standard (single-reference) coupled-cluster theory, which - in the case of hydrogen loss from a cation - provides a perfectly good description of the bond-breaking process. Ultimately, HEAT level calculations were done for formic acid and its isotopomers; this study provides accurate thermochemical results, using powerful experimental (TPEPICO) and theoretical (HEAT) methods, for the enthalpies of formation of formic acid, and the HOCO and HCO cations (-371.0, 600.3 and 827.6 kJ mol^{-1} for the normal isotopic species at 0 K), the latter of which helps to establish accurate enthalpies of protonation for carbon dioxide and carbon monoxide[1].

Our work in theoretical spectroscopy, using diabatic representations for cases of strong vibronic coupling and various approaches for the adiabatic nuclear motion problem, have also been used to assist the interpretation of vibrational spectra for the overtone region of the important propargyl radical[2] as well as the curious diazirinone (N_2CO) species[3] that represents a (meta)stable complex of the two most stable molecules known: molecular nitrogen and CO. In addition, the electronic spectrum of propadienyldene (H_2CCC:)[3], a molecule of interest, and important, to fields ranging from combustion science to the chemistry of the universe, has been successfully simulated and analyzed by means of high-level vibronic coupling calculations. The simulations effectively rationalize the very short lifetime found for the upper state levels in the strongly coupled $\tilde{A}^1A_2$ (dark) and $\tilde{B}^1B_1$ (bright) electronic states, and show that there is profound vibronic level congestion; approximately three hundred individual vibronic states manage to borrow intensity (*via* either Franck-Condon or non-adiabatic mechanisms) from the bright state origin, a process which leads to a quite complicated electronic spectrum[4].

In other work, we have been collaborating with John Barker (Michigan) on implementation of, and extensions to, the semi-classical transition state (SCTST) approach developed by Hernandez and Miller. In this method, the fact that good action-angle variables exist at a transition state is exploited to develop expressions for the tunneling probability analagous to the WKB treatment but allowing for anharmonicity in the reaction coordinate, as well as anharmonic coupling between the reaction coordinate and other modes belonging to the orthogonal complement. Initial results obtained with this method are excellent, and improvements in the implementation have been, and continue to be, worked out that will allow application of this approach to systems with approximately a dozen atoms. Also relevant here is that this work has also involved the first use of the HEAT methodology for the study of transition states[5].

Ongoing Research and Future Plans

A current focus of quantum chemical method development is towards methods that are applicable to "biradicals". These comprise two techniques that belong to the class of methods known as equation-of-motion coupled-cluster (EOM-CC) theory. In the first method, which we have implemented efficiently, carried out some initial pilot applications and analyzed in some detail, the reference state associated with the method is that of the molecule with two more electrons than the target state(s) of interest. This method, known as EOMDIP-CC, has been implemented at the (rather useless, honestly) EOMDIP-CCSD level as well as EOMDIP-CCSDT, which can be comparably accurate to single reference CCSD for simple systems not involving significant multireference character (and much better for more complicated systems like those involving e^2 or π^2 electronic configurations. This method, which has also been reported recently by Musial *et al.* does however have a few serious problems ultimately related to the fact that the reference state is a most unhappy molecule indeed; the requirement that two extra electrons are included has devastating consequences for studies that might wish to use extended basis sets, and these problems (also being looked at by A. Krylov (USC)) are lacking for a good solution at the present time. Another approach is to start with two *fewer* electrons, which does not have the same basis set issues. This has also been implemented, and preliminary work on the electronic spectrum of the Si_3 molecule (which involves a transition from an e^2e^0 configuration to an even more complicated e^1e^1 configuration.

[3] J.P. Maier, G.A.H. Walker, D.A. Bohlender, F.J. Mazziotti, R. Raghunandan, J. Fulara, I. Garkusha and A. Nagy *Astrophys. J.* 726, 41 (2011).

[4] J.F. Stanton, *Faraday Discussions*, in press.

[5] T.L. Nguyen, J.F. Stanton and J.R. Barker *Chem. Phys. Lett.* 499, 9 (2010).

References supported by DE-FG02-07ER15884 (2009-)

[1] Nicholas S. Shuman, Melanie Johnson, William R. Stevens, Michael E. Harding, John F. Stanton and Tomas Baer. Tunneling in a Simple Bond Scission: The Surprising Barrier in the H Loss from HCOOH+, *J. Phys. Chem. A*, 114, 10016 (2010).

[2] Xu Zhang, Stanley P. Sander, Adam Chaimowitz, G. Barney Ellison, and John F. Stanton. Detection of Vibrational Bending Mode ν_8 and Overtone Bands of the Propargyl Radical, $HCCCH_2$ *J. Phys. Chem. A* 114, 12021 (2010).

[3] Xiaoqing Zeng, Helmut Beckers, Helge Willner and John F. Stanton. Elusive Diazirinone, N_2CO *Angew. Chem. Intl. Ed.* 50, 1720 (2011).

[4] John F. Stanton. An unusually large nonadiabatic error in the BNB molecule, *J. Chem. Phys.* 133, 174309 (2010).

[5] Mathias Pabst, Andreas Koehn, Juergen Gauss and John F. Stanton. A worrisome failure of the CC2 coupled-cluster method when applied to ozone *Chem. Phys. Lett.* 495, 135 (2010).

[6] Ryan C. Fortenberry, Rollin A. King, John F. Stanton and T. Daniel Crawford. Crawford, T. Daniel. A benchmark study of the vertical electronic spectra of the linear chain radicals C_2H and C_4H, *J. Chem. Phys.* 132, 144303 (2010).

[7] Barney Ellison, Evan Jochnowitz, Xu Zhang, Mark Nimlos, Bradley Flowers, and John Stanton. Infrared Spectrum of the Propargyl Peroxyl Radical *J. Phys. Chem. A* 114, 1498 (2010).

[8] Etienne Garand, Kerstin Klein, John F. Stanton, Jia Zhou, Tara I. Yacovitch, and Daniel M. Neumark. Vibronic Structure of the Formyloxyl Radical (HCO_2) via Slow Photoelectron Velocity-Map Imaging Spectroscopy and Model Hamiltonian Calculations. *J. Phys. Chem. A* 114, 1374 (2010).

[9] Juergen Gauss Juana Vazquez, Michael E. Harding and John F. Stanton. High-Accuracy Extrapolated ab Initio Thermochemistry of the Propargyl Radical and the Singlet C_3H_2 Carbenes. *J. Phys. Chem. A* 113, 12447 (2009).

[10] Mychel E. Varner, Michael E. Harding, Juana Vazquez, Juergen Gauss, and John F. Stanton. Dissociation Energy of the HOOO Radical. *J. Phys. Chem. A* 113, 11238 (2009).

[11] Takatoshi Ichino, Juergen Gauss, and John F. Stanton. Quasidiabatic states described by coupled-cluster theory. *J. Chem. Phys.* 130, 174105 (2009).

[12] John F. Stanton. On the vibronic level structure in the NO_3 radical: II. Adiabatic calculation of the infrared spectrum. *Mol. Phys.* 107, 1059 (2009).

[13] Sandra L. Hobson, Edward F. Valeev, Attila G. Csaszar, and John F. Stanton. Is the adiabatic approximation sufficient to account for the post-Born-Oppenheimer effects on molecular electric dipole moments? *Mol. Phys.* 107, 8 (2009).

[14] John F. Stanton and Mitchio Okumura. On the vibronic level structure in the NO_3 radical Part III. Observation of intensity borrowing via ground state mixing. *Phys. Chem. Chem. Phys.* 11, 4742 (2009).

[15] Devin A. Matthews and John F. Stanton. Quantitative analysis of Fermi resonances by harmonic derivatives of perturbation theory corrections. *Mol. Phys.* 107, 213 (2009).

Universal and State-Resolved Imaging Studies of Chemical Dynamics

Arthur G. Suits
Department of Chemistry, Wayne State University
5101 Cass Ave
Detroit, MI 48202
asuits@chem.wayne.edu

I. Program Scope

The focus of this program is on combining universal ion imaging probes providing global insight, with high-resolution state-resolved probes providing quantum mechanical detail, to develop a molecular-level understanding of chemical phenomena. Particular emphasis is placed upon elementary reactions important in understanding and predicting combustion chemistry. This research is conducted using state-of-the-art molecular beam machines, photodissociation, reactive scattering, and vacuum ultraviolet lasers in conjunction with ion imaging technqiues. An ongoing parallel effort is made to develop new tools and experimental methods with which to achieve these goals.

II. Recent Progress

Systematic studies of polyatomic reaction dynamics

We continue our systematic studies of crossed-beam DC slice imaging of hydrocarbon reactions. These studies have been made possible by our intense radical source that gives very strong reactive scattering signal and minimal background. Our most detailed studies to date have focused on chlorine atom reactions with a wide variety of hydrocarbon target molecules, chosen to highlight various aspects of polyatomic reaction dynamics. In general, Cl atom reactions with hydrocarbons are fast, affording good signal-to-noise in challenging scattering studies. Moreover, the reaction energetics lie in an intermediate regime, i.e., some are endoergic, others thermoneutral or exoergic, and with either a modest barrier or no barrier to reaction. In addition, there are different abstraction sites and the possibility to investigate the associated reactivity. Finally, the H abstraction process leads to the diatomic product HCl, which can be detected with quantum state specificity and good sensitivity using resonance-enhanced multiphoton ionization (REMPI). In the past we reported an initial investigation of these reactions using state-resolved imaging of HCl from the Cl + ethane reaction. A systematic state-resolved series of investigations, complementing the VUV probed imaging, is described in future work below.

Last year we reported our systematic investigation of the isomer dependent dynamics in reaction of Cl with n-pentane, isopentane and neopentane. We have recently extended this to imaging Cl atom reactions with a series of monounsaturated hydrocarbons: 1-pentene, 1-hexene, 2-hexene, and cyclohexene at collision energies of 4 and 7 kcal/mol. The chemistry of Cl + alkene reactions is very rich, and more complicated than the saturated hydrocarbons owing to the presence of the double bonds and the dramatic variations in C-H bond energies across the various reaction sites (see Fig. 1). To date, numerous kinetic studies of chlorine with simple alkenes have been reported, but no detailed dynamical investigations. The rate constants reported in thermal studies represent three dynamically distinct processes: (1) addition to the double bond with stabilization of the adduct by a third body, (2) addition-elimination giving HCl and an alkenyl radical, (3) direct hydrogen abstraction the molecule giving the same products as (2).

$$Cl + C_nH_{2n} + M \rightarrow C_nH_{2n}Cl\cdot + M \quad (1)$$

$$Cl + C_nH_{2n} \rightarrow (C_nH_{2n}Cl)^* \rightarrow C_nH_{2n-1}\cdot + HCl \quad (2)$$

$$\rightarrow C_nH_{2n-1}\cdot + HCl \quad (3)$$

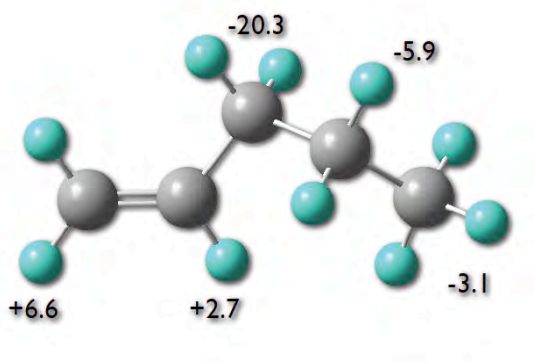

Figure 1. CBS-QB3 enthalpies (0 K) for Cl reaction with 1-pentene at the indicated site to give HCl and the associated radical.

Abstraction of an allylic H atom is strongly exoergic owing to the formation of the resonantly stabilized radical product, so this is the energetically preferred path. The addition channel (1) produces a chloroalkyl radical and is barrierless and exoergic (-20 kcal mol^{-1}). The products of addition-elimination (2) and direct abstraction (3) mechanisms are identical on the basis of chemical formula, but formation of distinct product isomers for these two pathways is clearly possible.

The results of our experiments show two distinct mechanisms for the reaction of chlorine atoms the molecules studied. At low collision energy, the angular distributions are highly isotropic with small (~3%) forward component. This suggests the formation of a long-lived intermediate that indicates addition-elimination mechanism with minimal direct H-atom abstraction contribution. At higher collision energy, the contribution of direct H-atom abstraction increases to ~13.5% of the product flux. The dynamics associated with the interaction of chlorine atoms with unsaturated hydrocarbons present a rich ground that merits further dynamical research.

In addition to the alkene studies, we recently reported the first crossed-beam imaging study directly probing primary vs. secondary H abstraction in the reaction of Cl with butane-1,1,1,4,4,4-d_6. The H- and D-atom abstraction channels were studied over a range of collision energies: 10.4 kcal/mol and 12.9 kcal/mol; 5.2 kcal/mol to 12.8 kcal/mol, respectively, using crossed molecular beam dc slice ion imaging techniques. These two channels manifest distinct dynamics principally in the translational energy distributions, while the angular distributions are remarkably similar. The reduced translational energy distribution for the primary abstraction showed marked variation with collision energy in the backward direction, while the secondary abstraction showed this variation in the forward direction. At the collision energies studied, no strong correlation between abstraction site and differential cross section was seen, perhaps accounting for inconsistent conclusions on this point arising from more indirect approaches over the years.

Roaming dynamics in NO_3

In collaboration with the North group at Texas A&M, we reexamined the photodissociation of the nitrate radical to give NO + O_2 in light of recent insights into roaming dynamics. The nitrate radical, NO_3, plays an important role in atmospheric chemistry, photolyzing in the visible region to yield two product channels:

$$NO_3 + h\nu \rightarrow NO + O_2 \quad (1)$$

$$\rightarrow NO_2 + O \quad (2)$$

The thresholds for both channels are close in energy (0.82 kcal/mol)[1] resulting in a narrow wavelength range (585-595 nm) for the molecular channel (1), since the higher energy radical channel (2) dominates once it is energetically accessible. The molecular channel threshold has been assumed to arise from a tight transition state involving a 3-center mechanism. However, no theoretical transition state of photochemically relevant energy has been identified, and roaming appears to be a likely mechanism. This state-correlated imaging study showed bimodal vibrational distribution was in the O_2 cofragment for some specific probed NO rotational levels, reminiscent of the CO product of H_2CO dissociation. For the major component, the O_2 was highly vibrationally excited as expected for a roaming-type intramolecular abstraction. The precise nature of the broader, large translational energy component is not yet clear.

Strong-Field Slice Imaging. A key aspect of our work has been the use of high-resolution slice ion imaging methods to obtain detailed velocity distributions for reaction products. Typically, these studies have detected products by resonance-enhanced ionization for small molecules, while in our reactive scattering studies we also have made extensive use of "universal" ionization of C-4 and larger hydrocarbon radicals using an F_2 excimer laser at 157nm. In many cases, however, we are interested in photochemistry of polyatomic molecules in an intermediate regime, in which the products are too large or complex to have assigned REMPI spectra, and too small (or closed shell) so that they cannot be readily detected at 157nm. We are now developing such an approach, termed "Strong Field Slice Imaging" (SFSI) using strong-field non-resonant ionization as a probe strategy. Numerous studies of the strong field ionization phenomenon have been reported over the years, with a comprehensive investigation reported in a feature article from the Dantus group.[1] Their extensive study examined a suite of 16 polyatomic molecules exposed to shaped femtosecond laser pulses at peak powers from 10^{13} to 10^{16} W/cm^2. They clearly demonstrated two features of control of femtosecond ionization by shaped pulses: 1) the total ion yield closely tracked the second harmonic signal, implying a two-photon bottleneck in the ionization process; 2) all pulse shape dependence of the ion mass spectrum could be reduced to a single parameter, the pulse duration, with transform limited pulses favoring minimal ion fragmentation. This suggests that no elaborate pulse shaping will be required for our purposes, in which we simply wish to minimize fragmentation of the detected species.

One issue with a universal imaging detection strategy is that one must minimize interaction with the molecular beam itself. This is a challenge for imaging, in which the probe is usually focused into the beam. To circumvent this, we are using a doubly differentially pumped beam source, collimated into a narrow rectangular cross section, which is employed in a "raster slice imaging" configuration as shown in Fig. 2. The probe laser is displaced downstream from the photodissociation laser, and translated through the recoiling photofragment cloud using an automated stepper motor. This is readily programmed to bypass the beam itself, minimizing background and excessive ionization. We have successfully demonstrated this approach for a number of systems, and we are currently investigating the strong-field ionization properties for small radical and atomic products of these reactions. Results for SO_2 dissociation at 193 nm are shown in Fig. 3, in which our stong field detection of SO is compared to imaging of the O atom cofragment by Brouard and coworkers.[2]

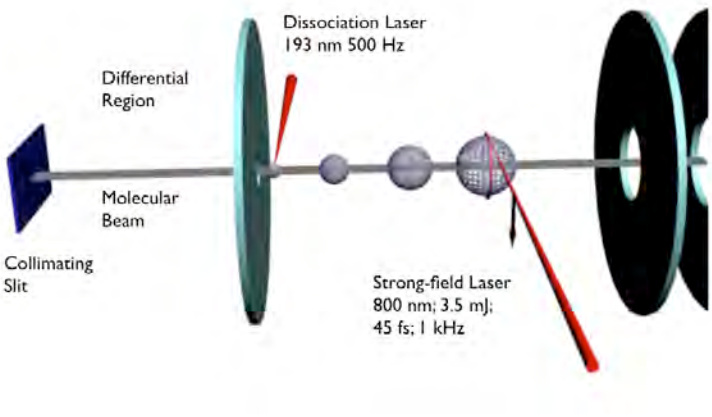

Figure 2. Schematic of SFSI approach showing interaction region.

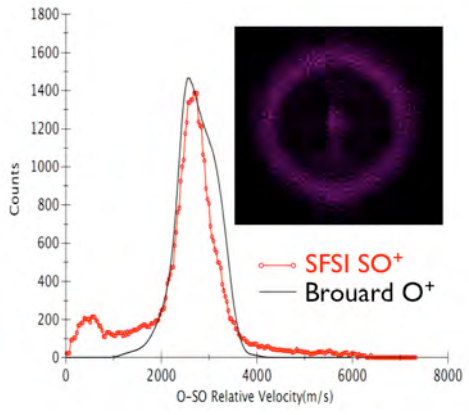

Figure 3. SFSI image of SO^+ and velocity distribution compared to O^+ REMPI imaging.

III. Selected Future Plans

State-resolved and universal crossed-beam DC slice imaging. We have plans to continue exploring a range of systems using our crossed-beam sliced imaging approach. We will finish an extended series of studies of Cl atom reactions, looking at alcohols as a function or isomer and chain length. An important aspect of our effort in the coming year is to implement fully state-selective detection

using our two-color reduced Doppler (TCRD) probe of the HCl product of these reactions. We were successful with state-resolved HCl detection for the Cl+ethane reaction using a single laser source in the past. With the TCRD probe, we anticipate enhanced sensitivity in the state-resolved imaging. In addition to exploring subtle features of the isomer dependent reactivity that did not appear strongly with the non-selective probe, we can look for differences in the rotationally-selected scattering for primary vs. secondary H abstraction, and compare HCl (v=0) and (v=1) distributions in the alkene reactions, in which we expect some interesting effects.

We also plan to extend the state-resolved TCRD imaging to study radical-radical reactions. Our first target will be the $O+CH_3$ reaction, a fascinating system that showed a novel H_2 elimination pathway which anticipated the roaming dynamics seen in formaldehyde.[3] For this system we can use TCRD REMPI detection of H_2 and CO products. We will prepare the O atoms photolytically, and the methyl radicals using flash pyrolysis.

j-j Correlations in Formaldehyde Roaming. We will revisit the rich formaldehyde system that has shown us so much concerning roaming dynamics. There is some suggestion in the data to-date that rotational excitation in CO is correlated to rotational excitation in H_2 for the roaming product. In the past we focused on the distinct correlations for roaming and non-roaming products. In the future we will "zoom in" to achieve maximal resolution for the slow roaming products and examine correlated H_2 rotation.

IV. References

1. V. V. Lozovoy, X. Zhu, T. C. Gunaratne, D. A. Harris, J. C. Shane, and M. Dantus, *J. Phys. Chem. A* **112** (17), 3789 (2008); C. Uiterwaal, C. R. Gebhardt, H. Schroder, and K. L. Kompa, *Euro. Phys. J. D* **30** (3), 379 (2004).

2. M. Brouard, R. Cireasa, A. P. Clark, T. J. Preston, and C. Vallance, *J. Phys. Chem. A*, 2004, *108* 7965.

3. T. P. Marcy, R. R. Diaz, D. Heard, S. R. Leone, L. B. Harding, and S. J. Klippenstein, *J. Phys. Chem* **105**, 8361 (2001).

V. DOE Publications 2009-present

V. Goncharov, N. Herath, A. Arregui, L. Banares, A. G. Suits, "Masked velocity map imaging: A one-laser-beam Doppler-free spectroscopic technique," *J. Phys. Chem A*, (2009) DOI: 10.1021/jp809711n.

A. D. Estillore, L. M. Visger, and A. G. Suits, "Imaging the dynamics of chlorine atom reactions with alkenes," *J. Chem. Phys.* **133,** 7 (2010).

M. P. Grubb, M. L. Warter, A. G. Suits, S. W. North, "Evidence of roaming dynamics and multiple channels for molecular elimination in NO_3 photolysis," *J. Phys. Chem. Lett.* **1**, 2455 (2010).

A. D. Estillore, L. Visger and A. G. Suits, "Crossed-beam DC slice imaging of chlorine atom reactions with pentane isomers," *J. Chem. Phys.* **132** 164313 (2010).

A. D. Estillore, L. M. Visger-Kiefer, T. A. Ghani. A. G. Suits, "Dynamics of H and D abstraction in the reaction of Cl atom with butane-1,1,1,4,4,4-d6," *Phys. Chem. Chem. Phys.* DOI:10.1039/c1cp20137a (2011).

N. Herath and A. G. Suits, "Roaming radical reactions," *J. Phys. Chem. Lett.*, **2** 642 (2011).

Elementary Reaction Kinetics of Combustion Species

Craig A. Taatjes
Combustion Research Facility, Mail Stop 9055, Sandia National Laboratories, Livermore, CA 94551-0969
cataatj@sandia.gov

SCOPE OF THE PROGRAM

This program aims to develop new methods for studying chemical kinetics and to apply these methods to the investigation of fundamental chemistry relevant to combustion science. One central goal is to perform accurate measurements of the rates at which important free radicals react with each other and with stable molecules. Another goal is to characterize complex reactions that occur via multiple potential wells by investigating the formation of products. Increasingly, these investigations are moving towards simultaneous time-resolved detection of multiple species in well-characterized photolytically-initiated reaction systems where multiple consecutive and competing reactions may occur. Understanding the reactions in as much detail as possible under accessible experimental conditions increases the confidence with which modelers can treat the inevitable extrapolation to the conditions of real-world devices. Another area of research is the investigation and application of new detection methods for precise and accurate kinetics measurements. Absorption-based techniques and mass-spectrometric methods have been emphasized, because many radicals critical to combustion are not amenable to fluorescence detection.

An important part of our strategy, especially for complex reaction systems, is using experimental data to test and refine detailed calculations (working in close cooperation with Stephen Klippenstein at Argonne and Ahren Jasper and Judit Zádor at Sandia), where the theory offers insight into the interpretation of experimental results and guides new measurements that will probe key aspects of potential energy surfaces. This methodology has been applied in our investigations of the reactions of alkyl radicals with O_2, where the combination of rigorous theory and validation by detailed experiments has made great strides toward a general quantitative model for alkyl oxidation. The focus of our laboratory is shifting to include investigations of the reactions oxygenated molecules relevant to biofuel combustion as well as studies of the effects of unsaturation on the chemistry leading to autoignition.

RECENT PROGRESS

We continue to apply frequency-modulation and direct absorption spectroscopy to measurements of product formation in reactions of alkyl radicals with O_2 and kinetics of unsaturated hydrocarbon radicals. In addition, the multiplexed photoionization mass spectrometric reactor at the Advanced Light Source (ALS), a close collaboration with David Osborn (see his abstract), has become a major part of our investigations of low-temperature hydrocarbon oxidation chemistry. Several highlights of the recent work are described briefly below.

Low-temperature oxidation chemistry of butanol. Butanol is an important emerging biofuel, and many groups around the world are investigating butanol combustion. Calculation and measurements of the high-pressure oxidation chemistry of butanol are also a focus of the Argonne-Sandia Consortium on High-Pressure Combustion Chemistry (see also the ASC-HPCC abstract).[1] In coordination with those efforts, measurements of low-pressure Cl-initiated oxidation of *n*-butanol have been undertaken in the multiplexed kinetics reactor at the ALS. Similarly to the oxidation of ethanol and isopentanol, substantial contributions from C-C bond fission channels are observed. These pathways are related to isomerization of hydroxybutylperoxy radicals via internal abstraction of an H atom from the hydroxyl group, resulting in formation of OH and two carbonyl species.

Oxidation of unsaturated C_5 alcohols. Isopentanol has been proposed as a potentially useful biofuel; efficient biochemical pathways exist to produce it from biomass and its performance in a HCCI engine is comparable to gasoline.[2,3] The production of unsaturated isoprenoid alcohols, of which the simplest are prenol (3-methyl-2-buten-1-ol) and isoprenol (3-methyl-3-buten-1-ol), is also favorable (in fact isopentanol is obtained by bioconversion of the unsaturated alcohols). We have investigated the effects of the unsaturation of the C_5 alcohols on the initial oxidation steps, measuring Cl- and OH-initated oxidation of prenol and isoprenol at low pressures in the ALS machine. The OH-initiated oxidation exhibits reactions from radicals formed by OH addition to the C=C double bonds, but similar addition pathways are negligible in Cl-initiated oxidation. The Cl-initiated oxidation is dominated by formation of allylic radicals in the initiation step. Because of the substantially smaller well depth for addition of oxygen, allylic radicals are generally less reactive with O_2. However the formation of HO_2 from reactions of alpha-hydroxyalkyl radicals with O_2 is so favorable that it remains facile for the alpha-radical formed in prenol oxidation, and the dominant initial reaction product in Cl-initiated oxidation of prenol is prenal (3-methyl-2-butenal).

Mechanism of ring-opening in OH-initiated oxidation of cyclohexene. Earlier experiments demonstrated that the OH-initiated oxidation of cyclohexene included a prominent ring-opening channel that is absent in oxidation of cyclopentene.[4] In collaboration with Giovanni Meloni at the University of San Francisco, we examined the mechanism of that ring opening by measuring the isomeric and isotopic products of OH-initiated oxidation of partially and fully deuterated cyclohexene, employing the technique of tunable synchrotron photoionization mass spectrometry. The ring-opening channel from the radical formed by OH-addition, hex-5-enal, was found to primarily result from C−C bond scission between the α and β carbons (along the former double bond) with an additional minor formation pathway in which the C−C bond scission occurs between the α and ζ carbons.

Chemistry of QOOH radicals. The reactions of hydroperoxyalkyl radicals "QOOH" with O_2 are responsible for chain branching in low-temperature hydrocarbon oxidation. However, although products of their reactions have been observed, no QOOH species has ever been directly detected by any means. We have continued our efforts to directly detect QOOH, but have also continued to explore indirect methods of experimentally characterizing these critical reactions.[5] Most recently we have used Cl atom reactions with alkylhydroperoxides to form QOOH radicals and investigated the

subsequent formation of products. Abstraction of the hydroxyl H is more favorable, but abstraction by Cl is not particularly site-specific, and a substantial fraction of the reaction forms the QOOH rather than the ROO isomers. For Cl + *t*-butyl hydroperoxide, only one QOOH isomer can be formed, $(CH_3)_2C(CH_2)OOH$. By far the most favorable channel for decomposition of this radical is to form OH + 2,2-dimethyloxirane.[6] On the other hand, the ROO isomer, *t*-butylperoxy radical, readily eliminates HO_2 to produce isobutene. Measurements of the products of Cl + *t*-butyl hydroperoxide in the ALS apparatus show rapid production of 2,2-dimethyloxirane even at room temperature, with little isobutene formation below 600 K. In laser absorption experiments we have found rapid production of OH following photolysis of Cl_2/*t*-butyl hydroperoxide mixtures. Addition of oxygen to the Cl + *t*-butyl hydroperoxide reaction showed a reduction in 2,2-dimethyloxirane yields and increased formaldehyde production, possibly related to QOOH + O_2 reactions.

Reaction of Cl with cyclohexylhydroperoxide can produce several QOOH species that have differing dissociation rate coefficients and products;[7] in principle the changes in *m*/*z* = 98 isomeric product ratios with added O_2 can be related to relative reaction and dissociation rate coefficients of the various QOOH isomers. Preliminary results on Cl-initiated oxidation of cyclohexylhydroperoxide indeed show changes in the isomer distribution with increasing oxygen, but it remains to be seen whether the results can be profitably deconvolved. Nevertheless we have demonstrated that Cl + alkylhydroperoxides are a useful avenue for explicit investigation of QOOH reactions.

FUTURE DIRECTIONS

Our analysis of the effects of unsaturation and oxygenation on low-temperature oxidation chemistry will also continue. Measurements of elementary oxidation reactions of representative biofuel molecules in the temperature region 500 K – 800 K will prove particularly important in developing a more general understanding of the ignition chemistry of alternative fuels.

The study of QOOH reactions will continue, with further efforts in the longstanding quest to directly detect QOOH. One key difficulty is simply making a high enough concentration of QOOH. The reactions of Cl with alkyl hydroperoxides may overcome this difficulty. I have referred before to the reactions of QOOH with molecular oxygen as the most important unmapped area in autoignition chemistry. Advanced theoretical kinetics has begun to develop rigorous predictions for these reactions; I hope that experiment can soon step up to test these predictions directly.

References

1 Vranckx, S. *et al.* Role of Peroxy Chemistry in the High Pressure Ignition of n-Butanol - Experiments and Detailed Kinetic Modelling. *Combust. Flame* **in press**, doi:10.1016/j.combustflame.2010.12.028 (2011).

2 Taatjes, C. A., Welz, O., Dec, J. E. & Yang, Y. Analysis of Advanced Biofuels. (Sandia National Laboratories, Livermore, California, 2010).

3 Yang, Y., Dec, J. E., Dronniou, N. & Simmons, B. A. Characteristics of Isopentanol as a Fuel for HCCI Engines. *SAE technical paper* **2010-01-2164** (2010).

4 Meloni, G., Selby, T. M., Osborn, D. L. & Taatjes, C. A. Enol Formation and Ring-Opening in OH-Initiated Oxidation of Cycloalkenes. *J. Phys. Chem. A* **112**, 13444-13451 (2008).

5 Fernandes, R. X., Zádor, J., Jusinski, L. E., Miller, J. A. & Taatjes, C. A. Formally direct pathways and low-temperature chain branching in hydrocarbon autoignition: The cyclohexyl + O_2 reaction at high pressure *Phys. Chem. Chem. Phys.* **11**, 1320-1327, doi:DOI:10.1039/B819825J (2009).

6 DeSain, J. D., Taatjes, C. A., Miller, J. A., Klippenstein, S. J. & Hahn, D. K. Infrared Frequency-Modulation Probing of Product Formation in Alkyl + O_2 Reactions: IV. Reactions of Propyl and Butyl Radicals with O_2. *Faraday Discuss.* **119**, 101-120 (2001).

7 Knepp, A. M. *et al.* Theory, measurements, and modeling of OH and HO_2 formation in the reaction of cyclohexyl radicals with O_2. *Phys. Chem. Chem. Phys.* **9**, 4315-4331 (2007).

Publications acknowledging BES support, 2009 –

1. Judit Zádor, Craig A. Taatjes, Ravi X. Fernandes, "Kinetics of Elementary Reactions in Low-Temperature Autoignition Chemistry," *Prog. Energy Combust. Sci.* in press, doi:10.1016/j.pecs.2010.06.006 (2011).

2. Haifeng Huang, Daniel J. Merthe, Judit Zádor, Leonard E. Jusinski, and Craig A. Taatjes, "New experiments and validated master-equation modeling for OH production in propyl + O_2 reactions," *Proc. Combust. Inst.* **33**, 293–299 doi:10.1016/j.proci.2010.06.039 (2011).

3. Satchin Soorkia, Craig A. Taatjes, David L. Osborn, Talitha M. Selby, Adam J. Trevitt, Kevin R. Wilson and Stephen R. Leone, "Direct detection of pyridine formation by the reaction of CH (CD) with pyrrole: a ring expansion reaction," *Phys. Chem. Chem. Phys.* **12,** 8750–8758 doi:10.1039/c002135k (2010).

4. Satchin Soorkia, Adam J. Trevitt, Talitha M. Selby, David L. Osborn, Craig A. Taatjes, Kevin R. Wilson and Stephen R. Leone, "Reaction of the C_2H radical with 1-butyne (C_4H_6): Low temperature kinetics and isomer-specific product detection," *J. Phys. Chem. A* **114**, 3340–3354 (Benoît Soep festschrift) doi:10.1021/jp911132r (2010).

5. Craig A. Taatjes, David L. Osborn, Talitha M. Selby, Giovanni Meloni, Adam J. Trevitt, Evgeny Epifanovsky, Anna Krylov, Baptiste Sirjean, Enoch Dames, Hai Wang, "Products of the Benzene + O (^{3}P) Reaction," *J. Phys. Chem. A* **114**, 3355–3370 (Benoît Soep festschrift) doi:10.1021/jp9114145 (2010).

6. Adam J. Trevitt, Fabien Goulay, Craig A. Taatjes, David L. Osborn and Stephen R. Leone, "Reactions of the CN Radical with Benzene and Toluene: Product Detection and Low Temperature Kinetics," *J. Phys. Chem. A* **114**, 1749–1755 doi:10.1021/jp909633a (2010).

7. Erin E. Greenwald, Buddhadeb Ghosh, Katie C. Anderson, Kristin S. Dooley, Peng Zou, Talitha Selby, David L. Osborn, Giovanni Meloni, Craig A. Taatjes, Fabien Goulay, and Simon W. North, "Isomer-Selective Study of the OH Initiated Oxidation of Isoprene in the presence of O_2 and NO: I. The Minor Inner OH-Addition Channel," *J. Phys. Chem. A* **114**, 904–912 doi:10.1021/jp908543a (2010).

8. T. Kasper, P. Oßwald, U. Struckmeier, K. Kohse-Höinghaus, C. A. Taatjes, J. Wang, T. A. Cool, M. E. Law, A. Morel, and P. R. Westmoreland, "The combustion chemistry of propanol isomers investigated by electron ionization and VUV-photoionization molecular-beam mass spectrometry," *Combust. Flame* **156**, 1181–1201 doi:10.1016/j.combustflame.2009.01.023 (2009).

9. Huzeifa Ismail, Paul R. Abel, William H. Green, Askar Fahr, Leonard E. Jusinski, Adam M. Knepp, Judit Zádor, Giovanni Meloni, Talitha M. Selby, David L. Osborn, and Craig A. Taatjes, "Temperature-Dependent Kinetics of the Vinyl Radical (C_2H_3) Self Reaction," *J. Phys. Chem. A* **113**, 1278–1286 doi:10.1021/jp8096132 (2009).

10. Fabien Goulay, Adam J. Trevitt, Giovanni Meloni, Talitha M. Selby, David L. Osborn, Craig A. Taatjes, Luc Vereecken and Stephen R. Leone, "Cyclic Versus Linear Isomers Produced by Reaction of the Methylidyne (CH) Radical with Small Unsaturated Hydrocarbons," *J. Am. Chem. Soc.* **131**, 993–1005 doi:10.1021/ja804200v (2009)

11. Adam J. Trevitt, Fabien Goulay, Giovanni Meloni, David L. Osborn, Craig A. Taatjes and Stephen R. Leone, "Isomer specific product detection of CN radical reactions with ethylene and propene by tunable VUV photoionization mass spectrometry, *Int. J. Mass Spectrom.* **280,** 113–118 doi:10.1016/j.ijms.2008.07.033 (Zdenek Herman festschrift) (2009).

12. Judit Zádor, Ravi X. Fernandes, Yuri Georgievskii, Giovanni Meloni, Craig A. Taatjes, and James A. Miller, "The reaction of hydroxyethyl radicals with O_2: a theoretical analysis and experimental product study," *Proc. Combust. Inst.* **32,** 271–277 doi:10.1016/j.proci.2008.05.020 (2009).

Elementary Reactions of PAH Formation

Robert S. Tranter
Chemical Sciences and Engineering Division, Argonne National Laboratory
Argonne, Il-60439
tranter@anl.gov

I. Program Scope

This program is focused on the experimental determination of kinetic and mechanistic parameters of elementary reactions, in particular those involved in the formation and destruction of the building blocks for aromatic species. Recently, the program has also encompassed the study of ethers and cyclic species and their dissociation products that are representative of oxygenated intermediates in combustion mechanisms. In addition, thermal sources of radicals are investigated and characterized for use in more complex reaction systems where secondary chemistry can be significant. The approach involves a diaphragmless shock tube (DFST) equipped with laser schlieren (LS) and a time-of-flight mass spectrometer (TOF-MS) and the development of a low pressure, fast flow, reactor equipped with a quadrupole MS. The combination of these techniques permits a wide range of reaction temperatures and pressures to be accessed.

II. Recent Progress

A. Dissociation of dimethyl ether and roaming

Pyrolysis and oxidation of dimethyl ether, DME, have been extensively studied, most recently by Sivaramarkrishnan et al.[i] They conducted an experimental and theoretical study of the initial dissociation and considered the possibility that the initial dissociation may not only occur by reaction (1) yielding radical products but that a second channel reaction (2), involving a roaming pathway exists leading to molecular products. At the conditions of their experiments OCH_3 readily dissociates by reaction (3) yielding H-atoms and therefore, assuming no other secondary reactions are significant, the H-atom concentration can be used to determine the branching ratio between reaction (1) and (2). Experimentally, Sivaramakrishnan et al. found $k_2/(k_1+k_2) = 0.19 \pm 0.07$ however, their theoretical analysis predicted $k_2/(k_1+k_2) < 0.03$.

$$CH_3OCH_3 \rightarrow CH_3 + OCH_3 \quad (1)$$

$$CH_3OCH_3 \rightarrow CH_4 + H_2CO \quad (2)$$

$$OCH_3 \rightarrow H + H_2CO \quad (3)$$

LS experiments are sensitive to the heat of reaction and rate of reaction. Reaction (1), the radical channel, is ~84 kcal/mol endothermic while the roaming pathway, reaction (2), is essentially isothermal, $\Delta H_{r,298K}$=0.2 kcal/mol. Thus if reaction (2) is strongly favored only weak initial density gradients would be observed. Furthermore, if reaction (1) is dominant but there is a reasonably large amount of DME removed by the roaming channel then the observed initial density gradients should be reduced.

DFST/LS experiments have been performed with reagent mixtures containing 2% and 4% DME dilute in krypton at incident shock pressures of 57 ± 4 Torr and 125 ± 5 Torr over the temperature range1500 – 2450 K. In these experiments secondary reactions are significant, in contrast to the work of Sivaramakrishnan et al., but the density gradient at t_0 , the start of reaction, is due solely to dissociation of DME. Example density gradient plots are shown in Fig. 1 for experiments with initial concentrations of 2% DME. At low temperatures only positive density gradients are observed whereas at higher temperatures and particularly higher pressures the profiles switch from positive to negative indicating that exothermic processes eventually dominate. Also shown in Fig. 1 are the results of simulations which show very good agreement with the experimental data and similar agreement is found over the complete range. Dissociation of DME generates H-atoms and CH_3 radicals and removal of DME by these species are the most important exothermic reactions (H+DME,$\Delta H_{r,298K}$=-7.9 kcal/mol; CH_3+DME, $\Delta H_{r,298K}$=-8.9 kcal/mol) in the early stages of reaction. Later, after most of the DME has been consumed reactions

involving H_2CO and HCO are the main sources of negative density gradients. The rate expression for H + DME was taken from reference[i] and that for CH_3 + DME was taken from Zhao et al.[ii] This latter rate produced excessively negative gradients and was subsequently reduced by a factor of 3 which is reasonable considering the uncertainties in the rate and the need to extrapolate to high temperatures.

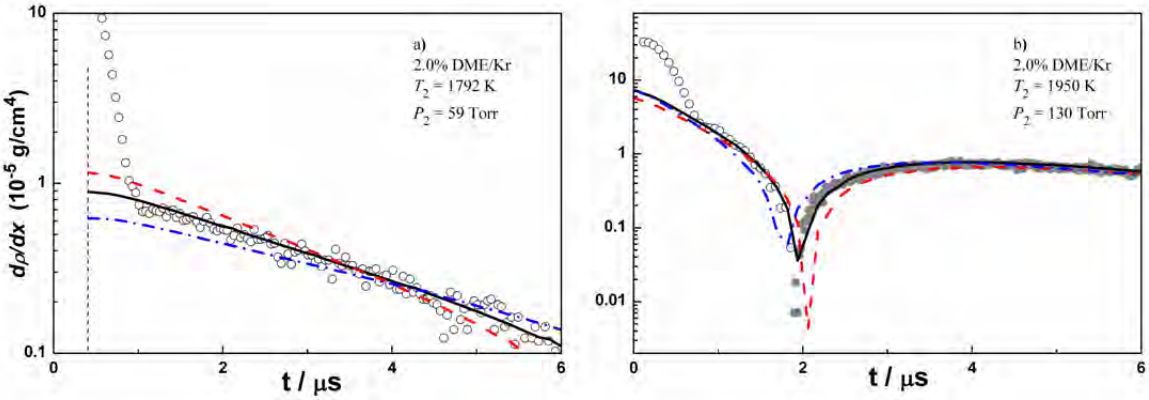

Figure 1: Semi-log plots of density gradients from LS experiments. Fig. (a) shows a small incubation delay (vertical dotted line). Points represent experimental data and absolute values are plotted, ○ +ve; ● -ve. Solid black lines are the results of simulations with $k_2/(k_1+k_2)$=0.01. a) Red dash line: (k_1+k_2) ×1.3, Blue dash dot line: 0.7× (k_1+k_2); b) Red dash line, $k_2/(k_1+k_2)$ = 0.2; blue dash dot line $k_2/(k_1+k_2)$ = 0.2 and (k_1+k_2)*1.3 .

The simulations shown in Fig. 1 were performed with $k_2/(k_1+k_2)$ = 0.01 and the excellent agreement with experiment suggests that reaction (2) plays only a minor role under the conditions of these experiments. The sensitivity of the simulations to both the branching ratio and magnitude of total rate of dissociation of DME, (k_1+k_2), are also shown in Fig.1. The effect of increasing the branching ratio to 0.2 while keeping (k_1+k_2) fixed clearly has a marked effect on the agreement between experiment and simulation. If (k_1+k_2) is increased to compensate for the increased branching ratio then the simulations drop faster than the experiments. Thus it appears that the LS experiments favor a small branching ratio for initial of DME with little dissociation by the roaming path. Of course there may be pressure and temperature dependencies in the branching ratio that have not been accounted for. However, there is significant overlap in the temperature range of these experiments and those of Sivaramakrishnan et al. and their lower pressures are similar to the high pressures of this work. Clearly, additional effort is required to resolve the apparent discrepancies in branching ratios and certainly further examination of secondary reactions, in particular CH_3+DME, which influence the LS experiments is necessary.

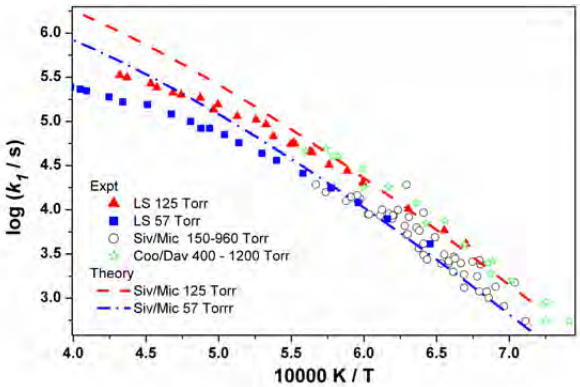

Figure 2 First order rate coefficients for DME → CH_3 + OCH_3. Siv/Mic: Ref. 1; Coo/Dav: Ref. 2.

From the values of (k_1+k_2) obtained it is clear that dissociation of DME is close to the low pressure limit at the reaction conditions in these experiments. The derived k_1 are compared in Fig.2 with the high temperature experimental results of Sivaramakrishan et al.,[i] Cook et al.,[iii] and values calculated from Troe parameters provided by Sivaramakrishnan et al. Clearly, there is very good agreement between all the experiments and the predicted k_1 agree extremely well with the current work up to 1800 K where greater falloff is found in the experimental results than predicted.

B. Dissociation of phenyl fluoride, chloride and bromide

Previous work on the self-reaction of phenyl radicals revealed that disproportionation reactions of phenyl will generate significant amounts of *o/m/p*-benzynes and suggest that the role of o-benzyne radicals may be much more important in the formation of PAH and soot than previously thought. The only high temperature kinetic study of *o*-benzyne dissociation is reflected shock H-ARAS experiments by Xu et al.[iv] Their results indicate that o-benzyne primarily dissociates to diacetylene and acetylene in agreement with Zhang et al.[v] who investigated the products of o-benzyne pyrolysis. DFST/LS/TOF-MS experiments have been conducted to investigate pyrolysis and self-reaction of *o*-benzyne at high temperatures. The monohalobenzenes were used as precursors for phenyl and benzyne radicals and due to the scarcity of data on the high temperature dissociation of these species a secondary aspect of the work was the investigation of pyrolysis of the precursors. C_6H_5I dissociates almost exclusively by C-I scission and the DFST experiments with C_6H_5(Br/Cl/F) indicate that HX elimination becomes increasingly dominant as the C-X bond strength increases and C_6H_5F dissociates only by HX elimination. Rate coefficients for HF elimination from C_6H_5F are shown in Fig. 3 where they are compared with the results of RRKM calculations (E_0 = 91 kcal/mol, $\langle\Delta E_{down}\rangle$ = 800 cm^{-1}) Analysis of the C_6H_5Br and C_6H_5Cl experiments is ongoing but the initial analysis indicates that dissociation of C_6H_5Br favors dissociation by C-Br scission at lower reaction temperatures with a switch to HBr elimination at higher temperatures. In the LS experiments with C_6H_5(Br/Cl/F) the temperatures are sufficiently high to immediately convert any C_6H_5 formed into o-benzyne + H. Consequently, as the halobenzenes dissociate at different but overlapping temperature ranges it is possible to probe both recombination and dissociation of *o*-benzyne radicals and preliminary dissociation rates have been obtained from the C_6H_5F work. These results show strong falloff and are about a factor of 8 lower than the 2bar predictions of Xu et al.[iv]

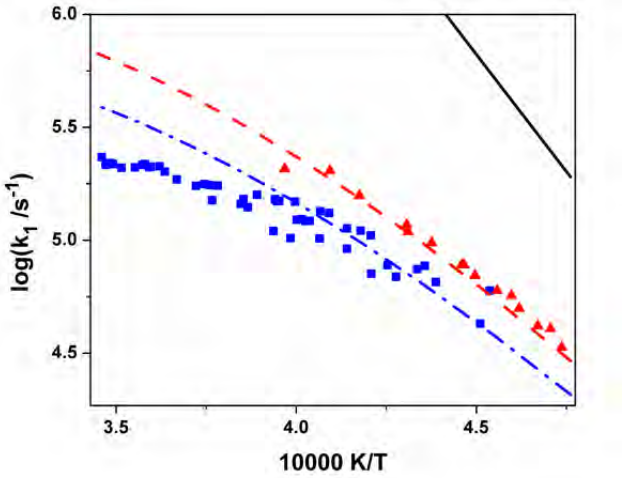

Figure 3 First order rate coefficients from LS experiments for $C_6H_5F \rightarrow$ o-C_6H_4 + HF. Symbols represent experiments and lines RRKM calculations. Red; 120 Torr; Blue 60 Torr; Black H.P.L.

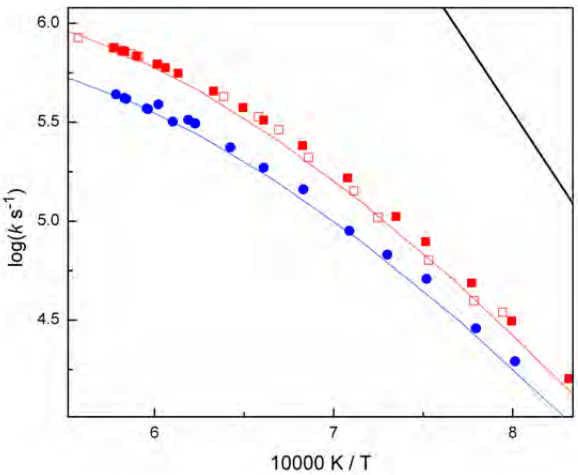

Figure 4 First order rate coefficients from LS experiments for EGVE $\rightarrow$ $HOCH_2CH_2$ + $OCH=CH_2$. Symbols represent experiments and lines RRKM calculations. Red; 120 Torr; Blue 60 Torr; Black H.P.L.

C. Ethylene glycol vinyl ether, EGVE

EGVE, $HOCH_2CH_2OCH=CH_2$, is one of the primary dissociation products of 1,4-dioxane and in an earlier DFST study of the dioxane[vi] it was concluded that EGVE was not stabilized when formed but dissociated immediately. Theoretical investigations of EGVE dissociation suggested that two routes were available one leading to stable molecular products, reaction (4) and the other to radical species reaction (5).

EGVE $\rightarrow$ $CH_3CHO + C_2H_3OH$ (4)

EGVE $\rightarrow$ $HOCH_2CH_2 + OCH=CH_2$ (5)

However, due to the number of coupled internal rotors in EGVE accurate master equation predictions of the rates for each channel could not be made although the radical channel was favored. The branching between

reactions (4) and (5) is of significance because the products of (5) readily dissociate yielding OH and H and promote chain reaction whereas the products of reaction (4) are thermally stable. A DFST/LS/TOF-MS study of EGVE pyrolysis has been carried out and the branching between reactions (4) and (5) investigated. The branching is temperature dependent and over the range of the LS experiments (1200-1800 K; 57 and 122 Torr) the radical channel is strongly favored and becomes increasingly dominant as the temperature increases. However, if the results are extrapolated to lower temperatures then below 1100 K reaction (4) the molecular channel dominates which is consistent with the only other shock tube investigation of a vinyl ether, ethylene vinyl ether.[vii] Rate coefficients for reaction (5) obtained from the LS experiments are shown in Fig. 4 where they are compared with the results of a Gorin model RRKM calculation. E_0=66.0 kcal/mol and was taken from a theoretical estimate by A.W. Jasper. $<\Delta E_{down}>$ = 600 cm^{-1} and the hindrance parameter, $\eta = 1\text{-}0.1\times T^{0.2}$ treated as adjustable.

III. Future Work

The DFST studies of pyrolysis and self-reaction of o-benzyne radicals will be completed and in addition to the monohalobenzenes additional precursors will be investigated. Additional experiments are planned to study reactions of phenyl and o-benzyne radicals with small molecules such as C_2H_2 and CH_3. Work has started to investigate precursors of allyl radicals and the self-reaction of allyl radicals as part of an ongoing study of the high temperature reactions of resonantly stabilized radicals. A study of CH_3 + DME will be carried out in the DFST utilizing diacetyl as the source of methyl radicals. Diacetyl was previously studied in the DFST and dissociates at a significantly lower temperature than DME.

Installation of a new TOF-MS and interface between the TOF-MS and DFST will be completed. The new TOF-MS should improve the temporal resolution and mass resolution and improvements to the data acquisition hardware and software for the TOF-MS will be investigated.

IV. References

i. Sivaramakrishnan R., Michael J.V., Wagner A.F., Dawes R., Jasper A.W., Harding L.B., Georgievskii Y., Klippenstein S. J., Combust. Flame, **158**, 618-632, 2011

ii. Zhao Z., Chaos M. Kazakov A., Dryer F. L., Int. J. Chem. Kinet., **40**, 1-18, 2008

iii. Cook R.D., Davidson D. F., Hanson R. K., J. Phys. Chem. A, **113**, 9974–9980, 2009

iv. Xu, C.; Braun-Unkhoff, M.; Naumann, C.; Frank, P. *Proc. Combust. Inst.* **2007,** *31*, 231.

v. Zhang, X.; Maccarone, A. T.; Nimlos, M. R.; Kato, S.; Bierbaum, V. M.; Ellison, G. B.; Ruscic, B.; Simmonett, A. C.; Allen, W. D.; Schaefer, H. F.; III *J. Chem. Phys.* **2007,** *126* (4), 044312-044320

vi. Yang X., Jasper A. W., Giri B. R., Kiefer J. H. Tranter R. S, Phys. Chem. Chem. Phys., **2010**, 13, 3686.

vii. Shimofuji, K.; Saito, K.; Imamura, A. *J. Phys. Chem.* **1991,** *95*, 155.

V. Publications and submitted journal articles supported by this project 2009-2011

1. Tranter R. S., Yang X. ,Kiefer, J. H. 'Dissociation of C_3H_3I and rates for recombination of C_3H_3 high temperatures' Proc. Combust. Inst.**, 2011,** 33, 259.
2. Yang X., Jasper A. W., Giri B. R., Kiefer J. H. Tranter R. S.'A shock tube and theoretical study on the pyrolysis of 1,4-dioxane' Phys. Chem. Chem. Phys., **2010**, 13, 3686.
3. Tranter R. S., Klippenstein S. K., Harding L. B., Giri B. R., Yang X., Kiefer J. H., "An experimental and theoretical investigation of the self-reaction of phenyl radicals" J. Phys. Chem. A, March **2010,** 114, 8240**.**
4. Yang X., Jasper A.W., Kiefer J. H., Tranter R. S., "The Dissociation of Diacetyl: A Shock Tube and Theoretical Study" J. Phys. Chem. *A*, **2009**, 29, 8318.
5. Yang X., Goldsmith C. F. and Tranter R. S., "Decomposition and Vibrational Relaxation in CH3I and Self-Reaction of CH3 Radicals" J. Phys. Chem. A, **2009**, *113*, 8307.

Variational Transition State Theory

Donald G. Truhlar
Department of Chemistry, University of Minnesota
207 Pleasant Street SE, Minneapolis, Minnesota 55455
truhlar@umn.edu

Program scope

This project involves the development of variational transition state theory (VTST) [Garrett and Truhlar 2005] including optimized multidimensional tunneling contributions and its application to gas-phase reactions with a special emphasis on developing reaction rate theory in directions that are important for applications to combustion. The further development of VTST/OMT as a useful tool for combustion kinetics also involves developing and applying new methods of electronic structure calculations for the input potential energy surface, which is typically an implicit surface defined by a level of electronic structure theory, and methods to interface reaction-path and reaction-swath dynamics calculations with electronic structure theory. The project also involves the development and implementation of practical techniques and software for applying the theory to various classes of reactions and transition states and applications to specific reactions, with special emphasis on combustion reactions and reactions that provide good test cases for methods needed to study combustion reactions.

The application of VTST to gas-phase reactions is carried out by direct dynamics [Truhlar and Gordon 1990, Truhlar 1995], and it involves electronic structure calculations of potential energy surfaces and the use of these surfaces to calculate generalized free energies of activation and multidimensional tunneling probabilities. A key emphasis is the interface of electronic structure calculations with dynamics algorithms as achieved in the POLYRATE computer program and its various RATE interfaces to electronic structure packages.

Recent progress

One of the challenges of modeling combustion and atmospheric chemistry is determining the reaction rates of intermediate species because their kinetics is often difficult to study directly. Quantum chemistry is playing an increasingly important role in this process. Enols have been implicated as intermediates in combustion [Taatjes et al. 2005], but the calculation of its reaction rates is very difficult because the electronic wave function has high multireference character. Therefore we adopted a multireference approach to calculate barrier heights for the various possible reaction channels possible reaction channels of OH with ethenol. Six barrier heights for abstracting H from a C–H bond range from 3.1 to 7.7 kcal/mol, two barrier heights for abstracting H from an O–H bond are both 6.0 kcal/mol, and two barrier heights for OH addition to the double bond are –1.8 and –2.8 kcal/mol. Thus we expect abstraction at high-temperature and addition at low temperature. The factor that determines which H is most favorable to abstract is an internal hydrogen bond that constitutes part of a six-membered ring at one of the abstraction saddle points (as illustrated in the figure); the hydrogen bond contributes about 3 kcal/mol stabilization.

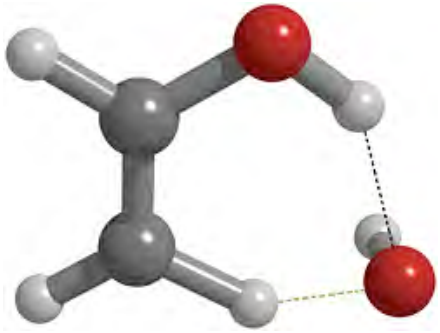

In order to generate reactive potential energy surfaces with minimal computational effort, we have introduced an algorithm called multiconfiguration Shepard interpolation (MCSI, formerly called multiconfiguration molecular mechanics, MCMM). MCSI describes polyatomic potential energy surfaces in terms of interacting molecular mechanics configurations (each of which is the analog of a valence bond configuration) and this provides a specialized interpolation formalism that is particularly powerful. MCSI fitting involves the reactant, product, and saddle point stationary points and a small number of non-stationary points. We developed a general strategy for placement of the non-stationary points for fitting potential energy surfaces in the kinetically important regions and for calculating rate constants for atom transfer reactions by variational transition state theory with multidimensional tunneling. The new method is proving robust and efficient for everyday use.

Software distribution

We have developed several software packages for applying variational transition state theory with optimized multidimensional tunneling coefficients to chemical reactions and for carrying out MCCM calculations, density functional theory calculations with new density functionals, direct dynamics, and MCSI applications. The URL of our software distribution site is comp.chem.umn.edu/Truhlar. The license requests that we fulfilled during the period Jan. 1, 2009–Apr. 5, 2011 for software packages developed wholly or partially under DOE support is as follows:

	Total	*academic*	*government//DoD/non-profit/industry*
POLYRATE	267	230	67
GAUSSRATE	144	130	14
GAMESSPLUSRATE	18	13	5
NWCHEMRATE	12	8	4
5 other RATE programs	34	27	7

The total number of requests fulfilled for the four explicitly named programs in the table above since Jan. 1, 1995 is 1665.

Future plans

The general objective of this project is to develop and employ improved methods for calculating the rate constants of gas-phase chemical reactions. Our current plans are as follows:

(1) We aim to improve the implementation of interpolated VTST algorithms in the POLYRATE computer program and to further develop multi-configuration Shepard interpolation as an efficient tool for the semiautomatic fitting of potential energy surfaces for large systems.

(2) Second, we aim to improve the interface of rate theory with electronic structure methods, especially to develop improved multi-coefficient correlation methods and density functionals for using electronic structure theory to calculate potential energy surfaces. We are especially interested in developing methods applicable to radicals, reactive intermediates, and complex organic molecules, as required for modeling combustion of real fuels.

(3) Third, plan to incorporate more reliable methods for including anharmonicity at variational transition states, with a special emphasis on torsions and mode coupling. For this purpose we propose to calculate benchmark converged partition functions for molecules with multiple torsions and to use them to test new approximation schemes.

(4) Fourth, we propose to continue the development, documentation, and distribution of software for carrying out calculations based on the methods developed in this project.

(5) We plan to add pressure-dependent modeling capability to POLYRATE.

(6) Finally, we plan to continue calculate rate constants for specific applications that are important in combustion.

References Cited

[Garrett and Truhlar 2005] "Variational transition state theory," B. C. Garrett and D. G. Truhlar, in *Theory and Applications of Computational Chemistry: The First Forty Year*s, edited by C. E. Dykstra, G. Frenking, K. Kim, and G. Scuseria (Elsevier, Amsterdam, 2005), pp. 67-87.

[Taatjes et al. 2006] "Combustion Chemistry of Enols: Possible Ethenol Precursors in Flames," C. A. Taatjes, N. Hansen, J. A. Miller, T. A. Cool, J. Wang, P. R. Westmoreland, M. E. Law, T. Kasper, and K. Kohse-Höinghaus, J. Phys. Chem. A **110**, 3254-3260 (2006).

[Truhlar and Gordon 1990] "From force fields to dynamics: classical and quantal paths," D. G. Truhlar and M. S. Gordon, Science **249**, 491–498 (1990).

[Truhlar 1995] "Direct dynamics method for the calculation of reaction rates," D. G. Truhlar, in *The Reaction Path in Chemistry: Current Approaches and Perspectives*, edited by D. Heidrich (Kluwer, Dordrecht, 1995), pp. 229–255. [Understanding Chem. React. **16**, 229–255 (1995).]

Publications supported by this grant, 2009-present

1. "The DBH24/08 Database and Its Use to Assess Electronic Structure Model Chemistries for Chemical Reaction Barrier Heights," J. Zheng, Y. Zhao, and D. G. Truhlar, Journal of Chemical Theory and Computation 5, 808-821 (2009). http://dx.doi.org/10.1021/ct800568m (John Perdew 2009 special issue)
2. "Efficient Diffuse Basis Sets: cc-pVxZ+ and maug-cc-pVxZ," E. Papajak, H. R. Leverentz, J. Zheng, and D. G. Truhlar, Journal of Chemical Theory and Computation 5, 1197-1202 (2009). dx.doi.org/10.1021/ct800575z. Errata and addendum: 5, 3330 (2009). dx.doi.org/10.1021/ct9004905.
3. "Thermochemical Kinetics for Multireference Systems: Addition Reactions of Ozone," Y. Zhao, O. Tishchenko, J. R. Gour, W. Li, J. J. Lutz, P. Piecuch, and D. G. Truhlar, Journal of Physical Chemistry A 113, 5786–5799 (2009). dx.doi.org/10.1021/jp811054n.
4. "Non-Hermitian Multiconfiguration Molecular Mechanics," O. Tishchenko and D. G. Truhlar, Journal of Chemical Theory and Computation 5, 1454-1461 (2009). dx.doi.org/10.1021/ct900077g.
5. "The Muonic He Atom and a Preliminary Study of the 4Hem + H2 Reaction," D. J. Arseneau, D. G. Fleming, O. Sukhorukov, J. H. Brewer, B. C. Garrett, and D. G. Truhlar, Physica B: Condensed Matter 404, 946-949 (2009). dx.doi.org/i:10.1016/j.physb.2008.11.13 (Proceedings of the Eleventh International Conference on Muon Spin Rotation, Relaxation and Resonance).
6. "Direct Dynamics Study of Hydrogen-Transfer Isomerization of 1-Pentyl and 1-Hexyl Radicals," J. Zheng and D. G. Truhlar, Journal of Physical ChemistryA 113, 11919-11925 (2009). dx.doi.org/10.1021/jp903345x.

7. “Steric Effects and Solvent Effects on SN2 Reactions,” Y. Kim, C. J. Cramer, and D. G. Truhlar, Journal of Physical Chemistry A 113, 9109-9114 (2009). dx.doi.org/10.1021/jp905429p
8. “Homogeneous Nucleation with Magic Numbers: Aluminum,” S. L. Girshick, P. Agarwal, and D. G. Truhlar, Journal of Chemical Physics 131, 134305/1-11 (2009). dx.doi.org/10.1063/1.3239469
9. “Phase Space Prediction of Product Branching Ratios: Canonical Competitive Nonstatistical Model,” J. Zheng, E. Papajak, and D. G. Truhlar, Journal of the American Chemical Society 131, 15754-15760 (2009). dx.doi.org/10.1021/ja904405v.
10. “Least-Action Tunneling Transmission Coefficient for Polyatomic Reactions,” R. Meana-Pañeda, D. G. Truhlar, and A. Fernández-Ramos, Journal of Chemical Theory and Computation 6, 6-17 (2010). dx.doi.org/10.1021/ct900420e
11. “Efficient Diffuse Basis Sets for Density Functional Theory,” E. Papajak and D. G. Truhlar, Journal of Chemical Theory and Computation 6, 597-601 (2010). dx.doi.org/10.1021/ct900566x. (Letter)
12. “Kinetics of Hydrogen-Transfer Isomerizations of Butoxyl Radicals,” J. Zheng and D. G. Truhlar, Physical Chemistry Chemical Physics 12, 7782-7793 (2010). dx.doi.org/10.1039/b927504e.
13. “Communication: Energetics of Reaction Pathways for Reactions of Ethenol with the Hydroxyl Radical: The Importance of Internal Hydrogen Bonding at the Transition State,” O. Tishchenko, S. Ilieva, and D. G. Truhlar, Journal of Chemical Physics 133, 021102/1-4 (2010). dx.doi.org/10.1063/1.3455996
14. “Direct Dynamics Implementation of the Least-Action Tunneling Transmission Coefficient. Application to the CH4/CD3H/CD4+CF3 Abstraction Reactions,” R. Meana-Pañeda, D. G. Truhlar, and A. Fernández-Ramos, Journal of Chemical Theory and Computation 6, 3015-3025 (2010). dx.doi.org/10.1021/ct100285a
15. “Minimally Augmented Karlsruhe Basis Sets,” J. Zheng, X. Xu, and D. G. Truhlar, Theoretical Chemistry Accounts 128, 295-305 (2011). dx.doi.org/10. 1007/s00214-010-0846-z
16. “Kinetic Isotope Effects for the Reactions of Muonic Helium and Muonium with H2,” D. G. Fleming, D. J. Arseneau, O. Sukhorukov, J. H. Brewer, S. L. Mielke, G. C. Schatz, B. C. Garrett, K. A. Peterson, and D. G. Truhlar, Science 331, 448-450 (2011). dx.doi.org/10.1126/science.1199421
17 “Computational Study of the Reactions of Methanol with the Hydroperoxyl and Methyl Radicals. Part I: Accurate Thermochemistry and Barrier Heights,” I. M. Alecu and D..G. Truhlar, Journal of Physical Chemistry A 115, 2811–2829 (2011). dx.doi.org/dx.doi.org/10.1021/jp110024
18. “High-Level Direct-Dynamics Variational Transition State Theory Calculations Including Multidimensional Tunneling of the Thermal Rate Constants, Branching Ratios, and Kinetic Isotope Effects of the Hydrogen Abstraction Reactions from Methanol by Atomic Hydrogen,” R. Meana-Pañeda, D. G. Truhlar and A. Fernández-Ramos, Journal of Chemical Physics 134, 094302/1-14. dx.doi.org/10.1063/1.3555763
19. “Practical Methods for Including Torsional Anharmonicity in Thermochemical Calculations on Complex Molecules: The Internal-Coordinate Multi-Structural Approximation,” J. Zheng, T. Yu, E. Papajak, I, M. Alecu, S. L. Mielke, and D. G. Truhlar, Physical Chemistry Chemical Physics, accepted Feb. 11, 2011. dx.doi.org/10.1039/C0CP02644A

Dimerization of polycyclic aromatic hydrocarbons and their collision efficiency

Angela Violi
Department of Mechanical Engineering, University of Michigan
Ann Arbor, MI 48109-2125
avioli@umich. edu

I. Program Scope

The dimerization of polycyclic aromatic hydrocarbons has been regarded as one of the most important processes in soot formation. In particular, the dimerization of pyrene is widely used as a nucleation process in many soot modeling studies. In this work, we report on a theoretical study using molecular dynamics simulations to investigate the role of various polycyclic aromatic hydrocarbon molecules, including pyrene, in the soot formation process [1-4]. Our simulation results indicate that the collision efficiency is primarily influenced by two major factors, temperature and molecular mass, and the pyrene dimerization route is more dependent on the flame temperature conditions than those of larger polycyclic aromatic hydrocarbons. There are also other important factors that influence collision efficiency, such as molecular curvature, that can induce complex behaviors in various temperature conditions. The results from this study can be utilized to obtain accurate nucleation rates for soot models.

II. Recent Progress

In order to predict the soot nucleation rate, we calculate the collision efficiency of dimerization between various hydrocarbons. We can define the nucleation rate through dimerization in terms of the collision rate and the collision efficiency of two molecules. The PAH collision rate for the nucleation can be expressed as [21]

$$r_{coll} = r_{nuc} \times N_{avo} = \frac{1}{2} \sum_{i=1}^{\infty} \sum_{j=1}^{\infty} \beta_{ij} N_i N_j \tag{1}$$

where r_{nuc} is the nucleation rate, N_{avo} is Avogadro's number, and N_i is the number density of *i* species. Assuming a free-molecular regime, β_{ij} can be expressed as

$$\beta_{ij} = \beta \times \sigma_{ij} \sqrt{\frac{8 k_B T}{\pi \mu_{ij}}} \tag{2}$$

where β is the collision efficiency, σ_{ij} is the reaction cross section between species *i* and *j*, and μ_{ij} is the reduced mass of species *i* and *j*. It should also be mentioned that β is not a constant, but highly dependent on temperature because the energy level of two colliding molecules is one of the important factors that determines β. Obtaining β is not straightforward. Therefore, we evaluate the dimerization of various PAH molecules using Molecular Dynamics (MD) simulations to provide more detailed nucleation rates of these compounds and to identify the effect of parameters, such as temperature and morphology.

An important component of this study is to accurately indentify collision and dimerization events. A collision criterion solely based on distance cannot be used to detect collision events, since it is unable to distinguish between mere collisions and effective collisions that lead to dimerization. Therefore, we use an additional lifetime cutoff, based on 20 ps, to distinguish between collision types.

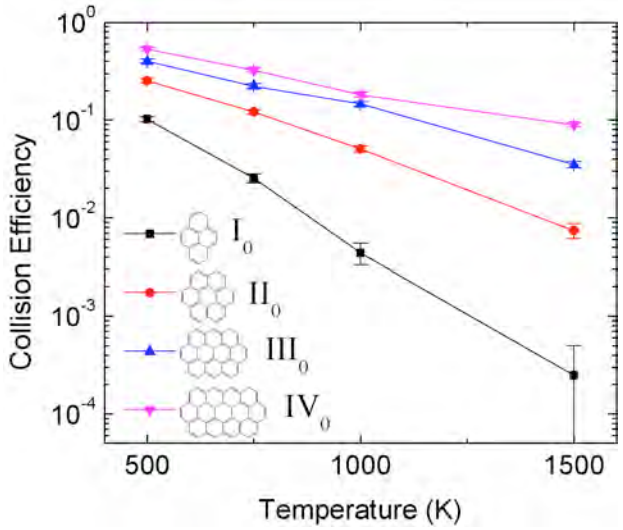

The figure on the left reports the collision efficiency, obtained with MD simulations, for four flat PAH molecules (I0, II0, III0, and IV0). Two major factors contribute to the results: temperature and molecular mass. In addition, it is important to note that there is a difference in the magnitude of variation depending on molecular mass in this temperature range. For example, in the case of IV0, the collision efficiency drops from 0.53 at 500 K to 0.089 at 1500 K, so the variation is within an order of magnitude. In contrast, in the case of I0, the collision efficiency drops from 0.10 at 500 K to 0.00025 at 1500 K, which is an almost three order of magnitude drop in collision efficiency. Since the temperature of the soot zone is usually within this temperature range, the pyrene (I0) dimerization route as a soot nucleation process is expected to be highly dependent on the flame conditions such as the temperature of soot nucleation zone, while the IV0 dimerization route is expected to be more consistent at various temperature conditions.

Morphological effects

While temperature and molecular mass are the two most important factors, molecular morphological effects such as the presence of an aliphatic chain or curvature in the PAH surface also influence the collision efficiency. The figure on the right shows I_0 with its corresponding structures having an aliphatic chain attachments – I_1, and I_2. The collision efficiency of II_0, which has a molecular mass (300 amu) comparable to that of I_2 (286 amu) is also plotted for comparison. Similarly, the lower panel in the figure below presents the collision efficiencies for II_0 with its corresponding structures with aliphatic chain attachments – II_1, and II_2, and the collision efficiency for III_0 is shown for comparison. The addition of an aliphatic chain to these PAH molecules produces different dimerization trends depending on the temperature. We suggest two possible explanations that may contribute to these trends: the addition of low frequency internal vibrational modes and the steric hindrance. At 1500 K, the collision efficiency values of I_1, I_2, II_1, and II_2 are lower than those of corresponding PAH molecules I_0 for I_1 and I_2, and II_0, for II_1 and II_2. and these results demonstrate that the addition of an aliphatic chain lowers collision efficiency. This is observed despite the fact that

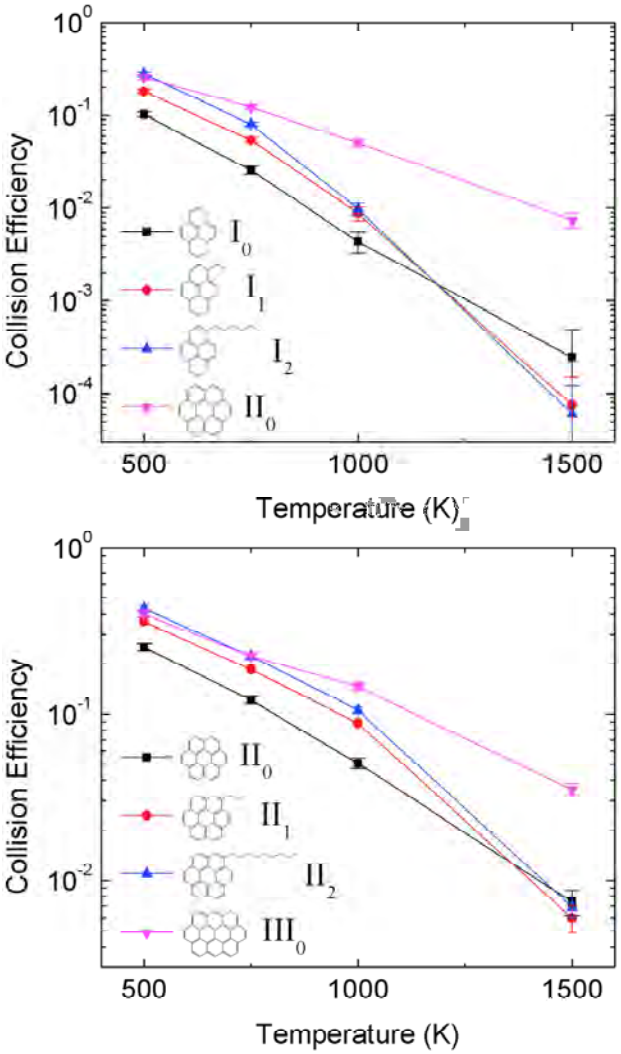

the addition of an aliphatic chain increases the total mass of the molecules, which should help increasing the collision efficiency. This effect is likely due to the steric hindrance introduced by an aliphatic chain, which limits the range of effective collision angles that can accommodate PAH stacking. However, the trend becomes opposite when temperature decreases. At lower temperatures such as 500 K, I_1, I_2, II_1, and II_2 have higher collision efficiency than the corresponding I_0 and II_0 molecules. I_2 has an even higher collision efficiency value than II_0, even though II_0 is heavier than I_2.

Next, the effect of curvature in the PAH surface is examined. In the figure below, the collision efficiency of V_0, which has three five-membered rings that result in a curved PAH surface, is compared with that of III_0 and IV_0, which are flat PAH molecules. The curved V_0 molecule has a different trend in changes of the collision efficiency compared to the flat PAH molecules. While V_0 (444 amu) is heavier than III_0 (398 amu) and lighter than IV_0 (496 amu), the collision efficiency of V_0 is lower than that of III_0 at temperatures higher than 750 K. We suggest two possible factors that may contribute to this trend: the direction of dimerization and the difference in binding energy for a wide range of collision angles. Firstly, the low collision efficiency of V_0 is due to the curvature in the PAH surface, because there is a preferential direction for dimerization unlike the planar PAH surface. However, if the temperature is low enough (e.g. 500 K) to accommodate the dimerization in an unfavorable direction, curvature in the PAH surface may help to increase the collision efficiency.

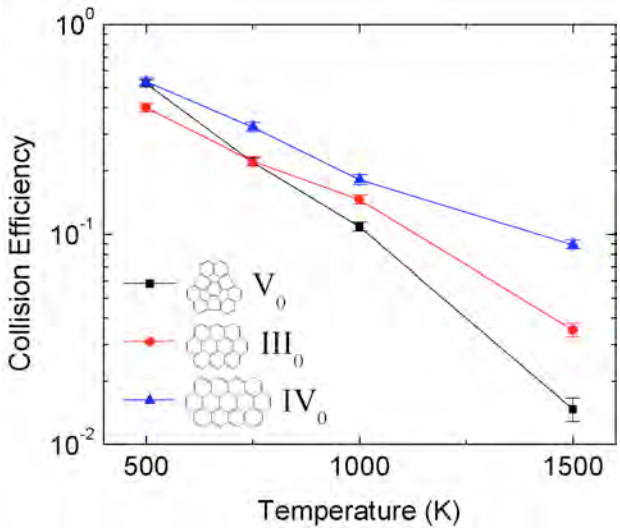

III. Future Work

Simulation work is in progress to investigate the effect of mass, temperature and morphology on various systems spanning a wide range of conditions to include nanoparticles. Our study show that pyrene dimerization route as a soot nucleation process is expected to be highly dependent on the various flame temperature conditions, while the larger PAH dimerization route is expected to be more consistent for various temperature conditions. We plan to investigate also the behavior of heteromolecular systems to determine a comprehensive model for nucleation.

IV. References

[1] Frenklach M. Reaction mechanism of soot formation in flames. Physical Chemistry Chemical Physics **2002**; 4(11):2028-37.

[8] Stein SE, Fahr A. High-temperature stabilities of hydrocarbons, Journal of Physical Chemistry **1985**; 89(17):3714-25.

[12] Miller JH, Smyth KC, Mallard WG. Calculations of the dimerization of aromatic hydrocarbons: Implications for soot formation. Symposium (International) on Combustion **1985**; 20(1):1139-47.

[18] Sabbah H, Biennier L, Klippenstein SJ, Sims IR, Rowe BR. Exploring the Role of PAHs in the Formation of Soot: Pyrene Dimerization. Journal of Physical Chemistry Letters **2010** Oct;1(19):2962-7.

V. Publications and submitted journal articles supported by this project in 2010

1. S. H. Chung, A. Violi "Nucleation of Fullerenes as a Model for Examining the Formation of Soot ", *Journal of Chemical Physics* **132**: 174502 (2010).
2. 48. S.H. Chung, A. Violi, "Peri-condensed aromatics with aliphatic chains as key intermediates for the nucleation of aromatic hydrocarbons" Proceedings of the Combustion Institute **33**(1): 693 (2011).

Ultrafast Structural Dynamics in Combustion Relevant Model Systems

Peter M. Weber
Department of Chemistry
Brown University, Providence, Rhode Island 02912
Peter_Weber@brown.edu

I. Program Scope

We have found that Rydberg electron binding energies are quite useful measures that relay a molecular ion core's geometrical structure. One can understand the structure sensitivity of the Rydberg electron by realizing that its orbit is defined by the charge distribution of all components of the ion core molecule. In the experiment we measure the electron binding energy, i.e. the energy difference between the electron in the Rydberg state and the electron at infinite distance. If the ion core changes its structure then the Rydberg electron has to adjust its energy. This provides us with a handle to observe, in real time, the structural dynamics of molecules.

Several features make this spectroscopy uniquely applicable. For one, the Rydberg electron is very large, and therefore encompasses the entire molecule. Secondly, the ionization does not change vibrational quantum numbers, so that even complicated and large molecules provide spectra with comparably high resolution. Important also is that any vibrational excitation is not seen in the spectrum. This has the interesting consequence that the spectra are blind toward internal, vibrational energy. For the study of chemical dynamics, where the molecules invariably are very energetic, this is a tremendously advantageous feature. It implies that, as a tool to probe the time-dependent structural dynamics of chemically interesting molecules, Rydberg spectroscopy may well be better suited than diffraction techniques. At this point, we can only qualitatively interpret the Rydberg spectra, but anticipating that in the future one may be able to calculate Rydberg binding energy spectra, the technology may indeed be developed into a structure determination method.

We implement Rydberg ionization spectroscopy using a time-resolved pump-probe multi-photon ionization/photoelectron scheme in which a first laser pulse excites the molecule to a Rydberg state, and a probe pulse ionizes the molecule. A time-of-flight detector measures the kinetic energy spectrum of the photoelectrons. The photoelectron spectrum directly provides the binding energy of the electron, and thereby reveals the molecule's time-dependent structural fingerprint. The time resolution of the measurement is given by the duration of the laser pulses, which in our experiment is on the order of 100 fs. To measure structural dynamics in Rydberg-excited states we time-delay the ionization photon from the pump photon. To measure the dynamics in ground or excited valence states we induce the dynamics using a near UV laser pulse, and use a multi-photon ionization scheme via the Rydberg states as a probe process.

II. Recent Progress

Several studies have been completed in the past year. They include work on methylated cyclopentadienes [7], phenyl ethyl N,N di-methyl amine [6],[2], amyl nitrite [5], and triethylamine [1]. We also published a review on the dynamics of 1,3-cyclohexadiene [3]. In the following we report on the ongoing work on the latter system.

Electronic curve crossing dynamics

Electronic curve crossings through conical intersections are important in the opening and closing of hydrocarbon rings containing double bonds. These mechanisms are very important in the formation of soot during combustion processes. Electrocyclic reactions are a mainstay of organic chemistry and important in energy conversion processes.

The application of the Rydberg photoionization technique to systems with conical intersections has been extremely rewarding. In previous years, we have explored the curve crossing dynamics of cyclopentadiene and cyclohexadiene systems through their conical intersections. Following the Rydberg spectra as a function of time has yielded accurate time constants, which are in the range of 50 to 200 fs, depending on the molecular system. More recently, we have extended these studies to explore how the electronic curve crossing dynamics depends on the electronic energy of the excited state. For this study we use cyclohexadiene as a model system.

While 268 nm excitation into the 1B valence state opens the ring to form hexatriene, we have found little evidence for this reaction upon excitation with 207 nm. This is even though the molecule contains 1.36 eV more energy. The analysis of the Rydberg spectra, figure 1, shows that the largest part of the wave packet bypasses the reactive electronic surfaces and goes directly to the ground electronic state.

The difference in the photochemical activity of the states excited at 268 and 207 nm is reflected in the different time dependencies of the Rydberg electron binding energies, figure 2. The photochemically stable state shows a fairly modest variation of the binding energy with delay time, while the opening of the ring is associated with a much larger binding energy shift. Structural distortions associated with 3p-excitation cause a dynamical shift in the p_x- and p_y-binding energies by 10 and 26 meV/ps respectively, whereas after excitation into 1B more severe structural transformations along the ring-

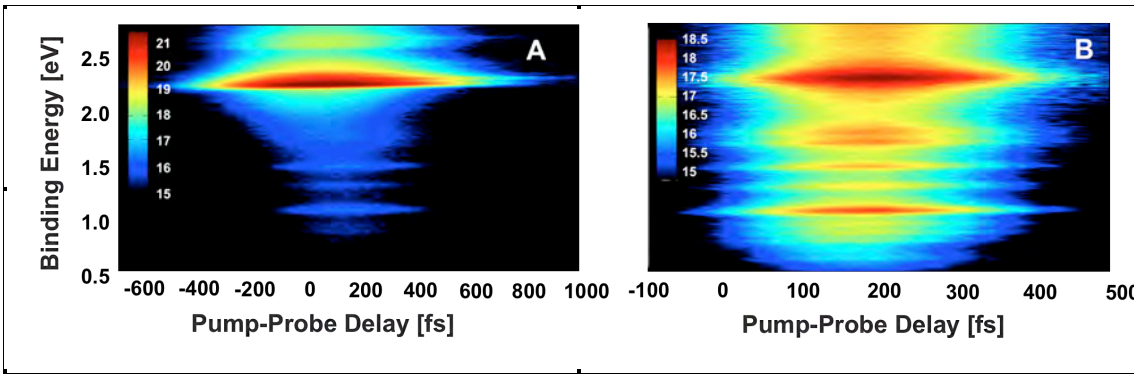

Figure 1: Time-resolved binding energy spectra of 1,3-cyclohexadiene. Part A shows the spectrum with 207 nm excitation, part B represents the result with 268 nm excitation. The color encodes the intensity on a (natural) logarithmic scale.

opening coordinate produce shifts at a rate of 40 to 60 meV/ps.

It is noteworthy that broadening of the Rydberg lines during the time window of observation is not seen in either experiment. However, the 3p Rydberg signal in the 268 nm experiment is broadened compared to that arising from direct excitation. Previous work has associated the spectral width to dispersion of molecular structure. The lack of observed broadening in the time resolved Rydberg spectra is consistent with the theoretically derived notion that the wavepacket remains well focused during the transition to the ground state. Challenges in the near future include the time and energy deconvoluted analysis of the peak shifts in order to extract the true molecular binding energy variations. These could then be compared to wavepacket dynamics calculations that others have performed.

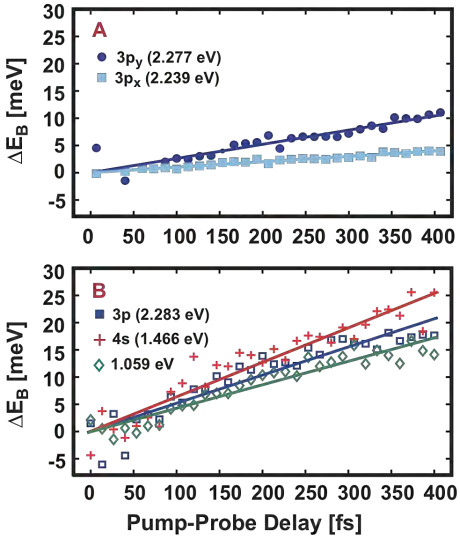

Figure 2: Shifts of peak maxima as a function of time. A: 207 nm + 414 nm ionization: The peak centers of the p_x (light blue squares) and p_y (dark blue circles) signals. Linear fits are included as solid lines in the respective colors. B: 268 m + 400 nm experiment: The shifts of peak centers of the 3p, the 4s and the 1.06 eV peaks as a function of delay time.

From these experiments we conclude that the structural dynamics is sensitively dependent on the excited electronic state. This is surprising as one would have expected that the 3p Rydberg state rapidly decays into the lower, reactive valence state. Further, one would have speculated that the 3p state decays first into 3s, which in turn is suspected to evolve into the doubly excited state that opens the ring. None of those mechanisms appear to be at work in CHD. Instead, the molecule finds a very different conical intersection and ends up directly in the ground state, bypassing the reactive channel that is so widely studied by spectroscopists, and used by organic chemists.

Ultrafast Dynamics of flexible model systems

In the past year we have continued our explorations of the structural motions in molecular systems with conformeric degrees of freedom. We have concluded our work on the formation of an intramolecular cation – pi bond, where we watch the formation of this bond in real time [2] and [6]. In addition, we finished our studies of the conformeric motions in triethyl amine, where we follow in real time the change of the amine from a pyramidal to a planar structure, which then induces structural motions of the ethyl arms that covers three distinct minima in the potential energy landscape [1].

III. Future Plans

Ongoing work continues to take advantage of the power inherent in the Rydberg ionization spectroscopy. We continue to explore model systems that are relevant to

combustion and that test the limits of applicability. This includes systems that exhibit conformeric motions and molecular clusters. Systems in the former category include cyclic diamines, such as morpholene, where we already have observed interesting temporal dynamics that relate to structural motions. In the latter category are clusters of large molecules, in particular tetramethyl ethyl diamine, where we continue to learn interesting aspects of the cluster dynamics.

In collaboration with theorists, we attempt to calculate the Rydberg electron binding energies from two vantage points. First, we use model systems to gain insights into the physical parameters that determine the binding energies in large molecules. Secondly, we work toward calculating Rydberg electron binding energies using ab initio methods.

IV. Publications resulting from DOE sponsored research (2009 - 2011)

1. "Structural Dynamics in Floppy Systems: Ultrafast Conformeric Motions in Rydberg-Excited Triethylamine," Brian Bayes, Sanghamitra Deb, Michael P. Minitti and Peter M. Weber, J. Phys. Chem. A. J. Phys. Chem. A **2011**, 115, 1804–1809.
2. "Dissociative energy flow, vibrational energy redistribution and conformeric structural dynamics in bifunctional amine model systems," Joseph C. Bush, Michael P. Minitti and Peter M. Weber, *J. Phys. Chem. A* **2010**, 114, 11078–11084.
3. "The Ultrafast Pathway of Photon-Induced Electrocyclic Ring Opening Reactions: The case of 1,3-cyclohexadiene" Sanghamitra Deb and Peter M. Weber, Annu. Rev. Phys. Chem. **2011**. 62, 19–39.
4. "Electron Diffraction with Bound Electrons: the Structure Sensitivity of Rydberg Fingerprint Spectroscopy" Xiao Liang, Michael G. Levy, Sanghamitra Deb, Joseph D. Geiser, Richard M. Stratt, and Peter M. Weber, Journal of Molecular Structure 978 (**2010**), pp. 250-256.
5. "Probing the Lifetimes of Internally Excited Amyl Nitrite Cations" Martin Rosenberg, Michael P. Minitti, Nerijus Rusteika, Christer Z. Bisgaard, Sanghamitra Deb, Peter M. Weber, Theis I. Sølling, *J. Phys. Chem. A* **2010**, *114*, 7021–7025.
6. "Ultrafast Formation of an Intramolecular Cation-Pi Bond," Joseph C. Bush, Michael P. Minitti and Peter M. Weber. Journal of Photochemistry and Photobiology A: Chemistry 213 **2010**, 70–72.
7. "Ultrafast Curve Crossing Dynamics through Conical Intersections in Methylated Cyclopentadienes," Fedor Rudakov and Peter M. Weber, J. Phys. Chem. A, **2010**, 114 (13), pp 4501–4506.
8. "Ground State Recovery and Molecular Structure upon Ultrafast Transition through Conical Intersections in Cyclic Dienes," Fedor Rudakov and Peter M. Weber, Chemical Physics Letters 470, **2009** 187-190.
9. "Excited-state ions in femtosecond time-resolved mass spectrometry: An investigation of highly excited chloroamines", R. Y. Brogaard, N. Rusteika and T. I. Sølling, F. M. Rudakov and P. M. Weber, *J. Phys. Chem. A*, **2009**, *113* (1), pp 40–43.

Detailed Studies of Hydrocarbon Radicals: C_2H Dissociation Dynamics

Curt Wittig
Department of Chemistry
University of Southern California
Los Angeles, CA 90089-1062
wittig@usc.edu

Program Scope

We have initiated a detailed examination of C_2H excited state properties and dynamics throughout the energy range that begins at dissociation threshold, $D_0(C_2\text{–}H)$, and extends as far above D_0 as possible. The central role played by this species in hydrocarbon chemistry cannot be overstated. It is also an excellent prototype for examining important properties and phenomena: electronic states; curve crossings and associated nonadiabatic transitions; intramolecular and dissociation dynamics; and so on. It is small enough to provide experimental parent and product state resolution, and it is tractable at a high level of theory — both electronic structure and quantum mechanical nuclear dynamics, including nonadiabatic couplings. It is an excellent example of a system in which more than two conical-type intersections need to be taken into account simultaneously. Complex issues range from couplings among its electronic states (conical intersection) to its ultraviolet spectrum. It dissociates to $C_2 + H$, which is certain to require care in theoretical descriptions because of the large number of C_2 electronic states that must be taken into account.

The research plan consists of complementary experimental studies, and theoretical calculations that complement the experimental effort. The absorption spectrum of expansion-cooled C_2H will be obtained via the yield spectrum for the dissociative channel: $C_2H + h\nu \rightarrow C_2 + H$. This will be achieved by monitoring the C_2 product using soft ionization (*e.g.*, electron energies of ~ 16 eV are incapable of producing C_2^+ from C_2H or its precursor) while varying $h\nu$. Because of the large geometry change in going from the $\tilde{X}^2\Sigma^+$ ground state to the *B* state (the CC bond length increases by 0.21 Å and the CCH angle goes from 180° to 116°), and because only low $3^2A'$ vibrational levels fluoresce, the dissociative channel dominates the UV absorption spectrum. This will constitute a benchmark for theoretical calculations.

The next set of experiments uses Rydberg time-of-flight spectroscopy to examine C_2H dissociation dynamics. This is a familiar tool in our laboratory. The low-lying C_2 electronic states: $X^1\Sigma_g^+$ and $a^3\Pi_u$ (which lies only 715 cm^{-1} above $X^1\Sigma_g^+$), as well as vibrations in each, will be resolved easily. Many rotations can be resolved, and the distributions of the lowest rotations can be obtained. It will also be possible to discern how C_2H

vibrational excitations are manifest in product distributions, ensuring an accurate $D_0(C_2–H)$ value. Though the experimental challenges are not to be underestimated, the planned approaches are well suited to detailed studies of the photoinitiated reaction dynamics of this species. The theoretical part is also quite challenging, but aided greatly by Anna Krylov's *iOpenShell Center* at USC.

Recent Progress

The grant arrived in August 2010, and the order for an electron-impact time-of-flight mass spectrometer (TOFMS) that operates at repetition rates up to 200 kHz (*i.e.*, a complete mass spectrum every 5 μs) was placed in September. It arrived in November and was promptly incorporated into the apparatus, where it has worked well ever since. The pulsed molecular beam uses a solenoid valve. After ~ 10 hours of operation, it emits a large (unwanted) burst of gas following the main pulse. This is a common problem. We can live with it, as the source chamber is evacuated using a large diffusion pump. Figure 1 illustrates the effect. Note that diagnosis is instant because of the high repetition rate TOFMS. This is not a big deal, but in the past it would have taken considerably more time to figure out what is happening. Let's now move on to data that are germane to the scientific goals.

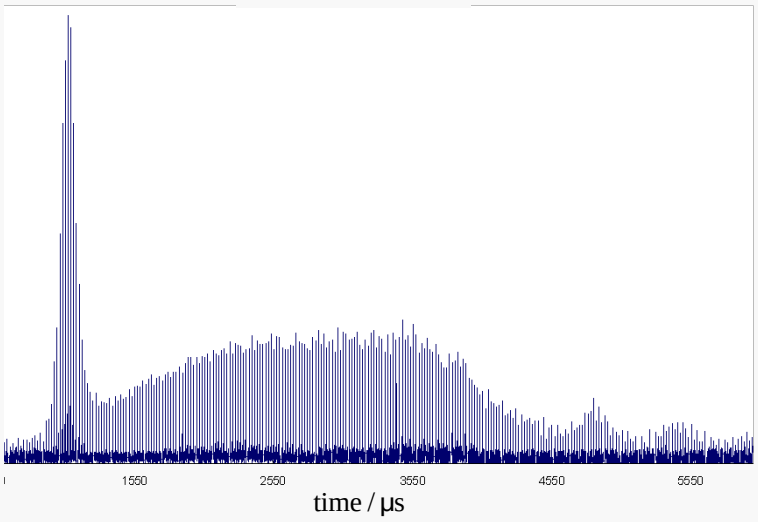

Figure 1. After many hours of operation, the pulsed solenoid valve fatigues, resulting in the release of a large amount of gas following the main pulse. Each vertical line represents a complete mass spectrum (see Fig. 2). The situation is diagnosed immediately.

At an electron energy of 60 eV, the expansion-cooled Ar/C_2H_2 mixture yields $C_2H_2^+$ parent ion, as well as daughter ions C_2H^+, C_2^+, and even some C^+, as seen in Fig. 2. This figure illustrates the simplicity of the region of concern (m / e = 24 – 26). By itself, it is not important, as any mass spectrometer could be used to obtain it. The advantage of the TOFMS is its uniquely well-suited compatibility with the pulsed (10 Hz) photoexcitation experiments that follow.

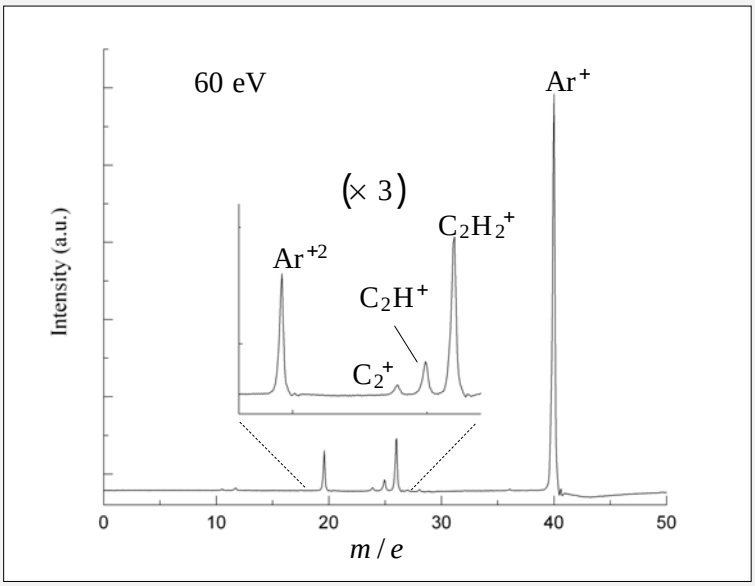

Figure 2. At 60 eV, the system behaves as expected. This spectrum was obtained using an Ar/C_2H_2 mix. The ×3 inset shows the $C_2H_2^+$, C_2H^+, and C_2^+ features. This is one of the many spectra recorded with a single valve opening (see Fig. 1).

Referring to Fig. 3, as the electron energy is lowered, daughter ions eventually disappear, *e.g.*, below approximately 17 eV, only $C_2H_2^+$ remains, *i.e.*, the C_2H^+ peak disappears. As mentioned above, this makes it possible to detect C_2H. In the next experiments, 193 nm photons will be used to dissociate C_2H_2. The nascent C_2H will be ionized at electron energies < 17 eV, in order that C_2H^+ daughter ions are not forthcoming from C_2H_2. Note that absorption cross sections can be obtained with good accuracy, including spatial anisotropy, because the fractional change of a given ion signal can be determined to within a couple percent. Thus, we will be able to obtain the photodissociation efficiency straightaway.

The same idea applies to C_2H and C_2. Specifically, with C_2H present, the electron energy will be turned down until the C_2^+ daughter ion signal goes away. The C_2H will then be photodissociated and C_2^+ will be monitored. In other words, the absorption spectrum of C_2H will be recorded by monitoring C_2^+ as the C_2H photodissociation frequency is varied. It is important that C_2H photodissociation occurs at lower frequencies than those of the C_2H_2 absorption spectrum.

The immediate goal is an accurate, high-resolution absorption spectrum of gas phase, expansion-cooled C_2H throughout a broad UV spectral range. Despite the importance and ubiquitous nature of this species, this will be a first. It sets the stage for the dynamics studies that use the Rydberg tagging technique.

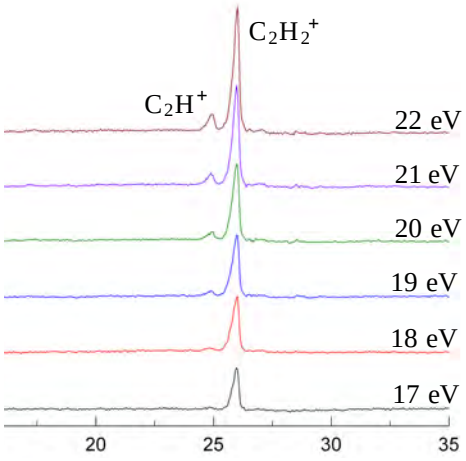

Figure 3. As the electron energy is lowered, the C_2H feature decreases, disappearing at approximately 17 eV.

In summary, the experiments commenced a few months ago and progress has been good. The graduate student, Jordan Fine, is doing an excellent job. We are focusing on the goals that were described in the proposal and no departure is anticipated. An additional student will join the project in Fall 2011.

Theoretical studies

The electronic structure theory part of the program has not yet commenced. This will get into high gear in Fall 2011. The part about myriad intersections of surfaces and the resulting geometric phases, though more conceptually sophisticated, is further along, as discussed below.

In parallel with the *ab initio* calculations is an effort to understand complex surface intersections and dynamics, *e.g.*, the triple intersections discussed by Yarkony, Matsika, and others. The approach is that of gauge field theory, which is premised on a fundamental redundancy of quantum mechanics, *e.g.*, a particle wave function can be multiplied by a phase factor having an argument that depends on spacetime without changing the probability. The cases of U(1), SU(2), and SU(3) gauge symmetries will be outlined and correspondence with double and triple intersections will be discussed. In the theory of fundamental particles, charges arise as strengths of particle-field interactions. No such charges exist when dealing with potential energy surfaces. The key to the latter as a gauge theory is geometrc: identification of gauge connections acting on the parameter space of the nuclear tuning coordinates. This yields results immediately and intuitively, albeit following some homework.

All of this material, and then some, will be presented at the contractors meeting. There have been no publications yet. One paper is in preparation;[1] the other two references[2,3] are related to ref. 1, but they were not suported by DOE.

References

1. C. Wittig, Spins and other Phases, Phys. Chem. Chem. Phys., International Year of Chemistry Perspective Article, in preparation.
2. C. Wittig, Photon and Electron Spins, Vincenzo Aquilanti Festschrift, J. Phys. Chem. A **113**, 15320 (2009)
3. C. Wittig, Statistics of Indistinguishable Particles, R. Benny Gerber Festschrift, J. Phys. Chem. A **113**, 7244 (2009).

Experimental Ignition Studies of Oxygenated Hydrocarbons

Margaret S. Wooldridge
Departments of Mechanical and Aerospace Engineering, University of Michigan
Ann Arbor, MI 48109-2121
mswool@umich.edu

I. Program Scope

The chemical physics of oxygenated fuels is an area which, until recently, has seen little scrutiny from the fundamental combustion science community. The chemistry of oxygenates presents an exciting area to apply our learning from hydrocarbons and adapt our methods to develop a similar level of predictive capabilities for elementary reaction theory and combustion reaction mechanisms. This research program uses ignition studies to investigate combustion and flame chemistry from the initiation and fuel oxidation phase to the heat release phase of combustion. Ignition delay time data provide valuable information on fuel reactivity for a range of state conditions, and speciation data provide direct insight into the dominant reaction pathways. The University of Michigan (UM) rapid compression facility (RCF) is used to create the temperature and pressure conditions of interest for the ignition studies. UM RCF studies focus on intermediate temperatures (600 – 1200 K) and high pressures (1-25 atm) where there are high uncertainties in the combustion chemistries.

During the past year, a comprehensive study of *n*-butanol ignition has been completed, as well as initial ignition studies of methyl3hexenoate. Ignition delay time data were acquired using the UM RCF for both species over a range of temperatures. Mass sampling and gas chromatography were applied to quantify the stable intermediates present during *n*-butanol/air ignition. Speciation studies are currently in progress for the methyl3hexenoate system.

II. Recent Progress

The long test times of the UM RCF allow application of rapid gas sampling methods to simultaneously measure a large number of stable species during ignition experiments. Details on the dimensions, components and performance characterization of the UM RCF can be found in Donovan *et al.* [1]. Previous UM RCF studies have considered iso-octane ignition [2] and radical growth during iso-octane ignition [3], H_2/CO ignition [4], particle nucleation [5], and C_5 ester ignition [6]. Previous gas sampling studies on iso-octane can be found in He *et al.* [7] and on methyl butanoate in Walton *et al.* [8].

Since these earlier studies, the gas sampling system has been modified to allow multiple sampling events to occur within one ignition experiment, and the trapped residual volume in the gas sampling system has been reduced to improve the accuracy of the species measurements.

A. Ignition delay time studies of methyl3hexenoate and *n*-butanol

We recently completed ignition studies of methyl3hexenoate and *n*-butanol. Pressure time histories were used to determine ignition delay times as a function of test gas composition and experimental conditions. High-speed optical images were acquired using a color CMOS camera. For the methyl3hexenoate study, mixture compositions were held constant using ϕ = 0.3 (based on fuel to oxygen ratio) and a fixed dilution ratio of inert/O_2 = 3.76, where the inert gases were nitrogen, argon, and carbon dioxide. The ignition delay time data for methyl3hexenoate span temperatures from 899 to 1102 K at a nominal pressure of 10.5 atm. Figure 1 compares the relative reactivity of this unsaturated ester with other saturated and unsaturated esters and iso-octane at comparable conditions (ϕ = 0.3-0.4 and P ≅ 10.5 atm). All the data presented in Figure 1 are for fuels and conditions that were in the strong ignition regime, and excellent homogeneity was observed in the high speed imaging data for each experiment. The results show the progression in ignition properties as a function of alkyl chain length and saturated versus unsaturated structures for these C5 and C7 ester species.

Ignition delay times for stoichiometric *n*-butanol/O_2 mixtures with an inert/O_2 ratio of 5.64 were measured over a temperature range of 920–1040 K and a pressure range of 2.86-3.35 atm. Typical results

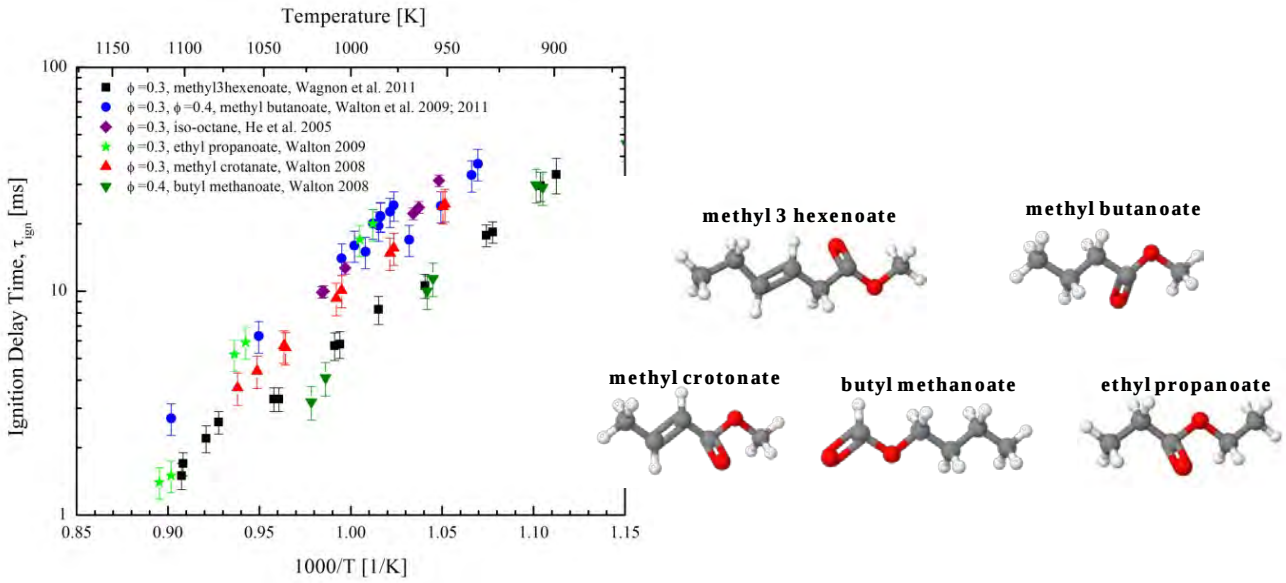

Figure 1: Comparison of experimental measurements of ignition delay times for C5 and C7 esters and iso-octane. All data were acquired at P ≅ 10.5 atm. The figure on the right shows the chemical structure of the esters studied.

for pressure time history and imaging for an ignition experiment are presented in Figure 2. The imaging data acquired during UM RCF ignition experiments provide vital qualitative and quantitative information on the homogeneity of the reaction in the test section. The data document the ignition regime of the mixture (defined after Zeldovich) as strong or weak. Such information is particularly important to understand the effects of heat transfer physics (such as boundary layer growth) on the sampling and ignition data. The experimentally measured ignition delay time data were in excellent agreement with model predictions (within 20% throughout the temperature range studied) using the recent reaction mechanism developed by Black *et al.* **[**9**]**.

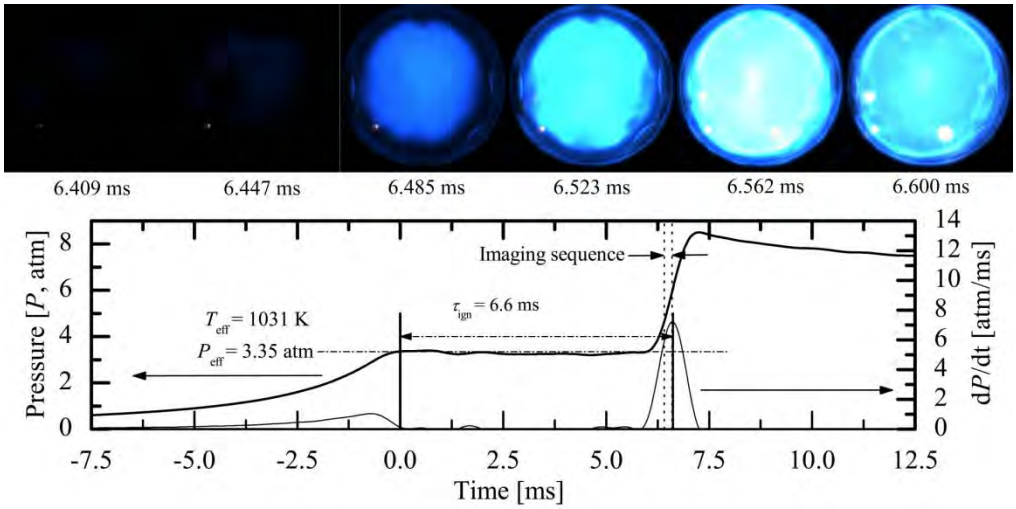

Figure 2. Results for a typical *n*-butanol ignition experiment with P_{eff} = 3.35 atm, T_{eff} = 1031 K, ϕ = 1, inert/O_2 = 5.64 and τ_{ign} = 6.6 ms. The lower panel shows the pressure and the rate of pressure rise (d*P*/d*t*) in the UM RCF test section. End of compression is set as *t* = 0 ms. The upper panel shows the corresponding still images (end view), acquired at 26,000 fps, of the chemiluminescence during ignition (no color adjustment).

B. Speciation studies of stable intermediates formed during *n*-butanol ignition

Direct measurements of intermediates of ignition are challenging experimental objectives, yet such measurements are critical for understanding fuel decomposition and oxidation pathways. High-speed gas sampling and gas chromatography techniques were used to acquire and analyze gas samples of intermediate species during the ignition delay of $\chi_{n\text{-butanol}} = 0.025$, $\chi_{O2} = 0.147$, $\chi_{N2} = 0.541$, $\chi_{Ar} = 0.288$ mixtures at P = 3.25 atm and T = 975 K. Quantitative measurements of mole fraction time histories of methane, carbon monoxide, ethene, propene, acetaldehyde, n-butyraldehyde, 1-butene and n-butanol were compared with model predictions using the Black *et al.* [9] mechanism. A subset of these results is presented in Figure 3. In general, the predicted trends for species concentrations were consistent with measurements. Sensitivity analyses and rate of production analyses were used to identify reactions important for predicting ignition delay time and the intermediate species time histories. Modifications to the mechanism by Black *et al.* [9] were explored based on recent contributions to the literature on the rate constant for the key reaction, *n*-butanol+OH by Zhou *et al.* **[**10**]**. The results improved the model agreement with some species (e.g. propene see Figure 3); however, the comparison also indicates some reaction pathways, particularly those important to C_2H_4 formation and removal, are not well captured.

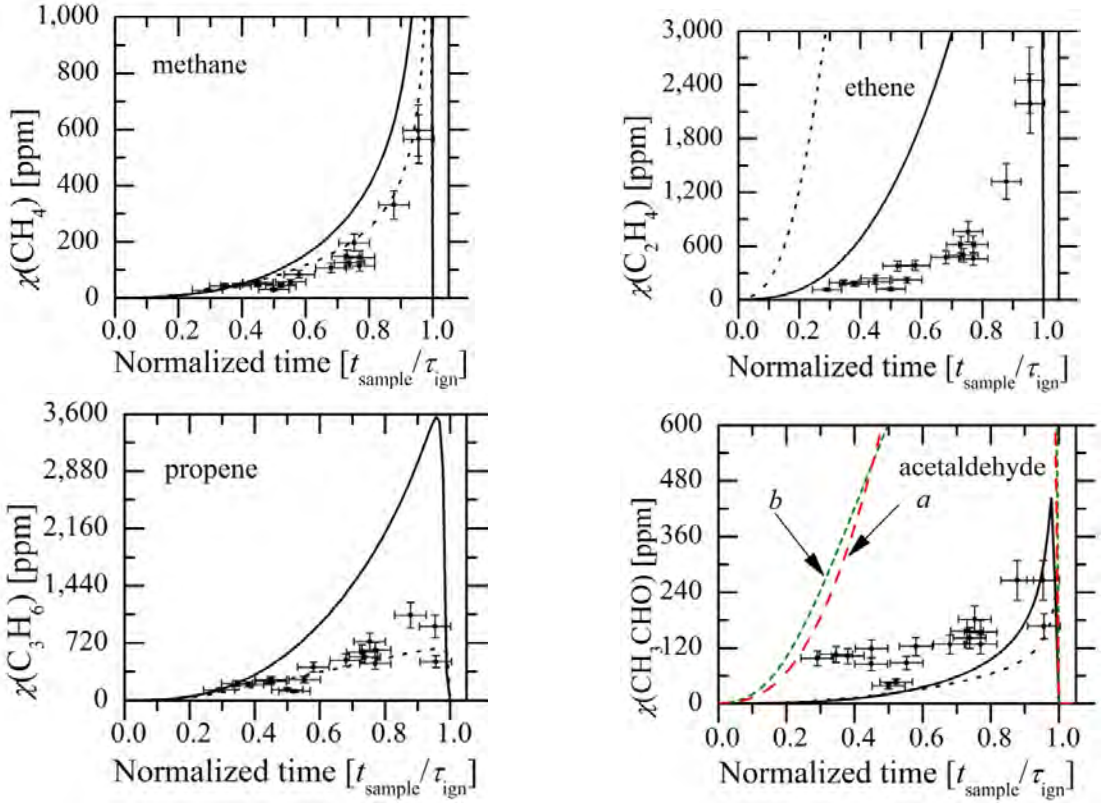

Figure 3. Comparison between measured and model predictions of intermediate species formed during *n*-butanol ignition. The model predictions are based on the reaction mechanism of Black et al. [9] and the conditions of P = 3.25 atm, T = 975 K, inert/O_2 = 5.64, and *n*-butanol = 2.45% ($\tau_{ign,predicted}$ = 18.6 ms). The unmodified mechanism predictions are shown with solid lines. The mechanism predictions when the recommended rate coefficients by Zhou et al. [10] are substituted for the *n*-butanol + OH channels are shown as the dotted black lines. The average experimental conditions are P_{eff} = 3.29 atm, T_{eff} = 975 K, inert/O_2 = 5.63, and *n*-butanol = 2.44% ($\tau_{ign,average}$ = 15.7 ms). The error bars represent the experimental uncertainties. The time domain has been normalized from t = 0 (end of compression) to the time of ignition, t/τ_{ign} = 1.

Recent studies, like the important works by Vasu *et al.* [11] and Zhou *et al.* [10] on the overall reaction rate and specific branching channels of the *n*-butanol+OH reaction, have improved the understanding of the reaction pathways important to *n*-butanol combustion. However, more experimental and theoretical work is needed to improve the fidelity of our predictive understanding of *n*-butanol combustion chemistry.

Future Work

Our future work includes ignition and speciation studies of longer chain esters, as well as speciation studies of the intermediates formed during ignition of methyl3hexenoate. We have installed new columns in our gas chromatographs that expand the intermediate species we can identify and measure as well as provide vital information to quantify the carbon balance in the speciation measurements. We will also continue to leverage our support to study blends of hydrocarbon and oxygenate compounds to understand the synergies between hydrocarbon and oxygenated hydrocarbon combustion chemistry.

III. References

1. Donovan, M.T., He, X., Zigler, B.T., Palmer, T.R., Wooldridge, M.S., Atreya, A. (2004) "Demonstration of a Free-Piston Rapid Compression Facility for the Study of High Temperature Combustion Phenomena" *Combust. Flame* **137** 351.
2. He, X., Donovan, M.T., Zigler, B.T., Palmer, T.R., Walton, S.M., Wooldridge, M.S., Atreya, A., (2005) "An Experimental and Modeling Study of Iso-octane Ignition Delay Times under Homogeneous Charge Compression Ignition Conditions," *Combust. Flame* **142** 266.
3. He, X., Zigler, B.T., Walton, S.M., Wooldridge, M.S., Atreya, A., (2006) "A Rapid Compression Facility Study of OH Time Histories During Iso-octane Ignition," *Combust. Flame* **145** 552.
4. Walton, S.M., He, X., Zigler, B.T., Wooldridge, M.S., (2007) "An Experimental Investigation of the Ignition Properties of Hydrogen and Carbon Monoxide Mixtures for Syngas Turbine Applications," *Proc. Combust. Inst.* **31** 3147.
5. Donovan, M.T., He, X., Zigler, B.T., Palmer, T.R., Walton, S.M., Wooldridge, M. S., (2005) "Experimental Investigation of Silane Combustion and Particle Nucleation Using a Rapid Compression Facility," *Combust. Flame* **141** 360.
6. Walton, S. M., Wooldridge, M. S., and Westbrook, C. K., (2009) "An Experimental Investigation of Structural Effects on the Auto-Ignition Properties of Two C5 Esters" *Proc. Combust. Inst.* **32** 255.
7. He, X., Walton, S.M., Zigler, B.T., Wooldridge, M.S., Atreya, A., (2007) "An Experimental Investigation of the Intermediates of Iso-octane During Ignition," *Int. J. Chem. Kinet.* **39** 498.
8. Walton, S.M., Karwat, D.M., Teini, P.D., Gorny, A., and Wooldridge, M.S., (2011) "Speciation Studies of Methyl Butanoate Ignition," *Fuel* **90** 1796.
9. Black, G.; Curran, H. J.; Pichon, S.; Simmie, J. M.; Zhukov, V. *Combust. Flame* **2010**, *157*, 363-373.
10. Zhou, C.-W.; Simmie, J. M.; Curran, H. J. *Combust.Flame* **2011**, *in press*.
11. Vasu, S. S.; Davidson, D. F.; Hanson, R. K.; Golden, D. M. *Chem. Phys. Lett.* **2010**, *497*, 26-29.

IV. Publications supported by this project 2008-2011

1. Karwat, D. M. A., Wagnon, S., Teini, P. D., Wooldridge, M. S., "On the chemical kinetics of n-butanol: ignition and speciation studies," submitted to the *Journal of Physical Chemistry A*, January 2011, revised and resubmitted, March 2011.
2. Walton, S. M., Karwat, D. M., Teini, P. D., Gorny, A., and Wooldridge, M. S., (2011) "Speciation Studies of Methyl Butanoate Ignition," *Fuel*, **90**, pp. 1796-1804.
3. Wagnon, S., Karwat, D. M. A., Wooldridge, M. S., "Chemical Kinetics of an Unsaturated Ester: Methyl Trans-3-hexenoate," 7th U.S. National Combustion Meeting, Atlanta, Georgia, March 2011.
4. Karwat, D. M. A., Wagnon, S., Teini, P. D., Wooldridge, M. S., "N-butanol ignition and speciation studies,".7th U.S. National Combustion Meeting, Atlanta, Georgia, March 2011.
5. Karwat, D. M. A., Wagnon, S., Lai, J. Y. W., Wooldridge, M. S., Westbrook, C. K. "An Experimental and Computational Investigation of n-Dodecane Ignition and Chemical Kinetics," AIAA Conference, Orlando, Florida, January 2011.

THEORETICAL STUDIES OF THE REACTIONS AND SPECTROSCOPY OF RADICAL SPECIES RELEVANT TO COMBUSTION REACTIONS AND DIAGNOSTICS

DAVID R. YARKONY
DEPARTMENT OF CHEMISTRY, JOHNS HOPKINS UNIVERSITY, BALTIMORE, MD 21218
yarkony@jhu.edu

We continued our work on anion photoelectron spectra that describe states of a neutral that are strongly coupled by conical intersections. As part of a study of alkoxide photoelectron spectra, we have finished simulations of the photoelectron spectrum (PES) of ethoxide and isopropoxide. A simulation of the related hydroxymethoxide anion is in progress. We have also completed a study nonadiabatic photodissociation of the 1-hydroxyethyl radical, which builds on our previous work on hydroxymethyl radical.

As part of other funded research, we are developing a new, general, method to describe strongly coupled adiabatic potential energy surfaces and their interstate interactions, based on quantifiably quasi-diabatic coupled state Hamiltonians, $\mathbf{H}^{d}$. This tool will enable us to study the dynamics of nonadiabatic photodissociation. As part of our DoE funded research, initally we will use this approach to develop an accurate representation of the $1,2^1A$ potential energy surfaces needed to describe the vibrationally mediated photodissociation of NH_3. We will also extend this approach to treat fragmentation in more complex molecules. Further, we will implement a recently developed formalism for describing anion electron photodetachment that is valid for low-energy detached electrons which leave a neutral molecule whose states are strongly coupled by conical intersections. The theory takes full account of electron exchange and nonorthogonality effects. It uses the solution to a Lippmann-Schwinger equation, constructed with only standard electronic structure techniques.[1] This will enable us to determine the partial photodetachment cross sections needed for a completely first principles simulation of a PES. A brief overview of these methods and their implications for our DoE funded research is provided.

I. Work Completed

A. Photodissociation of the 1-hydroxyethyl radical.

The 1-hydroxyethyl radical, CH_3CHOH, is relevant to the combustion of ethanol and the photochemistry of ethoxy.[2] Recently Reisler and coworkers, [2] denoted KEWR below, studied the nonadiabatic photodissociation of 1-hydroxyethyl to CH_3CHO + H (onset at 19,600 cm^{-1}) or CH_2CHOH + H (onset at 31, 250 cm^{-1}). Much of KEWR's analysis of the nonadiabatic aspects of this photodissociation was based on our earlier studies of the role of conical intersections in the photodissociation of hydroxymethyl, H_2COH.[3] We extended that work, studying, the 1^2A-3^2A states of 1-hydroxyethyl and the conical intersections that couple them.[4] These results are compared with previous results for hydroxymethyl and the 1-hydroxyethyl cation. The 2^2A and the 3^2A states are nominally the 3s and lowest 3p Rydberg states of 1-hydroxyethyl, built on the bound 1-hydroxyethyl cation. Our equilibrium structures of the 1^2A and 3^2A states are in good accord with CCSD(T) determinations of the equilibrium geometries of the ground state of the 1-hydroxyethyl radical and its *cation*, respectively.[5] This serves to confirm the characterization of the 3^2A state, as a 3p Rydberg state based on the bound 1-hydroxyethyl cation. Interestingly the 2^2A state, nominally a 3s Rydberg state built on the 1-hydroxyethyl cation, is dissociative, despite the fact that the cation is bound. The absence of a bound 2^2A state is attributed to a conical intersection connecting the 1^2A and 2^2A states, similar to the situation found in hydroxymethyl. KEWR were unable to observe a REMPI transition involving the 2^2A state and indicated conical intersections as the likely cause. We attributed this specifically to the region of 1^2A - 2^2A conical intersection seam with a stretched O-H bond. We further explained how the products and recoil anisotropy of time-of-flight measurements by KEWR, in the spectral region of the 3s Rydberg state, are consistent with dynamics mediated by that conical intersection.

However questions remain. We found the lowest energy 2^2A - 3^2A point of conical intersection is ~ 4,200 cm^{-1} above the 3^2A state minimum energy structure, suggesting that the low-lying vibrational levels of this state should be visible in REMPI spectroscopy. The analogous levels in CH_2OH were indeed observed by REMPI spectroscopy.[6] However KEWR report no REMPI signal in the spectral region where they expect the 3^2A state. One possible explanation is strong indirect predissociation. In indirect predissociation, coupling of nominally bound vibrational levels of the 3^2A state to the dissociated 2^2A state through the derivative couplings destabilizes the vibrational levels of the 3^2A state on the time scale of the REMPI experiments, without coupling from an accessible conical intersection. The reassignment of the observed spectra should also be considered.

The differences in the observed spectra for hydroxymethyl and 1-hydroxyethyl, in the region of the 3p-Rydberg states raise questions of general interest, concerning the stability of vibrational levels in regions where nonadiabatic effects are expected. The competition between indirect and conical intersection induced dissociation merit further study. It is hoped that the results of the present investigation will motivate further studies of nonadiabatic effects in this molecule.

II. Work in Progress

A. Photoelectron Spectrum of Hydroxymethoxide.

Hydroxymethoxy can be viewed as a derivative of methoxy with a hydrogen replaced by an OH group. Hence one would expect conical intersections to play a role in the electronic structure of the low-lying states of this molecule and perhaps contribute to the photoelectron spectrum. Indeed a recent, very high quality theoretical study of the low-lying electronic states of hydroxymethoxy found the excited $\tilde{A}$ state to be only 3142 cm^{-1} above the ground state minimum.[7] However, that theoretical study did not address the issue of the conical intersesction seam and the PES has yet to be measured experimentally. We have determined several points of conical intersection on the 1^2A-2^2A seam. The *g-h* plane of the minimum energy crossing point, at 3100 cm^{-1}, only ~400 cm^{-1} above the $\tilde{A}$ state minimum, is shown below.

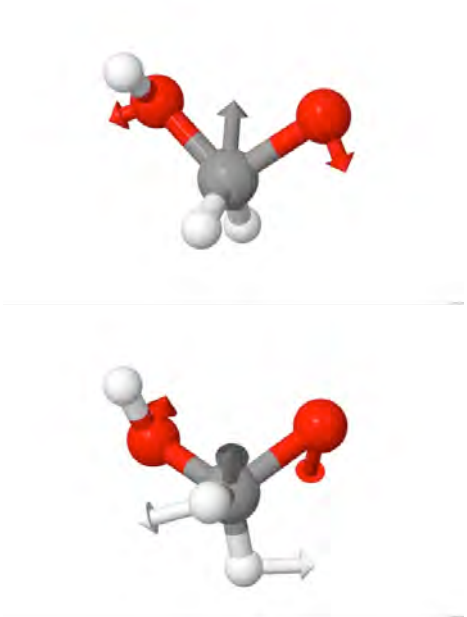

Figure 1: **g and h** vectors for minimum energy conical intersection of hydroxymethoxy.

The involvement of hydroxy oxygen in the *g-h* plane will serve to distinquish this methyoxy derivative from those previously studied. We are currently developing an $\mathbf{H}^d$ to simulate the photoelectron spectrum of the corresponding anion, hydroxymethoxide. It has emerged that the description of the OH motion requires the use of our recently developed higher order technology for representing $\mathbf{H}^d$ for bound molecules.[8] See below.

C. Coupled Potential Energy Surfaces for Nonadiabatic Processes from Quasi-diabatic Hamiltonians

As a result of other funded research, we have developed a procedure for describing coupled adiabatic potential energy surfaces and their interstate interactions using a quasi-diabatic Hamiltonian, $\mathbf{H}^d$,[9-11] of the form:

$$\mathbf{H}^d = \sum_{n=1}^{N^C} V_n \mathbf{M}^{(n)} \qquad (1)$$

The matrix elements of a given, $N^{state}xN^{state}$, matrix $\mathbf{M}^{(n)}$, reflect the proper symmetry properties of the molecule. For bound states the $\mathbf{H}^d$ are constructed from nonredundant internal coordinates. For dissociative states, motivated by the work of Bowman and coworkers[12] and of Collins and coworkers,[13] the matrix elements are given by symmetry adapted $\mathbf{M}^{(n)}$ constructed from primitive (unsymmetrized) matrix elements that have the monomial form:

$$f_n = \prod_{m=1}^{3} \prod_{i<j} w_m(r_{i,j})^{\alpha^{(n)}_{m,i,j}} \prod_{(i,j,k,l)} \phi^{\beta^{(n)}_{i,j,k,l}}_{i,j,k,l} \qquad (2)$$

Here $\mathbf{r}_{i,j} = \mathbf{R}^i - \mathbf{R}^j$, $r_{i,j} = |\mathbf{r}_{i,j}|$ $1 \le i, j \le N^{at}$, $\mathbf{R}^i$ are the atom centered cartesian coordinates of the i^{th} of N^{at} nuclei and (i,j,k,l) denotes an allowed combinations of four atoms. The w_j, j =1 – 3, have the form:

- Exponential $w_1(r_{i,j}) = e^{-s_1(r_{i,j}-r^{(a)}_{i,j})}$ (3)
- Gaussian $w_2(r_{i,j}) = e^{-s_2(r_{i,j}-r^{(b)}_{i,j})^2}$
- Reciprocal $w_3(r_{i,j}) = e^{-s_3(r_{i,j}-r^{(c)}_{i,j})^2} / (r_{i,j} + r^{(d)}_{i,j})$

and

- Dot-Cross product functions

$$\phi_{i,j,k,l} = \mathbf{r}_{i,j} \times \mathbf{r}_{i,k} \cdot \mathbf{r}_{i,l} / \sqrt{r_{i,j} r_{i,k} r_{i,l} r_{j,k} r_{j,l} r_{k,l}}$$

The $\mathbf{V}_n$ are determined from the pseudo constrained normal equations:

$$\begin{pmatrix} \mathbf{W}^{lsq\dagger}\mathbf{W}^{lsq} + \mathbf{t} & \mathbf{W}^{node\dagger} \\ \mathbf{W}^{node} & \mathbf{0} \end{pmatrix} \begin{pmatrix} \mathbf{V} \\ \boldsymbol{\lambda} \end{pmatrix} = \begin{pmatrix} \mathbf{W}^{lsq\dagger}\mathbf{L}^{lsq} \\ \mathbf{L}^{node} \end{pmatrix} \qquad (4)$$

where the λ_i are Lagrange multipliers. The right hand side involves, *ab initio* determined energies, energy gradients and derivative couplings. Here we introduced the idea of nodes, points in nuclear coordinate space at which the $\mathbf{H}^d$ derived energies, energy gradients and derivative couplings are required to agree exactly with the *ab initio* results.

The inclusion of nodes increased considerably the general accuracy of the fit. Further since we include derivative couplings in the fitting procedure our $\mathbf{H}^d$ are quantifiably quasi diabatic. Illustrative of the potential of this approach, is the excellent reproduction of the derivative coupling for the $1,2^1A$ states of NH_3 in the range 10^0 to 10^6 (see Fig. 2) justifying the attribute quasi-diabatic. The newest version of this algorithm for constructing $\mathbf{H}^d$ which employs the distributed origin approach illustrated in eq. (2) reproduces ~727 points, with an energy range of > 60, 000 cm^{-1}, with an RMS error of ~ 45 cm^{-1}.

We are currently extending this work on the $1,2^1A$ states of NH_3 to produce an $\mathbf{H}^d$ with full permutational symmetry, suitable for simulating Crim's studies of ammonia photodissociation[14,15]

$NH_3(\tilde{X},\mathbf{n})+hv \rightarrow NH_3(\tilde{A}) \rightarrow NH_2(\tilde{X},\tilde{A})+H$

where **n** denotes the vibrational quantum numbers. Crim's studies revealed a pronounced dependence of the final state of NH_2 produced on **n**, with the observed differences attributed to near conical intersection dynamics. These observations have yet to be fully explained by existing studies,[16] based on an alternative method of describing and fitting[17] the $1,2^1A$ states of NH_3.

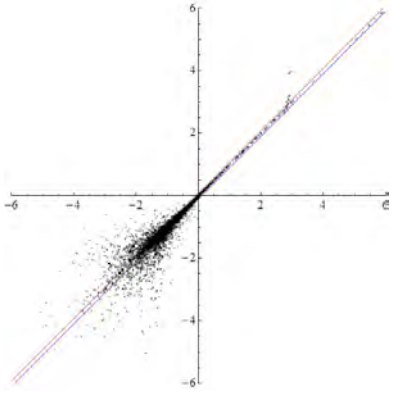

Figure 2: Comparison of *ab initio* and $\mathbf{H}^d$ determined derivative couplings from NH_3, $1,2^1A$. x-axis *ab initio* value and y-axis $\mathbf{H}^d$ determined value, of a nonzero component of the derivative coupling. For points on the diagonal agreement is exact. Solid lines enclose 20% error.

D. Partial Differential Cross Sections for PES

When simulating a PES where the molecule from which the electron has been detached has nondegenerate electronic states strongly coupled by conical intersections, a first principles simulation of the spectrum requires the transition moments to the individual diabatic electronic states. The determination of these transition moments is a complex problem in electron scattering and is routinely ignored in current simulations. In our work, see also Ref. [18], we have estimated the transition moments (assumed geometry independent) by comparing the simulated and measured photoelectron spectra. This procedure breaks down for SEVI experiments where the measured intensities may also reflect the Wigner threshold law.

We have developed, as part of other funded research, a formalism, for determining the partial differential cross sections for anion photodetachment using a Lippmann-Schwinger equation approach. In this case the wave function for the target plus outgoing electron is expanded as in an $N+1$ electron basis

$$\Psi^{(N+1)}_{\varepsilon,\mathbf{k}_\varepsilon} = \sum_{\alpha=1}^{N^{state}} A^c[\Psi^d_\alpha(\mathbf{r}^N;\mathbf{R})\phi^c_{\mathbf{k}_\varepsilon,\varepsilon}(\mathbf{r}_{N+1})]\zeta^\varepsilon_\alpha(\mathbf{R}) \quad (5)$$

where $\phi^c_{\mathbf{k}_\varepsilon,\varepsilon}$, which is to be determined, is the orbital that describes the outgoing electron, $\zeta^k_\alpha(\mathbf{R})$ is a vibrational function, Ψ^d_α is an N electron quasi-diabatic electronic state, A^c is the coupling antisymmetrizer, for which $A^{(N+1)} = \boldsymbol{A}^c A^{(N)}$, where $A^{(N)}$ is the N electron antisymmetrizer and

$$\Phi^{tar}_\varepsilon = \sum_{\alpha=1}^{N^{state}} \Psi^d_\alpha(\mathbf{r}^N;\mathbf{R})\zeta^\varepsilon_\alpha(\mathbf{R}) \quad (6)$$

is the, known, ε^{th} solution to the N electron total *vibronic* Schrödinger equation, as determined for example in our anion electron detachment simulations, described above. In this description the scattering orbital, which depends on the vibronic state of the target, is *not* orthogonal to the target electrons, but is geometry independent . Our approach takes full account of the antisymmetrizer,

The equation to be solved is the $(N+1)$ electron time independent Schrödinger equation

$$(H^{T,N+1} - E)\Psi^{(s),\pm}_E(\mathbf{r}^{N+1},\mathbf{R}) = 0 \quad (7a)$$

which using a Lippmann-Schwinger approach can be written[19]

$$\Psi^{(s),\pm}_{\varepsilon,\mathbf{k}_\varepsilon} = A^c(1 - G^{(\pm)}_0 V^{(s)}_{N+1})^{-1}\tilde{\Psi}^0_{\varepsilon,\mathbf{k}_\varepsilon} \quad (7b)$$

where the Green's function is given by

$$G^{(\pm)}_0(\mathbf{r}^{N+1},\mathbf{R};\mathbf{r}'^{N+1},\mathbf{R}') \quad (8)$$
$$= \sum_\varepsilon \Phi^{tar}_\varepsilon(\mathbf{r}^N,\mathbf{R})\Phi^{tar}_\varepsilon(\mathbf{r}'^N,\mathbf{R}')g^{k_\varepsilon,(\pm)}_0(\mathbf{r}_{N+1},\mathbf{r}'_{N+1})$$

where $g^{k_\varepsilon,(\pm)}_0(\mathbf{r},\mathbf{r}') = -\dfrac{\exp(\pm ik_\varepsilon|\mathbf{r}-\mathbf{r}'|)}{2\pi|\mathbf{r}-\mathbf{r}'|}$ (9)

and $k_\varepsilon = \sqrt{2(E-E_\varepsilon)}$. We showed[1,19] that eq. (7b) can be determined from, the following result

$$[1+G^{(-)}_0 V^{(s)}_{N+1}](\Phi^{tar}_\varepsilon(\mathbf{r}^N,\mathbf{R})e^{i\mathbf{k}\cdot\mathbf{r}_{N+1}}) = \sum_{\varepsilon'}\Phi^{tar}_{\varepsilon'}(\mathbf{r}^N)$$

$$[\delta_{\varepsilon',\varepsilon}e^{i\mathbf{k}\cdot\mathbf{r}_{N+1}} + < g^{k_{\varepsilon'},(-)}_0(\mathbf{r}_{N+1},\mathbf{r})V^{\varepsilon',\varepsilon}(\mathbf{r})e^{i\mathbf{k}\cdot\mathbf{r}_{N+1}} >_{\mathbf{r}}] \quad (10)$$

where

$$V^{\varepsilon',\varepsilon}(\mathbf{r}_{N+1}) \equiv \quad (11)$$

$$\left\langle \Phi_{\varepsilon'}^{tar}(\mathbf{r}^N,\mathbf{R}) \left| V_{N+1}^{(s)}(\mathbf{r}^{N+1},\mathbf{R}) \right| \Phi_{\varepsilon}^{tar}(\mathbf{r}^N,\mathbf{R}) \right\rangle_{\mathbf{r}^N,\mathbf{R}}$$

and

$$V_{N+1}^{(s)}(\mathbf{r}^{N+1},\mathbf{R}) = -\sum_K \frac{Z_K}{|\mathbf{r}_{N+1}-\mathbf{R}_K|} + \sum_{k=1}^{N} \frac{1}{|\mathbf{r}_{N+1}-\mathbf{r}_k|}$$

Note, $V_{N+1}^{(s)}(\mathbf{r}^{N+1},\mathbf{R}) \rightarrow 0$ as $|\mathbf{r}_{N+1}| \rightarrow \infty$ since the precursor is an anion. Key to the utility of this approach, which avoids the use of complex scaling techniques, is that the electronic integrals in eq. (11) can be evaluated using standard electronic structure techniques. A more complete analysis of the solution to eq. (6b) is found in Refs. [1,19] . Extension to photoionization is in progress.

As part of our DoE funded research the algorithms necessary to determine the partial differential cross sections above will be implemented. Molecules including 1-propynide[20] and ethoxide.[21] will be considered. In our previous analyses of those systems, the transition moments were estimated by comparing calculated and measured spectra. As pointed out in those works the estimates of the transition moments contained therein, will provide valuable benchmarks for these first principles calculations.

Literature Cited

[1] S. Han and D. R. Yarkony, J. Chem. Phys., submitted (2011).

[2] B. Karpichev, L. Edwards, J. Wei, and H. Reisler, J. Phys. Chem. A 112, 412 (2008).

[3] B. C. Hoffman and D. R. Yarkony, J. Chem. Phys. 116, 8300 (2002).

[4] K. Samanta and D. R. Yarkony, Chem. Phys. 378, 110 (2010).

[5] B. Karpichev, H. Reisler, A. I. Krylov, and K. Diri, J. Phys. Chem. A 112, 9965 (2008).

[6] L. Feng, X. Huang, and H. Reisler, J. Chem. Phys. 117, 4820 (2002).

[7] W. Eisfeld and J. Francisco, J. Chem. Phys. 131, 134313 (2009).

[8] J. J. Dillon, D. R. Yarkony, and M. S. Schuurman, J. Chem. Phys. 134, 044101 (2011).

[9] X. Zhu and D. R. Yarkony, J. Chem. Phys. 132, 104101 (15 pages) (2010).

[10] X. Zhu and D. R. Yarkony, Molec. Phys. 108 (19), 2611 (2010).

[11] X. Zhu and D. R. Yarkony, J. Chem. Phys., manuscipt in preparation (2011).

[12] B. J. Braams and J. M. Bowman, Int. Rev. Phys. Chem. 28, 577 (2009).

[13] O. Godsi, C. R. Evenhuis, and M. A. Collins, J. Chem. Phys. 125, 104105 (2006).

[14] A. Bach, J. M. Hutchison, R. J. Holiday, and F. F. Crim, J. Chem. Phys. 118, 7144 (2003).

[15] M. L. Hause, Y. H. Yoon, and F. F. Crim, J. Chem. Phys. 125, 174309 (2006).

[16] D. Bonhommeau and D. G. Truhlar, J. Chem. Phys. 129, 014302 (2008).

[17] Z. H. Li, R. Valero, and D. G. Truhlar, Theor. Chem. Acc. 118, 9 (2007).

[18] T. Ichino, A. J. Gianola, W. C. Lineberger, and J. F. Stanton, J. Chem. Phys. 125, 084312 (2006).

[19] S. Han and D. R. Yarkony, J. Chem. Phys., to appear (2011).

[20] B. N. Papas, M. S. Schuurman, and D. R. Yarkony, J. Chem. Phys. 130, 064306 (12 pages) (2009).

[21] J. J. Dillon and D. R. Yarkony, J. Chem. Phys 131, 134303 (12 pages) (2009).

PUBLICATIONS SUPPORTED BY DE-FG02-91ER14189: 2009 – present

1.*The Photoelectron Spectrum of 1-propynide. Nonadiabatic Effects*
Brian N. Papas, Michael S. Schuurman and David R. Yarkony, J. Chem. Phys. **130**, 064306 (2009).

2.*The simulated spectrum of isopropoxide. Nonadiabatic effects due to conical intersections and the spin-orbit interaction*
Joseph J. Dillon and David R. Yarkony, J. Chem. Phys. 130 154312 (11 pages) (2009)

3.*The Photoelectron Spectrum of the Ethoxide Anion: Conical Intersections, the Spin-Orbit Interaction and Sequence Bands*
Joseph J. Dillon and David R. Yarkony, J. Chem. Phys. 131, 134303 (12 pages) (2009)

4. On the Role of Conical Intersections and their Local Topography in the Photodissociation of 1-Hydroxyethyl Radical,
Kousik Samanta and David R. Yarkony, Chem. Phys. 378, 110-117 (2010)

GAS-PHASE MOLECULAR DYNAMICS: THEORETICAL STUDIES IN SPECTROSCOPY AND CHEMICAL DYNAMICS

Hua-Gen Yu (hgy@bnl.gov) and James T. Muckerman (muckerma@bnl.gov)
Chemistry Department, Brookhaven National Laboratory, Upton, NY 11973-5000

Program Scope

The main goal of this program is the development and application of computational methods for studying chemical reaction dynamics and molecular spectroscopy in the gas phase. We are interested in developing rigorous quantum dynamics algorithms for small polyatomic systems and in implementing approximate approaches for complex ones. Particular focus is on the dynamics and kinetics of chemical reactions and on the rovibrational spectra of species involved in combustion processes. This research also explores the potential energy surfaces of these systems of interest using state-of-the-art quantum chemistry methods, and extends them to understand some important properties of materials in condensed phases and interstellar medium as well as in combustion environments.

Recent Progress

Kinetics and dynamics study of the reaction of HOCO radical with other small molecules and radicals, and of the Chaperone mechanism for three-body reaction

During the past years, in collaboration with J. Francisco (Purdue), we have carried out a systematical study of the structure, spectroscopy, and reactivity of HOCO radical using a combined high level *ab initio* calculations, direct dynamics and/or RRKM (Rice-Ramsperger-Kassel-Marcus) approaches. The main results are shown in Fig. 1. Basically, the HOCO radical has two stable conformers: *trans*- and *cis*-HOCO, with *trans*-HOCO being more stable by about 1.8 kcal/mol. Both conformers have been identified by high-level *ab initio* calculations and experimental spectroscopy. The heat of formation of HOCO (298 K) was determined to be -43.0±0.5 kcal/mol, giving a potential well depth of 30.1±0.5 kcal/mol relative to the OH + CO asymptote. The adiabatic ionization potential of *trans*-HOCO is 8.01±0.05 eV, while its adiabatic electron affinity is about 1.30 eV. It is also evident that the HOCO radical is very reactive. A general feature of HOCO reactions with atoms and radicals is that the HOCO radical acts as a hydrogen donor to reaction partners. The mechanism by which the hydrogen is transferred is generally through the formation of an association intermediate, which then proceeds through a molecular elimination step to produce the reaction

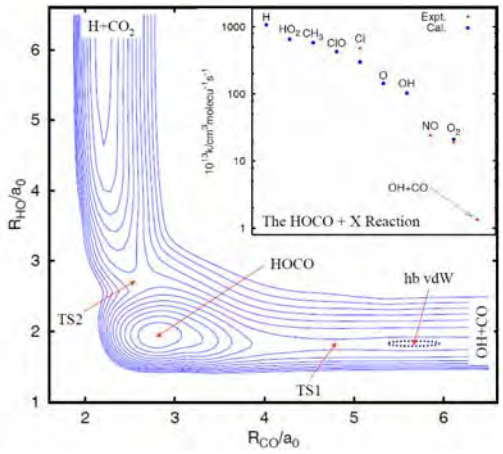

Figure 1 The potential energy surface for the OH + CO → H + CO_2 reaction, showing two barriers (TS1 and TS2) and the deep HOCO well along the minimum energy pathway. The insert figure shows the experimental and theoretical reactivity of HOCO with selected collision partners.

products. The reaction rates of HOCO with some small radicals fall in the range of 10^{-11} – 10^{-10} cm^3 $molec^{-1}$ s^{-1}. These results clearly illustrate that the HOCO radical can play an important role in the conversion of CO into CO_2 not only via the OH + CO reaction, but also its reactivity with other molecules.

The classical trajectory method has been used to study the kinetics of the (S + S_2 + Ar) three-body recombination via the Chaperone mechanism. Its thermal rate coefficient is determined as $2.67\times10^{-33}\exp[143.56(1/T-1/298.150)]$ $cm^6mol^{-1}s^{-1}$.

Molecular dynamics study of the roaming mechanism in molecule-ion reaction

The direct *ab initio* molecular dynamics method was employed to study the *p*-/*o*-H_2 + HOC^+ reaction, based on a scaling all correlation second-order Möller–Plesset perturbation theory (SAC-MP2) method with the cc-pVTZ basis set. Calculated thermal rate coefficients for the $H_2 + HOC^+ \rightarrow H_2 + HCO^+$ isomerization reaction are in good agreement with the experimental results. Results also predict that the $H_2 + H'OC^+ \rightarrow HH' + HOC^+$ exchange reaction can play an important role at low temperatures. The nuclear spin effect of H_2 on the reactivity is clearly demonstrated.

Reaction mechanisms have been extensively explored. In particular, it is found that the roaming mechanism is important for the isomerization reaction. About 10% of total reactive trajectories occur via this mechanism. The driving forces behind the roaming mechanism have been investigated in detail for the molecular ion-molecule reaction by using the trajectory dynamics method. Results show that the roaming reaction mechanism is largely promoted by several key factors including the long-range attractive forces, the late vdW complex H_3OC^+, the V-type of scattering orientation, the role of the orbital angular momentum and CO internal rotation, and the low relative collision energy. A roaming trajectory is often characterized by the non-intrinsic reaction coordinate pathway with a large amplitude motion. Besides the Cl^- + CH_3I SN2 reaction, it is another example for the roaming mechanism occurring in a molecular ion-molecule reaction in the gas-phase although such a reaction mechanism has been identified for a few radical reactions.

Quantum dynamics study of sympathetic cooling of polyatomic radicals in a magnetic trap

A rigorous quantum dynamics study has been performed for the low-temperature collisions of polyatomic molecular radicals with $^1S_0$ atoms in the presence of an external magnetic field using the CCSD(T) *ab initio* and scaled potential energy surfaces. The quantum scattering calculations show that collision-induced spin relaxation of the prototypical methylene molecule $CH_2(X^3B_1)$ and nine other triatomic radicals in cold ^{3}He gas occurs at a slow rate, demonstrating that cryogenic buffer-gas cooling and magnetic trapping of those molecules is feasible with current technology. The calculations also suggest that it may be possible to create ultracold gases of polyatomic molecules by sympathetic cooling with alkaline-earth atoms in a magnetic trap. This work was done in collaboration with Tscherbul and Dalgarno at Harvard.

Optical properties of GaN/ZnO solid solution nanocrystals

In collaboration with Dr. Han at BNL CFN, we have carried out some electronic structure calculations to understand the optical properties of GaN/ZnO solid solution nanocrystals, an important solar fuel material. Results show that the solid solutions have an even

distribution of (ZnO) units among the (GaN) wurtzite frameworks. The GaN/ZnO nanocrystals have the narrowest band gap of 2.21 eV. The Raman spectra strongly imply the occurrence of oxide states at nanocrystal surfaces. It requires more future work to illustrate the mechanism of band gap narrowing and the stability of nanocrystal surfaces.

Future Plans

Kinetics and dynamics study of combustion-related reactions

We will continue to study some important combustion reactions using the direct *ab initio* molecular dynamics program. An interesting direction will focus on the kinetics and dynamics of cyclic, N- and O-containing fuel molecules. The concentration of cyclic compounds in diesels and other future transportation fuels, produced largely from non-traditional sources such as oil shales and sand oils, are much higher than those in current fuels. There are only limited kinetics data on cyclic fuel molecules, yet they are required to design future internal combustion engines using such fuels. A new unique step in the chemistry is the ring-opening processes resulting in, for example cyclopentoxy (cyc-C_5H_9O) radicals discussed by us before. Such radicals may well contribute to enhanced formation of soot without a ring-opening reaction. In this work, we will start this project with the reactions of morpholine (1-oxa-4-aza-cyclohexane, i.e. cyclic $-OCH_2CH_2NHCH_2CH_2-$) and its derivatives with small radicals such as O_2, HO_2 and OH. Westmoreland et al. have recently demonstrated that morpholine is an ideal compound for modeling those hydrocarbon, oxygenated and N-containing fuels. Here, we will address the energies, geometries, and vibrational frequencies of the stationary points on the ground-state surfaces, and the reaction mechanism. The dynamics will be carried out using the DualOrthGT program, together with variational RRKM theory.

Vibronic spectrum calculations of CH_2 and its interactions with He

In our GPMD group, Sears and Hall have observed rich and complicated rovibronic levels of CH_2 near the C + H_2 and CH + H dissociation limits. They provide a challenge for multiple surface dynamics theory, with relevance to the reactive system as well as CH_2 spectroscopy. We have calculated five low-lying electronic potential energy surfaces of CH_2 using a multireference CI (MRCI) method. The adiabatic surfaces will be transformed into a set of diabatic ones using the quasi-adiababatic approximation of Koppel et al. Full-dimensional quantum dynamics will then be performed on the five coupled surfaces. The principal interest is in the energy levels and non-adiadiabatic coupling effects, for detailed comparison with experimental observations. In addition, we have calculated the singlet and triplet potential energy surfaces of the He-CH_2 (*X/A*) interaction system using the CCSD(T)/aug-cc-pVQZ level of theory. The surfaces will be used for investigating the dynamics of singlet and triplet states of CH_2 in collaboration with Tscherbul at Harvard.

Non-adiabatic molecular dynamics studies of polyatomic molecular reactions

Electronically excited species such as $^1CH_2$ also play an important role in combustion chemistry. However, the studies of their reactivity are rather limited, partially due to the non-adiabatic dynamics effects because those reactions often occur on multiple potential energy surfaces. In this research, we will extend the surface hopping direct *ab initio* molecular dynamics algorithm, developed for the SECH MD studies, to simulate the bimolecular reactions and the photo-dissociation chemistry. The first application would

be the photodissociation dynamics of acetone at 193-230 nm. This system has been investigated by Suits et al. using a universal ion imaging technique. The photon excited acetones produce two major types of products: $CH_3CO + CH_3$ and $CO + 2CH_3$. The latter products result from poorly understood dissociation mechanisms. Here we will attempt to explore the dissociation pathways of acetone on its three low-lying electronic states.

An optimal DFT method for GaN and ZnO

The standard DFT methods using the LDA and/or GGA approach have a typical flaw that often predicts a rather small band gap for semiconductors such as GaN and ZnO. This severely hampers the theoretical study of the properties of GaN/ZnO solid solutions. In this work, we are going to develop a DFT method optimized for the GaN and ZnO systems. The optimal method is expected to be capable of describing both the correct band gaps of GaN and ZnO, and the properties of those important molecules related to the photocatalytic water splitting processes. The method will be used to explore the GaN/ZnO nanocrystals.

Publications since 2009

H.-G. Yu, *Product branching ratios of the reaction of CO with H_3^+ and H_2D^+*, Astrophys. J. Lett., **706**, L52 (2009).

H.-G. Yu, *Spherical electron cloud hopping molecular dynamics simulation on dissociative recombination of protonated water*, J. Phys. Chem. A, **113**, 6555 (2009).

H.-G. Yu, *A general rigorous quantum dynamics algorithm to calculate vibrational energy levels of pentaatomic molecules*, J. Mol. Spectrosc. **256**, 287 (2009).

H.-G. Yu and J.S. Francisco, *A theoretical study of the reaction of CH_3 with HOCO radicals* , J. Phys. Chem. A, **113**, 3844 (2009).

H.-G. Yu and J.S. Francisco, *Ab initio and RRKM study of the reaction of ClO with HOCO radicals*, J. Phys. Chem. A, **113**, 12932 (2009).

J.S. Francisco, J.T. Muckerman, and H.-G. Yu, *HOCO radical chemistry*, Acc. Chem. Res. **43**, 1519 (2010).

W.-Q. Han, Z. Liu and H.-G. Yu, *Synthesis and optical properties of GaN/ZnO solid soulution nanocrystals*, App. Phys. Lett. **96**, 183112 (2010).

T.V. Tscherbul, H.-G. Yu, and A. Dalgarno, *Sympathetic cooling of polyatomic molecules with S-state atoms in a magnetic trap*, Phys. Rev. Lett. **106**, 073201 (2011).

H.-G. Yu, *An ab initio molecular dynamics study of the roaming mechanism of the H_2 + HOC^+ reaction*, Physica Scripta (accepted, 2011).

S.-Y. Du, T. Germann, J. Francisco, K. Peterson, H.-G. Yu, and J. Lyons, *The kinetics study of the $S + S_2 \rightarrow S_3$ reaction by the Chaperon mechanism*, J. Chem. Phys. (accepted, 2011).

Chemical Kinetics of Elementary Reactions

Judit Zádor
Combustion Research Facility, Mail Stop 9055, Sandia National Laboratories
Livermore, CA 94551-0969
jzador@sandia.gov

I. Program Scope

This program focuses on the theoretical determination of rate coefficients and branching fractions relevant in combustion chemistry. A particular aspect of the program is the close collaboration with experimental groups in order to minimize the effects of inherent uncertainties in the theoretical methods and also to reveal the parts of our current models causing most of these uncertainties. Up to now the program is centered on peroxy chemistry at low-temperatures associated with autoignition processes and on reactions of fuel molecules with OH radicals. The work involves quantum chemical calculations, application of transition-state theory, solution of the master equation and modeling of small reaction systems related to the experimental conditions.

II. Recent Progress

Propene + OH

It is well known that OH radicals play a central role in combustion especially at lower temperatures, where OH is the main chain carrier and is ultimately responsible for autoignition. OH radicals are usually thought of as simple H-abstractors, but depending on the other reactant the kinetics can be much more complex. We investigated several reactions involving OH radicals, which for certain reasons deviate from the behavior observed in alkane + OH reactions.

Propene is an important intermediate in many combustion mechanisms and is also a prototype alkene, which exhibits a richer combustion chemistry than ethene and yet is simple enough to permit a detailed theoretical analysis. In collaboration with Ahren W. Jasper and James A. Miller, rate coefficients at 50–3000 K temperature and from zero to infinite pressure were calculated using an RRKM-based multiwell master equation. The topography of the entrance channel required an effective two-transition-state model to be used to calculate accurate association rate coefficients.[i]

Almost perfect agreement with all available experimental data was achieved in this large temperature and pressure range by changing the inner barrier height for addition within its uncertainty limits. Our model also reproduces the change in the dominant mechanism as a function of temperature. Below ~550 K addition, while above ~700 K abstraction dominates. In the intermediate, ~550-700 K temperature range addition, backdissociation of the adducts and abstraction are all significant. The major abstraction channel leads to allyl radical + H_2O, and the major non-abstraction bimolecular product is vinyl alcohol + CH_3. Both the interest in this reaction as well as the predictive force of our model has been further demonstrated in two recent experimental papers, which found very good agreement with our published data.[ii,iii]

We also calculated dissociation rate coefficients based on the propene + OH potential energy surface (PES). The C_3H_7O isomers found on this surface correspond to the isomers obtained from propanol by H abstraction. The derived pressure and temperature dependent unimolecular dissociation rate coefficients can be readily used in combustion models of propanol ignition, where these parameters play a crucial role in establishing the composition of the low-temperature (i.e. initial) radical pool. We found several interesting pathways, such as the formation of vinyl alcohol and the ones contributing to the catalytic dehydration of alcohols.

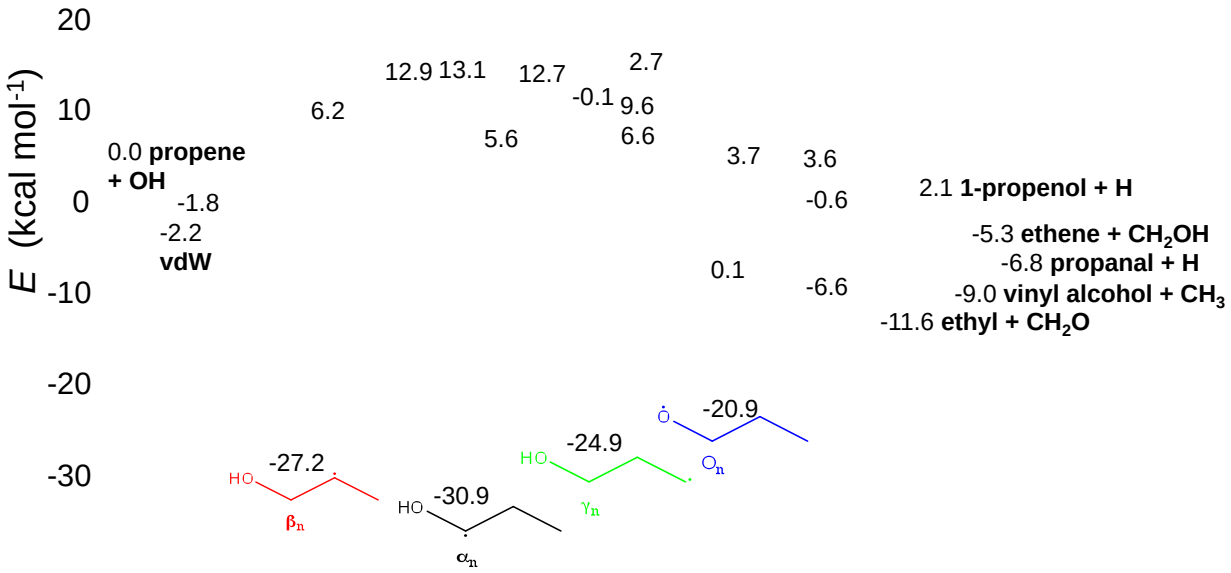

Figure 1. Part of the potential energy surface of OH + propene: addition to the terminal carbon atom.

1,3-butadiene + OH

In collaboration with Ron Hanson at Stanford University and James A. Miller the H-abstraction reactions from 1,3-butadiene by OH radical were studied. Below ~1000 K, the formation of *i*-C_4H_5 is more favored; however, above ~1000 K, the differences in the barrier heights become less important, and the fact that there are twice as many hydrogen attached to the terminal carbon atoms than to the nonterminal ones drives the branching ratio in favor of the *n*-C_4H_5 isomer. Adduct formation of course also takes place in this reaction. Our thermodynamic analysis has shown that because of the resonance stabilization of the $CH_2CHC^{\bullet}HCH_2(OH)$ adduct it is likely that at the lower end of the experimental temperature range (~1000 K) backdissociation is not instantaneous compared to the addition reaction, therefore, the observed loss of OH is faster than the abstraction rate alone.

Propanol + OH and butanol + OH

In collaboration with James A. Miller hydrogen-abstraction rate coefficients were calculated for the *n*- and *i*-propanol + OH reactions. We successfully applied the methodology previously used for the ethanol + OH reaction.[iv] The good agreement of our results with the experimental literature values for the total rate coefficients as well as for the branching fractions and kinetic isotope effects are encouraging, and suggests that this can be a way forward to larger alcohols to determine accurate abstraction rate coefficients.

However, we also calculated the rate coefficients for hydrogen abstractions from *n*-butanol by OH and found significant discrepancies compared to the experimental results at low temperatures mainly due to the γ channel. The analysis of the 2D hindering potentials revealed that in the case of the γ channel the strong interaction between the alcoholic and the radical OH groups leads to significant coupling between the rotors. This causes the overestimation of the number and densities of states. We also showed that it is very likely that higher energy conformers with larger entropy (compared to the lowest energy conformer) also contribute significantly to the rate coefficients, therefore, the 1D hindered rotor treatment is not accurate enough for this reaction.

Hydroxyethyl + O_2

In collaboration with James A. Miller and Craig A. Taatjes the possible reaction pathways for the α-hydroxyethyl + O_2 and β-hydroxyethyl + O_2 reactions were studied and zero- and high-pressure

limit rate coefficients for these systems were calculated. The α conformer produces exclusively acetaldehyde and HO_2, and because of the very low-lying exit channel the pressure dependence of this reaction is small. On the other hand, the β conformer has numerous competing channels, which are closer to each other than the expected uncertainty of our quantum chemical calculations. In the absence of detailed experimental results it is therefore difficult to predict the branching fractions.

In order to get more information on some of the product channels we carried out experiments at the Advanced Light Source in Berkeley using the molecular beam photoionization mass spectrometer. Amongst other products we showed for the first time experimentally that vinyl alcohol is a product of the β-hydroxyethyl + O_2 reaction.

Propyl + O_2 and ethyl + O_2

In collaboration with Craig A. Taatjes we modeled new chlorine-atom initiated propane oxidation experiments using the previously established PES for these reactions.[v] The goal of the work was to eliminate previously existing discrepancies between theory and experiment for the OH production. Using a better Cl-atom source and absolute OH-concentration measurements we achieved good agreement between the calculated and measured OH concentrations when the $RO_2 \leftrightarrow QOOH$ barrier heights were reduced by 0.25 kcal mol^{-1}. We also showed that these new low-pressure experiments are sensitive to the long-range part of the potential governing rate constants for $R+O_2$ addition, to the $RO_2 \leftrightarrow QOOH$ isomerization and $QOOH \leftrightarrow OH$ + cyclic ether dissociation barriers, and indirectly to the energy transfer processes. In the case of the ethyl + O_2 reaction there is a strong indication that the $CH_3CH_2O_2$ + HO_2 reaction produces a significant amount of OH radicals above 600 K.

III. Future Work

We continue our efforts to calculate more rigorous and accurate kinetic parameters to be used in combustion models. We plan to make progress on reactions involving OH radicals, especially in the context of oxygenated biofuels, where hydrogen-bonding influences the kinetics. We also plan to extend our investigations to the HO_2 radical, and to determine its role in abstraction and addition reactions. The addition reactions of HO_2 to alkenes or to aldehydes for instance are known to be important in combustion models, but are very difficult to study experimentally. To complement the propanol + OH research, we will also investigate the propanol + H and propanol + HO_2 reactions.

We also plan to explore possibilities to efficiently calculate state densities for coupled hindered rotors with multiple important minima in order to improve our results on the *n*-butanol + OH calculations. It is currently unknown how important this coupling is in terms of rate coefficients. However, based on our current calculations these might be important and can have a general importance for H abstractions from alcohols and other oxygenated compounds by OH.

As a continuation of the propene + OH investigations, we will analyze experimental data taken in the laboratory of Craig A. Taatjes together with previous experimental data from the laboratory of Frank P. Tully at Sandia and recent experimental data from the group of Matthias Olzmann at the Karlsruhe Institute of Technology on propene + OH in the intermediate, ~550-700 K range. The goal of this work is to test our previous theoretical results. The difficulty of the analysis arises due to the double exponential OH decay curves as well as the consolidation of the data originating from the various experimental setups. The result of the work will be a simplified set of reactions with validated rate coefficients to be used in combustion models for this reaction.

IV. References

i. Miller, W. H., *J. Chem. Phys.* **1976**, *65*, 2216-2223.

ii. Daranlot, J.; Bergeat, A.; Caralp, F.; Caubet, P.; Costes, M.; Forst, W.; Loison, J.-C.; Hickson, K. M., *ChemPhysChem* **2010**, *11*, 4002-4010.

iii. Krasnoperov, L. N.; Butkovskaya, N. I.; Le Bras, G., *J. Phys. Chem. A* **2011**, *111*, 2498-508.

iv. Sivaramakrishnan, R.; Su, M. C.; Michael, J. V.; Klippenstein, S. J.; Harding, L. B.; Ruscic, B., *J. Phys. Chem. A* **2010**, *114*, 9425-9439.

v. DeSain, J. D.; Klippenstein, S. J.; Miller, J. A.; Taatjes, C. A., *J. Phys. Chem. A* **2003**, *107*, 4415-4427.

V. Publications acknowledging BES support, 2009 – 2011

1. Ismail, H.; Abel, P. R.; Green, W. H.; Fahr, A.; Jusinski, L. E.; Knepp, A. M.; Zádor, J.; Meloni, G.; Selby, T. M.; Osborn, D. L.; Taatjes, C. A., Temperature-dependent kinetics of the vinyl radical (C_2H_3) self-reaction. *J. Phys. Chem. A* **2009,** *113*, 1278-1286.
2. Zádor, J.; Fernandes, R. X.; Georgievskii, Y.; Meloni, G.; Taatjes, C. A.; Miller, J. A., The reaction of hydroxyethyl radicals with O_2: A theoretical analysis and experimental product study. *Proc. Combust. Inst.* **2009,** *32*, 271-277.
3. Zádor, J.; Jasper, A. W.; Miller, J. A., The reaction between propene and hydroxyl. *Phys. Chem. Chem. Phys.* **2009,** *11*, 11040-11053.
4. Huang, H.; Merthe, D.; Zádor, J.; Jusinski, L. E.; Taatjes, C. A., New experiments and validated master-equation modeling for OH production in propyl + O_2 reactions. *Proc. Combust. Inst.* **2010,** *33*, 293-299.
5. Vasu, S. S.; Zádor, J.; Davidson, D. F.; Hanson, R. K.; Golden, D. M.; Miller, J. A., High-temperature Measurements and a theoretical study of the reaction of OH with 1,3-butadiene. *J. Phys. Chem. A* **2010,** *114*, 8312-8318.
6. Zádor, J.; Taatjes, C. A.; Fernandes, R. X., Kinetics of elementary reactions in low-temperature autoignition chemistry. *Prog. Energ. Combust. Sci.* **2011,** *available online*.

Isomer-specific Spectroscopy and Isomerization in Aromatic Fuels

Timothy S. Zwier
Department of Chemistry, Purdue University, West Lafayette, IN 47907-2084
zwier@purdue.edu

Program Definition and Scope

Under fuel-rich conditions, reactions that lead toward soot formation occur, with aromatic molecules and resonance-stabilized radicals playing key roles as intermediates. A key objective of this research program is to develop and utilize laser-based methods to characterize the spectroscopy and isomerization dynamics of conformational and structural isomers of aromatic derivatives and resonance-stabilized free radicals that play a role in soot formation. We are also characterizing the spectroscopy of model lignin compounds with the goal of providing deeper insight to the chemistry involved in the combustion and pyrolysis of wood and biofuels. Finally, we continue to study molecules in which two or more electronic states are in close proximity, and are coupled by vibrational motion involving low frequency torsions.

Recent Progress

A. Monolignols

The monolignols (shown below) form the three building blocks for lignin, and appear as breakdown products in the combustion/pyrolysis of wood and biofuels. A first manuscript on the conformer-specific spectroscopy of p-coumaryl alcohol, coniferyl alcohol, and sinapyl alcohol has just appeared in JACS.[7] In all three molecules, two conformers are observed. A combination of experimental data and calculations on the three monolignols and simpler derivatives is used to establish that the conformational preferences of the monolignols reflect the preferences of each of the ring substituents separately, enhanced by the presence of the intramolecular $OH^{\cdots}OCH_3$ H-bond.

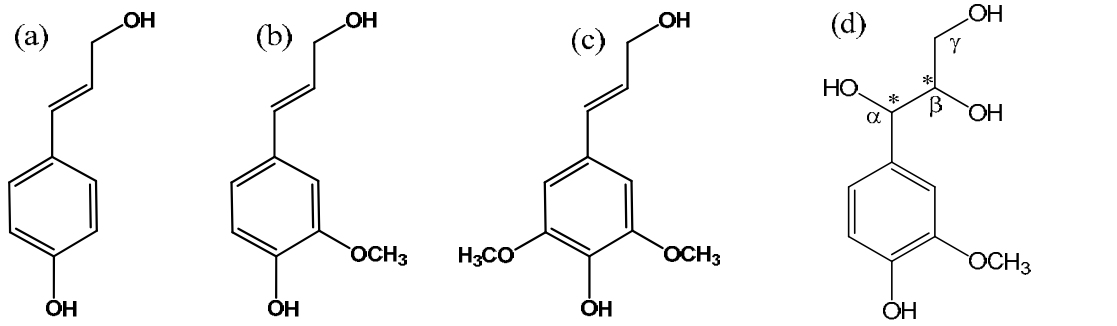

p-coumaryl alcohol | coniferyl alcohol | sinapyl alcohol | 1-(4-hydroxy-3-methoxyphenyl) propane-1,2,3-triol (HMPPT)

HMPPT (shown to the right) is the triol analog of coniferyl alchol that more closely resembles it's structure in lignin oligomers. Our collaborator, P.V. Ramachandran, a synthetic organic chemist at Purdue, has synthesized HMPPT in both (R,R) and (R,S) diastereomers. We are presently writing up a detailed study of the conformation and diastereomer-specific spectroscopy of HMPPT. In the process, we have implemented a laser desorption source that uses etched silicon as the surface from which desorption occurs. We have also utilized infrared ion-gain spectroscopy as a means for recording infrared spectra containing contributions from all conformers. It is used to identify new conformers that would otherwise be difficult to observe.

We also used it to obtain fractional abundances, providing an alternative to infrared population transfer spectroscopy for this purpose. The triol chain shows interesting H-bonded networks, including H-bonded chains that go from outer to inner OH groups or vica versa, and H-bonded cycles. The infrared spectroscopic signatures are clear in the infrared.

B. Flexible Bichromophores

Bis-(4-hydroxyphenyl)methane (b4HPM) is a model flexible bichromophore containing four flexible coordinates (two phenyl torsions and two OH torsions). In collaboration with Dr. David Plusquellic (NIST), we have explored both the ground state conformational isomerization and the excited state multi-mode vibronic coupling of b4HPM. A first paper, currently in press in J. Chem. Phys.,[8] describes the vibronic spectroscopy of jet-cooled bis-(4-hydroxyphenyl)methane (b4HPM), combining the results of fluorescence excitation (FE), dispersed fluorescence (DFL), UV-UV holeburning (UVHB), UV depletion (UVD), and fluorescence-dip infrared (FDIR) spectroscopies. Two conformers were identified which have nearly identical vibronic spectra and hydride stretch infrared spectra. The S_0-S_2 origin transitions are assigned to bands located 132 cm^{-1} above the S_0-S_1 origins of both conformers. The S_2 zero-point levels of both conformers display evidence for state-specific vibronic coupling involving S_1 vibronic levels of two types: (i) those nearby that are coupled by virtue of their close proximity, and (ii) select levels aromatic ring vibrations much further away that have large vibronic coupling matrix elements. One of the more notable aspects of this work is the development, in collaboration with David Plusquellic of NIST, of a multi-mode vibronic coupling program based on earlier theoretical descriptions of molecular dimers, here applied to flexible bichromophores.

High resolution ultraviolet spectra of both electronic origins and several other vibronic bands of the two conformers have also been recorded at NIST, again in collaboration with D. Plusquellic. These spectra provide further insight to the vibronic coupling via the dependence of the transition dipole moment on the vibronic transition involved. A paper describing this work is in press in J. Phys. Chem.[9]

Finally, SEP-population transfer spectroscopy has been used to determine the barrier heights separating the minima in the ground state. Barriers of less than 50 cm^{-1} are determined, about ten times smaller than other barriers we have studied by these methods. A calculated two-dimensional phenyl torsional potential energy surface is used to predict the vibrational energy levels both below and above the barriers to isomerization.

C. Resonance-stabilized free radicals

We are beginning studies aimed at spectroscopically characterizing resonance-stabilized aromatic radicals using the isomer-specific tools available to us. To that end, we have recently mapped out the vibronic spectroscopy of the 1-phenylallyl radical created and cooled in an electric discharge supersonic expansion source. This spectrum was recorded using two-color R2PI spectroscopy, with first photon in the middle of the visible where the first electronic transition of the radical occurs. We have also recorded the first resonant ion-dip infrared (RIDIR) spectrum of a free radical, which is shown in Figure 1. This spectrum was crucial to identification of the isomer. As can be seen from the figure, the match-up between experiment and theory is unequivocal in assigning the observed isomer as *trans*-1-phenylallyl radical. This radical gains importance as a doubly-resonance-stabilized radical in which the (nominal) radical site bridges the phenyl and vinyl groups.

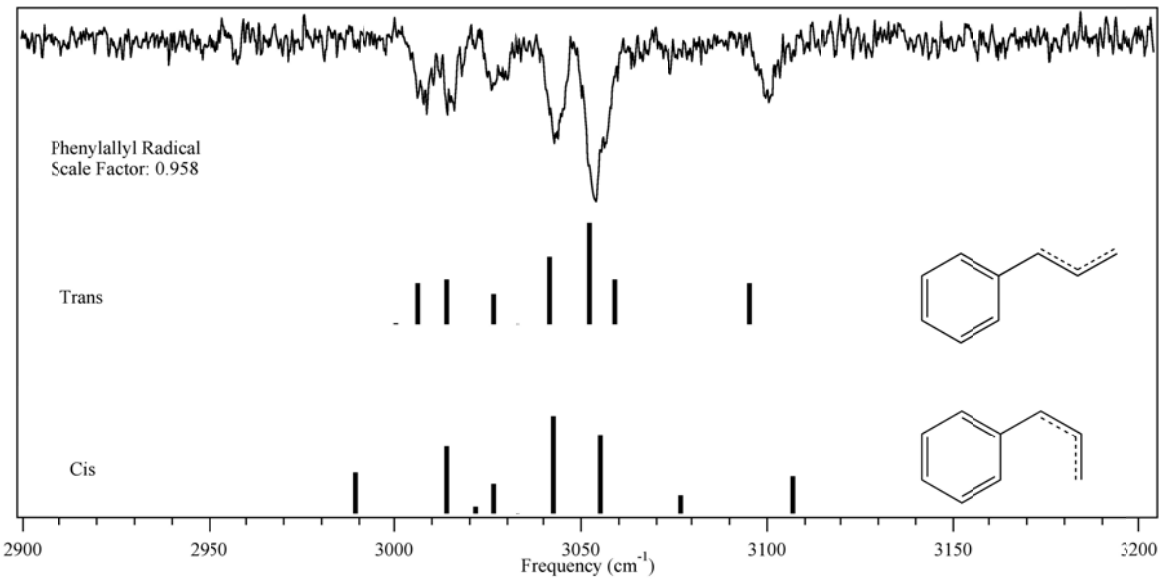

Figure 1: RIDIR spectrum of 1-phenylallyl radical in the CH stretch region (top trace). Calculated IR spectra for *cis* and *trans* isomers (below).

Future work

We plan to study the conformation-specific spectroscopy of three model lignin dimers. Our collaborators, P.V. Ramachandran and his group, have synthesized two of the three dimers shown below, containing different chemical linkages (-O-4 and) for this purpose. Electronic coupling between the chromophores should also manifest itself in the spectroscopy, making a nice linkage with our on-going studies of flexible bichromophores.

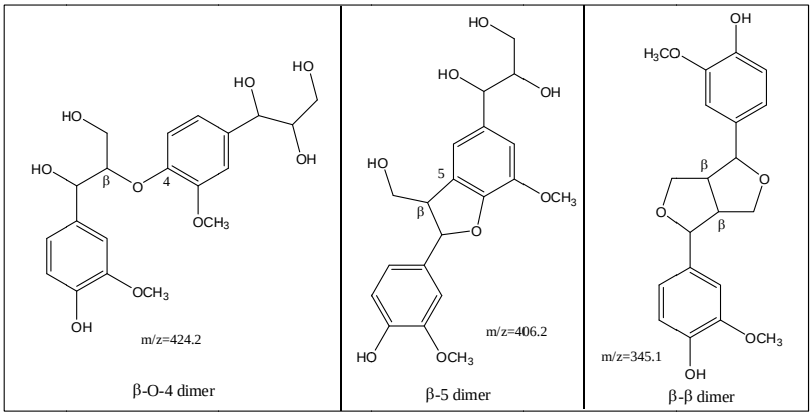

Our new multi-stage mass spectrometer for cold ion spectroscopy is nearly complete, and is undergoing final testing. We plan to test out electrospray ionization of lignin oligomers with the goal of studying the spectroscopy and photofragmentation of larger lignin oligomer ions under cold conditions.

We also plan to extend our studies of the vibrational spectroscopy of resonance-stabilized free radicals, focusing attention on the 1-hydronaphthyl, 2-hydronaphthyl, benzylallenyl, and phenylpropargyl radicals. We will record RIDIR spectra first in the CH stretch region, where calculations predict significant differences between the isomers. We hope to expand our spectroscopy down into the mid-infrared using a new medium-resolution IR OPO/OPA that can

scan broadly throughout this region with sufficient power. We also plan to take excited state RIDIR spectra of these radicals, since IR spectroscopy may be one of the most effective tools for characterizing the excited states of these radicals. Calculations are still challenging on excited states of free radicals, and standard methods (e.g., TDDFT) often have significant errors in predicting the energies and structures of the excited states. We would like to provide tests for theory on excited states of radicals with our spectroscopy. Finally, we will extend our studies of radicals to include radicals with longer alkyl chains, where conformation-specific methods are needed.

Publications acknowledging DOE support, 2008-present

1. Nathan R. Pillsbury, Jaime A. Stearns, Aloke Das, Talitha M. Selby, David F. Plusquellic, and Timothy S. Zwier, "State-specific studies of Internal Mixing in a Prototypical Flexible Bichromophore: Diphenylmethane", J. Chem. Phys. **129** 114301 (2008).

2. Nathan R. Pillsbury and Timothy S. Zwier, "Conformation-specific spectroscopy and excited state photophysics of 5-phenyl-1-pentene", J. Phys. Chem. A **113**, 118-125 (2009).

3. Nathan R. Pillsbury and Timothy S. Zwier, "Conformational isomerization of 5-phenyl-1-pentene probed by SEP-population transfer spectroscopy", J. Phys. Chem. A **113**, 126-134 (2009).

4. Jaime A. Stearns, Nathan R. Pillsbury, Christian W. Müller, Kevin O. Douglass, Timothy S. Zwier, and David F. Plusquellic, "Rotationally resolved studies of S_0 and the exciton coupled S_1/S_2 origin regions of diphenylmethane and its d_{12} isotopologue", J. Chem. Phys. **129**, 224305 (2009).

5. Nathan R. Pillsbury, Christian W. Muller, and Timothy S. Zwier, "Conformational Effects on Excitonic Interactions in a Prototypical H-bonded Bichromophore: Bis(2-hydroxyphenyl) methane", J. Phys. Chem. A **113**, 5000-5012 (2009).

6. Nathan R. Pillsbury and Timothy S. Zwier, "The Conformational Isomerization and Collisional Cooling Dynamics of Bis-(2-hydroxyphenyl)methane", J. Phys. Chem. A **113**, 5013-5021 (2009).

7. Chirantha P. Rodrigo, William H. James III, and Timothy S. Zwier, "Single-conformation ultraviolet and infrared spectra of jet-cooled monolignols: p-coumaryl alcohol, coniferyl alcohol, and sinapyl alcohol", J. Am. Chem. Soc. **133**, 2632-2641 (2011).

8. Chirantha P. Rodrigo, Christian W. Müller, Nathan R. Pillsbury, William H. James III, Timothy S. Zwier, and David F. Plusquellic, "Conformer-specific vibronic spectroscopy and vibronic coupling in a flexible bichromophore: bis-(4-hydroxyphenyl)methane", J. Chem. Phys. (in press).

9. Chirantha P. Rodrigo, Christian W. Müller, Timothy S. Zwier, and David F. Plusquellic, "Rotationally resolved studies of S_0 and the exciton coupled S_1/S_2 origin regions of bis-(4-hydroxyphenyl)methane", J. Phys. Chem. A (accepted).

Participant List

32nd Annual Combustion Research Meeting Participation List

Last Name	First Name	Organization	Email
Ahmed	Musahid	Lawrence Berkeley National Laboratory	mahmed@lbl.gov
Alexander	Millard	University of Maryland	mha@umd.edu
Allen	Wesley	University of Georgia	wdallen@uga.edu
Baer	Tomas	University of North Carolina	baer@unc.edu
Bellan	Josette	Jet Propulsion Laboratory, California Institute of Technology	josette.bellan@jpl.nasa.gov
Bowman	C. Tom	Stanford University	ctbowman@stanford.edu
Bowman	Joel	Emory University	jmbowma@emory.edu
Brown	Nancy	Lawrence Berkeley National Lab	NJBrown@lbl.gov
Bunel	Emilio	Argonne National Laboratory	ebunel@anl.gov
Butler	Laura	University of Chicago	L-Butler@uchicago.edu
Casassa	Michael	Office of Basic Energy Sciences, U.S. Department of Energy	michael.casassa@science.doe.gov
Chandler	David	Sandia National Laboratories	chand@sandia.gov
Chen	Jacqueline	Sandia National Labs	jhchen@sandia.gov
Continetti	Robert	University of California, San Diego	rcontinetti@ucsd.edu
Cool	Terrill	Cornell University	TAC13@CORNELL.EDU
Crim	Fleming	University of Wisconsin-Madison	fcrim@chem.wisc.edu
Dagdigian	Paul	Johns Hopkins University	pjdagdigian@jhu.edu
Daily	John	University of Colorado	john.daily@colorado.edu
Davis	Floyd	Cornell University	hfd1@cornell.edu
Davis	Michael	Argonne National Laboratory	davis@tcg.anl.gov
Debusschere	Bert	Sandia National Laboratories	bjdebus@sandia.gov
Dibble	Theodore	SUNY-ESF	tsdibble@syr.edu

Driezler	Andreas	Technische Universitaet Darmstadt	dreizler@csi.tu-darmstadt.de
Ellison	Barney	University of Colorado at Boulder	barney@jila.colorado.edu
Ervin	Kent M.	University of Nevada, Reno	ervin@unr.edu
Fiechtner	Greg	Office of Basic Energy Sciences, U.S. Department of Energy	Gregory.Fiechtner@science.doe.gov
Field	Robert	MIT	rwfield@mit.edu
Flynn	George	Columbia University	gwf1@columbia.edu
Frank	Jonathan	Sandia National Laboratories	jhfrank@sandia.gov
Frenklach	Michael	Lawrence Berkeley National Lab	myf@me.berkeley.edu
Green	William	MIT/Dept. of Chemical Engineering	balkwill@mit.edu
Guo	Hua	University of New Mexico	hguo@unm.edu
Hall	Gregory	Brookhaven National Lab	gehall@bnl.gov
Hansen	Nils	Sandia National Laboratories	nhansen@sandia.gov
Hanson	Ronald	Stanford University	rkhanson@stanford.edu
Harding	Lawrence	Argonne National Laboratory	harding@anl.gov
Harris	Alexander	Brookhaven National Lab	alexh@bnl.gov
Head-Gordon	Martin	Lawrence Berkeley National Lab	m_headgordon@berkeley.edu
Hershberger	John	North Dakota State University	john.hershberger@ndsu.edu
Hirata	So	University of Florida	hirata@qtp.ufl.edu
Hoffmann	Mark	University of North Dakota	mhoffmann@chem.und.edu
Jasper	Ahren	Sandia National Laboratories	ajasper@sandia.gov
Kaiser	Ralf	University of Hawaii	ralfk@hawaii.edu
Kellman	Michael	University of Oregon	kellman@uoregon.edu
Kerstein	Alan	Sandia National Laboratories	arkerst@sandia.gov
Khokhlov	Alexei	The University of Chicago	ajk@oddjob.uchicago.edu
Kliewer	Chris	Sandia National Laboratories	cjkliew@sandia.gov
Klippenstein	Stephen	Argonne National Laboratory	sjk@anl.gov
Krylov	Anna	University of Southern California	krylov@usc.edu
Lansdon	Connie	Oak Ridge Associated Universities	Connie.Lansdon@orise.orau.gov

Leone	Stephen	Lawrence Berkeley National Lab	srl@berkeley.edu
Lester	Marsha	University of Pennsylvania	milester@sas.upenn.edu
Lester, Jr.	William	Lawrence Berkeley National Lab	walester@lbl.gov
Lignell	David	Brigham Young University	davidlignell@byu.edu
Long	Marshall	Yale University	marshall.long@yale.edu
Lucht	Robert	Purdue University	Lucht@purdue.edu
Macdonald	Robert	Argonne National Laboratory	rgmacdonald@anl.gov
McCarthy	Michael	Harvard-Smithsonian Center for Astrophysics	mccarthy@cfa.harvard.edu
McCunn	Laura	Marshall University	mccunn@marshall.edu
McIlroy	Andrew	Sandia National Laboratories	amcilr@sandia.gov
Mebel	Alexander	Florida International University	mebela@fiu.edu
Michael	Joe	Argonne National Laboratory	jmichael@anl.gov
Michelsen	Hope	Sandia National Laboratories	hamiche@sandia.gov
Miller	Terry	Ohio State University	tamiller+@osu.edu
Miller	William	Lawrence Berkeley National Lab	millerwh@berkeley.edu
Mullin	Amy	University of Maryland	mullin@umd.edu
Najm	Habib	Sandia National Laboratories	hnnajm@sandia.gov
Nesbitt	David	JILA, NIST, Department of Chemistry and Biochemistry	djn@jila.colorado.edu
Neumark	Daniel	Lawrence Berkeley National Lab	dneumark@berkeley.edu
Ng	Cheuk-Yiu	University of California, Davis	cyng@chem.ucdavis.edu
Oefelein	Joseph	Sandia National Laboratories	oefelei@sandia.gov
Osborn	David	Sandia National Laboratories	dlosbor@sandia.gov
Parish	Carol	University of Richmond	cparish@richmond.edu
Pantano-Rubino	Carlos	University of Illinois at Urbana-Champaign	cpantano@illinois.edu
Pederson	Mark	Office of Basic Energy Sciences, U.S. Department of Energy	Mark.Pederson@science.doe.gov
Perry	David	The University of Akron	dperry@uakron.edu
Piecuch	Piotr	Michigan State University	piecuch@chemistry.msu.edu
Pitz	William	Lawrence Livermore National Laboratory	pitz1@llnl.gov

Pope	Stephen	Cornell University	s.b.pope@cornell.edu
Pratt	Stephen	Argonne National Laboratory	stpratt@anl.gov
Reisler	Hanna	University of Southern California	reisler@usc.edu
Ruscic	Branko	Argonne National Laboratory	ruscic@anl.gov
Schaefer	Henry	University of Georgia	sch@uga.edu
Sears	Trevor	Brookhaven National Laboratory	sears@bnl.gov
Settersten	Thomas	Sandia National Laboratories	tbsette@sandia.gov
Shepard	Ron	Argonne National Laboratory	shepard@tcg.anl.gov
Sheps	Leonid	Sandia National Laboratories	sheps@jila.colorado.edu
Sisk	Wade	Office of Basic Energy Sciences, U.S. Department of Energy	wade.sisk@science.doe.gov
Sivaramakrishnan	Raghu	Argonne National Laboratory	raghu@anl.gov
Smooke	Mitchell	Yale University	mitchell.smooke@yale.edu
Stanton	John	University of Texas at Austin	jfstanton@mail.utexas.edu
Suits	Arthur	Wayne State University	asuits@chem.wayne.edu
Sutherland	James	University of Utah	James.Sutherland@utah.edu
Sztáray	Bálint	University of the Pacific	bsztaray@pacific.edu
Taatjes	Craig	Sandia National Laboratories	cataatj@sandia.gov
Tranter	Robert	Argonne National Laboratory	tranter@anl.gov
Truhlar	Donald	University of Minnesota	truhlar@umn.edu
Vander Wal	Randy	Penn State University	ruv12@psu.edu
Wagner	Albert	Argonne National Laboratory	wagner@anl.gov
Weber	Peter	Brown University	Peter_Weber@brown.edu
Westbrook	Charles	Lawrence Livermore National Laboratory	westbrook1@llnl.gov
Wilson	Kevin	Lawrence Berkeley National Lab	krwilson@lbl.gov
Wittig	Curt	University of Southern California	wittig@usc.edu
Wooldridge	Margaret	University of Michigan	mswool@umich.edu
Yarkony	David	Johns Hopkins University	yarkony@jhu.edu
Yu	Hua-Gen	Brookhaven National Laboratory	hgy@bnl.gov

Zádor	Judit	Sandia National Laboratories	jzador@sandia.gov
Zwier	Timothy	Purdue University	zwier@purdue.edu